Physical and Catalytic Properties of High Silica Faujasites

Nicholas Henry John Stanbridge, B.Sc.

Thesis submitted to the University of Nottingham for the degree of Doctor of Philosophy, October 1995.

Abstract

The research described in this thesis was conducted over a total of three years during the period October 1990 to October 1994, and is the sole work of the author, unless indicated otherwise by reference.

A series of mildly dealuminated Y zeolites has been prepared by hydrothermal treatment using a low partial pressure of water vapour. These materials, together with samples previously dealuminated under more severe conditions, were characterised by the temperature programmed desorption of ammonia and the catalytic activity for suitable test reactions.

Advances in technique permitted simultaneous monitoring of both the deammoniation and dehydroxylation processes. Interesting features were observed in the dehydroxylation traces which were related to changes in the acid site strength and amount of extraframework aluminium.

The activity for both n-hexane cracking and toluene disproportionation reaches a maximum, corresponding to a framework concentration of 25-30 structural aluminium atoms per unit cell, consistent with the maximum number of strong acid sites. Slight deviation from this behaviour was noted, with the mildly steamed catalysts having lower activities than would be expected on the basis of their framework compositions alone. An in-depth analysis of the cracking of n-hexane has revealed that the extent of reaction is also critically dependent on the density of the available acid sites, which is explained in terms of the reaction mechanism.

The disproportionation of toluene has highlighted differences in the nature of the extrastructural aluminium. The catalytic activity of the materials is either decreased or enhanced on extraction depending on whether the catalysts have been prepared by mild or severe dealumination. Variations in product distribution with time on stream have been observed and accounted for by changes in the reaction. The lifetime and activity profile of the catalyst could be altered by exposure of the catalyst to small amounts of toluene prior to the main reaction. This supports the concept of active coke enhancing this reaction.

Cumene dealkylation was found to proceed on weaker acid sites than the cracking of n-hexane and the disproportionation of toluene, although a maximum in activity was still observed. This indicates that the weakest sites are not capable of catalysing this reaction, and that some heterogeneity of site strength exists between strong and weak acid sites.

The dehydration of propan-2-ol was confirmed as a reaction which assesses the total number of acid sites, regardless of strength. However, changes in the selectivity of the products with the strength of the acid sites were found, implying that the formation of di-isopropylether is favoured by strong sites. Deliberate coking of the catalyst surface by exposure to propan-2-ol at elevated temperatures was found to increase the measured activity, in addition to changing the selectivity almost entirely in favour of propene.

Extraframework aluminium was found to play an important role in all of the reactions studied. This emphasises the view that although structural aluminium has the larger influence on the overall activity of a catalyst for a particular reaction, the nature of the extraframework aluminium cannot be overlooked.

Acknowledgements

I would like to express my gratitude to Dr R.Rudham, under whose supervision this research was carried out, for his advice, encouragement and friendship.

I would like to thank my parents for giving me the opportunities and desire to further my education, and finally, I would also like to thank Liesel Carrington, for all her support and encouragement, given unreservedly at the times when they were needed most.

This work was funded by the award of a Quota grant from the Science and Engineering Research Council.

1 Introduction

1.1 General Introduction 1

1.2 Physical Properties of Y Zeolite 3

1.21 Structure and Composition: 3

Structural Investigation 6

Surface Acidity: 8

Generation and Detection of Acid Sites 9

Strength of Acid Sites 13

1.22 Modification: 15

Ion Exchange 15

Dehydroxylation 15

Dealumination 19

1.3 Catalytic Properties of Y Zeolite 29

1.31 Alcohol Reactions 32

1.32 Alkene Reactions 33

1.33 Alkylaromatic Reactions 34

1.34 Alkane Reactions 38

2 Experimental

2.1. Catalyst Preparation 41

2.11 Hydrothermal Dealumination 41

2.12 Extraction of Extraframework Aluminium 42

2.2. Catalyst Characterisation 43

2.21 Temperature Programmed Desorption 43

Theory and Principles of Mass Spectrometry 43

Apparatus: 45

The Service Section 46

The Experimental Section 47

The Control Section 48

Experimental Procedure 49

Mass Spectrometer Bakeout: 49

The TPD Experiment 50
Computer Programs: 52
Control Programs 52
Analysis Programs 53
2.22 Mid Infrared Spectroscopy 53
2.23 X-ray Diffraction 53
2.24 Thermogravimetric Analysis 54
2.3 Catalysis 55
2.31 Pulse Flow Apparatus: 55
2.32 n-Hexane Cracking Experiments 57
2.33 Cumene Dealkylation Experiments 59
2.34 Toluene Disproportionation Experiments 61
2.35 Continuous Flow Apparatus: 63
2.36 Toluene Disproportionation Experiments 64
Coking Experiments 66
2.37 Propan-2-ol Dehydration Experiments 66
Temperature Dependent Experiments 66
Pressure Dependent Experiments 67
Coking Experiments 68

3 Results
3.1 Characterisation 70
3.11 Infrared Spectroscopy and X-ray Crystallography 71
3.12 Temperature Programmed Desorption 78
3.2 Catalysis 87
3.21 n-Hexane Cracking 89
Toluene Disproportionation
3.22 Pulse Flow Experiments 119
3.23 Continuous Flow Experiments 133
Coking Experiments 145
3.24 Cumene Dealkylation 149
3.25 Propan-2-ol Dehydration 178
Temperature Dependent Experiments 180

Pressure Dependent Experiments 194
Coking Experiments 206

4 Discussion

4.1 Preparation and Characterisation 207
4.2 Temperature Programmed Desorption 210
Deammoniation Studies 211
Dehydration and Dehydroxylation Studies 216
4.2 n-Hexane Cracking 225
4.3 Toluene Disproportionation
Pulse Flow 247
Continuous Flow 251
4.4 Cumene Dealkylation 256
4.5 Propan-2-ol Dehydration 270

5 Conclusions 283

References 288

Appendix

Computer Programs 305

1 Introduction

1.1 General Introduction

Natural zeolites are crystalline aluminosilicates and comprise a group of around forty members, to which over one hundred and twenty synthetic types have been added in the last forty years. Interest in zeolites was mainly geological until the twentieth century when it was discovered that natural occurrence was much more widespread than had previously been thought. The second half of the century brought synthetic methods of preparation, which allowed specific tailoring of the structure of the zeolite; this led to an explosion in the research dedicated to zeolites, their chemistry and their applications.

All zeolites consist of an aluminosilicate framework which plays host to cations and water molecules. This may be represented by the general formula

$$M_{x/n}[(AlO_2)_x(SiO_2)_y]zH_2O$$

where M is a cation of valency n and y/x is the silicon/aluminium ratio of the framework. The charge balancing cations are necessary to offset the single negative charge introduced on the inclusion of each AlO_2 unit. Although the cations can be exchanged, eg. sodium for ammonium, they can never be removed. In contrast, all physically adsorbed water can be removed from the zeolite to produce a highly hydrophilic material. Many different framework structures exist, resulting in materials of widely differing properties. Details of many modern zeolites have been collated by Dyer.[1]

Zeolite nomenclature has two components, reflecting the inorganic framework and the resident cations. Natural zeolites are usually referred to by historical names, whereas synthetic zeolites use a Roman or Greek letter to signify structural type (eg. A, X, Y, ZSM-5, Rho, Omega). The identity of the cations is indicated by prefixing their chemical symbol, eg. Na-A, Ca-A. In addition, the treatment to which a zeolite may have been subjected can also be included in the name. Thus a zeolite may be referred to as dehydroxylated, deammoniated or dealuminated HY. Some basic rules on nomenclature have been proposed by Breck.[2] Full details of the definitions and processes leading

to these, and other types of zeolite, are included in the relevant section.

The first syntheses of zeolites, carried out as early as the middle of the nineteenth century, are now thought to be unreliable due to the lack of suitable experimental techniques available to characterise and verify the products obtained. The first successful syntheses, of mordenite in 1948,[3] and synthetic zeolite A in 1956, [4] required conditions of high pressure and temperature. More modern methods use lower temperatures and pressures. A zeolite synthesis requires a silica source and an aluminium source, which, when combined with water under high pH conditions, generate a homogeneous gel from which the product can be crystallised. Varying the silica/alumina ratio in the gel determines the framework composition of the zeolite; all the available aluminium is normally utilised. The silica is supplied in the form of hydrated soluble silicates, or from sols made from fumed silica, and the aluminium is provided by metal aluminates, or possibly aluminium hydroxides or salts. Alkalinity has been shown to effect crystallisation times. Barrer[5] has shown that optimum production of mordenite is obtained at alkalinities between pH 12 and pH 13, with the shortest crystallisation times at pH 12.85. Charge balancing cations are required to maintain electronic neutrality, and so, combined with the need to preserve a high pH, alkali metals and alkaline earth hydroxides are usually employed. Some syntheses[6] have used organic cations such as tetramethylammonium and the use of other substituted ammonium molecules has been reviewed.[7]

The cations present can have the secondary function of templating or controlling the crystallisation. It is thought that different cations can have diverging roles, eg. sodium disrupts the water structure allowing crystallisation to occur, whereas calcium increases the structure in the water.[1] Water molecules can be arranged into large polymolecular clusters with specific symmetries which can fit inside zeolitic cavities. It has also been suggested that some cations have a stabilising effect on the structural building blocks. Organic cations can exhibit structure directing properties; it is believed that the zeolite would form around the cation, which, when removed, leaves the cavities and pores of the structure.

In addition to aluminosilicate zeolites, recent years have seen the development of aluminophosphates, AlPOs[8], and silico-aluminophosphates, SAPOs[9]. These materials are of interest because, as well as being catalytically active, some structures have been reported as being identical to those of well established zeolites. Three AlPO structures are directly analogous to zeolites, namely, AlPO-17, offretite type, AlPO-20, sodalite type and AlPO-24, anaclime type. Similarly, SAPO-37 has the faujasite structure, SAPO-20 the sodalite structure, and SAPO-42 the structure of Zeolite A.

1.2 Physical Properties of Y Zeolite

1.21 Structure and Composition.

All zeolite frameworks consist of an infinite three dimensional array of silica and alumina tetrahedra, with the silicon or aluminium atoms lying at the centre of tetrahedra, and an oxygen atom at each of the four vertices. Different types of zeolite have different arrangements of the tetrahedra, although certain common elements persist from type to type. The basic building block of zeolite Y is the double six ring (D6R). Four such rings when linked tetrahedrally, enclose a void, the sodalite unit (figure 1.1). This consists of twenty four tetrahedra linked to form a truncated octahedron, with 8 hexagonal faces and 6 square faces. The tetrahedral atoms lie at the intersections of the lines in the diagram, and the oxygen are displaced slightly from the midpoint of each line to allow a true tetrahedral environment around the central atom. Although all the tetrahedral sites are identical, there are four different types of oxygen, distinguishable from their position within the sodalite unit: these are labelled O_I to O_{IV} on the diagram. Each sodalite unit is linked to four others tetrahedrally via the double six rings (figure 1.2): eight sodalite units thus linked form the unit cell.

The distribution of aluminium within the framework can be described by two rules. Loewenstein[10] postulated that direct Al-O-Al groups are forbidden, and Dempsey[11] concluded that the number of Al-O-Si-O-Al groups within the framework are minimised. These rules are thought to apply equally

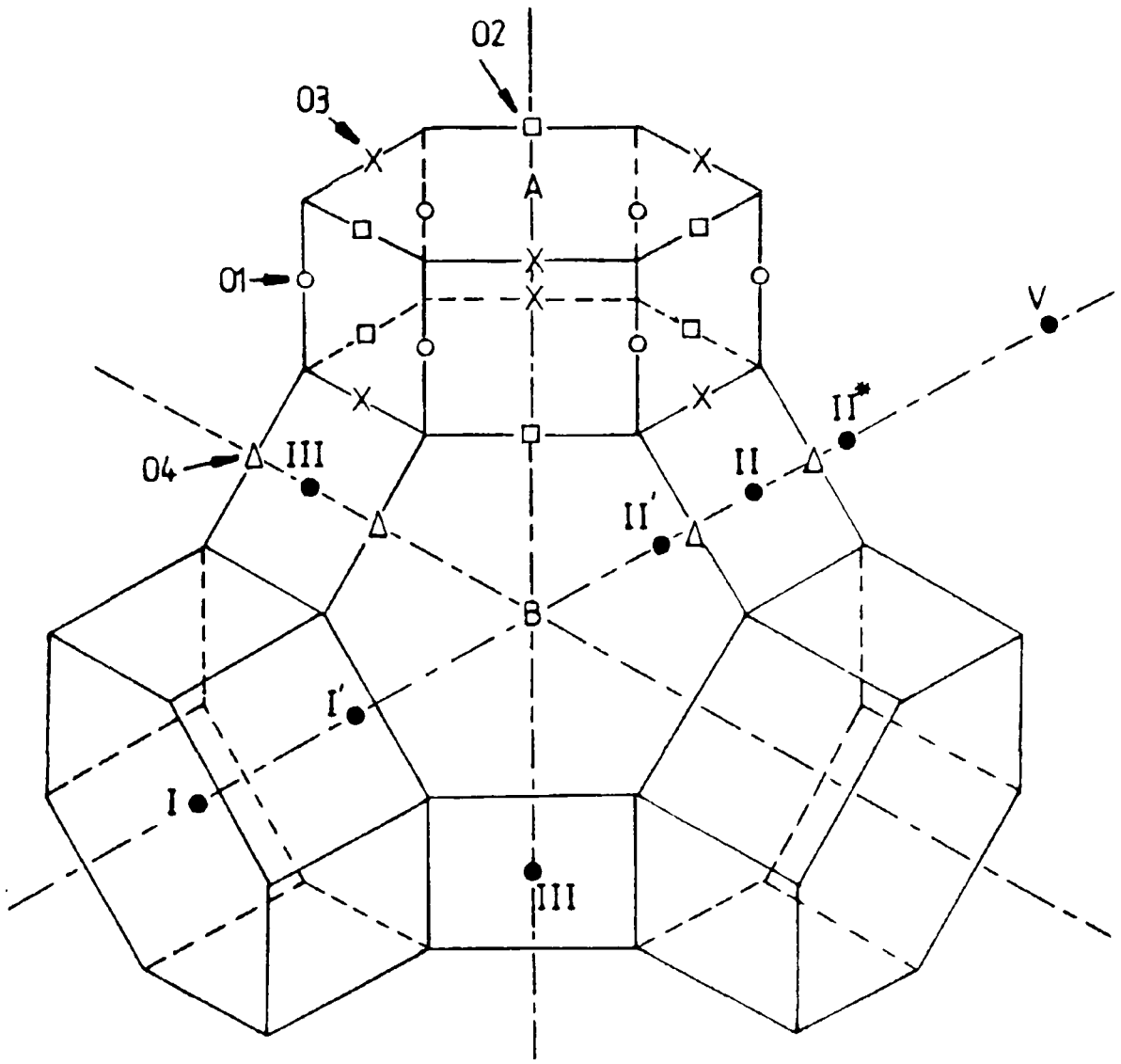

Figure 1.1: Idealised representation of three of four hexagonal prisms, A, surrounding the sodalite unit, B. Cation sites and distinguisable oxygen atoms are included.

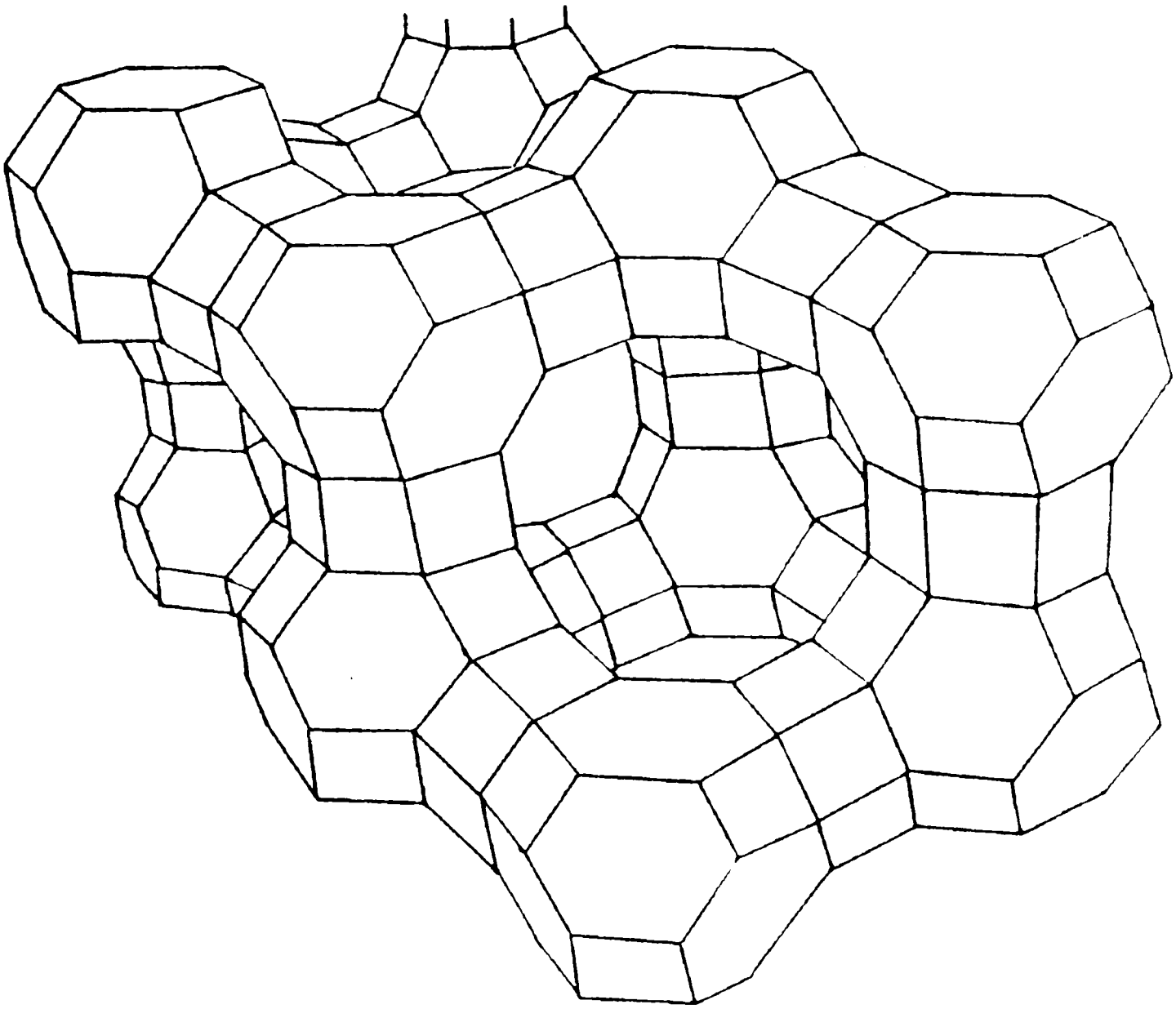

Figure 1.2: Line drawing of the faujasite structure.

to any aluminosilicate framework structure, be it natural, synthesised or altered by post synthesis methods. However, recent *ab initio* calculations have shown that it is possible to violate these postulations[12,13] and the synthesis of small fragments which transgress these rules has been claimed.[14]

The three dimensional structure of the framework leads to a complex series of cavities interlinked by channels. The smaller cavities lie within the sodalite units and are termed ß-cages, having a internal free diameter of 0.66nm. However, the smaller pore opening of 0.22nm in the distorted six membered ring excludes all but the smallest molecules eg. water carbon dioxide. The space enclosed by the sodalite units when building up the unit cell is called the α-cage or supercage, which has an internal free diameter of approximately 1.3nm. This is accessed through four distorted twelve membered rings of diameter about 0.74nm permitting entry of larger molecules eg. aromatic and branched chain hydrocarbons. The α-cages are tetrahedrally linked, and the resulting extensive internal network gives the material a very high surface area per unit mass and a void space which approaches half of the total volume of the dehydrated crystal.[15] When the zeolite is in the hydrated form these pores are filled with water molecules, approximately two hundred and fifty in each unit cell, or thirty per supercage.

As-synthesised zeolite Y has between fifty and seventy five aluminium atoms in the unit cell, giving a typical composition of

$$Na_{56}(AlO_2)_{56}(SiO_2)_{136}.250H_2O$$

and exhibits cubic symmetry. Each unit cell has eight sodalite units, eight supercages, thirty two free hexagonal rings and sixteen hexagonal prisms. The amount of aluminium contained in the framework is expressed either as the Si/Al ratio or as the framework aluminiums per unit cell, Al_F puc. These two expressions of framework content are related by the equation:

$$Al_F = \frac{192}{1 + Si/Al}$$

The inclusion of aluminium in the framework introduces negative charge, so that each aluminium necessitates the presence of a counterbalancing positive charge to preserve electronic neutrality. The position of the cations

within the framework structure was first described in simple terms by Breck.[16] He identified three positions, namely at the centre of the hexagonal prism, at the centre of the free hexagonal face, and within the supercage. Smith[17] extended and amplified this classification into the following, which has become accepted as the model for cation location. These are marked in figure 1.1 and are as follows:

I. Centre of hexagonal prism

I'. In the sodalite unit next to the hexagonal face between the sodalite unit and the hexagonal prism.

II. In the supercage next to the unshared hexagonal face of the sodalite unit.

II'. In the sodalite unit next to the unshared hexagonal face of the sodalite unit.

II*. As II, but further into the supercage.

III. In the supercage, next to the four ring group in the sodalite unit.

V. Near the centre of the twelve membered ring in the supercage.

U. At the centre of the sodalite unit.

The situation is further complicated by differences in nomenclature used by authors, and the grouping together of some of the sites[18] due to confusing x-ray data. The occupancy of the sites is determined by hydration and electrostatic co-ordination factors. For example, a cation in site I can be octahedrally co-ordinated by a slight movement of the six oxygen atoms in position O_{III}. Similarly, trigonal coordination can be achieved by a cation at site I' by slight movement of three O_{III} oxygens, as it can be at sites II and II' by movement of O_{II} oxygens. Cations at site III can obtain distorted square planar coordination from the four membered ring of the sodalite unit. Other sites are too far away from the framework for bonding interactions.

Attempts to produce computer models of the structure and properties of zeolites have been made;[19,20,21] this particular field can only increase in importance as computational techniques increase in refinement.

Structural Investigation

The highly crystalline nature of zeolites allows the production of very well defined x-ray diffractograms. Although natural zeolites produce large enough crystals for single crystal studies, synthetic crystals are too small. However, the detail in the x-ray powder diffractograms is high enough to permit detailed analysis of the structure, based on either the (331) peak, thought to be unaffected by cation and hydration levels[22] or a number of peaks,[23] resulting in information on the unit cell size and crystallinity.

The unit cell decreases as aluminium is removed from the framework and replaced by silicon, primarily due to the Si-O bond being shorter than that of Al-O (0.161nm cf 0.174nm). In theory the unit cell size can be used as an indicator of the aluminium content of the framework, as has been shown in a number of studies,[24,25,26] reviewed by Kerr.[27] When considering x-ray data it is essential to use a well defined standard, ie. a highly crystalline sample of known composition. Furthermore, it is necessary to ensure that the samples are in as similar a state as possible. Fritz *et al*[28] have shown that both dehydration and extent of exchange of sodium for ammonium increase the cell constant by the equivalent of up to ten aluminium atoms per unit cell, indicating that potentially misleading results can be obtained. These results support the findings of others,[24,29] but run counter to those of Klinowski and Anderson.[30] The crystallinity of a zeolite sample can be assessed from the integrated intensities of certain lines,[23] but once again results must be compared with a standard.

Mid range infrared [24,31,32] and Raman[33,34] spectroscopy have both been used to aid the investigation of zeolite structures. The region of the infrared spectrum between 200 and 1300cm^{-1} contains features common to all aluminosilicates. These peaks can be divided into two classes proposed by Flanigen *et al*[35]: those originating from vibrations within the tetrahedra and those from without. The first group are found in all aluminosilicates and are insensitive to structural variations. The second group, as they are generally weaker than the first and are subject to changes due to structure, are of less interest. Flanigen[36] has reviewed work on the linear relationships between the

aluminium content and the wavenumber of four vibrations, namely the external symmetric and asymmetric stretches, and the double six ring, D6R, and twelve ring, 12R, breathing modes. Kubelková et al[31] reported linear relationships between the wavenumber of the bands at *ca* 1050cm^{-1} and *ca* 820cm^{-1} and the aluminium content of a series of dealuminated HY samples. It was found that the equations derived could only be used for samples with a Si/Al ratio of less than 10, as the error for more siliceous frameworks was as much as 10%, and increased with increasing aluminium content. Similarly the wavenumber of the D6R band was found to exhibit non-linear behaviour with respect to aluminium content. It was further found that removal of the non framework aluminium species (by EDTA treatment) did not affect the linearity of the dependence, although it did highlight the need for internal standardisation of the method. This demonstrated the importance of structural factors in the tetrahedral stretching vibrations. Attempts have also been made to relate the intensity of the bands to aluminium content.[32] The variation in the area of the 730cm^{-1} band was found to be linearly related to the aluminium content. This band was assigned to isolated AlO_4 tetrahedra, and the other main bands were found not to vary in intensity with aluminium content.[32] Various studies have calculated the infrared spectra of zeolites using *ab initio* methods and, with the advent of increasingly powerful computers, are able to use more advanced models.[37,38,39,40]

Both x-ray crystallography and infrared spectroscopy rely heavily on the original determination of the framework composition, which until recently was determined by wet chemical methods. Furthermore, they are derivative techniques, in that the experimental value of the wavenumber of the unit cell is applied to an equation from which an answer is obtained. The applicability, or otherwise, of the equation over the range of samples, and the different conditions used by different workers combine to produce uncertainties in the final result. In addition, these methods require a homogenous distribution throughout the framework for best results, a condition that cannot be always assumed.[21,41,42]

Since the early applications of magic angle spinning nuclear magnetic resonance (masnmr) to the characterisation of zeolite frameworks,[43,44] its use

has become widespread,[45,46,47,48] and it is now accepted as the best method for determining the framework composition. An excellent review of the earlier work in the field has been written by Thomas and Klinowski.[49] Masnmr detects the local environment of the nucleus under investigation, so that ^{29}Si masnmr of Y zeolite generates five peaks,[48] one each for silicon atoms with one, two, three, four, or no near aluminium neighbours, denoted as Si(nAl) where n= 0 to 4. A near neighbour is defined as an atom in the next but one tetrahedral site away from the designated atom. The intensities of these lines are directly proportional to the populations of silicon atoms in the relevant position, allowing the framework composition to be deduced from the relative intensities.[49,50,51] Recently Newsam[52] has proposed an alternative method of determining the Si/Al ratio from the isotopic chemical shift of ^{29}silicon.

^{27}Al masnmr can establish the symmetry of the environment of the aluminium in the sample and can therefore distinguish between tetrahedrally co-ordinated aluminium in the framework and non framework aluminium in other symmetries. Complexation with acetylacetone renders all extraframework aluminium visible, including that in tetrahedral and 'nmr invisible' environments,[53] thus allowing accurate determination of the amount and locality of aluminium species to be made.

Surface Acidity

The generation, detection and characterisation of the surface acidity is of fundamental importance in the study of acidic catalysts. This is especially so in zeolite catalysis as the highly ordered framework allows subtle changes to be made to and detected in the framework. Ultimately, acidity in zeolites comprises two forms, Brønsted acidity associated with protons electrostatically counterbalancing the negative charge on the framework due to the inclusion of aluminium, and Lewis acidity resulting from trigonal aluminium or silicon at defect sites in the framework, from extraframework aluminium species, or from other metallic cations. A recent paper[54] has suggested that the Brønsted acid sites formed are not planar but bent in nature; therefore the hybridisation of the oxygen should be considered to be nearer sp^3 than sp^2.

Generation and Detection of Acid Sites

Brønsted acidity can be generated in a number of ways, depending on the exact nature of the zeolite in question.

i) Deamination of an amine- or ammonium-exchanged sample will lead to a proton being left on the framework and the evolution of the amine into the gaseous phase. Ammonia and small primary amines can be reversibly desorbed, whereas secondary and tertiary amines suffer irreversible desorption. For instance, Ghosh and Curthoys[55] reported that the desorption of n-butylamine at elevated temperatures resulted in the production of butene. Therefore ammonium salts are preferred for clean protonation of the framework, without any accompanied surface fouling.

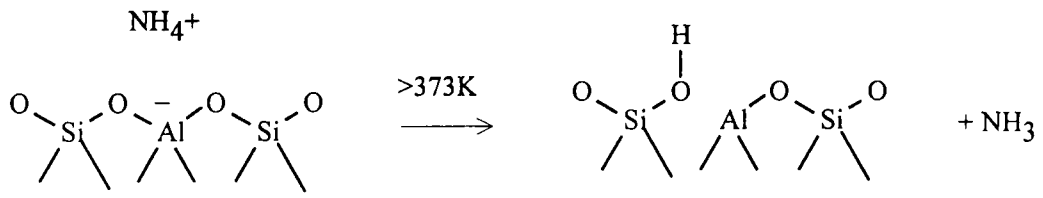

ii) Direct introduction of protons via a dilute mineral acid. This method is only applicable for zeolites with highly siliceous frameworks or structural dealumination will occur.

iii) Reduction of transitional metal ion exchanged zeolite by hydrogen has the effect of introducing protons into the zeolite. Platinum, palladium and copper have been extensively studied in this field due to their use as dual function catalysts. The metal ions are introduced by ion exchange and are then reduced in situ by hydrogen gas, producing metal atoms and protons.

This can be shown by the example of a sample exchanged with copper (II) ions:

$$Cu^{2+} + \tfrac{1}{2}H_2 \text{ ---> } Cu^{+} + H^{+}$$

$$Cu^{+} + \tfrac{1}{2}H_2 \text{ ---> } Cu^{0} + H^{+}$$

iv) At elevated temperatures, any molecular water can hydrolyse cations, which in addition to generating acidity distributes the charge more evenly over the framework.

$$M(H_2O)_x^{n+} \text{ ---> } MOH(H_2O)_{x-1}^{(n-1)+} + H^+$$

v) Interaction of bivalent cation zeolites with certain inorganic gases results in the creation of acid sites.[56] Carbon dioxide reacts reversibly with monohydrolysed cations freeing the proton and forming a metal carbonate complex.[57] Sulphur dioxide and halide compounds can also be used in this respect.[58,59]

In addition to the above, a further source of acidity exists which only becomes apparent during a catalytic reaction. Hydrocarbon residues, deposited on the framework during the course of a reaction, can in some circumstances enhance the catalytic function of the zeolite.[60,61] It is believed that this enhancement is related to the increased number of protons available during the reaction. However, this method is dependent on there being some initial Brønsted acidity to start the reaction in the first place. It is a lot harder to quantify as it is only evident under operating conditions, and therefore it cannot be considered as a primary method of acid generation.

The method used to generate the acidity is strongly dependent on the nature of the sample and the purpose for which the catalyst is intended. As noted, acid treatment can only be used on highly siliceous frameworks. Likewise, ammonium ion exchange followed by deammoniation should only be attempted on samples which are known to be thermally stable at the deammoniation temperature.

The Brønsted acid sites present in zeolites can be detected and quantified by studying the hydroxyl region of the infrared spectrum, 3000cm^{-1} to 3800cm^{-1}, alone, or in conjunction with well chosen probe molecules. There are typically three stretching bands in the hydroxyl region, found at

approximately 3740cm^{-1}, 3650cm^{-1} and 3560cm^{-1}. The first of these bands is found in all dehydrated faujasites and is associated with terminal hydroxyl groups at crystal faces and possibly with silica impurities. It does not interact with adsorbed molecules and had the same frequency and intensity over a range of samples studied by Angell and Schaffer.[62] The other two bands are only present in samples which have undergone protonation by one of the methods outlined above. The band at 3650cm^{-1} is assigned to hydroxyls involving O_I oxygens, and is termed the high frequency (HF) band, and the 3560cm^{-1} band to those involving O_{III} oxygens, the low frequency (LF) band.[63,64] The narrowness and the symmetry of the higher wavenumber band is explained by the unhindered vibrations of the hydroxyl group into the supercage, a fact corroborated by the ease of access of other molecules to these hydroxyls. Later work[65] showed that the 3560cm^{-1} band contained contributions from O_{II}, OIII, and O_{IV} hydroxyls, with O_{III} predominating. The acid strength of the high frequency band has been shown to increase with dealumination, by studying the shift in wavenumber of the hydroxyl stretching vibration on adsorption of ethene.[66] Improvements in this technique[67] have allowed the HF band to be deconvoluted into four components of differing strength, the relative intensities of which depended on the Si/Al ratio. As these were linked to four ^{29}Si masnmr peaks - the fifth, Si(0Al), does not have an associated hydroxyl peak in the infrared as it has no hydroxyl group - the acid strength distribution can be deduced directly from the silicon masnmr data.

There are two major types of interaction when basic molecules are allowed to come into contact with the zeolitic surface; those between the probe molecule and the proton from one of the framework hydroxyl groups, and those between the probe molecule and other positively charged entities, such as alumina conglomerates or metallic cations.

When pyridine is adsorbed onto a zeolite the characteristic band at 1545cm^{-1} is observed which is due to the pyridinium ion formed from the interaction of the pyridine molecule with the proton from a Brønsted acid site; a band at *ca.* 1440cm^{-1} is attributable to Lewis acid site interactions. However, interactions between the pyridine and any metallic cations which may be

present will also give rise to bands in the same region.[56] The wavenumber of these bands is proportional to the ionic radius of the cation concerned;[68] in material with two types of cation present, two close peaks will be observed, and it has been shown that changing the cation species in the same sample shifts the peak. Therefore these peaks can be used to provide evidence of ion exchange efficiency and as the cations have no other effect on the spectra, can be ignored. Ammonia adsorbed onto the surface gives bands at 3250cm^{-1}, 1623cm^{-1} and 1425cm^{-1}.[55] The last of these bands is due to the ammonia adsorbed onto a Brønsted site giving an ammonium ion whilst the 1623cm^{-1} band is due to ammonia residing on a Lewis acid site.

Hughes *et al*[69] reported that when piperidine was added to a sample of deaminated ammonium-Y at 423K and 2x10^{-6} torr the hydroxyl bands at both 3650 and 3550cm^{-1} were removed. However, with pyridine under the same conditions only the 3650^{-1} band was effected, and that this decrease and the growth in intensity of the 1545cm^{-1} band is proportional to the amount of pyridine added. These bands therefore arise from the hydroxyl groups which are the source of the Brønsted acidity, and the hydroxyl groups associated with the 3650cm^{-1} band are of higher acidity as only they reacted with the weaker base, pyridine. Similar results regarding the relative acidity of the two bands were obtained by Ward[70] and Eberly.[71]

Recent work[72] studied the interaction between pyridine and the zeolitic protons by introducing small amounts of deuterium oxide into the system. From shifts in the spectra it was shown that the exchangeable proton spectrum was positively identified as a broad band in the 3400-2600cm^{-1} region. The large range in energy of this proton is attributed to the fact that the pyridine molecule has an adsorbed lifetime of 5x10^{-7}s at 313K. This is long compared to the timescale of measurement (1x10^{-14}s) and so a fixed image of the surface is obtained. This work claimed to be the first to present infrared spectra of the LF hydroxyls without physisorbed interference. The LF spectrum was seen to show enough similarities to the HF spectrum for the authors to conclude that the pyridine was protonated to some degree, with the proton coming out of the sodalite cage to meet the pyridine molecule. Thus the pyridinium ion is less

stable and the pyridine would be more easily desorbed.[72]

Batamack *et al*[73] have advanced a new method for assessing Brønsted acidity, based on proton nmr. By examination of the proton spectra at ultra low temperatures, the extent of hydrogen bonding to a water molecule, or proton transfer in the case of a strong site, can be determined.

Strength of Acid Sites

The strength of any acid site is influenced by only two variables, which are respectively geometric and chemical in nature. The geometric factor relates to the Si-O and Al-O bond lengths and the angles between the atoms; since all tetrahedral sites in Y zeolite are equivalent, this factor can be disregarded. The chemical factor is dependant on the environment of the hydroxyl group.

It has been proposed that the acidic nature of a zeolite is dependant on the number of single occupancy aluminium four rings.[74,75] This was subsequently extended to the number of aluminium atoms in the second neighbour position[76] and is now known as the Dempsey-Mikovsky-Marshall theory (DMM theory). Aluminium atoms further away are too distant to influence the acid site. The number of such sites reaches a maximum when there are thirty two aluminium atoms per unit cell;[76,77] thereafter further dealumination only reduces the number of sites without any increase in strength of acidity. Quantum chemical calculations have confirmed the decrease in intrinsic acidity with increasing aluminium concentration.[78] Therefore, in a sample with more than 32 Al_F puc a degree of heterogeneity among the acid sites should be expected.

The hydroxyl peak at *ca* 3650cm^{-1} has been deconvoluted into as many as seven peaks,[79] but Datka *et al*,[80] by studying the shift in wavenumber on the hydrogen bonding interaction with chlorobenzene, were able to show that the HF peak could be resolved into three separate peaks. In a similar exercise, Makarova *et al*[81] has shown that the hydroxyl region can be split into acidic and non-acidic parts, and that the acidic part can be further subdivided into four peaks, the three highest wavenumber bands probably being identical to those of Datka. Other studies, centring on the temperature programmed

desorption of basic molecules, have found evidence of variable site strengths.

In addition to strong acidity generated by the framework alone, some authors have postulated acidity enhancement by interaction between Brønsted and Lewis sites. Originally, Lunsford[82] proposed interaction with framework Lewis sites, but, as the existence of these sites was doubted, the interaction with nonframework sites was suggested.[83,84] This enhancement, creating 'superacid sites', is thought to follow partial electron transfer from the hydroxyl bond, thus enabling greater delocalisation and stabilisation of the negative charge on the framework. Evidence to support this view was provided by dealumination studies.[85] Very careful hexafluorosilicate treatment produced a sample with very little nonframework aluminium; this was found to have negligible catalytic activity, as measured in the cracking of n-hexane, when compared to a sample of the same framework composition prepared by hydrothermal methods. When the chemically treated sample was subjected to a very mild steaming procedure a dramatic rise in activity was noted, resulting in a higher activity than the sample steamed to a similar framework composition. This was attributed to a few aluminium atoms becoming dislodged from the framework, promoting the remaining framework sites by a synergic interaction.

1.22 Modification

Modification of the chemical composition, structure and cation content of zeolites can be carried out after the initial synthesis.

Ion Exchange

Ion exchange has been the subject of many reviews[eg 86,87,88] which consider both the thermodynamic and kinetic aspects. In view of the catalytic effect of changing the cations, much work has been undertaken to determine their position within the structure in order to help elucidate possible reaction pathways.[17,18,89,90,91,92,93] More recently double rotor nmr[94,95,96] has provided additional information to that obtained from nmr.[97]

The charge balancing cations can be easily exchanged by refluxing the zeolite in a solution containing an excess of a salt of the desired cation. The extent of exchange depends on the zeolite in question, the nature and concentration of the cations involved in the exchange, and the temperature; repeated exchanges allow the theoretical maximum limit to be approached, which has been predicted for the equilibrium between different cations.[86,98] As well as mono-, di- and polyvalent metal ions, organic amines and metallic complexes[99] and metallic clusters[100] can be incorporated into the pore system. Changing the cation in any zeolite can have a marked effect on its properties; thermal stability,[101] adsorption,[102] catalytic activity[103,104,105] and sieving potential can all be influenced by judicious choice of cation.

Dehydroxylation

An understanding of the stability of the hydroxyl groups at elevated temperatures is central to the study of acidic catalysts. Early work on Y zeolite, using infrared spectroscopy has been reviewed by Ward.[106] Physically adsorbed water desorbs from the zeolite at *ca* 473K leaving a dehydrated protonated framework. Whilst protons are essentially immobile at temperatures below 473K, higher temperatures permit proton mobility where they hop from site to site.[107] More extreme heating results in water loss from the structure by the process of dehydroxylation. This involves the destruction of two Brønsted

sites, and the scheme proposed by Uytterhoeven *et al*[108] was accepted as the model dehydroxylation:

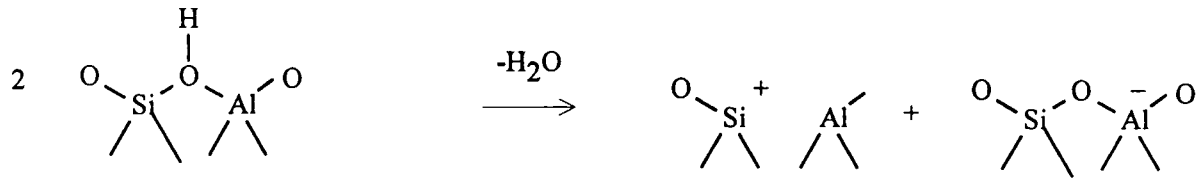

Thus two Brønsted sites were removed and one Lewis site created, namely the trigonal aluminium in the framework. The infrared band at 3600cm^{-1}, which had been shown to be acidic by its interaction with ammonia, decreased as the sample was heated above 773K. However, later work using ^{27}Al nmr[109] and x-ray spectroscopy[110] found no evidence of the trigonal aluminium in the framework as demanded by the model of Uytterhoeven. Kühl[110] reported that 28-44% of the aluminium in a dehydroxylated HY zeolite was hexacoordinated, and proposed a scheme involving the removal of some aluminium to extraframework positions:

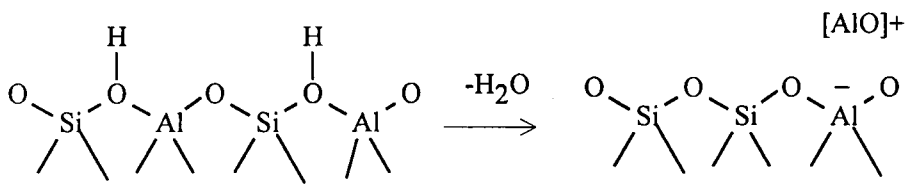

The general premise, that in the reaction one Lewis site is produced at the expense of two Brønsted sites is valid,[70,111,112] although the nature of the Lewis sites remains debatable. Jacobs *et al*[113] have presented work on Cu-Y zeolite which shows that $[AlO]^+$ groups act as the Lewis acid. This work suggests that the Uytterhoeven model Lewis site may be a metastable intermediate in the formation of the Lewis site suggested by Kühl. Bosáček *et al*[109] found that the amount of symmetrically coordinated aluminium in the zeolite is independent of the degree of dehydroxylation, and that after complete dehydroxylation, only an increased amount of hexacoordinated aluminium could be found. Furthermore, these authors determined the amount of extrastructural aluminium by coordinating it with acetylacetone and measuring the intensity of the ^{27}Al masnmr signal. It was

concluded that the amount of extrastructural aluminium was proportional to the degree of decationisation, and whether the sample was activated under deep bed or shallow bed conditions. The temperature of the activation determined where in the unit cell the extrastructural aluminium was located.

Other work by the same group[114,115] demonstrated that dehydroxylation of HY zeolites is always accompanied by dealumination of the structure. Using masnmr they were able to resolve three peaks due to hydrogen, and they were also able to separate framework aluminium from non-framework species. They were therefore able to conclude that trigonal lattice aluminium does not appear during the dehydroxylation process and that dehydroxylation in the vicinity of a framework aluminium atom always results in its expulsion from the lattice. The authors conclude that in the deep bed studies the dealumination is effected by hydrothermal damage, with a healing process involving the transfer of silicon atoms. This prevents the formation of hydroxyl nests, a fact verified by the lack of any increase in the signal due to terminal hydroxyl groups. Under shallow bed conditions no hydrothermal action can occur as the water and ammonia are swiftly removed. Consequently there is not much damage to the structure at temperatures below 723K; the damage present being due to the breakdown of the shallow bed conditions. Since thermal stability is not obtained, the lattice starts to breakdown above 723K. The appearance of AlOH groups similar to those on γ-Al_2O_3 supported this view.

Cattanach *et al*[116] have shown that the rate of dehydroxylation is highly dependent upon the ambient water vapour pressure. They also reported that the nitrogen atom to aluminium atom ratio, based on ammonia, dropped from 1.0 to 0.5 on dehydroxylation which is entirely consistent with the dehydroxylation models outlined above. The dehydroxylated form was found to be very unstable with respect to water and any attempt to regenerate the starting material lead to a loss in crystallinity and a reduction in adsorption capacity.

Wang *et al*[117] concluded that under the conditions employed in their study, only two percent of the structural aluminium was removed under self-steaming conditions at 673K. It was reported that only the aluminium ions associated with ammonium ions are susceptible to expulsion from the

framework, thus the extent of damage could theoretically be controlled by the extent of cation exchange, confirming the work of Bosáček *et al.*[109]

The infrared spectrum of the hydroxyl region of partially dehydroxylated zeolites show many similarities to that of the hydrogen form of the same zeolite.[106] The frequencies of the wavebands may move slightly, but the major change is in the intensities of selected bands and the appearance of two new bands. An extensive study of the effects on the infrared spectra of different pretreatments was carried out by Jacobs and Uytterhoeven.[65,118] The resulting spectra were then deconvoluted into six components which were compared. The most obvious change was the increase in the intensity of the 3740cm^{-1} band as the conditions become more severe. Comparison of the intensities of the bands show that there is a tenfold increase in intensity for the component at ca. 3620cm^{-1} and the appearance of a band at 3685cm^{-1}. Of the other bands, the 3650cm^{-1} band decreased in intensity while the 3550cm^{-1} increases slightly. This differs from earlier work by the same authors,[119] which showed that the lower frequency band was less stable under vacuum conditions. This implies that the conditions employed remove hydroxyls from the O_I site (3650cm^{-1}) which agrees with the x-ray work of Maher *et al.*[120] The slight change in the 3550cm^{-1} band assigned to O_{III} oxygens shows that these sites are not affected by deep bed calcination. The assignment of the bands at 3685cm^{-1} and 3600cm^{-1} is somewhat contentious, with some workers[121] being of the opinion that they can be attributed to hydroxyls associated with nonframework aluminium.

The relationship between number of acid sites and calcination temperature has been studied by Ward.[122] The number of Brønsted sites as detected by infrared measurements on the absorption of pyridine show that the number of sites rises until a calcination temperature of 623K is reached, after which there is no change in the concentration until the sample had been treated at 773K; thereafter there was a dramatic decrease so that by 1073K all the Brønsted sites had been removed. Paralleling this, the Lewis acidity concentration remained constant at a low level until 723K and then grew linearly to 1073K.

Dealumination

Until recently it has been impossible to synthesise zeolites with a framework Si/Al ratio of greater than about four, although in the last few years higher silica faujasite frameworks have been synthesised. Using organic templates, both cubic and hexagonal forms have been reported[123] and a new zeolite ZSM-20, consisting of intergrowths of the two structures has been claimed.[124] Given that highly siliceous frameworks are known to have high thermal and hydrothermal stability, coupled with different acidic and catalytic properties, much energy has been expended in preparing highly siliceous samples that retain the structural characteristics of the as-synthesised samples.

Dealumination, the process by which aluminium is removed from the framework of a pre-synthesised sample can be achieved by two distinctly different methods. The first involves removal of aluminium from the framework followed by migration of silicon from other parts of the crystallite to complete structural healing. The second type of dealumination concerns reaction of the framework with a reagent containing silicon, resulting in isomorphic substitution and hence negating the need for silicon transport.

Mineral acids and chelating agents were found to be effective in dealumination at an early stage. Early work had removed aluminium from clinoplitolite[125] and erionite[126] with hydrochloric acid. Kerr[127] reported that the treatment of faujasite with hydrogen EDTA removed aluminium from both the framework and the pore system in one experimental process.

The first step was shown to be partial ion exchange to produce the hydrogen form of the zeolite, followed by removal of a framework aluminium atom. The resultant nonframework aluminium cation is then chelated by the EDTA and removed in solution, figure 1.3. Materials prepared in this way were found to be more thermally and hydrothermally stable and capable of adsorbing about 20% more water and cyclohexane than the as-synthesised sample.[128] With up to 50% of the framework aluminium removed highly crystalline samples were achieved; increasing the extent of dealumination lead to loss of crystallinity, with aluminium free samples being totally amorphous.[127] Other organic acids, namely diethylenetriaminepentaacetic acid

(DTPA) and diaminocyclohexane-tetraacetic acid (DCTA) have been shown to have very similar dealumination characteristics as EDTA,[129] although reaction with acetylacetone was shown to only remove at maximum thirty percent of the available framework aluminium atoms. This restriction has been linked to the number of weak acid sites in the framework. Dealumination of Y zeolite with orthophosphoric acid decreased the number of acid sites, but surprisingly decreased their acid strength.[130] This was shown to arise from structural dealumination coupled with the formation of aluminium phosphates from extraframework aluminium and the acid.

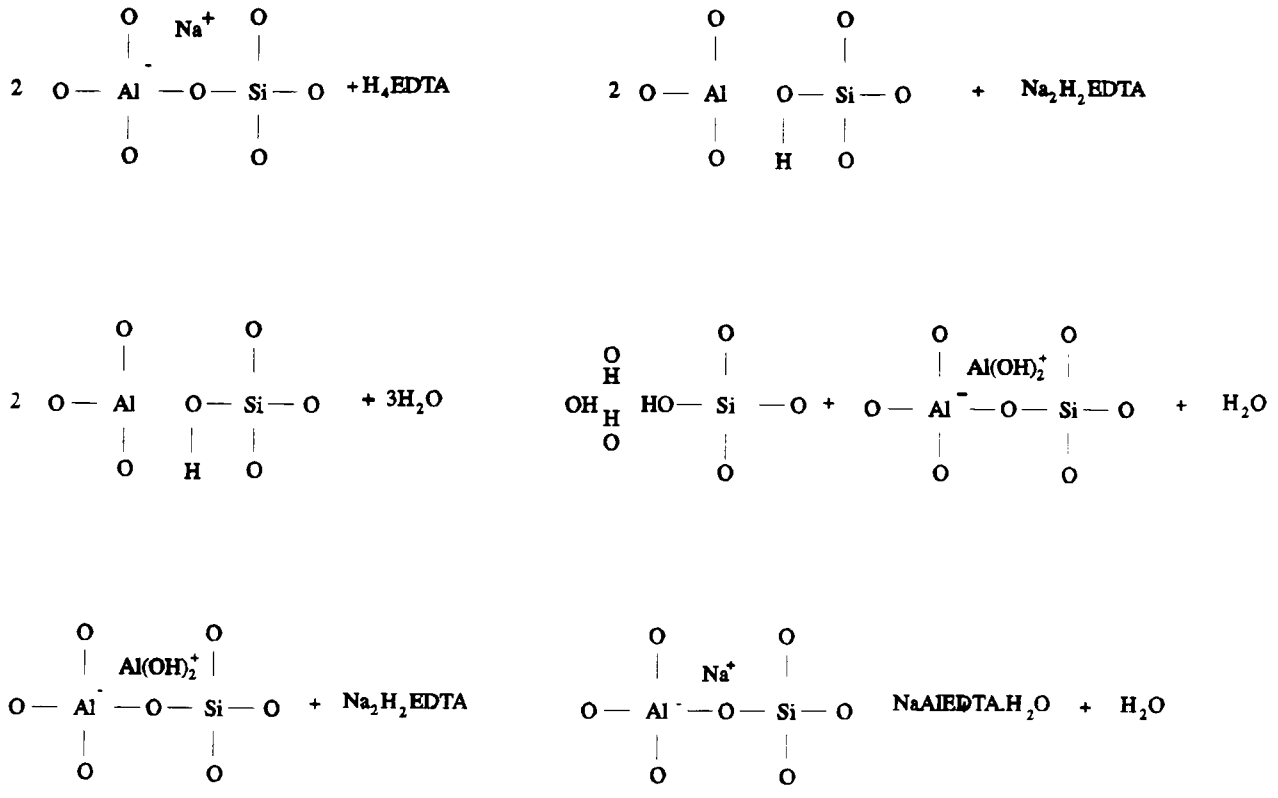

Figure 1.3: First Kerr mechanism.

Kerr[131] noted that thermal decomposition of ammonium Y produced two distinct products depending on the experimental conditions. When a shallow bed was employed HY zeolite was obtained, but when the decomposition was carried out in a deep bed an ultrastable product was obtained. The removal of water and ammonia from a deep bed is naturally impeded, a restriction which does not apply in a more shallow bed. It had previously been noted[132] that a

sample heated *in vacuo* has poor thermal stability compared to one heated at atmospheric pressure. The mechanism in figure 1.4 was proposed, in which interaction between the framework and water resulted in removal of aluminium from the framework as aluminum hydroxide, creating hydroxyl nests. Further reaction with the hydroxide could lead to charged hydroxyalumina species which would be progressively chemically reduced by the water. A similar product had been obtained by McDaniel[133] which exhibited high thermal stability and modified ion exchange, x-ray diffraction and adsorption properties.

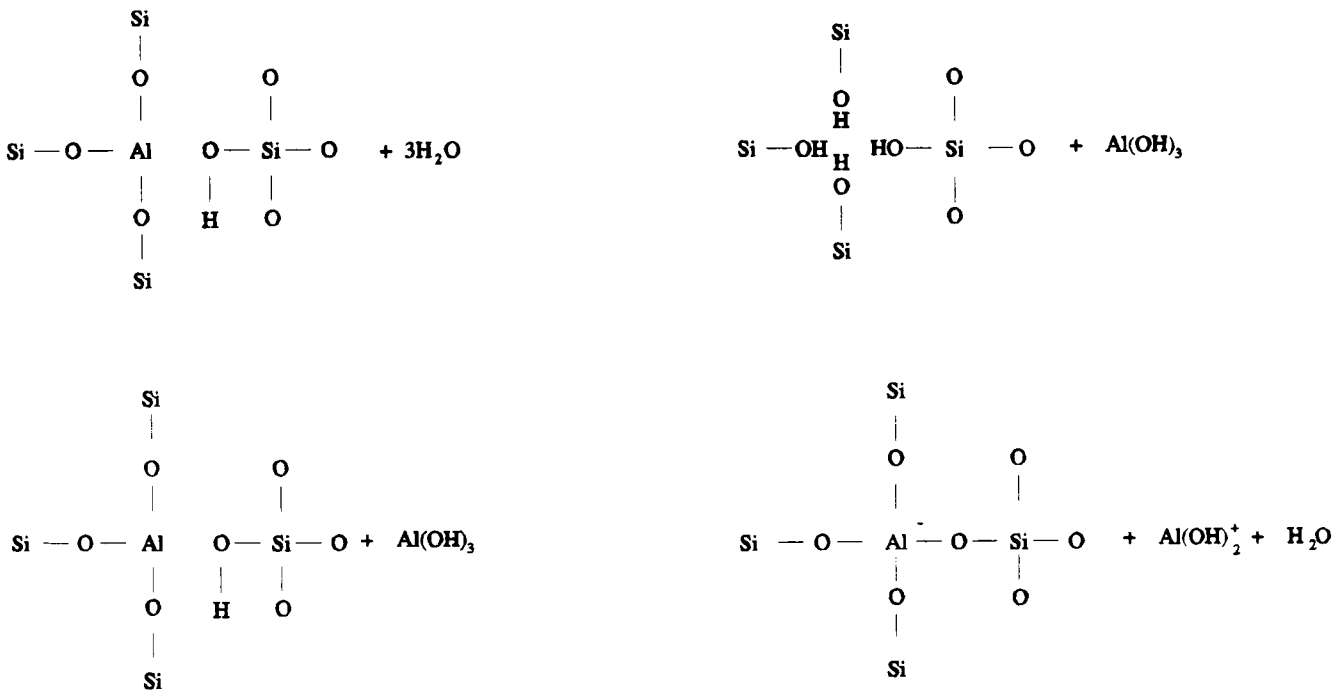

Figure 1.4: Second Kerr mechanism.

The role of water in the ultrastablisation process was confirmed by Ward[134] in a study of the calcination of Y zeolite under different atmospheres. Production of ultrastable Y zeolite (USY) was found to be possible under shallow bed conditions as long as the calcination was carried out under a flowing atmosphere of steam. The presence of steam is thought to promote the

structural healing process by rendering the silicon volatile. Normal dehydroxylation is known to result in the expulsion of aluminium from the framework, but this is always accompanied by a breakdown in the structure, leading to a loss of crystallinity in the sample.

Contrary to dehydroxylation, dealumination does not create any vacancies in the framework; that is, the occupancy factor of the tetrahedral atoms (silicon and aluminium are indistinguishable in x-ray scattering experiments) remains one after dealumination of half the available sites.[135] Removal of vacancy sites can be accomplished by transportation of silicon from other, remote sites of the crystallite, or by a relaxation of the framework. Breck[15] proposed structural healing by silicon tetrahydroxide insertion into the hydroxyl nests; the migration of which, it is argued, is facilitated by both high temperature and the presence of water vapour. Subsequent work[136] challenged the mechanism for the removal of aluminium postulated by Kerr in the case of an ammoniated zeolite. Whereas Kerr removes the ammonium hydroxide by reaction with water, Vedrine *et al*,[136] on the basis of ESR, evidence suggested the following:

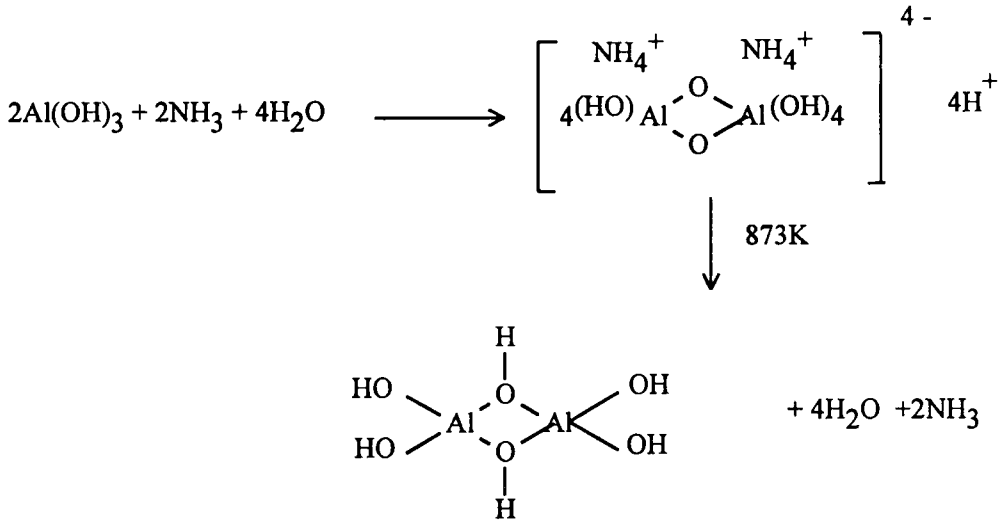

Figure 1.5: Vedrine mechanism

The progress of the dealumination reaction has been shown to be dependant on almost all experimental parameters. Reaction time, temperature and the partial pressure of steam were all found to be important factors affecting the extent of dealumination.[137] A very high apparent activation energy

for crystal destruction, 525 kJmol^{-1}, emphasises the extreme temperature dependence of the reaction.[137] Van Brockhoven *et al*[138] have shown that a 1.6 wt% loading of Na_2O was associated with 18 wt% formation of nonframework aluminium, but that this fell to 11% when the soda level increased to 3.9 wt%. These results mirror those reported earlier regarding the extent of dehydroxylation.[109,117]

Numerous reports have concluded that the first aluminium atoms to be removed are those associated with weak acidity. The Dempsey-Mikovsky-Marshall model proposes that the distribution of aluminium atoms in the framework will always be as such to minimise the number of Al-O-Si-O-Al units. This implies that during dealumination, aluminium atoms in close vicinity to other aluminium atoms will be the first removed, leaving a more stabilised, more strongly acid, isolated site. This view was challenged by Bodart *et al*[139] who concluded that, in the case of mordenites, dealumination progresses by extraction of the most closely spaced pairs of aluminium atoms, ie in the first instance two aluminium atoms in the four membered ring.

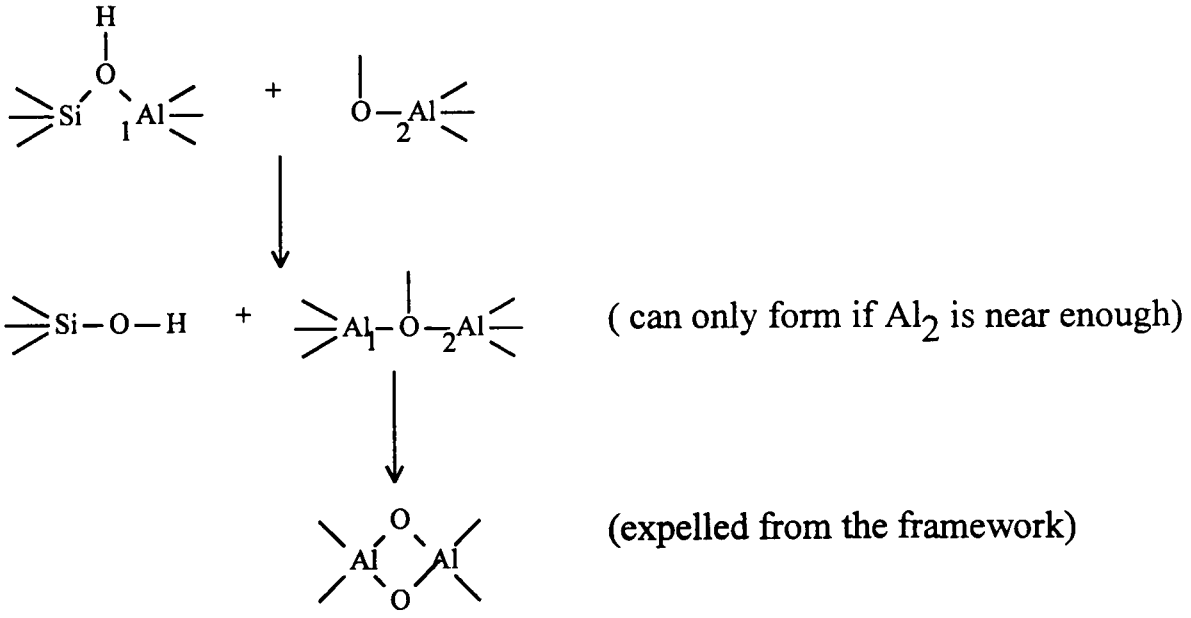

Figure 1.6: Pelmenschikov mechanism.

Pelmenschikov[140] claims that it is the chemical attraction of these pairs, resulting in the formation of mullite or kaolinite fragments which causes their expulsion from the framework, and not the repulsion between two closely spaced charged entities. This mechanism therefore accounts for the removal of

weak acid sites at the start of the dealumination process. In an earlier paper, Klinowski[141] implicitly refutes the possibility that the environment of silicon can progress from three or two aluminium neighbours to none directly: stepwise progression was observed as claimed by Englehardt *et al.*[142]

The silicon consumed in the healing process must come from elsewhere in the crystallites, as none is supplied by the reagents. Adsorption data shows that hydrothermal treatment results in the production of a new class of porosity, intermediate between the microporosity of the supercages and the macroporosity between crystallites. These mesopores, which are distributed inhomogeneously throughout the crystallite,[42] range in size from 2 to 50nm,[143,144] appear after silicon is removed and transported to other parts of the crystallite to participate in structural healing. This implies that the silicon is not sourced randomly from the crystallites, nor is it taken from the outside; rather removal is concentrated from certain areas. These might well be at sites of pre-existing faults in the framework which are more susceptible to hydrothermal attack. Once started a cascade effect will result in the formation of a mesopore.

Vacancy migration through the crystal provides an alternative mechanism for structural healing.[165] Silicon atoms would hop from site to site, causing the vacancy to migrate in the opposite direction. As the vacancies coalesce their movement becomes restricted and they are trapped, leading to the formation of mesopores. The vacancies could well be trapped by pre-existing faults.

The second approach to dealumination comprises processes in which the reactant is also the source of silicon. The two predominant reagents, silicon tetrachloride and ammonium hexafluorosilicate, offer products with slightly different properties. Silicon tetrachloride dealumination, introduced by Beyer and Belenykaja,[145] is effected by passing the vapours, carried on an inert gas, over the sample at elevated temperatures. In contrast to the hydrothermal methods, this method does not significantly alter the adsorption characteristics or the crystallinity of the zeolite. The masnmr peak generated by silicon with no aluminium neighbours, the Si(4Si) peak,[146] of a sample dealuminated in this

way was found to be half the width of the same peak in a sample dealuminated to the same extent by hydrothermal means,[43,147] implying that the tetrachloride treatment is less destructive to the framework crystallinity.

The reaction products, sodium chloride and aluminium trichloride can combine to form an involatile solid residue, sodium chloroaluminate, which remains in the pore system after the first stage of the process. Washing the zeolite hydrolyses this chloride, removing it from the system, but at the same time produces in situ hydrochloric acid, which can result in secondary acid leaching of the framework.[26] This results in the formation of hydroxyl nests which, in much the same way as earlier, can only be removed by the migration of silicon during subsequent steaming.[148] The extraction of the displaced aluminium means that the level of extraframework aluminium after these treatments is considerably less than after hydrothermal dealumination[149] although some octahedrally coordinated aluminium has been detected by masnmr, possibly due to the secondary acid leaching.[26,148]

Accumulation of the chloride complex in the pores, effectively blocking them and causing the reaction to cease, has been noted by Grobet *et al.*[148] This would seem to set an upper limit on the extent of dealumination possible in a single treatment, although Anderson *et al*[30] reported 96% dealumination of NaY. Ion exchange of sodium for lithium allows a greater extent of dealumination to be achieved. Sulikowski and Klinowski[141] rationalised this by noting that the lithium-aluminium tetrachloride salt is less stable than the sodium analogue, and may even be volatile. This was evident in the reduced amount of amorphous material in the lithium exchanged sample.

Evidence for a two step mechanism in the silicon tetrachloride dealumination process has been presented by Martens *et al*[150] (figure 1.7). The first step is the addition of oxybound $SiCl_3$ unit to the framework, with the contemporaneous formation of the chloride salt of the charge balancing cation. Masnmr data has been used to conclude that this step is responsible for the exothermicity noted by a number of workers.[26,141,145] It was claimed that the isomorphic substitution of aluminium by silicon does not take place at low reaction temperatures, but only after calcination at 623K which explains the

observation of Anderson *et al*[30] that dealumination at 423K produces a less crystalline material than dealumination at temperatures up to 773K. At lower temperatures hydrolysis of the O-$SiCl_3$ group takes place instead of silicon insertion leading to what amounts to a low temperature strong acid dealumination.

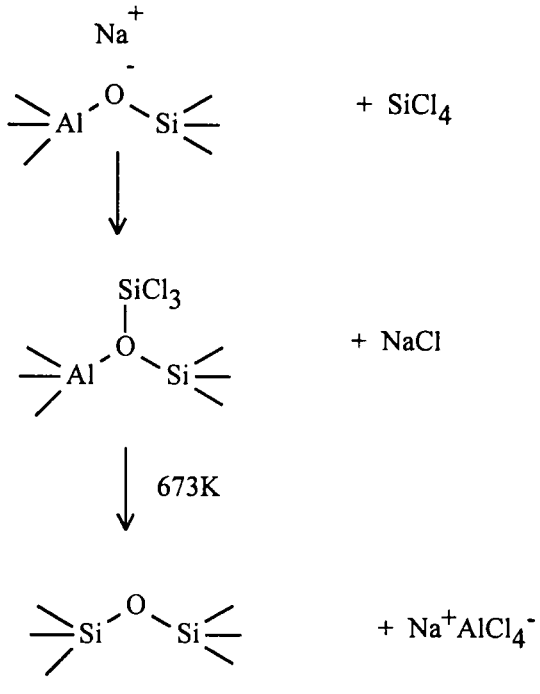

Figure 1.7: Silicon tetrachloride dealumination.

Dealumination with ammonium hexafluorosilicate has the distinct experimental advantage of being carried out at much lower temperatures than either hydrothermal or silicon tetrachloride treatment. Additionally, when the ammonium exchanged form of the zeolite is used, the extraframework aluminium is produced as a soluble product, and as the reaction is carried out in aqueous solution, extraction occurs in the same process, leaving little or no extraframework aluminium.[151] The standard procedure, introduced by Skeels and Breck,[152] involves slurrying the zeolite with an appropriate concentration of ammonium hexafluorosilicate solution at 363K. Samples prepared in this way exhibit high crystallinity,[153] but once again the exact reaction conditions and immediate post reaction procedures have been shown to have a bearing on the final product.[154,155] The surface of hexafluorosilicate treated samples was

found to be relatively deficient in aluminium, with a steeply increasing concentration gradient into the crystallite[138] implying that this is a fast, contact reaction, which is effectively diffusion controlled.[156]

The rate of insertion of silicon must be commensurate with that of the removal of aluminium if the integrity of the structure is to be preserved. Similar results have been obtained for this reactant as for the tetrachloride method, ie. low temperature reactions lead to products with a marked loss in crystallinity and low levels of dealumination;[154] once again these observations are reversed at slightly higher temperatures. This, together with the facts that high fluorosilicate to zeolite ratios in the reaction process result in collapse of the structure and the observation of hydroxyl nests, leads to the conclusion that this is also a two step, and not isomorphic reaction. Wang *et al*[155] have shown that residual reagent, which is very difficult to remove completely by washing, can cause the increased dealumination and loss of crystallinity under hydrothermal conditions noted by them and by others. They surmised that this dealumination was caused by thermal decomposition and then hydrolysis of the hexafluorosilicate, resulting in the in situ formation of hydrogen fluoride. Subsequent attack on the framework without the insertion of silicon explains the drop in crystallinity.

A reaction mechanism for the dealumination by ammonium hexafluorosilicate has been proposed.[157] The reagent is hydrolysed producing six fluoride ions and silicon tetrahydroxide. The fluoride ions extract the aluminium from the framework as the hexafluoride ion, allowing the silicon tetrahydroxide to insert into the vacancy. Both these species were detected as reaction intermediates in the reaction mixture. This mechanism neatly explains the observations of the other workers mentioned, and parallels the tetrachloride mechanism.

Once the aluminium has been removed from the framework, if it is not in a soluble form, it is deposited in the pore system. The nature and location of this material is of considerable interest, since it can have profound affects on the acidic and physical, and therefore catalytic, properties of the zeolite. The use of magic angle spinning nuclear magnetic resonance (masnmr) as a

diagnostic tool is widespread, and extraframework aluminium with octahedral and tetrahedral symmetries is well established.[114,158,159] However, Klinowski[160] found that the sum of the aluminium in these two environments was less than that removed from the framework and, as removal from the system was impossible he concluded that the deficit must be accounted for by 'nmr invisible' aluminium. These species were made visible by the addition of acetylacetone which forms $Al(acac)_3$ complexes with all available extrastructural aluminium without disturbing the framework.[53] In this way, Bosáček[109] found that at 573K most of the extraframework material was located in the supercages, but that with increasing temperature this migrates into the sodalite units.

In addition a third masnmr line has been reported, which has also been shown to originate from nonframework aluminium.[161] This has been assigned to penta-coordinate[162] and distorted tetrahedral[163] symmetries generated in studies of hydrothermal dealumination. Other authors[164,165] have proposed the formation of octahedrally coordinated nonframework aluminium associated with an amorphous silica/alumina phase. Very recent work has claimed that this peak is due to two[166] (one a spinning sideband) or even three separate species.[167] The populations of the differently coordinated species was found to vary with the method of dealumination, with penta- and octa-hedral coordination preferred in the case of hydrothermal dealumination, while silicon tetrachloride treatment produces nonframework aluminium predominately in a tetrahedral environment. With increasing severity of hydrothermal treatment, the nonframework aluminium was seen to progress to 'nmr invisible' species.[151]

The possibility of the nonframework aluminium possessing hydroxyl groups must not be neglected. As mentioned earlier, other bands at 3675-3700cm^{-1} and 3610cm^{-1} have been reported.[121,149,168,169,170,171] Claims of superacidity on behalf of the lower wavenumber band have been made on the basis of its interaction with pyridine, although a band at 3602cm^{-1} has been attributed[171] to a Brønsted site in the presence of Lewis site.

Different groups have drawn various conclusions as to the precise

location of the extraframework aluminium. Van Brockhoven[138] noted that upon steaming, a layer of nonframework aluminium approximately 5nm thick migrated to the surface of the crystallite. This is in broad agreement with other workers who have found octahedrally coordinated nonframework aluminium at, or near, the surface,[41,42,117,172,173,174] or in the mesopores[175.176] which might be considered as pseudo-surfaces. Polymeric hydroxyalumina species produced at high temperatures, have been located in the α-cages.[168,177] All these results can probably be summarised in the findings of Chevreau *et al*[178] who concluded that 65% of the nonframework aluminium is resident in the supercages, with the balance in the sodalite cages or on the surface.

As the objective of dealumination is to provide materials with highly siliceous frameworks, some of which are now available by direct synthesis methods[123,124] it is instructive to compare and contrast material of similar composition arrived at by direct or post synthesis methods. The major difference, disclosed by ^{29}Si masnmr, appears to be in the aluminium distribution within the framework.[179] Primary synthesis produces materials which have a greater proportion of silicon atoms with one near aluminium neighbour, and smaller proportion with no such neighbours, indicating a more uniform composition. This confirms the general mechanism of pairwise dealumination reported earlier,[139,140] as dealumination by single sites should produce materials with isolated framework aluminium atoms.

1.3 Catalytic Properties of Y Zeolite

The most important property of acidic zeolites is their ability to catalyse a variety of economically significant reactions. In addition to providing an energetically favourable pathway, zeolites can also determine the selectivity for different products from a single reactant. It is relevant to consider, in general terms, the contributions arising from the different physical properties of zeolites. Attention will be focused on Y zeolite, as it is the material under investigation in this study, although examples will be drawn from other systems where appropriate.

The presence of acid sites in the catalyst does not alone guarantee that

any particular reaction will proceed. Other factors, dependant on the physical structure of the zeolite, can determine the products formed during a particular reaction. This function, the selectivity of the zeolite, can be broken down into three separate components:

i) Reactant selectivity - if minimal surface reaction is ignored, for a reactant molecule to be protonated, it must enter the pore system of the zeolite. Synthetic zeolite A has an internal pore system accessed by eight membered rings. These have a free diameter of 0.4nm when the zeolite is in the full sodium form, but when eight sodium ions are replaced by four calcium ions these windows are freed and the free diameter increases to 0.5nm. n-Butanol is readily dehydrated by CaA, as it can fit through the pore windows; the more bulky branched isomer, is excluded from the catalyst and therefore is not dehydrated.[180]

ii) Transition state selectivity - the transition state species of a reaction is invariably larger than the final products. Thus the cages of the structure must be sufficiently large enough to accommodate the transition state, and to allow the molecules to approach in the correct orientation. If there is not enough room in the cages of the structure for the transition state to form, its products, no matter how favoured by other circumstances, will not form. The reaction of longer chain alkylaromatics combines dealkylation, isomerisation and cracking. As the side chain increases in length, geometric factors become increasingly important. In the cracking of 1-phenylheptane bicyclic products were detected over HY zeolite, but not over ZSM-5,[181] a medium pore zeolite. This is a good example of transition state selectivity.[182]

iii) Product selectivity - if the products of a reaction are to be observed downstream of the reactor, in addition to being sufficiently stable to exist outside of the high electrostatic field within the zeolite

structure, they must be physically small enough to pass through the pore mouths. The alkylation of cumene with propene on HZSM-12 results in the preferential formation of *para*-di-isopropylbenzene,[183] the catalytic yield of 69-80% being higher than that predicted by thermodynamic equilibrium, 32%. The *para* isomer has the smallest minimum dimension and so can diffuse out of the pores easily, whereas the other isomers are retained within the catalyst for longer, and therefore more likely to isomerise to the *para* isomer.

The primary reason for the catalytic activity of zeolites is the availability of protons, the strength of which can be controlled to suit the particular reaction. Reactant molecules differ widely in their ease of protonation and the ability of the zeolite to be tuned to provide protons of appropriate strength is of considerable utility. Jacobs[184] has ranked various test reactions in order according to their acid strength requirements. Starting with reactions which require the weakest acidity, they are:

i) dehydration of alcohols
ii) isomerisation of alkenes
iii) alkylation of aromatics
iv) isomerisation of alkylaromatics
v) transalkylation of alkylaromatics
vi) cracking of alkylaromatics
vii) cracking of alkanes

This list follows generally accepted principles in that protonation of a hydroxyl group is facile, after which protonation becomes increasingly difficult in the order carbon-carbon double bond, aromatic bond, carbon-carbon single bond.

Continuing improvements in catalyst design creates a need for reliable methods of assessing and comparing catalytic activity of both new and well established catalysts. Many reactions have been proposed as suitable test reactions; however, it is now realised that one universal reaction, capable of totally describing a catalyst's function is unattainable. The progressive development of highly crystalline, acidic catalysts has given catalysts that are

essentially too reactive for the earlier test reactions. Therefore, when studying catalysts which span a range of acidities, or that have more than one strength of acid site, it is necessary to consider the results from more than one set of reactions. In principle this will allow total characterisation of catalysts with a wide range of acid site strengths.

Before considering some particular reactions in greater detail, it is necessary to define the nomenclature used. Any positively charged hydrocarbon species is a carbocation, but can be either a penta-coordinated carb*onium* ion or a tri-coordinated carb*enium* ion. The former has an electronic octet and a two electron three centre bond and the latter has an electronic sextet and an empty p-orbital. The simplest visualisation is that a carb*onium* ion is a protonated alkane, and a carb*enium* ion is a protonated alkene.

1.31 Alcohol Reactions

Early work on alcohol dehydration has been reviewed by Venuto and Landis.[185] The intramolecular dehydration of alcohols results in alkene formation, whereas the intermolecular reaction culminates in the production of ethers. Both reactions, which occur simultaneously, require weak acidity and are thought to proceed via a common carbenium ion intermediate formed on the elimination of water from an alcohol molecule.[186] Water formed during the reaction could ionise the structural hydroxyl groups, essentially converting the catalyst to a ceramic material containing mobile hydroxonium ions.[187] The reactivity sequence for the higher alcohols, $R_3COH>R_2CHOH>RCH_2OH$, reflects the decreasing stability of the carbenium ion formed on the elimination of the hydroxyl group.

Rudham *et al*[187] have suggested that the dehydration of propan-2-ol can be used to assess the total amount of Brønsted acidity present in a catalyst. By titration of a fully hydrogen exchanged HY zeolite with an organic base they showed that the drop in activity was linearly proportional to the amount of base added. Therefore, all the sites that are initially active were shown to have equal activity, although the possibility that some sites were totally inactive was not dismissed.

1.32 Alkene Reactions

Alkenes can undergo four simple reactions: skeletal, positional and geometric isomerisation, and polymerisation. Additionally, longer chain alkenes have been studied in cracking reactions.[188,189] All these reactions are thought to proceed via a common carbenium ion, formed by simple protonation of the double bond. A general reaction scheme for these reactions, showing the common intermediate, is presented as figure 1.8. Disappearance of all double bond character in the infrared spectrum of 1-hexene was noted by Eberly,[63] on contact with Y zeolite at 366K. Once again, the stability of the carbenium ion formed has a direct bearing on the reactivity, with tertiary alkenes forming the most stable carbenium ions.

Simple skeletal isomerisation without a change in the degree of branching is accomplished by alkyl transfer; progression to a branched chain has been shown to occur via protonated cyclopropane intermediates.[190]

Double bond migration and cis/trans isomerisation generally progress much faster than skeletal isomerisation. Once a double bond has been protonated, there is free rotation about the carbon-carbon bond axis, and the loss of a proton from either side of the charge is likely. The activity of but-1-ene isomerisation over a series of HY zeolites was found to be proportional to the intensity of the high frequency band in the infrared,[191] thus suggesting a simple protonation mechanism. Unfortunately, the facile nature of the reactions being studied leads to complex inter-reactions resulting in a number of products.[189] Therefore, reactants which lead to fewer possible isomers are preferred for ideal test reactions, such as in the case of methyl transfer, 3,3-dimethyl -1-butene or cyclohexene to methylcyclopentene transformations.[192]

The study of these three reactions can be impeded by the last class of reaction, polymerisation. The build-up of polymeric species on the surface and at the pore mouths can cause deactivation of the catalyst by site suppression and pore mouth choking. As the polymerisation reaction is a straight addition of an alkene molecule to a surface carbenium ion, steps, such as very low partial reactant pressure, can be taken to minimise its effect. However, the low

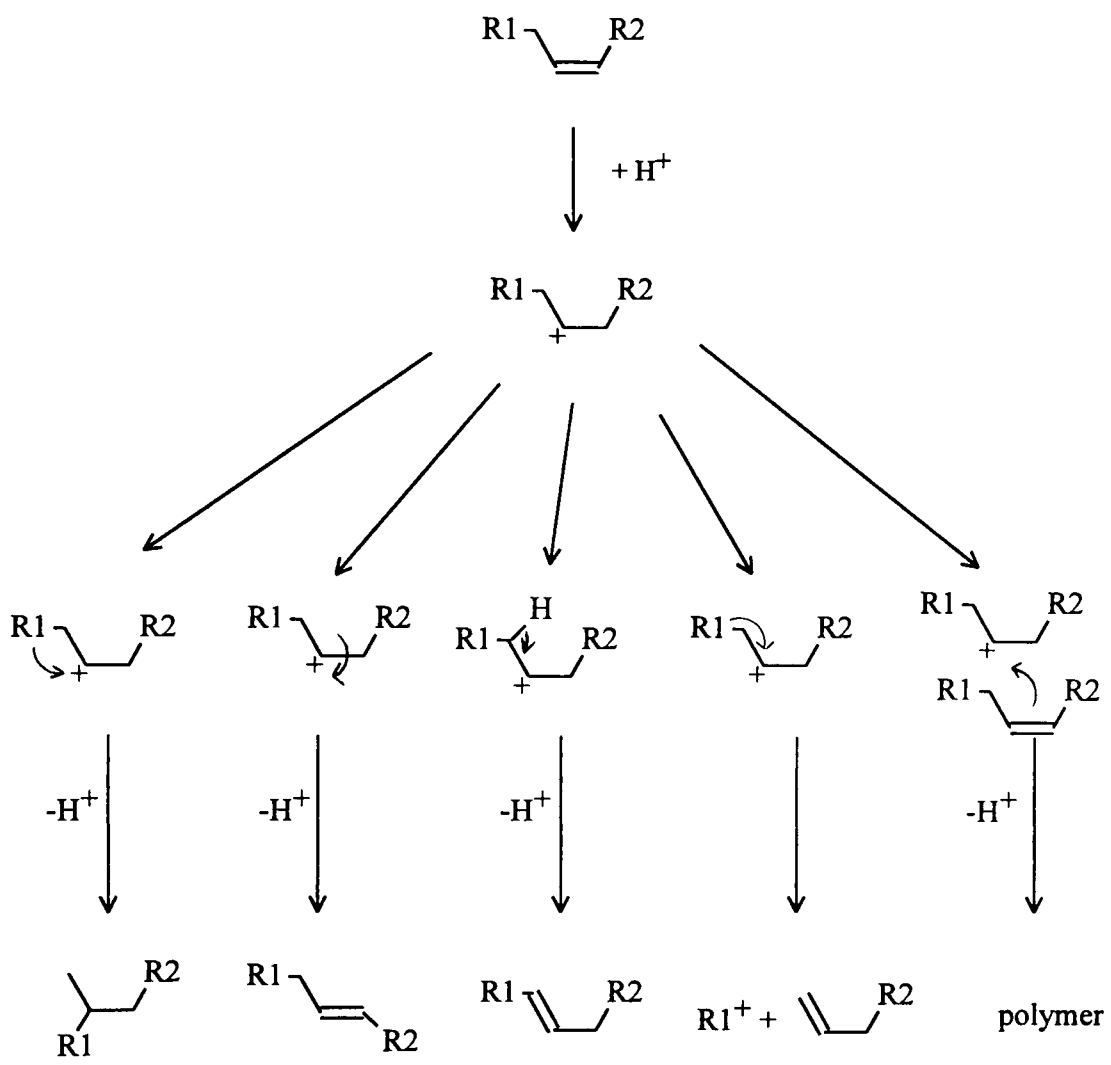

Figure 1.8: General scheme for alkene reactions showing common intermediate.

temperatures used in these reactions, when coupled with the highly acidic sites present in dealuminated zeolites can result in polymerisation due to the increased lifetime of the carbenium ion: Eberly[63] noted the onset of polymerisation of 1-hexene over deammoniated HY zeolite at the comparatively low temperature of 423K. Although the sample employed had a nominal Si/Al ratio of 2.33, the activation procedure may have dislodged some framework aluminium leading to the generation of some strong acid sites, which could effect the polymerisation process.

The direct study of the polymerisation reaction has been attempted by Weeks and Bolton[193] who studied the polymerisation of isotopically labelled but-1-ene over HY. Low temperatures (323K) were found to favour dimerisation leading to various isomers of octane, where hydride transfer had increased the level of saturation. However, higher temperatures (473K) produced shorter, branched molecules, presumably from the catalytic cracking of large polymeric molecules within the pore system. Although polymerisation reactions are interesting in their own right, they are more important in furthering the understanding of deactivation processes in other reactions, such as the dealkylation of alkylaromatics, where considerable amounts of alkene molecules are produced. In this respect, the polymerisation of propene has been studied[194,195,196,197] giving an insight into the deactivation processes in cumene dealkylation.

1.33 Alkylaromatic Reactions

The reactions which are grouped under this heading can be subdivided into addition reactions (alkylation), elimination reactions (dealkylation) and a combination of the two reactions (disproportionation). Di-substituted aromatic molecules can also undergo isomerisation to form different isomers. Once dealkylation has occurred, longer side chains are also prone to undergo other independent reactions, such as alkane and alkene isomerisation and cracking. Clearly, all these reactions cannot be considered to be totally discrete; some reaction competition is inevitable.

It is well known that mixtures of an alkene and benzene, when passed

over an acidic zeolite, will produce the appropriate substituted aromatic molecule.[198] Attack of the π-system of the benzene molecule by the carbenium ion formed on protonation of the alkene molecule will lead to an alkylaromatic carbenium ion. This, on elimination of a proton from the benzene ring, regains aromaticity and is free to desorb from the surface. It is obvious from the preceding section that the addition to the aromatic molecule is in direct competition to the reaction with another molecule of alkene. The latter would be more likely to form polymeric species, leading to the unavoidable deactivation of the catalyst. Weeks and Bolton[199] noted that butylbenzene was only formed when but-1-ene was added to HY zeolite with preadsorbed benzene and not when the reactants were added in the opposite manner. This they took as evidence that the polymerisation of but-1-ene was purely detrimental to the desired reaction, and did not produce additional or more active sites.

The stability of the carbenium ion determines the relative rate of the reaction. In a study of the alkylation of toluene,[200] the reaction was found to proceed one thousand times faster with propene than with ethene. The stability of the alkyl carbenium ion formed from the side chain also determines the nature and mechanism of the dealkylation /disproportionation reaction. For instance, the cracking of the alkylaromatic bond to give benzene and the appropriate alkene is negligible in the reaction of toluene,[201] present for that of ethylbenzene,[201] and the main reaction for cumene.[202]

The formation of the alkylaromatic carbenium ion is an essential starting point for all the reactions mentioned, and is generally thought to occur by protonation of the aromatic ring. A general reaction scheme for the alkylaromatic reactions is outlined in figure 1.9. Jacobs *et al*[118] reasoned that only a few of the Brønsted sites were catalytically active, with toluene disproportionation requiring sites of very high acidity. This last observation is in line with those of Wang and Lunsford,[203] who found that toluene disproportionation activity was greater on HY than on silica alumina. For toluene disproportionation, in which the methyl cation is unlikely to exist as a stable entity, two mechanisms have been proposed.[60] After protonation a

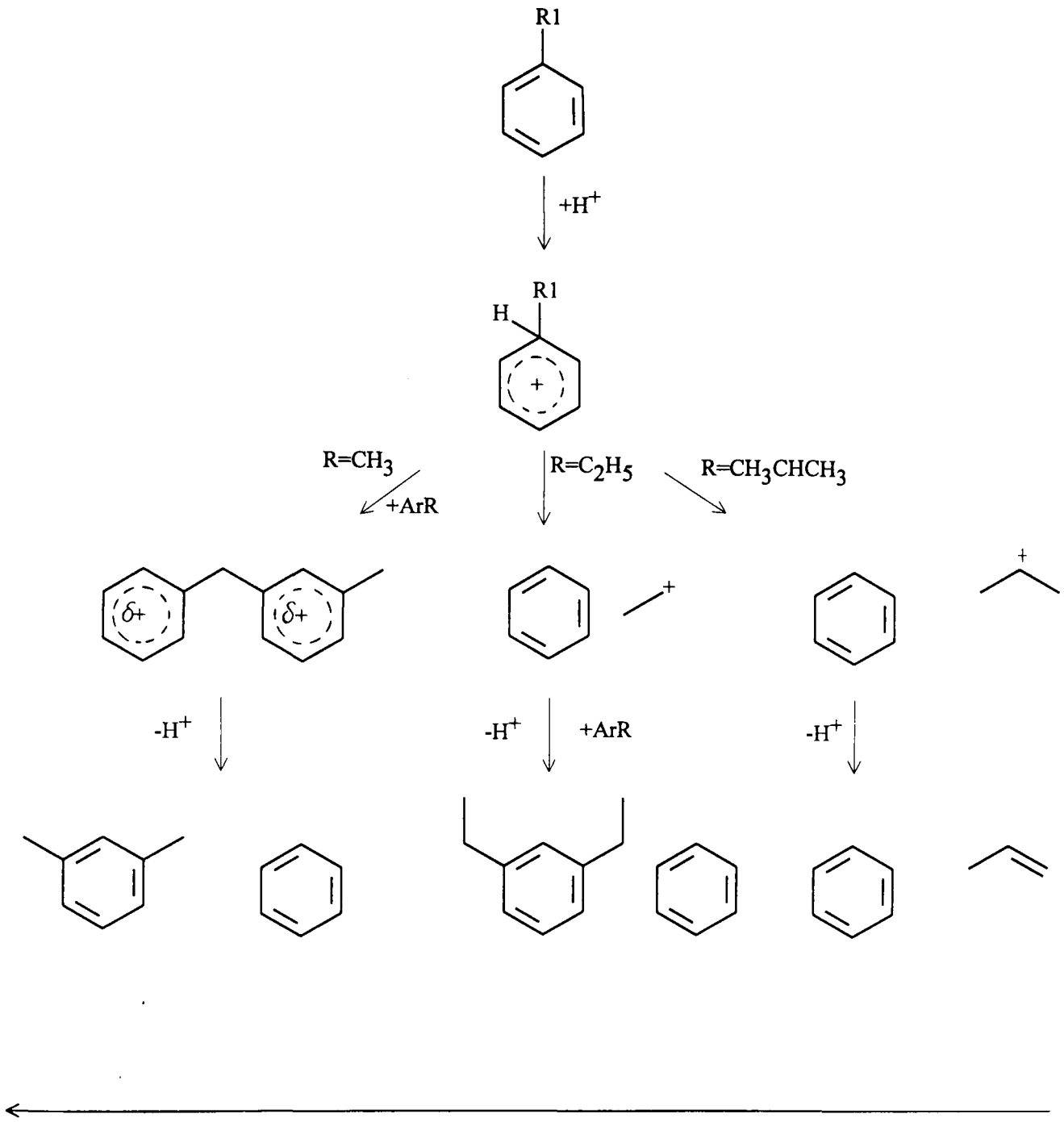

Figure 1.9: General scheme for alkylaromatic reactions.

methyl bridged intermediate is formed, followed by cleavage of the original methyl bond. A similar method, but initiated by hydride abstraction from the methyl group was also proposed.

At low levels of conversion only benzene and xylenes would be expected, the concentrations of each in the product stream being low enough to preclude any secondary reactions. However, at higher temperatures Benesi[204] reported appreciable amounts of trimethylbenzene, obviously formed by methyl transfer from toluene to xylene.

Although the initial activity in toluene disproportionation has been linked to the concentration of strong acid sites,[60,203,204] a recent study has proposed the existence of catalytically active coke.[60] Rhodes and Rudham[60] found that a maximum in activity for this reaction was observed after 4-20 hours on stream, the exact position of which was shown to vary with the catalyst and the amount of hydrogen in the carrier gas. After some elegant experiments in which the carbon content of the sample was measured at different points during the lifetime of the catalyst, it was concluded that the gradual deposition of coke was increasing the catalytic activity of the sample. Furthermore, the discrimination between the activities of samples with and without extrastructural aluminium on initial activity was completely lost when comparing the maximum activity achieved. It was proposed that the reaction was being maintained and enhanced by the coke, possibly because the proton was recycled without being returned to the zeolite framework.

Other molecules in the alkylaromatic series react at much lower temperatures than toluene, reflecting the more facile nature of the reactions concerned. Clean disproportionation of ethylbenzene has been reported at 473K.[176,205] The lack of any rapid catalyst deactivation, arising from possible ethene polymerisation, makes this an excellent reaction for assessing Brønsted acidity. Rhodes and Rudham reported[176] that the activity after five hours on stream could be related to the acid concentration, with maximum efficiency corresponding to $\approx 30Al_F$ puc. This agrees with Karge *et al*[205] who concluded, after titration of catalysts with butylamine, that only the acid sites of highest strength were responsible for the catalytic activity.

In contrast to the mechanism proposed for the toluene disproportionation, the reaction of ethylbenzene is thought to proceed via a two step dealkylation/alkylation process. The mechanism proposed[176] centres on the existence of a discrete ethyl carbenium ion. This accounts for the production of a small amount of other substituted alkylaromatics and short chain hydrocarbons, species not detected in the toluene study.[60] Dealkylation followed by alkylation in the same manner as indicated earlier, produces benzene and diethylbenzene.

A similar, but shorter, induction period has been noted[176,206,207] for the ethylbenzene reaction than had previously been reported for toluene disproportionation. In this case the enhancement of activity is considerably less marked than when toluene was the reactant.[60] During the induction period it was noted that the rate of formation of diethylbenzene was exceeded by that of benzene, a fact which was put down to the greater volatility of the unsubstituted molecule. Calculations showed that the shortfall in diethylbenzene could easily be accommodated in the pore system of the sample. Thus the apparent rise in activity with time is attributable to physical and not catalytic properties of the zeolite.

The final alkylaromatic under consideration, cumene, exhibits the most extreme behaviour. Under similar reaction conditions to ethylbenzene disproportionation, the major reaction is the fission of the alkylaromatic bond, forming benzene and propene, although a range of minor products have also been reported.[202] This dealkylation reaction is considered to be catalysed by acid sites of medium to weak strength.[118,208] The presence of a considerable amount of propene causes additional problems of catalyst deactivation, due to the build-up of polymeric coke molecules. Disproportionation to di-isopropylbenzene and benzene has been reported over a variety of catalysts.[183,209,210]

The activity sequence outlined above is in complete agreement with that proposed almost forty years ago.[211] In a study of the disproportionation of various alkylbenzenes in a homogeneous system in which aluminium tribromide and hydrogen bromide were dissolved in the alkylbenzene in

question, Brown and Smoot[211] found that the order of reactivity was t-butyl > i-propyl > ethyl > methyl. It can be seen from the reactions given that this can be entirely rationalised by the stability of the carbenium ion formed during the reaction.

1.34 Alkane Reactions

It is generally accepted that the cracking of alkanes proceeds via two distinct mechanisms; high temperature thermal cracking by free radical formation, and lower temperature, catalytic cracking with cationic intermediates. Thermal cracking is initiated by hydrogen atom abstraction from an alkane molecule to form a hydrocarbon radical, which, by successive ß-scission steps forms smaller radicals and alkanes. The chain is continued by hydrogen abstraction from a feedstock molecule forming a larger radical and an alkane molecule. This reaction path is typified by high yields of methane and ethane/ethene, low yields of molecules with more than three carbon atoms, and no skeletal isomerisation. In contrast, catalytic cracking proceeds via cationic species and provides more higher molecular weight products, fewer C_1 and C_2 molecules, and a high degree of skeletal isomerisation.

Strong Brønsted sites were found to be necessary for n-hexane and n-heptane cracking over a variety of acidic zeolites.[212] The activity for both hexane and heptane cracking was found to increase with activation temperature, peaking at around 823K; the fall thereafter being attributed to the destruction of Brønsted sites. More recent work[213,214] has reinforced this view, and combined it with the theory that strong acid sites are those with no second neighbour aluminium atoms.

The reaction could conceivably be initiated by four separate paths, which are:

i) protonation of an alkene impurity at a π-bond, to produce a carbenium ion,

ii) thermal cracking to produce an alkene molecule, which can then be protonated,

iii) protonation of an alkane molecule, at either a C-H σ-bond,

followed by hydrogen elimination to form a carbenium ion, or at C-C σ-bond to give a non-classical pentacoordinated carbonium ion, which on cleavage forms a carbenium ion,

iv) hydride abstraction by a Lewis site.

Initiation by mechanism iii) requires further consideration. Although postulated by comparison with liquid superacids,[215] the existence of the pentacoordinated carbonium ion in zeolite catalysis is becoming accepted, although the direct observation of carbenium ions formed from straight chain alkanes has yet to be reported. Nevertheless, the formation of such ions on Brønsted sites under operating conditions is proposed[213,216] and their subsequent protolytic cracking provides an additional source of carbenium ions.

Once formed, the carbenium ion can suffer one of five fates:

i) immediate desorption as an alkene molecule,

ii) hydride transfer from another hydrocarbon molecule and desorption as an alkane molecule

iii) skeletal isomerisation,

iv) ß-scission to a smaller carbenium ion and an alkene molecule,

v) addition to a feedstock (or other molecule) to produce a larger carbocation.

These reactions will be considered in greater detail in Section 4.2, the discussion on n-hexane cracking. At once the lack of small molecules in the product stream can be appreciated. The energetically most favourable carbenium ion will be formed, the most stable being tertiary and the least stable primary. Therefore the statistical chances of forming methane are small, especially when one considers that a propyl carbenium ion is more likely to desorb as propene or hydride abstract to propane, than to crack to smaller molecules. Short chain molecules are more likely to isomerise rather than crack; indeed in some cases, eg. an isobutyl carbenium ion, cracking by ß-scission is not possible. Long chain molecules predominately crack, but the number of products leads to a myriad of possible secondary reactions, highly

complicating the reaction mechanism.

This reaction pathway, with its predisposition to produce more saturated hydrocarbons, has its own product profile. Therefore the relative contributions from the protolytic and classical pathways can be determined.[217] Wielers *et al*[217] have proposed the cracking mechanism ratio (CMR) which provides a measure of the relative importance of each mechanism. Increasing values of the CMR imply an increasing dominance of the non-classical method.

As has been mentioned with previous reactant systems, it is advantageous to reduce the number of potential reactions to a minimum, although some catalytic and theoretical studies have been carried out on long ($C \geq 9$) molecules.[218,219,220] With this in mind, most alkane reactions investigated involve reactants with less than eight carbon atoms, with possibly the most effort centred on n-hexane.[212,213,221,222,223] The cracking of n-hexane is the basis for the long established α-test,[224,225] in which the cracking activity rate constants of the catalyst under study are compared with that of a highly active amorphous silica-alumina. This reference standard is fixed as having an α-value equal to one. However, the advent of highly siliceous, crystalline zeolites with activities magnitudes higher than that of the reference resulted in meaningless data when taken at the same temperature. Fortunately, similar activation energies allows the conversion to be determined at suitable temperatures and then extrapolated to give a theoretical value at 811K. In this way α-values in excess of 10,000 were obtained for hydrogen faujasites.[224,225] Although this would seem to be a convenient method for assessing activity variations between different catalysts, doubts have been expressed over its simplistic nature.[222]

Careful consideration of the results obtained from catalytic testing, when combined with information gained from direct study of the framework composition, will allow an understanding of some of the chemical processes involved in catalysis. The research reported in this thesis has attempted to unify the information obtained from a number of the processes outlined above.

2 Experimental

2.1 Catalyst Preparation

All the samples used in this study were generated from a NaY zeolite (Crosfield Chemicals, Batch No. 1034) with a hydrated composition:

$$Na_{48}Ca_{2.7}Mg_{2.3}(AlO_2)_{56}(SiO_2)_{136}.255H_2O$$

This sample was converted to the ammonium form by ion exchange with ammonium sulphate solution to give a sample designated NH_4YAS with a hydrated composition:

$$(NH_4)_{43.5}Ca_{0.5}Na_{12}(AlO_2)_{56}(SiO_2)_{136}.211H_2O$$

A sample with a very low sodium content (<0.4 Na^+ per unit cell), designated NH_4YLS, has been derived from NH_4YAS by heating to bring the remaining sodium ions from inaccessible positions to supercage sites where they were extracted by further ammonium exchange. NH_4YLS was the starting material for the extensively dealuminated Y zeolites prepared by Rhodes[201] and for the less aggressively dealuminated samples prepared by the present author. The samples were stored above a saturated solution of sodium hydrogen sulphate to ensure that they remained fully hydrated.

2.11 Hydrothermal Dealumination

Dealuminated Y zeolite samples with a framework aluminium content of between 25 and 13 per unit cell were prepared in bulk by heating NH_4YLS to temperatures between 823K and 1073K in 100% water vapour at atmospheric pressure. These samples are designated HYST x, where x is the maximum temperature at which the sample was steamed. A further series of samples were dealuminated in a partial pressure of water vapour under less forcing conditions, and are designated HYMST x.

The mild steaming apparatus is shown schematically in figure 2.1. A double saturator, each reservoir half filled with glass spirals and to the same level with de-ionised water, was placed in a large oven. A thermocouple port in the wall of the saturator allowed direct measurement of the water temperature via a chromel-alumel thermocouple. A stainless steel tube lead from the outlet of the saturator through a hole in the top of the oven directly

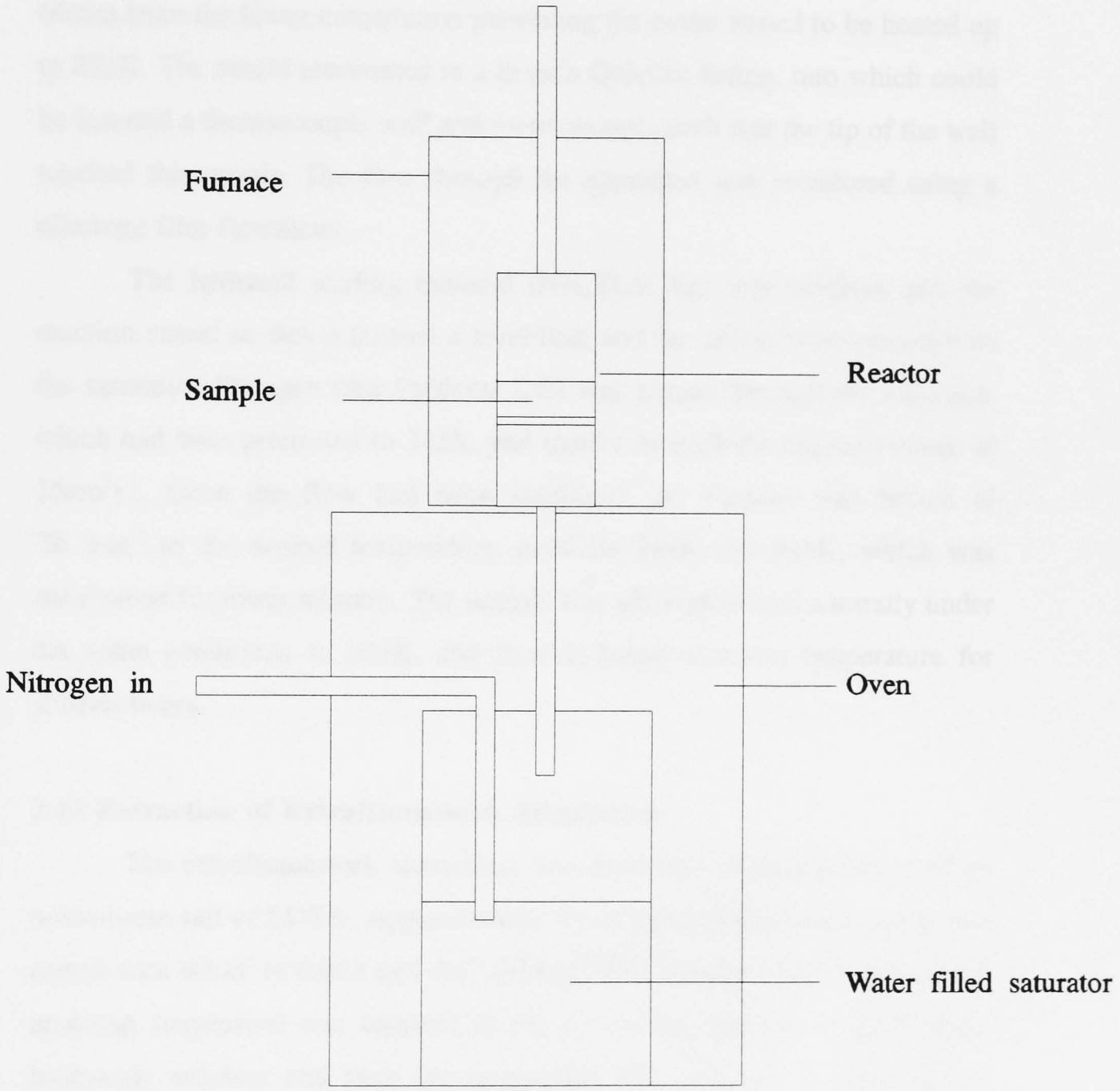

Figure 2.1: Mild steaming apparatus.

into a furnace where it was connected to the bottom of a vertical silica glass reaction vessel. A programmable controller (Eurotherm Digi) regulated the furnace via a chromel-alumel thermocouple inserted in furnace. The reaction vessel consisted of a silica tube (35mm o.d.) which narrowed to smaller tubing (6mm i.d.) at the lower end. A sintered silica disc was fused across the tube 60mm from the lower constriction permitting the entire vessel to be heated up to 873K. The vessel terminated in a female Quickfit fitting, into which could be inserted a thermocouple well and thermocouple such that the tip of the well touched the sample. The flow through the apparatus was monitored using a climbing film flowmeter.

The hydrated starting material (NH_4YLS, 8g) was weighed into the reaction vessel so that it formed a level bed, and the vessel was connected to the saturator. Nitrogen (Air Products Ltd) was passed through the saturator, which had been preheated to 343K, and thence through the reaction vessel at 25cm^3s^{-1}. Once the flow had been stabilised, the furnace was heated at 7K min^{-1} to the desired temperature, between 748K and 848K, which was maintained for thirty minutes. The sample was allowed to cool naturally under the same conditions to 323K, and then hydrated at room temperature for sixteen hours.

2.12 Extraction of Extraframework Aluminium

The extraframework aluminium was extracted using a solution of an ammonium salt of EDTA. Approximately 4g of the dealuminated sample was mixed with 80cm^3 of 0.023 mol dm^{-3} $(NH_4)_4$EDTA solution. The acidity of the resulting suspension was adjusted to pH 4.3 by the addition of ammonium hydroxide solution and then the suspension was refluxed for four hours. Acidity measurements of the solution were made both before and after reflux. The zeolite was recovered by vacuum filtration and washed with trebly distilled water (170cm^3). The washings were made up to a constant volume and analysed for aluminium using atomic adsorption spectroscopy. Extraction performed using the ammonium salt instead of the di- or tetra-sodium salt negated the requirement to carry out a second ion exchange reaction, thus

preserving the known low sodium content of the samples.

2.2 Catalyst Characterisation

In all the experiments performed, unless explicitly mentioned otherwise, the catalysts were presented in the form of broken pressed discs. Small pieces of pressed material are more analogous to preparations used in industry, and are much easier to handle and accurately weigh than a fine powder. It is also advantageous to perform as many as possible of the characterisation and catalytic tests with the samples in the same physical condition. Therefore the fully hydrated sample (0.3g) was pressed in an 25mm diameter infrared disc die for two minutes under a pressure of 0.6 GPa and broken up into small pieces (maximum dimension <5mm).

2.21 Temperature Programmed Desorption.

The extent and strength of the acidity of solid catalysts can be probed by the technique of temperature programmed desorption (TPD). In the apparatus used in this research, shown schematically in figure 2.2, ammonia desorbed from the catalyst into a high vacuum system was detected by mass spectrometry.

Theory and principles of Mass Spectrometry

Positive ions, formed in a ionisation chamber by bombardment of molecules with electrons from a rhenium filament, are accelerated towards a negatively charged plate which has a small hole through which some of the ions pass into a curved second chamber. This chamber is surrounded by a permanent magnetic field and has an ion detector at the end. Assuming that all the ions have the same energy, only those of the correct velocity, and hence mass, will impinge on the detector; those travelling too slowly will be attracted to the inner wall of the chamber, and those travelling too fast will not deviate enough in the magnetic field and will hit the outer side of the chamber.

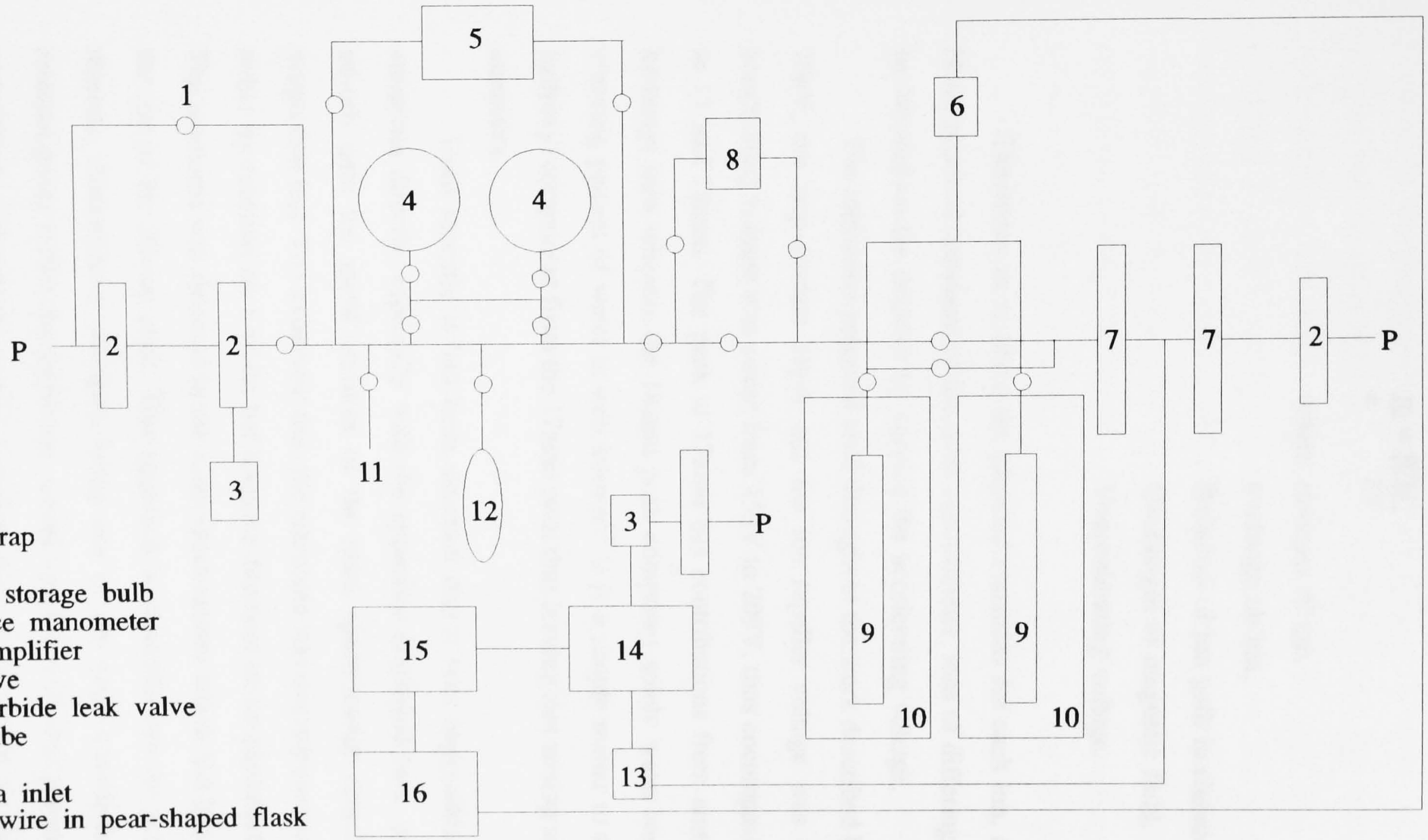

1. Teflon tap
2. Nitrogen trap
3. Ion gauge
4. Ammonia storage bulb
5. Capacitance manometer
6. Voltage amplifier
7. Metal valve
8. Silicon carbide leak valve
9. Sample tube
10. Furnace
11. Ammonia inlet
12. Sodium wire in pear-shaped flask
13. Leak valve
14. Mass spectrometer
15. Mass spectrometer control unit
16. Computer

P. To pumping system

Figure 2.2: Schematic diagram of the temperature programmed desorption apparatus.

The equation relating these properties is:

$$\frac{m}{e} = \frac{R^2H^2}{2V}$$

where m=mass of ion,
e=charge on ion,
R=radius of ion path in chamber,
H=strength of magnetic field,
V=accelerating voltage.

Therefore, as m and e are physical constants for each ion, and R and H are physical constants of the mass spectrometer, ions of differing mass can be focused on the detector by varying the accelerating voltage.

The ionisation potential used throughout the work described below was 70eV, the trap current 10μA and the ion repeller voltage was +1V. The accelerating voltage was swept from 253V to 209V, thus encompassing peaks at 17 and 18amu. The peak at 17amu has contributions from ammonia and hydroxyl ions whereas the 18amu peak comprises solely water ions. As the cracking pattern of water is well known[226] it is a simple matter to extract the hydroxyl component from the 17amu peak thus leaving that arising solely from ammonia.

Until recently it had been assumed that it was impossible to detect ammonia directly, especially with the apparatus employed here, as it would adsorb onto the metal surfaces of the mass spectrometer chamber and a proportion lost. To circumvent this, the ammonia was decomposed to nitrogen, either by reaction on a white hot tungsten filament or on platinised alumina. The ammonia was detected in the mass spectrometer which had been tuned to the top of the 28amu peak. This approach is unsatisfactory for a number of reasons. Atmospheric nitrogen, being one of the main constituents of the residual gases within the apparatus, would interfere with that produced in the experiment. Corrections would therefore have to be made to account for variations in the day to day pumping efficiencies of the pumps and quality of the seals around the sample tubes. In addition, if a small leak developed during

an experimental run, the run would have to be abandoned. Decomposition of ammonia to nitrogen depended on the temperature of the wire or platinised alumina, and the action of the former could also be diminished by the build up of a tungsten oxide layer or evaporation of the tungsten onto the glass presenting a smaller surface area of hot tungsten for the reaction. The assumption has to be made that the time for the adsorption and reaction of the ammonia, and desorption of the nitrogen is negligible, otherwise the temperature measured at the sample could not be related to the nitrogen signal measured by the mass spectrometer. This effect would be particularly noticeable at high heating rates, which in turn could also cause problems of swamping the decomposition catalyst. Monitoring the top of the 28 amu peak created additional problems as a very small drop in the accelerating voltage would cause the detector to 'fall off the top of the peak'. To counter this, the operator would observe the experiment, but as this problem could only be rectified by eye after it had occurred, experiments would sometimes have to be aborted before completion. These problems were solved by introducing computer control to the experiments. By sweeping the 17 and 18 amu peaks the problems of atmospheric leakage and accelerating voltage oscillation were instantly removed as the 18amu peak, being due to water, acted as an internal pressure standard as long as water was not being desorbed from the sample, and sweeping the voltage *through* the peaks ensured that none of the signal was lost.

Apparatus

The apparatus can be divided conveniently into three sections, the service section, the experimental section and the control section. The service section allows for ammonia and sample preparation, and for ammonia to be admitted to the sample. The experimental section permits the controlled thermal desorption of ammonia from the sample, and the detection of the ammonia by mass spectrometry. The control section consisted of an 'IBM clone' personal computer which has been programmed to control the mass spectrometer and to read, store and process the experimental data, together

with equipment to measure the pressure inside the apparatus and to control the furnaces. The entire apparatus was constructed from Pyrex glass tubing (13mm o.d.) and Young's taps, unless otherwise stated.

The Service Section

The vacuum is maintained in the service section by a mechanical rotary pump (Edwards Speedivac) and a two stage mercury diffusion pump (Jencons Electric) connected by wide bore (26mm o.d.) glass tubing. The pumps could be isolated from each other, and from the rest of the vacuum frame, by greased stopcocks (Apiezon N grease). It was possible to bypass the mercury pump totally so that ammonia could be evacuated from the apparatus. The reduced pressure generated could be measured using an ion gauge (Edwards IG5G) connected to a control unit (Mullard) and was generally found to be less than $1x10^{-2}$Pa. A liquid nitrogen cold trap was placed on the exit side of the ion gauge to prevent mercury vapour and rotary pump vapours from back-diffusing into the rest of the system. This, and a second cold trap under the ion gauge, protected the mercury pump and the ion gauge from exposure to ammonia, and the ion gauge from exposure to mercury. Similarly, a third cold trap positioned at the exit to the rotary pump collected any excess ammonia and prevented the majority of the rotary pump vapours from entering the apparatus.

Approximately 8000cm^3 of ammonia, sufficient for at least one hundred experiments, was admitted to the apparatus from a high pressure gas cylinder (Air Products Ltd) connected to a port on the apparatus by strengthened nylon tubing, and stored in two glass bulbs. The pressure of ammonia in the bulbs was monitored by a mercury manometer and a blowout safety valve guaranteed that a dangerous pressure of ammonia could not build up. Condensation of the ammonia into a pear shaped flask containing 5g of freshly wound sodium wire, surrounded by an propanone/CO_2 slush bath, removed any water by reaction to sodium hydroxide and hydrogen. This and any other gaseous impurities could then be removed from the solid ammonia by pumping. This freeze/thaw cycle was repeated at least three times with fresh ammonia, and when the apparatus had been up to air for sometime, to purify the ammonia. Three

additional pear shaped flasks were available for the storage of liquid bases. A bypass, including a silicon carbide leak, was situated between the service section and the experimental section, and allowed a small pressure of gas to be maintained in the experimental section for calibration purposes.

The Experimental Section

The experimental section of the apparatus, which could be isolated from the service section by PTFE taps (Young's 'O' ring), comprised two silica sample tubes which could be connected, either independently or jointly, to either the service section or to the mass spectrometer. Each sample tube, shown in figure 2.3, was manufactured of silica glass (11mm o.d.),rounded at the bottom, and was connected to the vacuum frame by a cylindrical joint (Young's). One sample tube had a stainless steel sheathed chromel-alumel thermocouple encased in a silica tube (4mm i.d.) which passed through the female end of the cylindrical joint, such that the tip of the thermocouple protruded 23mm from the silica sheath and rested 10mm from the end of the sample tube during an experiment. The join between the thermocouple and the glass was made vacuum tight with Araldite. A T-junction made in the sheath just below the metal/glass joint lead to another cylindrical joint and a T-junction on the exit line from the sample tube ending in a third cylindrical joint enabled helium to be passed over the sample at atmospheric pressure whilst a series of PTFE taps allowed the rest of the apparatus to be maintained at the operating vacuum. In this way, the sample could be prepared at atmospheric pressure under an inert gas, or under vacuum. The other sample tube was arranged in much the same way, except that there was no facility for atmospheric pressure treatment. The sample tubes were heated by electric furnaces, controlled by temperature controller/programmers (John Burdon/CRL, and Eurotherm Digi) and chromel-alumel thermocouples. Experimental reproducibility was ensured by using the same furnace and temperature controller for each experiment (John Burden/CRL) and smooth temperature ramping was achieved by inserting a wide bore silica tube into the furnace used for all the desorption experiments. The relative pressure in the

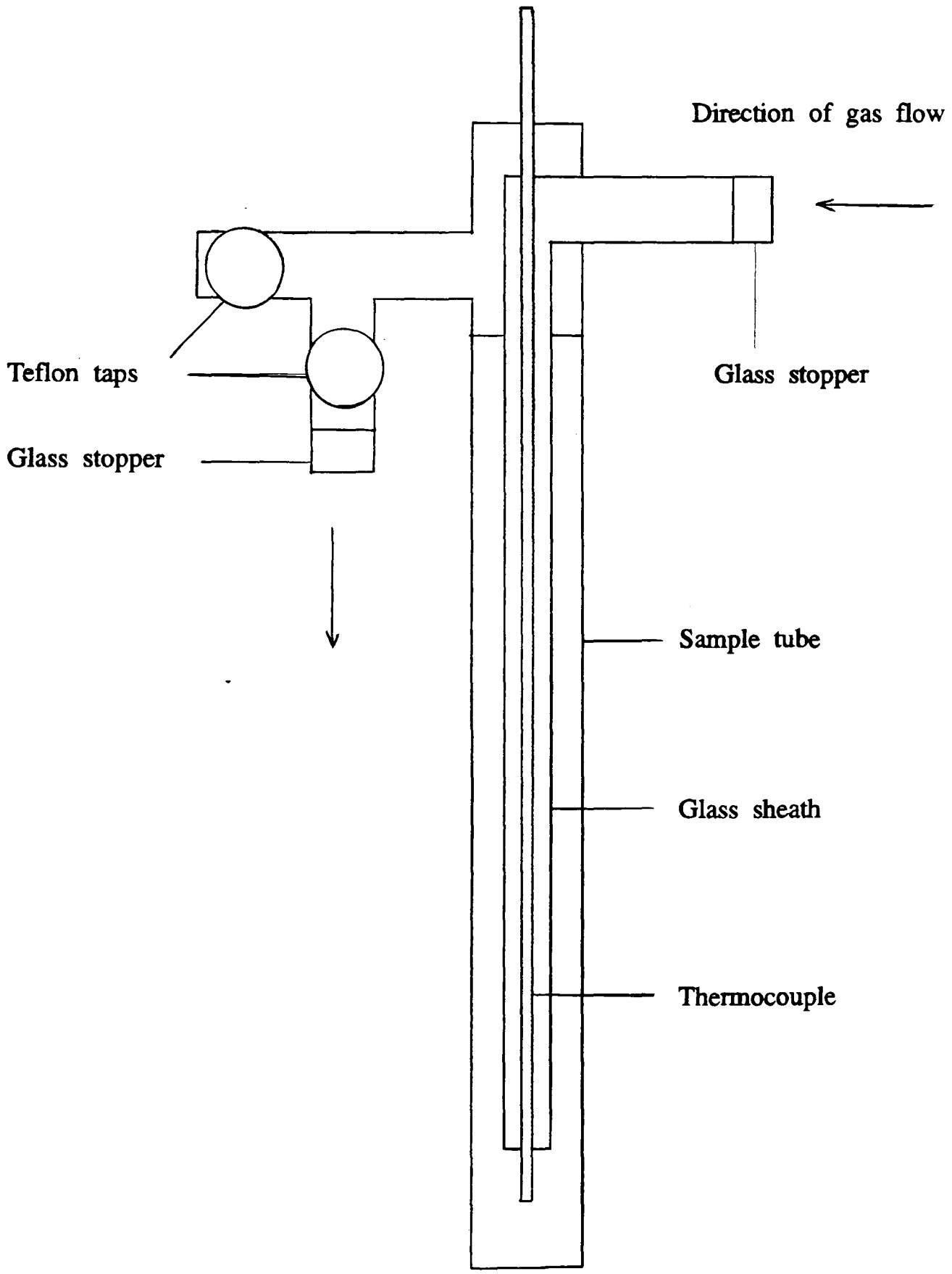

Figure 2.3: Apparatus for atmospheric pressure bakeout (detail).

experimental section of the apparatus over that of the service section vacuum was measured by a capacitance manometer (Baratron Type170, MKS Instruments Inc.) A second pumping system comprising a rotary pump, mercury diffusion pump and liquid nitrogen cold trap allowed rapid evacuation of the sample tubes without contamination of the service section. Two high vacuum metal valves (Vacuum Generators, RDP) connected with wide bore glass tubing (25mm o.d.), joined the second set of pumps to the sample tubes and the mass spectrometer (AEI MS10). A leak valve (Vacuum Generators MD6A) was situated on the inlet to the mass spectrometer. The mass spectrometer chamber was pumped by a rotary pump and an oil diffusion pump (AEI, Metrovac High Vacuum 033) connected in series. Crude measurements of the pressure within the mass spectrometer, which could be obtained from an external thermocouple gauge unit (AEI VC12) situated on the backing line, ie. between the rotary pump and the oil diffusion pump, allowed the detection of any serious leaks. Two electric heaters enabled the mass spectrometer chamber to be baked out at 623K to remove as much physically desorbed water as possible. A stainless steel liquid nitrogen cold trap between the oil diffusion pump and the mass spectrometer chamber further reduced the internal pressure and prevented backstreaming of oil vapours into the rest of the system. A background pressure of $1x10^{-5}$Pa was attainable in the chamber, measured by an ion gauge inserted directly into the chamber (Bayard-Alpert gauge, Vacuum Generators 7CS6 Control Unit). Opening the two metal valves by predetermined amounts meant that the same fraction of gas desorbed from the samples entered the mass spectrometer through the controlling leak valve during each experiment.

The Control Section

A temperature programmed desorption experiment requires the two experimental variables, temperature and amount of desorbing gas, to be known accurately. Computer control greatly enhances these experiments as each experiment comprises at least seven hundred data sets and can last up to twelve hours. More detailed subsequent data analysis is then possible.

Each thermocouple is connected to a signal amplifier (Nottingham University) which amplifies the signal from the thermocouple by a factor of 25. This signal is fed to an A/D conversion card (Cil Group) installed in an IBM clone personal computer. The signal from the mass spectrometer is preamplified by an electrometer head (AEI Type 1403) before amplification in the mass spectrometer control unit. A relay from the computer triggered the mass spectrometer control unit to start sweeping through the accelerating voltage, whilst the computer simultaneously started recording the output from the control unit. A description of the programs written by the author to control and run the TPD experiments can be found starting on page 52 and the program listings are contained in the Appendix.

Experimental Procedure

There follows a description of the bakeout procedure, used immediately after the mass spectrometer has been evacuated after having been let up to air, the general procedure for obtaining a TPD trace, the calibration of the system, and the modifications in experimental procedure developed within this project.

Mass Spectrometer Bakeout

The rotary pump was used to reduce the pressure in the mass spectrometer chamber to approximately 5Pa before the oil diffusion pump was started which took the pressure down to roughly 0.01Pa. Atmospheric water vapour, which adsorbs on the metal surfaces inside the mass spectrometer, will only be removed very slowly by pumping at ambient temperatures and its slow desorption creates a significant pressure. Therefore, to reduce the pressure, further it is necessary to bakeout the mass spectrometer at 623K for 48 hours whilst it is isolated from the rest of the system by closing the metal valves. At no time was the leak valve on the entry to the mass spectrometer closed. The cold trap above the oil diffusion pump was then filled with liquid nitrogen and the heating continued for a further hour before the chamber was allowed to cool and the rest of the cold trap filled. When the mass spectrometer was not being used for an experiment, it was isolated from the rest of the frame at the

metal valves as its pumps were more efficient than those serving the experimental and the service sides and continuous connection would increase the background pressure in the mass spectrometer.

The TPD Experiment

A few pieces of the sample were accurately weighed (*ca.*0.050g) into the sample tube, which was replaced on the apparatus and then evacuated through the service side at ambient temperature before being heated to 383K. The bakeout procedure which followed depended on the type of experiment being performed, and as such are summarised below:

i) ammonium exchanged samples were held at 383K for one hour.

Unextracted samples were:

ii) held at 383K for one hour,

iii) held at 673K for sixteen hours in flowing helium ($0.67cm^3s^{-1}$) then cooled in helium to 383K and then evacuated,

iv) held at 673K for sixteen hours in flowing helium ($0.67cm^3s^{-1}$) then evacuated before being crash cooled to 383K,

v) as iv), but held at 673K for two hours.

Ammonia was admitted into the sample tube until a steady pressure of 1.33kPa was attained, which was then maintained for fifteen minutes before the excess ammonia was removed via the service side pumps. The exit to the service side was closed and the metal valves to the mass spectrometer were opened the prescribed fixed amount. The sample was then evacuated for two hours or sixteen hours through the experimental and mass spectrometer side to allow complete desorption of physically adsorbed species. Next, the sample was allowed to cool to 373K, and if the computer confirmed that a low, level background had been obtained, the TPD experiment was run using the appropriate parameters of rise rate 7K min^{-1}, and final temperature 1173K, unless otherwise implicitly stated.

The mass spectrometer was calibrated for ammonia by running TPD

experiments using different masses of NH_4YAS, which has a known ammonia content. The results, shown in table 2.1 and figure 2.4, show that there is a linear response to ammonia in the range studied. Calibration of the system for water was achieved by analysing the dehydroxylation peaks of the same samples. It was found that the peak height above baseline was a better indicator of water content than the integrated area of the water peak because water desorbing from the chamber walls after the peak maximum had passed gave misleading results. The clear nonlinear relationship shown in figure 2.5 indicates that some of water is lost to the walls of the system, which is then slowly desorbed after the experiment; this amount is obviously a greater proportion of the water being desorbed from the smaller samples. The retained water slowly desorbs from the mass spectrometer walls, leading to a false interpretation of the hydroxyl content. The calibration was checked each time that the mass spectrometer had been brought up to air and was found to vary by less than seven percent, which can be attributed to changes in the relative pumping efficiencies of the mass spectrometer and experimental section pumps.

Dry mass / g	Ammonia /x10^{-6}mol	Ammonia signal area/A.U.	Water signal height/A.U.
0.0114	37.0	1169248	5290
0.0173	56.6	1723899	7543
0.0252	82.3	2397946	12057
0.0293	95.5	3057980	16961
0.0353	115.3	3860600	20680

Table 2.1: Mass spectrometer calibration.

A linear relationship of 3.26 x10^7 counts/mmol between the amount of ammonia contained in the sample and the integrated area of the temperature programmed desorption trace was obtained. The height of the water peak was found to have a more complex relationship to the hydroxyl content of the sample.

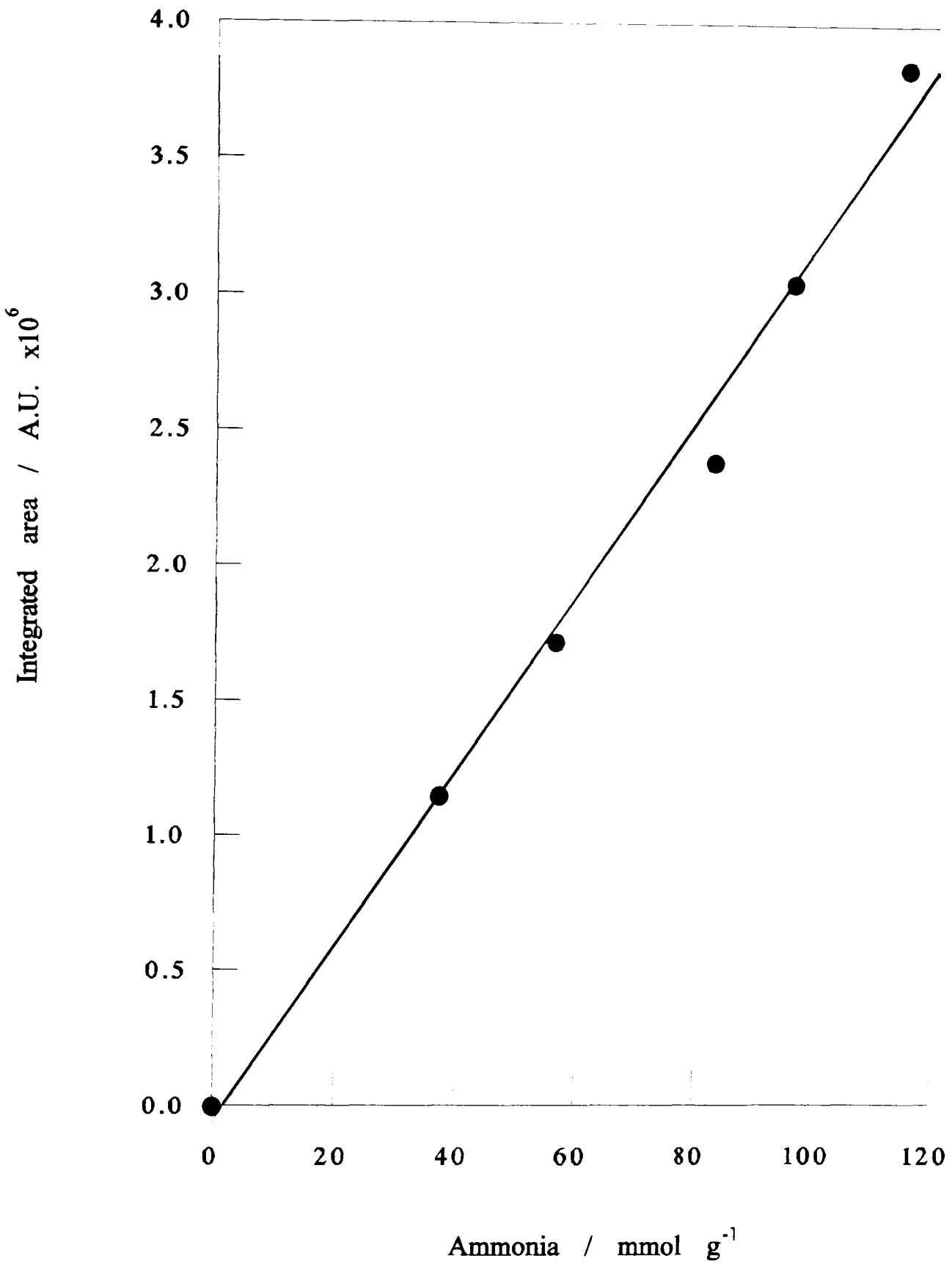

Figure 2.4: Mass spectrometer calibration for ammonia.

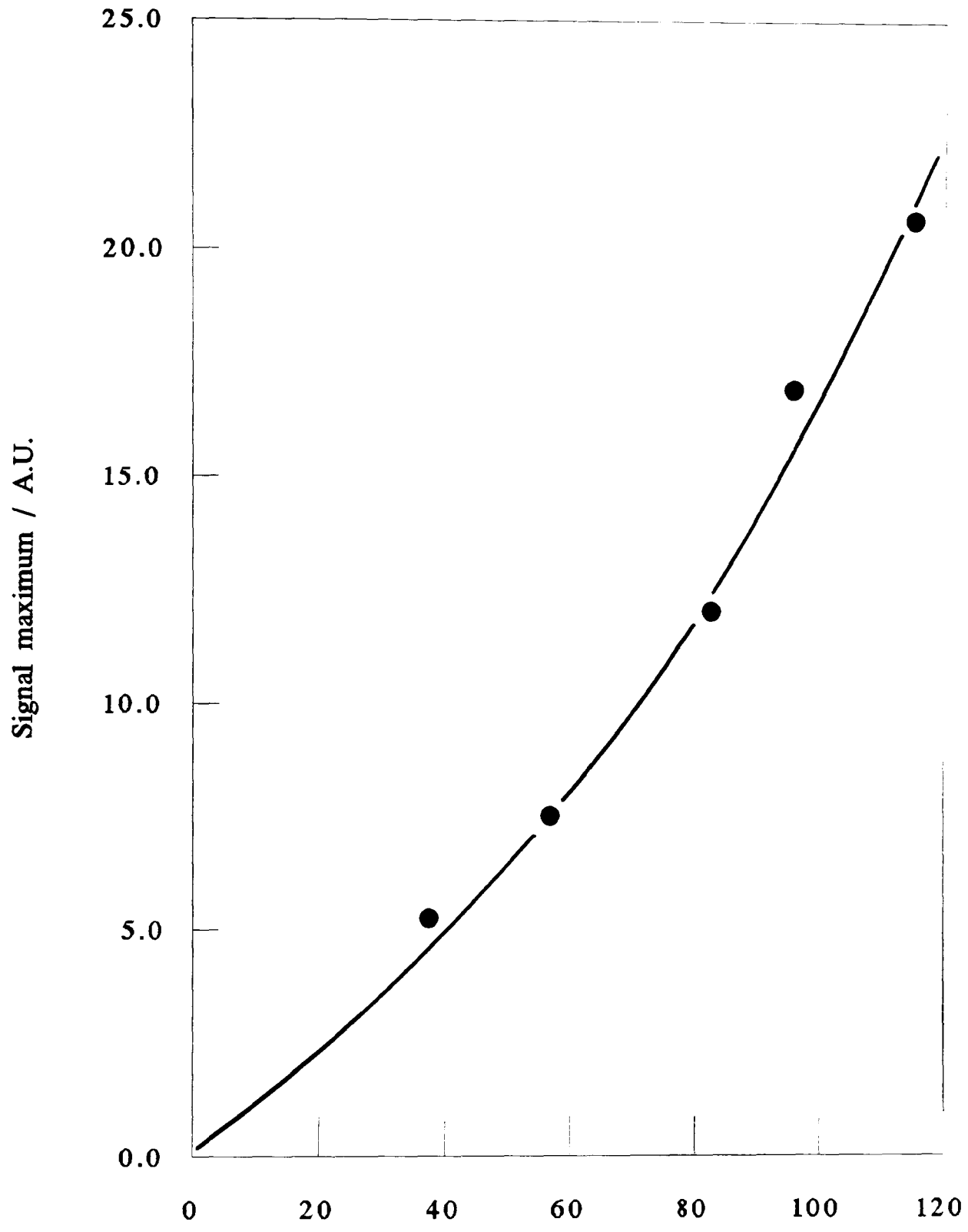

Figure 2.5: Mass spectrometer calibration for hydroxyl groups.

Computer Programs

The computer programs written by the author can be broken down into two sections; those involved with controlling the TPD experiment, and those concerned with processing and analysing the data. The set of programs are controlled by the program MENU and the program listings can be found in the Appendix.

Control Programs

The temperature of the sample during the bakeout procedure was monitored by program READOUT and displayed in large characters on the screen, together with a chart showing the recent relative change.

The temperature programmed desorption experiments were run by program SCAN. After entering the control parameters for the particular experiment a screen was generated which displayed the TPD trace as it was being produced. The right hand margin contained the experimental variables and a status bar across the bottom of the screen displayed the current value of the ammonia, water and temperature readings, and the estimated time remaining. The sequence of events for each reading was as follows. The input line from the thermocouple was monitored and an average reading taken. The relay from the computer to the mass spectrometer control unit was switched and the input line from the mass spectrometer was monitored while the accelerating voltage was swept from 253V to 205V. The signal was analysed, and the amplitudes of the peaks corresponding to 17 amu and 18 amu were registered. The water peak value was used to correct the ammonia value for the hydroxyl content: these two values were plotted against the temperature and all three values saved on the hard disc. The experimental time remaining was calculated and all values were displayed on the status bar. The program waited for the appropriate time and then repeated the cycle. The data took 12.5 seconds to collect, analyse and store and so the highest reading frequency was 0.08 Hz.

Analysis Programs

A series of programs were written to analyse the data, all of which were run in a menu format, its component parts being considered below.

The TPD trace could be geometrically modified using program PLOT. This program simply allowed the axes to be scaled, the ammonia, water, and temperature traces to be shown in any combination, and a hard copy produced. The difference trace between two traces could be obtained using program SUBTRACT. The TPD trace could be differentiated using program DIFF in which the degree of smoothing, and the number of differential points could be specified depending on the quality of the data used. The TPD trace maxima were reported from the x intercept on the differential trace. The TPD trace could be integrated using program INTEGRAT. The start and end point of each integration can be defined and was performed using the successive trapezoidal method, which has the advantage over the Simpson's method of allowing nonuniform increments of the x variable.

2.22 Mid Infrared Spectroscopy

The infrared transmission spectra of all the samples were measured in the 300 - 1350cm^{-1} range using a Nicolet 205 FT-IR spectrometer. Self supporting potassium bromide discs were prepared from an intimate mixture of finely ground potassium bromide (30mg, spectroscopic grade, BDH Chemicals Limited) which had been stored in an oven at 413K, and a very small quantity of the sample (*ca.*0.1mg). The mixture was pressed in an infrared die (13mm) for five minutes under a pressure of 0.6GPa before being transferred to the spectrometer for immediate recording of the spectrum.

2.23 X-ray Diffraction

X-ray powder diffraction patterns were obtained using Phillips PW series equipment. The powdered sample was loosely packed into the aluminium sample holder to a constant volume (0.45cm^3) with minimum pressure to form a flat surface. The cubic unit cell constant was determined by averaging the unit cell constants obtained from the Bragg equation using eight

peaks, the Miller Indices for which are presented in table 2.2. The crystallinity of the samples was estimated using the ASTM method of relative diffraction intensities.[23] The integrated areas of the eight peaks were calculated and the total area expressed as a percentage of that of the highly crystalline Y standard.

Peak	hkl	2θ
1	331	15.65
2	511,333	18.68
3	440	20.35
4	533	23.64
5	642	27.04
6	822,660	30.74
7	555,660	31.39
8	664	34.08

Table 2.2: Miller indices and 2θ values of peaks used to determine unit cell and crystallinity data.

$$a_o=(\frac{\lambda}{2\sin\theta})\sqrt{(h^2+k^2+l^2)} \qquad \text{Bragg equation}$$

where a_o = unit cell constant

h,k,l = Miller indices

θ = angle of radiation

λ = wavelength of radiation

2.24 Thermogravimetric Analysis

The water contents of the catalysts were determined using a Stanton Redcroft TG 750 thermogravimetric analyser consisting of a CI Mark 2C electronic microbalance accurate to $1x10^{-6}$g and a water cooled nichrome wound furnace controlled by a Pt/Pt13%Rh thermocouple connected to a temperature programmer. The sample temperature and weight were recorded simultaneously on a two pen chart recorder.

The sample (*ca* 10mg) was weighed directly into the platinum crucible on the balance and the furnace was raised carefully around it. The temperature was raised from ambient to 773K at 10K min^{-1} under normal atmospheric conditions. The sample was maintained at 773K until a constant weight was obtained. This process was repeated with fresh samples until consistent readings of water content, expressed as a percent of the fully hydrated weight, were obtained.

2.3 Catalysis

In all the experiments, unless explicitly mentioned otherwise, the catalyst was presented as sieved broken discs. The discs, prepared under the same conditions as for the characterisation studies, were broken and sieved such that the portion which passed through an 18 mesh but was retained on a 45 mesh was used.

2.31 Pulse Flow Apparatus

In systems where the catalysts experience deactivation with time on stream, pseudo-initial activities, taken at the first opportunity during continuous flow experiments, can prove misleading. Therefore, a pulse flow apparatus was developed which would allow initial activities and deactivation to be measured during the equivalent of the first minute of the time on stream of a continuous flow experiment.

The apparatus is shown schematically in figure 2.6. Stainless steel tubing (o.d. 3.2mm) was used throughout the apparatus, except for the portion between the end of the cold trap and the gas chromatograph where copper tubing was used (o.d. 3.2mm). Swagelok unions were used throughout the apparatus, except in the joins to the reaction vessel, where Swagelok nuts and 'O' rings were employed. The reaction vessel was a simple silica tube with a sheathed chrome-alumel thermocouple inserted through a T-piece from the bottom. The thermocouple was connected to a cold junction and accurate measurements of voltage and hence temperature were made using a digital multimeter (Keithley Model 175). The catalyst sample was contained between

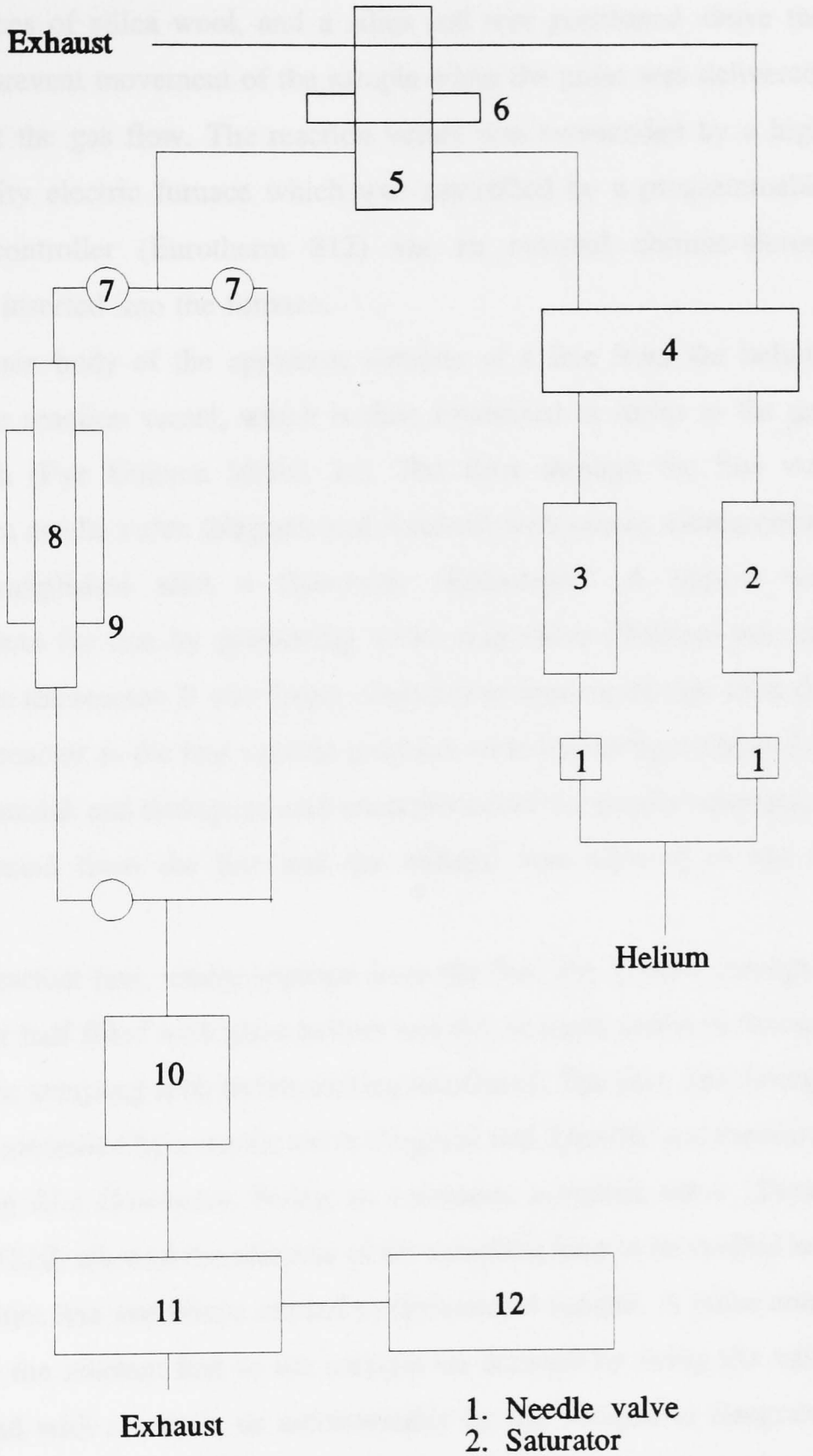

Figure 2.6: Schematic diagram of the pulse flow apparatus.

two small pieces of silica wool, and a silica rod was positioned above the upper pad to prevent movement of the sample when the pulse was delivered, and to preheat the gas flow. The reaction vessel was surrounded by a high thermal capacity electric furnace which was controlled by a programmable temperature controller (Eurotherm 812) via an external chrome-alumel thermocouple inserted into the furnace.

The main body of the apparatus consists of a line from the helium cylinder to the reaction vessel, which is then connected in series to the gas chromatograph (Pye Unicam Model 24). The flow through the line was controlled by a needle valve (Negretti and Zambra) with coarse measurement of flow accomplished with a flowmeter (Rotameter). A bypass was incorporated into the line by positioning a two-way valve (Whitey) into the line just before the reactor. It was found necessary to remove all taps from the line after the reactor as the less volatile products were becoming entrapped in the seating material, and during the activation procedure the gas chromatograph was disconnected from the line and the exhaust was allowed to run to atmosphere.

The reactant line, totally separate from the first line, passed through a glass saturator half filled with glass helices and the reactant, and then through a fixed volume sampling loop before exiting to exhaust. The flow rate through this line was controlled by a needle valve (Negretti and Zambra) and measured by a climbing film flowmeter. Firing an automatic sampling valve (Taylor Servomex SV220) allowed the contents of the sampling loop to be flushed into the main helium line and hence carried to the catalyst sample. A pulse could be sent from the reactant line to the catalyst on demand by firing the valve either by hand with a switch, or automatically by the computing integrator. The products and unreacted reactant were collected by condensation into the liquid nitrogen cold trap, from whence they were flash evaporated onto the gas chromatograph column by surrounding the trap with near boiling water. Details of the different columns used are given later in the specific reactant sections. The separated components of the gas stream were detected using flame ionisation, and the signal was measured by a computing integrator (Phillips

Pye Unicam PU4810). As the experiments were conducted with the gas chromatograph in series with the reaction vessel the total pressure inside the system was 228kPa. Accurate measurements of the flowrates were made on the exit side of the gas chromatograph column at atmospheric pressure using a climbing film flowmeter. A four port valve (Whitey) was positioned in the main helium line directly after the rotometer in the main line and after the saturator in the reactant line such that the two flows could be switched allowing the catalyst to experience a continuous flow of reactant.

2.32 n-Hexane Cracking Experiments

High purity helium was used as the purge gas during catalyst activation and the carrier gas in subsequent activity measurements, unless otherwise mentioned. Spectrophotometric grade n-hexane (Aldrich Chemical Company Limited), previously distilled and stored over fresh sodium wire, was used as the reactant during the experiments. The helium flow was saturated with n-hexane which was contained in a bubble-type saturator surrounded by an ice water bath at 273K. This provided a pressure of n-hexane of approximately 6000Pa in the helium carrier gas.

The products were separated at 438K on a glass column (i.d. 3.5mm x 2.1m) packed with Porapak Q (100-200 mesh size) using a helium carrier flow of $0.5cm^3s^{-1}$. These conditions separated the components of different size and isomerisation, but did not resolve similar unsaturated and saturated components in the product stream. The retention times obtained were ethene/ethane 1.8 minutes, propene/propane 2.9 minutes, i-butene/i-butane 4.7 minutes, n-butene/n-butane 5.3 minutes, i-pentene/i-pentane 9.6 minutes, n-pentene/n-pentane 10.6 minutes, and n-hexane 20.5 minutes.

The flame ionisation detector was calibrated for n-hexane by injecting solutions of n-hexane in propanone of known concentration (table 2.3, figure 2.7). Propanone was chosen as the diluent as it had a very short retention time, and thus allowed the n-hexane peak to be well resolved. As the products of n-hexane cracking are gaseous, their relative sensitivities had to be determined by injection of a known commercial gaseous mixture of each

component in nitrogen (Messer Griesheim, 1000ppm of each gas). Once the sensitivities of each component relative to n-hexane were obtained, the absolute sensitivity of each product could be determined by reference to the calibration obtained from the injected solution of n-hexane in propanone.

n-Hexane	
molecules / 10^{18}	Count
0.92	1767829
1.84	3752787
2.76	5515853
3.68	7442964
4.61	9971748
5.53	12245885
6.45	14020517

Table 2.3. n-Hexane calibration.

The calibration constants derived were:

n-hexane	4.53 $x10^{11}$	molecules/count
n-pentane	5.07 $x10^{11}$	molecules/count
n-butane	5.98 $x10^{11}$	molecules/count
propane	8.24 $x10^{11}$	molecules/count
ethane	11.41 $x10^{11}$	molecules/count
methane	23.19 $x10^{11}$	molecules/count

and it therefore follows that the reactant pulse contains 3.98 $x10^{18}$ molecules. The calibration constants for iso-hexane, iso-pentane and iso-butane were assumed to be identical to those for n-hexane, n-pentane and n-butane respectively.

The sample of the hydrated zeolite (*ca.* 20mg) was accurately weighed by difference into the vessel and carefully levelled off before a second plug of silica wool was pushed on top to prevent movement of the sample. The sample was activated by heating in flowing helium ($0.63cm^3s^{-1}$) from room

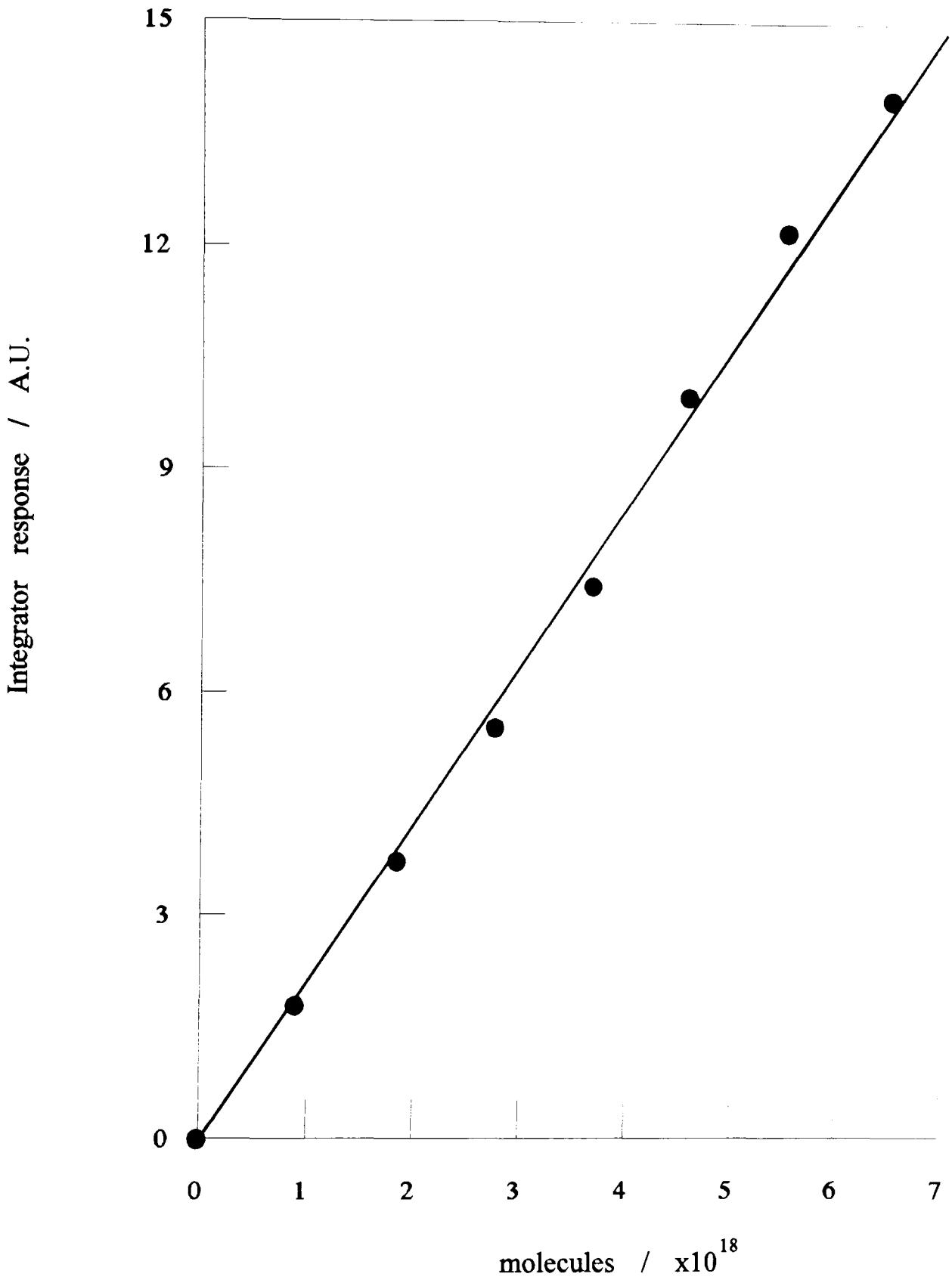

Figure 2.7: n-Hexane calibration

temperature to 673K at 7K min^{-1}; this temperature was then maintained for sixteen hours. To avoid the possibility of treating the sample in steam under pressure at elevated temperatures and to protect the gas chromatograph column from ammonia and water during the initial dehydration, the gas chromatograph was disconnected from the line, allowing the activation to be carried out at atmospheric pressure. The gas chromatograph was reconnected and the flow rate was adjusted to 0.5cm^3s^{-1} after the chromatograph oven had been given sufficient time to warm up. The sample loop was allowed to fill for at least two minutes before the pulse was taken to ensure that equilibrium between the gas phase and adsorption on the walls of the sample loop had been attained. Fifteen pulses of n-hexane were passed over the sample at thirty minute intervals and individually trapped for five minutes in the cold trap by surrounding it with liquid nitrogen before being flash evaporated with near boiling water onto the gas chromatograph column. Initial experiments indicated that five minutes was sufficiently long enough to allow all the reactant and products to desorb from the catalyst. The apparatus was then switched to the continuous mode and n-hexane was passed over the catalyst for sixteen hours after which the sample was degassed for two hours in pure helium before sufficient pulses were passed over, in the same manner as before, to assess the catalyst's activity. The sample was then degassed for 30 minutes at the reaction temperature in pure helium before the furnace was allowed to cool to room temperature. Day-to-day variations in the sensitivity of the flame ionisation detector were followed by injecting a known volume of a standard solution of n-hexane in propanone. The spent catalyst was analysed for coke (Perkin Elmer 240B elemental analyser operated by Mr T.Spencer).

2.33 Cumene Dealkylation Experiments

The cumene dealkylation experiments were carried out in a similar manner to those on n-hexane cracking, Section 2.32, but with the following alterations. The reaction temperature used was 468K and the interval between the pulses was ten minutes. Preliminary experiments confirmed the need to adhere to a strict timing regime as significant differences in activity were noted

when the time interval between the pulses was changed.

The products were separated on a stainless steel column (1.5m x 5mm i.d.) packed with 10% Apiezon L on diatomite C (100-120 mesh) at 413K which gave retention times of: aliphatic peak 1.1 minutes, dimethylbutane 1.54 minutes, benzene 2.2 minutes, toluene 2.9 minutes, ethylbenzene 4.3 minutes and cumene 5.5 minutes. During the degassing period at the end of the experiment the cold trap was used to collect any products which were desorbing slowly from the catalyst.

The flame ionisation detector was calibrated for the aromatic components by injection of a solution of the aromatics in propanone, table 2.4, and figures 2.8 and 2.9. The calibration for the aliphatic components, contained in table 2.4 and shown in figure 2.10, was achieved by injection of a known gas mixture (Speciality Gases Limited).

Benzene		Toluene		Ethylbenzene	
molecules $/10^{16}$	Count	molecules $/10^{16}$	Count	molecules $/10^{16}$	Count
2.16	48693	0.91	22231	0.78	23618
4.32	90459	1.85	44417	1.56	48033
6.48	17707	3.36	87413	3.06	87350
8.64	180690	5.04	122571	4.59	127473
10.80	228770	6.72	162761	6.12	168530
12.95	274645	8.40	194971	7.65	201166
15.11	318602	10.08	248546	9.18	239883
17.27	364221	11.76	281443	10.71	287640
19.43	410566	13.44	325376	12.24	331797
21.59	471066	15.12	363750	13.77	369162

Table 2.4: Calibration for cumene dealkylation experiments.

Aliphatic Carbon		Cumene	
molecules /10^{16}	Count	molecules /10^{16}	Count
9.54	18210	1.39	46132
26.22	42222	2.77	85553
30.99	71068	4.16	126899
42.91	95101	5.55	164884
57.22	131588	6.93	205757
71.52	163996	8.32	242373
90.59	209348	9.71	278048
159.73	325591	11.10	321442
290.85	518855	12.48	352692
419.58	699000	13.87	406737

Table 2.4 (cont.): Calibration for cumene dealkylation experiments.

The calibration constants derived were:

Cumene	3.51 $x10^{11}$	molecules/count
Ethylbenzene	3.76 $x10^{11}$	molecules/count
Toluene	4.16 $x10^{11}$	molecules/count
Benzene	4.67 $x10^{11}$	molecules/count
Aliphatic	4.31 $x10^{12}$	carbon atoms/count

and thus the reactant pulse contained approximately 4.0 $x10^{17}$ molecules.

2.34 Toluene Disproportionation Experiments

The toluene disproportionation experiments were carried out in a similar manner to those on n-hexane cracking, Section 2.32, but with the following modifications. The reaction was studied at 673K, the interval between pulses was 20 minutes and ten pulses were taken. The products were separated on a stainless steel column (1.5m x 5mm i.d.) packed with 10% Apiezon L on diatomite C (100-120 mesh) at 403K which gave retention times as follows: benzene 3.9 minutes, toluene 7.3 minutes, m/p- and

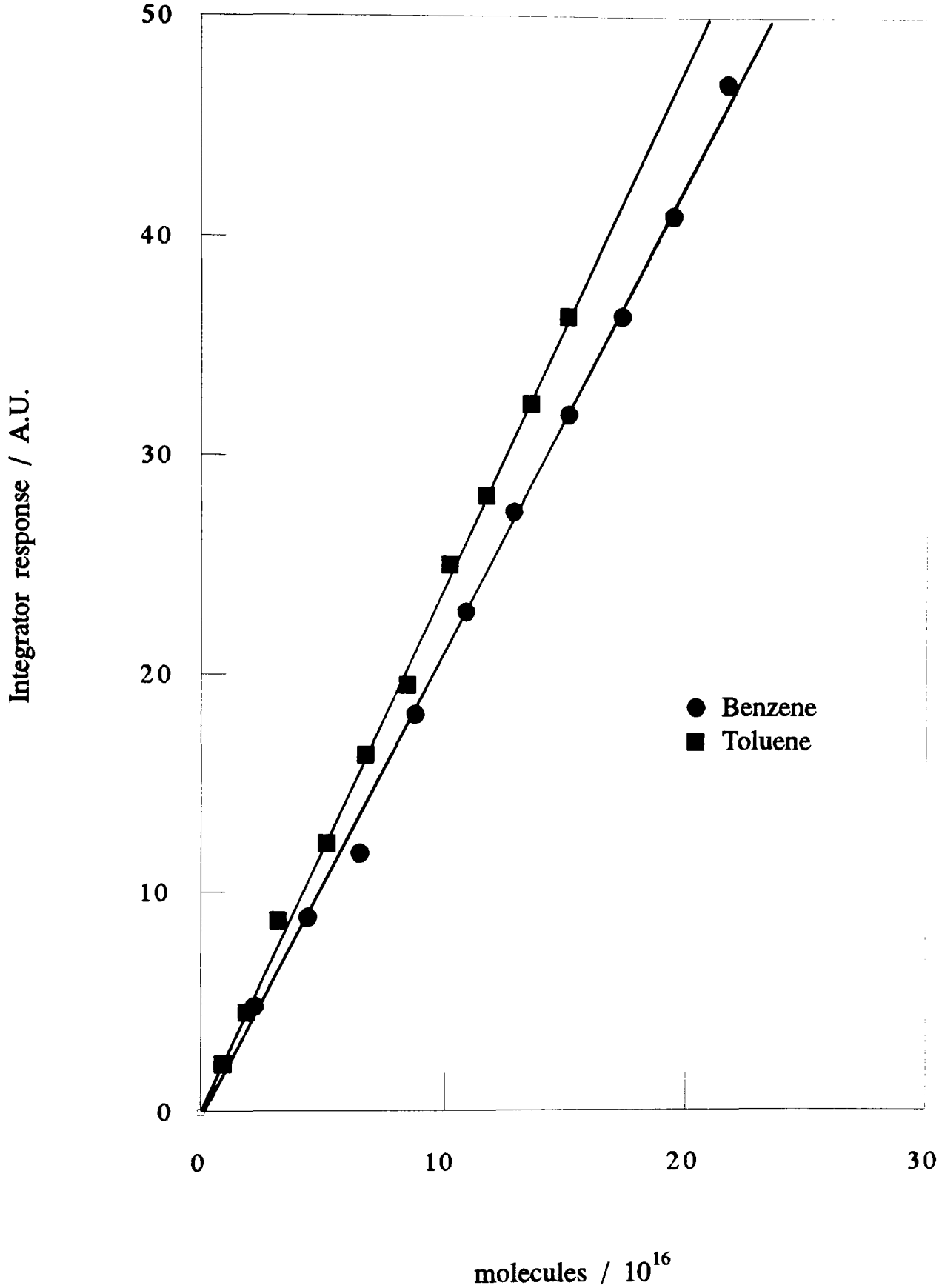

Figure 2.8: Calibration for cumene experiments (I)

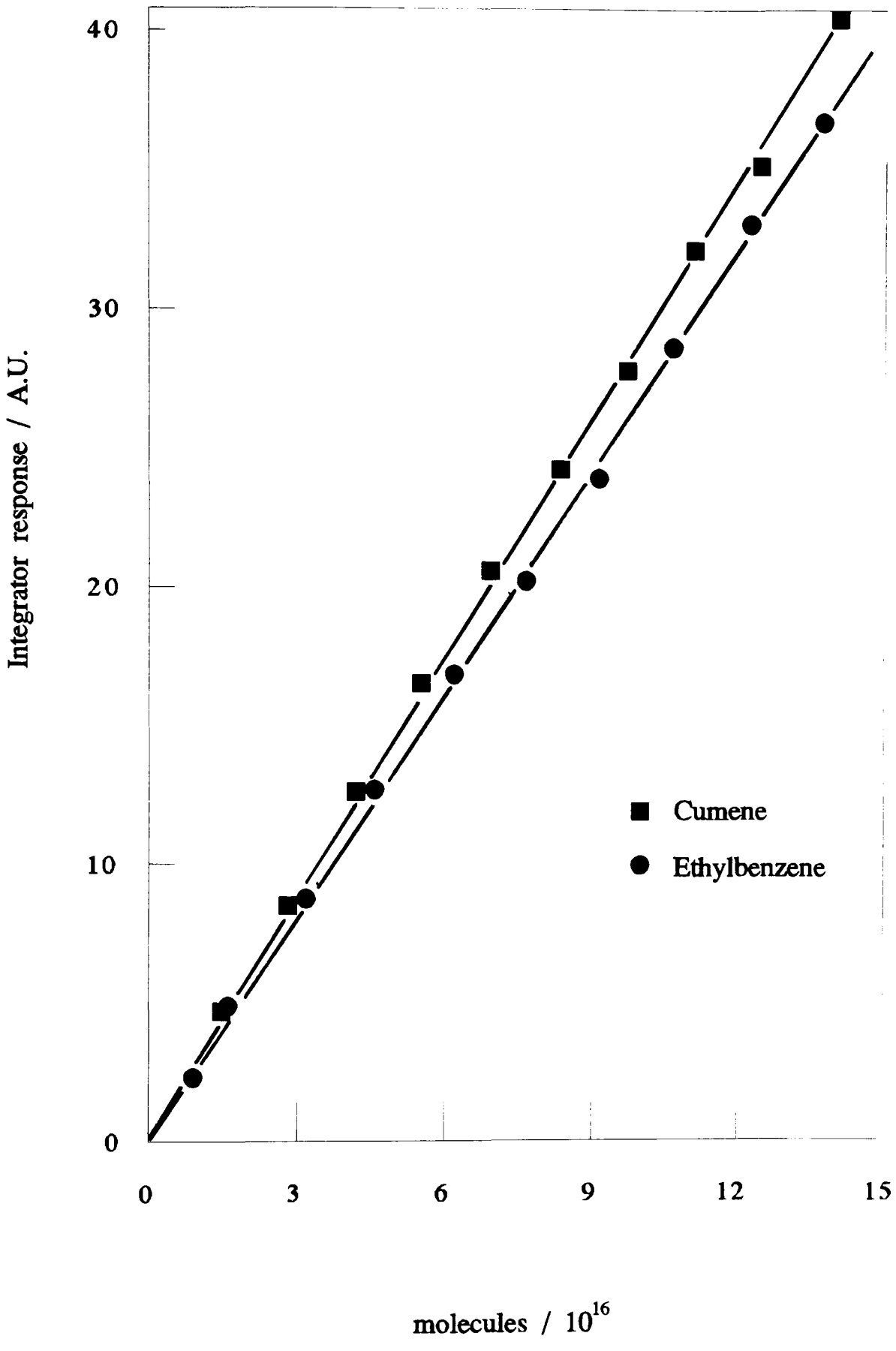

Figure 2.9: Calibration for cumene experiments (II)

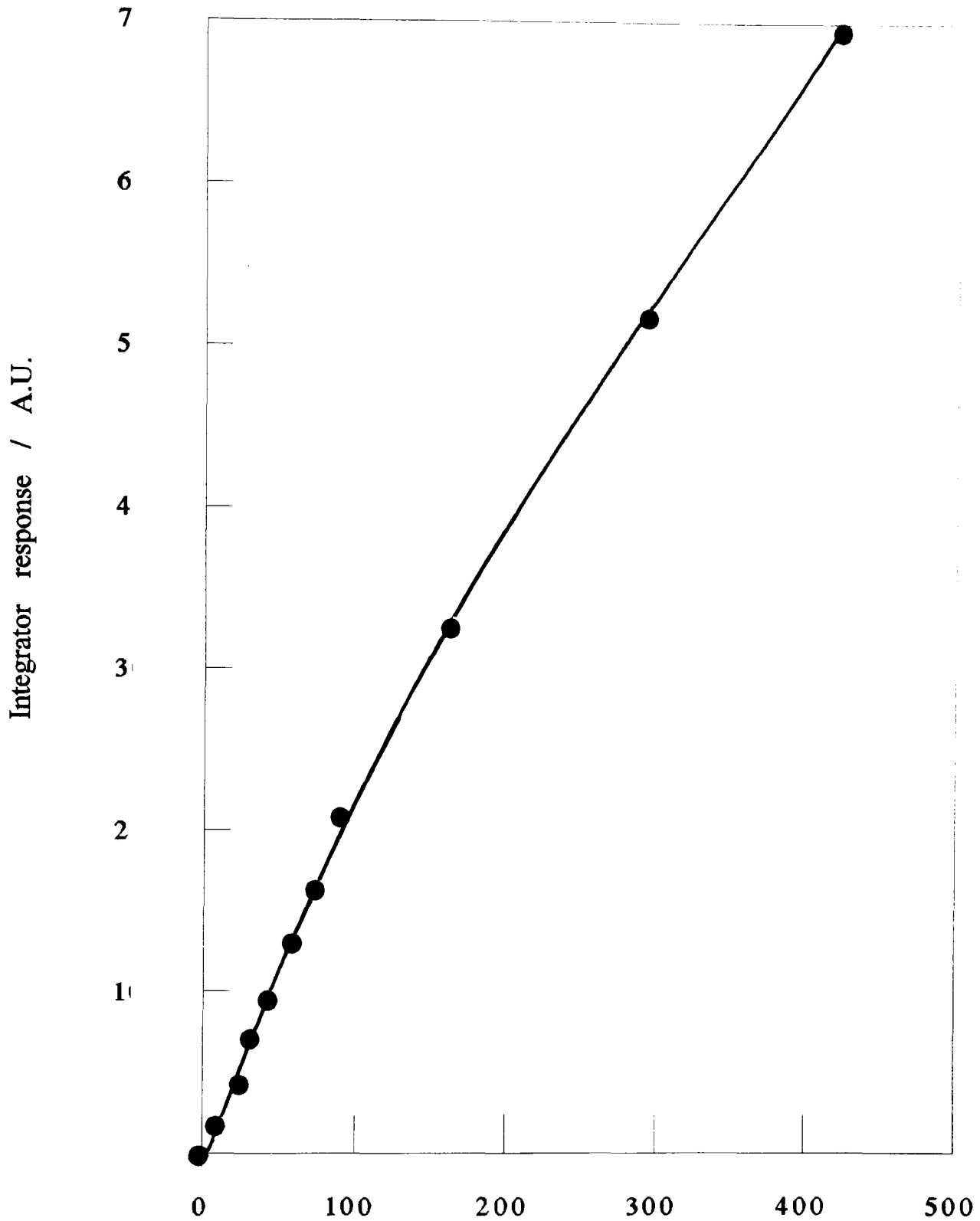

Figure 2.10: Aliphatic carbon calibration.

o-dimethylbenzene 13.8 and 14.2 minutes respectively.

The flame ionisation detector was calibrated for benzene, toluene and 1,2-dimethylbenzene by injection of a known solution of the three components in propanone. The results of this calibration are contained in table 2.5 and shown in figure 2.11.

Benzene		Toluene		1,2-dimethylbenzene	
molecules /10^{16}	Count	molecules /10^{16}	Count	molecules /10^{16}	Count
0.68	11382	0.57	11381	0.49	11440
1.35	24182	1.13	22378	0.99	22459
2.03	37279	1.70	34053	1.48	31724
2.70	46221	2.27	44846	1.98	43968
3.38	57942	2.84	56820	2.47	57344
4.05	68169	3.40	67007	2.96	68128
4.73	80048	3.97	77699	3.46	78888
5.40	92121	4.54	90038	3.95	91538
6.08	103203	5.10	100477	4.45	100685
6.75	115252	5.67	112396	4.94	113226

Table 2.5: Calibration for toluene disproportionation experiments.

The calibration constants obtained from these figures are:

benzene	5.92 x10^{11} molecules/count
toluene	5.07 x10^{11} molecules/count
1,2-dimethylbenzene	4.35 x10^{11} molecules/count

and so the reactant pulse contained 4.3 x10^{18} molecules of toluene.

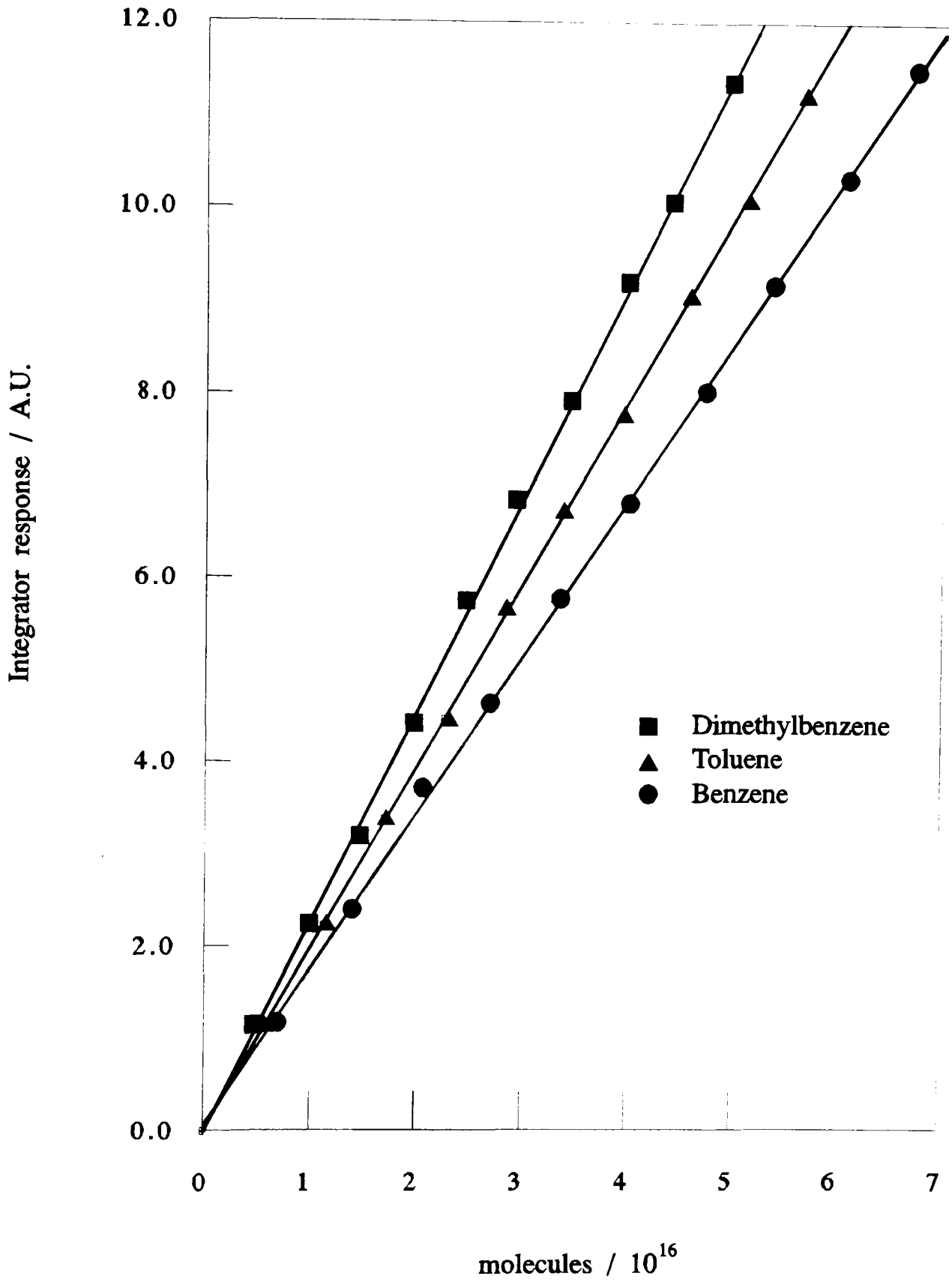

Figure 2.11: Calibration for toluene disproportionation - pulse flow experiments

2.35 Continuous Flow Apparatus

The experiments were carried out on a continuous flow microreactor previously developed,[201,227,228] but modified for the present application (figure 2.12). Two lines serviced the reactor; the pure helium bakeout line and the toluene reactant line. The reactant was contained in a glass saturator approximately half filled with small glass helices. The saturator was connected upstream to a helium cylinder (Air Products industrial grade) and downstream, to ensure that the vapour pressure was that of 273K, the flow was passed through a second empty saturator. The saturators were positioned in separate dewar vessels filled with a water/ice mixture at 273K. The gas flow through each line was controlled by a leak valve (Negretti and Zambra Limited), a flow meter (Gap Instruments Limited) and a stop valve (Whitey) before the two lines joined. The combined line led to the reactor which was held in a high thermal capacity electric furnace (Nottingham University), controlled by a programmable temperature controller (Eurotherm 812). The reaction vessel consisted of a silica glass tube (*ca.*40cm, i.d.7mm) joined to the apparatus at the top by a Swagelok elbow and at the bottom by a Swagelok t-piece. A chromel-alumel thermocouple was inserted through the t-piece and the seal was made gas-tight with rubber 'O' rings. The temperature of the inside of the reaction vessel was monitored using a digital display unit. A bypass facility was incorporated into the apparatus by placing valves (Whitey) before and after the reactor and on the bypass loop, thus allowing the reactor to be isolated. The product stream could be sampled on demand by an automatic valve (Taylor Servomex Type SV220) which was driven by using a high pressure nitrogen controlled by a magnetic valve (Asco). The product stream components were analysed by a gas chromatograph (Pye Unicam model GCD) equipped with a flame ionisation detector. The output from the gas chromatograph was monitored by a computing integrator (Phillips PU 4815) which also controlled the firing of the automatic sampling valve. The integrator was connected to a personal computer (Akhter) to allow easier data storage and manipulation.

A number of modifications were made to the apparatus in the course

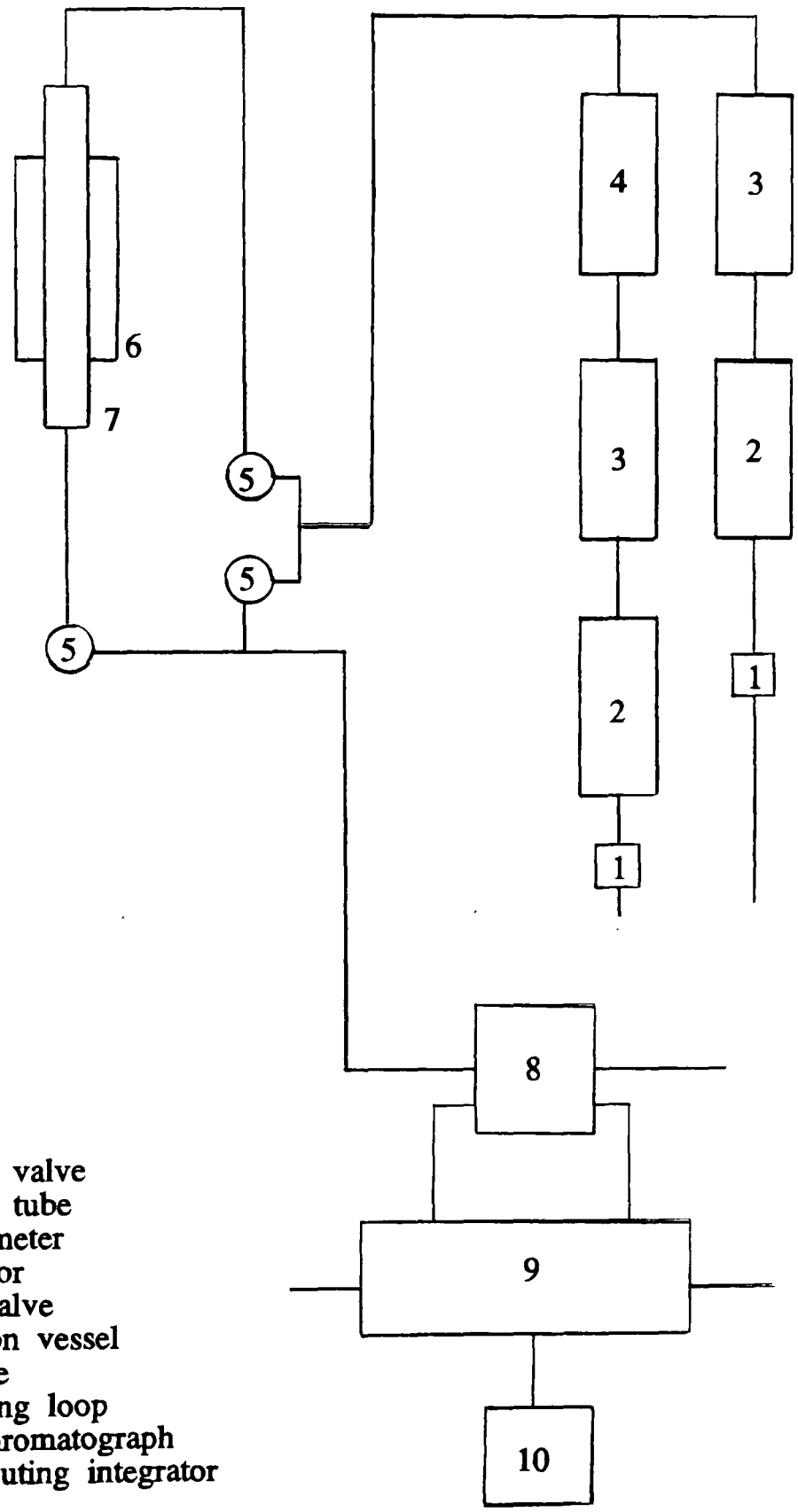

1. Needle valve
2. Drying tube
3. Flow meter
4. Saturator
5. Stop valve
6. Reaction vessel
7. Furnace
8. Sampling loop
9. Gas chromatograph
10. Computing integrator

Figure 2.12: Schematic diagram of the continuous flow apparatus.

of the research. A restricted steel tube (25mm i.d.x 150mm) filled with pelleted 3A zeolite was placed in the reactant line before the saturators and after the needle valve to dry the helium carrier gas. Two valves (Nupro Co.) at either end permitted sealing of the canister. Another steel tube (25mm i.d. x 300mm) filled with pelleted 3A zeolite was placed in the helium line. This canister was permanently fixed in a furnace controlled by a programmable temperature programmer (Pye Ether 'Digi') to allow in situ activation.

2.36 Toluene Disproportionation Experiments

Two reaction vessels were used, referred to as the bulb reactor and the tube reactor. The bulb style reactor, identical to that used in previous work,[201] consisted of a silica tube (7mm i.d.) which widened half way down its length to 10mm with a 10mm sintered glass disc to hold the catalyst sample fused across its bore at the widest point and the tube reactor was as described in Section 2.31. The sample, in either powder or pellet form, was accurately weighed by difference directly into the reactor and activated by heating at a rate of 7K min^{-1} to a final temperature of 673K under a helium flow of $0.66cm^3s^{-1}$; this temperature was then maintained for sixteen hours. A helium flow of $0.5cm^3s^{-1}$, saturated with toluene at 273K (pressure 884Pa) was passed over the sample and the product stream was analysed after five minutes and subsequently every twenty minutes on stream. The reaction products were separated at 403K on a stainless steel column (1.5m x 5mm i.d.) packed with Apiezon L on diatomite C (100-200 mesh) using nitrogen flowing at $0.67cm^3s^{-1}$ as the carrier gas. These conditions gave retention times of 3.1 minutes, 5.7 minutes and 13 minutes for benzene, toluene and 1,2-dimethylbenzene respectively. After the experiment the sample was purged with pure helium at the reaction temperature for half an hour before being allowed to cool under helium. The carbon content of the spent catalyst was determined by elemental analysis.

The response of the flame ionisation detector was determined for benzene, toluene and 1,2-dimethylbenzene by injecting varying amounts of an accurately known weak solution of the three components in propanone onto the

top of the column (table 2.6, figure 2.13). This method was preferred over the dilution of a saturated flow of the component because of uncertainties in the exact vapour pressure and therefore dilution of the components. Conversion to a rate calibration can be obtained using the data in Section 2.37 where the calibration of propan-2-ol was determined using both the injection and diluted flow methods.

The calibration constants obtained were:

benzene	5.34×10^{11} molecules/count
toluene	4.59×10^{11} molecules/count
1,2-dimethylbenzene	4.05×10^{11} molecules/count

The canisters containing 3A molecular sieve were periodically reactivated by being heated to 423K for sixteen hours under a helium flow ($0.67 cm^3 s^{-1}$). The temperature was then raised to 673K and the heating was continued until no sign of water could be found at the exit by condensation onto cold glass. The canister was then allowed to cool in the furnace under the flow of helium to room temperature, before being sealed or rejoined to the apparatus.

Benzene		Toluene		1,2-dimethylbenzene	
molecules $/10^{16}$	Count	molecules $/10^{16}$	Count	molecules $/10^{16}$	Count
0.81	14146	0.68	13887	0.59	14015
1.22	21800	1.02	21333	0.89	21133
1.62	29590	1.36	28449	1.19	29021
2.03	36418	1.70	35266	1.49	35625
2.43	44674	2.04	43921	1.78	43804
2.84	50255	2.38	49544	2.08	49210
3.24	58650	2.72	57318	2.38	57457
3.65	67673	3.06	66771	2.67	66259

Table 2.6: Calibration for toluene disproportionation.

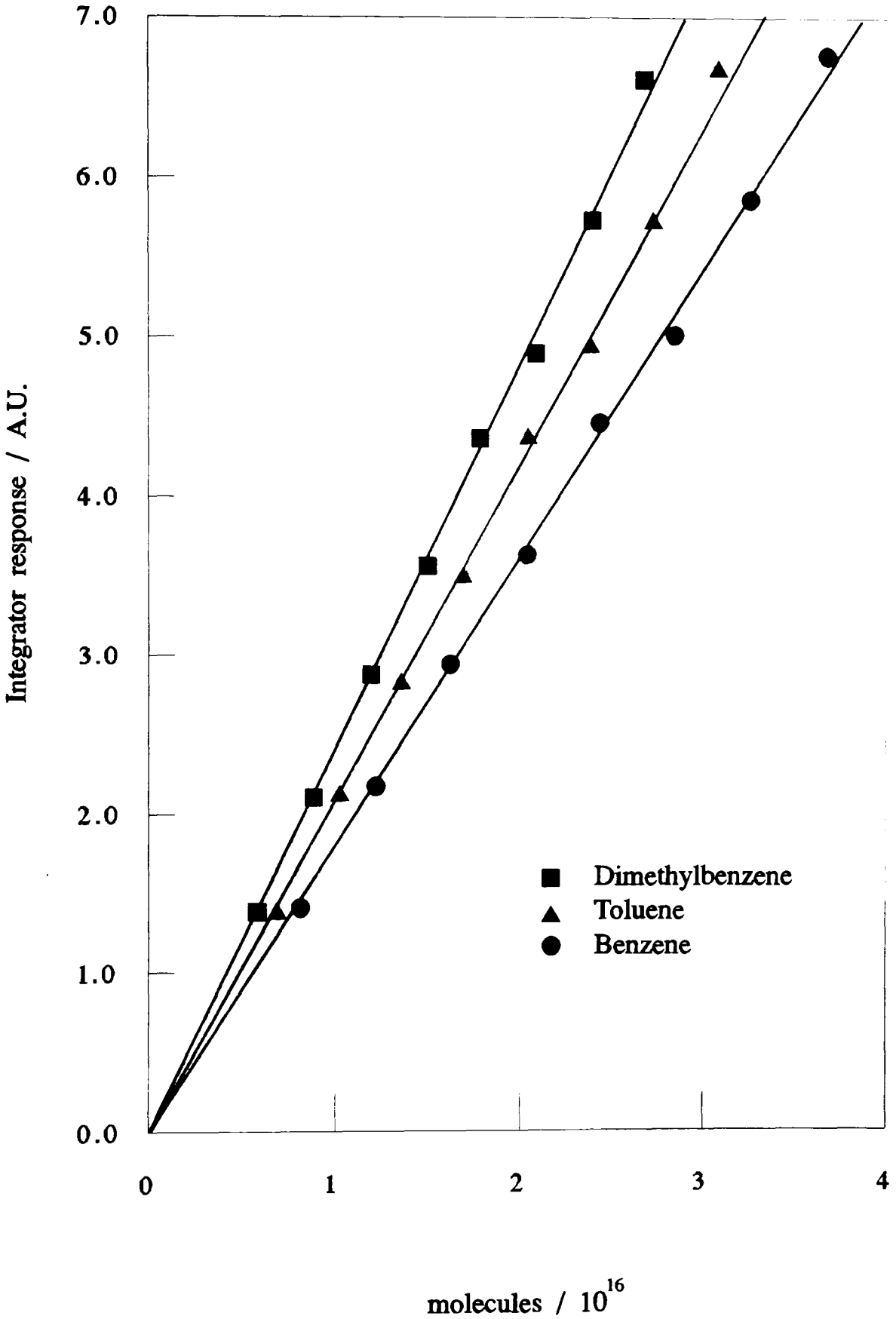

Figure 2.13: Calibration for toluene disproportionation - continuous flow experiments.

Coking Experiments

Catalyst samples were deliberately pre-coked in a variety of ways:

i) The sample was allowed to reach 673K and then exposed to the toluene for three minutes ($0.5cm^3s^{-1}$). The pure helium flow was then restored and the bakeout and the subsequent experiment conducted as usual.

ii) The sample was baked out using helium which had been passed through the toluene saturator whilst it had been held at 195K for sixteen hours and then the experiment conducted as usual.

iii) The sample was baked out as usual, except that for the first hour the helium was passed through the saturator held at 195K, and then after sixteen hours the sample was further treated with the cold toluene flow for four and a half hours before the experiment was commenced.

iv) The sample was baked out in the pulsed flow apparatus and exposed to eleven pulses of toluene before being transferred to the continuous flow apparatus with the furnace having already attained a temperature of 673K.

2.37 Propan-2-ol Dehydration

Temperature Dependence Experiments

The unextracted samples (*ca.* 10mg) were weighed directly into the tubular reactor. Activation was achieved by heating the sample to 375K for thirty minutes at 7K min^{-1}. The extracted samples were heated at the same rate to 673K and held for sixteen hours to fully desorb the ammonia present. After the samples had cooled to room temperature they were hydrated by passing helium ($0.67cm^3s^{-1}$) through a saturator containing water at 291K for thirty minutes, before being treated in a similar manner to the unextracted samples. A helium stream, ($0.5cm^3s^{-1}$), saturated with propan-2-ol was passed over the sample for two hours to achieve a steady activity, before activities in the temperature range 369-383K were measured. The products were separated at 378K on a glass column (5mm x 2.1m) packed with 12.5% Carbowax 20M on

Chromosorb using nitrogen as the carrier gas ($0.67cm^3s^{-1}$). The retention times for the products were propene 1.5 minutes, propan-2-ol 4.1 minutes and di-isopropylether 2.1 minutes. The flame ionisation detector was calibrated for propan-2-ol and di-isopropylether by injection of an accurately known solution of each in water and propan-2-ol respectively; the results can be found in table 2.7 and figure 2.14.

Calibration for propene, presented in table 2.8 and figure 2.15, was achieved by 100% conversion of propan-2-ol to propene over NH_4YAS (50mg) at 324K. No discolouration of the catalyst was noted, and so it can be assumed that the conversion was 100% efficient. The detector was found to be 89% as sensitive to propene as to propan-2-ol. Conversion between molecules injected and molecules s^{-1} can be achieved by combining the propan-2-ol calibrations.

Propan-2-ol		Di-isopropylether	
molecules /10^{17}	Count	molecules /10^{15}	Count
1.89	163288	1.71	7738
3.15	254475	3.42	15848
6.30	423276	5.13	23177
9.45	558733	6.85	29756
12.60	656399	8.56	36641
15.75	790271	10.27	43184
18.90	842663	11.98	51065
-	-	13.70	54620

Table 2.7: Calibration by injection for propan-2-ol dehydration experiments.

Pressure Dependence Experiments

The samples were prepared and activated in exactly the same manner as for the temperature dependence experiments. The partial pressure of propan-2-ol in the reactant stream was controlled by varying the temperature of the

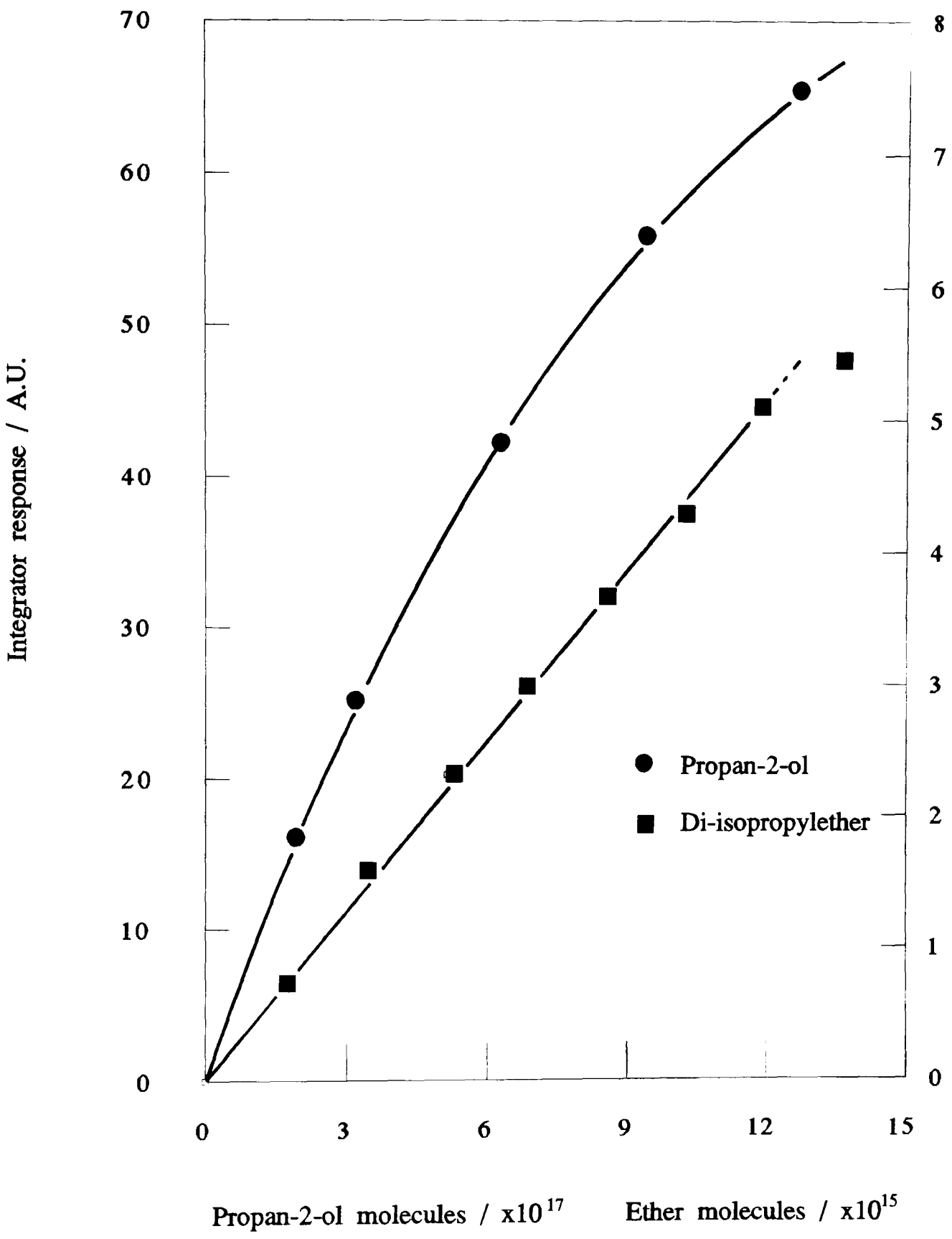

Figure 2.14: Calibration by injection for propan-2-ol experiments.

saturator bath. Ethanol was cooled by a compressor cooler (Cryocool CC-80II) allowing propan-2-ol vapour pressures of between 1.7kPa and 0.8kPa to be obtained. Preliminary experiments indicated that more reliable results could be obtained by starting from a high vapour pressure and cooling, rather than the reverse process.

A stabilisation period of half an hour was allowed at the desired temperature and vapour pressure of 1.3-1.7kPa before the reactant pressure was decreased at the approximate rate of 0.2kPa hr^{-1}; the product stream was monitored at regular intervals in the same manner as before. In this way the pressure dependence of the dehydration reaction was measured for selected catalysts for at least four temperatures in the range 369K to 381K.

molecules / 10^{17} s^{-1}	Count	
	Propan-2-ol	Propene
0.32	32783	27777
0.41	44768	39372
0.66	67755	60242
0.88	88148	79060
1.20	112743	101548
1.55	142884	124775
2.24	-	163784
3.16	268069	219417

Table 2.8: Calibration by flow dilution for propan-2-ol dehydration experiments.

Coking Experiments

The change in activity due to coke on the surface was investigated by deliberate precoking of the sample in situ. Catalyst HYST 1073Ex was used in all the precoking experiments.

The sample was deammoniated by being heated to 673K for half an

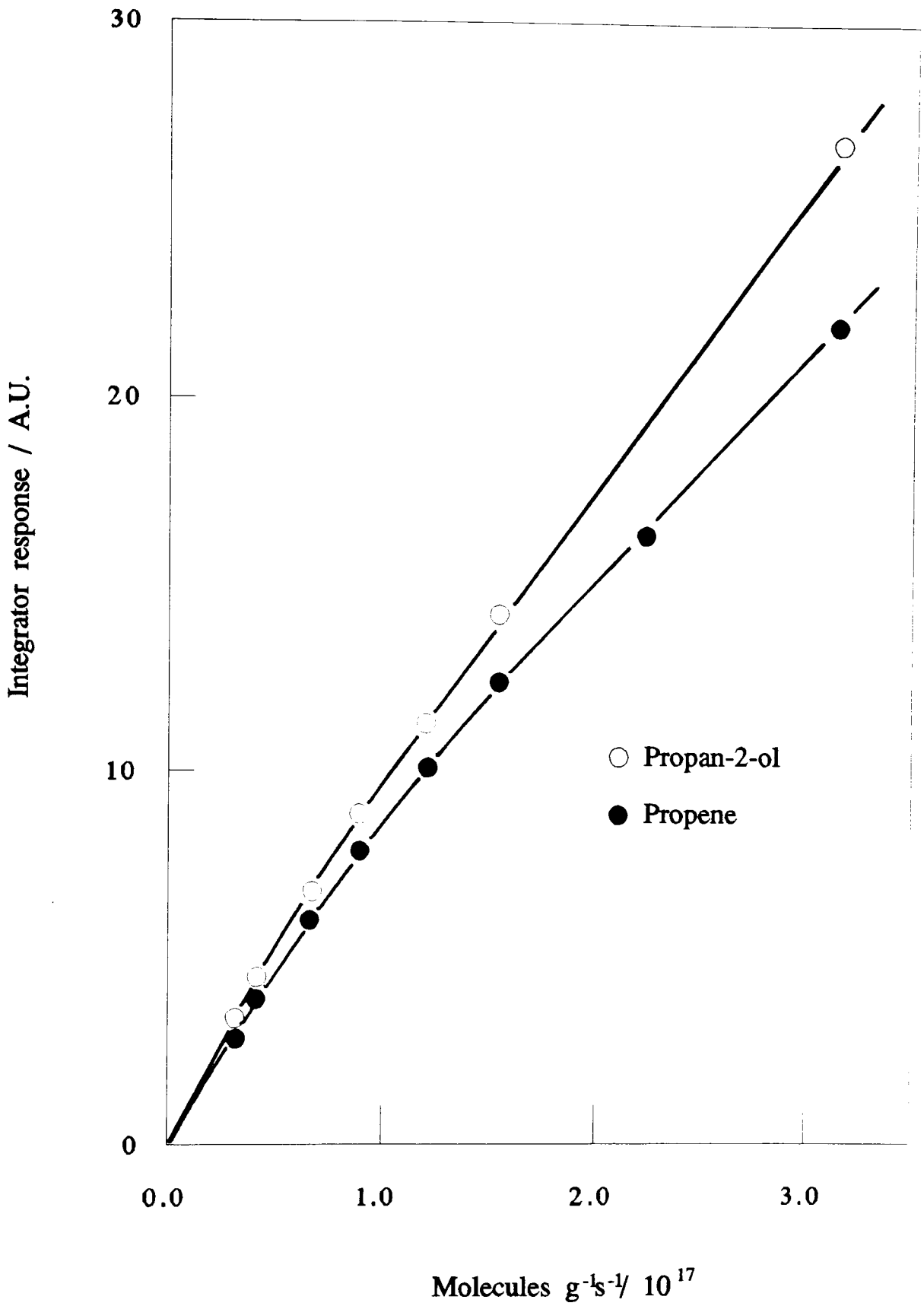

Figure 2.15: Calibration by flow dilution for propan-2-ol continuous flow experiments.

hour in flowing helium ($0.66cm^3s^{-1}$, $7K\ min^{-1}$). The reactant stream was then passed over the sample at a temperature between 673K and 376K for half an hour before the sample was allowed to cool to 376K without interruption to the reactant stream flow. The flowrate was checked at the reaction temperature, and the products were analysed at regular intervals over nineteen hours in the same manner as before. In addition, one experiment was carried out in as above, with the initial coking at 673K, but flushed at 673K for half an hour and cooled to 376K in flowing helium before the start of the experiment.

3 Results

3.1 Characterisation

The extent of structural dealumination can be determined by a variety of methods, as discussed in the introduction. Of the three methods used in the present study the temperature programmed desorption of ammonia is preferred over the framework aluminium content derived from either x-ray crystallography or infrared spectroscopy.

The reasons for this decision are twofold, one physical and one chemical in nature. Firstly, the temperature programmed desorption measurements are taken after the sample has undergone an activation program similar to that used in the catalytic experiments. Among other factors, this ensures that the water content of the samples is comparable to that of the catalytic experiments, rather than measurements made with the sample as fully saturated as possible as is the case with crystallography. The x-ray measurements are by necessity made on a finely powdered sample whereas the temperature programmed desorption measurements are conducted on broken pressed pellets, the same format as in the catalytic experiments.

The second reason concerns the properties that the two methods measure. By determining the unit cell, x-ray crystallography essentially counts the number of aluminium atoms resident in the framework of the catalysts; it makes no statement as to whether these aluminium atoms are associated with protons, and whether these protons are accessible to adsorbed molecules. In contrast, temperature programmed desorption assesses the interaction between base molecules and the catalytic sample, and hence the number of available acid sites. Therefore, if a framework aluminium is unable to interact with the base molecule for steric or electrostatic reasons, then it is disregarded by temperature programmed desorption.

If the assumption that the catalytic activity of the zeolites in their various forms is associated primarily with their acid content is valid, it is prudent to choose a method to distinguish between samples which relies directly on the acid content, and not one which in effect measures the theoretical total acid content.

3.11 Infrared Spectroscopy and X-ray Crystallography

Mid infrared spectroscopy is known to be sensitive to changes in the structural composition of zeolites, a subject which has been discussed in Section 1.21. The wavenumbers of selected vibrations are presented in table 3.1, together with a typical infrared spectrum in figure 3.1. Various groups have attempted to relate the wavenumber of certain vibrations to the aluminium content of the zeolite framework, perhaps the most widely used are those of Sohn *et al*[24], equation 3.1 and 3.2, and those of Kubelková *et al*[31], equation 3.3 and 3.4.

$$Al_F = 0.776(1086.7 - \upsilon_1) \qquad 3.1$$

$$Al_F = 1.007(838.8 - \upsilon_2) \qquad 3.2$$

$$Al_F = 0.778(1092.0 - \upsilon_1) \qquad 3.3$$

$$Al_F = 1.017(843.2 - \upsilon_2) \qquad 3.4$$

Similarly, the unit cell constant of the zeolite framework is known to decrease with increasing dealumination. A typical x-ray diffractogram is reproduced in figure 3.2. Sohn *et al*[24] and Kubelková *et al*[31] have also presented equations, 3.5 and 3.6 respectively, relating the unit cell constant, a_o, to the framework composition.

$$Al_F = 107.1(a_o - 24.238) \qquad 3.5$$

$$Al_F = 113.5(a_o - 24.205) \qquad 3.6$$

For reasons outlined in the Section 4.1, the equations derived by Sohn *et al*[24] are preferred. The unit cell constants of all the zeolites, together with the derived framework compositions using equation 3.5 are presented in table 3.2.

In addition to composition data, x-ray crystallography can also yield information on the degree of crystallinity of the catalysts. This is particularly useful in assessing the damage done to the framework by various procedures. Figure 3.3 shows the x-ray diffractograms of HYST 823 before and after an extraction performed with H_4EDTA in a solution of pH 2.8. The complete

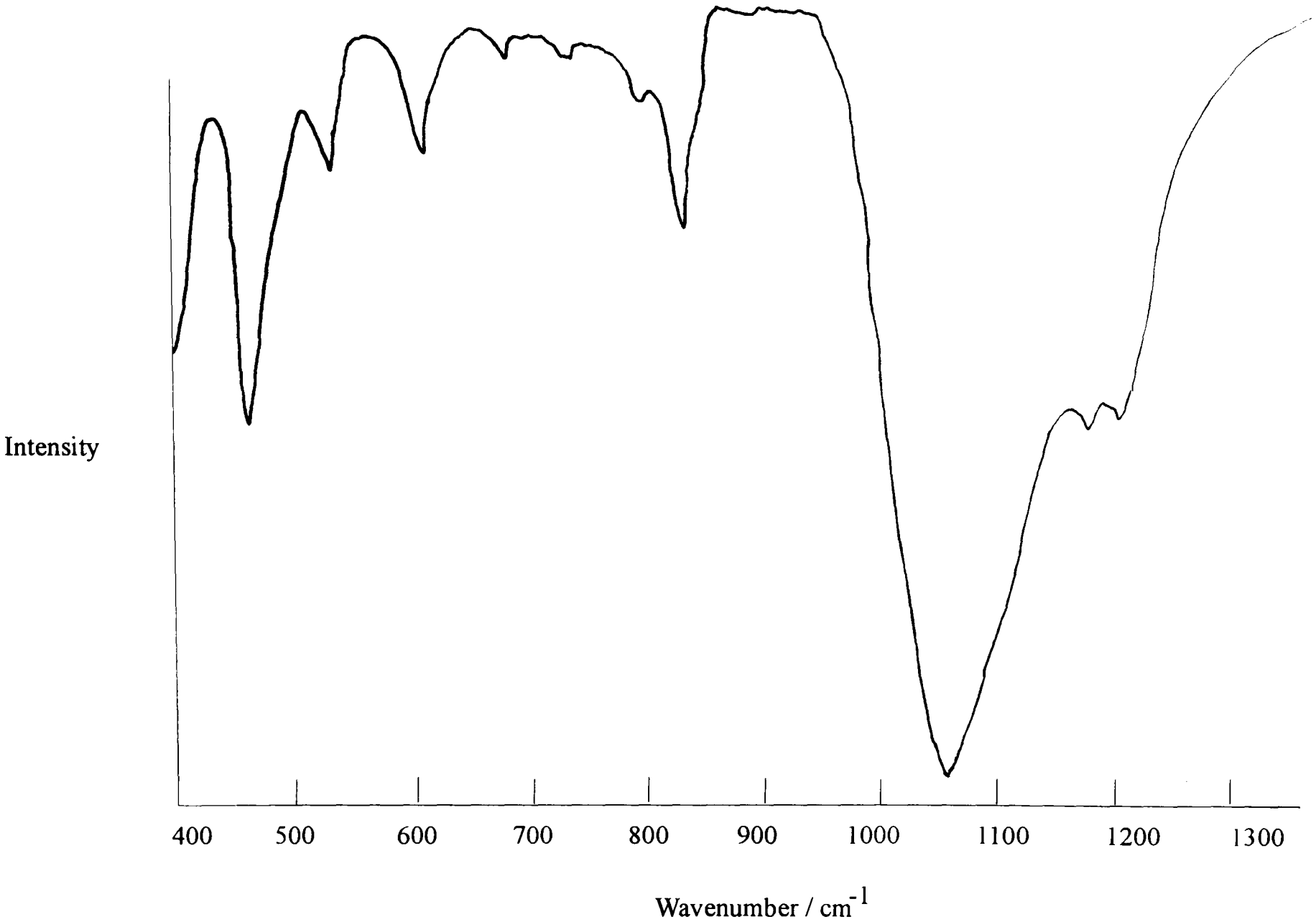

Figure 3.1: Infrared spectrum of HYST 923.

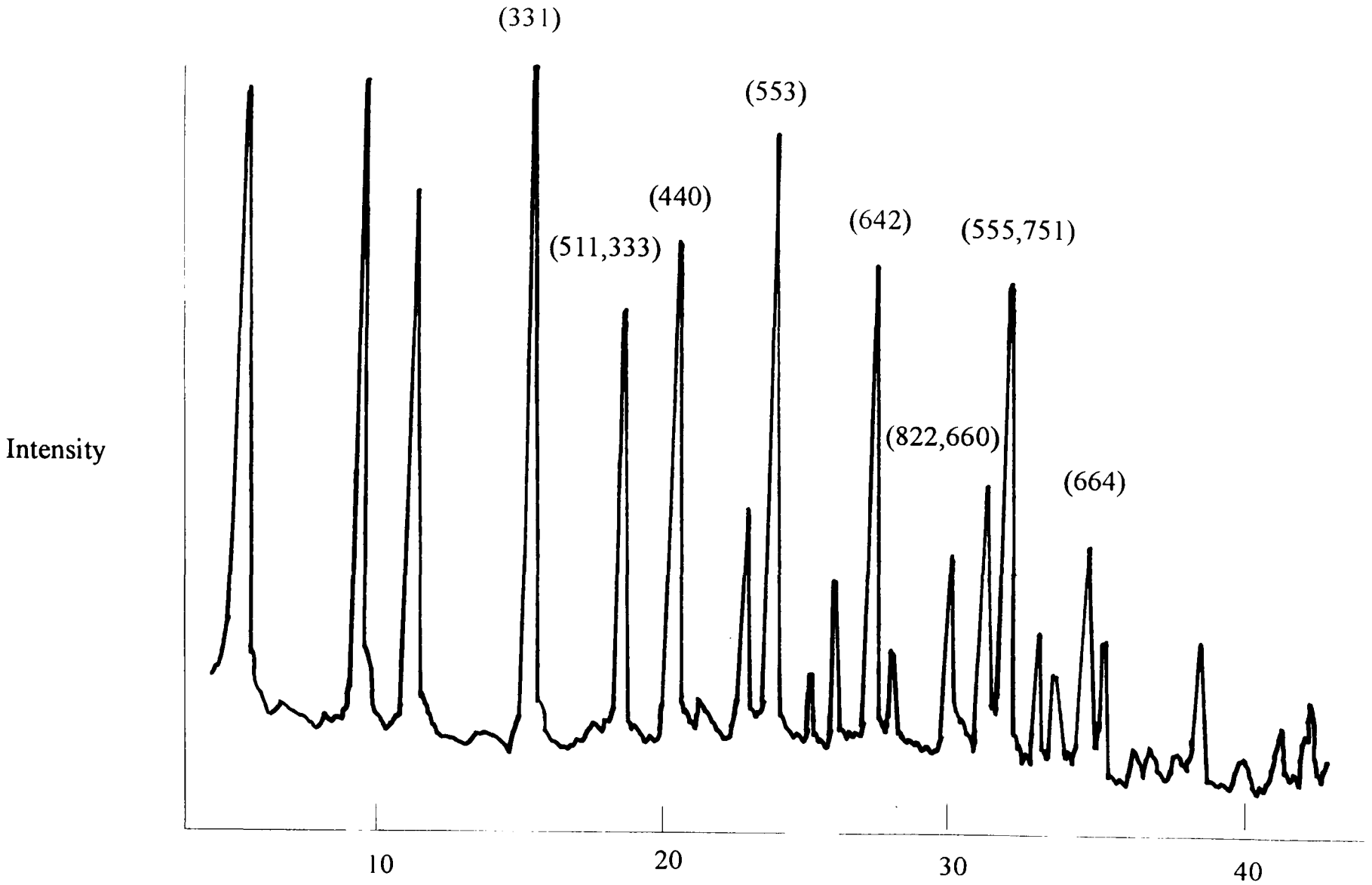

Figure 3.2: X-ray diffractogram of NH_4YAS

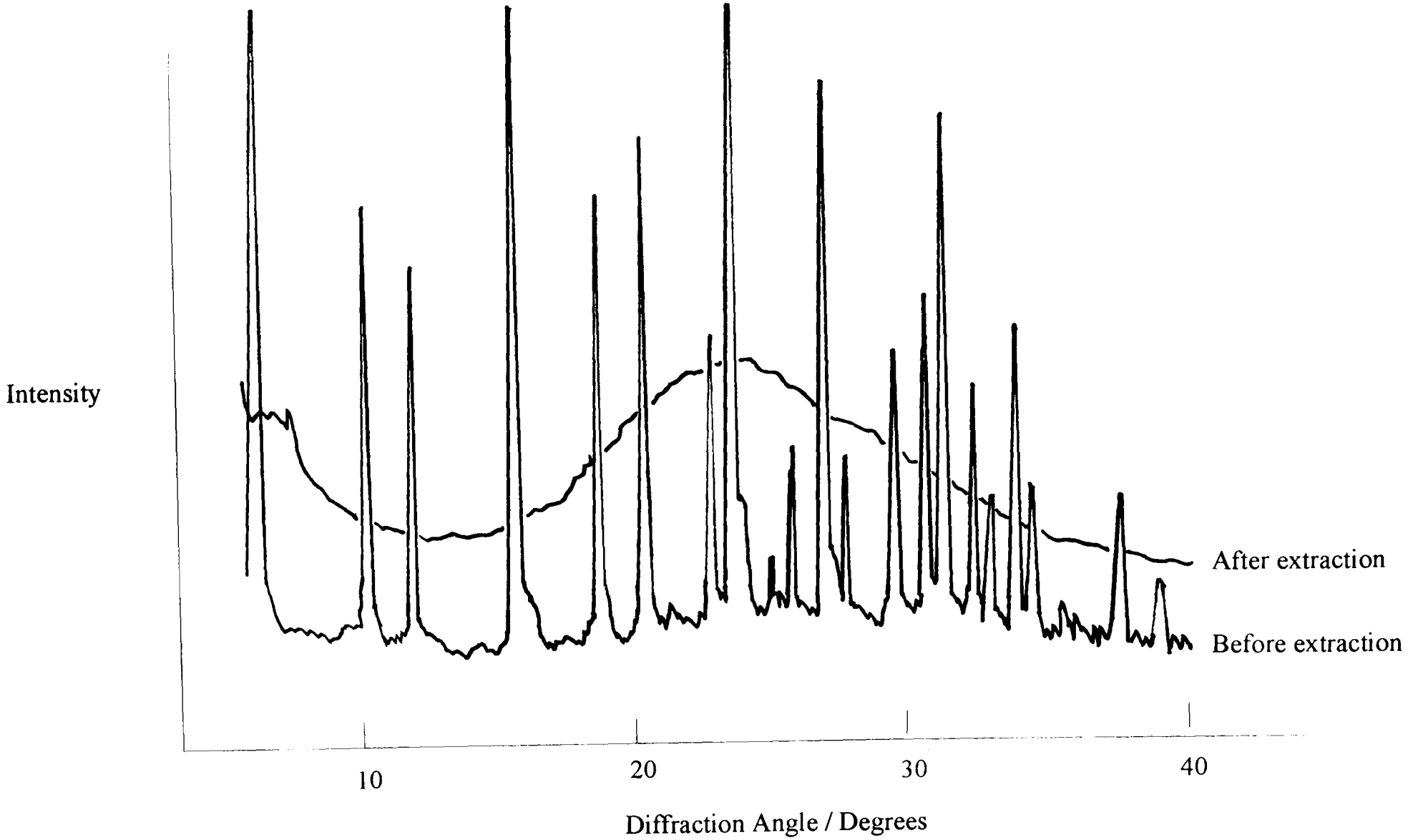

Figure 3.3: X-ray diffractogram of HYST 823 before and after EDTA extraction at pH 2.8.

breakdown of the structure is clearly evident from the formless ridge, attributable to amorphous material. The crystallinities of all the samples are shown in table 3.2, indicating that the revised extraction process, carried out in a solution of pH 4.3 does not dramatically harm the structure.

The crystallinity values obtained are somewhat disappointing. The intensities, when compared to the starting material, are generally lower. However, examination of the individual traces did not suggest that structural breakdown had occurred, which would undoubtedly lead to a loss in crystallinity. It must be emphasised that the drop in intensity does not effect the peak positions. Therefore, any unit cell size calculations based on this data are valid. Previous work,[201] has shown that the crystallinity of the strongly steamed unextracted samples to be ≈80% and the extracted samples ≈ 90%. It is worth noting that with only two exceptions, the crystallinity of all the samples increased on extraction, in accordance with previous work.[201] This is probably a physical manifestation of the technique. Measurements were made on a constant volume, and extraction might increase the density of unit cells, permitting more to be packed into the sample holder.

The water contents of the catalysts are reported in table 3.3. These allow the actual weight of the sample used in the catalytic experiments to be calculated, thus taking into account differences in water capacity.

The total amount of aluminium present in the catalysts can be calculated using

$$Al_T = \frac{192 - Al_F}{Si/Al} \qquad 3.7$$

and therefore the extraframework aluminium from the simple relationship

$$Al_{NF} = Al_T - Al_F. \qquad 3.8$$

The derived values for the aluminium distribution are presented in table 3.4, along with the nonframework values derived from the atomic adsorption spectroscopy measurements of the extraction washings. The values of Al_T

increase with dealumination, suggesting that aluminium is deposited within the catalysts during the dealumination procedure. This obvious fallacy can be traced to the decrease in the number of unit cells on hydrothermal treatment. The value of Al_T for the unextracted catalysts cannot change from that of the starting material, and when this is taken into account, the agreement between the calculated and measured Al_{NF} values is acceptable.

Sample	Pore Opening	T-O bend	D6R	ν_2	ν_1
NH_4YAS	456	502	573	786	1014
NH_4YLS	456	504	575	797	1035
HYMST 748	458	512	592	802	1050
HYMST 768	458	513	593	810	1050
HYMST 783	458	508	594	806	1049
HYMST 798	458	512	593	810	1051
HYST 823	458	517	596	820	1057
HYMST 848	458	512	593	816	1053
HYST 873	456	520	601	826	1060
HYST 923	455	520	603	829	1061
HYST 973	455	521	605	830	1060
HYST 1023	458	527	606	831	1068
HYST 1073	458	527	608	832	1072
HYMST 748Ex	458	514	592	816	1055
HYMST 768Ex	455	517	593	815	1055
HYMST 783Ex	458	515	590	812	1054
HYMST 798Ex	458	514	592	816	1055
HYST 823Ex	458	518	593	820	1056
HYMST 848Ex	458	518	593	818	1055
HYST 873Ex	455	518	600	825	1059
HYST 923Ex	458	518	601	827	1061
HYST 973Ex	458	520	601	828	1065
HYST 1023Ex	458	518	602	829	1067
HYST 1073Ex	458	518	605	829	1069

ν_1 Asymmetric stretch
ν_2 Symmetric stretch

Table 3.1: Infrared spectroscopy data.

Sample	a_0 / Å	nAl_F	% crystallinity
NH_4YAS	24.73	52.9	100
NH_4YLS	24.62	40.9	99
HYMST 748	24.58	36.2	71
HYMST 768	24.56	34.4	73
HYMST 783	24.54	32.3	44
HYMST 798	24.52	30.0	86
HYST 823	24.49	26.7	38
HYMST 848	24.47	25.1	44
HYST 873	24.44	21.3	46
HYST 923	24.41	18.6	37
HYST 973	24.40	17.6	50
HYST 1023	24.40	17.0	74
HYST 1073	24.39	15.9	74
HYMST 748Ex	24.57	35.7	94
HYMST 768Ex	24.51	28.8	73
HYMST 783Ex	24.53	30.9	80
HYMST 798Ex	24.51	29.3	74
HYST 823Ex	24.48	26.4	64
HYMST 848Ex	24.50	27.9	73
HYST 873Ex	24.46	24.2	53
HYST 923Ex	24.46	23.6	45
HYST 973Ex	24.44	21.4	66
HYST 1023Ex	24.43	20.9	61
HYST 1073Ex	24.40	16.9	81

Table 3.2: X-ray crystallography data.

Sample	%age Water
NH_4YAS	29.4
NH_4YLS	25.2
HYMST 748	25.7
HYMST 768	24.9
HYMST 783	26.6
HYMST 798	24.8
HYST 823	23.8
HYMST 848	23.2
HYST 873	24.5
HYST 923	22.7
HYST 973	22.4
HYST 1023	20.8
HYST 1073	20.1
HYMST 748Ex	24.8
HYMST 768Ex	24.1
HYMST 783Ex	25.4
HYMST 798Ex	24.7
HYST 823Ex	23.8
HYMST 848Ex	23.8
HYST 873Ex	23.8
HYST 923Ex	22.2
HYST 973Ex	22.4
HYST 1023Ex	23.0
HYST 1073Ex	25.5

Table 3.3: Water content of hydrated unextracted and extracted catalysts.

Sample	Al_F from unit cell, Sohn *et al*[24]			Al_{NF} removed
	Al_T	Al_F	Al_{NF}	
NH_4YAS	53.9	53	0.9	n/a
NH_4YLS	58.6	40.9	17.7	n/a
HYMST 748	60.4	36.2	24.2	24.4
HYMST 768	61.1	34.4	26.7	27.8
HYMST 783	61.9	32.3	29.6	23.6
HYMST 798	62.8	30.0	32.8	29.5
HYST 823	64.1	26.7	37.4	-
HYMST 848	64.7	25.1	39.6	29.3
HYST 873	66.2	21.3	44.9	-
HYST 923	67.2	18.6	48.6	-
HYST 973	67.6	17.6	50.0	-
HYST 1023	67.8	17.0	50.8	-
HYST 1073	68.2	15.9	52.3	-
HYMST 748Ex	/	35.7	/	n/a
HYMST 768Ex	/	28.8	/	n/a
HYMST 783Ex	/	30.9	/	n/a
HYMST 798Ex	/	29.3	/	n/a
HYST 823Ex	29.7	26.4	3.3	n/a
HYMST 848Ex	/	27.9	/	n/a
HYST 873Ex	27.5	24.2	3.3	n/a
HYST 923Ex	23.6	23.6	0	n/a
HYST 973Ex	22.1	21.4	0.7	n/a
HYST 1023Ex	20.2	20.9	-0.7	n/a
HYST 1073Ex	16.2	16.9	-0.7	n/a

Table 3.4: Aluminium distribution within catalysts.

n/a not applicable / Si/Al not available

3.12 Temperature Programmed Desorption

A substantial part of the work carried out in this project has involved the partial automation of the temperature programmed desorption experiments, and the development of methods of analysing the data produced. An example of the raw data is presented in figure 3.4, showing the deammoniation and dehydroxylation peaks. Figure 3.5 shows the differential trace of the same experiment which allows accurate assessment of the position of the peak maximum. It is also possible to subtract one peak from another, permitting the effect of changing the experimental conditions to be easily appreciated. Figure 3.6 clearly shows the position of the excess ammonia which is removed by extending the desorption time.

As seen in table 3.5, changing the bakeout procedure affects capacity of the catalysts to adsorb ammonia. The complete sets of deammoniation and dehydroxylation traces are shown in figures 3.7 to 3.10 for the HYMST 783 series and the HYST 1073 series of catalysts. The deammoniation and dehydroxylation traces generated in the partially dehydrated experiments (flowing helium) for all the catalysts are presented in figures 3.11 to 3.18. Other desorption experiments, conducted to investigate the deammoniation and dehydroxylation processes, are reported in tables 3.6 to 3.14.

The activation energy for the desorption of gas adsorbed on a solid surface can be obtained from desorption traces in which the change in the position of the maximum in the rate of desorption of the gas is monitored as a function of the rate of temperature increase. For simplicity it is assumed that all molecules are bonded to the surface with the same energy and that desorption occurs, without readsorption, by a first order process.

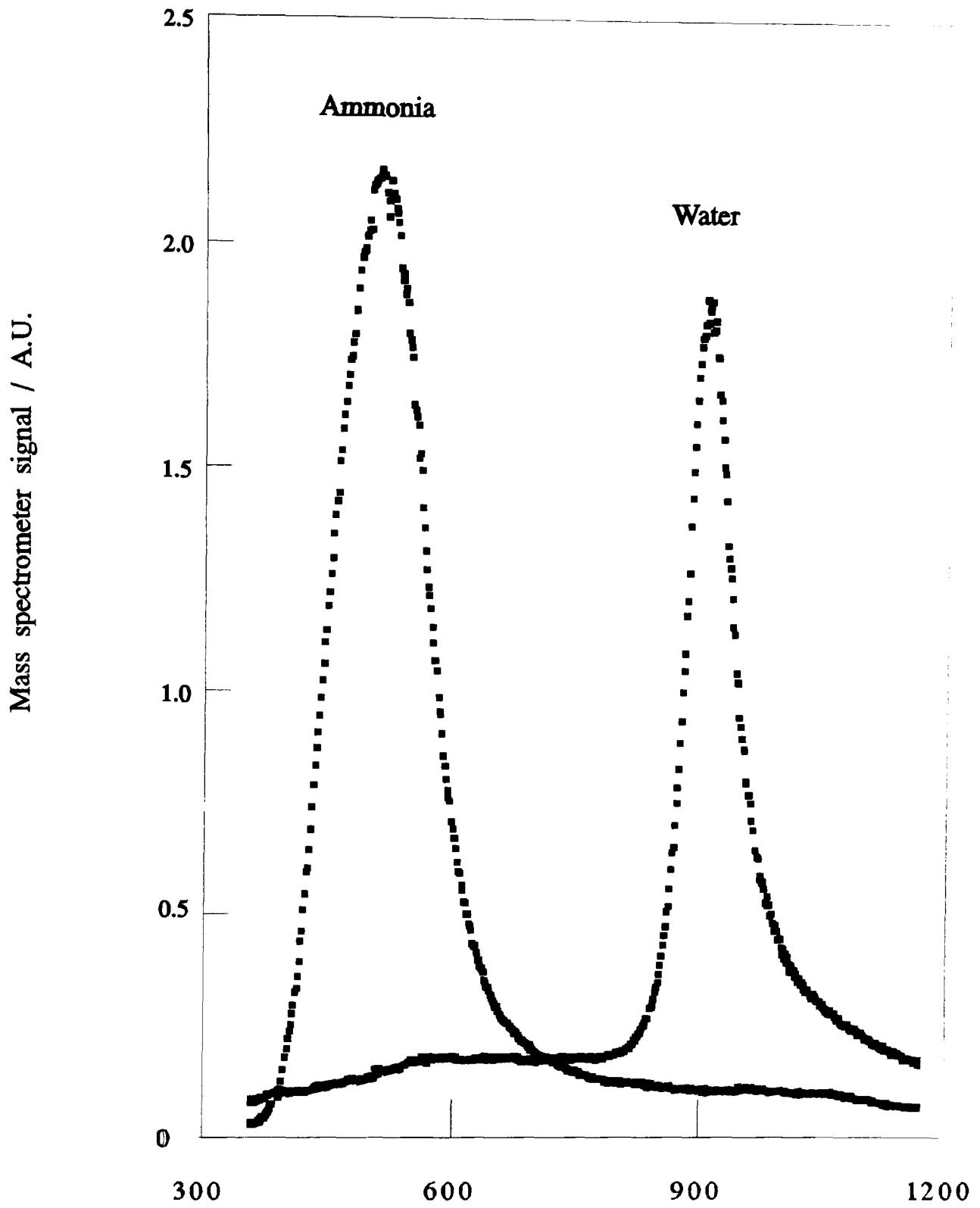

Figure 3.4: TPD traces of ammonia and water from NH_4YAS - generated using SCAN program.

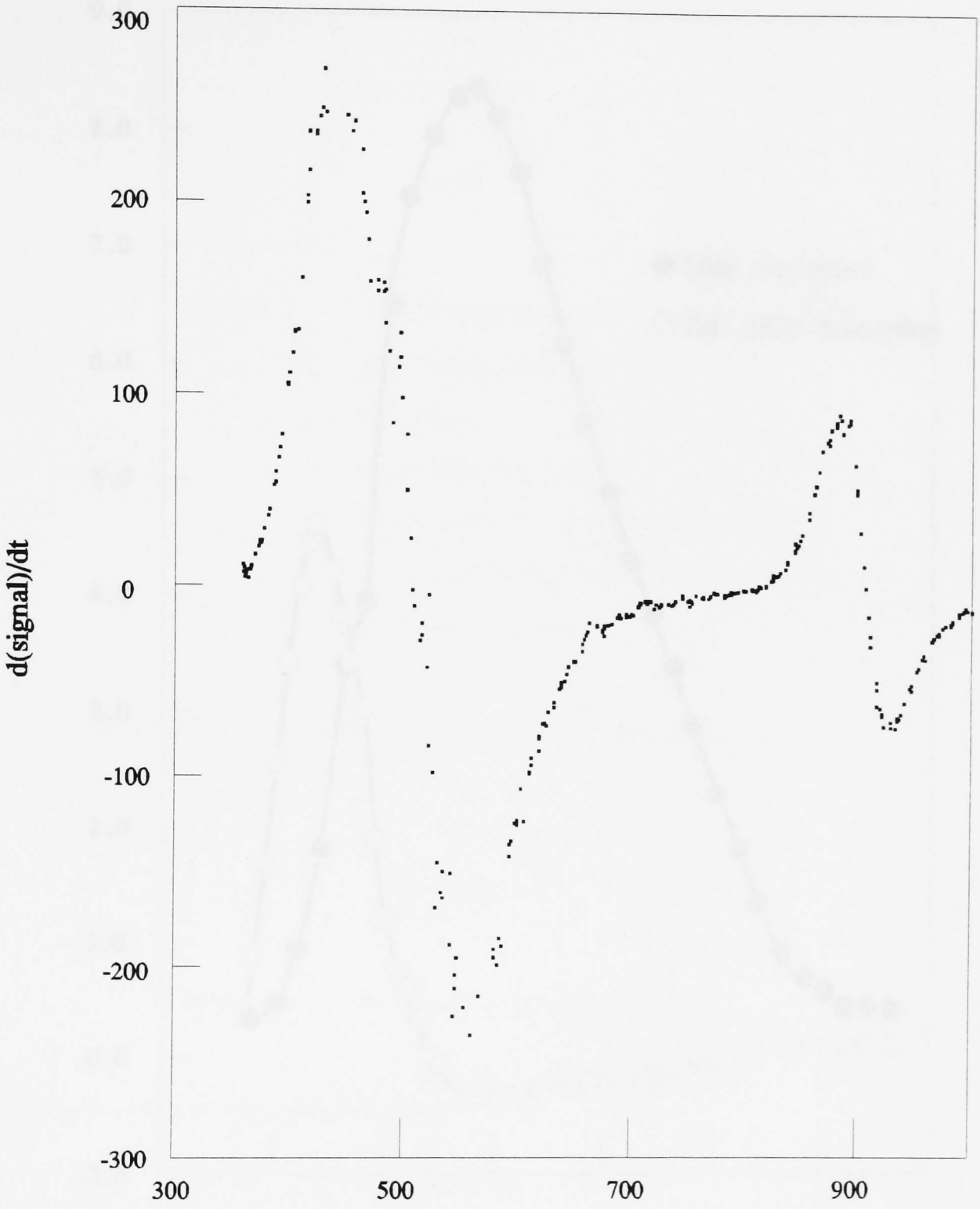

Figure 3.5: Differential trace of figure 3.4
- generated using DIFF program.

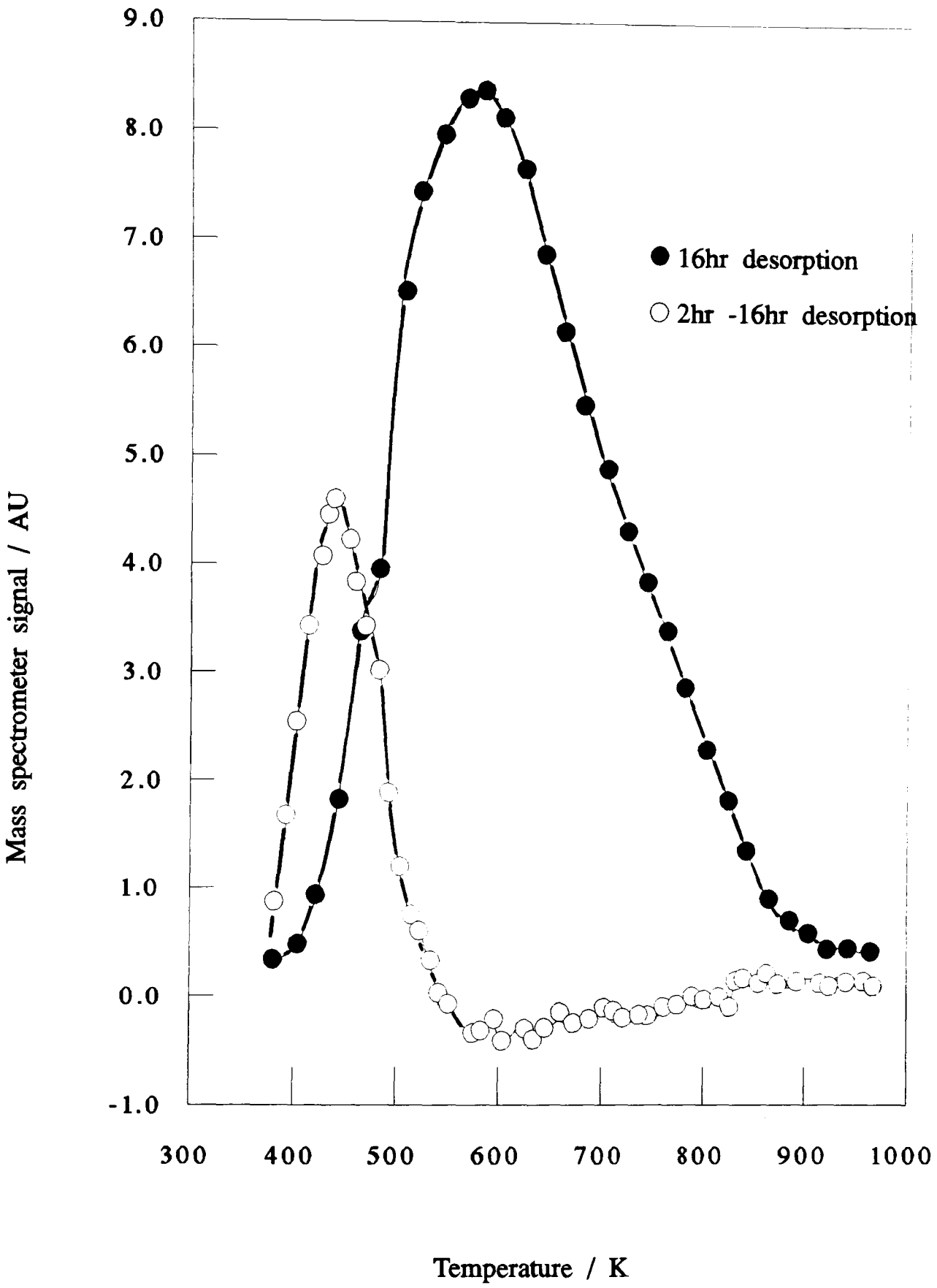

Figure 3.6: Effect of bakeout conditions on ammonia content of HYMST 768. Small trace generated using SUBTRACT program.

Therefore, the following equations can be applied:

$$T=T_o+\beta t \qquad 3.9$$

$$k_d=Ae^{-\frac{E_{Act}}{RT}} \qquad 3.10$$

where: T = temperature, (T_0 initial temperature),
β = temperature rise rate,
t = time,
k_d = rate constant,
A = Arrhenius pre-exponential factor,
E_{Act} = activation energy for desorption,
R = gas constant.

Under the conditions outlined, Cvetanovic and Amenomiya[229] have shown that

$$\frac{d\theta}{dt}=-A\theta e^{-\frac{E_{Act}}{RT}} \qquad 3.11$$

where: θ = surface coverage.

Differentiation of equation 3.9 gives

$$dT=\beta dt \qquad 3.12$$

which, on substitution into equation 3.11 gives

$$\frac{d\theta}{dt}=-\frac{A}{\beta}\theta e^{-\frac{E_{Act}}{RT}} \qquad 3.13$$

At the maximum rate of desorption $(d\theta/dt)_{max}$, occurring at a temperature T_{max}, the concentration, [C], of desorbed gas is at a maximum and so the rate of change of the concentration with respect to the temperature is zero, ie. d[C]/dT=0. The condition of no readsorption means that the concentration of the gas is proportional to -(dθ/dT) so, from equation 3.13 and differentiating with respect to temperature

$$\frac{d[C]}{dT} = \frac{d\theta}{dT} + \theta \frac{E_{Act}}{RT_{max}^{2}} = 0 \qquad 3.14$$

Combination of equations 3.13 and 3.14 gives

$$e^{-\frac{E_{Act}}{RT_{max}}} = \frac{\beta}{T_{max}^{2}} \cdot \frac{E_{Act}}{RA} \qquad 3.15$$

and taking natural logarithms yields

$$\ln \frac{T_{max}^{2}}{\beta} = \frac{E_{Act}}{RT_{max}} + \ln \frac{E_{Act}}{RA} \qquad 3.16$$

Therefore an experiment which varies β and measures T_{max} can be used to find the activation energy of the desorption process as the gradient of a graph of $2\ln T_{max} - \ln\beta$ against $1/T_{max}$ is equivalent to E_{Act}/R.

Sample	Unextracted Catalysts/mmol g^{-1}			Extracted Catalysts /mmol g^{-1}
	2hr	16hr	2hrHe	
NH_4YAS	3.47	-	-	-
NH_4YLS	2.56	-	-	-
HYMST 748	2.07	1.73	1.32	2.21
HYMST 768	2.10	1.52	1.11	1.91
HYMST 783	2.22	1.64	1.23	1.60
HYMST 798	1.93	1.22	0.85	1.67
HYST 823	1.76	1.27	0.80	1.57
HYMST 848	1.82	1.30	0.81	1.62
HYST 873	1.42	1.12	0.66	1.56
HYST 923	1.20	1.04	0.61	1.37
HYST 973	1.06	0.97	0.50	1.23
HYST 1023	0.88	0.78	0.48	1.18
HYST 1073	0.71	0.62	0.42	1.04

Table 3.5: Temperature programmed desorption - ammonia content.

Bakeout key:		duration/temperature/atmosphere
Unextracted:	2hr	2 hours/383K/vacuum
	16hr	16 hours/383K/vacuum
	2hrHe	2 hours/673K/helium
Extracted:		2 hours/383K/vacuum

NH_4YLS		HYST 1023Ex	
Evacuation time / min	Relative ammonia	Evacuation time / min	Relative ammonia
32	1.70	35	1.43
62	1.67	62	1.37
120	1.36	-	-
180	1.20	180	1.14
290	1.18	312	1.08
510	1.03	480	1.05
750	1.00	750	1.07
960	1.00	960	1.00

Table 3.6: Evacuation time experiments.

Treatment	Ammonia	
	mmol g^{-1}	T_{max}/K
Initial	1.27	505
1st repeat	0.30	485
2nd repeat	0.36	488
3rd repeat	0.35	484

Table 3.7: Reammoniation experiments on HYST 823.

Range /K	Ammonia /mmol g^{-1}	Hydroxyl /AU	Total Hydroxyl/AU
373-773	1.27	-	0
373-823	1.16	11	11
373-853	1.18	73	84
373-923	0.86	114	198
373-973	0.44	68	266
373-973	0.36	-	-

Table 3.8: Increased final temperature experiments - HYST 823.

HYMST 748			
Heating rate /K min^{-1}	Ammonia /AU	Hydroxyl /AU	T_{max}(OH) /K
5	45.0	1.22	949
7	56.4	1.53	955
9	68.2	1.56	958
11	108.0	2.59	973
13	115.5	2.77	981
15	136.8	3.27	998
19	179.5	3.89	992

Table 3.9: Temperature programmed desorption experiments.

HYMST 748Ex			
Heating rate /K min^{-1}	Ammonia /AU	Hydroxyl /AU	T_{max}(OH) /K
9	89.0	3.21	1015
11	112.7	4.15	1030
13	128.6	5.03	1042
15	162.6	6.01	1051
17	197.2	6.43	1048
19	193.3	6.74	1065

Table 3.10: Temperature programmed desorption experiments.

HYST 1023			
Heating rate /K min^{-1}	Ammonia /AU	Hydroxyl /AU	T_{max}(OH) /K
3	10.6	-	-
9	40.1	-	-
11	47.3	-	-
13	63.6	-	-
15	67.6	-	-
17	68.7	-	-
17	83.2	-	-
19	106.3	-	-

Table 3.11: Temperature programmed desorption experiments.

HYST 1023Ex			
Heating rate /K min^{-1}	Ammonia /AU	Hydroxyl /AU	T_{max}(OH) /K
5	26.9	0.74	-
9	43.2	1.22	1030
11	63.6	1.58	1043
13	60.4	1.49	1058
15	85.4	1.95	1064
17	91.8	2.16	1070
19	107.0	2.59	1079

Table 3.12: Temperature programmed desorption experiments.

NH_4YAS			
Heating rate /K min^{-1}	Ammonia /AU	Hydroxyl /AU	T_{max}(OH) /K
3	31.7	2.70	890
5	48.9	4.11	904
7	78.4	7.55	-
9	89.4	7.41	927
11	123.4	7.53	-
13	115.7	9.37	929
15	162.6	10.62	940
17	155.5	11.07	943

Table 3.13: Temperature programmed desorption experiments.

Sample	E_{des}/kJmol^{-1}
NH_4YAS	212
HYMST 748	216
HYMST 748Ex	122
HYST 1023Ex	110

Table 3.14: Dehydroxylation energies.

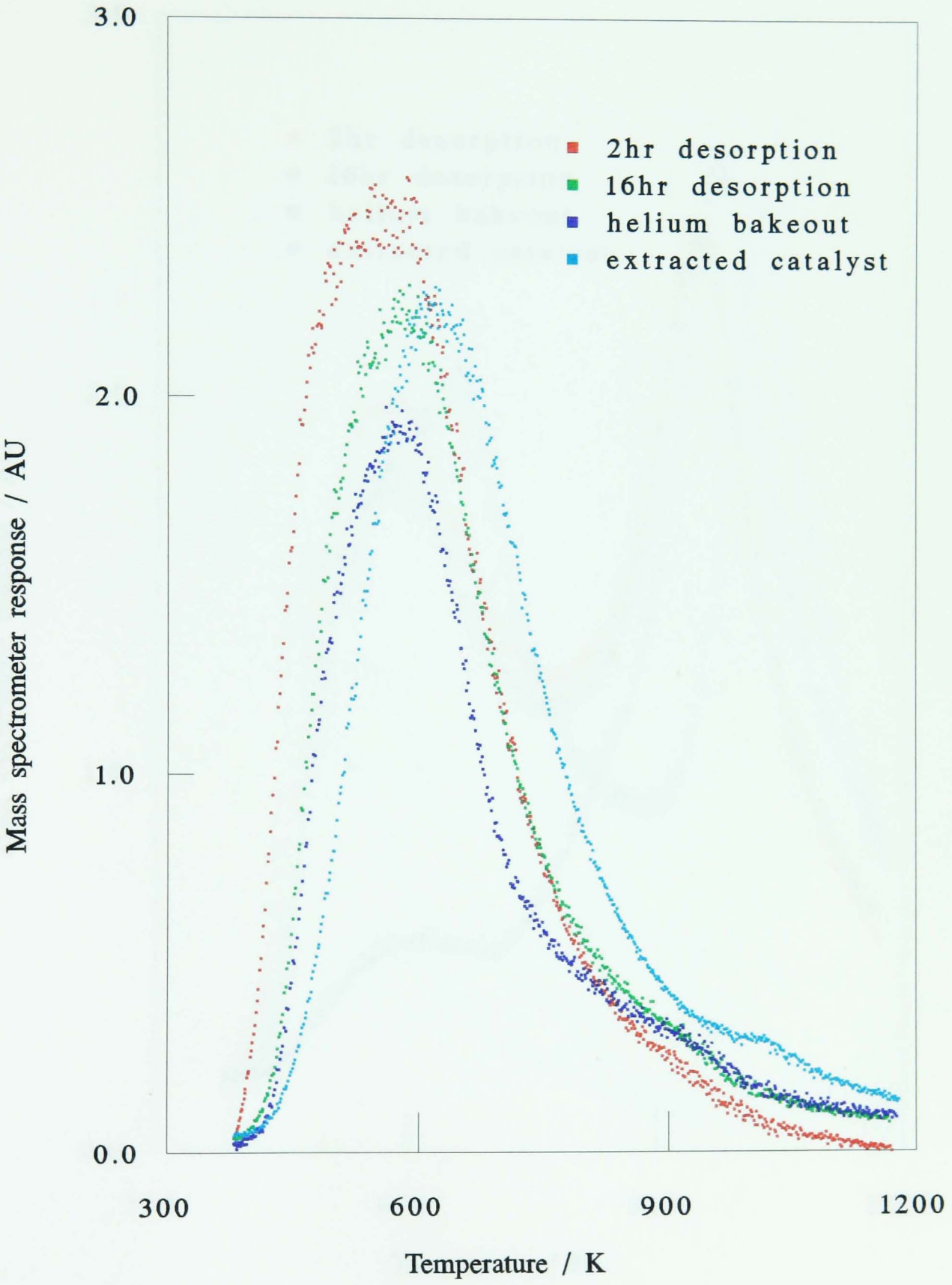

Figure 3.7: Effect of bakeout and desorption procedure on the ammonia capacity of HYMST 783.

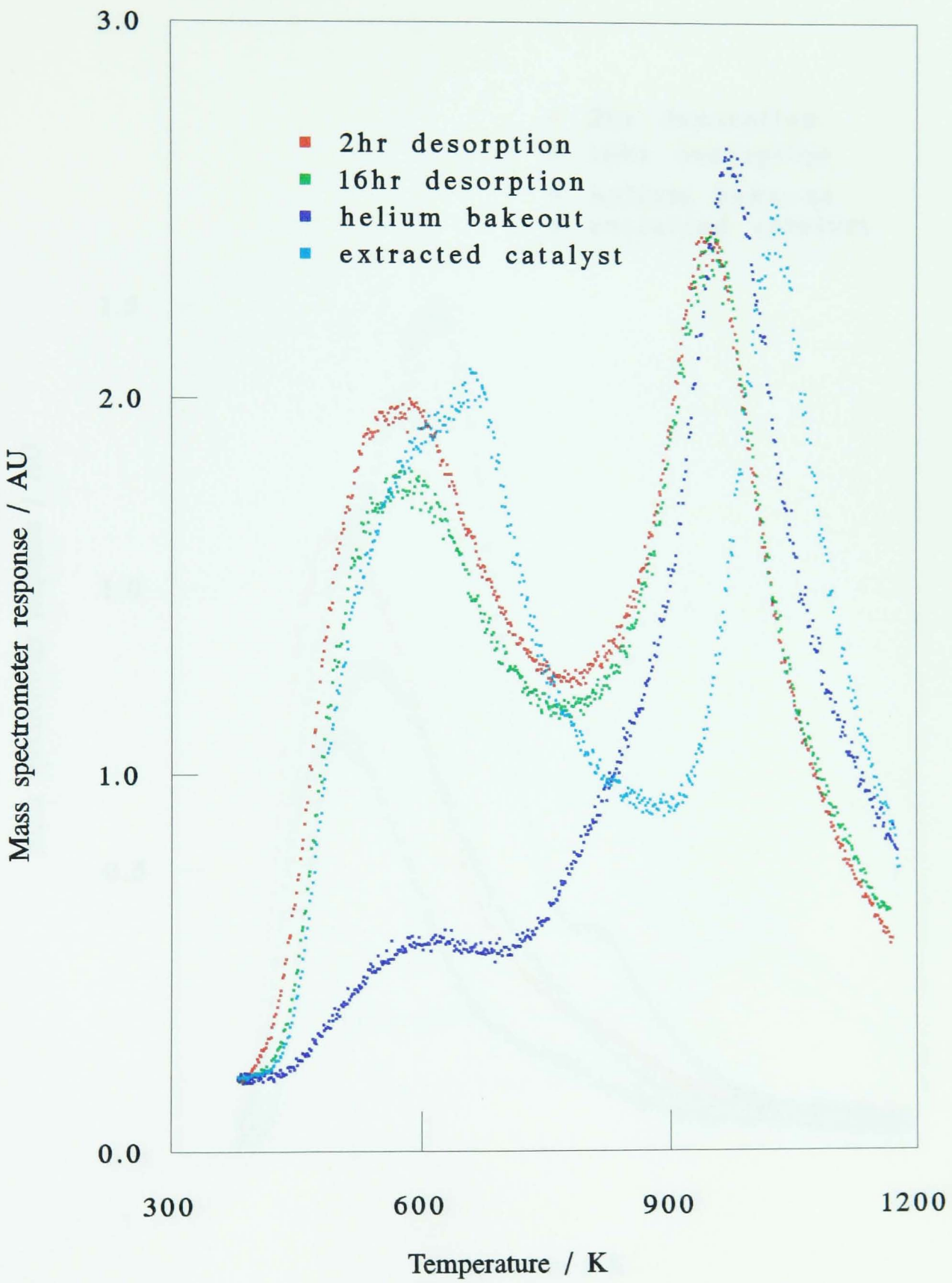

Figure 3.8: Effect of bakeout and desorption procedure on the hydroxyl content of HYMST 783.

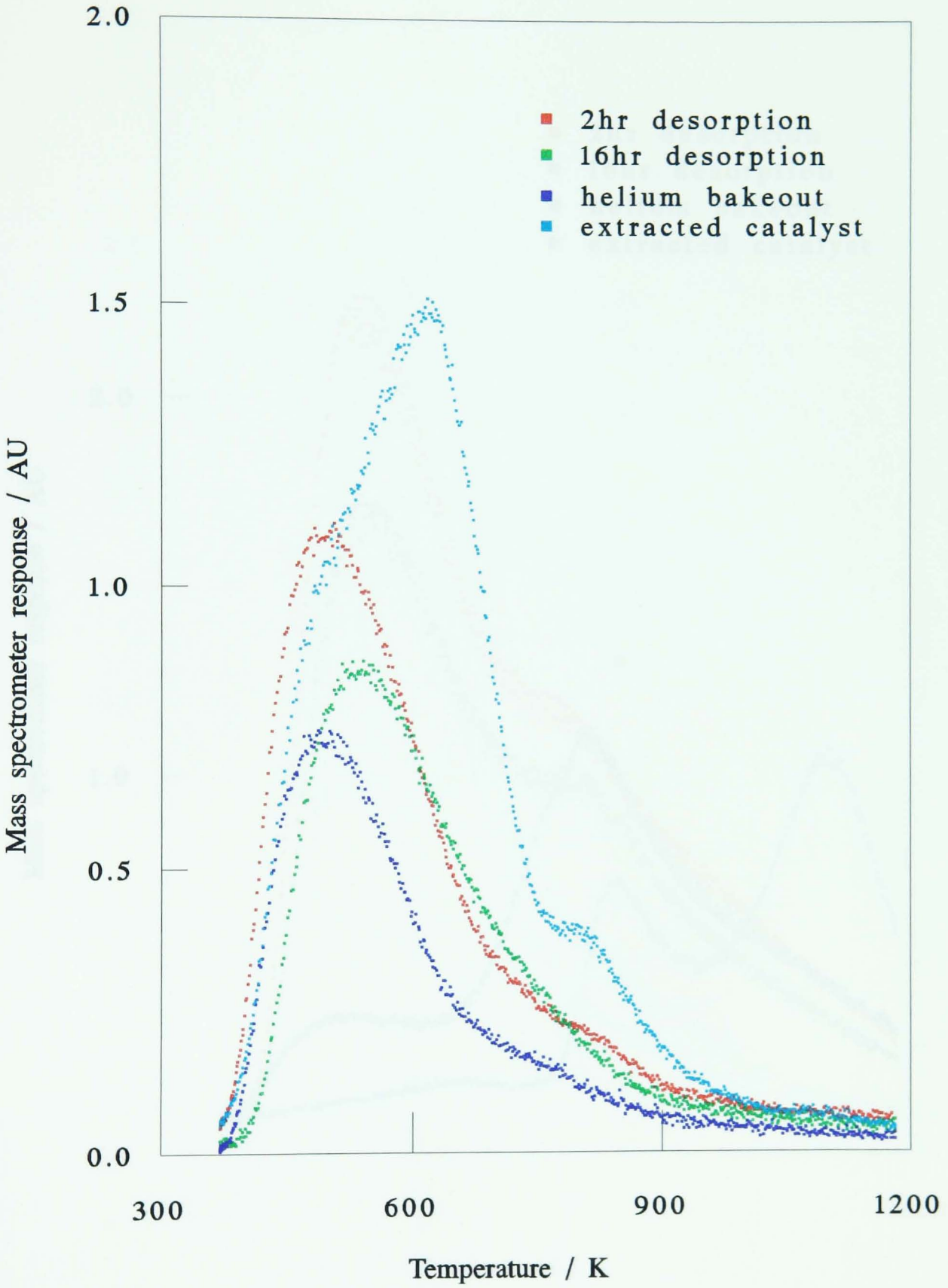

Figure 3.9: Effect of bakeout and desorption procedure on the ammonia capacity of HYMST 1073.

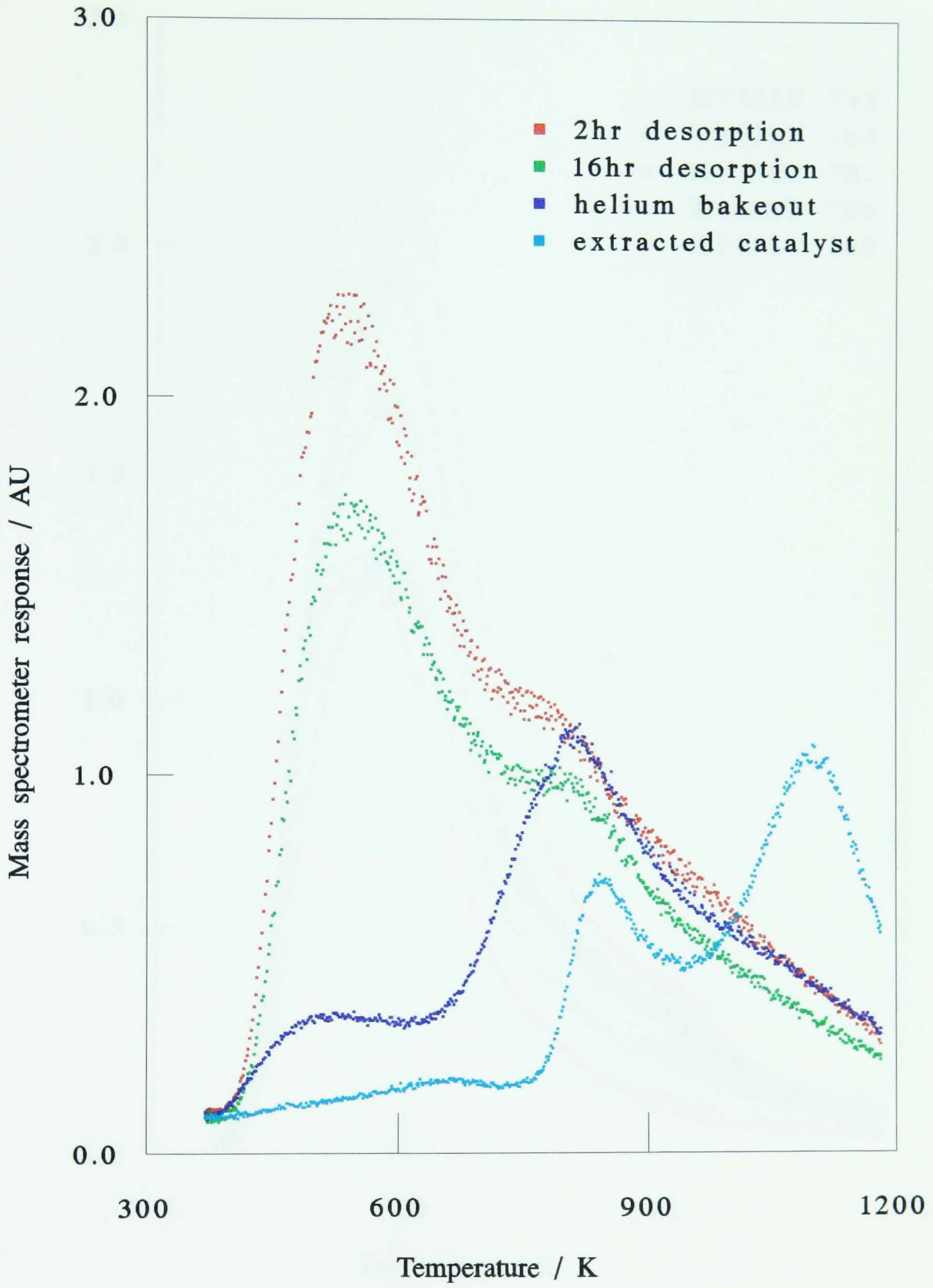

Figure 3.10: Effect of bakeout and desorption procedure on the hydroxyl content of HYMST 1073.

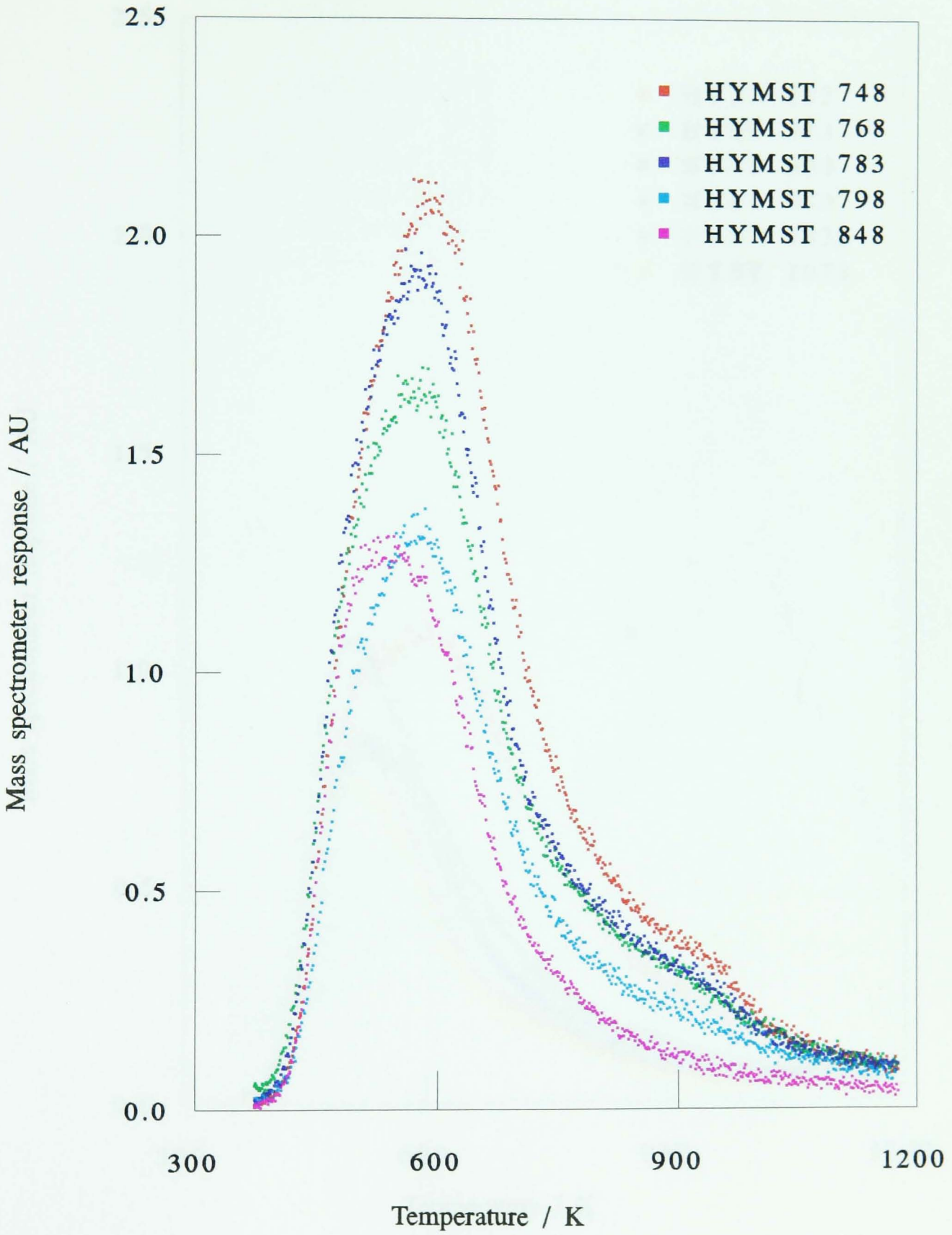

Figure 3.11: Temperature programmed desorption of ammonia from HYMST x samples.

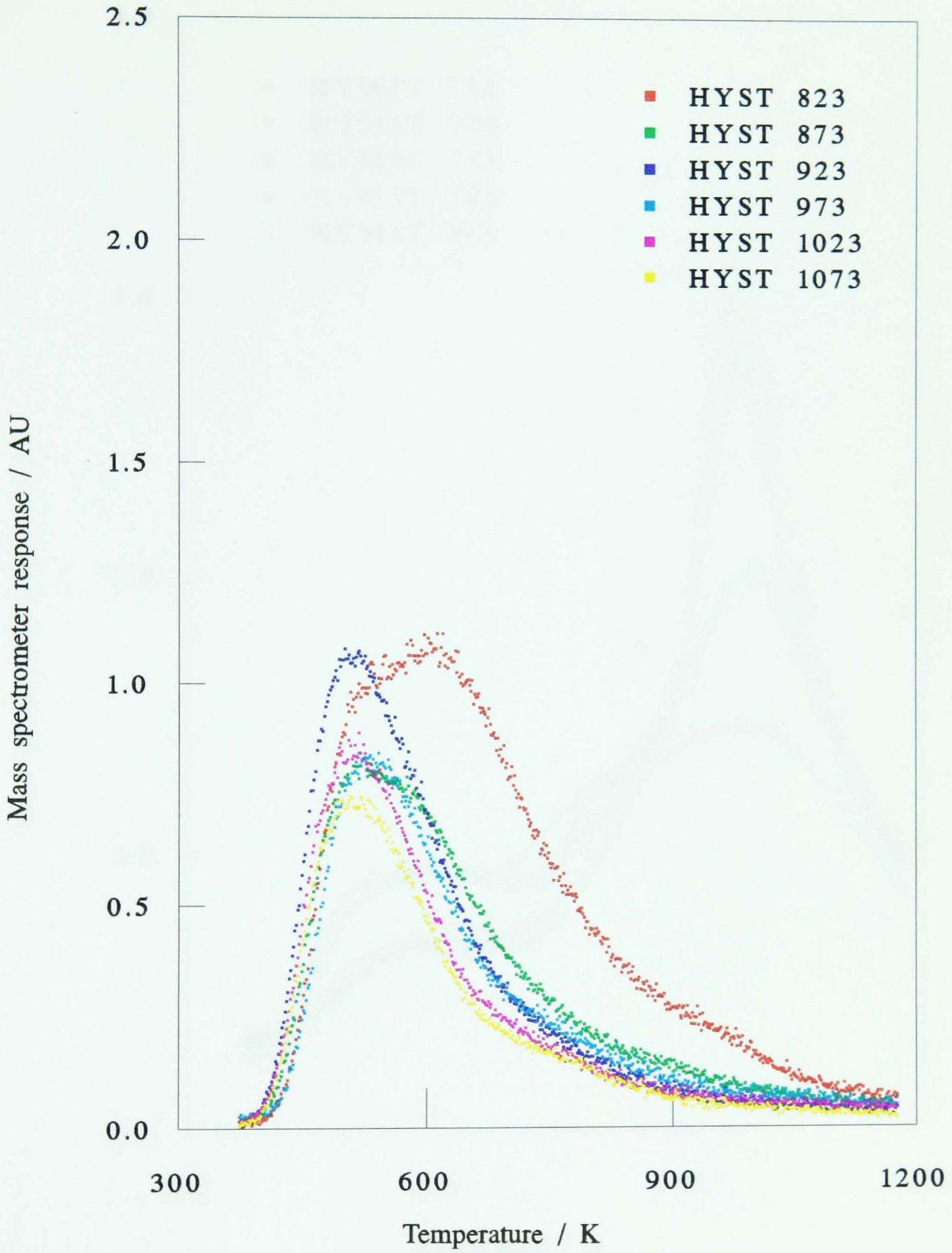

Figure 3.12: Temperature programmed desorption of ammonia from HYST x samples.

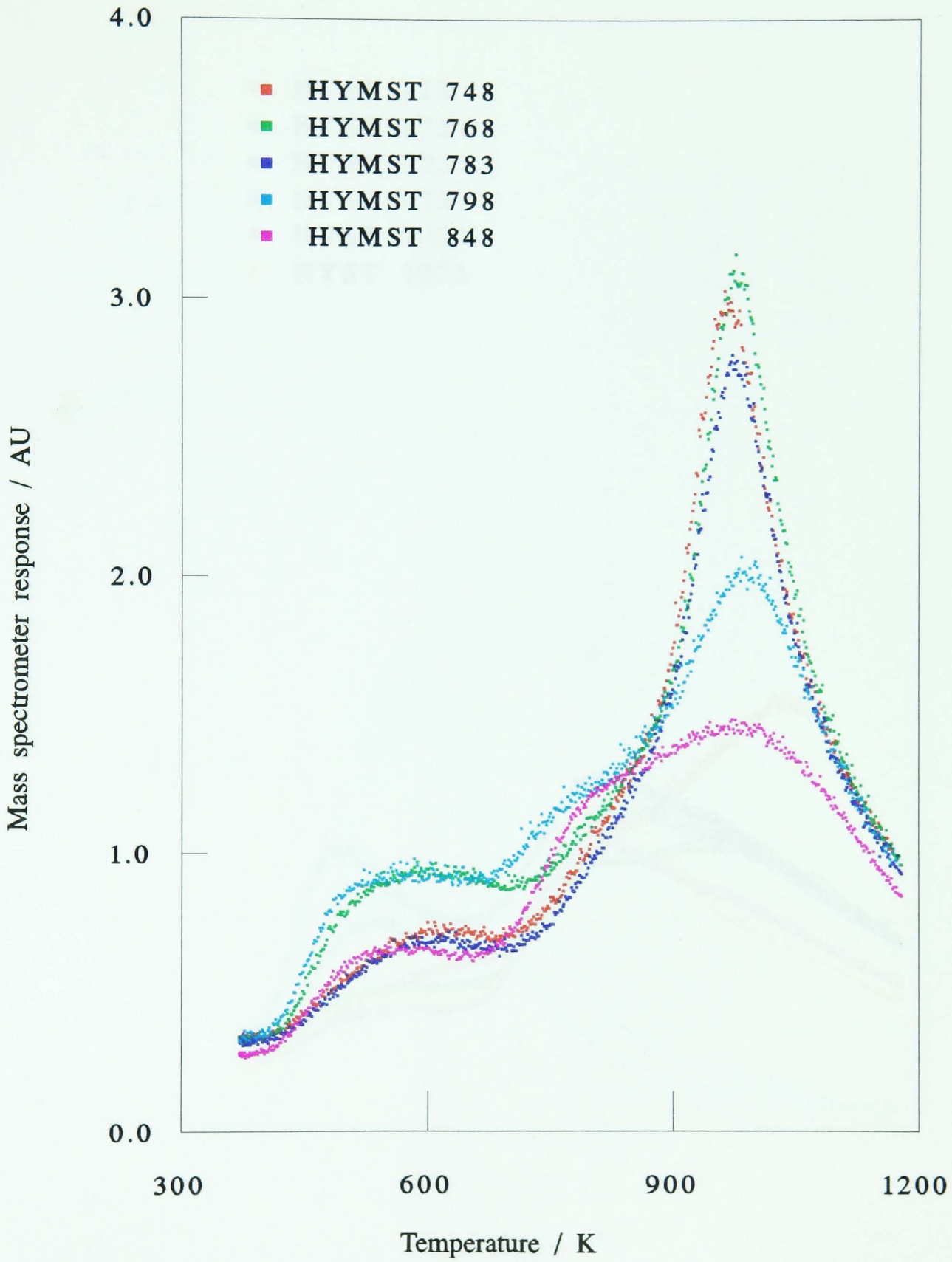

Figure 3.13: Temperature programmed desorption of water from HYMST x samples.

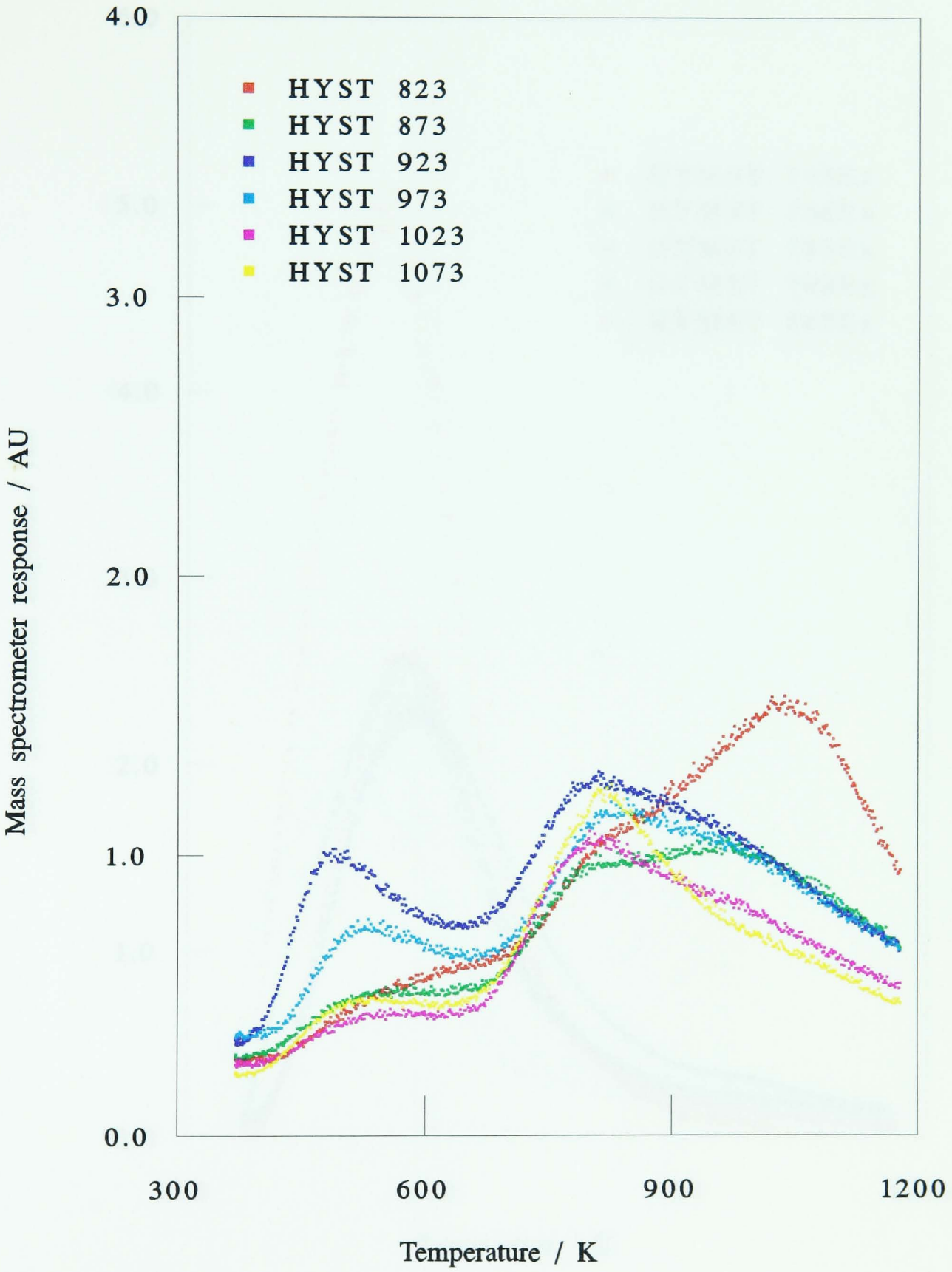

Figure 3.14: Temperature programmed desorption of water from HYST x samples.

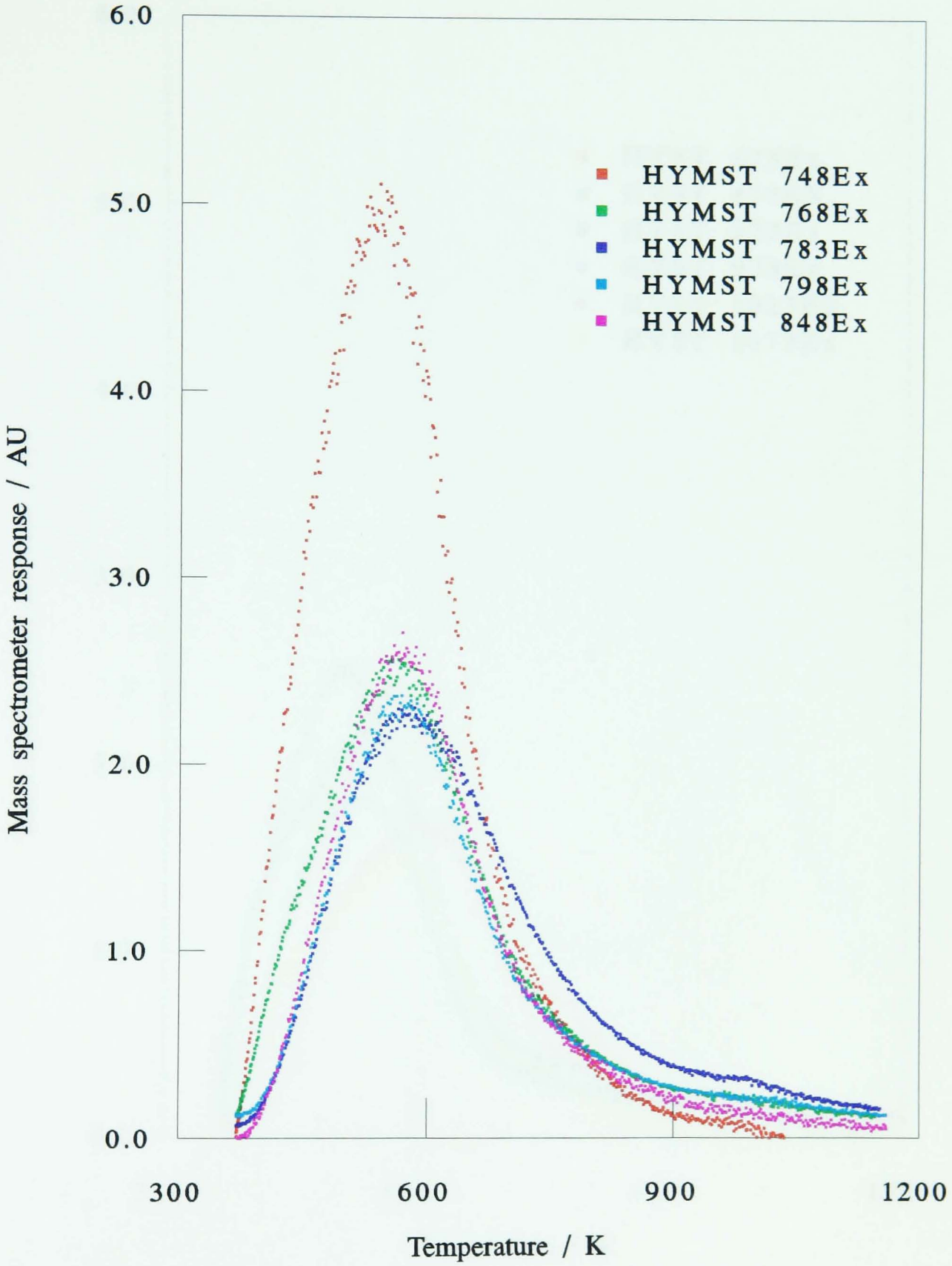

Figure 3.15: Temperature programmed desorption of ammonia from HYMST x Ex samples.

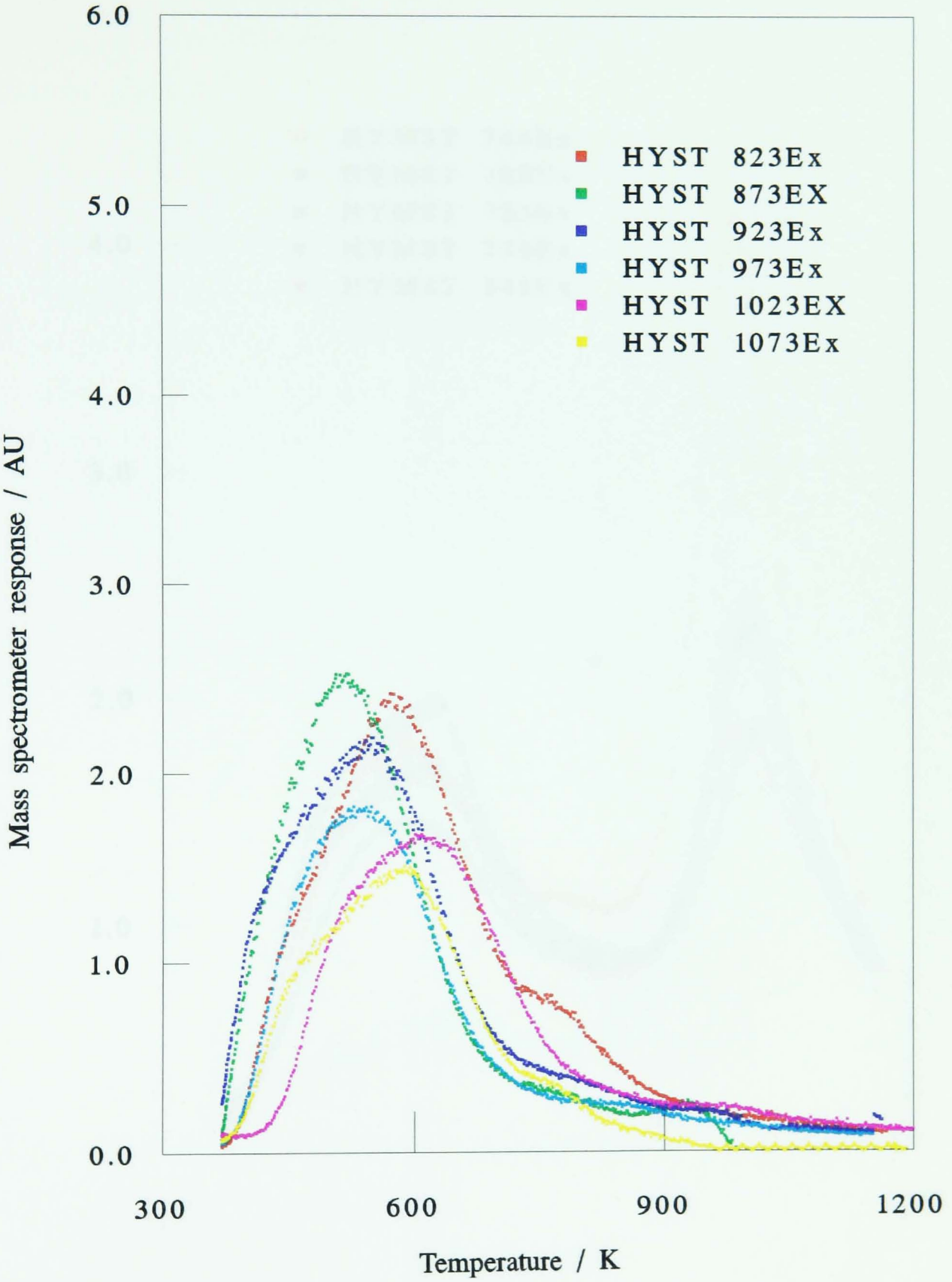

Figure 3.16: Temperature programmed desorption of ammonia from HYST x Ex samples.

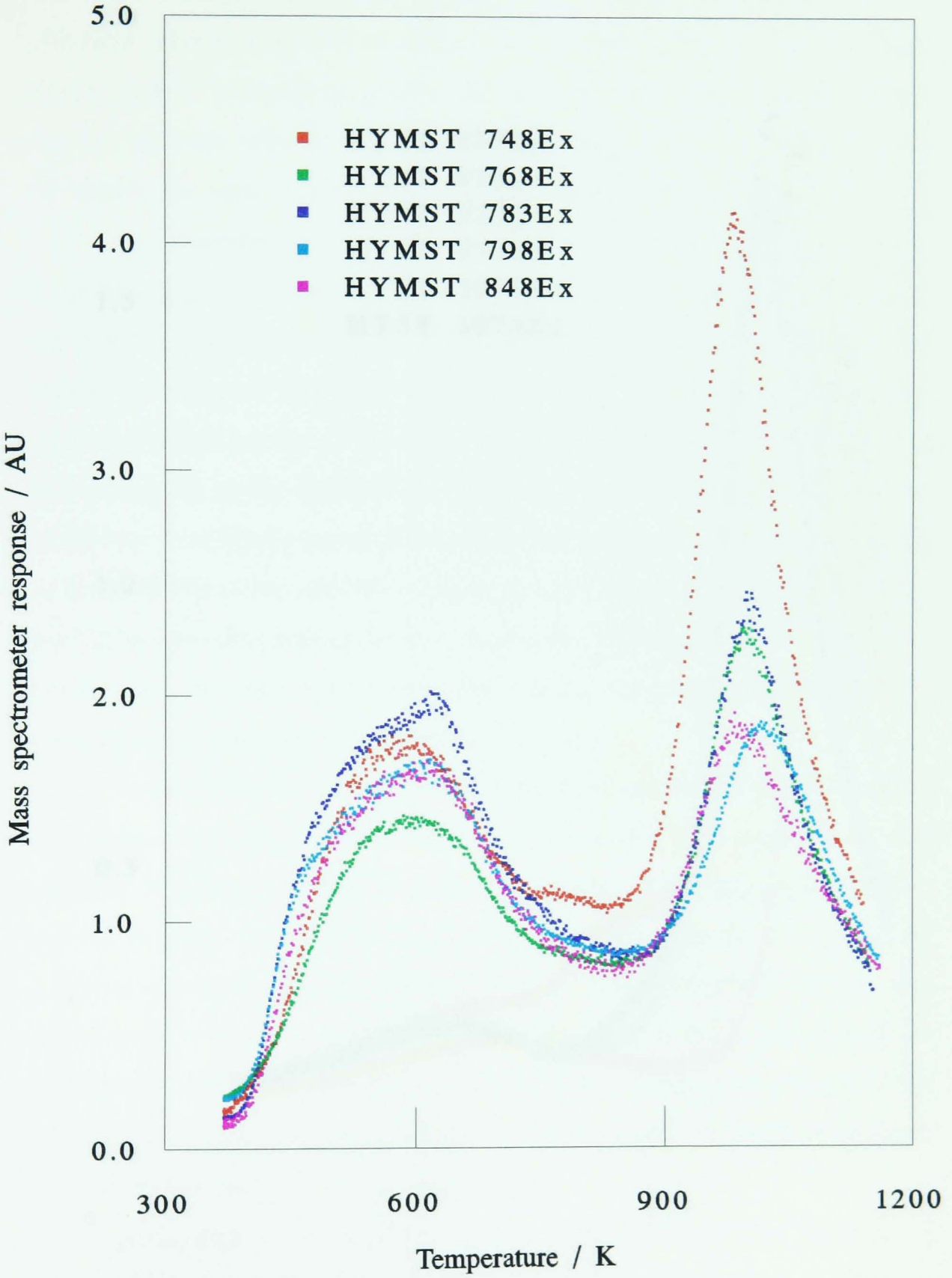

Figure 3.17: Temperature programmed desorption of water from HYMST x Ex samples.

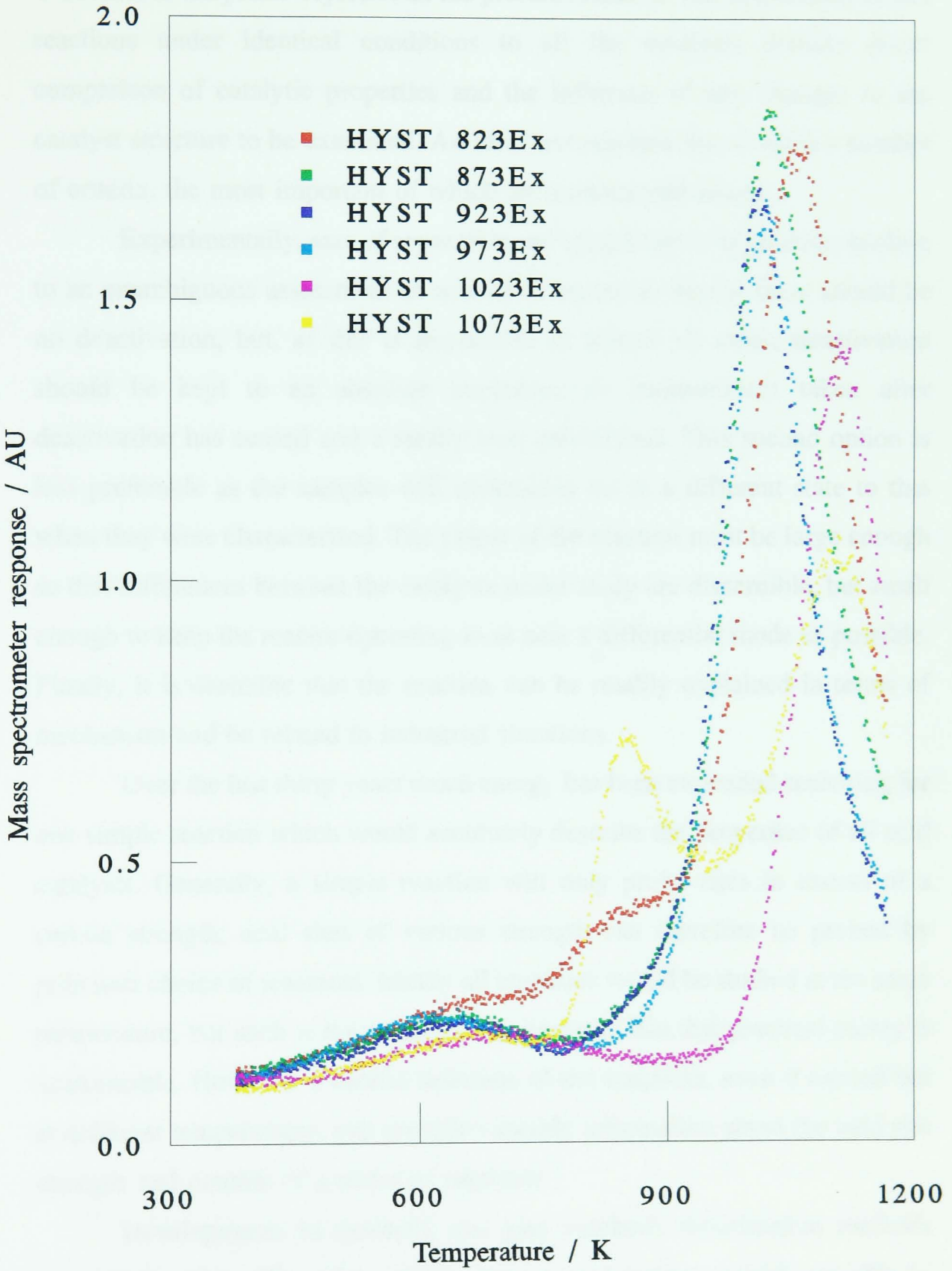

Figure 3.18: Temperature programmed desorption of water from HYST x Ex samples.

3.2 Catalysis

An understanding of the catalytic properties of the series of modified Y zeolites is the prime objective of the present research. The application of test reactions under identical conditions to all the catalysts permits direct comparison of catalytic properties and the influence of any changes to the catalyst structure to be examined. An ideal test reaction has to fulfil a number of criteria, the most important of which are summarised below.

Experimentally, ease of separation and identification of products leading to an unambiguous assessment of activity is essential. Ideally there should be no deactivation, but, as this is impossible in almost all cases, deactivation should be kept to an absolute minimum, or measurement taken after deactivation has ceased and a steady state established. This second option is less preferable as the samples will undeniably be in a different state to that when they were characterised. The extent of the reaction must be large enough so that differences between the catalysts under study are discernible, but small enough to keep the reactor operating in as near a differential mode as possible. Finally, it is desirable that the reaction can be readily explained in terms of mechanism and be related to industrial situations.

Over the last thirty years much energy has been expended searching for one simple reaction which would accurately describe the properties of all acid catalysts. Generally, a simple reaction will only probe sites in excess of a certain strength; acid sites of various strength can therefore be probed by judicious choice of reactants. Ideally all reactions would be studied at the same temperature, but such is the range of requirements that this practical nicety is unattainable. However, a careful selection of test reactions, even if carried out at different temperatures, can provide valuable information about the acid site strength and content of a series of catalysts.

Developments in synthetic and post synthesis modification methods have produced zeolites of increasing strong acid content, which are able to catalyse more demanding reactions at lower temperatures. The catalytic cracking of n-hexane is currently the favoured test reaction for strong acidity, and so will be considered first in the following discussion. The other test

reactions studied will be examined in what is generally considered to be order of decreasing acid strength requirement, that is toluene disproportionation, cumene dealkylation and propan-2-ol dehydration. Therefore the progression from a reaction which will occur on only strong sites to a reaction which will proceed on all sites can be studied.

The presentation of the catalyst will affect the extent of the reactions studied. The work contained in this thesis has for the most part centred on broken pressed pellets of pure catalyst, sieved to provide particles within a uniform band, contained within a tubular reactor. Pellets are preferred over the previously favoured fine powder as they are easier to handle, have greater similarity with industrial catalysts and, most importantly, have the same presentation as used in the temperature programmed desorption experiments. Reactions were studied in a tubular reactor to remove any uncertainties regarding the non uniform distribution across the sample bed, especially since preliminary experiments had shown that switching certain valves created a back pressure which redistributed the catalyst bed, potentially moving some of the sample to regions of different temperature.

The reactions were usually studied under pulse flow conditions in which a pulse of reactant is passed over the sample and the products collected in a liquid nitrogen trap. This allows the activity at the very start of a catalytic reaction to be assessed before any deactivation has occurred. The effects of adsorption and desorption on the activity can also be studied, as well as deactivation in the very first stages of the reaction. Care has to be taken when comparing the results from pulse flow experiments with those obtained under continuous flow conditions as full equilibrium between the gas phase and the surface of the catalyst cannot be assumed. One of the reactions chosen, the dehydration of propan-2-ol, is a wet reaction, and as the concentration of the water within the samples is known to be critical an equilibrium between water production and adsorption must be achieved. For this reason the reaction was studied under continuous flow conditions, and fortunately, as this is a clean reaction without any deactivation, the results can be treated as initial activities.

3.21 n-Hexane Cracking

The cracking of n-hexane was studied at 673K using the pulse flow system after the catalyst had been activated at 673K for sixteen hours in flowing helium. Fifteen pulses were individually collected in a nitrogen trap and analysed by gas chromatography. A continuous flow of n-hexane was then passed over the samples for sixteen hours after which sufficient pulses were taken until consistent results were obtained.

As this reaction produces many products, there are several ways of expressing the activity of the catalyst. In addition to monitoring the production of individual products, the total amount of n-hexane converted to volatile products can be utilised. This can be calculated from the observed products according to the following equation:

$$\Sigma_{hex} = \frac{(C_1 + 2C_2 + 3C_3 + 4C_4 + 5C_5 + 6iC_6)}{6} \quad 3.17$$

where C_x is the number of hydrocarbon molecules containing x carbon atoms. However, in this instance neither methane nor isohexane were observed. This calculation does not take into account the unquantifiable amount of coke produced in each pulse. The results from the individual experiments are presented in tables 3.17 to 3.40 and summarised in tables 3.41 to 3.44. Activity profiles representative of the range of activities are shown in figures 3.19 and 3.20. The results presented in table 3.41 are reported as total n-hexane converted and isobutane produced in the first pulse, or representative pulses thereof, total hexane converted in fifteen pulses, and the amount of n-hexane converted after sixteen hours of continuous exposure to n-hexane.

1/f xcm^{3}min^{-1}; iC$_6$ x 10^{16} molecules							
0.0132g		0.0193g		0.0289g		0.0383g	
1/f	iC$_6$	1/f	iC$_6$	1/f	iC$_6$	1/f	iC$_6$
0.077	0.00	0.061	0.00	0.033	0.00	0.022	0.00
0.094	5.79	0.071	6.02	0.053	7.10	0.040	7.22
0.116	6.94	0.073	6.54	0.069	9.62	0.062	11.53
0.128	7.62	0.093	8.62	0.093	11.61	0.071	13.25
0.154	8.74	0.135	10.33	0.107	12.37	0.114	15.16
0.192	10.25	0.151	12.25	0.128	13.89	0.151	15.48
-	-	-	-	0.151	14.60	0.182	15.52

Table 3.15: Detection of iso-hexane with varying contact time.

1/f /cm^{-1}min^{-1}	molecules / x10^{18}g^{-1}		
	C$_3$	C$_4$	C$_5$
0.017	0.66	-	-
0.025	1.98	0.27	0.11
0.037	4.51	1.04	0.35
0.052	8.11	2.48	0.65
0.077	13.52	5.32	1.29
0.094	16.89	7.17	1.55
0.116	20.31	9.96	1.95

Table 3.16: n-Hexane cracking activity of HYST 823 with varying contact time.

NH_4YAS			673K			Dry mass=0.0130g		
Product formation / 10^{19} molecules g^{-1}								
Pulse	C_2	C_3	iC_4	nC_4	iC_5	nC_5	iC_6	Σ_{hex}
1	0.13	1.34	0.29	-	-	-	-	0.91
2	0.13	1.32	0.27	-	-	-	-	0.88
3	0.13	1.29	0.24	-	-	-	-	0.85
4	0.09	1.31	0.25	-	-	-	-	0.85
5	0.13	1.26	0.23	-	-	-	-	0.83
6	0.14	1.37	0.27	-	-	-	-	0.91
7	0.14	1.33	0.23	-	-	-	-	0.87
8	0.14	1.33	0.26	-	-	-	-	0.89
9	0.14	1.34	0.26	-	-	-	-	0.89
10	0.14	1.35	0.20	-	-	-	-	0.86
11	0.15	1.38	0.28	-	-	-	-	0.93
12	0.14	1.30	0.17	-	-	-	-	0.81
13	0.14	1.39	0.27	-	-	-	-	0.92
14	0.14	1.30	0.23	-	-	-	-	0.85
15	0.14	1.32	0.25	-	-	-	-	0.87
16hr	0.23	1.71	0.23	0.13	0.14	-	-	1.29

Table 3.17: n-Hexane cracking activity as a function of pulse number.

NH_4YLS			673K			Dry mass=0.0144g		
Product formation / 10^{19} molecules g^{-1}								
Pulse	C_2	C_3	iC_4	nC_4	iC_5	nC_5	iC_6	Σ_{hex}
1	2.09	34.22	8.11	3.51	3.21	0.96	-	29.03
2	2.02	33.56	8.03	3.43	3.28	0.94	-	28.61
3	1.87	31.15	7.25	3.16	2.87	0.88	-	26.26
4	1.99	32.90	7.88	3.41	3.16	0.94	-	28.06
5	1.94	32.40	7.66	3.27	3.08	0.86	-	27.42
6	1.92	31.96	7.49	3.19	3.00	0.84	-	26.94
7	1.92	31.58	7.38	3.22	3.02	0.85	-	26.72
8	1.76	29.26	6.56	3.25	2.75	0.85	-	24.76
9	1.88	31.16	7.17	3.07	3.01	0.89	-	26.28
10	1.81	30.85	6.90	3.06	3.00	0.73	-	25.78
11	2.13	30.32	6.86	3.03	3.03	0.75	-	25.61
12	1.83	29.74	6.70	3.03	2.89	0.81	-	25.05
13	1.89	29.76	6.57	2.52	2.67	0.79	-	24.45
14	1.42	28.26	6.05	2.52	2.28	-	-	22.22
15	1.60	26.30	5.58	2.54	2.42	0.72	-	21.71
16hr	1.86	30.10	6.68	3.11	2.73	0.80	-	25.14

Table 3.18: n-Hexane cracking activity as a function of pulse number.

HYMST 748			673K			Dry mass=0.0157g		
Product formation / 10^{19} molecules g^{-1}								
Pulse	C_2	C_3	iC_4	nC_4	iC_5	nC_5	iC_6	Σ_{hex}
1	2.78	47.09	13.00	4.99	4.83	1.23	-	41.52
2	2.75	45.57	12.73	4.89	4.68	1.20	-	40.35
3	2.55	42.80	11.58	4.46	4.50	1.13	-	37.64
4	2.57	42.86	12.26	4.53	4.92	1.09	-	38.49
5	2.33	38.64	10.64	3.97	4.37	1.00	-	34.31
6	2.30	38.86	10.15	3.94	4.7	0.97	-	34.32
7	2.24	37.15	9.89	3.76	4.17	0.97	-	32.71
8	2.14	35.03	9.43	3.57	3.92	0.92	-	30.93
9	2.09	33.96	8.91	3.42	3.77	0.87	-	29.76
10	2.02	33.64	8.25	3.29	3.63	0.86	-	28.93
11	2.06	34.77	8.42	3.35	3.78	0.85	-	29.78
12	2.02	33.79	8.14	3.22	3.60	0.82	-	28.83
13	1.98	33.28	7.74	3.09	3.56	0.79	-	28.15
14	2.03	33.28	7.94	3.17	3.60	0.83	-	28.42
15	2.00	33.02	7.73	3.07	3.50	0.74	-	27.91
16hr	1.98	33.3	8.21	3.28	3.56	0.88	-	28.67

Table 3.19: n-Hexane cracking activity as a function of pulse number.

HYMST 768			673K			Dry mass=0.0152g		
Product formation / 10^{19} molecules g^{-1}								
Pulse	C_2	C_3	iC_4	nC_4	iC_5	nC_5	iC_6	Σ_{hex}
1	3.34	60.28	17.77	6.22	7.59	1.57	-	54.88
2	3.05	53.93	15.89	5.63	6.77	1.49	-	49.21
3	3.09	54.18	15.68	5.64	6.69	1.40	-	49.08
4	2.73	47.57	13.48	4.94	5.98	1.28	-	43.03
5	2.69	46.91	13.04	4.76	5.83	1.27	-	42.14
6	2.58	44.48	12.16	4.46	5.46	1.21	-	39.74
7	2.62	44.49	12.18	4.42	5.41	1.19	-	39.69
8	2.47	42.02	11.27	4.16	5.28	1.14	-	37.47
9	2.40	40.40	10.73	4.04	4.98	1.09	-	35.91
10	2.36	39.92	10.51	3.99	4.96	1.03	-	35.41
11	2.31	38.57	10.07	3.78	4.77	1.02	-	34.11
12	2.26	38.10	9.80	3.70	4.75	0.99	-	33.59
13	2.22	37.40	9.48	3.68	4.59	0.97	-	32.85
14	2.18	36.63	9.15	3.52	4.46	0.97	-	32.01
15	2.17	36.47	9.13	3.50	4.47	0.95	-	31.90
16hr	2.55	43.94	11.02	4.15	4.91	1.06	-	37.88

Table 3.20: n-Hexane cracking activity as a function of pulse number.

HYMST 783			673K			Dry mass=0.0158g		
Product formation / 10^{19} molecules g^{-1}								
Pulse	C_2	C_3	iC_4	nC_4	iC_5	nC_5	iC_6	Σ_{hex}
1	3.21	56.67	17.55	6.02	6.39	1.49	-	51.69
2	2.84	49.39	14.80	5.24	5.78	1.29	-	44.89
3	2.68	46.78	13.58	4.87	5.87	1.20	-	42.48
4	2.52	43.62	15.57	4.54	5.12	1.14	-	41.27
5	2.46	42.29	12.13	4.39	5.04	1.09	-	38.09
6	2.40	41.66	11.51	4.24	4.90	1.09	-	37.12
7	2.41	41.33	11.42	4.18	4.93	1.04	-	36.84
8	2.35	40.38	10.83	4.02	4.69	1.03	-	35.64
9	2.30	39.38	10.43	3.89	4.55	0.95	-	34.59
10	2.21	38.02	9.81	3.74	4.78	1.04	-	33.63
11	2.26	37.42	10.07	3.69	4.27	0.95	-	32.99
12	2.19	36.71	9.41	3.54	4.33	0.86	-	32.04
13	2.15	36.31	9.10	3.44	4.20	0.77	-	31.37
14	2.15	35.81	9.26	3.43	4.15	0.75	-	31.17
15	2.11	35.27	8.77	3.29	4.07	0.81	-	30.45
16hr	2.41	41.5	11.1	4.19	5.26	1.05	-	37.01

Table 3.21: n-Hexane cracking activity as a function of pulse number.

HYMST 798			673K			Dry mass=0.0153g		
Product formation / 10^{19} molecules g^{-1}								
Pulse	C_2	C_3	iC_4	nC_4	iC_5	nC_5	iC_6	Σ_{hex}
1	2.51	41.78	11.95	4.34	5.21	1.12	-	37.86
2	2.42	41.64	11.90	4.38	5.14	2.32	-	38.70
3	2.28	39.51	11.16	4.13	4.96	1.11	-	35.77
4	2.45	39.31	11.12	3.97	4.77	1.07	-	35.40
5	1.94	33.87	8.86	3.45	4.18	0.93	-	30.05
6	1.95	33.27	8.73	3.39	4.00	0.89	-	29.44
7	1.84	31.76	8.12	3.16	3.87	0.82	-	27.92
8	1.79	31.01	7.66	3.05	3.66	0.81	-	26.97
9	1.83	31.49	7.79	3.06	3.73	0.81	-	27.37
10	1.78	30.22	7.50	3.00	3.54	0.79	-	26.31
11	1.70	28.95	7.14	2.88	3.42	0.74	-	25.19
12	1.76	30.25	7.18	2.85	3.50	0.73	-	25.92
13	1.65	28.07	6.84	2.47	3.48	0.52	-	24.13
14	1.71	29.46	6.82	2.79	3.31	0.50	-	24.88
15	-	-	-	-	-	-	-	-
16hr	2.11	35.5	9.65	3.72	4.53	1.05	-	32.02

Table 3.22: n-Hexane cracking activity as a function of pulse number.

HYST 823		673K			Dry mass=0.0155g		
Product formation / 10^{19} molecules g^{-1}							
Pulse	C_2	C_3	iC_4	nC_4	iC_5	nC_5	iC_6	Σ_{hex}
1	5.75	109.4	37.75	11.11	10.48	2.23	-	99.78
2	5.13	98.11	32.50	9.61	10.27	2.72	-	89.66
3	5.03	95.31	29.35	8.88	9.35	1.89	-	84.19
4	4.77	90.46	27.00	8.41	9.07	1.79	-	79.48
5	4.49	83.57	24.14	7.56	8.49	1.71	-	72.92
6	4.25	77.35	21.83	6.96	7.75	1.52	-	67.01
7	3.97	71.99	19.69	6.47	7.48	1.39	-	62.15
8	-	71.46	19.48	6.15	7.48	1.35	-	60.18
9	3.85	67.98	18.19	5.94	7.11	1.32	-	58.39
10	3.72	65.42	17.14	5.62	7.02	1.23	-	56.00
11	3.69	63.10	16.37	5.41	6.85	1.05	-	53.88
12	4.32	73.60	16.66	5.59	7.13	1.29	-	60.09
13	4.16	71.51	15.73	5.25	6.77	1.25	-	57.81
14	4.60	77.33	16.79	5.66	7.06	1.25	-	62.09
15	4.33	74.28	16.10	5.48	7.04	1.35	-	59.96
16hr	3.76	59.81	14.72	5.22	7.40	1.49	-	51.86

Table 3.23: n-Hexane cracking activity as a function of pulse number.

HYMST 848			673K			Dry mass=0.0159g		
Product formation / 10^{19} molecules g^{-1}								
Pulse	C_2	C_3	iC_4	nC_4	iC_5	nC_5	iC_6	Σ_{hex}
1	-	-	9.18	3.25	2.82	0.66	-	11.19
2	1.40	25.08	6.15	2.45	2.91	0.64	-	21.70
3	1.33	23.73	5.79	2.28	2.83	0.69	-	20.62
4	1.31	23.20	5.69	2.34	2.78	0.65	-	20.25
5	1.27	22.61	5.51	2.22	2.71	0.64	-	19.67
6	1.24	22.12	5.30	2.20	2.59	0.62	-	19.15
7	1.28	22.64	5.43	2.20	2.72	0.61	-	19.61
8	1.27	22.45	5.32	2.14	2.89	-	-	19.03
9	1.21	21.41	5.05	2.00	3.13	-	-	18.42
10	1.22	21.60	5.06	2.08	2.48	0.57	-	18.51
11	1.17	21.03	4.87	2.00	2.48	0.61	-	18.06
12	1.18	20.99	4.80	1.98	2.39	0.51	-	17.83
13	1.16	20.56	4.67	1.88	2.39	0.53	-	17.47
14	1.15	20.52	4.60	1.93	2.27	0.50	-	17.31
15	1.07	19.24	4.18	1.76	2.73	0.59	-	16.70
16hr	1.20	21.3	5.16	2.19	2.56	0.61	-	18.59

Table 3.24 n-Hexane cracking activity as a function of pulse number.

HYST 873			673K			Dry mass=0.0152g		
Product formation / 10^{19} molecules g^{-1}								
Pulse	C_2	C_3	iC_4	nC_4	iC_5	nC_5	iC_6	Σ_{hex}
1	3.45	58.67	16.13	5.78	5.81	1.45	-	51.14
2	3.38	57.17	15.61	5.64	5.63	1.32	-	49.67
3	3.17	54.28	14.26	5.20	5.35	1.22	-	46.65
4	2.94	50.17	12.81	4.77	5.00	1.09	-	42.86
5	2.91	48.70	12.39	4.62	4.84	1.09	-	41.60
6	2.74	46.43	11.36	4.29	4.63	1.04	-	39.29
7	2.74	46.33	11.08	4.15	4.58	0.95	-	38.84
8	2.65	45.11	10.46	4.04	4.38	0.89	-	37.50
9	2.54	43.23	9.83	3.84	4.20	0.87	-	35.80
10	2.86	42.20	9.68	3.67	4.04	0.87	-	35.05
11	2.55	43.07	9.52	3.73	4.15	0.84	-	35.38
12	2.48	41.68	9.14	3.58	3.98	0.82	-	34.15
13	2.48	41.96	8.93	3.52	3.96	0.79	-	34.07
14	2.47	41.30	8.72	3.57	4.04	0.45	-	33.41
15	2.41	40.27	8.39	3.34	3.98	0.55	-	32.53
16hr	6.47	46.7	10.4	4.16	4.58	1.17	-	40.01

Table 3.25 n-Hexane cracking activity as a function of pulse number.

HYST 923			673K			Dry mass=0.0152g		
Product formation / 10^{19} molecules g^{-1}								
Pulse	C_2	C_3	iC_4	nC_4	iC_5	nC_5	iC_6	Σ_{hex}
1	0.52	8.83	0.95	0.57	0.64	-	-	6.14
2	0.52	8.79	0.95	0.56	0.50	-	-	5.99
3	0.53	8.94	0.99	0.58	0.39	-	-	6.02
4	0.51	8.46	0.90	0.56	0.36	-	-	5.67
5	0.54	9.12	1.00	0.59	0.52	-	-	6.23
6	0.49	8.19	0.85	0.52	0.45	-	-	5.55
7	0.48	7.93	0.83	0.53	0.45	-	-	5.41
8	0.52	8.75	0.99	0.57	0.48	-	-	5.99
9	0.53	8.86	1.02	0.59	0.57	-	-	6.16
10	0.52	8.73	1.01	0.59	0.58	-	-	6.09
11	0.48	8.03	0.90	0.54	0.71	-	-	5.73
12	0.50	8.51	0.98	0.57	0.40	-	-	5.79
13	0.49	8.84	0.89	0.55	0.50	-	-	5.96
14	-	-	-	-	-	-	-	-
15	0.50	8.34	0.88	0.52	0.37	-	-	5.58
16hr	0.43	6.86	0.67	0.46	0.26	0.29	-	4.79

Table 3.26: n-Hexane cracking activity as a function of pulse number.

HYST 973			673K			Dry mass=0.0151g		
Product formation / 10^{19} molecules g^{-1}								
Pulse	C_2	C_3	iC_4	nC_4	iC_5	nC_5	iC_6	Σ_{hex}
1	0.31	4.32	0.28	0.26	0.11	-	-	2.72
2	0.34	4.93	0.33	0.2	0.13	-	-	3.04
3	0.28	3.86	0.24	0.22	0.09	-	-	2.41
4	0.33	4.73	0.31	0.28	0.27	-	-	3.09
5	0.33	4.67	0.29	0.27	0.12	-	-	2.92
6	0.30	4.14	0.26	0.23	0.10	-	-	2.58
7	0.32	4.73	0.33	0.29	0.13	-	-	2.99
8	0.35	5.28	0.37	0.30	0.16	-	-	3.34
9	0.31	4.29	0.24	0.24	0.11	-	-	2.66
10	0.27	3.03	0.18	0.16	0.05	-	-	1.87
11	0.37	5.88	0.46	0.37	0.20	-	-	3.78
12	0.33	4.97	0.36	0.31	0.15	-	-	3.17
13	0.17	4.79	0.33	0.26	0.14	-	-	2.96
14	0.30	4.43	0.28	0.24	0.20	-	-	2.83
15	0.31	4.45	0.28	0.24	0.12	-	-	2.78
16hr	0.25	3.15	0.20	0.21	0.08	-	-	2.00

Table 3.27: n-Hexane cracking activity as a function of pulse number.

HYST 1023			673K			Dry mass=0.0161g		
Product formation / 10^{19} molecules g^{-1}								
Pulse	C_2	C_3	iC_4	nC_4	iC_5	nC_5	iC_6	Σ_{hex}
1	0.22	2.61	0.14	0.16	0.06	-	-	1.92
2	0.28	4.01	0.25	0.22	0.17	-	-	2.55
3	0.23	3.08	0.18	0.18	0.13	-	-	1.97
4	0.22	2.75	0.15	0.17	0.07	-	-	1.72
5	0.24	3.32	0.20	0.20	0.10	-	-	2.09
6	0.24	3.26	0.20	0.19	0.09	-	-	2.05
7	0.23	2.99	0.18	0.18	0.08	-	-	1.88
8	0.23	3.01	0.18	0.18	0.08	-	-	1.89
9	0.23	3.05	0.19	0.19	0.08	-	-	1.92
10	0.26	3.64	0.24	0.20	0.10	-	-	2.28
11	0.24	3.25	0.20	0.18	0.09	-	-	2.03
12	0.24	2.99	0.19	0.20	0.07	-	-	1.89
13	0.28	4.27	0.31	0.23	0.15	-	-	2.71
14	0.24	3.06	0.18	0.19	0.14	-	-	1.97
15	0.24	3.11	0.18	0.16	0.08	-	-	1.93
16hr	0.21	2.23	0.12	0.12	0.05	-	-	1.39

Table 3.28 n-Hexane cracking activity as a function of pulse number.

HYST 1073			673K			Dry mass=0.0157g		
Product formation / 10^{19} molecules g^{-1}								
Pulse	C_2	C_3	iC_4	nC_4	iC_5	nC_5	iC_6	Σ_{hex}
1	0.13	0.99	0.07	0.07	-	-	-	0.59
2	0.13	1.07	0.07	0.07	-	-	-	0.67
3	0.14	1.16	0.08	0.09	-	-	-	0.74
4	0.09	1.10	0.07	0.09	-	-	-	0.69
5	0.13	1.09	-	-	-	-	-	0.59
6	-	-	-	-	-	-	-	-
7	-	-	-	-	-	-	-	-
8	0.11	0.85	0.06	0.06	-	-	-	0.54
9	0.13	0.91	0.07	0.11	-	-	-	0.62
10	0.11	0.79	0.06	0.07	-	-	-	0.52
11	0.12	0.85	0.07	0.10	-	-	-	0.58
12	0.12	0.82	0.07	0.08	-	-	-	0.55
13	0.12	0.82	-	0.13	-	-	-	0.54
14	0.11	0.80	-	0.11	-	-	-	0.51
15	0.12	0.88	-	0.08	-	-	-	0.53
16	0.11	0.68	0.04	0.07	0.03	-	-	0.48

Table 3.29: n-Hexane cracking activity as a function of pulse number.

HYMST 748Ex			673K			Dry mass=0.0157g		
Product formation / 10^{19} molecules g^{-1}								
Pulse	C_2	C_3	iC_4	nC_4	iC_5	nC_5	iC_6	Σ_{hex}
1	3.43	59.80	17.45	6.02	3.89	1.32	-	51.03
2	3.65	56.84	16.12	5.49	5.83	1.29	-	49.98
3	3.23	55.39	15.57	5.44	5.82	1.31	-	48.72
4	3.07	51.52	14.46	5.02	5.41	1.14	-	45.23
5	2.97	50.44	13.76	4.88	5.53	1.18	-	44.23
6	2.98	50.35	13.29	4.77	5.41	1.18	-	43.70
7	3.03	51.21	13.58	4.75	5.61	0.99	-	44.34
8	2.85	47.37	12.40	4.43	6.13	-	-	40.96
9	2.87	47.25	12.32	4.44	5.17	1.09	-	40.97
10	2.79	46.50	11.72	4.27	4.97	1.07	-	39.87
11	2.80	47.19	11.78	4.27	5.09	0.99	-	40.30
12	2.74	46.08	11.27	4.12	4.91	1.03	-	39.16
13	2.71	44.92	11.08	4.00	5.68	-	-	38.15
14	2.81	46.88	11.38	4.13	5.00	1.06	-	39.77
15	2.69	44.64	10.79	3.92	4.67	0.99	-	37.74
16hr	2.59	42.1	10.2	3.88	4.64	1.02	-	36.02

Table 3.30: n-Hexane cracking activity as a function of pulse number.

HYMST 768Ex			673K			Dry mass=0.0148g		
Product formation / 10^{19} molecules g^{-1}								
Pulse	C_2	C_3	iC_4	nC_4	iC_5	nC_5	iC_6	Σ_{hex}
1	5.88	84.03	29.54	9.17	10.36	2.10	-	80.17
2	3.46	60.88	19.59	6.54	7.76	1.70	-	56.90
3	3.41	57.29	18.20	6.05	7.06	1.52	-	53.10
4	3.26	55.54	16.97	5.78	7.06	1.54	-	51.19
5	3.23	54.40	16.37	5.61	6.73	1.42	-	49.72
6	3.18	53.43	15.70	5.42	6.82	1.41	-	48.71
7	3.04	51.18	14.58	5.10	6.38	1.29	-	46.12
8	3.03	50.39	14.26	5.01	6.23	1.28	-	45.31
9	2.98	49.04	13.90	4.99	6.14	1.27	-	44.28
10	2.95	48.88	13.52	4.78	6.16	1.26	-	43.81
11	2.84	46.86	12.90	4.49	5.92	1.15	-	41.86
12	2.81	45.91	12.61	4.44	4.51	-	-	39.02
13	2.67	44.07	11.76	4.22	5.42	1.01	-	38.94
14	2.73	-	-	4.18	-	0.97	-	4.51
15	-	-	-	-	-	-	-	-
16hr	2.88	47.80	12.60	4.51	5.81	1.07	-	42.00

Table 3.31: n-Hexane cracking activity as a function of pulse number.

HYMST 783Ex			673K			Dry mass=0.0154g		
Product formation / 10^{19} molecules g^{-1}								
Pulse	C_2	C_3	iC_4	nC_4	iC_5	nC_5	iC_6	Σ_{hex}
1	4.29	76.04	25.99	8.38	8.87	1.90	-	71.34
2	4.14	73.05	24.34	7.87	8.51	1.93	-	68.08
3	-	-	-	-	-	-	-	-
4	3.87	63.71	20.08	6.69	7.93	1.75	-	59.06
5	3.60	61.66	18.96	6.41	7.51	1.58	-	56.52
6	2.71	60.28	18.63	6.34	7.32	1.48	-	55.02
7	-	-	-	-	-	-	-	-
8	2.73	59.75	17.68	6.08	7.25	1.41	-	53.84
9	3.30	56.90	16.86	5.76	7.10	1.34	-	51.66
10	3.21	54.32	15.81	5.45	6.79	1.25	-	49.10
11	3.23	53.56	15.43	5.33	6.71	1.22	-	48.31
12	3.18	52.65	14.89	5.13	6.52	1.14	-	47.12
13	3.15	51.50	14.47	5.08	6.42	1.20	-	46.18
14	2.97	49.49	13.62	4.81	6.84	1.76	-	45.19
15	3.09	50.02	13.77	4.83	6.22	1.18	-	44.61
16hr	2.98	50.6	13.90	4.98	6.29	1.76	-	45.59

Table 3.32: n-Hexane cracking activity as a function of pulse number.

HYMST 798Ex			673K			Dry mass=0.0153g		
Product formation / 10^{19} molecules g^{-1}								
Pulse	C_2	C_3	iC_4	nC_4	iC_5	nC_5	iC_6	Σ_{hex}
1	3.85	66.87	21.76	7.09	8.28	1.76	-	62.32
2	3.70	65.03	20.75	6.80	8.23	1.93	-	60.58
3	3.55	62.91	19.42	6.42	7.80	1.61	-	57.71
4	3.41	60.12	18.29	6.23	7.51	1.59	-	55.13
5	3.03	52.34	15.42	5.31	6.50	1.43	-	47.61
6	3.07	52.16	15.20	5.22	6.48	1.33	-	47.23
7	3.04	49.70	13.60	4.74	5.67	1.17	-	43.79
8	2.96	50.30	14.06	4.92	6.16	1.26	-	44.97
9	2.91	49.03	13.48	4.75	5.99	0.83	-	43.32
10	2.85	48.47	13.23	4.66	5.92	1.27	-	43.10
11	2.81	46.97	12.79	4.45	5.79	1.11	-	41.67
12	2.79	46.65	12.47	4.37	5.53	1.08	-	40.99
13	2.80	46.04	12.06	2.28	5.52	1.14	-	39.06
14	2.73	45.86	11.83	4.20	5.49	1.04	-	39.97
15	2.66	44.60	11.33	4.13	5.16	0.95	-	38.59
16hr	2.70	45.3	12.00	4.36	5.34	1.16	-	39.87

Table 3.33: n-Hexane cracking activity as a function of pulse number.

HYST 823Ex			673K			Dry mass=0.0156g		
Product formation / 10^{19} molecules g^{-1}								
Pulse	C_2	C_3	iC_4	nC_4	iC_5	nC_5	iC_6	Σ_{hex}
1	6.79	112.21	35.35	11.38	8.63	2.20	0.10	98.65
2	6.80	113.12	35.36	11.23	9.29	2.18	0.12	99.57
3	6.34	106.31	32.00	10.27	8.75	2.06	0.07	92.53
4	6.16	103.17	30.00	9.73	8.46	1.95	0.07	88.87
5	5.66	95.37	26.73	8.77	7.97	1.80	0.06	81.44
6	5.70	95.48	25.83	8.52	8.14	1.61	0.09	80.76
7	5.53	91.78	24.12	8.09	7.69	1.58	0.04	76.97
8	5.36	89.18	22.88	7.61	7.34	1.55	0.04	74.15
9	5.27	87.00	21.78	7.36	9.02	-	0.04	72.24
10	5.18	85.41	21.11	7.18	7.39	1.48	0.11	70.79
11	5.25	86.15	20.97	7.04	7.17	1.07	-	70.37
12	5.34	87.23	20.72	6.94	7.49	1.06	0.03	70.99
13	4.98	80.87	18.83	6.54	9.35	-	-	66.80
14	4.91	81.25	18.48	6.39	6.60	1.36	0.03	65.51
15	4.97	84.67	19.31	6.58	3.05	1.37	0.03	64.97
16hr	-	-	-	-	-	-	-	-

Table 3.34: n-Hexane cracking activity as a function of pulse number.

HYMST 848Ex			673K			Dry mass=0.0157g		
Product formation / 10^{19} molecules g^{-1}								
Pulse	C_2	C_3	iC_4	nC_4	iC_5	nC_5	iC_6	Σ_{hex}
1	3.68	66.99	20.54	6.67	7.83	1.67	-	60.78
2	3.45	61.39	18.71	6.31	7.43	1.62	-	56.07
3	3.47	61.30	18.54	6.22	7.41	1.59	-	55.81
4	3.21	56.43	17.00	5.67	7.14	1.44	-	51.55
5	3.12	54.32	16.01	5.44	6.91	1.39	-	49.42
6	3.21	54.97	16.03	5.47	6.75	1.41	-	49.69
7	3.08	52.81	15.05	5.14	6.61	1.31	-	47.49
8	3.03	51.94	14.61	5.08	6.42	1.28	-	46.52
9	2.84	48.05	13.27	4.77	6.02	1.28	-	43.08
10	2.78	47.17	12.70	4.55	7.08	-	-	41.91
11	2.89	49.40	13.29	4.72	6.12	1.20	-	43.77
12	2.83	47.46	12.82	4.57	5.98	1.18	-	42.23
13	2.84	47.62	12.48	4.45	5.79	1.22	-	41.89
14	2.62	44.16	11.28	4.08	5.40	2.12	-	39.46
15	2.64	44.67	11.33	4.13	5.38	1.09	-	38.91
16hr	1.71	28.2	6.62	2.61	3.37	0.74	-	24.25

Table 3.35: n-Hexane cracking activity as a function of pulse number.

HYST 873Ex			673K			Dry mass=0.0153g		
Product formation / 10^{19} molecules g^{-1}								
Pulse	C_2	C_3	iC_4	nC_4	iC_5	nC_5	iC_6	Σ_{hex}
1	5.57	91.18	27.32	9.36	7.81	1.90	-	79.99
2	5.47	88.71	25.91	8.89	7.49	1.87	-	77.18
3	5.34	87.02	24.46	8.49	7.30	1.79	-	74.83
4	-	-	-	-	6.93	1.65	-	7.15
5	4.99	80.98	21.37	7.58	6.82	1.60	-	68.47
6	4.85	77.76	20.08	7.10	6.58	1.56	-	65.40
7	4.64	75.13	19.93	6.77	6.43	1.57	-	63.58
8	4.68	75.43	18.53	6.70	6.76	1.22	-	62.75
9	4.56	72.88	17.67	6.34	6.28	1.27	-	60.26
10	4.46	71.28	16.94	6.11	5.91	1.27	-	58.48
11	4.44	71.00	16.64	6.03	6.01	1.30	-	58.19
12	4.29	68.16	15.42	5.69	6.61	1.57	-	56.40
13	4.45	70.16	16.00	5.99	5.72	1.36	-	57.12
14	4.36	69.00	15.43	5.70	5.80	1.31	-	55.97
15	4.30	67.54	15.07	5.52	5.61	1.23	-	54.63
16hr	4.35	70.1	15.7	5.81	5.99	1.32	-	56.93

Table 3.36: n-Hexane cracking activity as a function of pulse number.

HYST 923Ex			673K			Dry mass=0.0158g		
Product formation / 10^{19} molecules g^{-1}								
Pulse	C_2	C_3	iC_4	nC_4	iC_5	nC_5	iC_6	Σ_{hex}
1	2.94	50.26	13.66	4.71	5.58	1.28	-	44.07
2	2.86	48.62	13.83	4.64	5.60	2.13	-	44.02
3	2.68	45.88	12.90	4.43	5.43	1.13	-	40.85
4	2.67	45.13	12.59	4.39	5.35	1.14	-	40.18
5	2.65	44.64	12.22	4.26	5.31	1.09	-	39.52
6	2.66	44.72	12.01	4.25	5.12.	1.10	-	39.33
7	2.60	43.53	11.52	4.03	5.01	1.08	-	38.07
8	2.49	41.43	10.88	3.91	4.92	0.94	-	36.29
9	2.51	42.14	10.82	3.86	4.89	0.97	-	36.58
10	2.47	40.97	10.46	3.84	4.66	1.08	-	35.63
11	2.46	40.70	10.28	3.75	4.65	1.00	-	35.23
12	2.39	39.66	9.88	3.63	4.49	0.95	-	34.17
13	2.35	39.29	9.60	3.51	4.47	0.95	-	33.69
14	2.37	38.86	9.49	3.52	4.44	0.93	-	33.37
15	2.35	38.51	9.25	3.37	4.28	0.86	-	32.74
16hr	2.20	35.9	8.63	3.04	4.81	2.99	-	32.96

Table 3.37 n-Hexane cracking activity as a function of pulse number.

HYST 973Ex			673K			Dry mass=0.0162g		
Product formation / 10^{19} molecules g^{-1}								
Pulse	C_2	C_3	iC_4	nC_4	iC_5	nC_5	iC_6	Σ_{hex}
1	3.35	47.18	12.50	4.71	4.99	1.08	-	41.24
2	2.37	39.68	11.71	4.12	4.90	1.11	-	36.19
3	2.30	38.31	11.52	3.98	4.85	1.03	-	35.16
4	2.10	34.90	10.03	3.62	4.40	0.95	-	31.71
5	2.08	34.55	9.76	3.55	4.26	0.94	-	31.18
6	2.03	33.59	9.29	3.40	4.12	0.91	-	30.12
7	2.09	34.48	9.59	3.50	4.21	0.93	-	30.95
8	1.81	29.84	8.00	2.95	4.44	-	-	26.52
9	1.91	31.57	8.51	3.14	4.70	-	-	28.11
10	1.88	31.35	8.30	3.06	4.03	0.56	-	27.70
11	1.94	32.31	8.59	3.11	4.00	0.74	-	28.55
12	1.94	31.99	8.49	3.06	4.72	-	-	28.28
13	1.93	31.66	8.31	3.00	4.00	0.54	-	27.80
14	1.86	30.73	7.91	2.94	4.39	-	-	26.88
15	1.77	29.45	7.40	2.80	3.53	0.66	-	25.61
16hr	1.41	23.1	6.35	2.31	2.84	0.62	-	20.68

Table 3.38: n-Hexane cracking activity as a function of pulse number.

HYST 1023Ex			673K			Dry mass=0.0153g		
Product formation / 10^{19} molecules g^{-1}								
Pulse	C_2	C_3	iC_4	nC_4	iC_5	nC_5	iC_6	Σ_{hex}
1	2.29	37.84	9.67	3.81	3.98	1.08	-	32.89
2	2.33	37.40	9.78	3.82	3.90	0.98	-	32.61
3	2.67	35.75	9.37	3.69	3.71	0.98	-	31.38
4	2.1	32.74	8.81	3.43	3.67	0.89	-	29.03
5	1.84	27.94	7.09	2.83	3.04	0.78	-	24.38
6	1.80	26.10	6.70	2.78	2.95	0.77	-	23.07
7	1.98	30.07	7.60	2.99	3.23	0.80	-	26.11
8	2.01	30.61	7.75	3.02	3.26	0.84	-	26.57
9	1.86	28.61	6.93	2.81	3.63	0.76	-	25.08
10	1.91	29.07	7.03	2.85	3.04	0.82	-	24.98
11	1.85	27.64	6.57	2.71	2.90	0.75	-	23.67
12	1.64	24.68	5.28	2.32	2.40	0.65	-	20.50
13	1.89	28.64	6.81	2.77	3.00	0.75	-	24.46
14	1.67	25.11	5.49	2.33	2.43	0.4	-	20.68
15	1.71	25.89	5.52	2.40	2.55	0.67	-	21.48
16hr	1.84	27.5	6.54	2.67	2.82	0.74	-	23.47

Table 3.39: n-Hexane cracking activity as a function of pulse number.

HYST 1073Ex			673K			Dry mass=0.0147g		
Product formation / 10^{19} molecules g^{-1}								
Pulse	C_2	C_3	iC_4	nC_4	iC_5	nC_5	iC_6	Σ_{hex}
1	0.71	12.12	2.26	1.05	0.81	0.25	-	9.39
2	1.08	15.04	3.99	1.73	1.04	0.26	-	12.78
3	0.86	13.80	2.71	1.25	0.98	0.28	-	10.88
4	-	14.01	2.85	1.30	0.99	0.28	-	10.83
5	0.84	13.48	2.70	1.26	1.07	0.22	-	10.74
6	0.91	14.48	2.99	1.36	1.05	0.29	-	11.56
7	0.89	14.28	2.87	1.26	1.03	0.30	-	11.30
8	0.92	14.66	3.04	1.42	0.83	-	-	11.30
9	0.86	13.81	2.72	1.25	0.98	0.30	-	10.91
10	0.88	14.11	2.79	1.31	1.09	0.20	-	11.16
11	0.85	13.64	2.64	1.24	0.94	0.28	-	10.71
12	0.90	14.42	2.89	1.34	1.00	0.27	-	11.39
13	0.83	13.42	2.56	1.20	0.94	0.27	-	10.50
14	0.34	13.33	2.54	1.20	0.93	0.26	-	10.26
15	0.91	14.63	2.91	1.32	1.16	0.15	-	11.52
16hr	0.85	13.4	2.62	1.18	1.35	0.53	-	11.08

Table 3.40: n-Hexane cracking activity as a function of pulse number.

Sample	Product formation / x10^{19}molecules g^{-1}				% coke
	iC_4 1st pulse	Σ_{hex} 1st pulse	Σ_{hex} 15 pulses	Σ_{hex}16hr one pulse	
NH_4YAS	0.29	0.91	13.12	1.29	1.2
NH_4YLS	8.11	29.03	388.90	25.14	0.4
HYMST 748	13.00	41.52	485.38	28.67	0.6
HYMST 768	17.77	54.88	555.61	37.88	0.8
HYMST 783	17.55	51.69	554.26	37.01	0.5
HYMST 798	11.95	38.70	446.38	32.02	0.5
HYST 823	37.75	99.78	1023.58	59.96	4.8
HYMST 848	6.15	21.70	282.68	18.59	0.6
HYST 873	16.13	46.65	585.94	40.01	0.6
HYST 923	0.95	6.14	88.19	4.79	0.5
HYST 973	0.28	2.72	43.14	2.00	0.4
HYST 1023	0.18	1.92	30.80	1.39	0.3
HYST 1073	0.07	0.59	8.73	0.48	0.5
HYMST 748Ex	17.54	51.03	644.15	36.02	2.1
HYMST 768Ex	29.54	56.90	737.46	42.00	1.2
HYMST 783Ex	25.99	71.34	803.11	45.59	1.4
HYMST 798Ex	21.67	62.32	706.04	39.06	1.4
HYST 823Ex	35.53	98.65	1173.99	-	2.1
HYST 848Ex	20.54	60.78	708.58	24.25	1.6
HYST 873Ex	27.32	79.99	957.05	56.93	1.6
HYST 923Ex	13.66	44.07	563.74	32.96	1.4
HYST 973Ex	12.50	41.24	453.80	20.68	0.6
HYST 1023Ex	9.67	32.89	386.89	23.47	0.3
HYST 1073Ex	2.71	10.88	165.23	11.08	0.2

Table 3.41: Activity and coke content for n-hexane cracking.

	C_4/C_2			iC_4/nC_4		
	Pulse		After	Pulse		After
	1st	15th	16 hr	1st	15th	16 hr
NH_4YAS	2.23	1.78	1.57	-	-	1.77
NH_4YLS	5.56	5.07	5.26	2.31	2.20	2.15
HYST 748	6.47	5.05	5.81	2.60	2.52	2.51
HYMST 768	7.18	5.82	5.94	2.86	2.61	2.65
HYMST 783	7.34	5.71	6.34	2.91	2.65	2.65
HYMST 798	6.49	5.62	6.34	2.75	3.52	2.59
HYST 823	8.50	4.98	5.30	3.40	2.94	2.82
HYMST 848	6.14	5.55	6.12	2.82	2.37	2.36
HYST 873	6.35	4.86	2.25	2.79	2.51	2.50
HYST 923	2.92	2.80	2.63	1.67	1.69	1.46
HYST 973	1.74	1.68	1.64	1.08	1.17	1.00
HYST 1023	0.91	1.42	1.29	0.87	1.12	0.80
HYST 1073	1.08	-	1.00	1.00	-	0.57
HYMST 748Ex	6.84	5.53	5.44	2.90	2.80	2.63
HYMST 768Ex	6.58	5.98	5.94	3.22	2.79	2.79
HYMST 783Ex	8.01	6.01	6.34	3.10	2.85	2.79
HYMST 798Ex	7.49	5.81	6.06	3.07	2.74	2.75
HYST 823Ex	6.88	5.21	5.51	3.10	2.93	2.90
HYMST 848Ex	7.37	5.86	5.40	3.07	2.74	2.54
HYST 873Ex	6.58	4.79	4.94	2.92	2.73	2.70
HYST 923Ex	6.25	5.37	5.30	2.90	2.74	2.84
HYST 973Ex	5.14	5.76	6.14	2.65	2.64	2.75
HYST 1023Ex	5.87	4.63	5.01	2.54	2.30	2.45
HYST 1073Ex	4.66	4.63	4.47	2.15	2.24	2.20

Table 3.42: Reaction product ratios - n-hexane cracking.

	iC_5/nC_5			C_2/iC_4 'CMR'		
	Pulse		After	Pulse		After
	1st	15th	16hr	1st	15th	16 hr
NH_4YAS	-	-	-	0.45	0.56	1.00
NH_4YLS	3.34	3.36	3.41	0.26	0.27	0.28
HYMST 748	3.93	4.73	4.05	0.21	0.26	0.24
HYMST 768	4.83	4.70	4.63	0.19	0.24	0.23
HYMST 783	4.29	5.02	5.01	0.18	0.24	0.22
HYMST 798	4.65	6.02	4.31	0.21	0.25	0.22
HYST 823	4.70	5.21	4.20	0.15	0.27	0.26
HYMST 848	4.27	4.54	4.20	0.23	0.26	0.23
HYST 873	4.00	7.24	3.91	0.21	0.29	0.62
HYST 923	-	-	0.90	0.55	0.57	0.64
HYST 973	-	-	-	1.11	1.11	1.25
HYST 1023	-	-	-	1.51	1.33	1.75
HYST 1073	-	-	-	1.85	-	2.75
HYMST 748Ex	2.94	4.72	4.55	0.20	0.69	0.25
HYMST 768Ex	4.93	5.37	5.43	0.20	0.23	0.23
HYMST 783Ex	4.67	5.27	3.57	0.16	0.22	0.21
HYMST 798Ex	4.70	5.43	4.60	0.18	0.23	0.23
HYST 823Ex	3.80	4.81	-	0.19	0.26	0.24
HYMST 848Ex	4.69	4.93	4.55	0.18	0.23	0.26
HYST 873Ex	4.11	4.56	4.54	0.20	0.28	0.28
HYST 923Ex	4.35	4.98	1.61	0.21	0.25	0.25
HYST 973Ex	4.62	5.34	4.58	0.27	0.24	0.22
HYST 1023Ex	3.68	3.80	3.81	0.24	0.31	0.28
HYST 1073Ex	3.24	7.73	2.55	0.31	0.31	0.32

Table 3.43: Reaction product ratios - n-hexane cracking.

	Σ_{hex} 15 pulses		iC_4 1st pulse	
	molecules $/10^{19}g^{-1}$	%age	molecules $/10^{19}g^{-1}$	%age
HYMST 748	159	33	4.5	35
HYMST 768	181	33	8.2	48
HYMST 783	249	45	8.4	48
HYMST 798	260	58	9.7	1
HYST 823	151	15	-2.2	-6
HYMST 848	425	150	14.4	234
HYST 873	371	63	11.2	69
HYST 923	475	540	12.7	1338
HYST 973	410	953	12.2	4357
HYST 1023	356	1148	9.5	5272
HYST 1073	154	1170	2.6	3771

Table 3.44: Change in activity on extraction - n-hexane cracking.

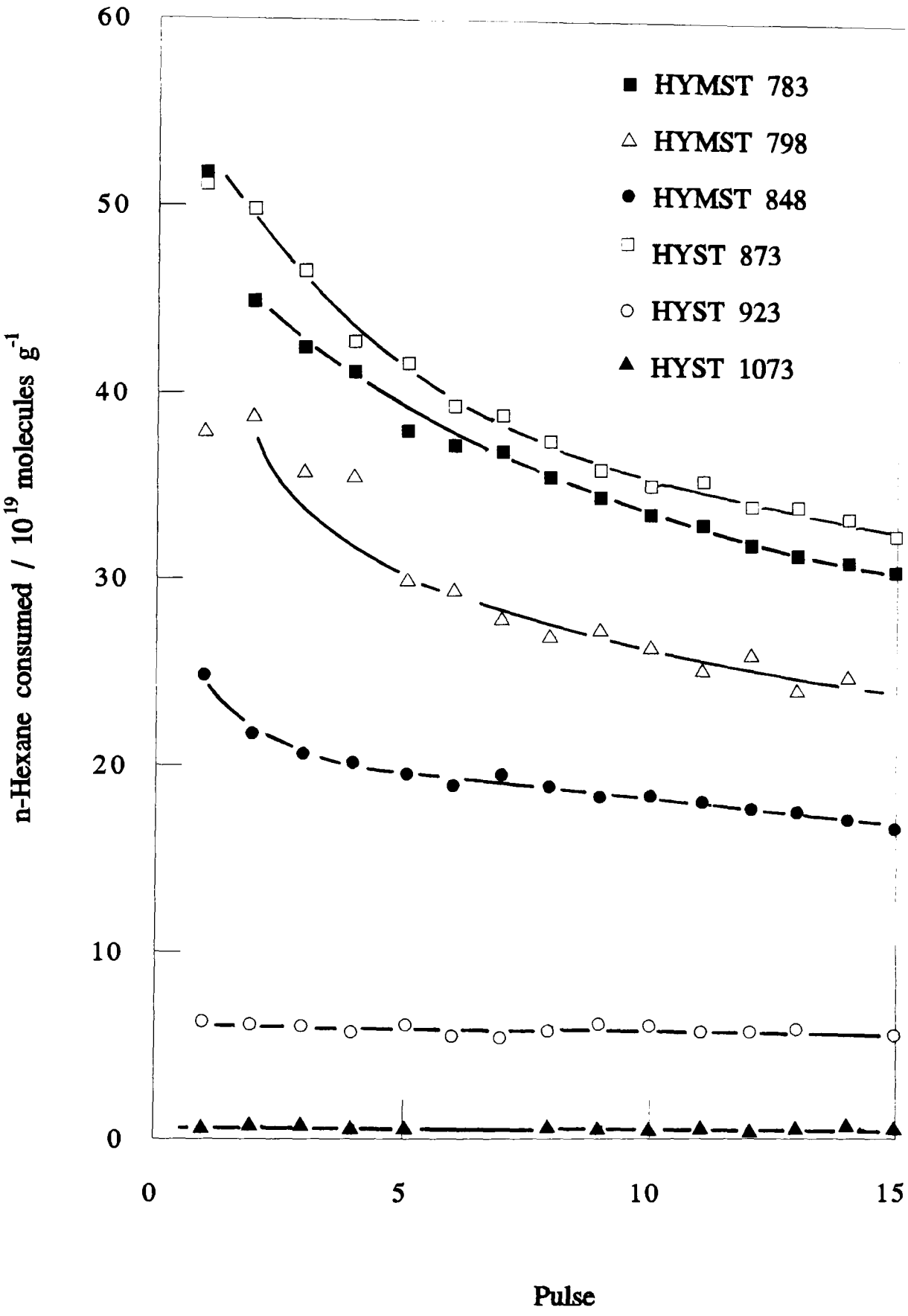

Figure 3.19: n-Hexane cracking - unextracted catalysts.

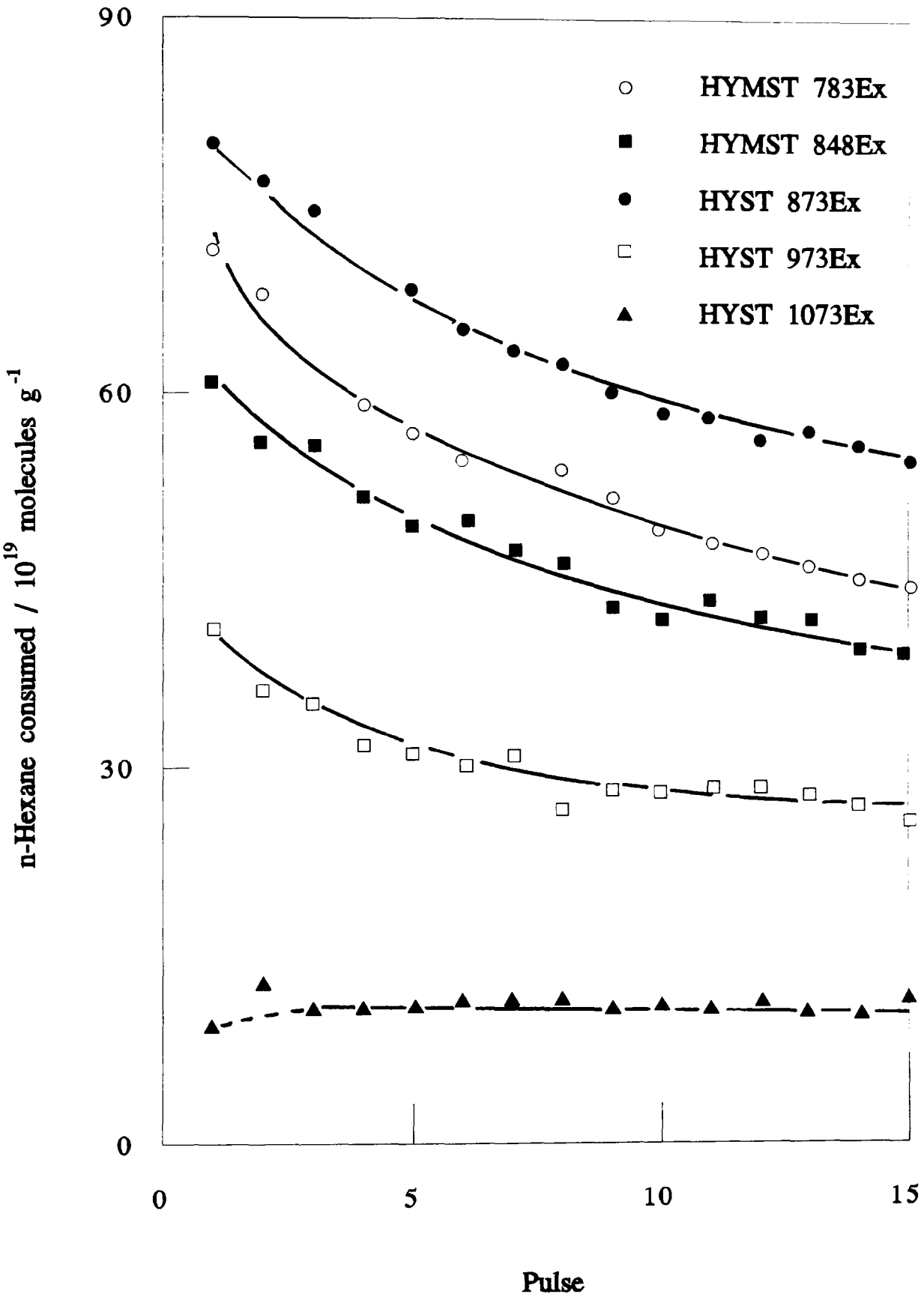

Figure3.20 : n-Hexane cracking - extracted catalysts.

3.22 Toluene Disproportionation - Pulse Flow Experiments

The disproportionation of toluene was studied at 673K using the pulse flow apparatus after the sample had been activated at 673K in flowing helium for sixteen hours. The results were obtained using the technique described in Section 2.34: constant masses and temperatures were used, the exact values of which are reported in the individual tables. As no deactivation was detected, ten pulses were deemed sufficient to assess the activity of each catalyst. The amount of benzene produced was chosen as the measure of activity as incomplete resolution of the dimethylbenzene isomers, from each other and from the tail of the unreacted toluene peak, made the sum of the products potentially unreliable. This problem could have been alleviated by changing the operating conditions of the gas chromatograph, but this would have been at the expense of other experimental variables.

The initial activity of each catalyst is therefore defined as the amount of detected benzene per pulse after ten pulses, which, where necessary, was averaged over the seventh to tenth pulse, a region in which the activity was essentially constant. This removes the possibility of any adsorption effects in the first few pulses distorting the reported activity. The results from the individual experiments are reported in tables 3.45 to 3.68, and are summarised in table 3.69. A selection of activity profiles spanning the range of activities are shown in figures 3.21 and 3.22.

$\overline{NH_4}$YAS	673K	0.0143g
Product formation /10^{18}molecules g^{-1}		
Pulse	Benzene	DMB	Total
1	5.04	1.67	6.71
2	4.35	1.63	5.98
3	4.79	1.79	6.58
4	4.32	1.71	6.03
5	4.74	2.48	7.22
6	4.66	2.51	7.17
7	4.85	2.68	7.53
8	5.12	3.11	8.23
9	5.27	2.70	7.97
10	6.82	3.58	10.40

Table 3.45: Toluene disproportionation activity as a function of pulse number.

NH_4YLS	673K	0.0155g
Product formation /10^{18}molecules g^{-1}		
Pulse	Benzene	DMB	Total
1	6.61	3.88	10.49
2	3.24	1.51	4.75
3	-	1.74	1.74
4	3.35	1.78	5.13
5	2.68	1.65	4.33
6	2.90	2.36	5.26
7	2.66	1.90	4.56
8	2.67	2.07	4.74
9	2.67	1.86	4.53
10	2.67	1.65	4.32

Table 3.46: Toluene disproportionation activity as a function of pulse number.

HYMST 748	673K	0.0124g
Product formation /10^{18}molecules g^{-1}		
Pulse	Benzene	DMB	Total
1	12.2	6.49	18.69
2	6.08	4.11	10.19
3	5.29	3.74	9.03
4	5.30	4.05	9.35
5	4.62	2.85	7.47
6	6.79	4.50	11.29
7	5.88	4.52	10.40
8	4.79	3.04	7.83
9	4.58	2.64	7.22
10	5.21	3.16	8.37

Table 3.47: Toluene disproportionation activity as a function of pulse number.

HYMSt 748Ex	673K	0.0144g
Product formation /10^{18}molecules g^{-1}		
Pulse	Benzene	DMB	Total
1	8.05	-	8.05
2	7.00	4.55	11.55
3	6.34	4.34	10.68
4	6.01	4.21	10.22
5	5.91	4.11	10.02
6	5.42	3.95	9.37
7	5.68	4.85	10.53
8	5.71	4.35	10.06
9	5.73	4.36	10.09
10	-	-	-

Table 3.48: Toluene disproportionation activity as a function of pulse number.

HYMST 768	673K	0.0157g	
Product formation /10^{18}molecules g^{-1}			
Pulse	Benzene	DMB	Total
1	27.0	11.50	38.50
2	9.63	4.98	14.61
3	11.20	7.38	18.58
4	7.31	4.02	11.33
5	6.99	4.10	11.09
6	7.74	4.44	12.18
7	6.88	3.74	10.62
8	6.89	3.75	10.64
9	6.88	3.62	10.50
10	6.81	3.73	10.54

Table 3.49: Toluene disproportionation activity as a function of pulse number.

HYMST 768Ex	673K	0.0162g	
Product formation /10^{18}molecules g^{-1}			
Pulse	Benzene	DMB	Total
1	7.13	4.33	11.46
2	6.45	4.47	10.92
3	6.31	4.31	10.62
4	6.16	4.31	10.47
5	6.05	4.30	10.35
6	5.93	4.40	10.33
7	6.09	4.31	10.40
8	5.91	4.43	10.34
9	5.86	4.43	10.29
10	5.86	4.58	10.44

Table 3.50: Toluene disproportionation activity as a function of pulse number.

HYMST 783	673K	0.0146g
Product formation /10^{18}molecules g^{-1}		
Pulse	Benzene	DMB	Total
1	8.29	5.53	13.82
2	5.48	3.85	9.33
3	4.99	3.40	8.39
4	5.01	3.56	8.57
5	4.85	3.79	8.64
6	4.79	3.76	8.55
7	4.80	3.75	8.55
8	4.78	3.29	8.07
9	4.93	3.52	8.45
10	4.81	3.19	8.00

Table 3.51: Toluene disproportionation activity as a function of pulse number.

HYMST 783Ex	673K	0.0154g
Product formation /10^{18}molecules g^{-1}		
Pulse	Benzene	DMB	Total
1	4.35	-	4.35
2	4.01	-	4.01
3	3.91	-	3.91
4	3.83	-	3.83
5	3.78	-	3.78
6	3.80	-	3.80
7	3.93	-	3.93
8	3.82	-	3.82
9	3.82	-	3.82
10	3.78	-	3.82

NB. Dimethylbenzene present although erratically resolved.

Table 3.52: Toluene disproportionation activity as a function of pulse number.

HYMST 798	673K	0.0152g	
Product formation /10^{18}molecules g^{-1}			
Pulse	Benzene	DMB	Total
1	10.70	7.49	18.19
2	5.13	3.58	8.71
3	4.61	3.48	8.09
4	4.52	3.31	7.83
5	5.42	3.99	9.41
6	4.59	3.44	8.03
7	4.51	3.79	8.30
8	4.48	3.50	7.98
9	5.83	4.68	10.51
10	4.58	3.56	8.14

Table 3.53: Toluene disproportionation activity as a function of pulse number.

HYMST 798Ex	673K	0.0164g	
Product formation /10^{18}molecules g^{-1}			
Pulse	Benzene	DMB	Total
1	10.60	6.93	17.53
2	8.16	5.48	13.64
3	9.85	7.02	16.87
4	7.74	5.44	13.18
5	7.61	5.36	12.97
6	7.57	5.36	12.93
7	8.88	6.45	15.33
8	7.70	5.11	12.81
9	7.74	5.46	13.20
10	7.89	4.86	12.75

Table 3.54: Toluene disproportionation activity as a function of pulse number.

HYST 823	673K	0.0161g
Product formation /10^{18}molecules g^{-1}		
Pulse	Benzene	DMB	Total
1	8.29	5.06	13.35
2	7.97	5.15	13.12
3	7.89	4.78	12.67
4	7.95	4.58	12.53
5	7.84	4.62	12.46
6	7.71	4.35	12.06
7	7.86	4.35	12.21
8	7.90	4.30	12.20
9	7.89	4.30	12.19
10	7.85	4.29	12.14

Table 3.55: Toluene disproportionation activity as a function of pulse number.

HYST 823Ex	673K	0.0155g
Product formation /10^{18}molecules g^{-1}		
Pulse	Benzene	DMB	Total
1	4.88	2.16	7.04
2	4.51	3.46	7.97
3	4.20	2.66	6.86
4	4.23	3.08	7.31
5	4.31	3.25	7.56
6	4.31	3.13	7.44
7	4.40	3.19	7.59
8	4.30	3.39	7.69
9	4.42	3.36	7.78
10	4.29	3.43	7.72

Table 3.56: Toluene disproportionation activity as a function of pulse number.

HYMST 848	673K	0.0154g	
Product formation /10^{18}molecules g^{-1}			
Pulse	Benzene	DMB	Total
1	4.29	3.28	7.57
2	3.72	2.49	6.21
3	3.55	1.79	5.34
4	3.50	2.43	5.93
5	3.54	2.17	5.71
6	3.89	2.60	6.49
7	3.49	1.93	5.42
8	3.44	2.23	5.67
9	3.42	2.38	5.80
10	3.40	2.25	5.65

Table 3.57: Toluene disproportionation activity as a function of pulse number.

HYMST 848Ex	673K	0.0152g	
Product formation /10^{18}molecules g^{-1}			
Pulse	Benzene	DMB	Total
1	8.96	5.55	14.51
2	8.35	5.55	13.90
3	8.11	5.43	13.54
4	7.92	5.73	13.65
5	7.77	4.94	12.71
6	7.56	5.17	12.73
7	7.50	5.06	12.56
8	7.53	4.92	12.45
9	7.60	5.19	12.79
10	7.57	4.94	12.51

Table 3.58: Toluene disproportionation activity as a function of pulse number.

HYST 873	673K	0.0155g
Product formation /10^{18}molecules g^{-1}		
Pulse	Benzene	DMB	Total
1	4.00	4.29	8.29
2	3.89	2.42	6.31
3	3.91	2.07	5.98
4	3.91	2.06	5.97
5	3.86	2.02	5.88
6	3.95	2.04	5.99
7	4.50	2.04	6.54
8	3.91	2.07	5.98
9	3.94	2.01	5.95
10	3.83	2.42	6.25

Table 3.59: Toluene disproportionation activity as a function of pulse number.

HYST 873Ex	673K	0.0155g
Product formation /10^{18}molecules g^{-1}		
Pulse	Benzene	DMB	Total
1	4.32	2.77	7.09
2	3.88	2.56	6.44
3	3.78	2.59	6.37
4	3.73	2.64	6.37
5	3.68	2.73	6.41
6	3.65	2.45	6.10
7	3.56	1.42	4.98
8	3.50	3.24	6.74
9	3.53	-	3.53
10	3.37	2.76	6.13

Table 3.60: Toluene disproportionation activity as a function of pulse number.

HYST 923	673K	0.0155g
Product formation /10^{18}molecules g^{-1}		
Pulse	Benzene	DMB	Total
1	1.90	4.29	6.19
2	2.54	2.42	4.96
3	2.66	2.07	4.73
4	2.72	2.06	4.78
5	2.37	2.02	4.39
6	2.36	2.04	4.40
7	3.25	2.04	5.29
8	2.51	2.07	4.58
9	2.52	2.01	4.53
10	2.42	2.13	4.55

Table 3.61: Toluene disproportionation activity as a function of pulse number.

HYST 923Ex	673K	0.0156g
Product formation /10^{18}molecules g^{-1}		
Pulse	Benzene	DMB	Total
1	2.12	1.28	3.40
2	2.07	1.24	3.31
3	2.07	1.26	3.33
4	2.00	1.25	3.25
5	2.04	1.23	3.27
6	2.04	1.22	3.26
7	1.99	1.22	3.21
8	1.99	1.20	3.19
9	1.97	1.20	3.17
10	1.98	1.20	3.18

Table 3.62: Toluene disproportionation activity as a function of pulse number.

HYST 973	673K	0.0153g
Product formation /10^{18}molecules g^{-1}		
Pulse	Benzene	DMB	Total
1	-	-	-
2	2.02	1.32	3.34
3	2.14	1.79	3.93
4	1.85	1.31	3.16
5	2.05	1.36	3.41
6	1.80	1.38	3.18
7	1.80	0.96	2.76
8	2.78	2.18	4.96
9	2.08	1.38	3.46
10	1.76	1.25	3.01

Table 3.63: Toluene disproportionation activity as a function of pulse number.

HYST 973Ex	673K	0.0153g
Product formation /10^{18}molecules g^{-1}		
Pulse	Benzene	DMB	Total
1	2.21	1.40	3.61
2	1.94	1.43	3.37
3	1.91	0.95	2.86
4	1.82	1.05	2.87
5	1.81	1.33	3.14
6	1.85	1.15	3.00
7	1.82	1.67	3.49
8	1.80	1.59	3.39
9	1.80	1.25	3.05
10	2.42	1.84	4.26

Table 3.64: Toluene disproportionation activity as a function of pulse number.

HYST 1023	673K	0.0160g
Product formation /10^{18}molecules g^{-1}		
Pulse	Benzene	DMB	Total
1	6.71	4.47	11.18
2	1.62	0.76	2.38
3	1.47	0.94	2.41
4	1.39	0.90	2.29
5	1.39	1.00	2.39
6	1.41	0.77	2.18
7	1.45	0.93	2.38
8	1.39	0.75	2.14
9	1.38	1.04	2.42
10	1.33	0.71	2.04

Table 3.65: Toluene disproportionation activity as a function of pulse number.

HYST 1023Ex	673K	0.0157g
Product formation /10^{18}molecules g^{-1}		
Pulse	Benzene	DMB	Total
1	1.93	1.10	3.03
2	1.80	1.35	3.15
3	1.71	0.84	2.55
4	1.70	0.93	2.63
5	1.72	0.97	2.69
6	1.72	0.97	2.69
7	1.70	1.52	3.22
8	1.72	1.02	2.74
9	2.05	1.30	3.35
10	1.75	1.13	2.88

Table 3.66: Toluene disproportionation activity as a function of pulse number.

HYST 1073	673K	0.0165g
Product formation /10^{18}molecules g^{-1}		
Pulse	Benzene	DMB	Total
1	0.72	0.54	1.26
2	0.70	0.76	1.46
3	0.73	0.27	1.00
4	0.66	0.34	1.00
5	0.82	0.45	1.27
6	0.66	0.37	1.03
7	0.70	0.65	1.35
8	0.66	0.36	1.02
9	0.68	0.55	1.23
10	0.67	0.36	1.03

Table 3.67: Toluene disproportionation activity as a function of pulse number.

HYST 1073Ex	673K	0.0155g
Product formation /10^{18}molecules g^{-1}		
Pulse	Benzene	DMB	Total
1	1.26	1.18	2.44
2	1.11	0.58	1.69
3	1.07	0.58	1.65
4	1.04	0.46	1.50
5	1.10	0.62	1.72
6	1.37	0.86	2.23
7	1.21	0.63	1.84
8	1.09	0.61	1.70
9	1.05	0.75	1.80
10	1.03	0.53	1.56

Table 3.68: Toluene disproportionation activity as a function of pulse number.

Sample	Benzene formation /10^{18}molecules g^{-1}		Coke / wt%	
	Unextracted	Extracted	Unextracted	Extracted
NH_4YAS	4.66	-	0.6	-
NH_4YLS	2.67	-	0.2	-
HYMST 748	5.11	5.63	0.9	0.5
HYMST 768	6.81	5.93	0.3	0.4
HYMST 783	4.83	3.84	0.2	0.3
HYMST 798	4.54	7.78	0.2	0.5
HYST 823	7.87	4.30	0.2	0.2
HYMST 848	3.44	7.55	0.3	0.5
HYST 873	3.91	3.54	0.2	0.1
HYST 923	20.6	1.99	0.3	0.2
HYST 973	1.86	1.82	0.3	0.1
HYST 1023	1.39	1.72	0.3	0.2
HYST 1073	0.67	1.09	0.1	0.1

Table 3.69: Activities and coke contents - toluene disproportionation

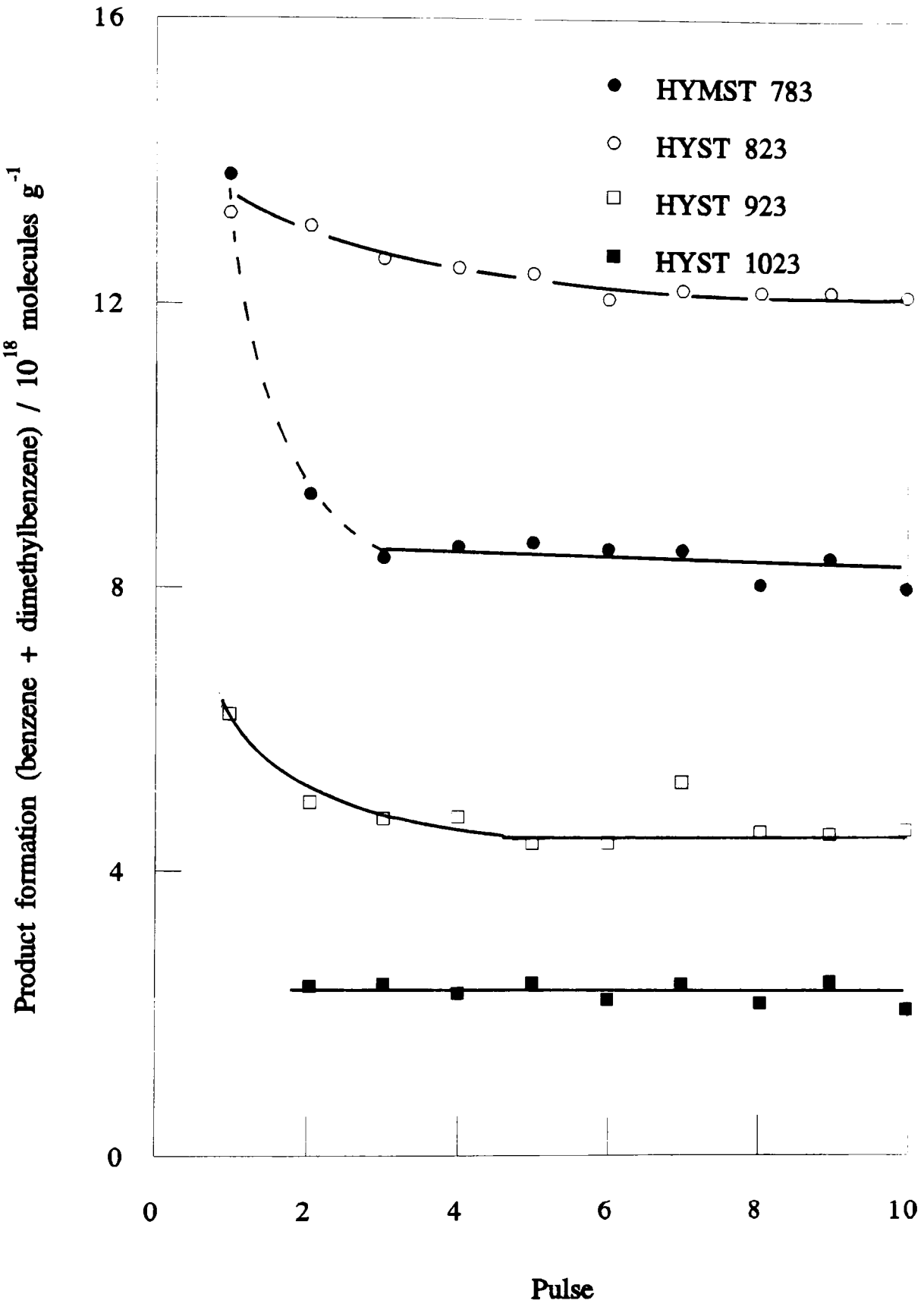

Figure 3.21: Toluene disproportionation - unextracted catalysts.

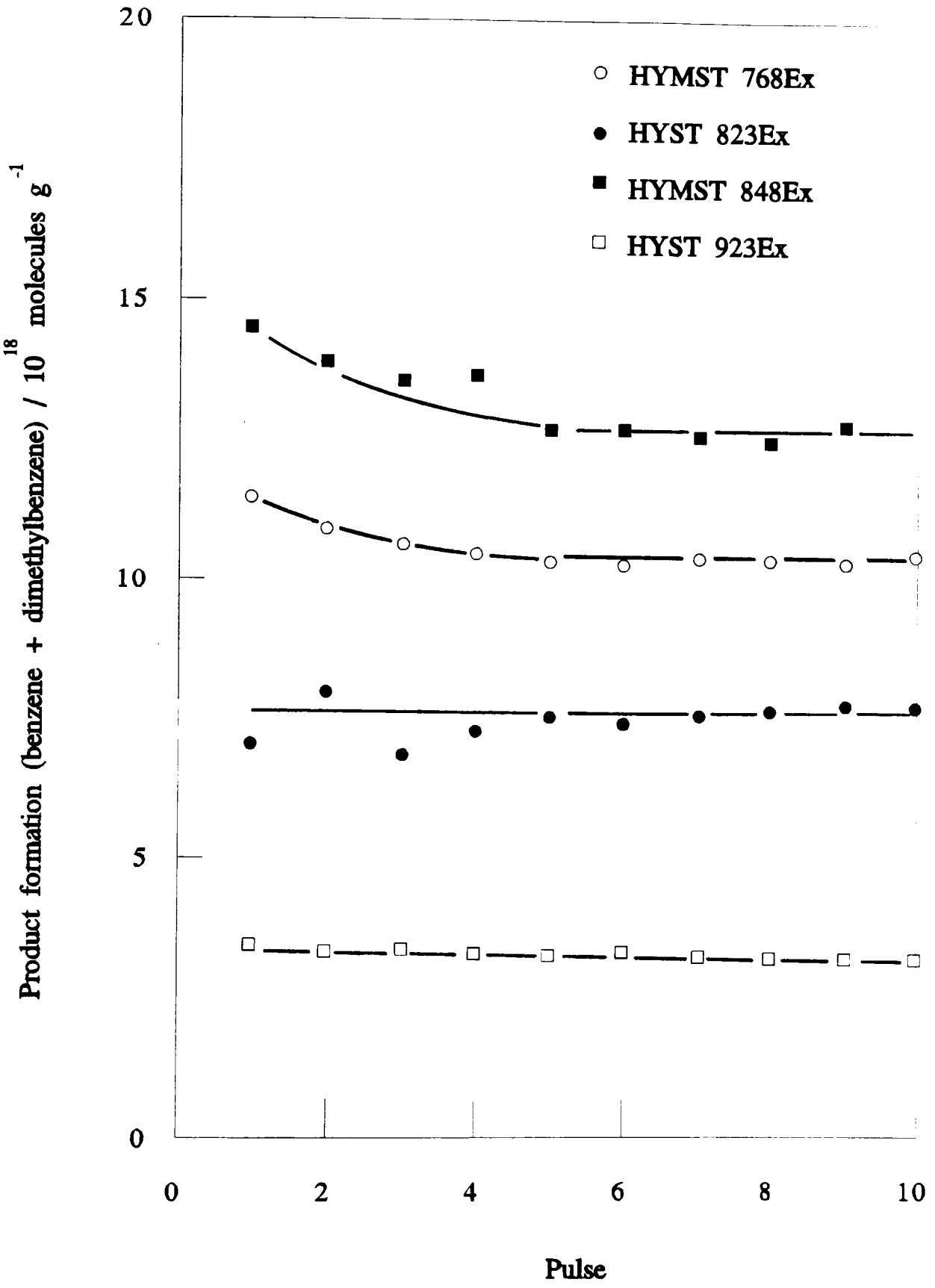

Figure 3.22: Toluene disproportionation - extracted catalysts.

3.23 Toluene Disproportionation - Continuous Flow Experiments

The work contained in this study encompassed a major shift in experimental procedure. Full details of the experimental procedure can be found in Section 2.36. Instead of presenting the catalyst as a fine powder supported on a sinter bed fused across a bulb reactor, broken pressed pellets were supported on a silica wool plug placed in a narrow tubular reaction vessel. Preliminary experiments were conducted to assess the extent of any change in the characteristics of the reaction. These experiments, performed on NH_4YAS and the extracted and the unextracted forms of HYST 873 and HYST 1073, are summarised in tables 3.70 to 3.74.

The period of time for total deactivation was found to decrease across the series: powder/bulb, pellets/bulb, powder/tube, pellets/tube. This is consistent with the proposition that a loose powder non-uniformly spread across a large surface area with respect to the sample bed depth is the least concentrated form of the catalyst, and compressed pellets contained within a tube - small surface area to bed depth - is the most concentrated. With the catalyst spread in a thin layer, it is probable that the bed is not of uniform thickness, and in some places might be absent completely.

The same argument explains the trend in the deactivation of the samples. If deactivation is caused by coke blocking up the mouths of the micropores, then it is obvious that if the activity is higher for the reason outlined above, and the reaction follows the same mechanism, the critical amount of coke will be formed quicker, hence speeding up the deactivation. The total reaction fell across the series above as far as can be determined, although in all cases the reaction ceased when the same amount of coke, $\approx$14 wt% for the unextracted catalysts and 18 wt% for the extracted catalysts, had been deposited. Either the activity has peaked within the first twenty minutes, and only the deactivation tail is observed, or the rate of deactivation proceeds at different rates depending on internal variables.

Since adsorption equilibrium was not attained early in an experiment, the initial activity is defined as the sum of the benzene and dimethylbenzene molecules detected after half an hour. This treatment of results is possible in

the continuous flow experiments because the performance of the gas chromatograph can be optimised since it is not connected in series with the reactor. In all but one case the initial activity increases across the same series, in the order above.

It was therefore concluded that the change in catalyst presentation or reactor geometry had the chemical consequence of "speeding up the reaction". This may be rationalised as follows. The weight of the sample used, to ensure that differential reactor conditions are maintained, is too small to cover the base of reactor uniformly, irrespective of whether powder or pellets are employed. Therefore, not all the reactant which passes through the reactor necessarily comes into contact with the sample. This results in lower conversions per gram of catalyst in the bulb reactor than in the tube reactor, where the bed is geometrically uniform. The increase in initial and maximum activity when proceeding from powder to pellets can be explained by assuming that the path length of a molecule within a powder crystallite is less than in a pellet, and so, once inside a pellet, the chances of a reactive interaction are increased.

Experiments were conducted across the range of unextracted catalysts in the pellet/tube form, unless otherwise indicated. Although the initial activity showed no consistent pattern, the catalysts remained active for longer as the total number of sites was decreased by dealumination, as can be seen from table 3.76 and figure 3.23. The coke content of the fully deactivated samples, measured by microanalysis, was found to be about 14.0 wt%, with one exception, implying that the reaction proceeds until a certain concentration of carbonaceous material retained within the pores of the catalyst causes deactivation by pore blockage or filling. In every case towards the end of the run the products cease desorbing from the catalyst in the order ortho-dimethylbenzene, meta- and para-dimethylbenzene, and finally benzene. This suggests that the reaction stops at some stage prior to the last of the benzene being eluted. Then, any products which remain within the pore structure can diffuse out, and as pore openings become increasingly restricted it is clear that only the benzene can diffuse out. Indeed the catalyst can be deemed to have

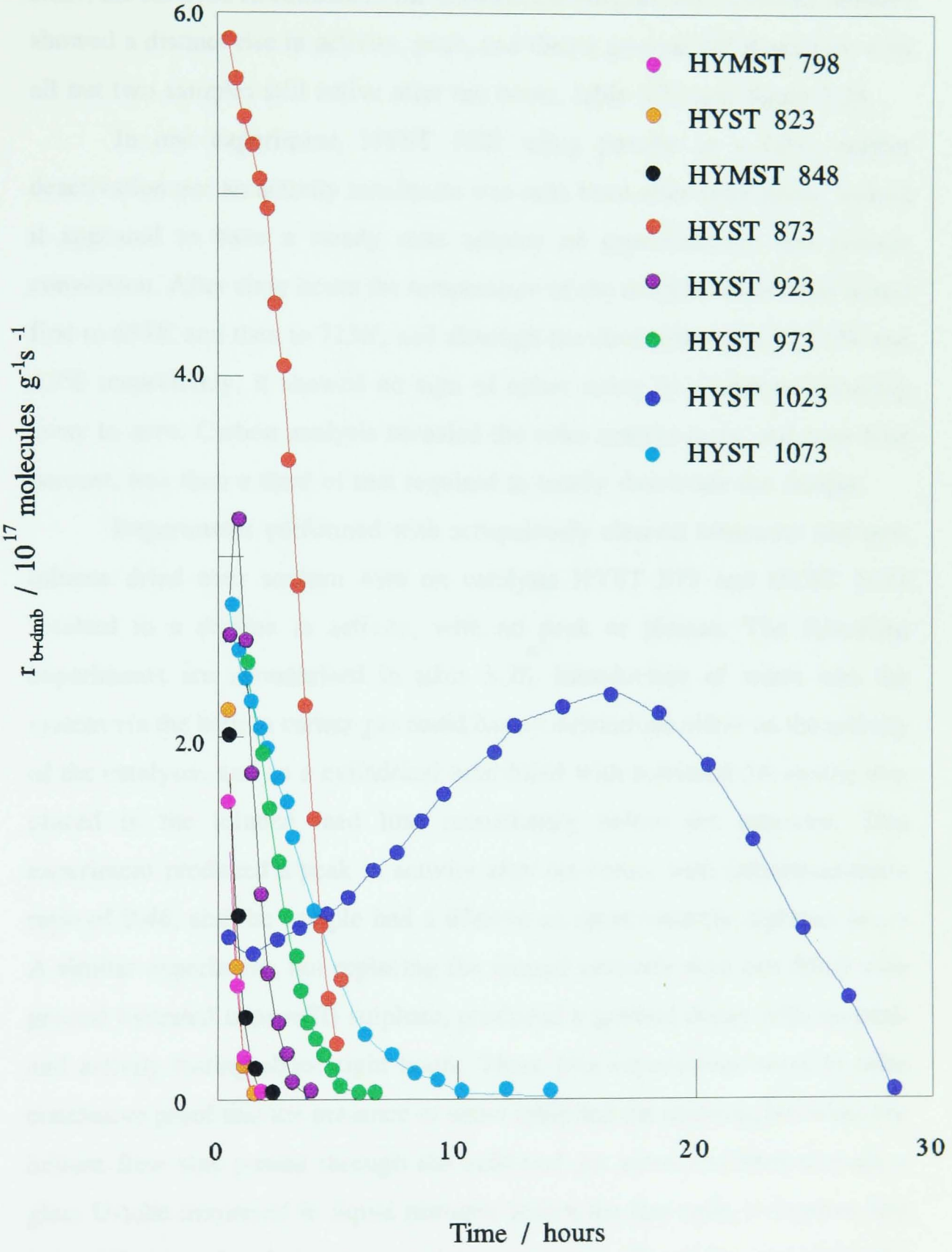

Figure 3.23: Toluene disproportionation over unextracted samples.

been deactivated not when the acid sites have become incapable of sustaining the reaction, but when the products cannot escape from, or the reactants cannot enter, the catalyst. In contrast to the unextracted samples, the extracted samples showed a distinct rise in activity, peak, and then a gradual fall in activity with all but two samples still active after ten hours, table 3.77 and figure 3.24.

In one experiment, HYST 1023 using powder in a tube, neither deactivation nor an activity maximum was seen even after sixty hours, indeed it appeared to have a steady state activity of approximately one percent conversion. After sixty hours the temperature of the reaction vessel was raised first to 693K and then to 713K, and although the conversion rose to 2.5% and 4.7% respectively, it showed no sign of either rising to a peak or decaying away to zero. Carbon analysis revealed the coke content to be just over four percent, less than a third of that required to totally deactivate the sample.

Experiments performed with scrupulously cleaned saturators and new toluene dried over sodium wire on catalysts HYST 873 and HYST 1023 resulted in a decline in activity, with no peak or plateau. The following experiments are summarised in table 3.78. Introduction of water into the system via the helium carrier gas could have a deleterious effect on the activity of the catalysts, and so a cylindrical tube filled with activated 3A zeolite was placed in the toluene feed line immediately before the saturator. This experiment produced a peak in activity after six hours, with initial/maximum ratio of 0.46, and the sample had a lifetime of approximately eighteen hours A similar experiment, but replacing the second saturator with one filled with ground hydrated copper(II) sulphate, produced a gradual decay with no peak and activity lasting about eight hours. These two experiments seem to offer conclusive proof that the presence of water inhibited the reaction, but when the helium flow was passed through the activated 3A sieve and then through a glass U-tube immersed in liquid nitrogen before the line split, to remove any traces of water, the effect on the activity was small. The slight increase in the activity in the second instance may be due to the Lewis acid sites being dehydrated to a greater extent,[230] thus having a different synergic effect with the framework aluminium. Alternatively, the experimental observation may be

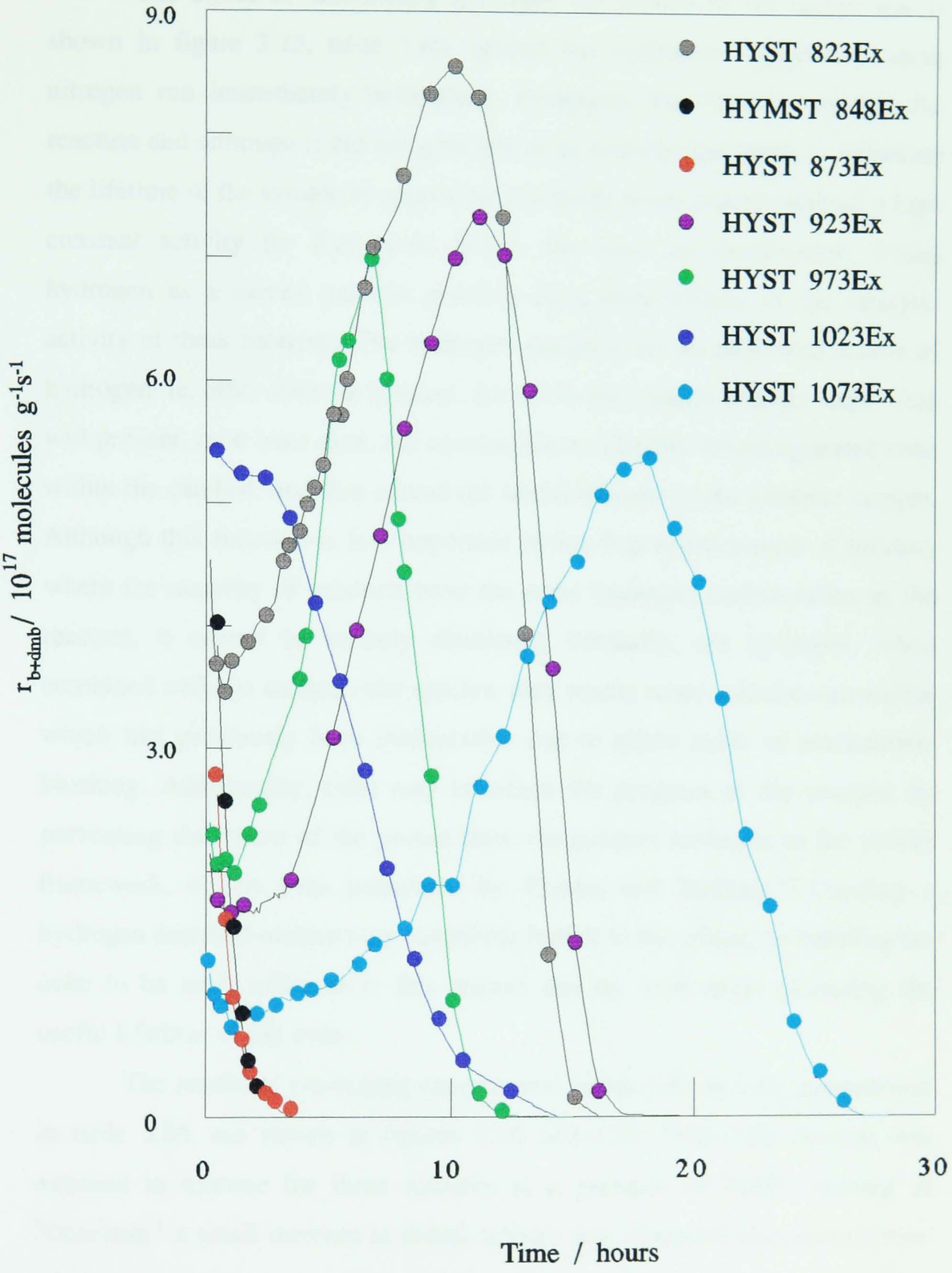

Figure 3.24: Toluene disproportionation over extracted samples.

due to what amounts to a further, very mild, low temperature steaming of the catalyst during the activation where wet helium is used.

The effect of substituting hydrogen for helium as the carrier gas is shown in figure 3.25, table 3.80, against the equivalent experiment using nitrogen run immediately beforehand. Hydrogen was found to sustain the reaction and although it did not give rise to an activity maximum, it increased the lifetime of the sample to approximately thirty hours and maintained a high constant activity for five hours before the onset of deactivation. Using hydrogen as a carrier gas can possibly have three effects of the catalytic activity of these catalysts. The hydrogen gas provides an additional source of hydrogen, ie. other than the reactant, for use in the hydride transfer steps. This will prevent, or at least slow, the accumulation of highly dehydrogenated coke within the catalyst, and thus extend the useful lifetime of the catalytic sample. Although this function is less important in the disproportionation of toluene, where the majority of products have the same hydrogen carbon ration as the reactant, it cannot be entirely dismissed. Secondly, the hydrogen, when combined with the surface coke species, may render some acid sites accessible which had previously been inaccessible due to either steric or electrostatic blocking. Additionally, coke may influence the progress of the reaction by preventing the return of the proton from the product molecule to the zeolite framework, as has been postulated by Rhodes and Rudham.[60] Creating a hydrogen enriched surface may contribute further to this effect, by enabling the coke to be more efficient in this respect and by once again extending the useful lifetime of the coke.

The results of pre-coking experiments, tables 3.81 to 3.84, summarised in table 3.85, are shown in figures 3.26 and 3.27. When the catalyst was exposed to toluene for three minutes at a pressure of 948Pa flowing at $30cm^3min^{-1}$ a small increase in initial activity was observed with deactivation taking three hours; an experiment following the normal procedure, but with a vapour pressure of toluene of approximately 1Pa in the bakeout stream produced a doubling in initial activity and deactivation in four hours was observed.

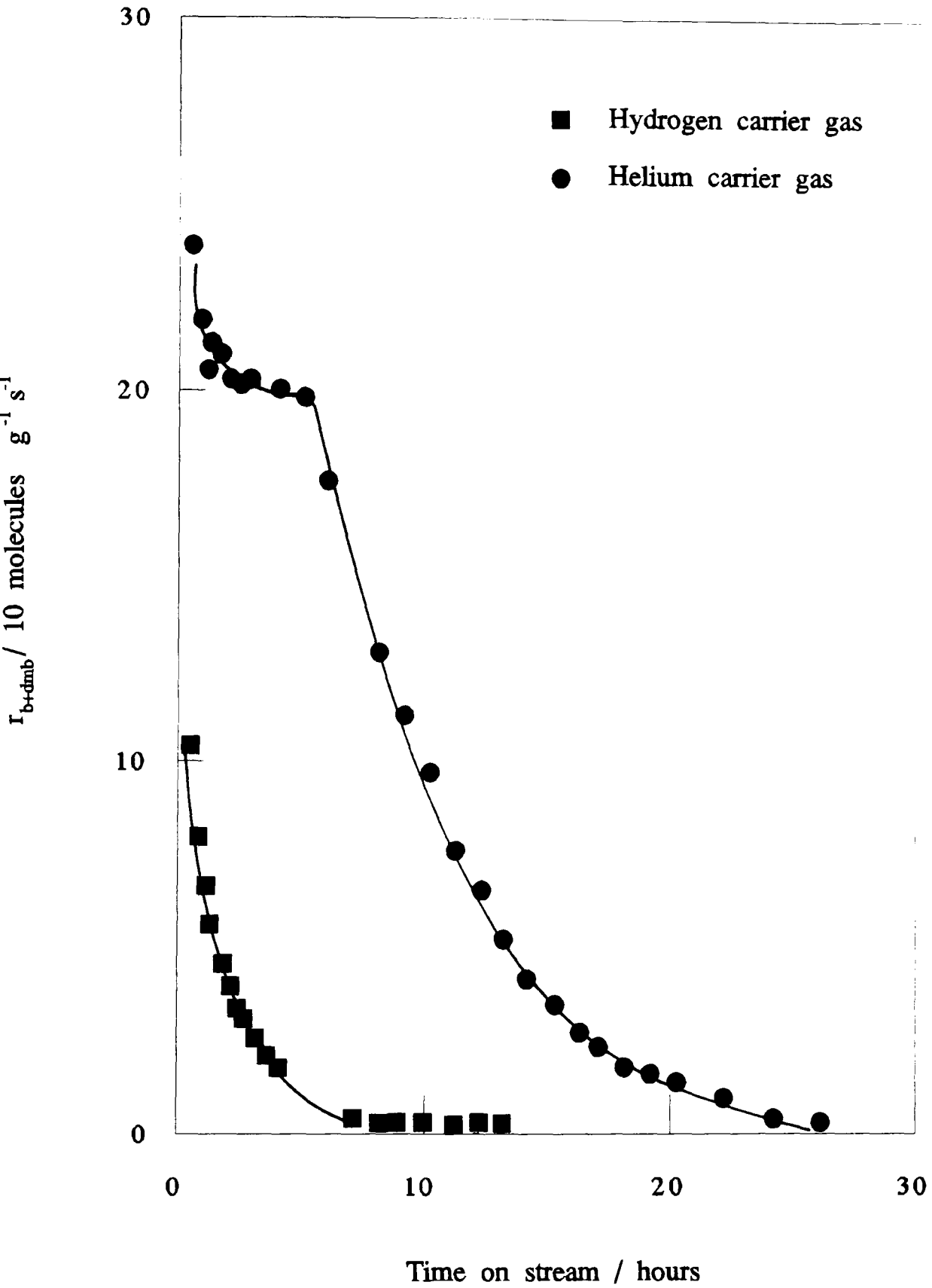

Figure 3.25: Toluene disproportionation - effect of carrier gas on the activity of HYST 1073.

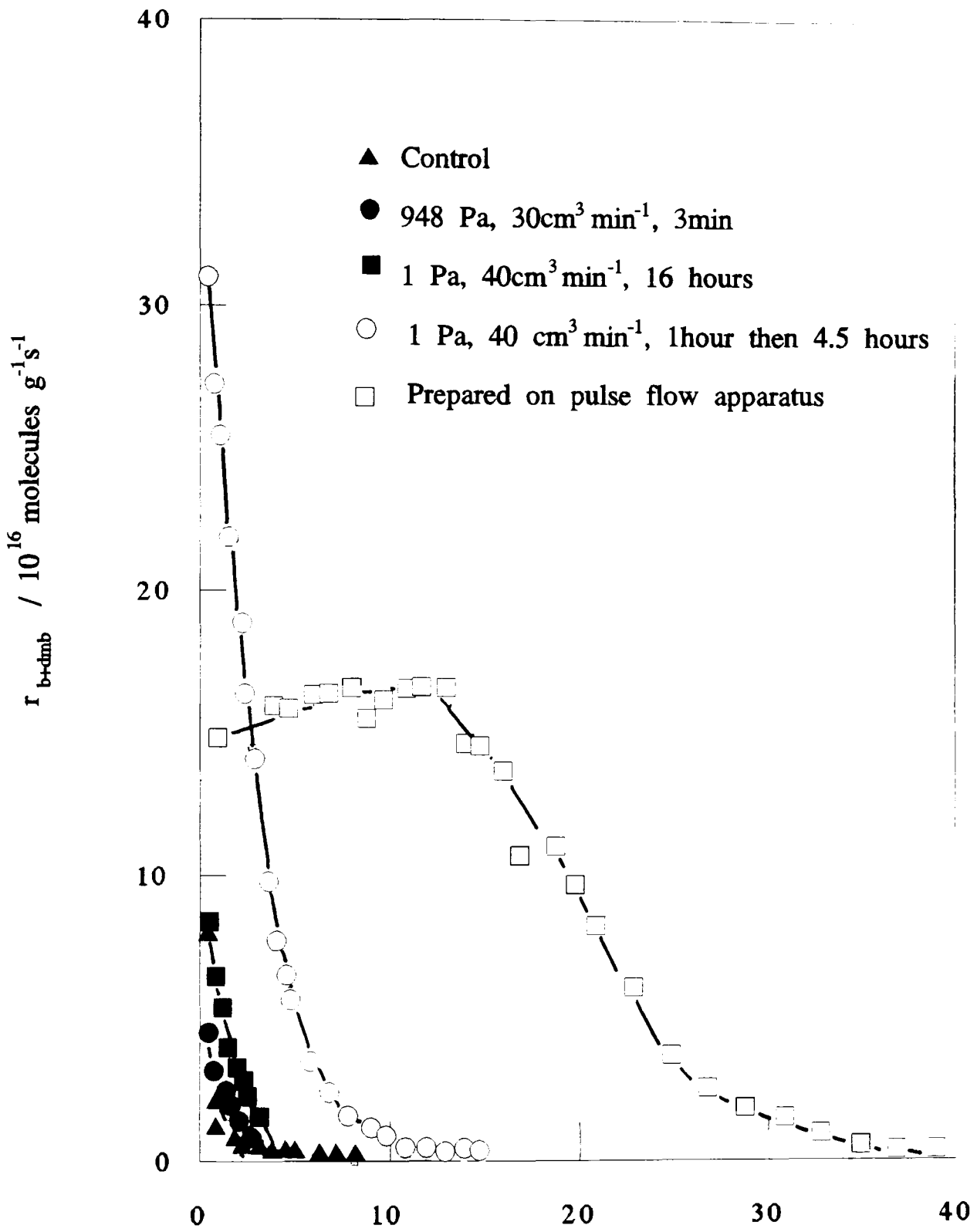

Figure 3.26: Toluene disproportionation on HYST 1073 precoking experiments.

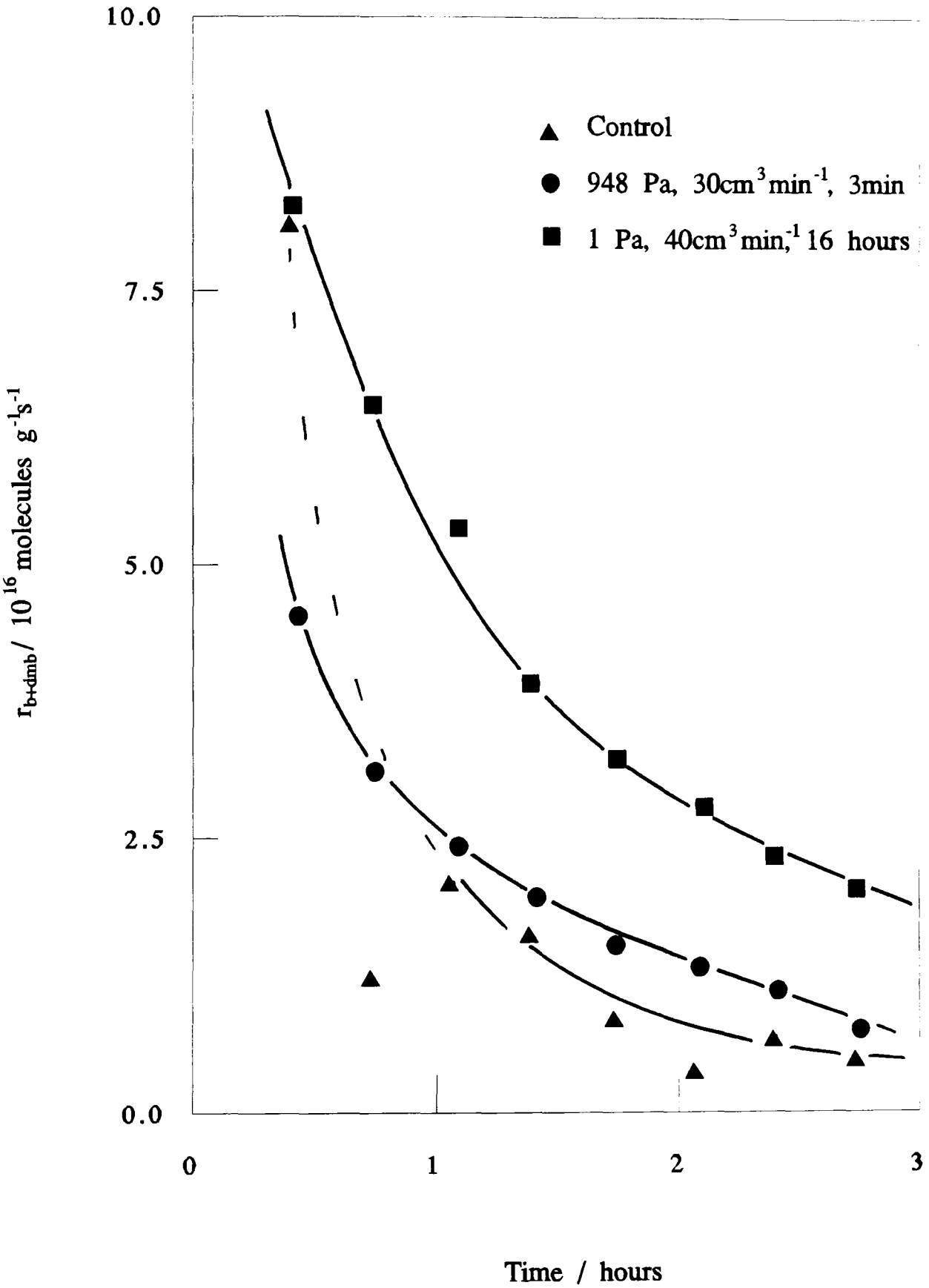

Figure 3.27: Toluene disproportionation on HYST 1073 precoking experiments - detail.

Analysis of the gas stream by gas chromatography implied that more toluene was getting to the catalyst during the bakeout than desired and so the sample was exposed to toluene (1Pa) for one hour at the start of the bakeout and then for a further four and a half hours after the sixteen hours had elapsed: this experiment produced a much higher initial activity and longer period of activity.

Finally, a sample was prepared on the pulse flow apparatus and subjected to eleven pulses of toluene delivered from the sampling loop at random intervals over a period of six hours. The reaction vessel was sealed and then rapidly transferred to the continuous flow furnace, preheated to 673K and after half an hour in flowing helium the reaction was started. Although the initial activity was only half that of the previously mentioned experiment, it persisted for about fifteen hours before undergoing a gradual deactivation: the reaction ceased after forty hours.

These results are corroborated by an observation from the pulse flow experiments where an increase in the activity of NH_4YAS over ten pulses was noticed. The experiment was repeated, without trapping the pulses in liquid nitrogen. Although this was a slight departure from the experimental procedure, it allowed far more pulses to be taken, and figure 3.28 shows that a distinct rise in activity, reaching a plateau approximately four times higher than the initial activity, was seen. These results will be considered in more detail, together with those from the pulse flow experiments, in Section 4.3, the discussion on toluene disproportionation.

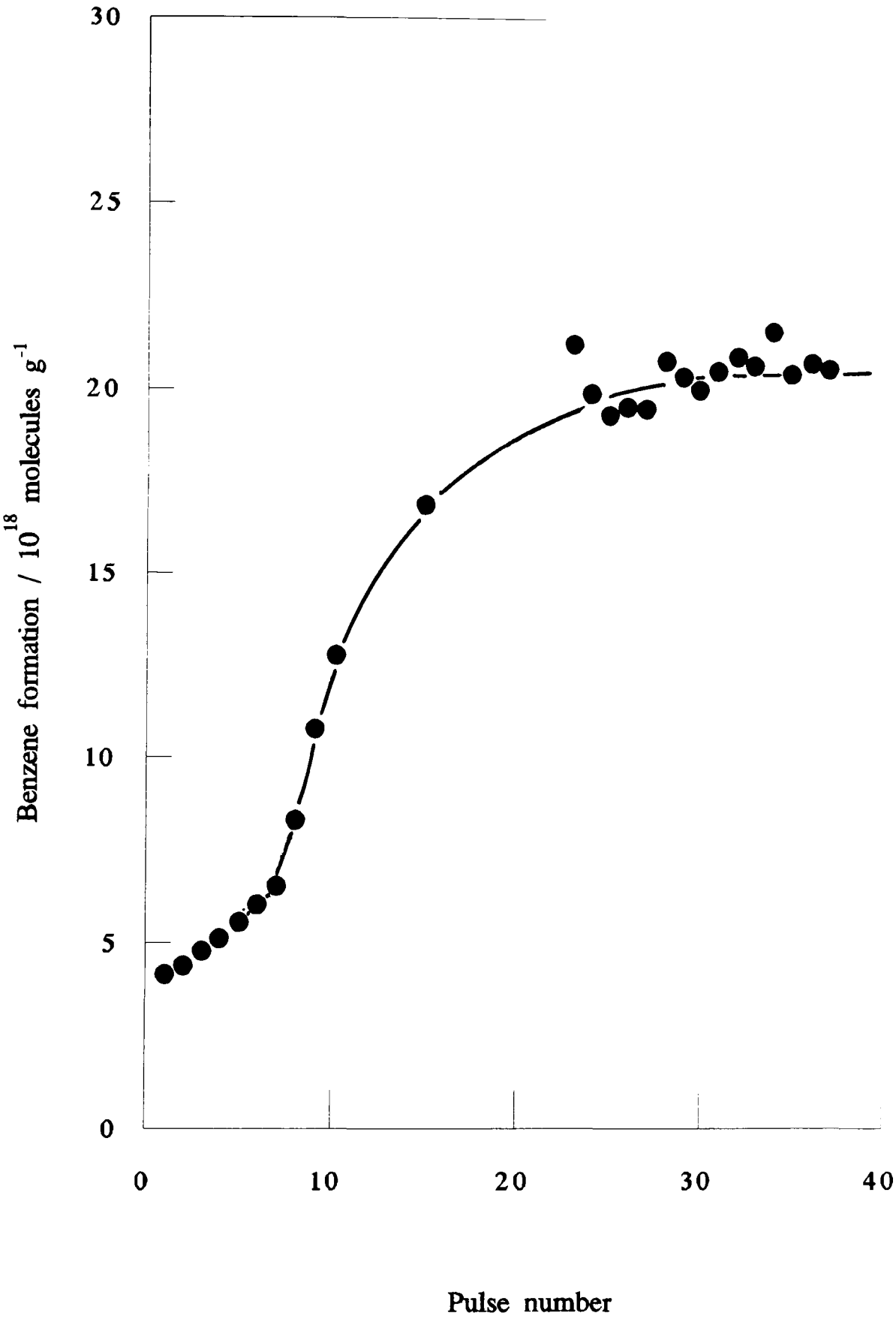

Figure 3.28: Repeated pulses over NH_4YAS

Format	Lifetime /hr	% Coke	Peak /hr	$r_{b+dmb}/10^{17}$molecules $g^{-1}s^{-1}$
Powder/bulb	3	14.5	-	1.55
Pellets/tube	6.5	14.6	-	5.87

Table 3.70: Toluene disproportionation over HYST 873 in different formats.

Format	Lifetime /hr	% Coke	Peak /hr	$r_{b+dmb}/10^{17}$molecules $g^{-1}s^{-1}$	
				½ hour	Peak
Powder/bulb	60	18.8	45	1.02	5.92
Pellets/bulb	24	18.0	18	1.58	9.42
Powder/tube	4.5	18.2	-	0.89	-
Pellets/tube	4.0	17.1	-	2.62	-

Table 3.71: Toluene disproportionation over HYST 873Ex in different formats.

Format	Lifetime /hr	% Coke	Peak /hr	r_{b+dmb}/ 10^{17}molecules $g^{-1}s^{-1}$	
				½ hour	Peak
Powder/bulb	80	15.0	48	0.33	1.27
Pellets/bulb	40	13.8	20	0.84	1.73
Powder/tube	?	4.1	?	0.86	-
Pellets/tube	28	14.4	16	0.86	2.35

Table 3.72: Toluene disproportionation over HYST 1023 in different formats.

Format	Lifetime /hr	% Coke	Peak /hr	r_{b+dmb}/10^{17}molecules $g^{-1}s^{-1}$	
				½ hour	Peak
Powder/bulb	53	18.5	35	0.70	4.31
Pellets/bulb	35	18.8	10	3.03	4.13
Powder/tube	22	19.5	7	3.64	5.02
Pellets/tube	14	18.2	-	5.43	-

Table 3.73: Toluene disproportionation over HYST 1023Ex in different formats.

Format	Lifetime /hr	% Coke	Peak /hr
Powder/bulb	2	16.0	-
Pellets/bulb	2	14.7	-
Powder/bulb	2	16.0	-
Pellets/tube	3	17.5	-

NB. No measurable activity after half an hour.

Table 3.74: Toluene disproportionation over NH_4YAS in different formats.

Time (hr)	Rate / 10^{16} molecules $g^{-1}s^{-1}$		
	r_b	r_{dmb}	r_{b+dmb}
0.4	5.95	9.82	15.77
1.4	5.51	9.49	15.00
2.3	5.80	9.91	15.71
3.3	5.96	10.06	16.02
4.3	6.34	11.02	17.36
5.2	7.23	12.35	19.58
6.2	7.98	13.87	21.85
7.1	9.55	16.23	25.78
8.1	10.66	18.57	29.23
9.1	12.14	22.03	34.17
10.0	14.17	24.91	39.08
11.0	16.28	29.05	45.33
11.9	18.77	34.09	52.86
12.9	21.31	38.36	59.67
13.8	24.72	44.65	69.37
14.8	28.03	51.09	79.12
15.8	30.93	57.78	88.71
16.7	32.23	61.22	93.45
17.7	31.64	62.58	94.22
18.7	28.52	57.85	86.37
19.6	22.06	43.68	65.74
20.6	13.70	25.88	39.58
21.5	4.89	9.36	14.25
22.5	1.06	2.05	3.11
23.5	0.31	-	0.31

Table 3.75: Toluene disproportionation on HYST 873Ex, pellets/bulb format.

Sample	Lifetime /hr	Peak /hr	% Coke	$r_{b+dmb}/10^{17}$molecules $g^{-1}s^{-1}$	
				½ hour	peak
NH_4YAS	<0.5	-	11.6	None	-
HYMST 768	<1	-	14.4	None	-
HYMST 798	1.5	-	14.1	1.65	-
HYST 823	1.5	-	15.1	2.16	-
HYMST 848	2	-	14.6	2.02	-
HYST 873	6.5	-	13.7	5.87	-
HYST 923	4.5	-	13.4	2.55	-
HYST 973	6	-	14.4	3.25	-
HYST 1023	28	16.5	14.4	0.90	2.29
HYST 1073	12	-	14.8	2.74	-

Table 3.76: Summary of toluene disproportionation experiments on unextracted catalysts carried out under continuous flow conditions - pellets/tube format.

Sample	Lifetime /hr	Peak /hr	% Coke	$r_{b+dmb}/10^{17}$ molecules $g^{-1}s^{-1}$	
				½ hour	peak
HYST 823Ex	16	10	16.2	3.67	8.60
HYMST 848Ex	3	-		3.44	-
HYST 873Ex	4	-	15.8	2.95	-
HYST 923Ex	17	11	16.0	1.74	7.25
HYST 973Ex	13	6	17.1	2.18	7.48
HYST 1023Ex	14	-	18.2	5.43	-
HYST 1073Ex	26	16	16.7	0.83	5.36

Table 3.77: Summary of toluene disproportionation experiments on extracted catalysts carried out under continuous flow conditions - pellets/tube format.

Expt	Sample	Lifetime /hr	% coke	Peak /hr	$r_{b+dmb}/10^{17}$ molecules $g^{-1}s^{-1}$	
					½ hour	Peak
1	1023	8	14.6	-	1.44	-
2	1023	18	13.6	6	2.06	2.75
3	1073	<1	-	-	0.14	-
4	1073	17	13.6	-	1.04	-
5	1073	30	12.2	?	2.30	-
6	1073	15	-	-	1.58	-
7	1073	15	14.1	-	2.62	-
8	1073	7	13.6	-	1.00	-

Table 3.78: Summary of addition toluene disproportionation experiments

1. Copper sulphate in second saturator.
2. Toluene passed through 3a sieve.
3. 3A sieve opened to air.
4. One saturator; toluene through 3A sieve.
5. Hydrogen carrier gas.
6. Toluene partial pressure 1191 Pa.
7. Toluene partial pressure 1528 Pa.
8. Helium through 3A sieve.

Time /hr	Rate /10^{16} molecules $g^{-1}s^{-1}$			
	r_b	$r_{m/p\ dmb}$	$r_{o\ dmb}$	r_{b+dmb}
0.41	4.26	5.34	0.78	10.38
0.74	3.23	4.09	0.59	7.91
1.07	2.67	3.45	0.51	6.63
1.41	2.32	2.88	0.37	5.57
1.74	1.97	2.52	0.03	4.52
2.08	1.77	2.16	-	3.93
2.41	1.56	1.76	-	3.32
2.74	1.36	1.68	-	3.04
3.08	1.25	1.39	-	2.64
3.41	1.01	1.16	-	2.17
3.74	1.00	1.11	-	2.11
4.08	0.85	0.99	-	1.84
4.41	0.80	0.51	-	1.31
4.74	0.65	0.67	-	1.32
5.08	0.63	0.65	-	1.28
6.08	0.44	0.35	-	0.79
7.08	0.35	-	-	0.35
8.08	0.26	-	-	0.26
9.08	0.25	-	-	0.25
10.08	0.26	-	-	0.26
11.08	0.25	-	-	0.25
12.08	0.26	-	-	0.26
13.08	0.26	-	-	0.26

Table 3.79: Toluene disproportionation control before hydrogen carrier gas experiment - HYST 1073.

Time /hr	Rate /10^{16} molecules $g^{-1}s^{-1}$			
	r_b	$r_{m/p\ dmb}$	$r_{o\ dmb}$	r_{b+dmb}
0.42	6.55	14.06	3.29	23.90
0.76	5.90	13.11	2.90	21.91
1.09	5.72	12.18	2.66	20.56
1.42	5.87	12.60	2.83	21.30
1.76	5.80	12.51	2.69	21.00
2.09	5.88	12.25	2.12	20.25
2.42	5.99	12.13	2.11	20.23
2.76	5.75	11.91	2.69	20.35
3.09	5.77	11.99	2.45	20.21
4.09	5.85	11.77	2.44	20.06
5.09	5.50	11.80	2.51	19.81
6.09	5.28	10.44	1.89	17.61
8.09	4.19	8.74	-	12.93
9.09	3.70	7.50	-	11.20
10.09	3.22	6.46	-	9.68
11.09	2.58	5.21	-	7.79
12.09	2.13	4.40	-	6.53
13.09	1.74	3.50	-	5.24
14.09	1.43	2.70	-	4.13
15.09	1.20	2.22	-	3.42
16.09	0.97	1.80	-	2.77
17.09	0.81	1.44	-	2.25
18.09	0.66	1.12	-	1.78
19.09	0.59	1.07	-	1.66
20.09	0.52	0.89	-	1.41
22.09	0.38	0.54	-	0.92
24.09	0.32	-	-	0.32
26.09	0.27	-	-	0.27

Table 3.80: Effect of hydrogen carrier gas on toluene disproportionation - HYST 1073.

Time /hr	Rate /10^{16} molecules $g^{-1}s^{-1}$			
	r_b	$r_{m/p\ dmb}$	$r_{o\ dmb}$	r_{b+dmb}
0.41	2.07	2.13	0.31	4.51
0.74	1.53	1.57	-	3.10
1.08	1.23	1.21	-	2.44
1.41	0.99	1.00	-	1.99
1.74	0.82	0.63	-	1.45
2.08	0.73	0.61	-	1.34
2.41	0.61	0.51	-	1.12
2.74	0.48	0.27	-	0.75
3.08	0.45	-	-	0.45

Table 3.81: Toluene disproportionation after coking sample by exposure to toluene at 948Pa for 3 minutes at the start of the bakeout - HYST 1073.

Time /hr	Rate /10^{16} molecules $g^{-1}s^{-1}$			
	r_b	$r_{m/p\ dmb}$	$r_{o\ dmb}$	r_{b+dmb}
0.41	2.93	4.57	0.86	8.36
0.74	2.28	3.55	0.65	6.48
1.08	1.93	2.91	0.53	5.37
1.41	1.64	2.28	-	3.92
1.74	1.52	1.70	-	3.22
2.08	1.25	1.58	-	2.83
2.41	1.08	1.22	-	2.30
2.74	0.95	1.10	-	2.05
3.08	0.89	0.56	-	1.45

Table 3.82: Toluene disproportionation after coking sample by exposure to toluene at 1Pa for 16 hours during the bakeout - HYST 1073.

Time /hr	Rate /10^{16} molecules $g^{-1}s^{-1}$			
	r_b	$r_{m/p\ dmb}$	$r_{o\ dmb}$	r_{b+dmb}
0.45	8.16	18.59	3.58	30.33
0.79	7.21	16.47	3.73	27.41
1.12	6.43	15.30	2.76	24.49
1.45	6.01	13.20	2.94	22.15
1.79	6.02	13.71	2.80	22.53
2.12	4.94	11.28	2.13	18.35
2.45	4.57	9.80	1.88	16.25
2.79	4.26	8.99	1.58	14.83
3.79	2.88	5.65	0.80	9.33
4.79	1.91	3.63	0.45	5.99
5.79	1.32	2.12	-	3.44
6.79	0.97	1.43	-	2.40
7.79	0.63	1.04	-	1.67
8.79	0.51	0.67	-	1.18
9.79	0.39	0.40	-	0.79
10.79	0.25	-	-	0.25
11.79	0.25	-	-	0.25
12.79	0.21	-	-	0.21
13.79	0.17	-	-	0.17
14.79	0.13	-	-	0.13

Table 3.83: Toluene disproportionation after coking sample by exposure to toluene at 1Pa for 1 hour at the start of the bakeout and 4.5 hours at the end - HYST 1073.

Time /hr	Rate /10^{16}molecules $g^{-1}s^{-1}$			
	r_b	$r_{m/p\ dmb}$	$r_{o\ dmb}$	r_{b+dmb}
0.41	4.18	9.40	1.77	15.35
0.75	4.04	8.75	2.08	14.87
2.75	3.92	8.78	1.77	14.47
3.75	4.18	9.70	1.97	15.84
4.75	4.04	9.78	2.03	15.85
5.75	4.04	10.24	2.02	16.30
6.75	4.06	10.30	1.98	16.34
7.75	4.23	10.35	2.06	16.64
8.75	4.10	9.58	1.74	15.42
9.75	4.19	10.02	1.95	16.16
10.75	4.37	10.20	2.01	16.58
11.75	4.34	10.28	1.98	16.60
12.75	4.15	10.26	2.00	16.41
13.75	4.06	9.10	1.44	14.60
14.75	3.83	9.48	1.12	14.43
15.75	3.52	8.95	1.11	13.58
16.75	3.39	6.16	1.04	10.59
18.75	3.18	6.51	1.35	11.04
19.75	2.85	5.85	1.00	9.70
20.75	2.53	4.91	0.67	8.11
22.75	1.87	3.68	0.54	6.09
24.75	1.41	2.33	-	3.74
26.75	1.04	1.53	-	2.57
28.75	0.70	1.10	-	1.80
30.75	0.55	0.77	-	1.32
32.75	0.46	0.45	-	0.91
34.75	0.34	-	-	0.34
36.75	0.24	-	-	0.24
38.75	0.20	-	-	0.20

Table 3.84: Toluene disproportionation after coking sample by exposure to 11 pulses on the pulse flow apparatus - HYST 1073.

Expt	Lifetime / hr	% Coke	Peak /hr	$r_{b+dmb}/10^{16}$molecules g^{-1} s^{-1}	
				½ hour	peak
1	ca 4	11.2	-	4.51	-
2	ca 4	9.9	-	8.36	-
3	15	13.0	-	30.33	-
4	40	13.7	12	15.35	16.60

Table 3.85: Summary of toluene pre-coking experiments.

1. 948Pa, 3 min, $30cm_3min^{-1}$ at start
2. 1Pa, 16 hours, $40cm^3min^{-1}$
3. 1Pa, 1 hour, then activation, then 4½ hours, $40cm^3min^{-1}$
4. 948Pa, 11 x 6 second pulses

3.24 Cumene Dealkylation.

The reaction conditions employed in the dealkylation of cumene are reported in Section 2.33. Preliminary experiments indicated the very facile nature of this reaction, resulting in very high percentage conversions for the most active samples. Therefore, different conditions to those used for the toluene and n-hexane experiments were used to minimise the extent of the reaction. The reaction was studied at 448K, although the activation procedure was the same as for the previous reactants; any further lowering of the reaction temperature caused the products to be retained on the sample on the timescale of the experiment. The amount of catalyst used (10mg hydrated mass) was as low as could be reproducibly measured, and diluting the catalyst with an inert matrix to further lower the active mass was deemed inappropriate as direct comparison with other reactant systems would be rendered void. Exact masses and temperatures used are reported in the individual tables.

The results from the individual cumene dealkylation experiments are presented in tables 3.86 to 3.109, and a selection of activity profiles representing the range of activities are shown in figures 3.29 and 3.30. These results are summarised in table 3.110 as benzene or aliphatic molecules formed from the fourth pulse of cumene. This pulse was taken as being indicative of the initial activity of the sample in that it is the first point which follows the trend of the rest of the experiment. Fitting all of the points to a mathematical equation, followed by extrapolation to zero would have yielded erroneous initial values due to benzene retention from the first three pulses. Extrapolation to zero after removal of these points sometimes led to unreasonably high values for the initial activity. An averaging procedure, as used in the toluene disproportionation experiments, was inappropriate as the samples underwent noticeable deactivation over the fifteen pulses.

The formation of benzene was taken as the measure of the reaction as it is considered, unlike the aliphatic molecules, not to contribute to the formation of coke. Therefore, in the first stages of the reaction after the retention of material noted in the first three pulses, benzene formation should provide a true and accurate measure of the activity of the catalysts.

The deactivation and coke contents of the catalysts, and the products desorbed from the catalysts, up to one hour after, but not including, the last pulse, are reported in table 3.111 and table 3.112 respectively.

NH_4YAS	468K		Dry Mass=0.0068g		
Product formation / 10^{19}molecules g^{-1}					
Pulse	Aliphatic	Benzene	Toluene	E'benzene	Aromatic
1	0.01	0.01	0.02	0.00	0.03
2	0.03	0.03	0.00	0.01	0.04
3	0.05	0.05	0.01	0.02	0.08
4	0.05	0.06	0.01	0.02	0.09
5	0.06	0.07	0.03	0.02	0.12
6	0.06	0.07	0.01	0.03	0.11
7	0.06	0.07	0.00	0.02	0.09
8	0.06	0.07	0.00	0.02	0.09
9	0.06	0.07	0.00	0.02	0.09
10	0.06	0.08	0.01	0.02	0.11
11	0.06	0.07	0.00	0.01	0.08
12	0.06	0.07	0.00	0.01	0.08
13	0.07	0.07	0.00	0.02	0.09
14	0.06	0.08	0.00	0.02	0.10
15	0.07	0.07	0.00	0.01	0.08

Table 3.86: Cumene dealkylation activity as a function of pulse number.

NH_4YLS	468K		Dry Mass=0.0070g		
Product formation / 10^{19}molecules g^{-1}					
Pulse	Aliphatic	Benzene	Toluene	E'benzene	Aromatic
1	0.60	1.38	0.35	-	1.73
2	1.60	2.20	0.04	0.03	2.27
3	2.04	2.43	0.03	0.14	2.60
4	1.88	2.43	0.04	0.30	2.77
5	1.66	2.23	0.03	0.27	2.53
6	1.99	2.46	0.04	0.30	2.80
7	2.11	2.50	0.04	0.30	2.84
8	1.84	2.30	0.04	0.31	2.65
9	1.90	2.46	0.05	0.41	2.92
10	1.89	2.41	0.06	0.41	2.88
11	2.11	2.53	0.05	0.46	3.04
12	1.79	2.40	0.07	0.47	2.94
13	1.70	2.28	0.07	0.38	2.73
14	1.90	2.01	0.13	0.28	2.42
15	1.91	2.20	-	0.26	2.46

Table 3.87: Cumene dealkylation activity as a function of pulse number.

HYMST 748		468K		Dry Mass=0.0079g	
Product formation / 10^{19}molecules g^{-1}					
Pulse	Aliphatic	Benzene	Toluene	E'benzene	Aromatic
1	1.11	2.41	-	0.04	2.45
2	2.35	4.09	0.02	0.24	4.35
3	2.35	3.15	0.04	0.37	3.56
4	2.46	3.49	0.04	0.41	3.94
5	2.55	3.24	0.34	0.80	4.38
6	2.46	3.13	0.47	0.58	4.18
7	2.44	3.07	0.46	0.66	4.19
8	2.29	2.95	0.18	0.42	3.55
9	2.26	2.91	0.40	0.59	3.90
10	2.43	2.96	0.41	0.61	3.98
11	2.51	2.97	0.41	0.58	3.96
12	2.31	2.85	0.42	0.51	3.78
13	2.32	2.81	0.43	0.54	3.78
14	2.36	2.77	0.44	0.54	3.75
15	2.34	2.74	0.49	0.75	3.98

Table 3.88: Cumene dealkylation activity as a function of pulse number.

HYMST 768		468K		Dry Mass=0.0074g	
Product formation / 10^{19}molecules g^{-1}					
Pulse	Aliphatic	Benzene	Toluene	E'benzene	Aromatic
1	1.41	3.99	-	0.04	4.03
2	2.33	3.29	0.02	0.31	3.62
3	2.41	3.21	0.04	0.36	3.61
4	2.48	3.21	0.06	0.37	3.64
5	2.36	3.45	0.07	0.36	3.88
6	2.47	3.22	0.07	0.55	3.84
7	2.38	2.99	0.17	0.40	3.56
8	2.04	2.80	0.50	0.64	3.94
9	2.48	3.00	0.17	0.36	3.53
10	2.29	2.93	0.45	0.50	3.88
11	2.33	2.88	0.43	0.55	3.86
12	1.96	2.70	0.42	0.58	3.70
13	2.33	2.87	0.42	0.46	3.75
14	2.19	2.87	0.41	0.48	3.76
15	2.30	2.80	0.43	0.50	3.73

Table 3.89: Cumene dealkylation activity as a function of pulse number.

HYMST 783		468K		Dry Mass=0.0073g	
Product formation / 10^{19}molecules g^{-1}					
Pulse	Aliphatic	Benzene	Toluene	E'benzene	Aromatic
1	1.02	2.48	-	-	2.48
2	2.16	3.32	0.01	0.23	3.56
3	2.19	2.90	0.03	0.31	3.24
4	2.19	2.81	0.04	0.38	3.23
5	2.39	2.96	0.04	0.64	3.64
6	2.24	2.77	0.07	0.46	3.30
7	2.21	2.74	0.04	0.35	3.13
8	2.17	2.53	0.14	0.42	3.09
9	2.28	2.71	0.35	0.55	3.61
10	2.34	2.72	0.41	0.54	3.67
11	2.23	2.64	0.39	0.52	3.55
12	2.14	2.57	0.34	0.51	3.42
13	2.21	2.55	0.33	0.65	3.53
14	1.96	2.44	0.54	0.48	3.46
15	2.13	2.34	0.14	0.40	2.88

Table 3.90: Cumene dealkylation activity as a function of pulse number.

HYMST 798		468K		Dry Mass=0.0074g	
Product formation / 10^{19}molecules g^{-1}					
Pulse	Aliphatic	Benzene	Toluene	E'benzene	Aromatic
1	1.08	2.31	0.03	0.05	2.39
2	2.17	3.40	0.01	0.24	3.65
3	2.06	2.73	0.03	0.30	3.06
4	2.11	2.75	0.05	0.35	3.15
5	2.14	2.65	0.04	0.36	3.05
6	2.08	3.32	0.04	0.37	3.73
7	2.21	3.33	0.05	0.40	3.78
8	2.19	3.28	0.05	0.39	3.72
9	2.19	3.04	0.32	-	3.36
10	1.95	2.88	0.35	0.38	3.61
11	2.14	2.92	0.36	0.47	3.75
12	1.84	2.84	0.38	0.37	3.59
13	2.04	2.88	0.40	0.25	3.53
14	1.99	2.74	0.30	-	3.04
15	-	-	-	-	-

Table 3.91: Cumene dealkylation activity as a function of pulse number.

HYST 823		468K		Dry Mass=0.0074g	
Product formation / 10^{19}molecules g^{-1}					
Pulse	Aliphatic	Benzene	Toluene	E'benzene	Aromatic
1	2.20	2.40	0.01	0.05	2.46
2	2.18	3.41	0.03	0.26	3.70
3	1.99	3.23	0.07	0.28	3.58
4	2.05	2.90	0.09	0.26	3.25
5	2.22	2.68	0.05	0.29	3.01
6	2.01	2.64	0.06	0.29	2.99
7	2.01	2.50	0.13	0.32	2.95
8	1.99	2.50	-	-	2.50
9	2.05	2.58	0.07	0.29	2.94
10	1.97	2.35	0.14	0.27	2.76
11	1.85	2.25	0.14	0.28	2.67
12	1.88	2.31	-	-	2.31
13	1.75	2.26	-	-	2.26
14	1.72	2.17	0.28	0.37	2.82
15	1.78	2.14	0.28	0.35	2.77

Table 3.92: Cumene dealkylation activity as a function of pulse number.

HYMST 848		468K		Dry Mass=0.077g	
Product formation / 10^{19}molecules g^{-1}					
Pulse	Aliphatic	Benzene	Toluene	E'benzene	Aromatic
1	0.68	2.23	0.09	0.08	2.40
2	1.87	3.26	0.05	0.19	3.50
3	2.01	2.83	0.05	0.34	3.22
4	1.74	2.16	0.04	0.34	2.54
5	1.85	1.95	0.08	0.41	2.44
6	1.63	20.2	0.06	0.38	20.64
7	1.62	2.03	0.05	0.32	2.40
8	1.59	1.88	0.03	0.31	2.22
9	1.52	1.88	0.09	0.31	2.28
10	1.55	1.91	0.18	0.32	2.41
11	-	-	-	-	-
12	1.44	1.67	0.09	0.31	2.07
13	1.46	1.56	0.05	0.44	2.05
14	1.28	1.69	0.29	0.35	2.33
15	1.48	1.67	0.12	0.31	2.10

Table 3.93: Cumene dealkylation activity as a function of pulse number.

HYST 873		468K		Dry Mass=0.0070g	
Product formation / 10^{19}molecules g^{-1}					
Pulse	Aliphatic	Benzene	Toluene	E'benzene	Aromatic
1	-	-	-	-	-
2	1.42	3.08	0.02	0.09	3.19
3	2.65	4.02	0.03	0.34	4.39
4	2.31	3.06	0.06	0.44	3.56
5	1.89	3.04	0.06	0.47	3.57
6	2.06	3.26	0.11	0.42	3.79
7	2.34	2.85	0.08	0.46	3.39
8	0.91	2.55	0.20	0.26	3.01
9	1.53	2.74	0.14	0.31	3.19
10	2.02	2.54	0.32	0.61	3.47
11	1.84	2.54	0.28	0.57	3.39
12	1.89	2.44	1.35	0.36	4.15
13	2.09	2.49	0.31	0.54	3.34
14	0.79	2.75	0.25	0.17	3.17
15	-	-	-	-	-

Table 3.94: Cumene dealkylation activity as a function of pulse number.

HYST 923		468K		Dry Mass=0.0079g	
Product formation / 10^{19}molecules g^{-1}					
Pulse	Aliphatic	Benzene	Toluene	E'benzene	Aromatic
1	0.51	1.52	0.03	0.04	1.59
2	1.54	2.20	0.06	0.16	2.42
3	1.40	1.79	0.03	0.26	2.08
4	1.38	1.74	0.01	0.30	2.05
5	1.40	1.71	0.03	0.36	2.10
6	1.38	1.85	0.03	0.31	2.19
7	1.17	1.73	0.03	0.28	2.04
8	1.29	1.52	0.02	0.25	1.79
9	1.22	1.48	0.04	0.26	1.78
10	1.38	1.52	0.19	0.33	2.04
11	1.23	1.51	0.16	0.29	1.96
12	1.23	1.42	0.09	0.26	1.77
13	1.08	1.47	0.06	0.18	1.71
14	1.13	1.33	0.08	0.20	1.61
15	1.07	1.36	0.17	0.29	1.82

Table 3.95: Cumene dealkylation activity as a function of pulse number.

HYST 973		468K		Dry Mass=0.0074g	
Product formation / 10^{19}molecules g^{-1}					
Pulse	Aliphatic	Benzene	Toluene	E'benzene	Aromatic
1	0.56	1.54	0.06	0.05	1.65
2	1.40	2.63	0.01	0.15	2.79
3	1.39	1.80	0.01	0.27	2.08
4	1.41	1.69	0.03	0.32	2.04
5	1.41	1.68	0.19	0.41	2.28
6	1.41	1.64	0.21	0.37	2.22
7	1.41	1.65	0.17	0.41	2.23
8	1.16	1.69	0.18	0.27	2.14
9	1.36	1.56	0.18	0.34	2.08
10	1.29	1.49	0.19	0.30	1.98
11	1.24	1.44	0.18	0.32	1.94
12	1.24	1.36	0.07	0.24	1.67
13	1.23	1.30	0.19	0.30	1.79
14	1.16	1.37	0.16	0.28	1.81
15	1.36	1.40	0.19	0.34	1.93

Table 3.96: Cumene dealkylation activity as a function of pulse number.

HYST 1023		468K		Dry Mass=0.0078g	
Product formation / 10^{19}molecules g^{-1}					
Pulse	Aliphatic	Benzene	Toluene	E'benzene	Aromatic
1	0.48	1.42	0.01	0.05	1.48
2	1.28	1.76	0.01	0.13	1.90
3	1.28	1.58	0.01	0.24	1.83
4	1.24	1.53	0.02	0.28	1.83
5	1.21	1.47	0.03	0.28	1.78
6	1.21	1.43	0.03	0.27	1.73
7	1.18	1.39	0.02	0.25	1.66
8	1.24	1.39	0.02	0.22	1.63
9	1.19	1.33	0.03	0.21	1.57
10	1.18	1.35	0.15	0.31	1.81
11	1.18	1.34	0.16	0.28	1.78
12	1.16	1.30	0.14	0.26	1.70
13	1.14	1.23	0.06	0.19	1.48
14	1.01	1.22	0.14	0.27	1.63
15	1.06	1.15	0.24	0.20	1.59

Table 3.97: Cumene dealkylation activity as a function of pulse number.

HYST 1073		468K		Dry Mass=0.0079g	
Product formation / 10^{19}molecules g^{-1}					
Pulse	Aliphatic	Benzene	Toluene	E'benzene	Aromatic
1	0.30	0.82	-	0.03	0.85
2	0.91	1.24	0.01	0.08	1.33
3	0.85	1.09	-	0.12	1.21
4	0.97	1.30	0.03	0.16	1.49
5	0.96	1.07	0.01	0.16	1.24
6	0.71	0.99	0.01	0.14	1.14
7	0.76	0.98	0.02	0.15	1.15
8	0.77	0.95	0.01	0.14	1.10
9	0.79	0.90	0.04	0.14	1.08
10	0.76	0.89	0.08	0.15	1.12
11	0.72	0.96	0.04	0.40	1.40
12	0.69	0.91	0.03	0.65	1.59
13	0.75	0.90	0.03	0.87	1.80
14	0.80	0.92	0.01	0.14	1.07
15	0.68	0.85	0.06	0.11	1.02

Table 3.98: Cumene dealkylation activity as a function of pulse number.

HYMST 748Ex		468K		Dry Mass=0.0074g	
Product formation / 10^{19}molecules g^{-1}					
Pulse	Aliphatic	Benzene	Toluene	E'benzene	Aromatic
1	2.02	3.22	-	0.07	3.29
2	2.99	3.99	0.05	0.36	4.40
3	2.92	3.72	0.08	0.45	4.25
4	2.85	3.61	0.08	0.46	4.15
5	2.89	3.67	0.11	0.52	4.30
6	2.63	3.44	0.12	0.47	4.03
7	2.69	3.48	0.52	0.80	4.80
8	2.63	3.40	0.39	0.72	4.51
9	2.65	3.34	0.52	0.82	4.68
10	2.61	3.36	0.49	0.83	4.68
11	2.64	3.14	0.19	0.46	3.79
12	2.59	3.08	0.19	0.46	3.73
13	2.61	3.08	0.23	0.43	3.74
14	2.60	2.96	0.21	0.41	3.58
15	2.53	2.96	0.21	0.43	3.60

Table 3.99: Cumene dealkylation activity as a function of pulse number.

HYMST 768Ex		468K		Dry Mass=0.0072g	
Product formation / 10^{19}molecules g^{-1}					
Pulse	Aliphatic	Benzene	Toluene	E'benzene	Aromatic
1	1.72	3.69	0.00	0.09	3.78
2	2.55	3.52	0.04	0.34	3.90
3	2.75	4.33	0.08	0.43	4.84
4	2.55	4.04	0.10	0.45	4.59
5	2.29	3.98	0.10	0.41	4.49
6	2.46	3.04	0.17	0.43	3.64
7	2.31	3.07	0.11	0.46	3.64
8	2.36	3.05	0.44	0.67	4.16
9	2.16	2.84	0.10	0.45	3.39
10	2.05	2.49	0.36	0.54	3.39
11	2.37	2.94	0.39	0.77	4.10
12	2.02	2.79	0.19	0.39	3.37
13	2.06	2.65	0.17	0.37	3.19
14	2.09	2.66	0.17	0.37	3.20
15	2.16	2.87	0.13	0.53	3.53

Table 3.100: Cumene dealkylation activity as a function of pulse number.

HYMST 783Ex		468K		Dry Mass=0.0073g	
Product formation / 10^{19}molecules g^{-1}					
Pulse	Aliphatic	Benzene	Toluene	E'benzene	Aromatic
1	2.05	3.81	0.01	0.08	3.90
2	2.49	3.46	0.04	0.27	3.77
3	2.72	3.43	0.07	0.39	3.89
4	2.73	3.35	0.08	0.40	3.83
5	2.67	3.30	0.18	0.43	3.91
6	2.71	3.37	0.10	0.44	3.91
7	2.59	3.22	0.19	0.42	3.83
8	2.46	3.35	0.51	0.64	4.50
9	2.61	3.28	0.51	0.65	4.44
10	2.60	3.26	0.52	0.62	4.40
11	2.54	3.26	0.49	0.57	4.32
12	2.70	3.26	0.47	0.55	4.28
13	2.56	3.19	0.53	0.56	4.28
14	2.88	3.15	0.49	0.56	4.20
15	2.56	3.13	0.54	0.60	4.27

Table 3.101: Cumene dealkylation activity as a function of pulse number.

HYMST 798Ex		468K		Dry Mass=0.0072g	
Product formation / 10^{19}molecules g^{-1}					
Pulse	Aliphatic	Benzene	Toluene	E'benzene	Aromatic
1	1.61	3.00	0.08	0.51	3.59
2	2.19	3.43	0.31	0.67	4.41
3	2.36	3.69	0.40	0.91	5.00
4	2.23	3.28	0.40	0.95	4.63
5	2.19	2.74	0.41	0.90	4.05
6	2.11	2.67	0.38	0.81	3.86
7	2.16	2.70	0.58	1.13	4.41
8	1.87	3.20	0.36	1.01	4.57
9	2.04	2.53	0.33	1.02	3.88
10	1.97	2.43	0.51	1.04	3.98
11	1.97	2.54	0.51	1.27	4.32
12	2.08	2.56	0.37	1.34	4.27
13	1.84	2.34	0.30	1.14	3.78
14	1.55	2.03	0.22	0.67	2.92
15	1.40	2.01	-	0.16	2.17

Table 3.102: Cumene dealkylation activity as a function of pulse number.

HYST 823Ex		468K		Dry Mass=0.0074g	
Product formation / 10^{19}molecules g^{-1}					
Pulse	Aliphatic	Benzene	Toluene	E'benzene	Aromatic
1	1.88	3.56	0.00	0.08	3.64
2	2.45	3.90	0.01	0.28	4.19
3	2.56	3.27	0.05	0.38	3.70
4	2.43	3.56	0.05	0.36	3.97
5	2.45	3.19	0.09	0.44	3.72
6	2.34	3.45	0.08	0.37	3.90
7	2.51	3.04	0.10	0.40	3.54
8	2.12	3.64	0.10	0.38	4.12
9	2.28	3.13	0.41	0.50	4.04
10	2.24	2.84	0.17	0.38	3.39
11	2.28	2.98	0.47	-	3.45
12	2.33	2.98	0.48	0.51	3.97
13	2.34	2.98	0.44	0.52	3.94
14	2.33	2.95	0.46	0.52	3.93
15	-	-	-	-	-

Table 3.103: Cumene dealkylation activity as a function of pulse number.

HYMST 848Ex		468K		Dry Mass=0.0072g	
Product formation / 10^{19}molecules g^{-1}					
Pulse	Aliphatic	Benzene	Toluene	E'benzene	Aromatic
1	2.06	3.09	0.00	0.12	3.21
2	2.43	3.83	0.02	0.30	4.15
3	2.85	4.09	0.05	0.43	4.57
4	2.82	3.46	0.04	0.56	4.06
5	2.58	3.17	0.15	0.39	3.71
6	2.47	3.18	0.38	0.54	4.10
7	2.61	3.20	0.41	0.58	4.19
8	2.53	3.13	0.40	0.54	4.07
9	2.56	3.11	0.39	0.53	4.03
10	2.34	3.03	0.39	0.52	3.94
11	2.60	3.10	0.38	0.51	3.99
12	2.24	2.79	0.16	0.40	3.35
13	2.11	2.65	0.16	0.34	3.15
14	2.14	2.65	0.15	0.36	3.16
15	-	-	-	-	-

Table 3.104: Cumene dealkylation activity as a function of pulse number.

HYST 873Ex		468K		Dry Mass=0.0074g	
Product formation / 10^{19}molecules g^{-1}					
Pulse	Aliphatic	Benzene	Toluene	E'benzene	Aromatic
1	1.99	3.73	0.00	0.08	3.81
2	2.80	4.37	0.03	0.37	4.77
3	2.83	4.60	0.07	0.44	5.11
4	2.82	3.64	0.32	0.68	4.64
5	2.84	3.57	0.30	0.54	4.41
6	2.74	3.52	0.42	0.63	4.57
7	2.12	3.26	0.29	0.61	4.16
8	2.59	3.36	0.32	0.55	4.23
9	2.43	3.19	0.31	0.58	4.08
10	2.41	3.14	0.29	0.58	4.01
11	2.43	3.13	0.27	0.57	3.97
12	2.47	3.14	0.37	0.70	4.21
13	2.36	3.10	0.36	0.59	4.05
14	2.38	3.06	0.34	0.56	3.96
15	2.50	3.13	0.36	0.69	4.18

Table 3.105: Cumene dealkylation activity as a function of pulse number.

HYST 923Ex		468K		Dry Mass=0.0074g	
Product formation / 10^{19}molecules g^{-1}					
Pulse	Aliphatic	Benzene	Toluene	E'benzene	Aromatic
1	1.65	3.25	0.07	0.07	3.39
2	2.83	3.83	0.46	0..41	4.70
3	2.55	3.37	0.55	0.49	4.41
4	2.33	3.18	0.51	0.46	4.15
5	2.38	3.14	0.52	0.47	4.13
6	2.25	3.03	0.49	0.44	3.96
7	2.36	2.99	0.48	0.44	3.91
8	2.31	2.89	0.78	0.70	4.37
9	2.23	2.91	0.43	0.39	3.73
10	2.31	2.84	0.81	0.73	4.38
11	2.24	2.86	0.46	0.41	3.73
12	2.48	2.99	0.46	0.41	3.86
13	2.08	2.69	0.72	0.65	4.06
14	2.15	2.77	0.45	0.41	3.63
15	2.22	2.79	0.41	0.38	3.58

Table 3.106: Cumene dealkylation activity as a function of pulse number.

HYST 973Ex		468K		Dry Mass=0.0076g	
Product formation / 10^{19}molecules g^{-1}					
Pulse	Aliphatic	Benzene	Toluene	E'benzene	Aromatic
1	0.72	1.47	0.04	0.04	1.55
2	1.72	2.47	0.17	0.15	2.79
3	1.97	2.48	0.36	0.32	3.16
4	1.84	2.63	0.42	0.38	3.43
5	1.84	2.67	0.38	0.35	3.40
6	1.80	2.26	0.39	0.35	3.00
7	1.94	2.24	0.41	0.37	3.02
8	1.99	2.22	0.38	0.35	2.95
9	1.95	2.37	0.28	0.46	3.11
10	1.90	2.21	0.35	0.32	2.88
11	1.79	2.25	0.48	0.43	3.16
12	1.98	2.25	0.49	0.44	3.18
13	1.93	2.27	0.48	0.44	3.19
14	1.80	2.19	0.44	0.40	3.03
15	1.69	2.02	0.39	0.35	2.76

Table 3.107: Cumene dealkylation activity as a function of pulse number.

HYST 1023Ex		468K		Dry Mass=0.0078g	
Product formation / 10^{19}molecules g^{-1}					
Pulse	Aliphatic	Benzene	Toluene	E'benzene	Aromatic
1	1.43	3.83	0.02	0.58	4.43
2	2.30	3.69	0.01	0.32	4.02
3	2.22	4.05	0.05	0.40	4.50
4	2.17	2.74	0.06	0.38	3.18
5	2.17	2.66	0.07	0.41	3.14
6	2.29	2.74	0.29	0.64	3.67
7	2.04	2.75	0.08	0.40	3.23
8	2.30	2.47	0.28	0.42	3.17
9	2.12	2.45	0.13	0.38	2.96
10	2.06	2.37	0.12	0.38	2.87
11	1.97	2.45	0.32	0.47	3.24
12	2.03	2.32	0.12	0.37	2.81
13	1.97	2.39	0.24	0.64	3.27
14	1.97	2.36	0.29	0.46	3.11
15	1.90	2.20	0.09	0.37	2.66

Table 3.108 Cumene dealkylation activity as a function of pulse number.

HYST 1073Ex		468K		Dry Mass=0.0071g	
Product formation / 10^{19}molecules g^{-1}					
Pulse	Aliphatic	Benzene	Toluene	E'benzene	Aromatic
1	1.23	1.78	0.00	0.08	1.86
2	1.64	1.96	0.01	0.20	2.17
3	1.47	1.75	0.01	0.21	1.97
4	1.43	1.72	0.03	0.27	2.02
5	1.32	1.57	0.03	0.23	1.83
6	1.46	1.64	0.03	0.24	1.91
7	1.40	1.57	0.08	0.26	1.91
8	1.31	1.55	0.18	0.38	2.11
9	1.28	1.44	0.08	0.22	1.74
10	1.24	1.47	0.15	0.28	1.90
11	1.24	1.46	0.15	0.28	1.89
12	1.14	1.45	0.09	0.32	1.86
13	0.96	1.37	0.13	0.27	1.77
14	1.26	1.44	0.11	0.27	1.82
15	-	-	-	-	-

Table 3.109 Cumene dealkylation activity as a function of pulse number.

	Product formation / 10^{19}molecules g^{-1}			
	Fourth pulse		%change on extraction	
	Benzene	Aliphatic	Benzene	Aliphatic
NH_4YAS	0.06	0.05	-	-
NH_4YLS	2.43	1.88	-	-
HYMST 748	3.49	2.46	3.4	6.5
HYMST 768	3.21	2.48	-5.3	2.0
HYMST 783	2.81	2.19	19.2	24.7
HYMST 798	2.75	2.11	0.0	4.7
HYST 823	2.90	2.05	22.8	18.5
HYMST 848	2.16	1.74	60.2	61.1
HYST 873	3.06	2.31	18.9	21.5
HYST 923	1.74	1.38	82.7	66.9
HYST 973	1.69	1.41	55.6	31.2
HYST 1023	1.53	1.24	80.3	75.0
HYST 1073	1.30	0.97	32.3	45.9
HYMST 748Ex	3.61	2.85	-	-
HYMST 768Ex	3.04	2.55	-	-
HYST 783Ex	3.35	2.73	-	-
HYMST 798Ex	2.74	2.23	-	-
HYST 823Ex	3.56	2.43	-	-
HYMST 848Ex	3.46	2.82	-	-
HYST 873Ex	3.64	2.82	-	-
HYST 923Ex	3.18	2.33	-	-
HYST 973Ex	2.63	1.84	-	-
HYST 1023Ex	2.74	2.17	-	-
HYST 1073Ex	1.72	1.43	-	-

Table 3.110: Summary of cumene dealkylation experiments.

	% Deactivation	% Coke
NH_4YAS	None	0.6
NH_4YLS	9	1.0
HYMST 748	13	1.2
HYMST 768	13	1.2
HYMST 783	19	1.2
HYMST 798	19	1.0
HYST 823	34	1.2
HYMST 848	23	0.9
HYST 873	19	1.2
HYST 923	24	0.7
HYST 973	22	0.7
HYST 1023	27	0.6
HYST 1073	22	0.7
HYMST 748Ex	20	1.4
HYMST 768Ex	24	1.7
HYMST 783Ex	10	1.6
HYMST 798Ex	33	1.6
HYST 823Ex	18	1.9
HYMST 848Ex	23	1.5
HYST 873Ex	14	1.6
HYST 923Ex	17	1.2
HYST 973Ex	19	1.1
HYST 1023Ex	20	0.8
HYST 1073Ex	18	0.8

NB. Approximate deactivation 4th to 15th pulse.

Table 3.111: Cumene dealkylation - deactivation and coke content.

Sample	Product formation / 10^{19}molecules g^{-1} molecules g^{-1} (%)				
	Aliphatic	Benzene	Toluene	E'benzene	Cumene
NH_4YAS	-	-	-	-	-
NH_4YLS	-	-	-	-	-
HYMST 748	3.94 (15)	0.96 (2)	0.15 (10)	0.66 (12)	0.75 (61)
HYMST 768	3.51 (15)	0.87 (2)	0.11 (9)	0.50 (13)	0.76 (61)
HYMST 783	4.55 (14)	1.14 (2)	0.16 (10)	0.78 (16)	1.28 (57)
HYMST 798	2.95 (15)	0.80 (14)	0.71 (5)	0.23 (10)	0.51 (57)
HYST 823	-	-	-	-	-
HYMST 848	1.32 (28)	1.49 (2)	0.11 (5)	0.28 (41)	2.20 (24)
HYST 873	-	-	-	-	-
HYST 923	1.12 (11)	0.25 (2)	0.05 (8)	0.19 (29)	0.66 (50)
HYST 973	1.41 (9)	0.26 (2)	0.06 (9)	0.25 (32)	0.94 (48)
HYST 1023	1.42 (10)	0.31 (2)	0.06 (8)	0.25 (36)	1.13 (45)
HYST 1073	-	-	-	-	-
HYMST 748Ex	3.64 (15)	0.94 (3)	0.16 (10)	0.63 (13)	0.82 (59)
HYMST 768Ex	3.58 (15)	0.93 (3)	0.16 (10)	0.63 (13)	0.80 (59)
HYMST 783Ex	3.71 (16)	1.06 (3)	0.18 (11)	0.71 (13)	0.82 (57)
HYMST 798Ex	3.49 (17)	1.15 (2)	0.15 (8)	0.55 (23)	1.57 (50)
HYST 823Ex	-	-	-	-	-
HYMST 848Ex	1.97 (34)	2.25 (2)	0.13 (11)	0.73 (24)	1.60 (29)
HYST 873Ex	2.77 (14)	0.66 (3)	0.16 (12)	0.58 (11)	0.51 (59)
HYST 923Ex	2.69 (14)	0.62 (2)	0.11 (11)	0.51 (14)	0.63 (59)
HYST 973Ex	2.35 (13)	0.52 (3)	0.11 (12)	0.48 (16)	0.67 (57)
HYST 1023Ex	3.00 (11)	0.83 (2)	0.13 (8)	0.60 (38)	0.28 (41)
HYST 1073Ex	-	-	-	-	-

Table 3.112: Products retained in cold trap after one hour degassing.

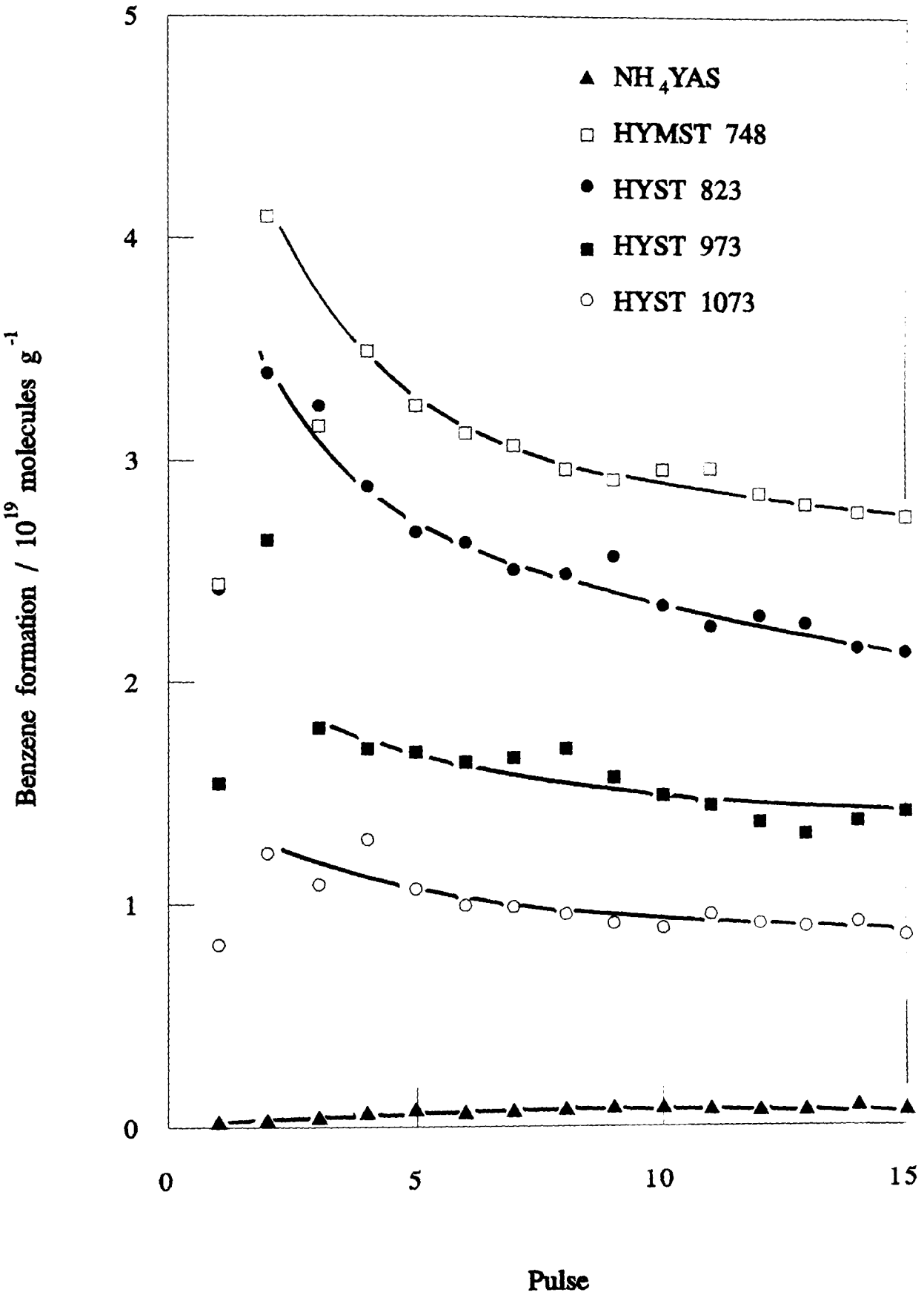

Figure 3.29: Cumene dealkylation - unextracted catalysts.

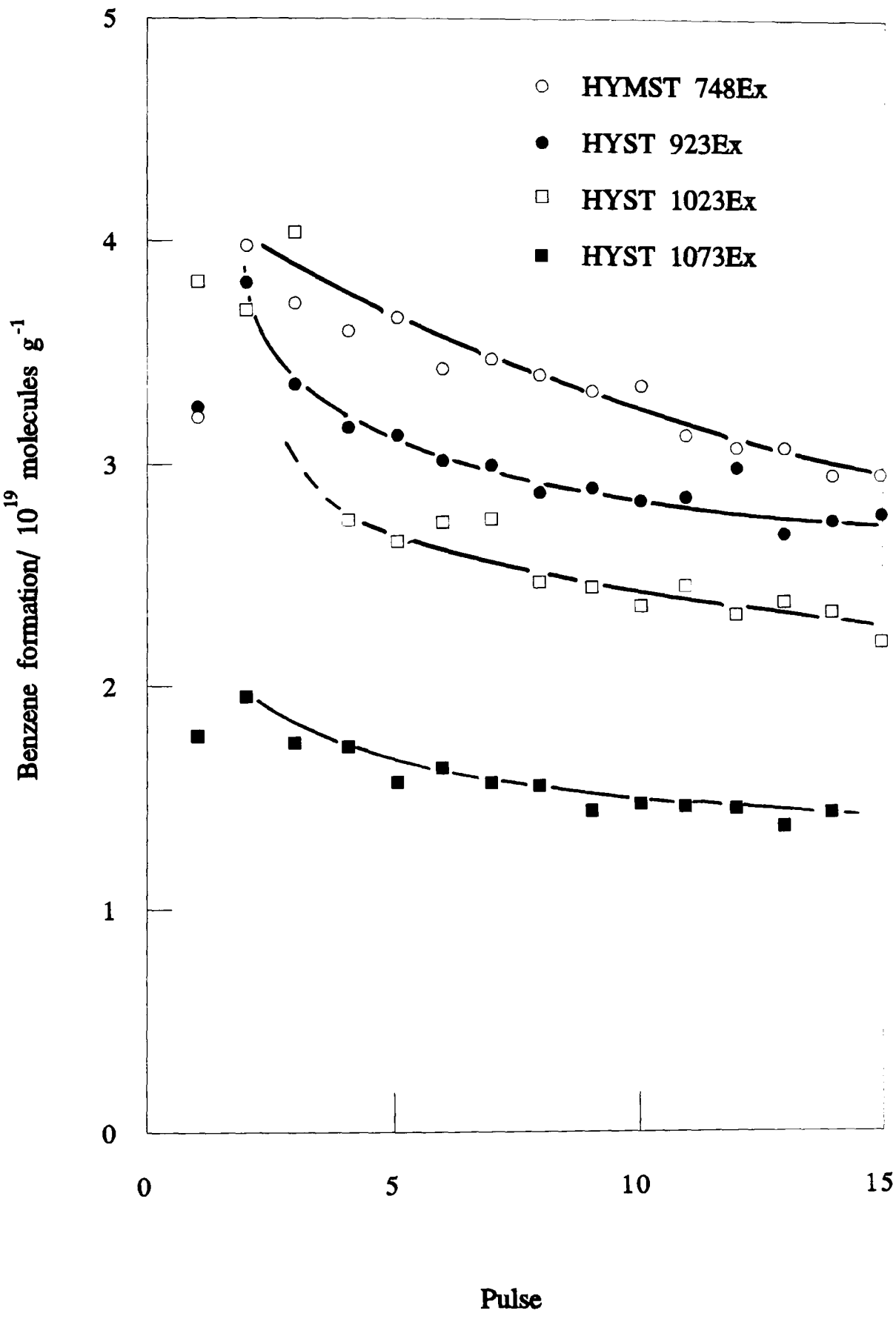

Figure 3.30: Cumene dealkylation - extracted catalysts.

3.25 Propan-2-ol Dehydration

The dehydration of propan-2-ol was studied at temperatures centred around 373K under continuous flow conditions. Full details of the experimental technique can be found in Section 2.37. As this reaction differs from the others studied in this work in that water is formed as a product, it is best studied under continuous flow conditions where it can be assumed that equilibrium between adsorbed water and water vapour in the product stream has been achieved. Misleading results could be obtained from pulse flow methods as the production of water, allied to the reaction temperatures used, could lead to a gradual build up of water in the pores of the sample. This could affect the catalytic and transport properties of the catalyst. The pressure dependence of the reaction was studied at reactant pressures of 1.00×10^3 Pa and 1.45×10^3 Pa and offered confirmation that the reaction was of zero order.

The temperature dependence of the reaction was investigated in the temperature range 367K-381K with a propan-2-ol pressure of 1.11×10^3 Pa, allowing activation energies and derived rate constants at set temperatures to be obtained. The zero order rate constant can be obtained from the following equation

$$k = \frac{1}{\tau} x \qquad 3.18$$

where k is the zero order rate constant, x is the fractional conversion of propan-2-ol and τ is the contact time between the reactant and the catalyst sample, defined as the volume of the catalyst divided by the flowrate of the reactant. However, as almost identical catalyst masses and flowrates were used the above equation reduces to a form which gives a pseudo zero order rate constant as equal to the natural logarithm of the fractional conversion. Using this assumption, the activation energy for the reactions can be obtained from the Arrhenius equation:

$$k = Ae^{-(EAct/RT)} \qquad 3.19$$

Therefore, a plot of ln x against 1/T will yield the activation energy of the reaction.

The results of the temperature dependence experiments are presented in tables 3.113 to 3.135, and graphically in figures 3.31 to 3.37. The activities

at 373K and the calculated activation energies are reported in table 3.136. The effect of removing the extraframework aluminium on the activity of the catalysts is reported in table 3.137. The results of the pressure dependence experiments are reported in tables 3.138 to 3.143 and a selection shown in figures 3.38 and 3.39; the derived activation energies can be found in table 3.144.

The results of a short study on the effects of pretreating the catalyst samples with propan-2-ol at various elevated temperatures are contained in table 3.145.

NH_4YLS	Rate / 10^{16}molecules g^{-1} s^{-1}		
Temperature/K	$r_{Propene}$	r_{DIPE}	$r_{propene+2DIPE}$
369	18.0	1.16	20.32
371	22.9	1.54	25.98
373	32.7	2.41	37.52
375	40.0	2.60	45.20
377	52.4	3.28	58.96
379	64.0	4.16	72.32
381	80.5	4.66	89.82

Table 3.113: Temperature dependence of propan-2-ol dehydration.

HYMST 748	Rate / 10^{16}molecules g^{-1} s^{-1}		
Temperature/K	$r_{Propene}$	r_{DIPE}	$r_{propene+2DIPE}$
369	6.01	3.19	12.39
371	7.84	3.99	15.82
373	9.56	4.31	18.18
375	12.35	5.08	22.51
377	14.39	6.03	26.45
379	19.12	6.86	32.84
381	23.52	7.84	39.20

Table 3.114: Temperature dependence of propan-2-ol dehydration.

HYMST 748Ex	Rate / 10^{16}molecules $g^{-1}s^{-1}$		
Temperature/K	$r_{Propene}$	r_{DIPE}	$r_{propene+2DIPE}$
369	18.77	2.40	23.57
371	23.47	3.10	29.67
373	29.88	3.84	37.56
375	41.08	4.83	50.74
377	51.08	5.84	62.76
379	58.94	7.30	73.54
381	75.38	8.48	92.34

Table 3.115: Temperature dependence of propan-2-ol dehydration.

HYMST 768	Rate / 10^{16}molecules $g^{-1}s^{-1}$		
Temperature/K	$r_{Propene}$	r_{DIPE}	$r_{propene+2DIPE}$
369	4.68	3.22	11.12
372	6.31	3.71	13.73
375	9.15	4.56	18.27
376	9.76	4.92	19.60
378	13.63	6.05	25.73
379	14.34	6.10	26.54
381	18.51	7.21	32.93

Table 3.116: Temperature dependence of propan-2-ol dehydration.

HYMST 768Ex	Rate / 10^{16}molecules $g^{-1}s^{-1}$		
Temperature/K	$r_{Propene}$	r_{DIPE}	$r_{propene+2DIPE}$
369	15.17	2.30	19.77
371	19.34	2.85	25.04
373	24.88	3.65	32.18
375	33.03	4.47	41.97
377	39.15	5.41	49.97
379	47.39	6.41	60.21
381	58.29	7.72	73.73

Table 3.117: Temperature dependence of propan-2-ol dehydration.

HYMST 783	Rate / 10^{16}molecules $g^{-1}s^{-1}$		
Temperature/K	$r_{Propene}$	r_{DIPE}	$r_{propene+2DIPE}$
369	5.88	2.72	11.32
371	7.72	3.33	14.38
373	9.56	3.84	17.24
375	12.56	4.73	22.02
377	16.13	5.62	27.37
379	19.58	6.56	32.70
381	24.54	7.61	39.76

Table 3.118: Temperature dependence of propan-2-ol dehydration.

HYMST 783Ex	Rate / 10^{16}molecules $g^{-1}s^{-1}$		
Temperature/K	$r_{Propene}$	r_{DIPE}	$r_{propene+2DIPE}$
369	16.62	1.94	20.50
371	21.03	2.61	26.25
373	25.63	3.45	32.53
375	36.96	4.26	45.48
377	44.69	5.04	54.77
379	52.04	6.07	64.18
381	64.42	7.30	79.02

Table 3.119: Temperature dependence of propan-2-ol dehydration.

HYMST 798	Rate / 10^{16}molecules $g^{-1}s^{-1}$		
Temperature/K	$r_{Propene}$	r_{DIPE}	$r_{propene+2DIPE}$
369	4.56	2.74	10.04
371	6.07	3.30	12.67
373	7.71	3.77	15.25
375	10.51	4.84	20.19
377	13.32	5.67	24.66
379	16.00	6.14	28.28
381	20.44	7.29	35.02

Table 3.120: Temperature dependence of propan-2-ol dehydration.

HYMST 798Ex	Rate / 10^{16}molecules $g^{-1}s^{-1}$		
Temperature/K	$r_{Propene}$	r_{DIPE}	$r_{propene+2DIPE}$
369	11.31	2.09	15.49
371	14.27	2.63	19.53
373	18.03	3.36	24.75
375	23.28	4.32	31.92
377	28.08	5.06	38.20
379	36.00	6.33	48.66
381	46.61	7.85	62.31

Table 3.121: Temperature dependence of propan-2-ol dehydration.

HYST 823	Rate / 10^{16}molecules $g^{-1}s^{-1}$		
Temperature/K	$r_{Propene}$	r_{DIPE}	$r_{propene+2DIPE}$
367	0.59	0.39	1.37
369	0.78	0.52	1.82
372	1.17	0.73	2.63
374	1.61	0.88	3.37
376	2.33	1.25	4.83
379	3.36	1.77	6.90
381	4.25	2.12	8.49
383	5.40	2.59	10.58

Table 3.122: Temperature dependence of propan-2-ol dehydration.

HYST 823Ex	Rate / 10^{16}molecules $g^{-1}s^{-1}$		
Temperature/K	$r_{Propene}$	r_{DIPE}	$r_{propene+2DIPE}$
367	6.22	1.60	9.42
369	8.25	2.15	12.55
370	9.08	2.22	13.52
371	9.51	2.34	14.19
373	13.02	3.33	19.68
376	18.52	4.45	27.42
378	23.10	5.62	34.34
381	32.23	7.35	46.93

Table 3.123: Temperature dependence of propan-2-ol dehydration.

HYMST 848	Rate / 10^{16}molecules $g^{-1}s^{-1}$		
Temperature/K	$r_{Propene}$	r_{DIPE}	$r_{propene+2DIPE}$
369	3.61	1.89	7.39
371	4.85	2.29	9.43
373	6.32	2.77	11.86
375	7.68	3.22	14.12
377	10.27	4.02	18.31
379	12.53	4.44	21.41
381	15.81	5.25	26.31

Table 3.124: Temperature dependence of propan-2-ol dehydration.

HYMST 848Ex	Rate / 10^{16}molecules $g^{-1}s^{-1}$		
Temperature/K	$r_{Propene}$	r_{DIPE}	$r_{propene+2DIPE}$
369	15.39	3.08	21.55
371	19.66	3.85	27.36
373	25.41	4.88	35.17
375	33.36	6.12	45.60
377	40.39	7.15	54.69
379	47.96	8.54	65.04
381	59.33	9.97	79.27

Table 3.125: Temperature dependence of propan-2-ol dehydration.

HYST 873	Rate / 10^{16}molecules $g^{-1}s^{-1}$		
Temperature/K	$r_{Propene}$	r_{DIPE}	$r_{propene+2DIPE}$
365	0.42	0.26	0.94
367	0.54	0.32	1.18
370	0.89	0.49	1.87
374	1.43	0.83	3.09
376	2.59	1.24	5.07
379	2.93	1.57	6.07
380	3.64	1.93	7.50
383	5.17	2.47	10.11
384	5.68	2.70	11.08

Table 3.126: Temperature dependence of propan-2-ol dehydration.

HYST 873Ex	Rate / 10^{16}molecules $g^{-1}s^{-1}$		
Temperature/K	$r_{Propene}$	r_{DIPE}	$r_{propene+2DIPE}$
366	5.94	2.76	11.46
368	7.34	3.08	13.50
370	10.23	4.16	18.55
372	13.13	5.20	23.53
373	15.17	5.93	27.03
375	18.60	7.04	32.68
379	29.09	10.18	49.45
381	36.87	12.18	61.23

Table 3.127: Temperature dependence of propan-2-ol dehydration.

HYST 923	Rate / 10^{16}molecules $g^{-1}s^{-1}$		
Temperature/K	$r_{Propene}$	r_{DIPE}	$r_{propene+2DIPE}$
366	0.62	0.47	1.56
368	0.78	0.59	1.96
369	0.95	0.66	2.27
370	1.18	0.72	2.62
371	1.28	0.84	2.96
372	1.45	0.96	3.37
373	1.62	1.07	3.76
375	2.30	1.39	5.08
378	3.60	2.04	7.68
380	4.30	2.34	6.64

Table 3.128: Temperature dependence of propan-2-ol dehydration.

HYST 923Ex	Rate / 10^{16}molecules $g^{-1}s^{-1}$		
Temperature/K	$r_{Propene}$	r_{DIPE}	$r_{propene+2DIPE}$
368	4.19	2.41	9.01
370	5.22	3.01	11.24
372	6.43	3.80	14.03
373	8.20	4.53	17.26
375	10.80	6.04	22.88
377	14.59	7.38	29.35
379	17.61	9.05	35.71
381	22.79	11.14	45.07
383	29.39	12.97	55.33

Table 3.129: Temperature dependence of propan-2-ol dehydration.

HYST 973	Rate / 10^{16}molecules $g^{-1}s^{-1}$		
Temperature/K	$r_{Propene}$	r_{DIPE}	$r_{propene+2DIPE}$
365	0.80	0.56	1.92
366	0.93	0.71	2.35
369	1.43	1.06	3.55
371	2.03	1.33	4.69
373	2.52	1.62	5.76
375	3.56	2.31	8.18
382	7.02	4.91	16.84

Table 3.130: Temperature dependence of propan-2-ol dehydration.

HY973Ex	Rate / 10^{16}molecules $g^{-1}s^{-1}$		
Temperature/K	$r_{Propene}$	r_{DIPE}	$r_{propene+2DIPE}$
367	4.62	2.60	9.82
369	6.05	3.42	12.89
371	8.13	4.50	17.13
373	10.29	5.58	21.45
375	13.45	6.87	27.19
377	17.59	8.73	35.05
379	21.61	10.99	43.59
381	27.47	13.19	53.85
383	36.28	16.15	68.58

Table 3.131: Temperature dependence of propan-2-ol dehydration.

HYST 1023	Rate / 10^{16}molecules $g^{-1}s^{-1}$		
Temperature/K	$r_{Propene}$	r_{DIPE}	$r_{propene+2DIPE}$
365	0.75	0.38	1.51
368	1.14	0.66	2.46
370	1.52	0.82	3.16
372	1.95	1.00	3.95
375	2.93	1.54	6.01
378	5.01	2.38	9.77
381	7.22	3.25	13.72

Table 3.132: Temperature dependence of propan-2-ol dehydration.

HYST 1023Ex	Rate / 10^{16}molecules $g^{-1}s^{-1}$		
Temperature/K	$r_{Propene}$	r_{DIPE}	$r_{propene+2DIPE}$
366	6.81	2.91	12.63
367	7.10	3.08	13.26
368	9.23	3.75	16.73
370	11.71	4.80	21.31
372	14.76	5.94	26.64
375	21.35	8.22	37.79
378	32.21	11.42	55.05
381	43.86	14.81	73.48

Table 3.133: Temperature dependence of propan-2-ol dehydration.

HYST 1073	Rate / 10^{16}molecules $g^{-1}s^{-1}$		
Temperature/K	$r_{Propene}$	r_{DIPE}	$r_{propene+2DIPE}$
367	0.72	0.42	1.56
371	1.17	0.69	2.55
373	1.52	0.82	3.16
376	2.67	1.35	5.37
378	3.20	1.57	6.34
379	3.74	1.60	6.94
382	5.34	2.31	9.96
383	5.93	2.53	10.99

Table 3.134: Temperature dependence of propan-2-ol dehydration.

HYST 1073Ex	Rate / 10^{16}molecules $g^{-1}s^{-1}$		
Temperature/K	$r_{Propene}$	r_{DIPE}	$r_{propene+2DIPE}$
368	4.04	1.44	6.92
370	4.56	1.86	8.28
372	6.10	2.33	10.76
375	8.06	3.14	14.34
381	15.77	5.84	27.45
383	20.16	7.26	34.68

Table 3.135: Temperature dependence of propan-2-ol dehydration.

Sample	Rate / 10^{16}molecules $g^{-1}s^{-1}$; E_{Act}/ $kJmol^{-1}$				
	$r_{Propene}$	r_{DIPE}	$r_{propene+2DIPE}$	$E_{Act}(p)$	$E_{Act}(e)$
NH_4YLS	32.7	2.41	37.52	146	135
HYMST 748	9.54	4.31	18.16	131	86
HYMST 768	7.03	3.99	15.01	136	81
HYMST 783	9.58	3.85	17.28	139	101
HYMST 798	7.69	3.77	15.23	146	96
HYST 823	1.36	0.82	3.00	165	140
HYMST 848	6.10	2.71	11.52	135	100
HYST 873	1.52	0.78	3.08	163	149
HYST 923	1.62	1.07	3.76	165	138
HYST 973	2.52	1.61	5.74	151	145
HYST 1023	2.38	1.26	4.90	165	150
HYST 1073	1.52	0.82	3.16	159	131
HYMST 748Ex	29.85	3.84	37.53	135	122
HYMST 768Ex	24.51	3.55	31.61	129	116
HYMST 783Ex	26.31	3.56	33.43	134	126
HYMST 798Ex	20.61	3.55	27.71	137	128
HYST 823Ex	13.02	3.33	19.68	137	129
HYMST 848Ex	25.34	5.05	35.44	131	115
HYST 873Ex	15.18	5.93	27.04	142	118
HYST 923Ex	8.21	4.45	17.11	155	135
HYST 973Ex	10.28	5.59	21.46	149	132
HYST 1023Ex	15.94	6.61	29.16	148	130
HYST 1073Ex	6.27	2.47	11.21	127	124

Table 3.136: Activities at 373K and activation energies for the dehydration of propan-2-ol.

Sample	Percent change on extraction	
	$r_{Propene}$	r_{DIPE}
HYMST 748	213	-18
HYMST 768	249	-13
HYMST 783	175	-7
HYMST 798	168	-6
HYST 823	857	306
HYMST 848	315	86
HYST 873	899	660
HYST 923	407	316
HYST 973	308	247
HYST 1023	570	425
HYST 1073	312	201

Table 3.137: Effect of extraction on product formation in the dehydration of propan-2-ol.

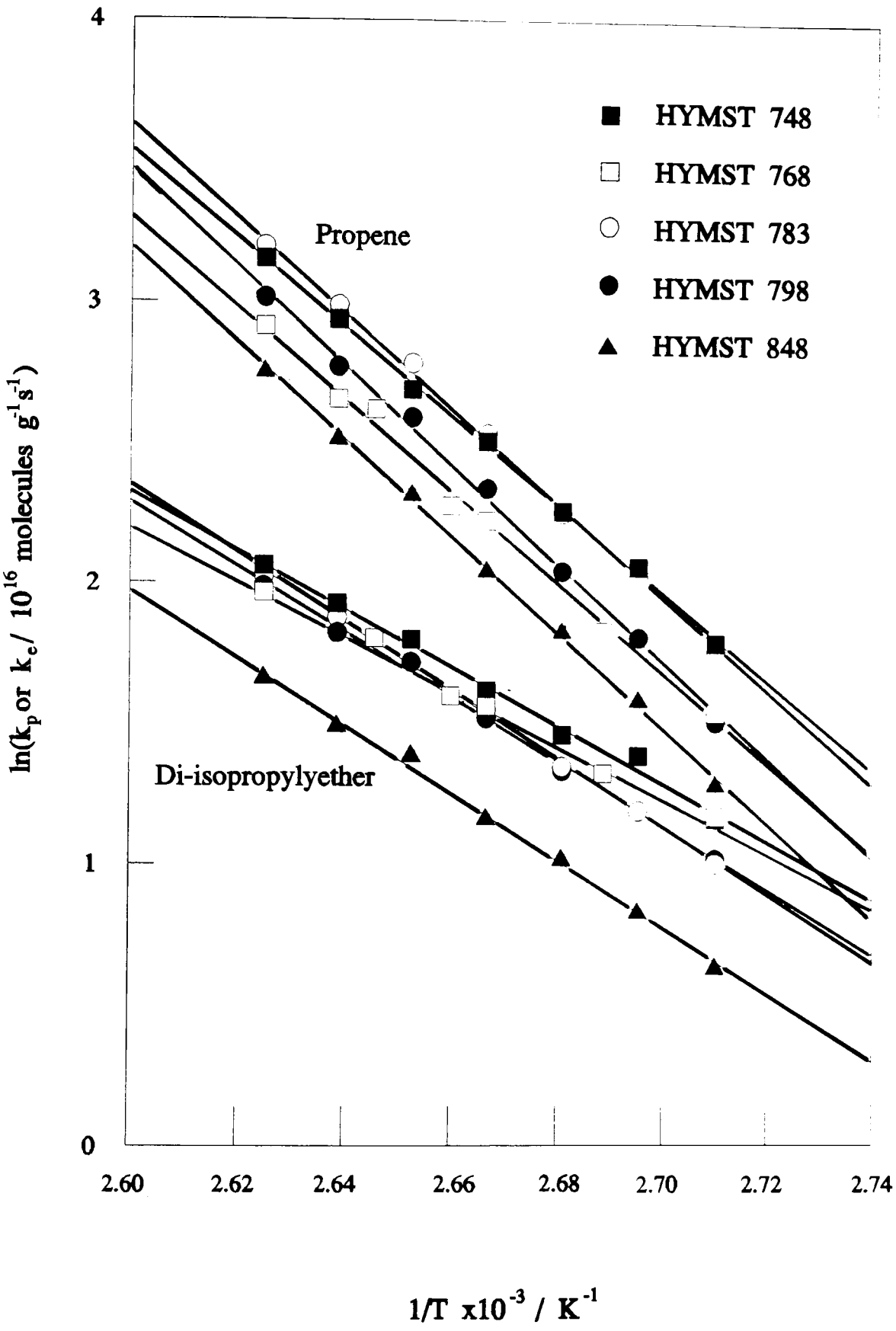

Figure 3.31: The temperature dependence for the formation of propene and di-isopropylether on HYMST x samples.

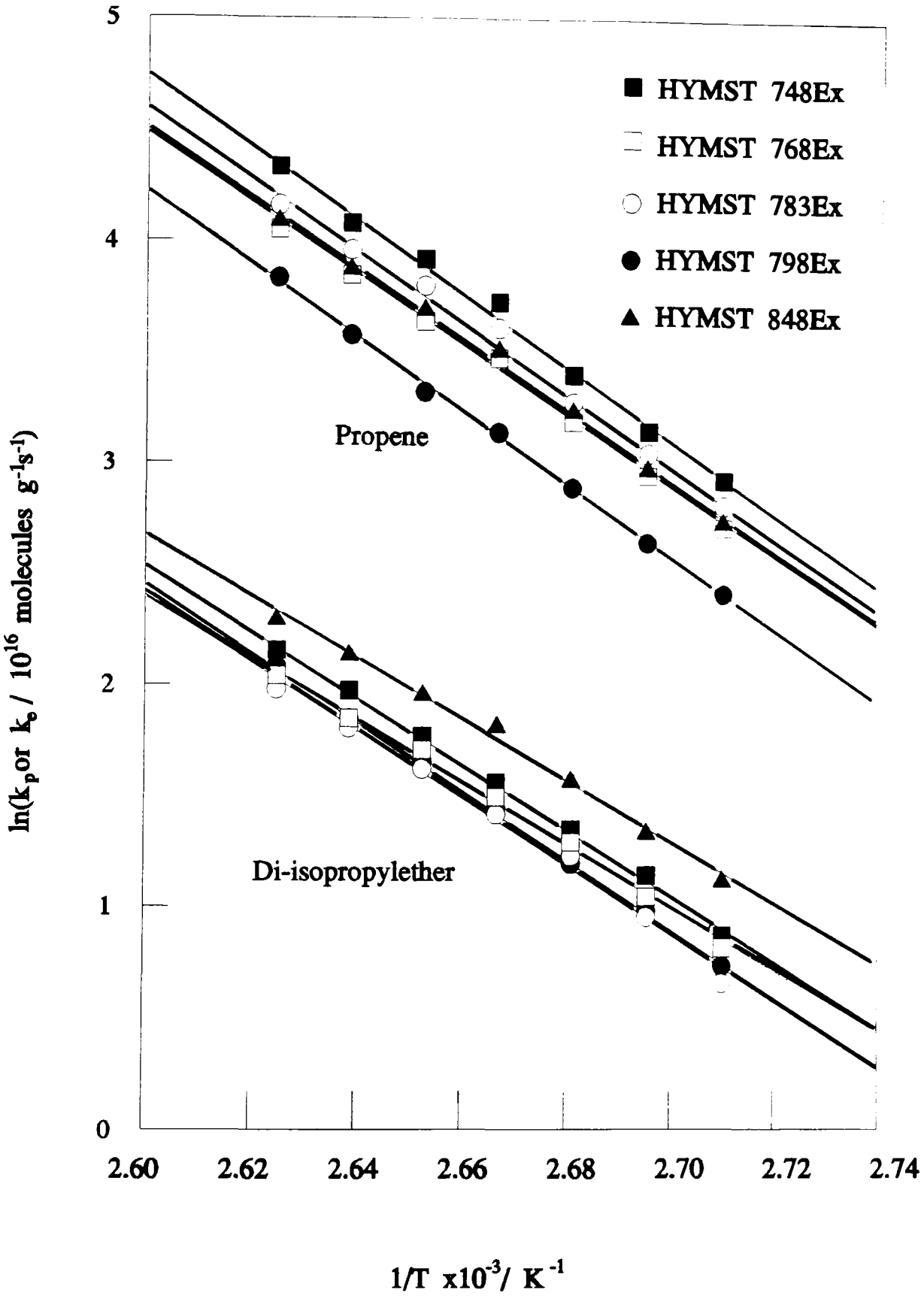

Figure 3.32:The temperature dependence for the formation of propene and di-isopropylether on HYMST x EX samples.

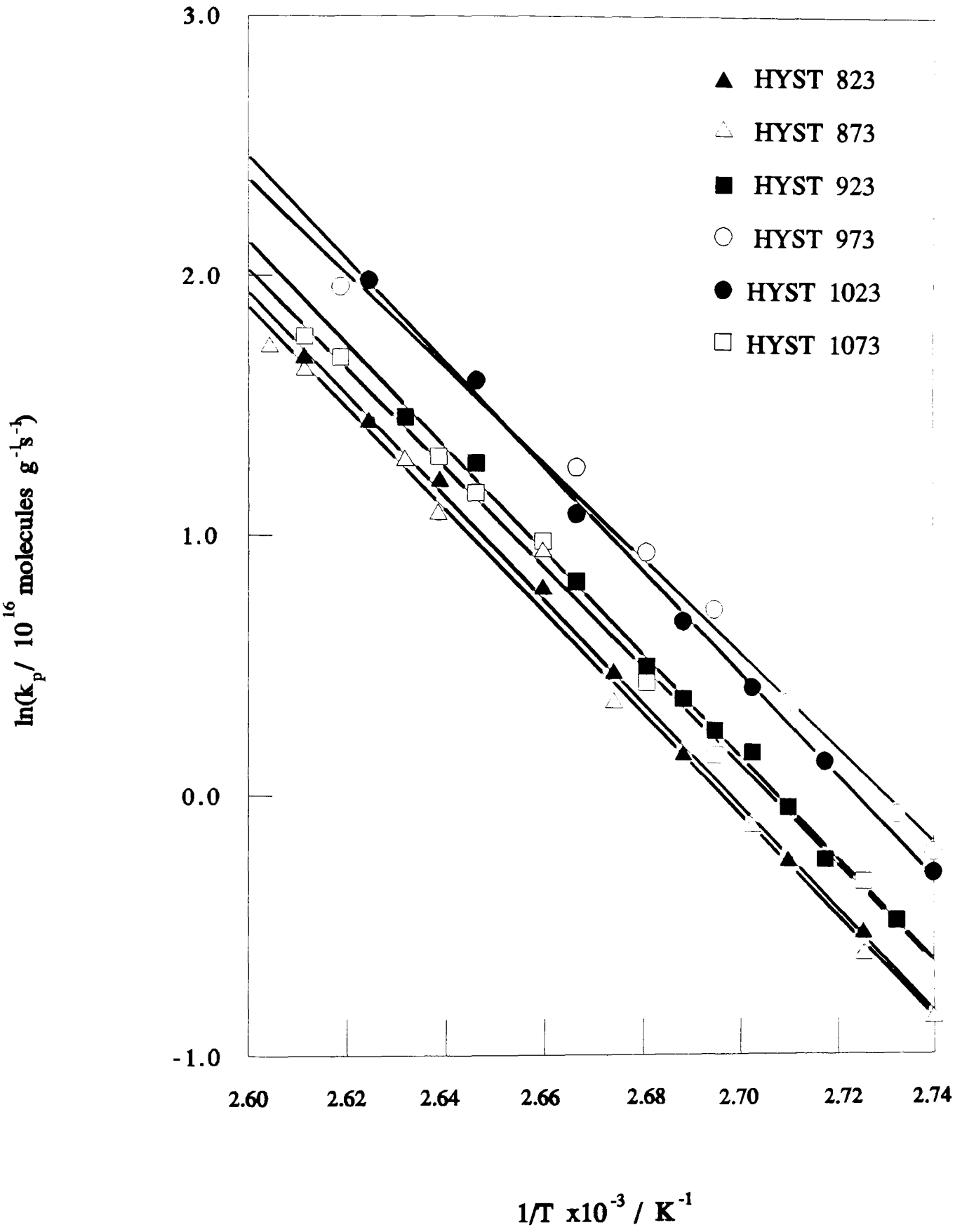

Figure 3.33: The temperature dependence for the formation propene on HYST x samples.

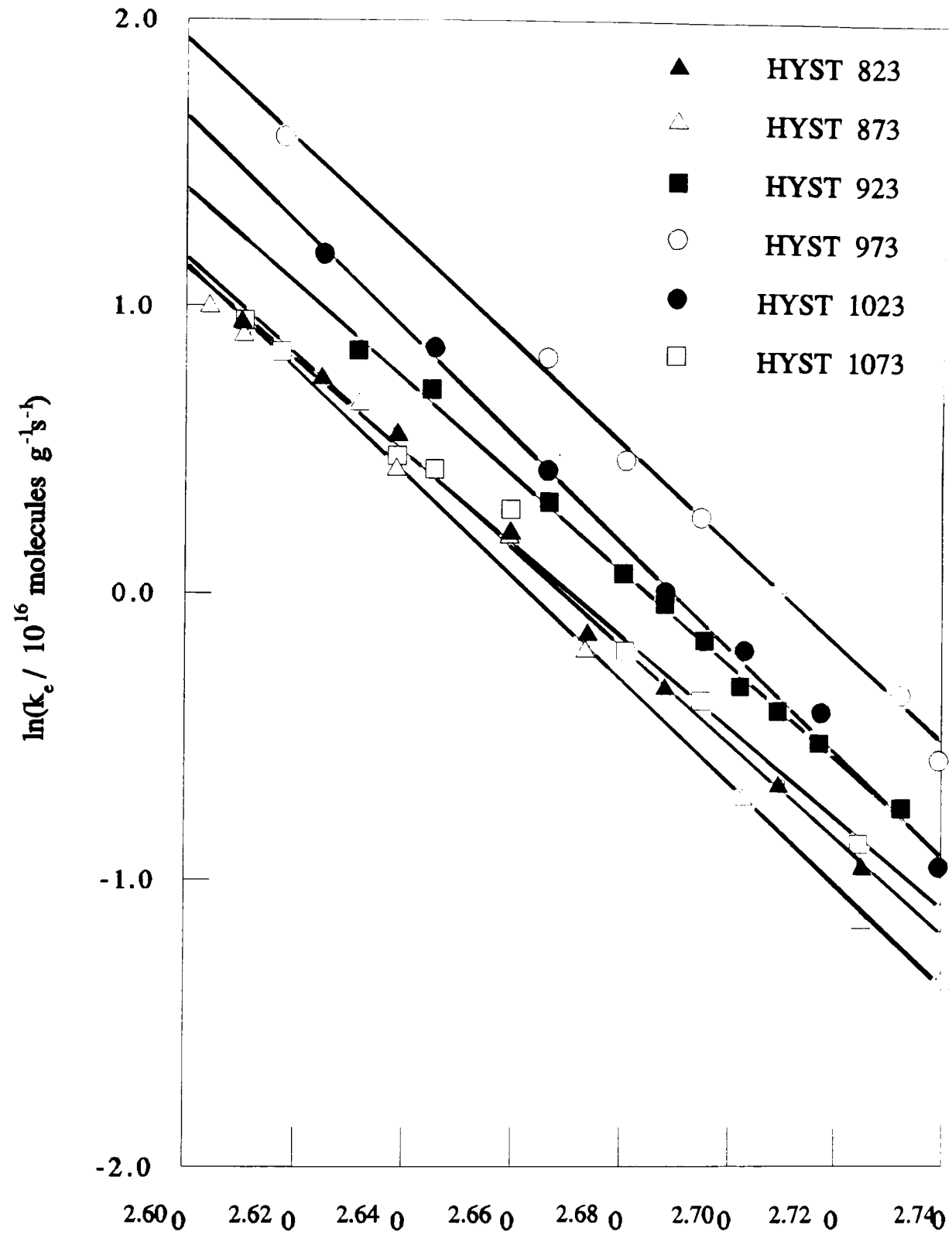

Figure 3.34: The temperature dependence for the formation di-isopropylether on HYST x samples.

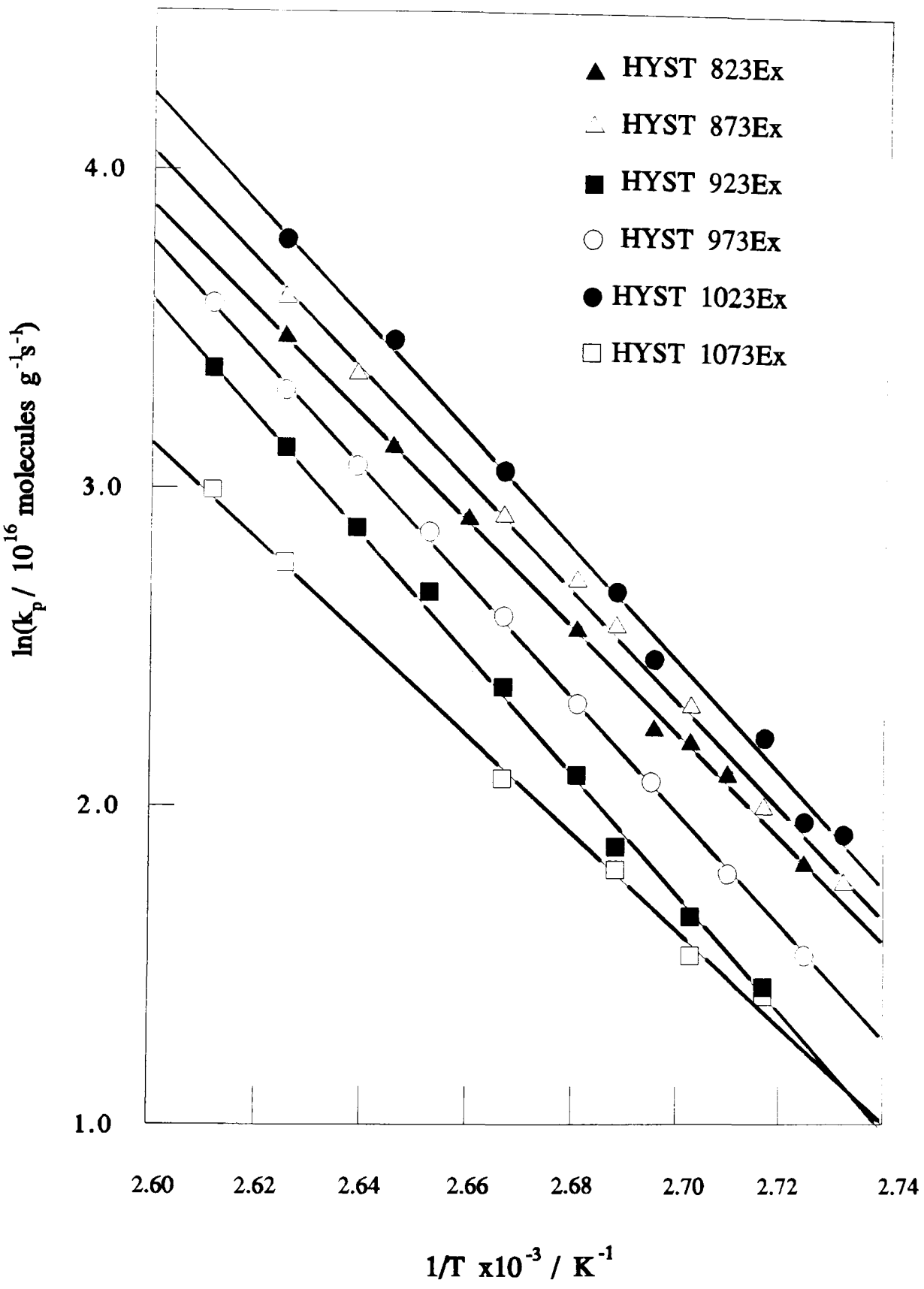

Figure 3.35: The temperature dependence for the formation propene on HYST x Ex samples.

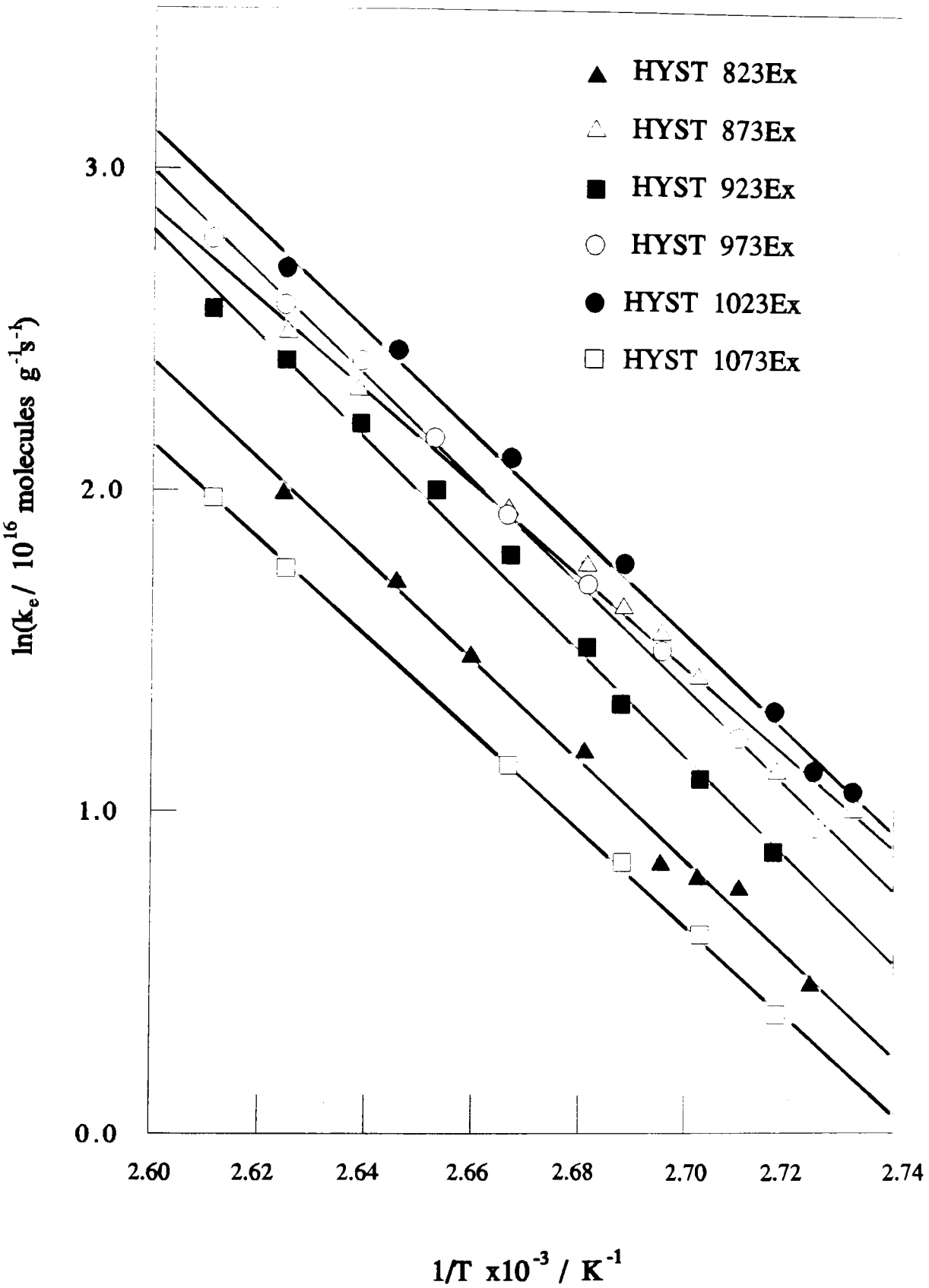

Figure 3.36: The temperature dependence for the formation di-isopropylether on HYST x Ex samples.

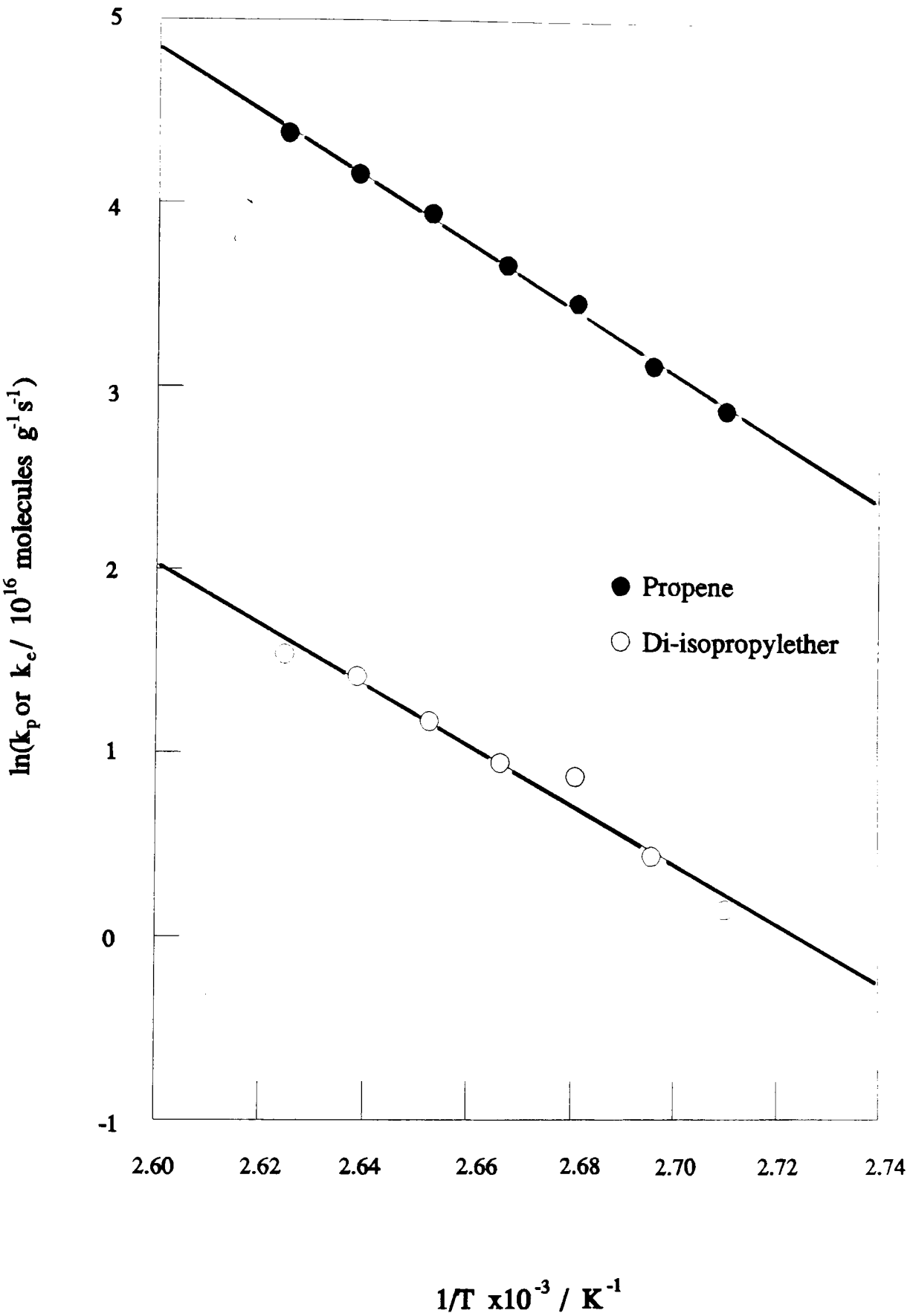

Figure 3.37: The temperature dependence for the formation of propene and diisopropylether on NH_4YLS.

HYMST 748		Mass = 0.0151g		
Pressure propan-2-ol /kPa	Rate / 10^{16} molecules $s^{-1}g^{-1}$			S_e
	$r_{Propene}$	r_{DIPE}	$r_{propene+2DIPE}$	
Reaction Temperature 369K				
1.13	1.63	0.44	2.51	0.27
1.08	1.67	0.41	2.49	0.25
1.03	1.67	0.46	2.59	0.28
0.96	1.64	0.43	2.50	0.26
0.83	1.67	0.41	2.49	0.25
0.68	1.69	0.41	2.51	0.24
Reaction Temperature 373K				
1.20	7.29	2.11	11.51	0.29
1.19	7.25	2.15	11.55	0.30
1.13	7.13	2.04	11.21	0.29
1.06	7.45	2.19	11.83	0.29
0.98	7.45	2.24	11.93	0.30
0.85	7.45	2.15	11.85	0.29
Reaction Temperature 378K				
1.08	12.90	3.61	20.12	0.28
1.06	12.28	3.48	19.24	0.28
0.95	12.77	3.61	19.99	0.28
0.90	13.02	3.59	20.20	0.28
0.89	12.65	3.69	20.03	0.29
Reaction Temperature 383K				
1.19	19.69	4.81	29.31	0.24
1.05	19.83	4.82	29.47	0.24
0.98	19.90	4.81	29.52	0.24
0.94	20.02	4.82	29.66	0.24
0.89	20.18	4.74	29.66	0.23

Table 3.138: Pressure dependence of propan-2-ol dehydration.

HYMST 748Ex		Mass = 0.0162g		
Pressure propan-2-ol /kPa	Rate / 10^{16} molecules $s^{-1}g^{-1}$			S_e
	$r_{Propene}$	r_{DIPE}	$r_{propene+2DIPE}$	
Reaction Temperature 369K				
1.37	9.64	1.46	12.56	0.15
1.37	9.59	1.46	12.51	0.15
1.35	9.66	1.46	12.58	0.15
1.31	9.73	1.47	12.67	0.15
1.27	9.78	1.48	12.74	0.15
1.23	9.95	1.49	12.93	0.15
1.20	10.00	1.50	13.00	0.15
1.17	10.13	1.49	13.11	0.15
1.15	10.20	1.51	13.22	0.15
1.12	10.29	1.52	13.33	0.15
Reaction Temperature 373K				
1.41	19.01	2.78	24.57	0.15
1.35	19.25	2.78	24.81	0.14
1.30	19.50	2.80	25.10	0.14
1.24	19.59	2.80	25.19	0.14
1.20	19.78	2.81	25.40	0.14
1.15	19.91	2.81	25.53	0.14
1.11	20.06	2.83	25.72	0.14
1.07	20.15	2.84	25.83	0.14
1.05	20.29	2.83	25.85	0.14
1.02	20.40	2.87	26.14	0.14
Reaction Temperature 375K				
1.40	28.36	3.48	35.32	0.12
1.33	28.72	3.51	35.74	0.12
1.27	28.94	3.51	35.96	0.12
1.23	29.25	3.52	36.29	0.12
1.18	29.50	3.53	36.56	0.12

Table 3.139: Pressure dependence of propan-2-ol dehydration.

HYMST 748Ex	Mass = 0.0162g			
Pressure propan-2-ol /kPa	Rate / 10^{16} molecules $s^{-1}g^{-1}$			S_e
	$r_{Propene}$	r_{DIPE}	$r_{propene+2DIPE}$	
Reaction Temperature 375K				
1.09	30.04	3.53	37.10	0.12
1.05	30.30	3.58	37.46	0.12
1.02	30.55	3.57	37.69	0.12
0.98	30.75	3.58	37.91	0.12
0.96	31.06	3.60	38.26	0.12
Reaction Temperature 378K				
1.43	35.74	4.79	45.32	0.13
1.38	36.08	4.80	45.68	0.13
1.29	36.86	4.83	46.52	0.12
1.25	37.22	4.84	46.90	0.13
1.17	38.03	4.93	47.89	0.13
1.13	38.34	4.89	48.12	0.13
1.10	36.63	4.85	46.33	0.13
1.07	39.04	4.89	48.82	0.13
1.03	39.48	4.86	49.20	0.12
1.00	39.55	4.90	49.35	0.12
Reaction Temperature 381K				
1.37	53.50	6.49	66.48	0.12
1.31	54.15	6.49	67.13	0.12
1.25	54.77	6.52	67.81	0.12
1.19	55.27	6.49	68.28	0.12
1.14	55.93	6.51	68.95	0.12
1.09	56.36	6.51	69.38	0.12
1.05	56.92	6.49	69.90	0.11
1.01	57.35	6.48	70.31	0.11
0.98	57.78	6.55	70.88	0.11
0.97	57.75	6.54	70.83	0.11

Table 3.139 (cont.): Pressure dependence of propan-2-ol dehydration.

HYST 823		Mass = 0.0174g		
Pressure propan-2-ol /kPa	Rate / 10^{16} molecules $s^{-1}g^{-1}$			S_e
	$r_{Propene}$	r_{DIPE}	$r_{propene+2DIPE}$	
Reaction Temperature 370K				
1.66	0.40	0.16	0.72	0.40
1.59	0.36	0.17	0.70	0.47
1.53	0.37	0.18	0.73	0.49
1.45	0.37	0.19	0.75	0.51
1.39	0.39	0.19	0.77	0.49
1.33	0.40	0.20	0.80	0.50
1.28	0.40	0.20	0.80	0.50
1.23	0.40	0.20	0.80	0.50
1.18	0.40	0.21	0.82	0.53
602	0.42	0.21	0.84	0.50
Reaction Temperature 372K				
1.39	0.52	0.28	1.08	0.54
1.34	0.52	0.26	1.04	0.50
1.30	0.56	0.26	1.08	0.46
1.24	0.56	0.27	1.10	0.48
1.20	0.56	0.28	1.12	0.50
1.16	0.57	0.28	1.13	0.49
1.12	0.59	0.29	1.17	0.49
1.09	0.59	0.29	1.17	0.49
1.07	0.60	0.29	1.18	0.48
1.04	0.59	0.29	1.17	0.49
Reaction Temperature 375K				
1.41	1.06	0.49	2.04	0.46
1.35	1.08	0.50	2.08	0.46
1.27	1.09	0.51	2.11	0.47
1.19	1.11	0.52	2.15	0.47
1.13	1.14	0.53	2.20	0.46

Table 3.140: Pressure dependence of propan-2-ol dehydration.

HYSY 823		Mass = 0.0174		
Pressure propan-2-ol /kPa	Rate / 10^{16} molecules $s^{-1}g^{-1}$			S_e
	$r_{Propene}$	r_{DIPE}	$r_{propene+2DIPE}$	
Reaction Temperature 375K				
1.08	1.16	0.54	2.24	0.47
1.06	1.16	0.55	2.26	0.47
1.04	1.20	0.55	2.30	0.46
1.02	1.18	0.55	2.28	0.47
1.00	1.20	0.54	2.28	0.45
Reaction Temperature 378K				
1.40	1.53	0.70	2.93	0.46
1.37	1.53	0.70	2.93	0.46
1.33	1.53	0.70	2.93	0.46
1.26	1.56	0.71	2.98	0.46
1.20	1.62	0.72	3.06	0.44
1.15	1.65	0.74	3.13	0.45
1.09	1.65	0.75	3.15	0.45
1.05	1.72	0.74	3.20	0.43
1.03	1.74	0.76	3.26	0.44
0.98	1.75	0.78	3.31	0.45
Reaction Temperature 382K				
1.51	2.26	1.01	4.28	0.45
1.43	2.26	1.00	4.26	0.44
1.46	2.29	0.99	4.27	0.43
1.16	2.41	1.02	4.45	0.42
1.12	2.42	1.03	4.48	0.43
1.09	2.46	1.05	4.56	0.43
1.06	2.51	1.06	4.63	0.42
1.03	2.54	1.07	4.68	0.42
1.01	2.57	1.08	4.83	0.42
0.99	2.61	1.08	4.77	0.41

Table 3.140(cont.): Pressure dependence of propan-2-ol dehydration.

HYST 823Ex	Mass = 0.0152g			
Pressure propan-2-ol /kPa	Rate / 10^{16} molecules $s^{-1}g^{-1}$			S_e
	$r_{Propene}$	r_{DIPE}	$r_{propene+2DIPE}$	
Reaction Temperature 373K				
1.41	19.14	2.36	23.86	0.12
1.35	19.26	2.38	24.02	0.12
1.29	19.22	2.38	23.98	0.12
1.24	19.38	2.39	24.16	0.12
1.19	19.66	2.43	24.52	0.12
1.15	19.70	2.41	24.52	0.12
1.11	19.64	2.43	24.50	0.12
1.07	20.07	2.46	24.99	0.12
1.04	19.89	2.44	24.77	0.12
1.00	20.14	2.48	25.10	0.12
Reaction Temperature 375K				
1.40	23.79	3.16	30.11	0.13
1.34	24.15	3.17	30.49	0.13
1.28	24.44	3.18	30.80	0.13
1.22	24.60	3.24	31.08	0.13
1.17	25.02	3.24	31.50	0.13
1.12	25.18	3.26	31.70	0.13
1.08	25.35	3.26	31.87	0.13
1.04	25.54	3.29	32.12	0.13
1.01	25.87	3.31	32.49	0.13
0.97	26.01	3.32	32.65	0.13

Table 3.141: Pressure dependence of propan-2-ol dehydration.

HYST 823Ex		Mass = 0.0152g		
Pressure propan-2-ol /kPa	Rate / 10^{16} molecules $s^{-1}g^{-1}$			S_e
	$r_{Propene}$	r_{DIPE}	$r_{propene+2DIPE}$	
Reaction Temperature 378K				
1.39	27.34	3.78	34.90	0.14
1.33	27.57	3.81	35.19	0.14
1.28	27.95	3.84	35.63	0.14
1.23	28.36	3.88	36.12	0.14
1.18	28.28	3.89	36.06	0.14
1.14	28.49	3.88	36.25	0.14
1.10	28.70	3.87	36.44	0.13
1.07	28.86	3.92	36.70	0.14
1.04	29.05	3.89	36.83	0.13
1.00	29.28	3.91	37.10	0.13
Reaction Temperature 381K				
1.37	45.76	5.57	60.70	0.12
1.30	44.57	5.66	55.89	0.13
1.25	44.53	5.66	55.85	0.13
1.20	44.76	5.66	56.08	0.13
1.16	44.95	5.63	56.21	0.13
1.12	44.86	5.69	56.24	0.13
1.08	45.01	5.59	56.19	0.12
1.05	45.20	5.59	56.38	0.12
1.02	45.26	5.57	56.40	0.12
0.99	45.49	5.59	56.67	0.12

Table 3.141(cont.): Pressure dependence of propan-2-ol dehydration.

HYST 1073		Mass = 0.0163g		
Pressure propan-2-ol /kPa	Rate / 10^{16} molecules $s^{-1}g^{-1}$			S_e
	$r_{Propene}$	r_{DIPE}	$r_{propene+2DIPE}$	
Reaction Temperature 369K				
1.30	1.35	1.06	3.47	0.79
1.26	1.35	1.02	3.39	0.76
1.23	1.37	1.03	3.43	0.75
1.20	1.33	1.00	3.33	0.75
1.17	1.35	0.99	3.33	0.73
1.13	1.35	0.98	3.31	0.73
1.10	1.37	0.94	3.25	0.69
1.06	1.35	0.91	3.17	0.67
1.02	1.35	0.91	3.17	0.67
1.0	1.33	0.90	3.13	0.68
Reaction Temperature 378K				
1.41	3.17	1.72	6.61	0.54
1.34	3.20	1.69	6.58	0.53
1.31	3.21	1.66	6.53	0.52
1.23	3.25	1.67	6.59	0.51
1.19	3.29	1.66	6.61	0.50

Table 3.142: Pressure dependence of propan-2-ol dehydration.

HYST 1073		Mass 0.0163g		
Pressure propan-2-ol /kPa	Rate / 10^{16} molecules $s^{-1}g^{-1}$			S_e
	$r_{Propene}$	r_{DIPE}	$r_{propene+2DIPE}$	
Reaction Temperature 378K				
1.15	3.34	1.66	6.66	0.50
1.09	3.34	1.64	6.62	0.49
1.06	3.38	1.64	6.66	0.49
1.02	3.36	1.60	6.56	0.48
1.00	3.38	1.59	6.56	0.47
Reaction Temperature 381K				
1.40	4.35	2.04	8.43	0.47
1.38	4.48	2.09	8.66	0.47
1.35	4.40	2.04	8.48	0.46
1.28	4.46	2.06	8.58	0.46
1.21	4.58	2.06	8.70	0.45
1.18	4.40	2.06	8.52	0.47
1.15	4.62	2.03	8.68	0.44
1.12	4.67	2.06	8.79	0.44
1.08	4.75	2.05	8.85	0.43
1.04	4.80	2.08	8.96	0.43

Table 3.142(cont.): Pressure dependence of propan-2-ol dehydration.

HYST 1073Ex		Mass = 0.0160g		
Pressure propan-2-ol /kPa	Rate / 10^{16} molecules $s^{-1}g^{-1}$			S_e
	$r_{Propene}$	r_{DIPE}	$r_{propene+2DIPE}$	
Reaction Temperature 369K				
1.39	6.48	1.53	9.54	0.24
1.36	6.50	1.54	9.58	0.24
1.34	6.54	1.55	9.64	0.24
1.32	6.56	1.55	9.66	0.24
1.29	6.58	1.55	9.68	0.24
1.23	6.63	1.57	9.77	0.24
1.18	6.68	1.58	9.84	0.24
1.13	6.68	1.56	9.80	0.23
1.09	6.72	1.58	9.88	0.24
1.05	6.74	1.59	9.92	0.24
Reaction Temperature 375K				
1.39	13.49	3.03	19.53	0.22
1.35	13.57	3.03	19.63	0.22
1.27	13.77	3.06	19.89	0.22
1.20	13.98	3.09	20.16	0.22
1.17	14.06	3.10	20.26	0.22
1.14	14.16	3.14	20.44	0.22
1.12	14.30	3.11	20.52	0.22
1.09	14.36	3.16	20.68	0.22
1.05	14.51	3.16	20.83	0.22
1.00	14.73	3.19	21.11	0.22

Table 3.143: Pressure dependence of propan-2-ol dehydration.

HYST 1073Ex		Mass = 0.0160g		
Pressure propan-2-ol /kPa	Rate / 10^{16} molecules $s^{-1}g^{-1}$			S_e
	$r_{Propene}$	r_{DIPE}	$r_{propene+2DIPE}$	
Reaction Temperature 378K				
1.39	16.81	3.83	24.49	0.23
1.34	16.88	3.84	24.54	0.23
1.28	16.99	3.88	24.75	0.23
1.23	17.07	3.86	24.79	0.23
1.18	17.14	3.89	24.92	0.23
1.14	17.18	3.89	24.96	0.23
1.11	16.72	3.90	24.52	0.23
1.05	16.96	3.92	24.80	0.23
1.01	17.16	3.93	25.02	0.23
0.96	17.40	3.96	25.32	0.23
Reaction Temperature 381K				
1.39	22.76	4.98	32.72	0.22
1.35	23.06	5.02	33.10	0.22
1.29	23.28	5.04	33.36	0.22
1.22	23.53	5.11	33.75	0.22
1.20	23.66	5.09	33.84	0.22
1.17	23.84	5.10	34.04	0.21
1.12	24.18	5.14	34.46	0.21
1.07	24.41	5.16	34.73	0.21
1.03	24.65	5.19	35.03	0.21
1.00	24.94	5.18	35.30	0.21

Table 3.143(cont.): Pressure dependence of propan-2-ol dehydration.

Sample	Activation Energy /kJmol^{-1}		Number of Points
	Propene	Ether	
HYMST 748	163	163	4
HYST 823	165	171	5
HYST 1073	175	72	3
HYMST 748Ex	116	136	5
HYST 823Ex	118	115	4
HYST 1073Ex	120	113	4

Table 3.144: Pressure dependence of propan-2-ol dehydration.

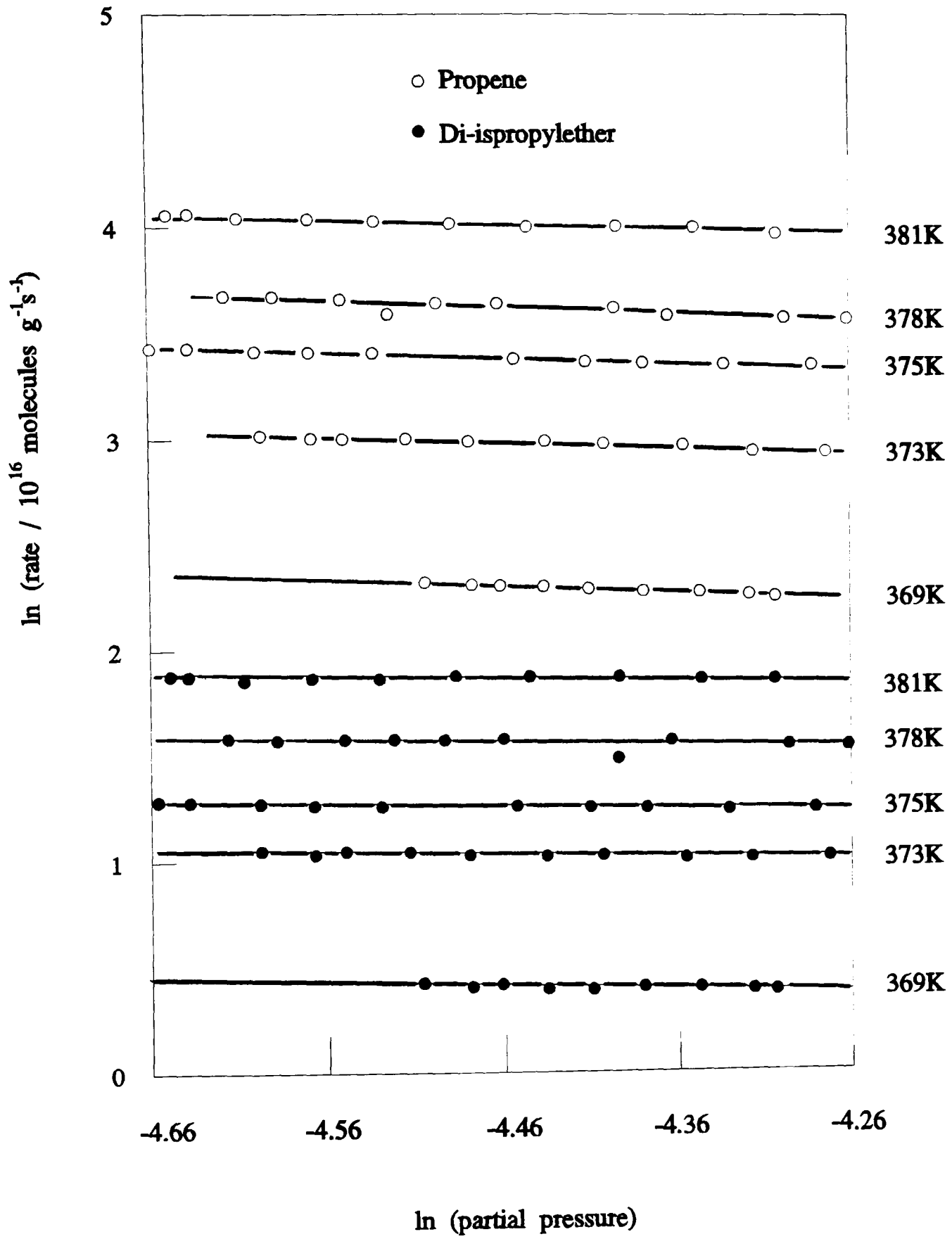

Figure 3.38: Pressure depenence of propan-2-ol dehydration - HYMST 748Ex.

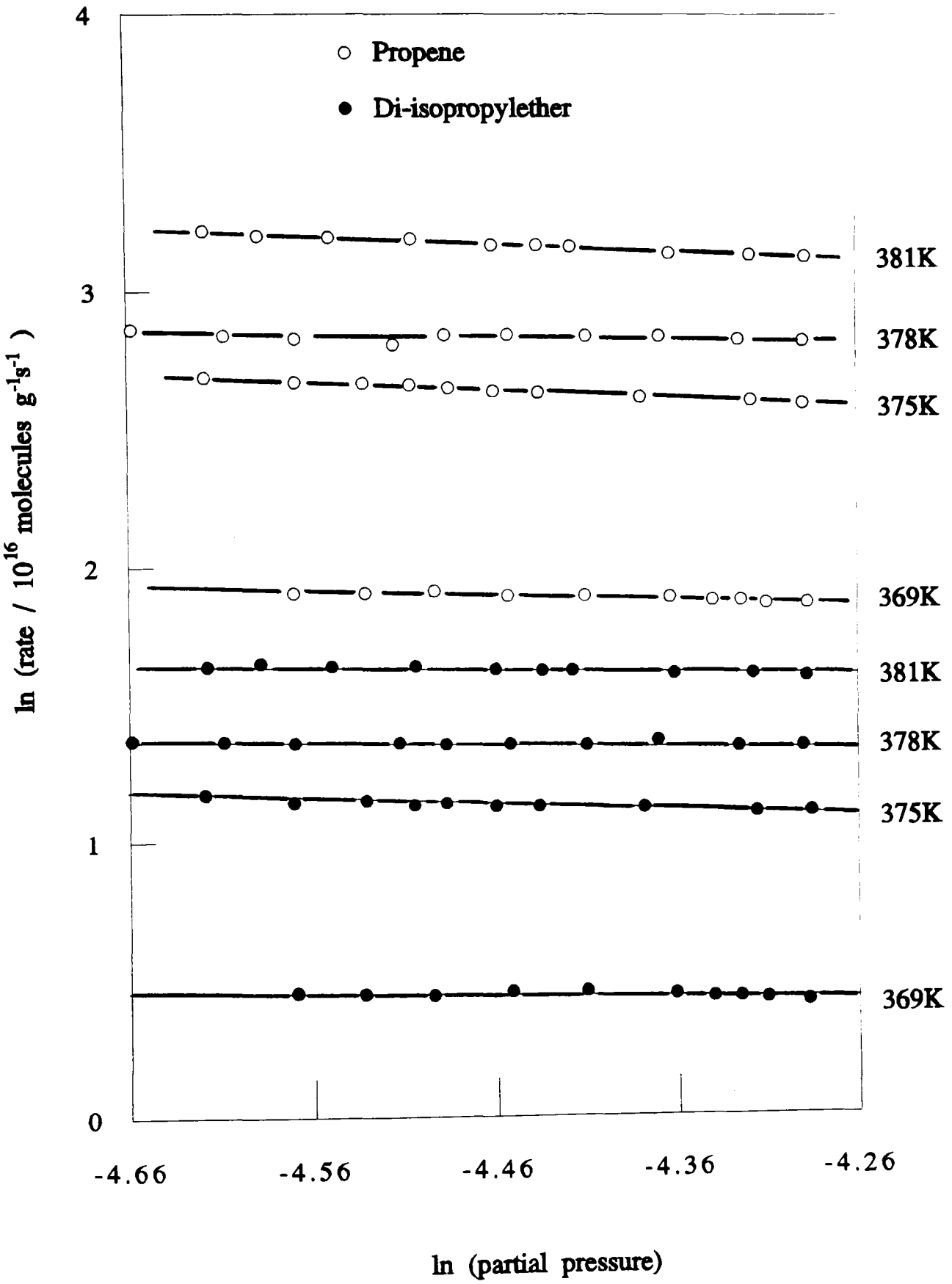

Figure 3.39: Pressure dependence of propan-2-ol dehydration - HYST 1073Ex.

Time/hr	$r_{Propene}/x10^{17}$ molecules $g^{-1}s^{-1}$					
	1	2	3	4	5	6
Initial	1.13	7.30	11.07	10.71	10.60	2.09
2	1.11	7.40	12.25	13.00	9.98	2.48
4	1.11	7.40	13.00	13.84	9.90	2.48
6	1.09	7.40	13.00	14.36	9.55	2.44
8	1.09	7.26	13.00	14.57	9.17	2.37
10	1.08	7.17	12.89	14.52	8.85	2.29
12	1.07	7.05	12.73	14.56	8.62	2.23
14	1.06	6.99	12.57	14.47	8.34	2.17
16	1.05	6.88	12.36	14.21	8.15	2.14
18	1.04	6.78	12.64	13.94	7.76	2.07
Coke /wt%	6.1	9.3	6.9	10.3	7.2	6.1
DIPE/Propene	0.213	0.039	-	0.028	0.001	0.103

Bakeout key:

1 673K ½hour helium.
2 673K ½hour helium, 673K ½hour propan-2-ol 1166Pa
3 673K ½hour helium, 582K ½hour propan-2-ol 1166Pa
4 673K ½hour helium, 479K ½hour propan-2-ol 1166Pa
5 673K ½hour helium, 419K ½hour propan-2-ol 1166Pa
6 673K ½hour helium, 673K ½hour propan-2-ol 1166Pa, degassed in helium

Table 3.145: Precoking experiments on HYST 1073Ex - propan-2-ol dehydration.

4 Discussion

The aim of the research was to produce a series of mildly dealuminated Y zeolite samples with framework aluminium contents of between 56 Al_F puc, the value of the parent sample, and 30 Al_F puc, the theoretical maximum concentration of strong acid sites.[77] Such sites are considered to be associated with those framework aluminium atoms that have no aluminium atoms in the second neighbour position. Removal of the extrastructural aluminium from these samples without drastically altering the framework constitution was investigated. The nature of these samples, together with those previously produced by a hydrothermal method and having a framework aluminium content of between 30 Al_F puc and 10 Al_F puc,[201] was probed by x-ray powder diffraction, infrared spectroscopy and temperature programmed desorption. Their catalytic activity was assessed by studying the test reactions of n-hexane cracking, toluene disproportionation, cumene dealkylation and propan-2-ol dehydration, reactions which are generally accepted to require acid sites of decreasing strength.[184]

4.1 Preparation and Characterisation

Five samples were prepared by mild hydrothermal dealumination of NH_4YLS, a material prepared from NH_4YAS by repeated ion exchange and thermal treatment cycles to produce a sample with a very low sodium content. X-ray crystallography established that the samples had retained crystallinity and the unit cell size was found to decrease with increasing temperature of dealumination, suggesting that structural dealumination and, more importantly, structural healing had also occurred, since the latter was a source of concern when using partial pressures of water vapour. Simply removing aluminium from the framework and depositing it as extraframework species would not affect the unit cell size, but would create hydroxyl nest vacancies in the fabric of the structure. The decrease in unit cell is brought about by the formation of additional Si-O bonds, which at 0.161nm are shorter than the Al-O bonds (0.174nm) that they have replaced. The new bonds can be formed either by the 'dehydration' of the hydroxyl nests, or by the transport of silicon from other

areas of the crystallite, creating mesoporosity. Both methods would result in a reduction in the total number of unit cells as aluminium has been expelled from the framework and no new material has been introduced.

The extraction of extraframework aluminium from the catalysts is considered desirable as it has been shown to increase both the total effective acidity and the catalytic activity of the samples.[201] Extraction can be performed using either mineral acid, or a suitable chelating agent such as EDTA.[31,231] However, with extraction there is also a risk of removing further structural aluminium, especially from samples which are not sufficiently dealuminated to be 'ultrastable'. Preliminary experiments assessing the effects of the extraction procedure on the framework and nonframework aluminium were performed. The strongly steamed samples, prepared by Rhodes,[201] had been extracted using the tetrasodium salt of EDTA; this was therefore a two stage extraction, as the sodium ions introduced would have to be re-exchanged using ammonium chloride. This involved procedure, together with the desire to retain the initial low sodium integrity of the samples, prompted investigation of other salts of EDTA. A useable concentration of tetrahydrogen EDTA was found to be too acidic (pH=2.8), causing the complete breakdown of the structure, as shown by the amorphous ridge shown in the x-ray trace, figure 3.3. The tetra-ammonium salt was more soluble, and the acidity of the solution could be decreased to pH 4.3 by the addition of ammonium hydroxide solution without precipitation of the salt, providing a less acidic medium for the extraction. These conditions were found to be effective in extraframework aluminium removal without drastically changing the unit cell constant. The pH of the suspension, monitored during the extraction procedure, revealed an immediate slight rise on the addition of the zeolite, with a final value of 5.2. This indicated that the ammonium EDTA was still in excess, and that there was no possibility of precipitation of EDTA within the zeolite. Analysis of the washings by atomic adsorption confirmed that the majority of the extraframework aluminium had been removed and x-ray crystallography verified that the composition and crystallinity of the structure had been essentially preserved. In view of the desire not to subject the samples to

another, possibly destructive, procedure, and as trial experiments removed most of the nonframework material from HYST 823, it was deemed sufficient to perform only one extraction procedure on the mildly dealuminated samples.

Both the mildly steamed and the severely steamed sets of catalysts were examined using x-ray crystallography and infrared spectroscopy. The infrared results are somewhat disappointing, with there being no discernable difference between the mildly dealuminated samples, although there is a slight increase in wavenumber on extraction. The strongly steamed samples however show a discrete change with increasing temperature of dealumination, and on extraction a slight drop in wavenumber is evident. The lattice vibrations may be influenced by the change in cation between the unextracted and extracted samples, and indeed the presence of the extrastructural framework aluminium itself. The failure to resolve the mildly dealuminated samples, as they are shown to be different by x-ray crystallography and temperature programmed desorption studies (see below), is more difficult to explain. It may be as simple as dealumination of the structure sharpens the peaks as it becomes more siliceous; in the region of the mildly steamed samples the peak is therefore too rounded to determine the wavenumber of the maximum with accuracy. Alternatively, the concentration of catalyst in the KBr disc may be too high, leading to very high absorbances.

Relationships have been established between the frequency of the asymmetric internal stretching vibration of the TO_4 tetrahedra to the aluminium content of the framework.[24,25,26] Of the available choices, the work of Sohn *et al*[24] is preferred as it used masnmr to determine the framework content of the reference samples. In the following discussion where the framework aluminium contents are quoted they are those derived from the unit cell data using the equation of Sohn *et al*:[24]

$$Al_F = 107.1(a_o - 24.238) \qquad 4.1$$

Provided that complete structural healing has taken place the total aluminium content of the unit cell can be obtained from equation.4.2

$$Al_T = \frac{192\text{-}Al_F}{Si/Al} \qquad 4.2$$

where the Si/Al ratio is that of the bulk analysis, 2.58.[201] This is the same for all the unextracted samples as they were all prepared from the same sample without any net loss of material. The figures obtained from this calculation using the value of Al_F derived from the unit cell size are contained in table 3.4, and it can be seen that Al_T for the unextracted catalysts is always in excess of the theoretical maximum of 56. This is an artefact, caused by the increase of the real Si/Al ratio of the framework and by the decrease in number of unit cells on dealumination, and the magnitude of this effect is indeed seen to increase with dealumination. The Al_F value used obviously applies to the framework whereas the Si/Al value applies to the bulk; it is not and cannot be made representative of the framework. The non framework aluminium values arrived at via this method are therefore higher than the values obtained from the analysis, and the negative values obtained for the highly dealuminated extracted samples are an artefact of the equation and have no physical meaning.

It is therefore possible to extract nonframework aluminium from the mildly steamed samples whilst retaining their structural integrity. The EDTA did not promote further leaching of aluminium from the framework and the concern that extraction would result in all of the mildly steamed samples possessing essentially the same framework composition was unfounded.

4.12 Temperature Programmed Desorption.

Temperature programmed desorption is a valuable characterisation technique since it directly measures those properties of the catalysts which are responsible for their catalytic activity. The choice of probe molecule for a series of desorption experiments is crucial, as the results can be as much a reflection of the chemistry of the probe as of the catalyst. For this reason ammonia was used in this study as its high mobility and small size ensures deep penetration into the catalyst, accessing all available sites, both in the small and large pores. The high basicity of ammonia guarantees that it is stabilised on the acid sites, and its simple structure allows it to adsorb and desorb without reaction, thus simplifying the detection process. The reaction

conditions employed also influence the results.[232] The high adsorption temperature used enables equilibrium to be achieved rapidly eliminating excessive broadness in the desorption peak, and it is generally accepted that better resolution between two overlapping peaks is obtained by using lower ($<10 K min^{-1}$) heating rates, although conditions exist where the reverse is true. To these ends, the standard procedure of ammonia adsorption at 383K and a heating rate of $7 K min^{-1}$ was adopted.

Deammoniation Studies

The trace generated from a typical temperature programmed desorption experiment of NH_4YAS, figure 3.4, shows a single well defined peak in the ammonia trace centred at around 500K, and a similar peak in the water trace at around 900K. NH_4YAS has received minimal treatment so is most likely to contain only one type of site. This is confirmed by the lack of any discernible shoulders on either peak showing that desorption of the relevant species is from essentially one type of site, even though, in the case of the dehydroxylation peak, three types of hydroxyl groups (low frequency infrared, high frequency infrared and terminal silanol) are well characterised.[65,70,108]

Multiple peaks in tpd traces can be attributed to desorption from different types of sites and other workers have reported one,[176,233,234,235] two,[236,237,238],three,[116,239] and four[153,240] peaks in the deammoniation of dealuminated Y zeolites. In most instances these anomalies arise from differences in the adsorption temperatures, pre- and post-adsorption treatment and to the mathematical deconvolution of one irregular peak into two or more individual components. Once the peaks have been deconvoluted or steps have been taken to ensure that authentic single site traces have been obtained, information regarding the energetics of the processes involved and changes in the site strength and site distribution can be acquired.

Generally, the total area under the trace, as it is indicative of the total amount of ammonia released by the sample during the experiments, can be related to the number of available sites, (refer to calibration graphs in Section 2.21). Examination of the tpd results shows a progressive decrease in

the area under the traces as the hydrothermal dealumination temperature increases, regardless of the bakeout procedure, figure 4.1. This is consistent with a concurrent decrease in the number of acid sites in the dealuminated material. There does not seem to be any differentiation between samples prepared by the two differing severities of dealumination. This is expected considering that Miessner[239] found no difference in the acid strength between isolated Brønsted sites in silicon tetrachloride treated and hydrothermally steamed samples. However, Anderson *et al*[149] reported marked differences in the general acidity of samples dealuminated by the same methods as Miessner. As the catalysts in the current work are prepared by one method of dealumination, albeit one with different severities, it can be concluded that no discontinuity is expected, nor was found, in the acid properties of the catalysts generated.

The position of T_{max} is thought to convey information regarding the strength of the acid sites present, with higher temperatures implying that more energy is necessary for the molecule to desorb. However, even with no time delay between exit of gas from the sample and detection of the same, that is direct sample temperature to detection correlation, there would still remain physical impediments inherent in the catalyst which effect the release of the gas from the sample into the vacuum. Possibly the largest factor is the change in porosity of the samples. It known that the mesoporosity increases on dealumination and further on extraction of extraframework aluminium.[201] Increased porosity causes the diffusion pathlength of the desorbed ammonia within the cages to decrease, thus theoretically lowering T_{max}. Counter to this is the increase in strength of the sites within one site type, which would increase T_{max}, but then the increase in scarcity of sites would result in the chances of readsorption decreasing, once again lowering T_{max}. Clearly, all these factors are contributory to the final value of T_{max}, and to quote changes in T_{max} as indicative of changes in the strength of sites without considering other structural factors is, at best, misleading.

It is constructive at this point to consider the differences between the shapes of the deammoniation and dehydroxylation traces, found in figures 3.11

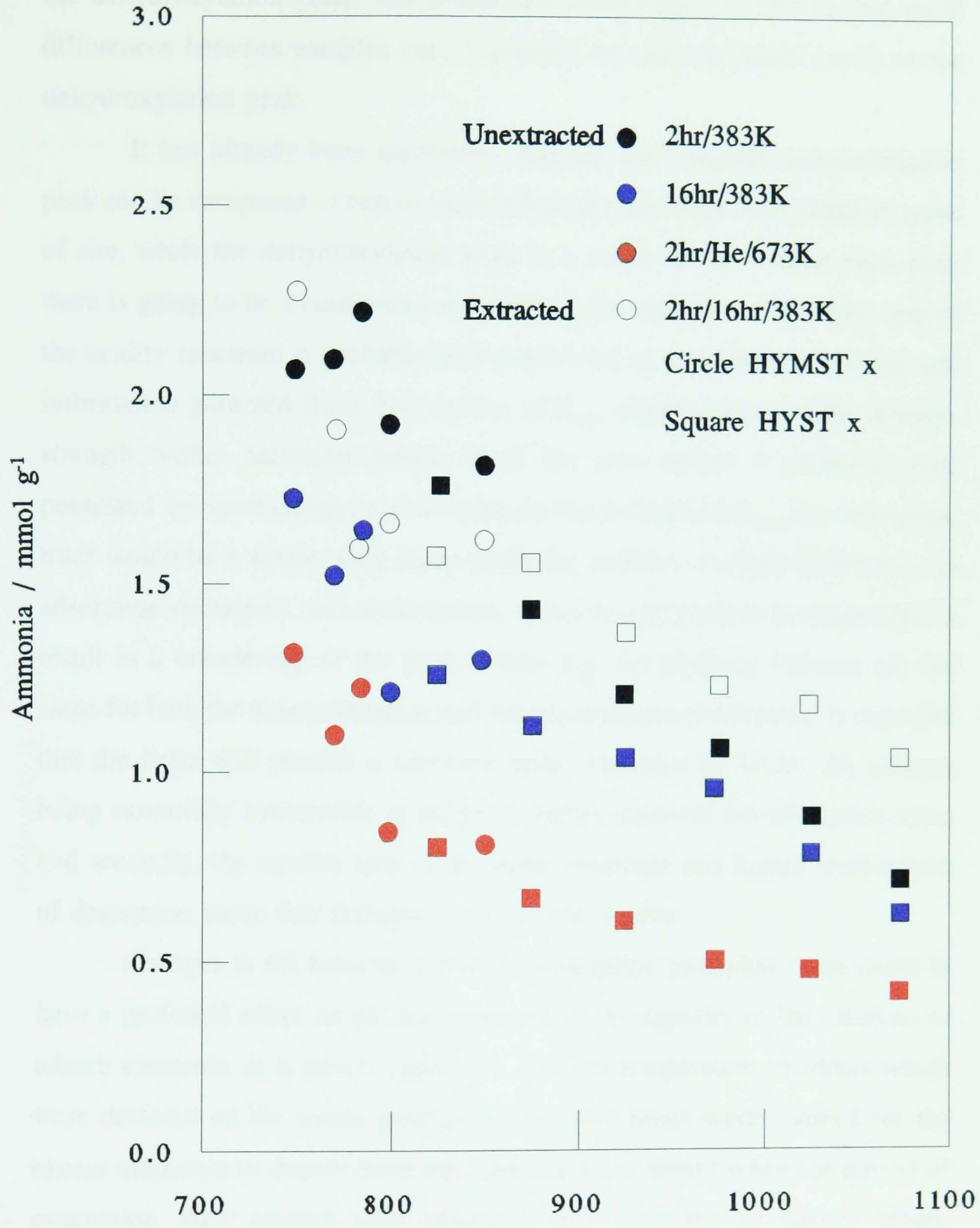

Figure 4.1: Temperature programmed desorption.

to 3.18. With the exception of NH_4YAS, the deammoniation peak is considerably more rounded, and hence has a more ill-defined maximum, than the dehydroxylation peak. The immediate consequence of this is that small differences between samples can, if present, be detected more easily in the dehydroxylation peak.

It has already been mentioned that the one irregular deammoniation peak can be composed of two or more sub peaks, deriving from different types of site, while the dehydroxylation peak is a single entity. Within each peak there is going to be a continuous variation in the strengths of the sites, and so the acidity spectrum is probably best considered as continuously varying and information garnered from the position of T_{max} representative of the average strength within particular limits. If all the sites within a particular type possessed the same energy, and no other factors influenced T_{max}, the desorption trace would be a single, very sharp peak: the addition of slight differences in adsorption enthalpies, and readsorption, diffusion and surface coverage effects result in a broadening of the peak. Given that the physical variants are the same for both the deammoniation and dehydroxylation processes it is expected that the latter will present a narrower peak. This due to firstly, the process being essentially irreversible as dehydroxylation destroys the adsorption sites, and secondly, the smaller size of the water molecule and higher temperature of desorption mean that diffusivity effects are smaller.

Changes in the bakeout and initial desorption procedure were found to have a profound effect on the measurement of the capacity of the catalysts to adsorb ammonia, as is seen in figure 4.1. The low temperature shoulders which were detected on the traces generated when two hours were allowed for the excess ammonia to desorb from the catalysts were absent when the period of evacuation after contact with ammonia was extended to sixteen hours. Subtraction of the sixteen hour desorption trace from that of two hours reveals a small peak, centred in the region of 460K which can be attributed to weakly bound ammonia, figure 4.2. This peak was attributed by Karge *et al*[240] and Miessner *et al*[239] to weak Brønsted and /or Lewis sites and by Niwa *et al*[232] to physically adsorbed or weakly chemisorbed molecules which could be more

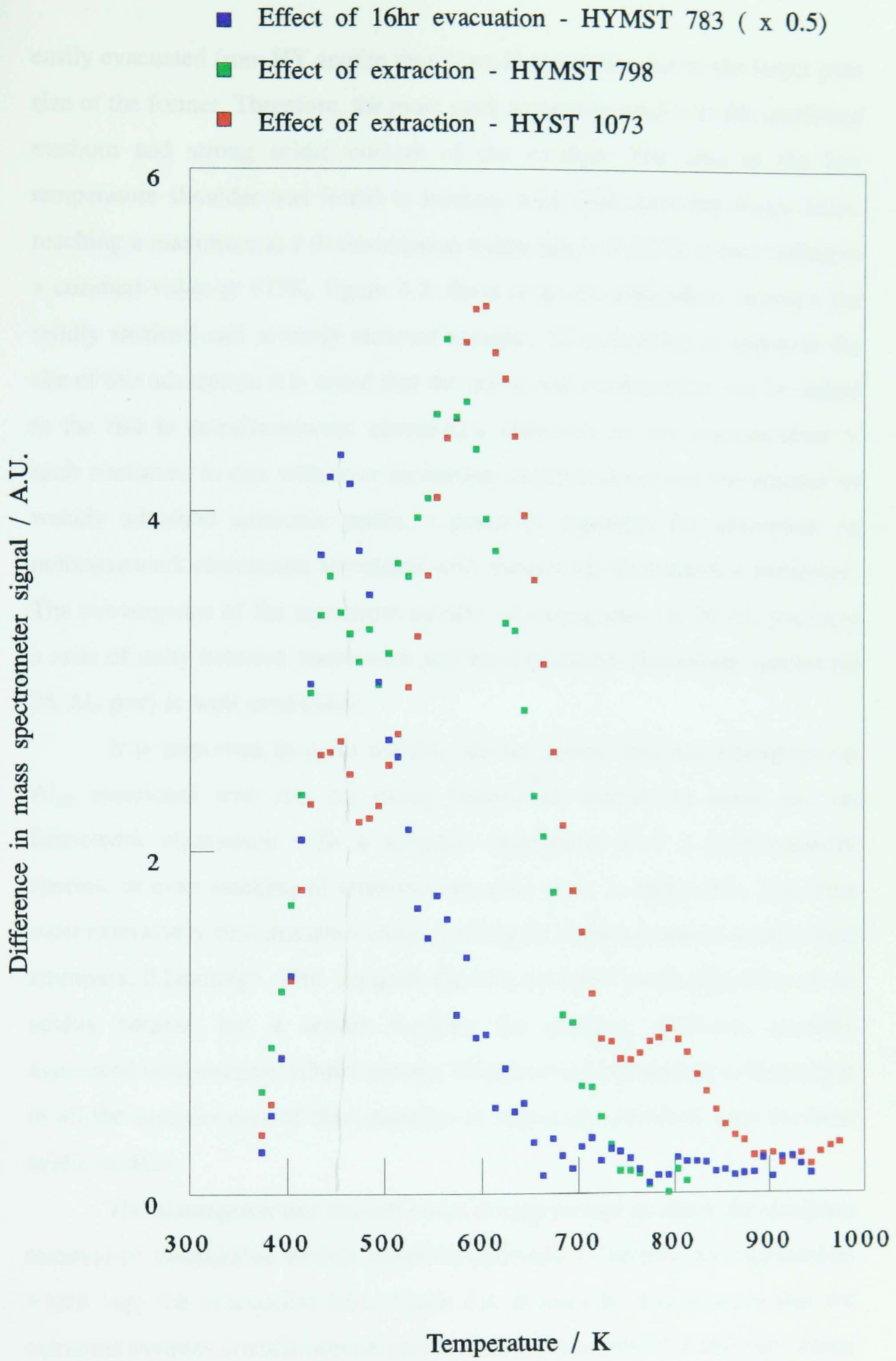

Figure 4.2: Subtraction traces showing the difference in ammonia content between extracted and unextracted catalysts, and the ammonia removed by the extended bakeout procedure.

easily evacuated from HY zeolite than from H mordenite due to the larger pore size of the former. Therefore, the main peak accurately evaluates the combined medium and strong acidic content of the catalyst. The area of the low temperature shoulder was found to increase with dealumination temperature, reaching a maximum at a dealumination temperature of 820K before falling to a constant value at 973K, figure 4.3; there is no discrimination between the mildly steamed and severely steamed samples. In attempting to ascertain the site of this adsorption it is noted that the initial rise in adsorption can be linked to the rise in extraframework aluminium. However, as the concentration of such continues to rise with ever increasing dealumination and the amount of weakly adsorbed ammonia peaks, a powerful argument for adsorption on nonframework aluminium associated with framework aluminium is presented. The convergence of the maximum number of strong sites (at 30 Al_F puc) and a ratio of unity between framework and nonframework aluminium species (at 28 Al_F puc) is well established.

It is important to point out that discrimination between adsorption on Al_{NF} associated with Al_F, on strong framework aluminium alone, and on framework aluminium with a synergic interaction with a nonframework species, or even stacking of ammonia on some sites, is impossible. The three most extensively dealuminated samples retain the same amount of weakly held ammonia, 0.2mmolg^{-1}. This suggests that the structure itself, regardless of its acidity content, has a certain capacity for retaining ammonia, possibly associated with terminal silanol groups. This provides convincing evidence that in all the samples part of this ammonia is physically adsorbed onto the non-acidic surface.

The assumption that sixteen hours is long enough to allow for complete removal of undesirable weakly adsorbed ammonia is verified by experiments which vary the evacuation time, figure 4.4. It must be remembered that the extracted samples contain approximately five nonframework aluminium atoms per unit cell, even after extraction, and are therefore liable to physically adsorb some ammonia. When this ammonia is added to the ammonia which is adsorbed irrespective of acidic strength, it can account for the drop registered

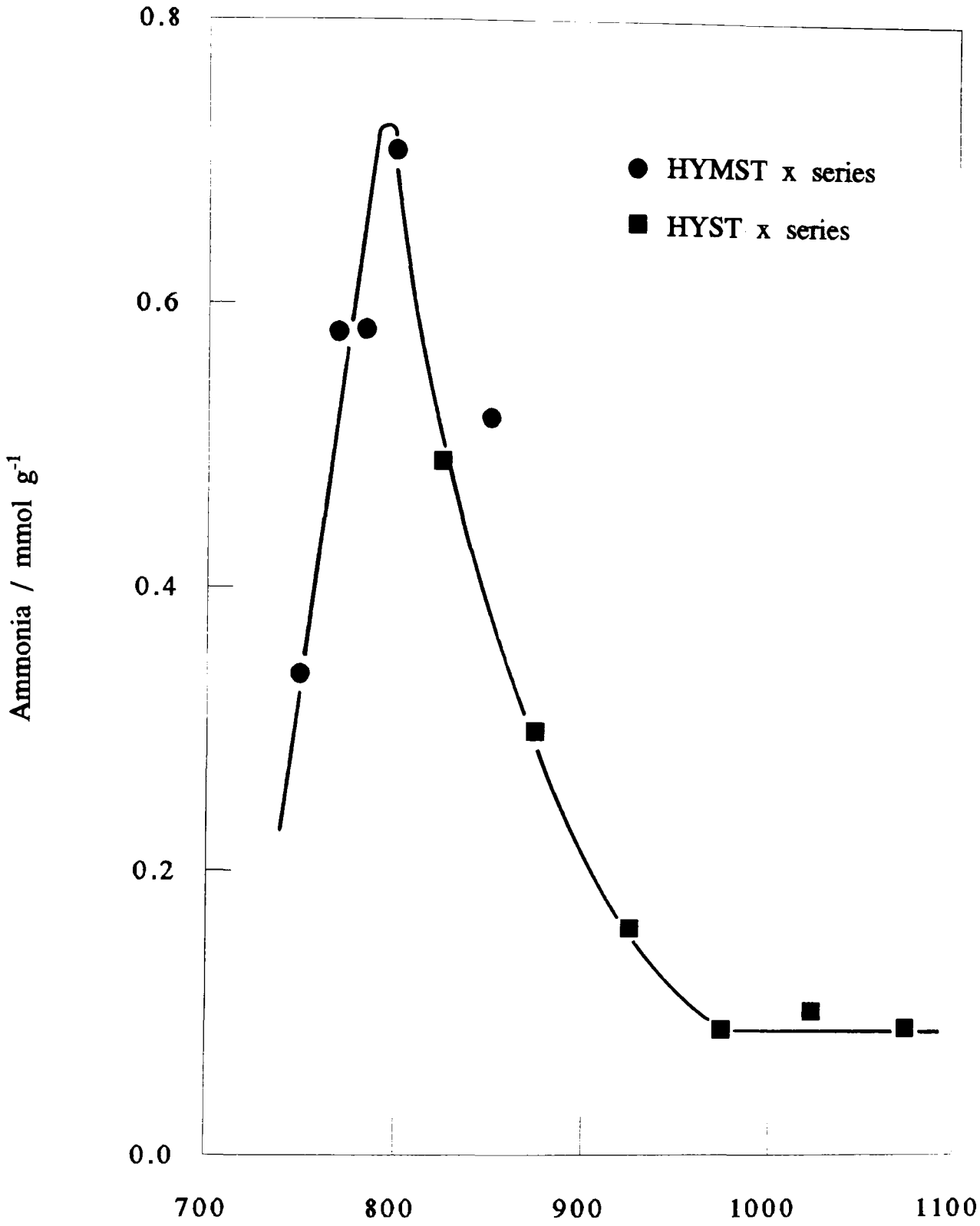

Figure 4.3: Excess physically adsorbed ammonia.

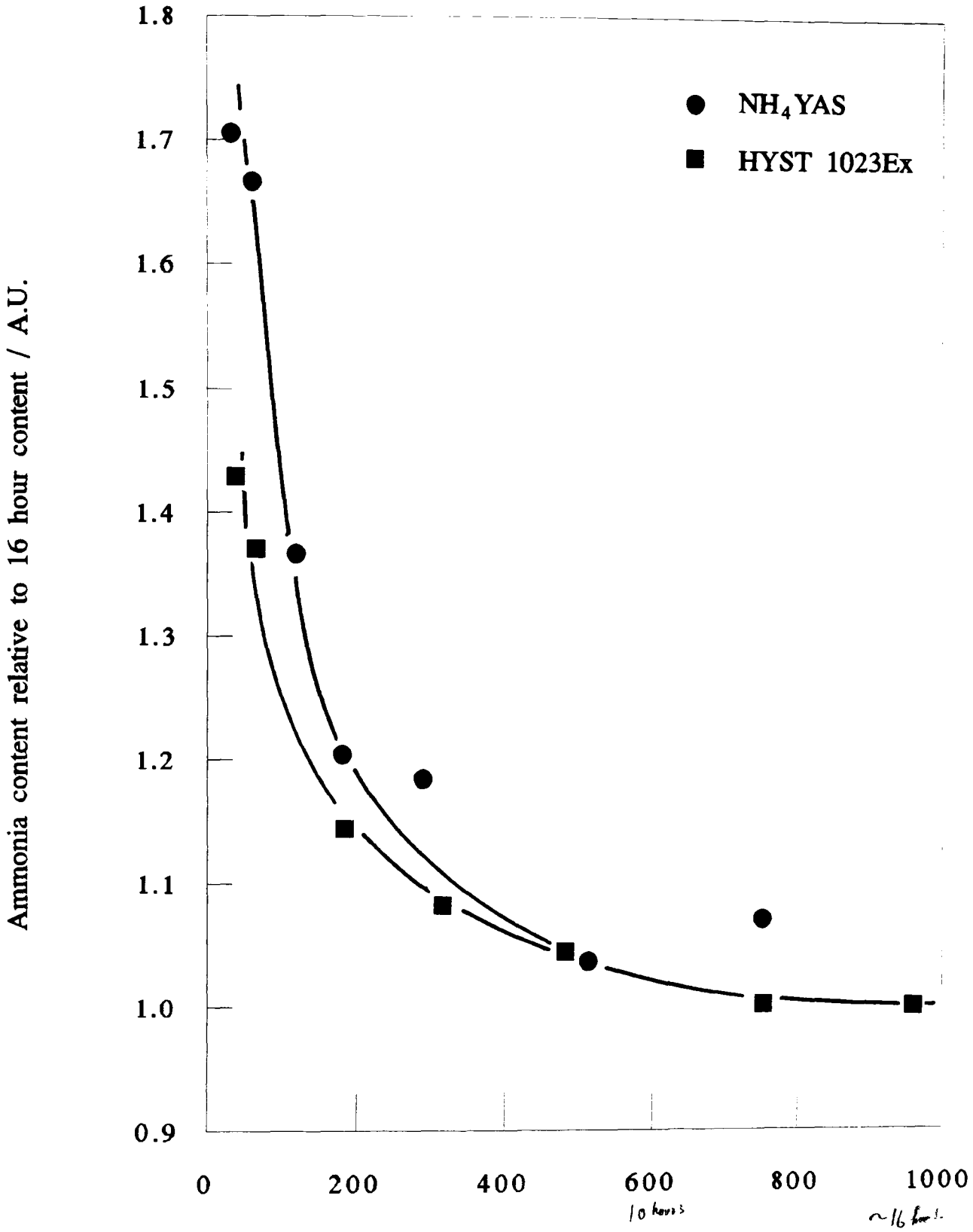

Figure 4.4: Variation of evacuation time.

when the ammonia is introduced in the gas phase. This, and the fact that the framework sites in HYST 1023Ex are stronger than those in NH_4YLS, explains why the former also suffers a drop in ammonia adsorption with extended evacuation time, even though it has been extracted.

In all but a very few cases the extracted sample possessed the highest number of available sites, and if the helium bakeout is taken as indicative of the true number of sites in the unextracted samples, extraction roughly doubles the number of available sites. The change in structural aluminium content, as measured by x-ray crystallography or infrared spectroscopy does not vary by nearly as much. Thus, confirmation is provided that the large amount of extrastructural aluminium present in the unextracted catalysts causes a reduction in the theoretical number of acids sites based on the x-ray data.[239] However, on the basis of this evidence alone, it is impossible to quantify how much of this reduction is due to pore blocking or cationic poisoning. The double effect of dealumination, ie. structural site diminishment and extraframework shielding of the remaining sites, causes the unextracted line to fall quicker than the extracted line; the difference between the two as a percentage of the extracted values increases with increasing dealumination until about 973K; thereafter it is constant, figure 4.1.

Subtraction of the 16hr/383K/vacuum unextracted ammonia trace from that obtained from the corresponding extracted sample reveals the additional ammonia that has been adsorbed on extraction, figure 4.2; the helium tpd was not employed as the extracted samples were activated under a vacuum and not flowing helium. The similarity between the two different traces shown, derived from the HYMST 798 series and the HYST 1073 series, offers further proof that there is basically no qualitative difference between catalysts dealuminated using mild or forcing conditions. Both exhibit one major peak, at T_{max} 573K and 608K for HYMST 798 and HYST 1073 respectively, with a small low temperature shoulder at about 450K.

The nature of the low temperature peak, which is in the same position as that which had previously been assigned to weakly adsorbed ammonia in the unextracted samples is uncertain. Clearly, in this instance it cannot result

from physically adsorbed ammonia as the extracted samples were ammoniated by ion exchange, and so this peak must be caused by weakly adsorbed ammonia only. The large peak maximum had not moved in the case of the weakly dealuminated sample and had shifted up temperature by 45K for HYST 1073 signifying that the former had gained sites across the range that it originally possessed, whereas the latter had gained sites of a (marginally) stronger nature. This is consistent with the view that cationic extraframework aluminium preferentially poisons the stronger sites: HYST 1073 has a higher number of strong sites and more extrastructural aluminium, and so the extraction of such is going to release a greater proportion of strong sites,[238] than in the more weakly dealuminated case. Therefore extraction increases the number of available sites and, importantly, in the case of the more strongly dealuminated samples, changes the 'acidity spectrum'.

Dehydration and Dehydroxylation Studies.

The water desorbed from the catalysts can be divided into three categories, depending on its temperature of desorption. By far the greatest volume of water is the pore filling water of hydration which desorbs at temperatures below 423K, and is removed in the standard bakeout procedure. Studying a typical severely steamed unextracted catalyst, HYST 873, figure 4.5, a second peak is then revealed with T_{max} at around 573K which has prominent shoulder starting at 773K. This is in contrast to the trace of NH_4YAS which has a sharp high temperature dehydroxylation peak. As this peak has been shown to be directly related to the capacity of the sample to adsorb ammonia, further investigations were made to explain the absence of, and hopefully recover this peak. Conducting the bakeout under flowing helium and increasing the final temperature to 673K reduced the size of the first peak by about two thirds and revealed a broad peak in the position of the original shoulder (green, figure 4.5). A similar experiment conducted *in vacuo* completely removed the low temperature peak and some of the high temperature peak (pink), interestingly a portion with desorption temperature greater than the bakeout temperature of 673K. Repetition of the helium

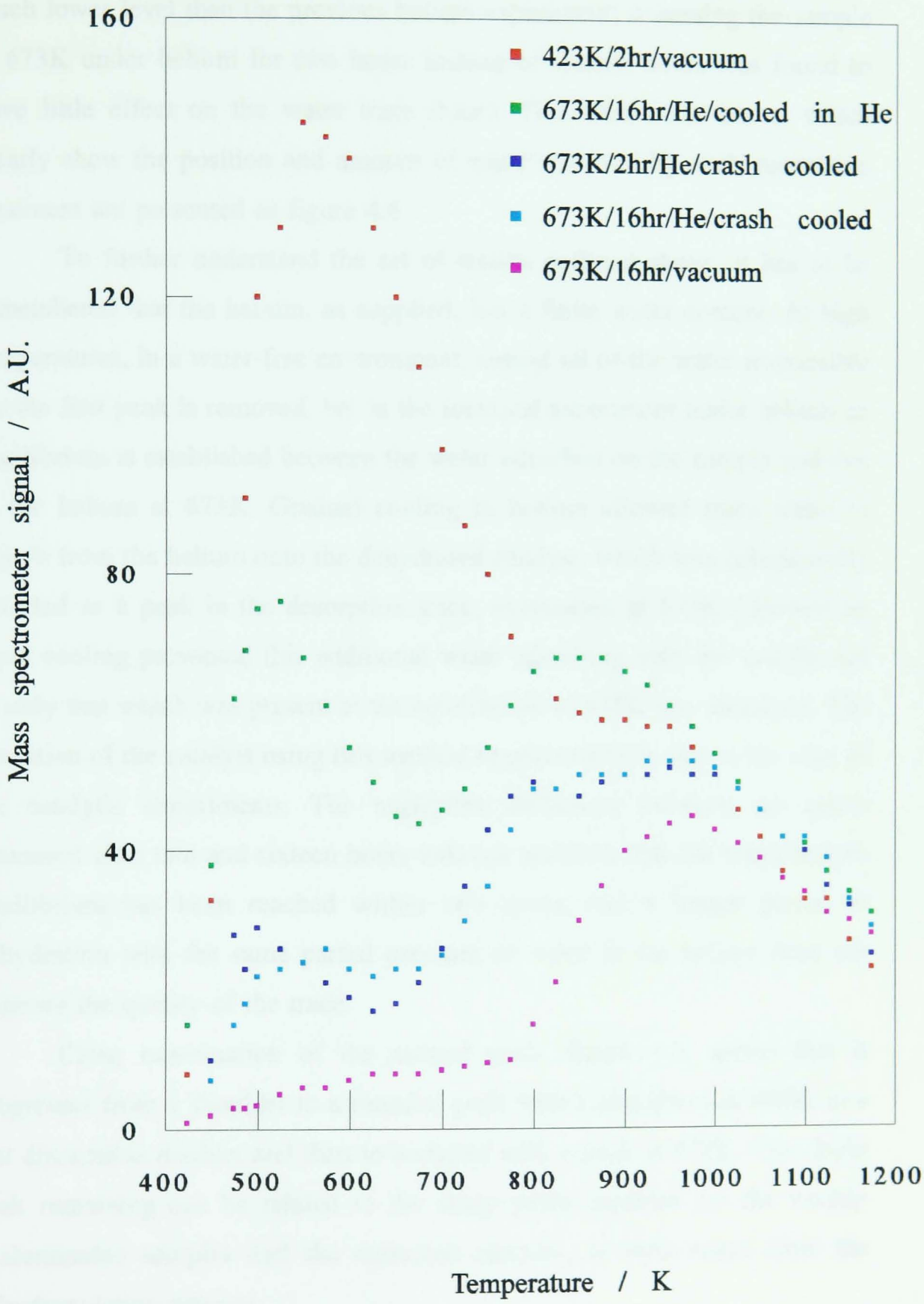

Figure 4.5: Water removed from successive bakeouts - HYST 873.

experiment, but with restoration of the vacuum at 673K and rapid cooling of the sample to 373K reinstated the low temperature peak (turquoise), but at a much lower level than the previous helium experiment; degassing the sample at 673K under helium for two hours instead of sixteen hours was found to have little effect on the water trace (blue). The subtraction traces, which clearly show the position and amount of water removed by each successive treatment are presented as figure 4.6.

To further understand the set of results outlined above, it has to be remembered that the helium, as supplied, has a finite water content. At high temperatures, in a water-free environment, almost all of the water responsible for the first peak is removed, but in the identical experiment under helium an equilibrium is established between the water adsorbed on the sample and that in the helium at 673K. Gradual cooling in helium allowed more water to adsorb from the helium onto the dehydrated catalyst, which was subsequently detected as a peak in the desorption trace; evacuation at 673K followed by rapid cooling prevented this additional water adsorbing onto the sample and so only that which was present at the equilibrium at 673K was measured. The condition of the catalyst using this method approximates to that at the start of the catalytic experiments. The negligible difference between the traces measured after two and sixteen hours bakeout confirms that the water/helium equilibrium has been reached within two hours, and a longer period of dehydration with the same partial pressure of water in the helium does not improve the quality of the trace.

Close examination of the second peak, figure 4.5, shows that it progresses from a shoulder to a rounded peak with a maximum at 850K, to a just discernible doublet and then to a singlet with a peak at 973K. The single peak remaining can be related to the sharp peaks reported for the weakly dealuminated samples and the extracted samples, as both result from the dehydroxylation process.

The effect of the hydration level of the catalyst on its capacity to adsorb ammonia was studied, using the helium bakeout with high temperature evacuation and rapid cooling, as this most closely resembled the state of the

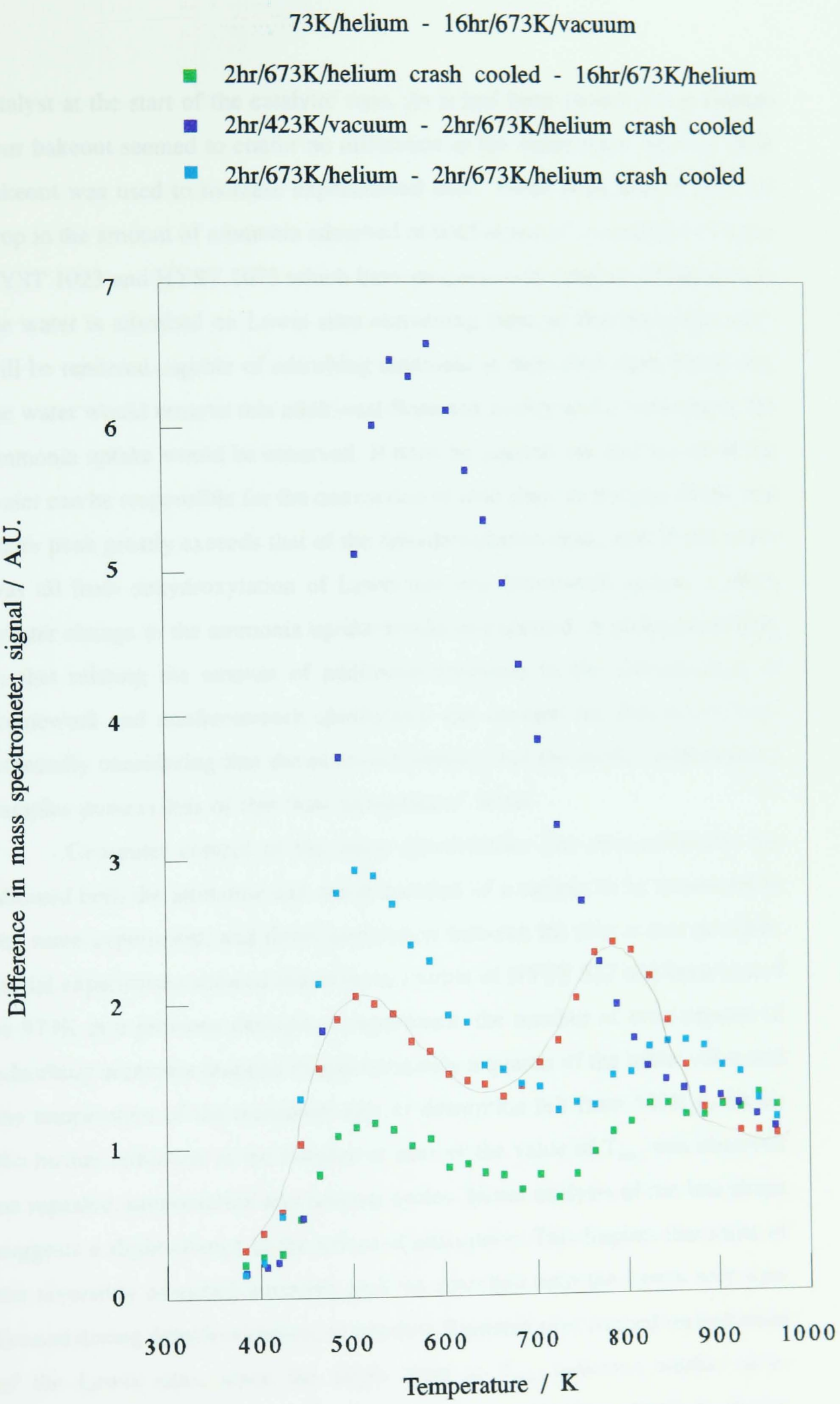

Figure 4.6: Subtraction traces showing the water removed by different bakeout procedures - HYST 873.

catalyst at the start of the catalytic runs. As it had been shown that a sixteen hour bakeout seemed to confer no difference in the water trace, the two hour bakeout was used to increase experimental ease. There is an almost uniform drop in the amount of ammonia adsorbed of 0.45 mmol g^{-1}, except for samples HYST 1023 and HYST 1073 which have progressively smaller differences. If the water is adsorbed on Lewis sites converting them to Brønsted sites, they will be rendered capable of adsorbing ammonia in their own right. Removing the water would remove this additional Brønsted acidity and a lowering of the ammonia uptake would be observed. It must be pointed out that not all of the water can be responsible for the conversion of acid sites, as the area of the mid water peak greatly exceeds that of the dehydroxylation peak, and, if this water was all from dehydroxylation of Lewis and non framework species a much greater change in the ammonia uptake would be expected. A similar argument to that relating the amount of additional ammonia to the concentration of framework and nonframework aluminiums can account for this observation, especially considering that the extracted samples and the mildly dealuminated samples possess less of this 'low temperature' water.

Computer control of the mass spectrometer and data collection has allowed both the ammonia and water contents of a sample to be monitored in the same experiment, and direct correlation between the two is now possible. Initial experiments showed that when a sample of HYST 823 had been heated to 973K in a previous desorption experiment, the number of sites capable of adsorbing ammonia dropped to approximately a quarter of the initial value and the temperature of the maximum rate of desorption fell from 505K to 485K. No further reduction in the number of sites or the value of T_{max} was observed on repeated ammoniation and heating cycles. Initial analysis of the line shape suggests a slight change in the nature of adsorption. This implies that some of the reversibly adsorbed ammonia may be adsorbed onto the Lewis acid sites formed during dehydroxylation, or possibly Brønsted sites formed on hydration of the Lewis sites, since the slight drop in T_{max} indicates weaker sites. However, the structure will have been extensively changed during dehydroxylation, leading to possible changes in the physical parameters which

are known to affect the position of T_{max}. Guimon *et al*[241] observed irreversible dissociative adsorption of ammonia after dehydroxylation to form a terminal amine group, and a new Brønsted site.

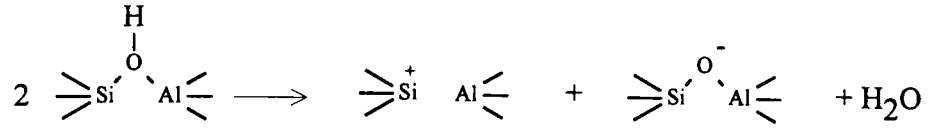

If it is assumed that ammonia will adsorb onto this 'new' Brønsted site, and that this site will be more stable, ie. will not be dehydroxylated at the temperatures reached, then it is a further possible site for the adsorption of ammonia. However, evidence presented below will show that an increased stability of Brønsted sites to dehydroxylation results in a concurrent shift in the T_{max} value of the deammoniation peak to higher values, and therefore this explanation is improbable.

More detailed experiments revealed that the ammonia capacity of the sample is related to the final temperature of the previous run, figure 4.7, and also the total amount of 'dehydroxylation water' detected in the previous stages of the experiment, figure 4.8. For the purpose of this discussion 'dehydroxylation water' is taken as that which desorbs from the catalyst at temperatures in excess of 773K, ie. water formed on dehydroxylation. Figure 4.8 shows that the first 75% of hydroxyl groups destroyed result in an almost linear decrease in the number of sites as measured by ammonia adsorption. These can be identified as the low frequency and high frequency hydroxyl groups associated with Brønsted sites as assigned by infrared spectroscopy as the work of Cattanach *et al*[116] has shown that a sharp loss of weight at around 953K coincides with the almost complete disappearance of the 3640cm^{-1} and 3545cm^{-1} bands. Both the low frequency and high frequency bands were shown

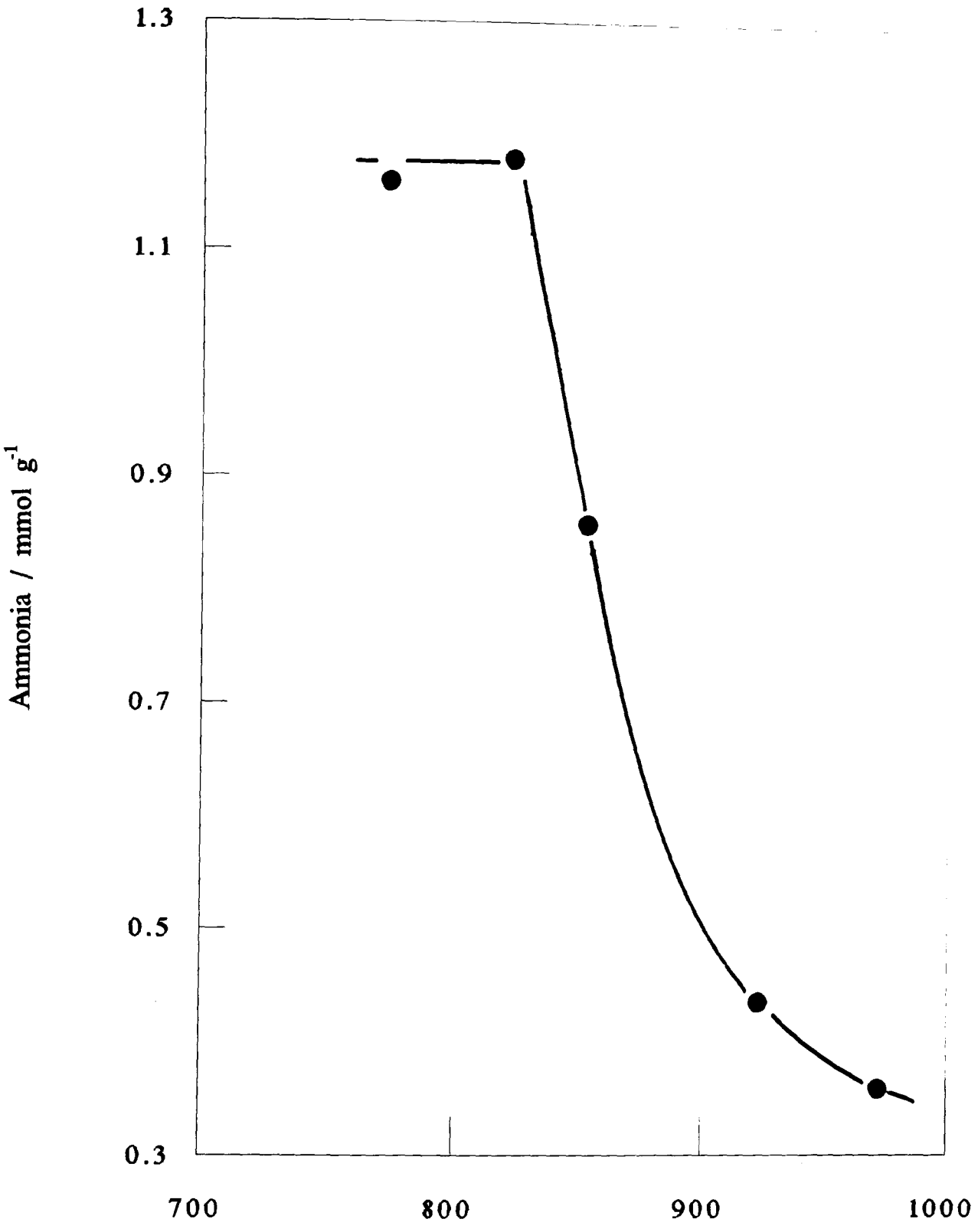

Figure 4.7: Ammonia content of HYST 823 against temperature history.

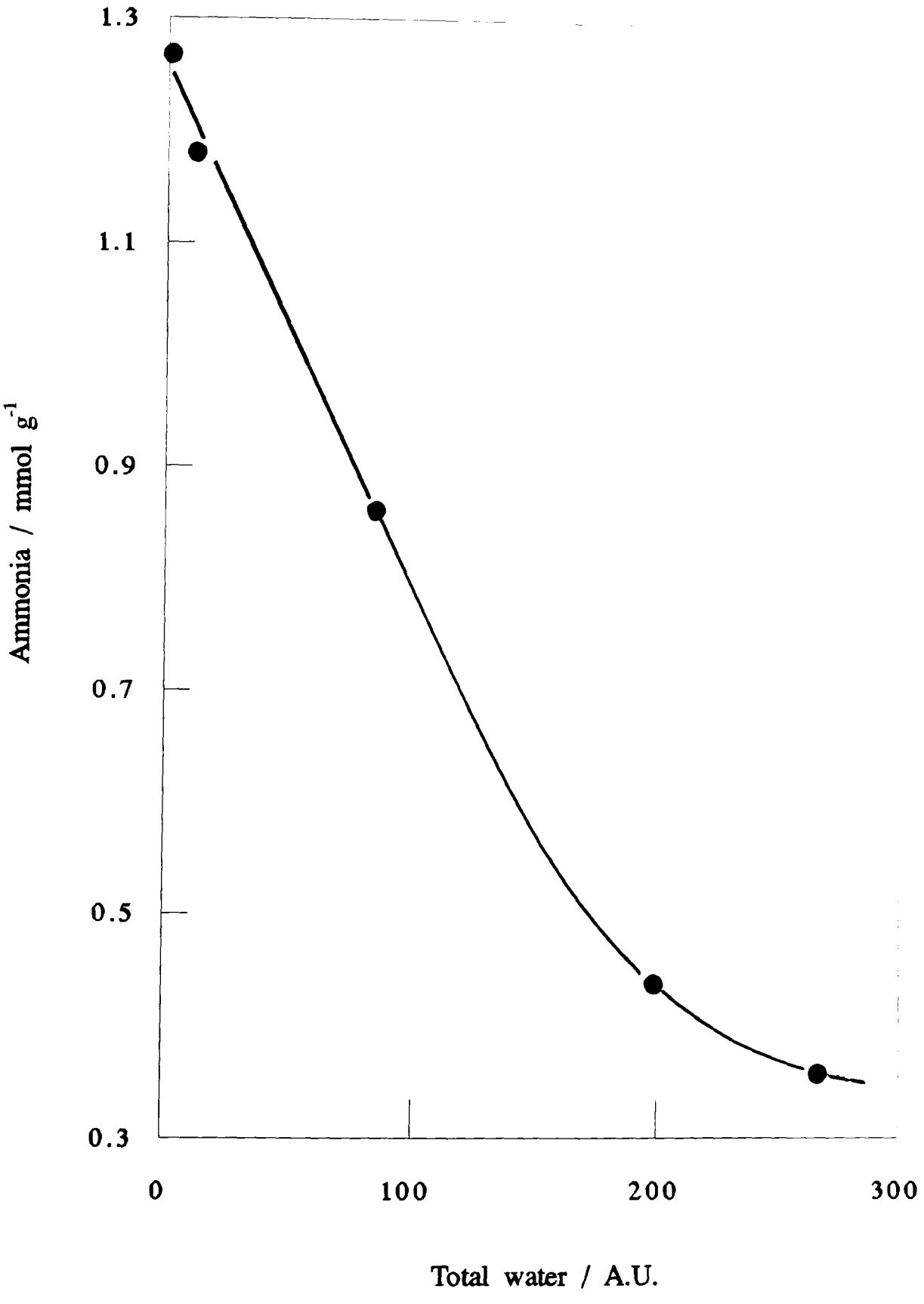

Figure 4.8: Ammonia capacity of HYST 823 against total amount of water previously desorbed from sample.

to contribute in the same way to ammonia adsorption, as they appeared simultaneously on calcination of an ammoniated HY zeolite, thus validating the assumption made in this work regarding the simultaneous destruction of both types of site. However, the last 25% of hydroxyl groups removed have less effect on the ammonia uptake, and therefore can be tentatively assigned, in part, to terminal silanol groups. The small discrepancy at the start, ie. the drop from 1.27 mmol NH_3/g to 1.16 mmol NH_3/g, is probably due to incomplete dehydration (not dehydroxylation) as the sample was heated, by necessity, to 673K in the first experiment, and higher temperatures in the subsequent experiments. Once again, the sample has a small residual capacity for ammonia which cannot be removed after repeated heating *in vacuo* to 973K.

The relationship between Brønsted site hydroxyl groups and ammonia adsorption has thus been proved, confirming that the measured ammonia in the normal experiment is adsorbed on Brønsted sites, with the possibility of a small amount of Lewis adsorption.

Close examination of the HYST 1073 series of deammoniation traces, shown in figures 3.9 and 3.10, reveals a shoulder at about 800K which is absent from the helium experiment, an effect which is not as marked in the HYMST 783 series, figure 3.7 and 3.8, indicating another hydration effect. The combination of the high temperature of desorption, the ameliorating effect of water, and the absence/ very slight evidence of this peak in the more weakly dealuminated sample imply that this ammonia is retained on a strong site formed by the hydration of a Lewis site. In the vacuum experiment, the lack of water leads to adsorption directly onto Lewis sites, which seems to be less effective causing a drop in the shoulder. Therefore, these desorption studies have identified four types of adsorption: on weak Brønsted and/or Lewis sites (Brønsted only in the case of the extracted samples), on medium and high strength Brønsted sites, and on strong Lewis sites.

The water traces, shown in figures 3.13 and 3.14, for the mildly steamed and strongly steamed samples confirm that the mid-temperature peak has been drastically reduced leaving the high temperature peak basically unaffected. Furthermore, the evolution of the high temperature peak is worth

considering in detail as the single sharp peak, which has shifted from 900K in NH_4YAS to 975K in HYMST 748, decreases in size and sharpness but shifts in position to 1050K by catalyst HYST 823. This change is accompanied by progressive emergence of a shoulder at 773K. Catalyst HYST 873 produces a 'square topped plateau' in lieu of a peak, and thereafter the shoulder at 773K becomes predominant and the peak assumes a equatorial triangle appearance with the total disappearance of the high temperature peak as a separate entity. With regards to the hydroxyl groups there is no acknowledgement of the different methods of dealumination, as the progressive change in nature of the dehydroxylation curve depends solely on the temperature of dealumination, with HYST 823 being more similar to the HYMST x series than HYMST 848.

At first sight it would seem that structural hydroxyl groups dehydroxylate at 973K and extrastructural groups do likewise at the lower temperature and so are responsible for the shoulder. However, if this were the case catalysts HYMST 848 and HYST 873 exhibit equal amounts of each hydroxyl type, implying by necessity that all of the extrastructural aluminium possessed hydroxyl groups which is in contrast to Lohse *et al*[121] who claim that only one tenth of the Al_{NF} possessed hydroxyl groups.

Examination of the water traces from the HYST 873/16hr/673K/vacuum and HYST 873/2hr/673K/He experiments, pink and blue lines respectively in figure 4.5, show that part of this peak can be considered to arise from adsorbed water, the difference arising from the finite water vapour pressure in the helium. The peak derived from the vacuum experiment is of a similar shape to those from the later helium experiments, validating the discussion. Extraction, although not affecting the total area, clearly depletes the peak at 800K and restores the higher temperature peak, indeed it is now centred at around 1100K, an increase over the most weakly dealuminated sample of 140K.

If the position of T_{max} was determined by the increase in porosity of the samples with dealumination one would expect a gradual shift in T_{max} to lower values with dealumination as the average diffusion pathlength gradually decreased, and not a distinct change from one type of behaviour to the other.

Furthermore, extraction would exacerbate the situation rather than reversing it as found. The initial shift in T_{max} value is opposite to that which would be expected if the controlling factor was indeed diffusion through the newly created mesopore system, and so it is totally correct to link this change to an increase in the strength of the sites, and it is only when substantial amounts of extrastructural aluminium are present that the position of T_{max} starts to fall.

It is concluded that extrastructural aluminium interacts with the remaining hydroxyl groups in a way such that they dehydroxylate at a lower temperature. This effect is always proportional to the extent of dealumination and is discrete in that each peak changes in intensity but not in position. The effect can be reversed by the extraction of the extrastructural aluminium, although a residual peak at 800K indicates incomplete extraction, as is known. The high temperature peak reverts to a higher position than the original unextracted samples, confirming that a decrease in structural aluminium produces strong sites which dehydroxylate at higher temperatures.

These results lead to the important conclusion that if, as accepted, dealumination of the parent material produces stronger acid sites, then extraction of the nonframework species produced also increases the strength of the sites. This is different from the increase in accessibility of previously existing strong sites by removing the effects of pore blockage, as these hydroxyl groups are present both before and after extraction, and the removal of extrastructural aluminium should reduce T_{max}, as already noted.

It is interesting to note that the total area of the dehydroxylation peak does not double on extraction suggesting that not much of the nonframework aluminium is cationic (cf deammoniation results) and bears direct comparison with the changes observed in the deammoniation traces.

Analysis of tpd traces can yield information about the desorption process. Of the many methods available,[242] the determination of the energy of desorption from the variation in the temperature of the maximum rate of desorption, T_{max}, with the heating rate, see Section 3.12, is possibly of most use. The dehydroxylation energies obtained from this treatment for four catalysts are presented in figure 4.9. Energies thus derived give the average for

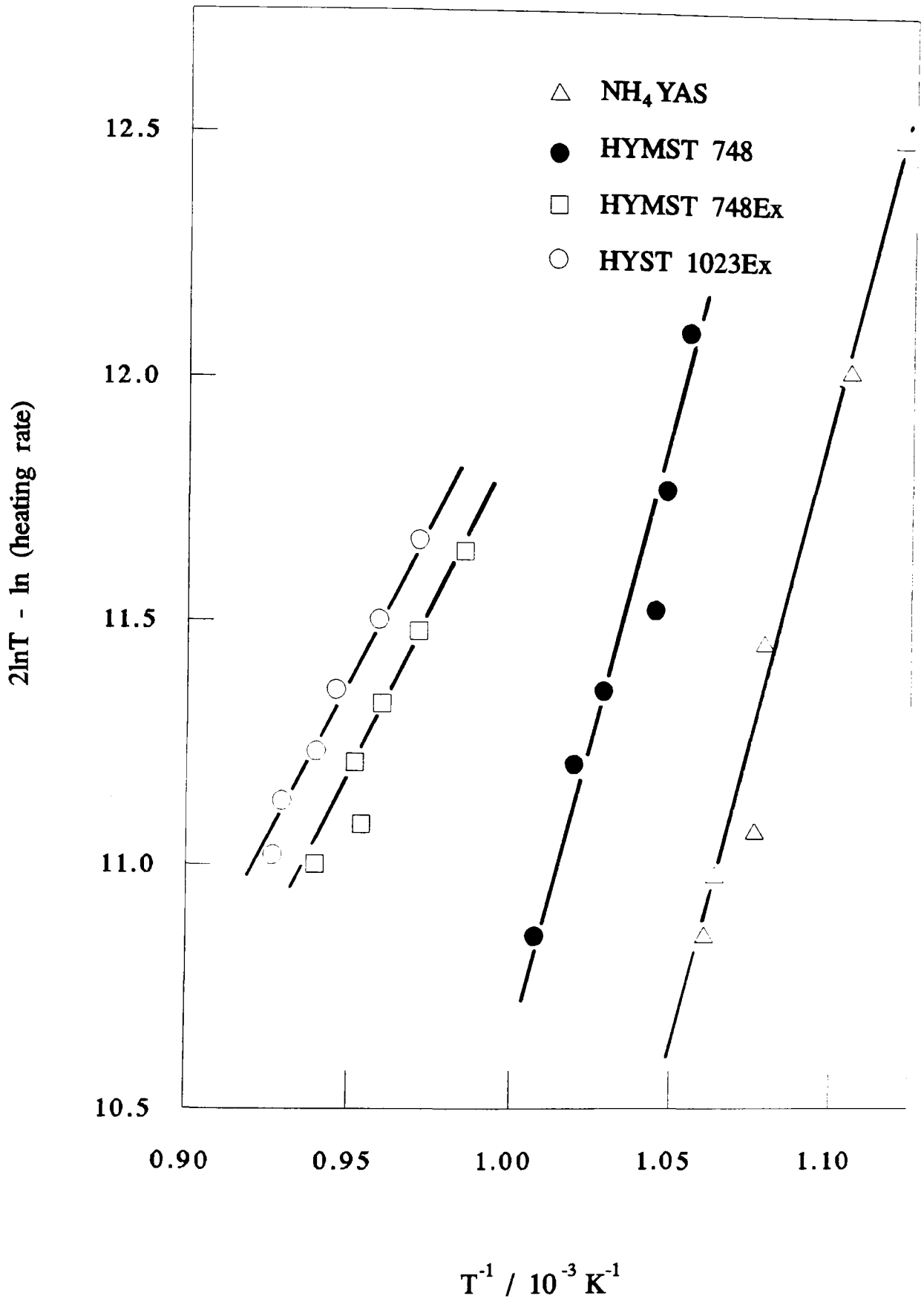

Figure 4.9: Desorption energies of hydroxyl groups.

desorption of that type of site. The wide variation of acid strength within that type may relate to differences in adsorption at different crystallographic sites[116] although isolated Brønsted sites have similar acid strengths.[239] The enthalpy of desorption of ammonia from NH_4YAS was determined as 105kJmol^{-1}, which is to the lower end of the spread of values contained in the literature,[116,236,243,244] but very similar to some recent work using single[234,240] and variable[234] heating rate techniques. Unfortunately, further attempts to establish the desorption enthalpies from the dealuminated catalysts were unsuccessful due to the broad peak and the inherent uncertainty in the value of T_{max}[245]. Heating the samples at the rates necessary to effect a reliable, measurable change in T_{max} were considered to be impractical due to the nature of the experimental setup.

Analysis of the dehydroxylation peak proved more successful, mainly due to the more pronounced nature of the peak leading to a greater certainty in the position of the peak maxima. The dehydroxylation process has been reported as first order[116] and the T_{max} value obtained from NH_4YAS, 915K, and the dehydroxylation enthalpy of 215kJmol^{-1} that was observed in both the cases of NH_4YAS and HYMST 748 are in good agreement with that work[116] when it is considered that they found the enthalpy of dehydroxylation to be dependant on the partial pressure of water. Their values of 420kJmol^{-1} for an atmosphere of helium and 293kJmol^{-1} for an absolute pressure of $\approx$ 1Pa are consistent with the findings of the present research which were obtained at absolute pressures of between 10^{-4} and 10^{-2}Pa. The dehydroxylation enthalpy was found to drop to 122kJmol^{-1} on extraction of nonframework material and identical experimentation on the HYST 1023 pair of catalysts, although revealing an enthalpy of 110kJmol^{-1} for the extracted sample, failed to return a value for the unextracted sample due to the lack, at every heating rate attempted, of a dehydroxylation peak. The values from the extracted catalysts are similar in magnitude to those obtained by Dima and Rees[246] for the removal of the last few water molecules in a study of the dehydration of a series of sodium exchanged Y zeolites.

A synergic interaction between the framework and nonframework aluminium, as claimed by other authors to increase the acidity of the hydroxyl

groups, probably accounts for the drop in enthalpy, as it has already been shown to that the non framework aluminium has a pronounced effect on the framework hydroxyl groups. The absence of any detectable dehydroxylation peak in the more strongly dealuminated unextracted samples, as reported earlier, confirms that it is impossible to detect reliably a small amount of water in the presence of a large amount of extraframework material/adsorbed water.

4.2 n-Hexane Cracking

The cracking of n-hexane has been used extensively as a model reaction in the examination of strong acidity in solid acid catalysts,[212] and as such was studied in this research over all the dealuminated and extracted samples at 673K using the pulse flow method. The products detected were ethane, propane, n-butane, i-butane, n-pentane, i-pentane and the corresponding unsaturated compounds, which although present, were not resolved. In addition, coke was formed on the catalyst, and although not a product in the normal sense, cannot be ignored as it accounts for some of the n-hexane consumed from each pulse.

In a study of n-heptane cracking over Y zeolite Wang *et al* [247] reported a maximum in the initial paraffin/olefin selectivity ratio of 28 at 30 Al_F puc and the value never dropped below 5. Gas oil cracking over HY zeolite studied by Corma *et al*[248] showed that under the extreme conditions of 65% conversion the butane/butene ratio was constant at 1.25 for steamed samples with aluminium contents of between 30 and 10 Al_F puc. Therefore it can be assumed that paraffinic products form the majority of those in the present work, but when a paraffin is mentioned, the presence of the unsaturated analogue is accepted.

Initial work found no evidence of reactant isomerism, although previous studies on these catalysts had detected isohexane as a reaction product in some cases.[201] As the catalyst presentation was different from that in the earlier work, a series of experiments was conducted to establish the relationship between product distribution and contact time. This was achieved by altering the flow rate or mass of catalyst used. These experiments suggested that reactant isomerisation was contact time dependent, and should only be expected at higher contact times than those used in the main experiments.

Although pulse flow methods are used to obtain a 'snap shot' of the activity, and as such the pulses are sometimes treated as instantaneous, they are, in reality, very small segments of a continuous flow. In the pulse experiments n-hexane flows over the catalyst for approximately six seconds per pulse if a carrier flow rate of $0.5cm^3s^{-1}$ is used. Therefore, changing the

flowrate will undoubtedly change the contact time, even in a pulse experiment.

In a study on HYST 823, iso-hexane was only detected when the flow rate was less than a critical rate, the exact value of which was inversely proportional to the mass of the catalyst, figures 4.10 and 4.11, thus confirming the contact time dependence. The C_3 and C_4 hydrocarbons exhibited similar behaviour, and seemed to imply that no reaction occurs at all with flow rates in excess of $1cm^3s^{-1}$, figure 4.12. Even if this is taken as evidence that no detectable reaction occurs at fast flow rates, there is still a clear discontinuity in the product formation. These results suggest that the product distribution is to some extent contact time dependent, or that the activity is nonlinear with respect to contact time,[179] and that under the conditions used no reactant isomerisation would be expected. This is in agreement with Dwyer *et al*,[179] and at first sight contrary to Anderson *et al*,[213] as the latter found no sudden change in activity with contact time. They, however, used far greater contact times and so did not study the appropriate region.

All the samples suffered some deactivation with a near steady activity being achieved after fifteen pulses, although in the range of the experiments the activity of the less active samples can be approximated to a straight line. Subsequent exposure to a continuous flow of n-hexane for sixteen hours, followed by flushing the surface in pure helium, did not show any significant further deactivation, the reasons for which will be discussed later.

The activity of the catalyst can either be expressed as the formation of certain products, or the total amount of n-hexane converted determined from the sum of the detected products. The activity can be taken at a certain point during the experiment or extrapolated to zero time on stream, or as total products formed over a period of time. These values are reported in table 3.41, and, as can be seen in figure 4.13, the choice of parameter has little effect as there is a simple relationship between each definition of activity. Plotting the amount of n-hexane converted in the first pulse against the framework aluminium or proton content, shown in figures 4.14 and 4.15, allows comparison of the activities of the samples before any deactivation has taken place: these might be considered as true initial activities. The total n-hexane

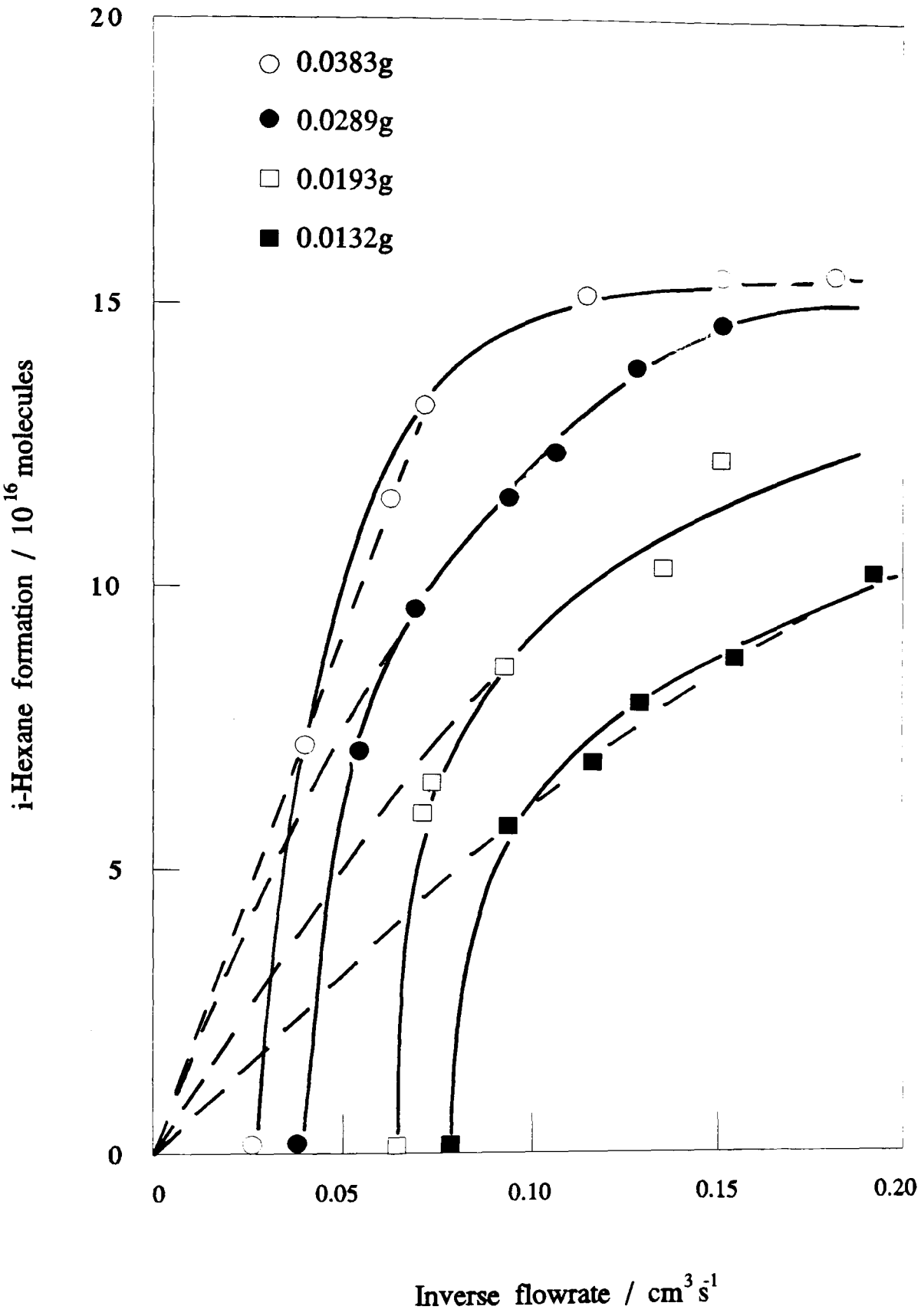

Figure 4.10: Contact time dependence of reactant isomerisation on HYST 823.

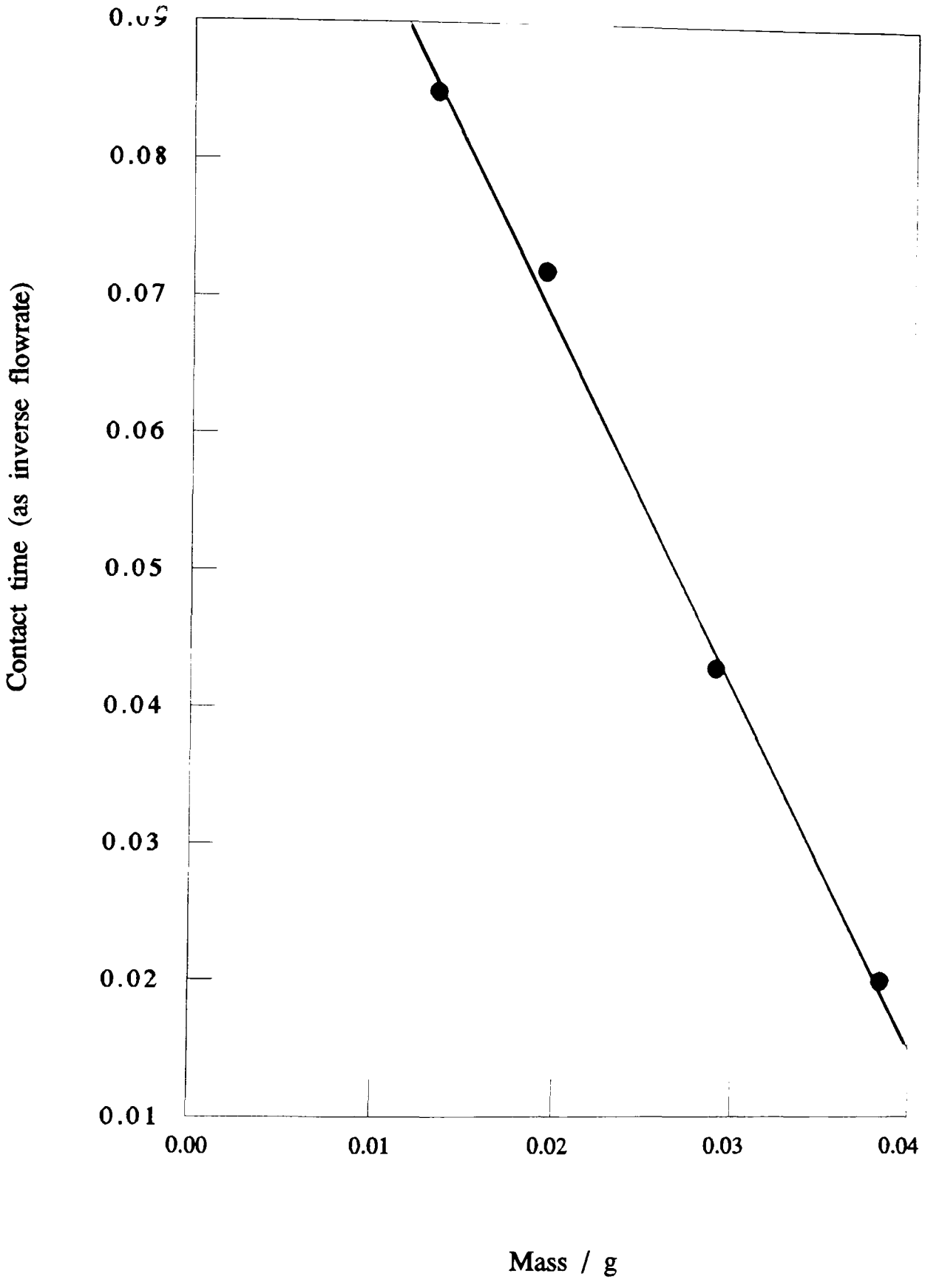

Figure 4.11: Contact time dependence of isohexane formation.

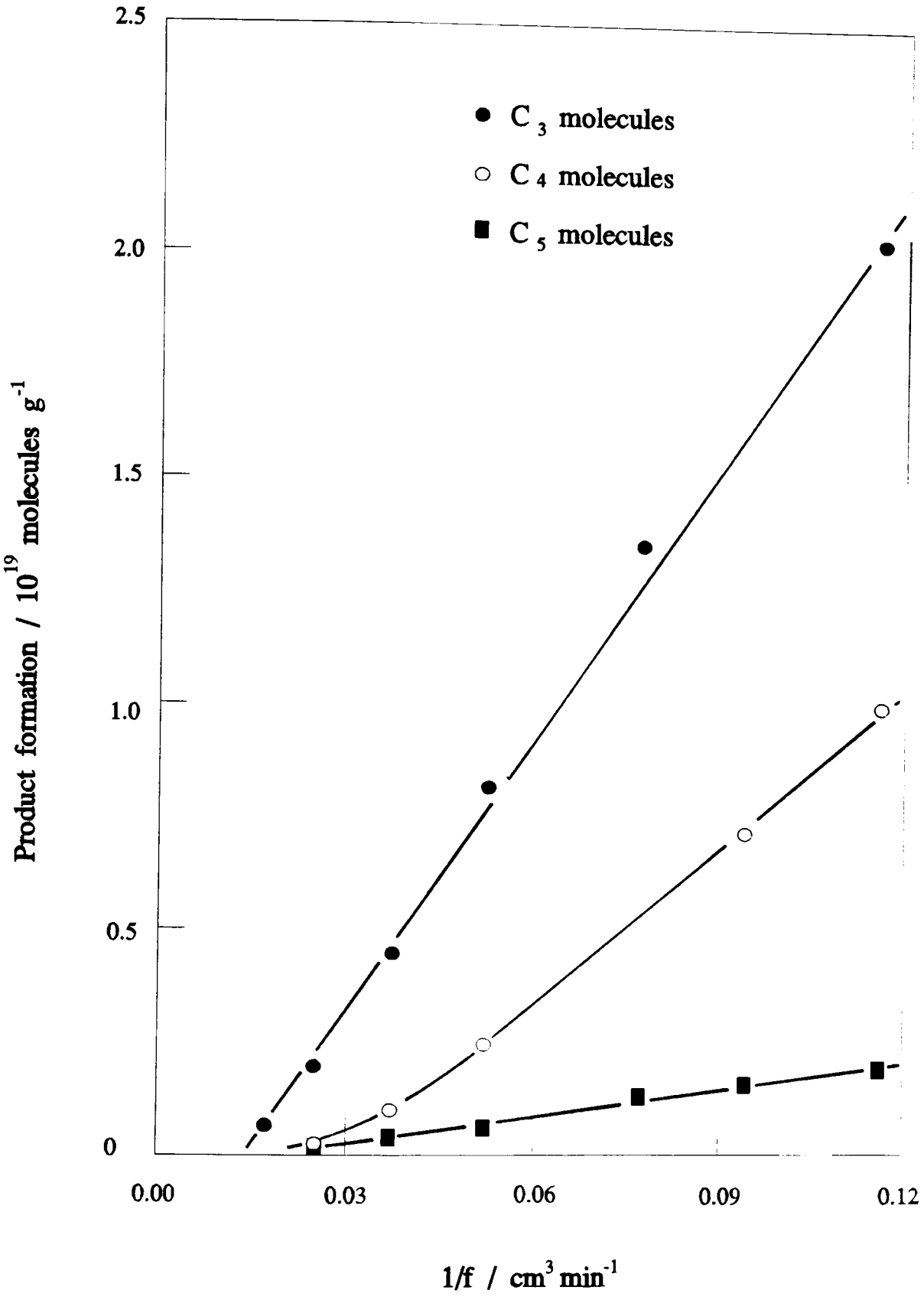

Figure 4.12: Variation in activity with contact time - HYST 823.

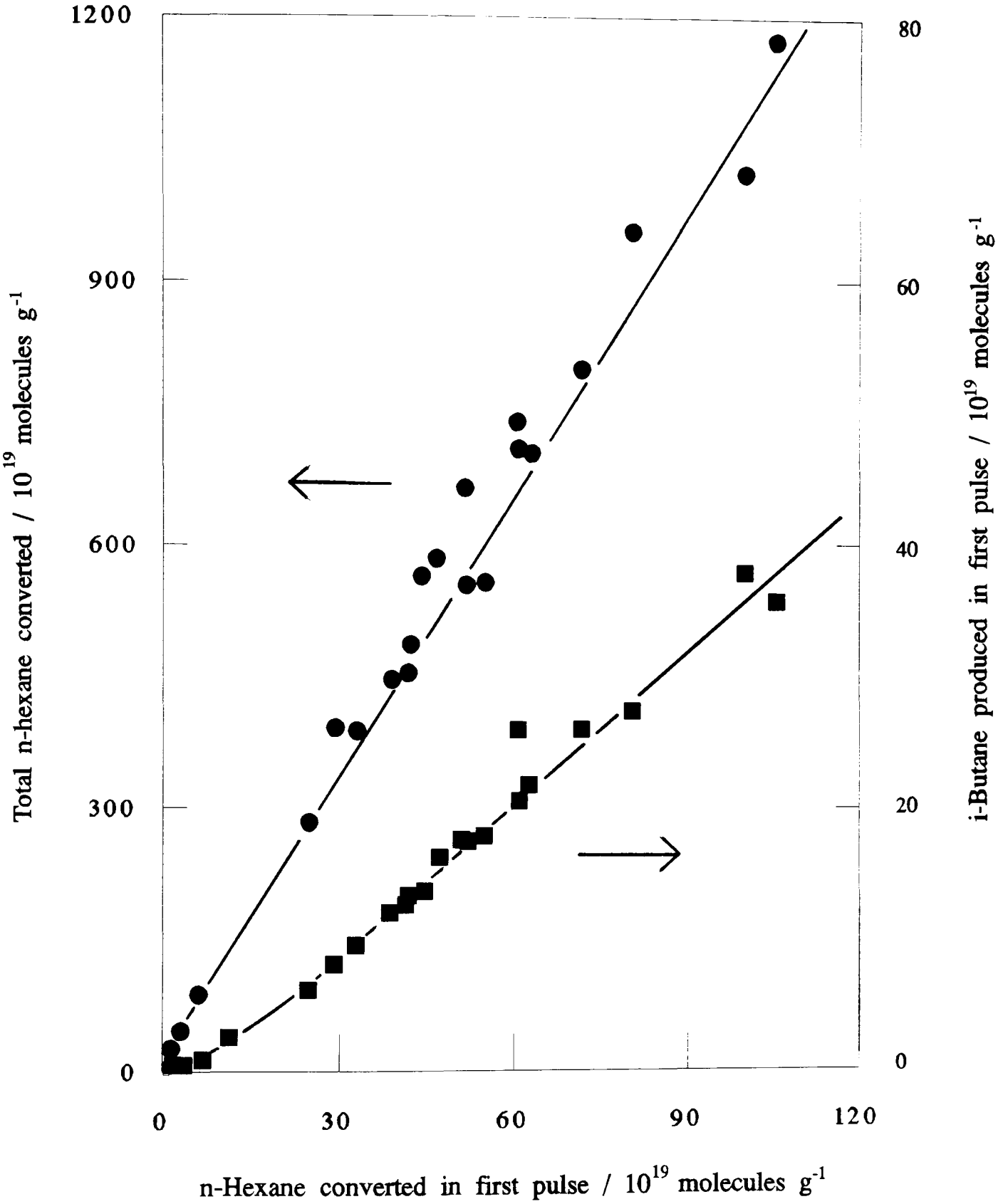

Figure 4.13: Comparison of different methods of denoting activity.

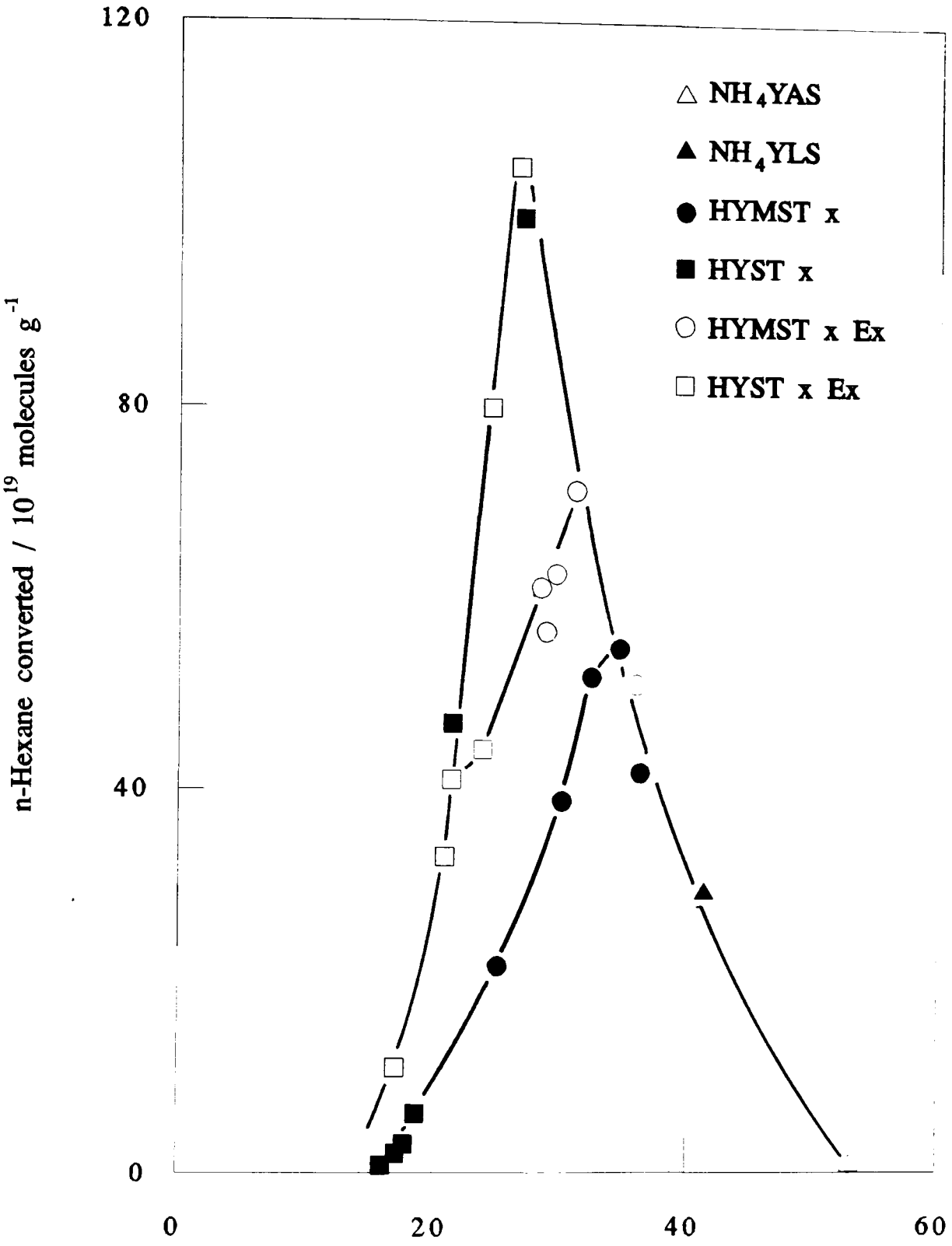

Figure 4.14: n-Hexane converted in the first pulse.

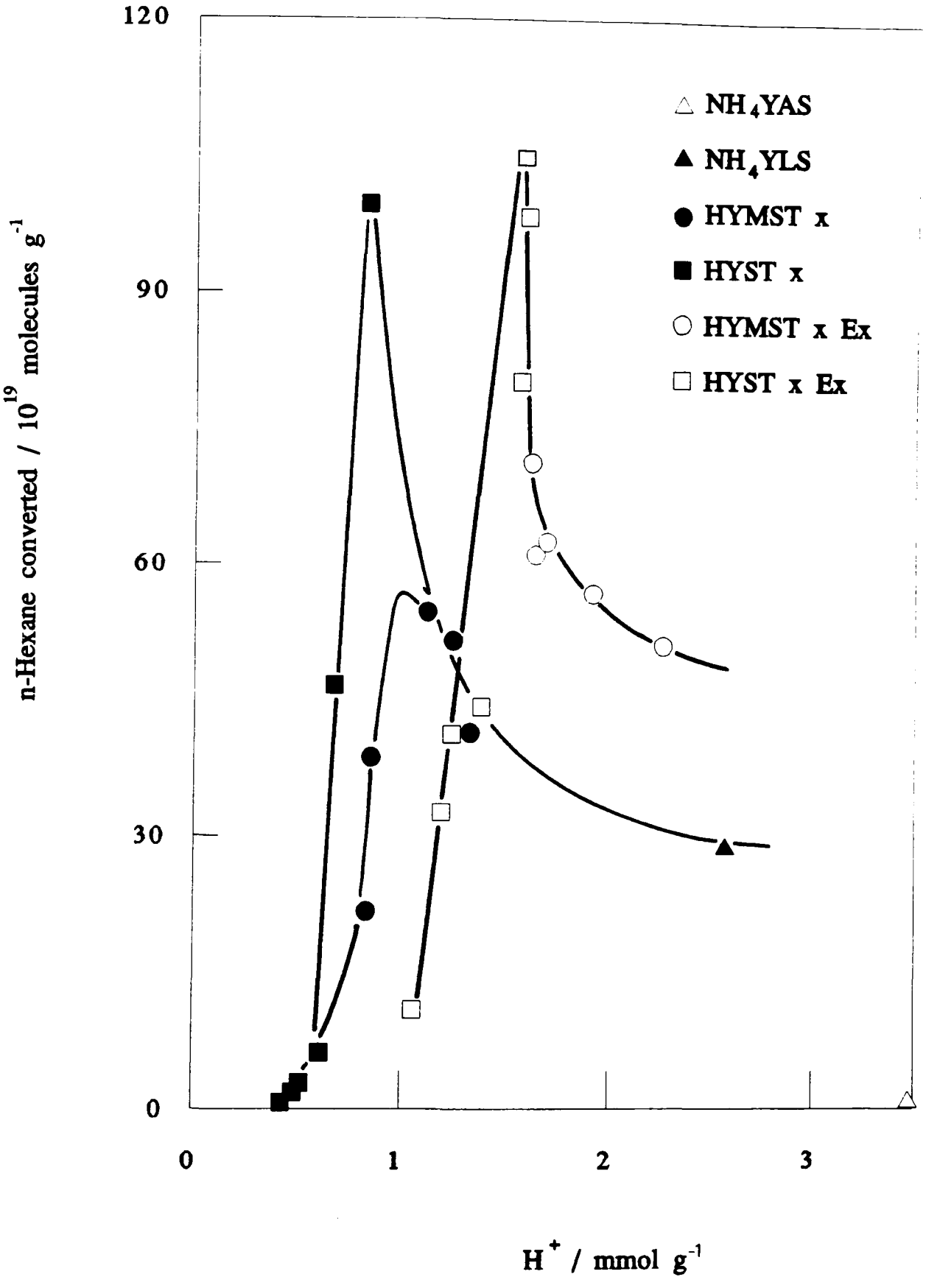

Figure 4.15: n-Hexane converted in the first pulse.

converted after fifteen pulses possibly offers a more accurate assessment of the catalysts' capabilities, as it takes into account the initial deactivation, and is based on more experimental points (figure 4.16). These values approximate to those of Rhodes[201] taken after five minutes in a flow reactor, which have previously been used as pseudo-initial activities.[201]

There is a maximum in activity when the initial activity is plotted against either framework aluminium or proton content, seen in figures 4.14 and 4.15, and when the activity after sixteen hours on stream is plotted against framework aluminium, figure 4.17. The mildly dealuminated samples exhibit lower activity than would be expected on the basis of the more extensively dealuminated samples. Extraction of the extraframework aluminium universally increases the activity of each catalyst and shifts the position of the maximum to a higher proton content, but not a higher framework aluminium content. Therefore, as mentioned in Section 3.1, x-ray data, although confirming that the extraction of extraframework aluminium does not dramatically alter the constitution of the framework, is of limited support to catalytic investigations.

NH_4YAS has very little activity, and this is associated with the preferential poisoning of active sites[236,249,250,251] with sodium. Titration of 10% of the active sites in HY with ammonia was found to be sufficient to remove all the activity for neopentane cracking.[252] This implies that it is the removal of sites by poisoning, be it with ammonia or sodium, which is responsible for the decrease in activity. NH_4YLS was considerably more active than NH_4YAS, followed by a more gradual rise in activity until the maximum activity is achieved with sample HYST 823; thereafter the activity decreases until sample HYST 1073, which is two-thirds as active as NH_4YAS. These results are in general agreement with the literature [77,84,179,208,214,253] and the well documented idea that an increase in activity is linked to the increase in strong acidity induced by removing aluminium atoms from the framework.[75,76,254] However, there is no linearity in the 0-15 Al_F region,[85] but rather a minimum aluminium content below which the activity is minimal. This agrees well with Anderson *et al*[213] who reported a dramatic rise in the activation energy when the unit cell contained less than four structural aluminium atoms. For a valid

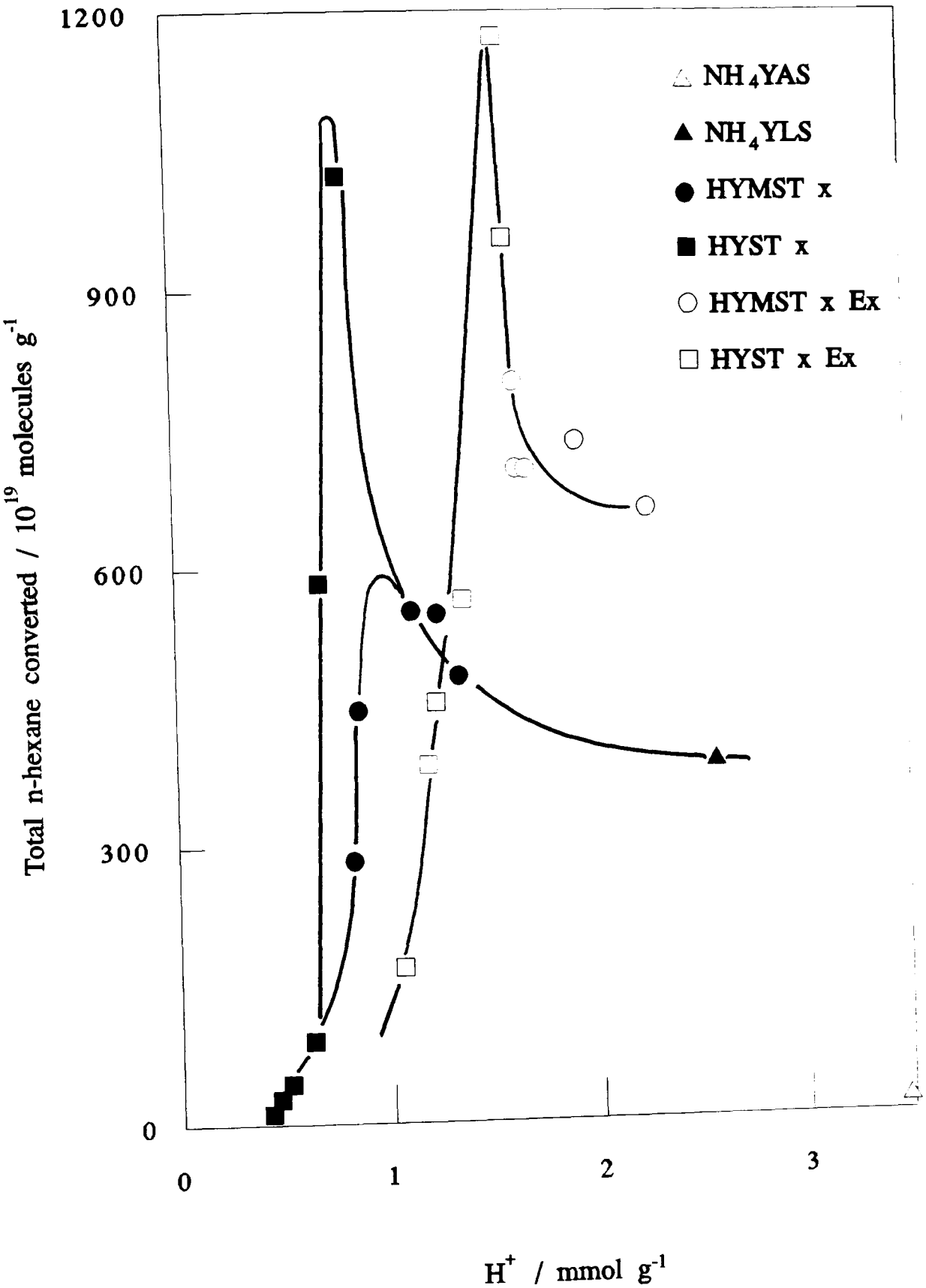

Figure 4.16: n-Hexane converted in the first fifteen pulses.

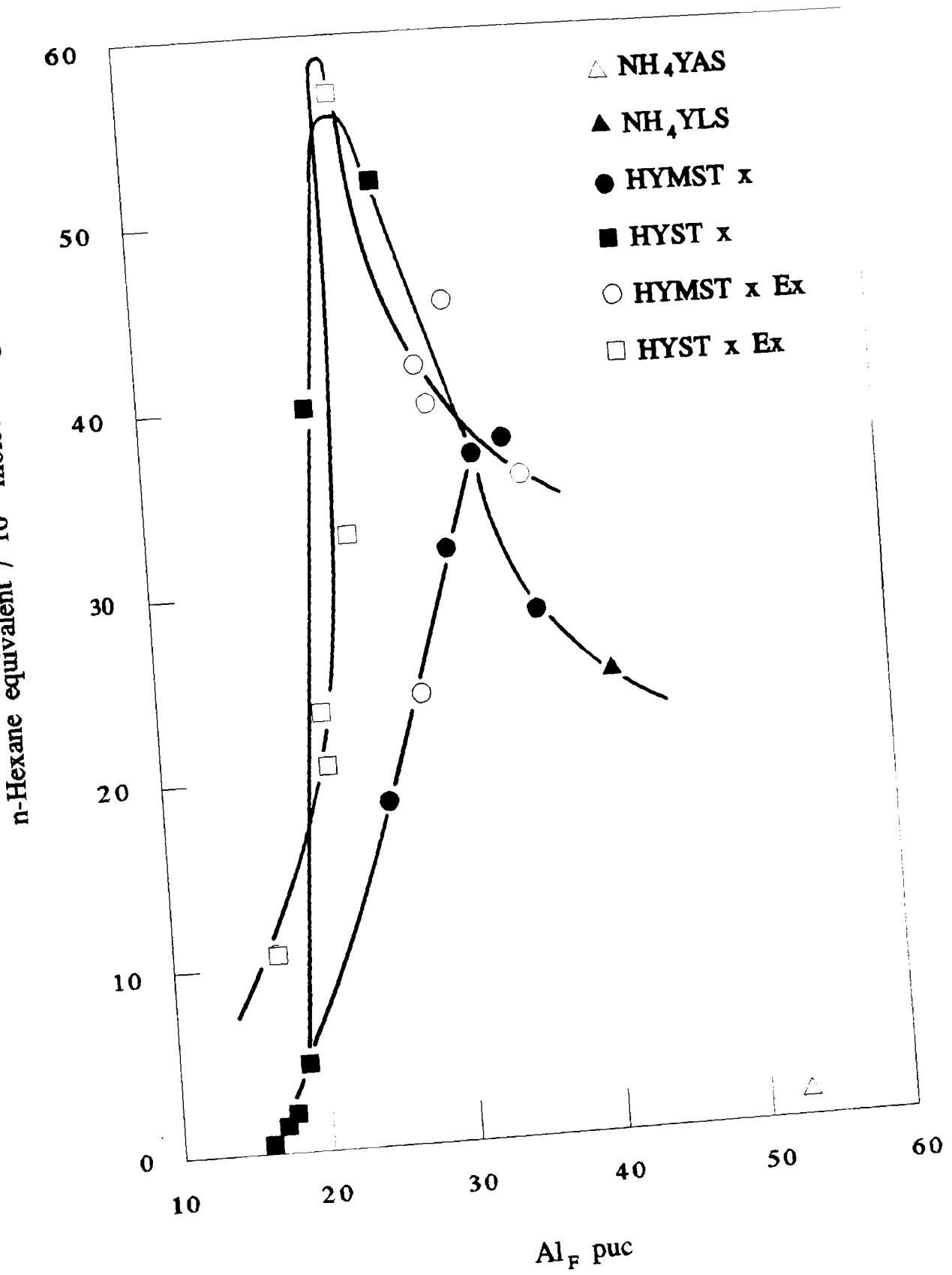

Figure 4.17: n-Hexane cracking activity after sixteen hours on stream

comparison of activities across a range of catalysts the activation energies should be similar. However, a change in activation energy can indicate a change in reaction mechanism, and so with this caveat in mind, a study across a range of samples can still be worthwhile from a mechanistic point of view.

Mechanistic Considerations

While the overall activity can yield information on the acidic nature of the catalysts, a detailed examination of the product distribution allows a greater understanding of the chemical processes involved in the reaction itself. Before such an analysis can be appreciated it is necessary to consider the mechanistic steps leading to the products observed. The consensus of opinion is that hydrocarbons crack by an ionic chain mechanism and as such the mechanism can be divided into the three classical steps: initiation, propagation and termination.

The initiation step is thought to be the formation of an adsorbed carbenium ion although there is debate as to the means of its formation. Two competing mechanisms have been postulated: the protolytic route and the hydride abstraction route; both routes rely on the formation of carbocations. The n-hexane molecule can either be directly protonated, forming a non-classical Olah type pentacoordinated carbonium ion, or undergo hydride abstraction and form a classical tricoordinated carbenium ion. As mentioned in Section 1.3, a carbonium ion can be visualised as an adsorbed alkane molecule and a carbenium ion as an adsorbed alkene molecule. Both these routes may involve Brønsted acid sites, but hydride abstraction could also result from interaction with Lewis acid centres. The adsorption of pre-existing olefinic molecules in the feedstock, which might arise either from impurities or from thermal cracking of the alkane prior to interaction with the catalyst, could provide a third source of initiation. Each of these options will now be studied in detail.

The formation[255] of pentacoordinated carbonium ions in solid superacids has been postulated.[256] Various workers, invoking the supposed similarity between dealuminated zeolites and superacids,[215] have postulated the formation

of these in zeolites.[83,216,257] The initiation step would therefore be the protonation of a carbon-carbon σ bond or carbon-hydrogen σ bond by a Brønsted site, as outlined in figure 4.18, forming a surface bound pentacoordinated carbonium ion.[171,258]

Attack at the carbon-carbon bond would result in protolytic bond fission yielding an adsorbed carbenium ion and a gas phase alkane molecule; protonation of the carbon-hydrogen bond would result in molecular hydrogen being evolved, and a hexylcarbenium ion being adsorbed onto the surface. There are three distinguishable sites for proton addition to a carbon-carbon bond and the energetics and the stabilities of the resultant cation for each can be calculated.[222] Under conditions approximating to those of the present research, Bassir *et al*[222] found that 76% of all protolysis reactions involved the cracking of the central bond and the remaining 24% cracked to give a C_4 and a C_2 fragment.

Hydride abstraction from the parent molecule to form an olefin could conceivably take place on either Brønsted or Lewis sites.[259] Hydrogen is evolved if the interaction is with a Brønsted site, or a hydride ion adsorbs onto a Lewis site, generating in either case a carbenium ion which would then be stabilised by adsorption onto the surface. Hydrogen was only found as a secondary product on HY,[260] not as a primary product as on HZSM-5.[261] It was therefore concluded that HY was not sufficiently acidic to protonate any C-H bonds and protolysis of hydrogen was reported to be so slow as to be unnoticeable in the reactions of n-hexane over HY at 673K.[222] Calculations[250] of the relevant activation energies for hydride abstraction (see following table) show that, if the bond energies are taken as activation energies for the bond fission process, the rate of removal of primary hydrogens is approximately $1x10^5$ times less than that of tertiary hydrogens (the authors concluded that paraffin chain length had little effect on the energies, although charge position did). Studies using neopentane [262] and isobutane [250] have confirmed that Brønsted sites do not attack primary hydrogens and that only tertiary hydrogens are sufficiently weakly bound to be removed.

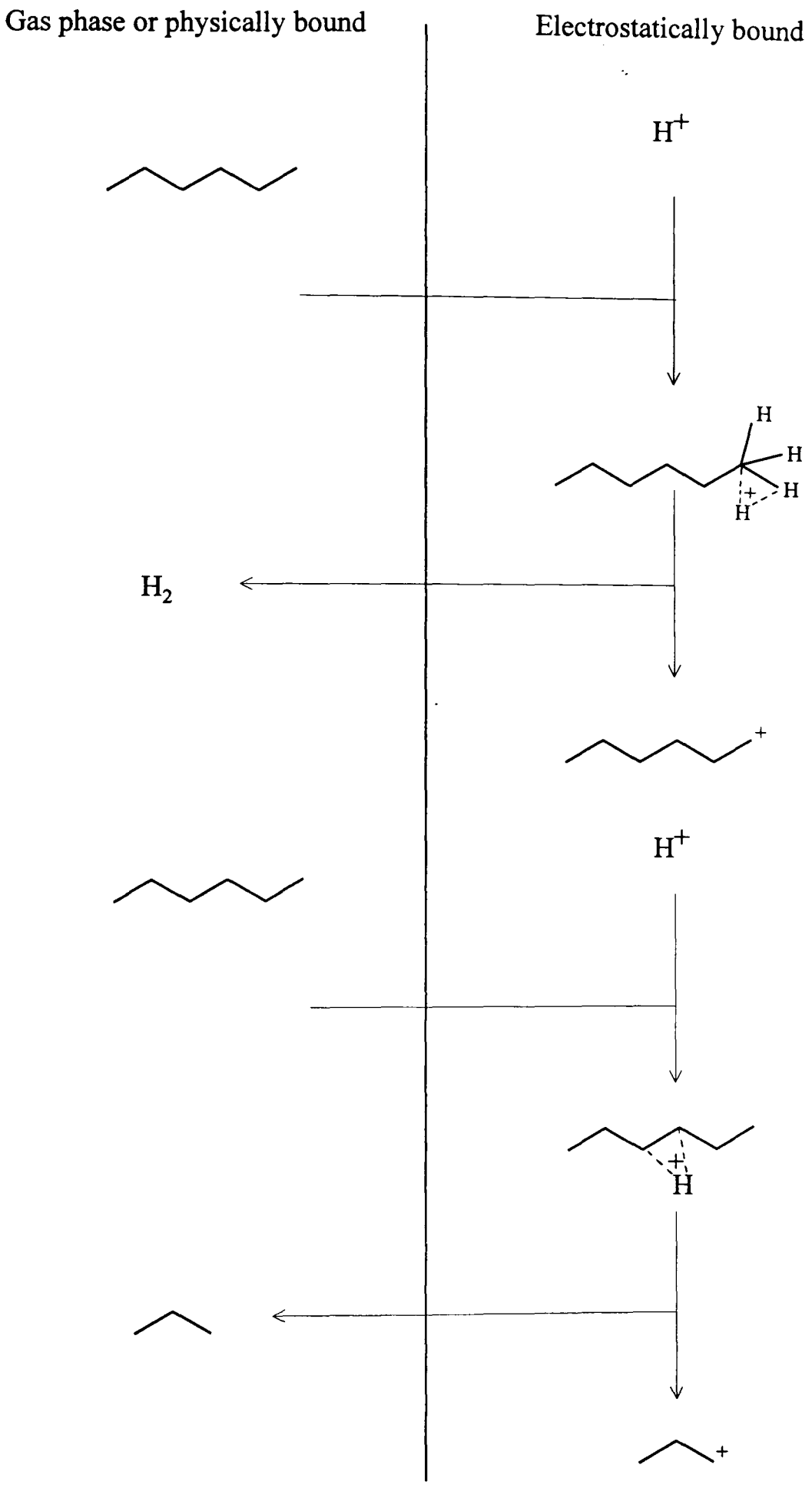

Figure 4.18: Protolytic cracking at a carbon-hydrogen bond and at a carbon-carbon bond.

Molecule	Bond Type	Bond Energy /kJmol^{-1}	Relative Rate (673K)
n-butane	Primary $C_3H_7C\underline{H}_3$	117	1
n-butane	Secondary $C_2H_5C\underline{H}_2CH_3$	87	$2.1x10^2$
n-hexane	Secondary $C_4H_9C\underline{H}_2CH_3$	83	$4.3x10^2$
2-methylpentane	Tertiary $C_3H_7C\underline{H}(CH_3)_2$	68	$6.3x10^3$
3-methylpentane	Tertiary $(C_2H_5)_2C\underline{H}CH_3$	54	$7.7x10^4$

Recent work has cast doubt on the classification of zeolites as solid superacids, claiming that HY is equivalent to 65% H_2SO_4 [263,264] or 90-98% H_2SO_4[265] and thus should be termed a strong acid. However, this work was conducted on a highly aluminous sample (Si/Al = 2.5) at only 373K, conditions which do not match catalytic conditions. A number of nmr studies conducted to try and assess the extent, if any, of hydrogen exchange between deuterated zeolites and alkanes [266,267] have concluded that exchange does not take place at the relatively low temperatures used (373K), though some exchange was noted at higher temperatures. Once again, it has been found that tertiary hydrogens were the most easily substituted.[268,269] Until in situ studies are carried out under catalytic conditions this argument will remain unresolved. Specifically, there seems to be little direct evidence presented, so far, for protolytic attack of a carbon-carbon bond.

The final category of initiation, the generation of olefinic species by non catalytic means, has also been investigated. Deliberate contamination of the feedstock with olefinic impurities has been shown to effect the rate of reaction, although the nature is undecided with arguments being propounded for beneficial[218,270,271] or detrimental[272,273] effects on the activity. Where bimolecular processes are thought to dominate, olefins facilitate the reaction,[223] but when the principal processes are monomolecular the presence of additional

olefins would either have no effect or a negative effect due to enhanced site suppression. Thermal cracking, or catalytic cracking on surfaces other than the catalyst would provide false results. It has been shown[272] that thermal cracking of n-hexane occurs to a negligible extent at 673K and less than 1 wt% at 773K.[223] This is confirmed by tests carried out within the present study using a set-up identical to the catalytic tests, but with a silica wool plug in place of the catalyst, which showed no conversion under the conditions employed. This, and the absence of any detectable impurity in the feedstock, allows the last category of initiation to be discounted in the present study.

The carbenium ion thus formed, independent of its genesis, will then, if possible, undergo rapid hydride transfer resulting in a more stable secondary carbenium ion. This can then suffer one of three fates:

i) desorption into the gas phase as an olefin molecule, whilst returning a proton to the catalyst surface,

ii) ß-scission to form a gas phase alkene and a smaller adsorbed carbenium ion,

iii) hydride abstraction from another molecule and subsequent/concurrent desorption/adsorption to form a gas phase alkane molecule and a larger adsorbed carbenium ion.

Step i) terminates and step iii) propagates the reaction chain.

There is a choice as to which fragment will form the carbenium ion and which will enter the gas phase as the olefin when a cracking event ii) has occurred, unless the central bond has been split. It has been claimed that the larger of the two fragments will be retained on the surface.[274] This is justified by assuming that the smaller olefin is more able to diffuse away from the site, and so will escape while the larger fragment is trapped. The lack of any change in the product distribution over a wide range of conversion in that study, and in a study by Nace,[275] further suggests that the smaller fragment, which is less likely to recrack, is released into the gas phase. These studies were conducted using longer straight chain paraffins, (C_6 to C_{15}) which may not necessarily be applicable in the present reaction. Presumably, where the sizes of the fragments produced are similar, other factors, such as carbenium

ion stabilisation have to be taken into consideration. A fourth reaction of the carbenium ion, progressive dehydrogenation to form coke, cannot be neglected. Although this forms no immediately detectable products, it contributes to the overall reaction by providing a source of hydrogen for use in the production of alkane molecules from other carbenium ions. This, therefore, is a termination step as a carbenium ion is consumed without the production of a replacement. It is assumed that the dehydrogenated carbenium ion is incapable of desorption from the surface. These reactions are summarised in figure 4.19.

Analysis of Results

As already mentioned, there are two competing reaction pathways, protolytic cracking with or without β-scission, and hydride abstraction followed by β-scission. Detailed analysis of the product distribution has allowed different workers to attempt to assess the relative contribution of each to the overall reaction in particular catalysts. The length of the cracking chain has been calculated[276] under differing conditions for several reactants. Chain length was defined as the ratio of the rate of bimolecular propagation to unimolecular initiation; short chain lengths indicate that initiation products form an important proportion of the total products and conversely the longer the chain length the less important the initiation products become. Shorter chain lengths were found for molecules without tertiary hydrogens[222] indicating that these reactants were more likely to have a greater contribution from monomolecular mechanisms. Detailed consideration of the possible routes for the formation of various products will yield information as to the nature of the reaction. Propane and n-butane can be formed from either the protolytic cracking of the appropriate carbon-carbon bond, or the hydride transfer from an alkane to a secondary propyl or n-butyl carbenium ion respectively; isobutane can only be formed by hydride transfer to a tertiary butyl carbenium ion, and so cannot be formed directly by normal protolytic cracking. For protolytic cracking to form a branched isomer, a larger branched paraffin must first be adsorbed, or a pre-existing carbenium ion rearranged. Although it is feasible that a molecule of methylpentane formed from the isomerisation of n-hexane at an earlier stage

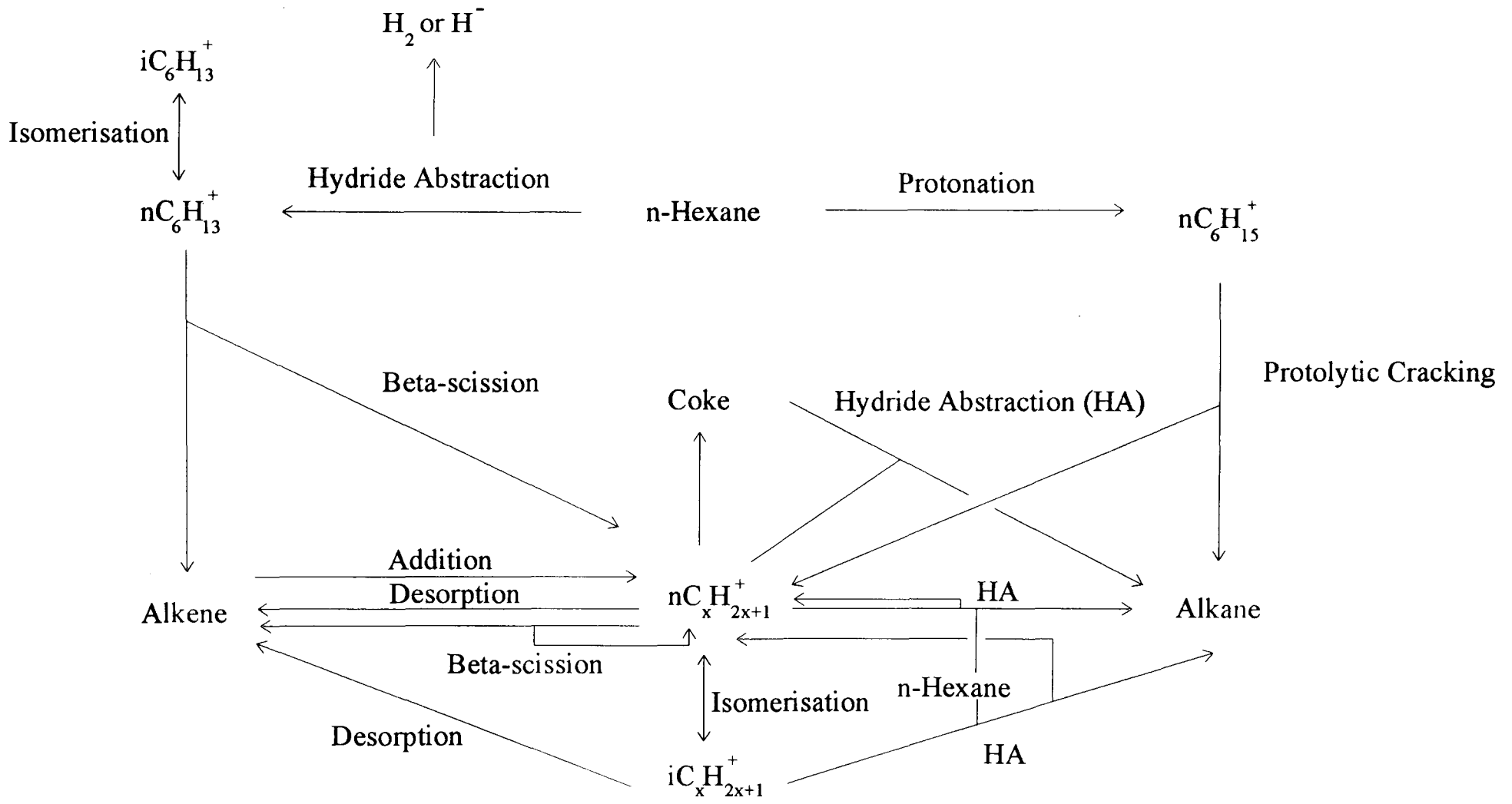

Figure 4.19: n-Hexane reaction scheme summary.

of the reaction can be reprotonated and crack protolytically to form the isobutane, this is unlikely given the negligible methylpentane concentration in the 'secondary' feedstock, for reasons given earlier.

If the reaction proceeded solely via a primary monomolecular route the amount of C_4 produced would never exceed that of C_2, but the figures in table 3.42 clearly show that the amount of C_4 produced is considerably higher than that of C_2 in all but three cases, implying that secondary and/or bimolecular processes are occurring. The evident loss of C_2 or excess of C_4 can be accounted for in three non mutually exclusive ways:

i) production of C_4 without associated production of C_2

ii) the initially produced C_4 fragment does not recrack

iii) most of the C_2 produced takes part in further reactions.

Options i) and iii) are indicative of bimolecular reactions which will now be considered in detail.

It is first necessary to define reaction nomenclature. A primary reaction is one which has involved only one adsorption event, as seen from the vantage point of the molecule concerned, whilst a secondary reaction is one that has seen two or more adsorption events. Monomolecular and bimolecular need no explanation. Thus, in figure 4.20 reaction i), the C_4 fragment is undergoing a secondary bimolecular reaction to form butane, whereas the n-hexane is experiencing a primary bimolecular reaction to form a hexyl carbenium ion. In reaction ii) this hexyl carbenium ion can now crack via ß-scission, here a primary monomolecular reaction. When a hydrocarbon molecule adds to a carbenium ion, the resulting ion must then undergo primary cracking reactions, as at no stage has there been a second desorption event. For a cracking reaction to be defined as secondary, desorption of a carbenium ion as an olefin, followed by readsorption must first occur.

Secondary cracking has been dismissed by Shendye *et al*[274] since no change in the product distribution with increasing conversion was observed, implying no further reaction of the cracking products. They used longer chain (n>6) paraffins and postulated that the smaller fragment escaped as the olefin. These smaller olefins are less prone to readsorption and hence further reaction.

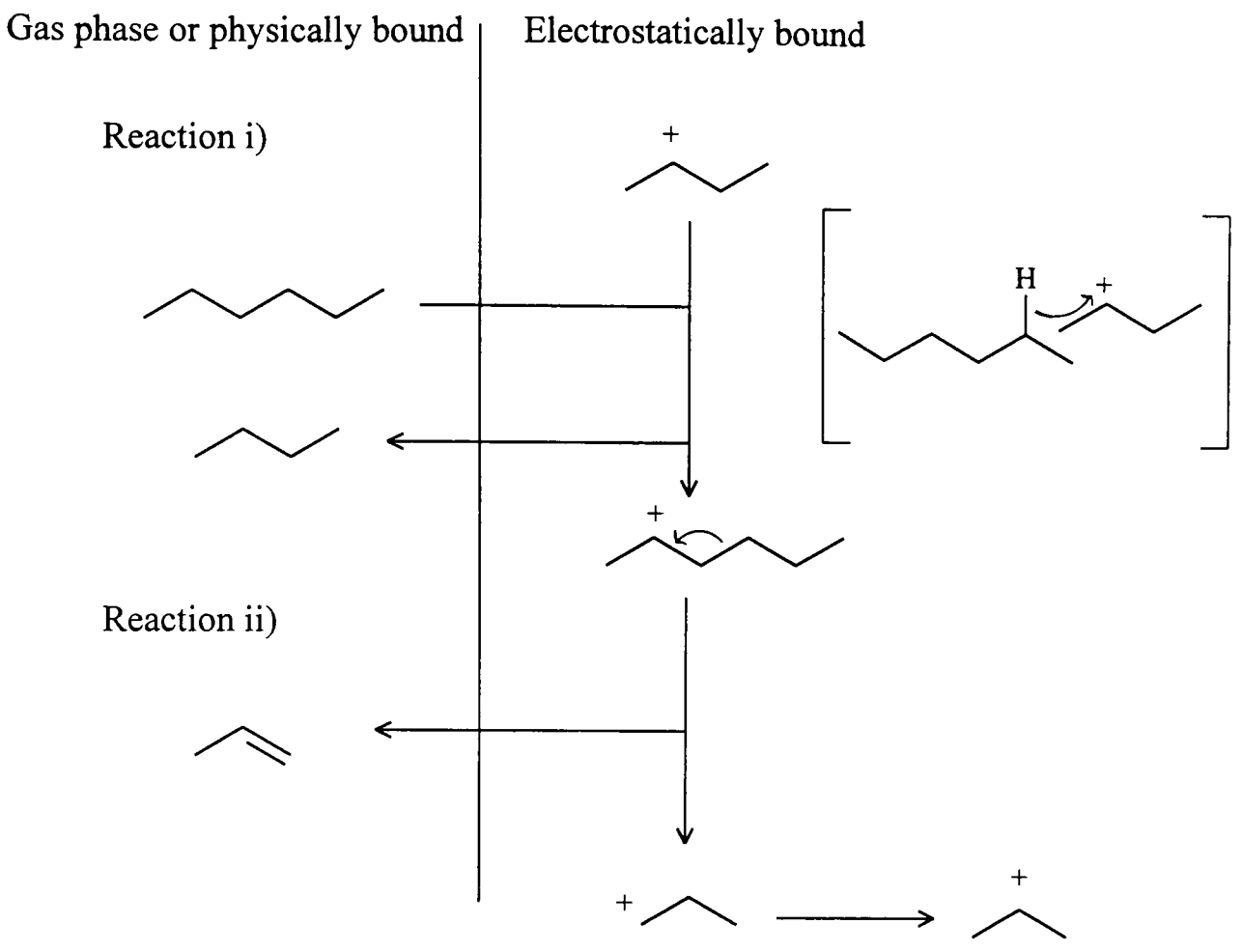

Figure 4.20: Primary and secondary reactions.

Reaction between the adsorbed carbenium ion and a gas phase olefin in which the carbenium ion acts as a Lewis acid, accepting an electron from the double bond, have been shown to exist using isotopic studies of isobutene cracking over silica/alumina.[277,278] The resulting larger carbenium ion could then experience ß-scission to produce a C_4 molecule without an associated C_2 molecule.[247] In additional, the carbenium ion could react with another n-hexane molecule.[213] Statistically, one would expect to form a C_9 cation, which has dimensions of 0.49 x 0.60 nm[279] and a length of 0.92 nm; formation of C_8 and C_7 cations can be ruled out due to the lifetimes of the C_2^+ and C_1^+ cation being too short to allow interaction with a n-hexane molecule.[213]

The rate of formation of propane and the butanes due to protolytic cracking was deduced by Lukyanova[280] by plotting the rates of their formation against the extent of n-hexane conversion. The intercept on the Y axis after extrapolation to zero conversion gave the cracking rate due to protolytic

cracking alone. It was shown that propane and n-butane had a contribution from protolytic cracking, whilst i-butane had none, and so was entirely due to hydride extraction, which is consistent with the mechanism outlined above. Therefore, the effects of the two mechanisms can be separated, and the rates of formation of products due to the two mechanisms calculated. The rate of hydride transfer from a gas phase alkane to an adsorbed carbenium ion can also be probed. Lukynova[281] showed that at low conversion levels the ratio between the rate of formation of an alkane and the concentration of its corresponding carbenium ion was constant, and the value of such could be used to characterise the hydride transfer capabilities of the ion. As has been shown earlier, isobutane cannot be formed by protolytic cracking, and so this forms the basis of the so called ß-test for hydride transfer activity.

In large pore zeolites, ie. those without steric constraints, it was shown[280] that the hydrogen transfer activity of isobutene, n-butene and propene is in the approximate ratio 6.5:1.3:1.0, in direct contradiction to Zhao *et al*[282] who, in a study of 2-methylpentane cracking over HY zeolite, reported that ethyl and propyl ions are active in abstraction processes, whereas butyl ions are not. For hydrogen transfer the two molecules involved must approach to within a certain distance. Under the conditions of the experiments carried out in this study there is at most one n-hexane molecule to every fifty supercages.[213]

In a further attempt to quantify the contributions of the two mechanisms Wielers *et al*[217] introduced the cracking mechanism ratio (CMR), defined as the sum of the amounts of the C_1 and C_2 products divided by that of isobutane. As the production of C_1 and C_2 molecules is considered typical of protolytic cracking and the formation of isobutane as indicative of the classical ß-scission mechanism, high values of the CMR suggest a greater contribution from the protolytic route whereas a smaller value (CMR<1) suggests that β-scission is more dominant. The authors also pointed out that a ratio of one did not necessarily imply equality between the mechanisms, as the cracking mechanisms by which the determining molecules have been obtained have been simplified. Unfortunately, the experimental conditions of

the present study did not permit the detection of methane, nor the separation of iosbutane from isobutene. The amount of methane produced over these catalysts has been shown[201] to be low enough to make no difference to the ratio determined, but the non resolution of the isobutyl compounds is more problematic. The result is that the ratios calculated cannot be considered true cracking mechanism ratios, in the sense of Wielers *et al*,[217] but rather apparent CMRs. However, valuable information can still be obtained from these ratios, and the changes in ratio discussed in what follows are of sufficient magnitude to be significant.

The cracking mechanism ratios for all the catalysts presently studied can be found in table 3.43. Samples up to and including HYST 873 have a low, constant CMR, which shows a slight rise after fifteen pulses and is then constant to sixteen hours. However, catalysts HYST 923 to HYST 1073 show a linear rise in the CMR when plotted against acidity, figure 4.21, and this can only be attributed to a progressive change in mechanism, with protolytic cracking becoming increasingly more dominant.[171,248] This trend is continued over fifteen pulses and after the following sixteen hours, and with time on stream. The extracted samples show a very slight rise, but this is negligible when compared to that of the unextracted samples.

Production of n-butane is enhanced with respect to isobutane after fifteen pulses, and sixteen hours on stream, as is shown by the i/n butane ratio for both the extracted and unextracted samples. The change in this ratio cannot be ascribed solely to coke or adsorbed n-hexane causing steric hindrance favouring production of the straight chain isomers, as the production of isopentane with respect to the straight chain isomer is enhanced after fifteen pulses. A surface populated with n-hexane promoting the production of isopentane could be regarded as evidence supporting the claim of Anderson *et al*[213] that surface species with nine carbon atoms readily form on the surface, as, both initially, and following flushing after sixteen hours, the concentration of such species is less than after fifteen pulses. The addition of an n-hexane molecule to a pre-existing propyl carbenium ion is shown in figure 4.22, resulting in the formation of a C_9 carbonium ion. Addition across

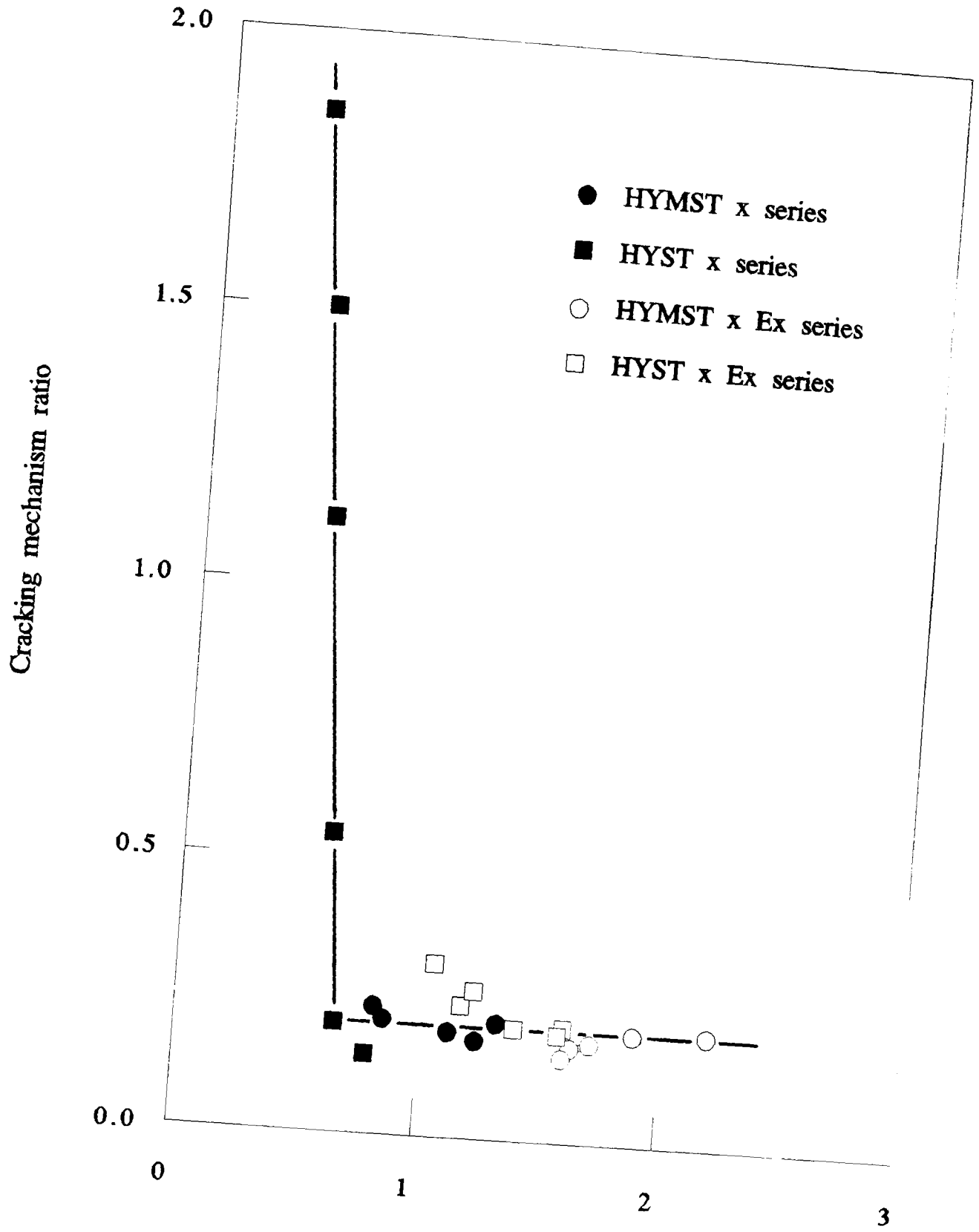

Figure 4.21: Cracking mechanism ratio.

the second carbon-carbon bond, as shown, followed by protolytic cracking, results in the production of isopentane. The fact that the butane ratio does not follow that of the pentane suggests that isobutane is not formed predominately by this method, via addition across the first carbon-carbon bond. Direct isomerisation of a butyl carbenium ion must be the more favoured method, although reasons for the ratio change, other than the steric argument, are difficult to propound. The isomerisation ratios vary with sample composition in a similar way to the overall acidity (figure 4.23) which clearly implies that both isomerisation processes are favoured by strong acidity. Both mechanisms outlined above will be enhanced by dealumination as an increase in acidic strength will increase the lifetime of the carbenium ion. It is worth pointing out that extraction seems to favour the production of isobutane more than that of isopentane, but if these figures are compared against the increase in acidity as measured by ammonia temperature programmed desorption an apparent drop in selectivity is noted.

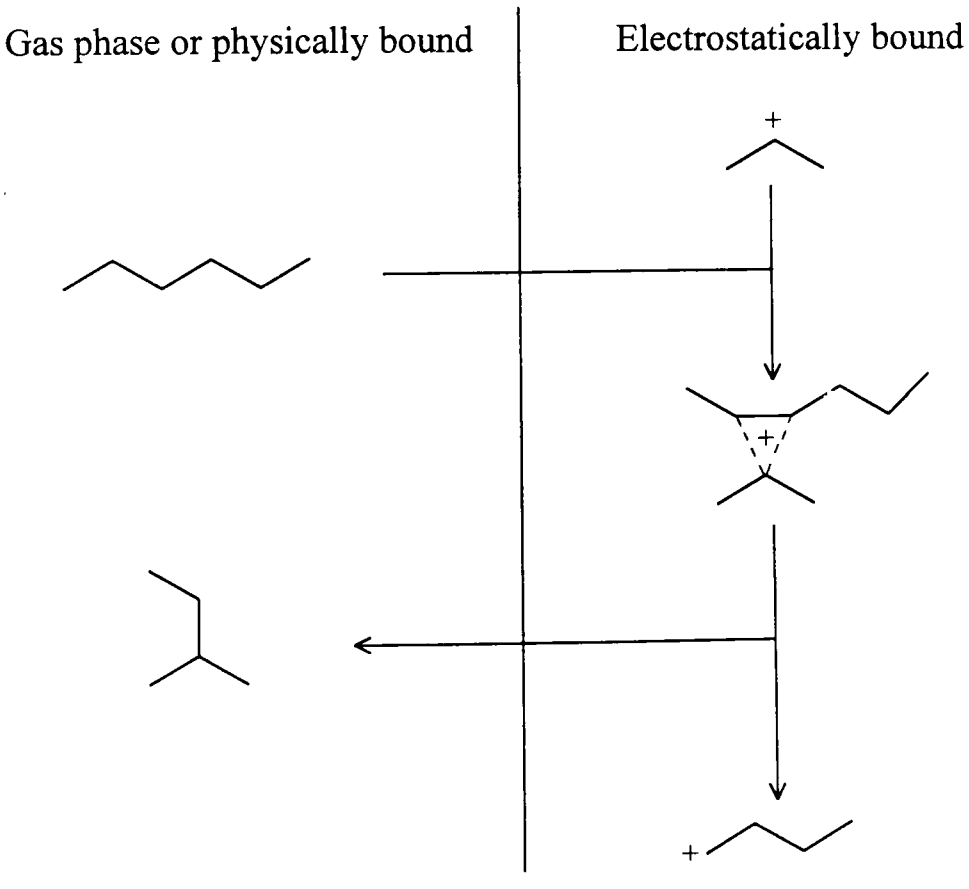

Figure 4.22: Formation and cracking of nonocarbonium ions.

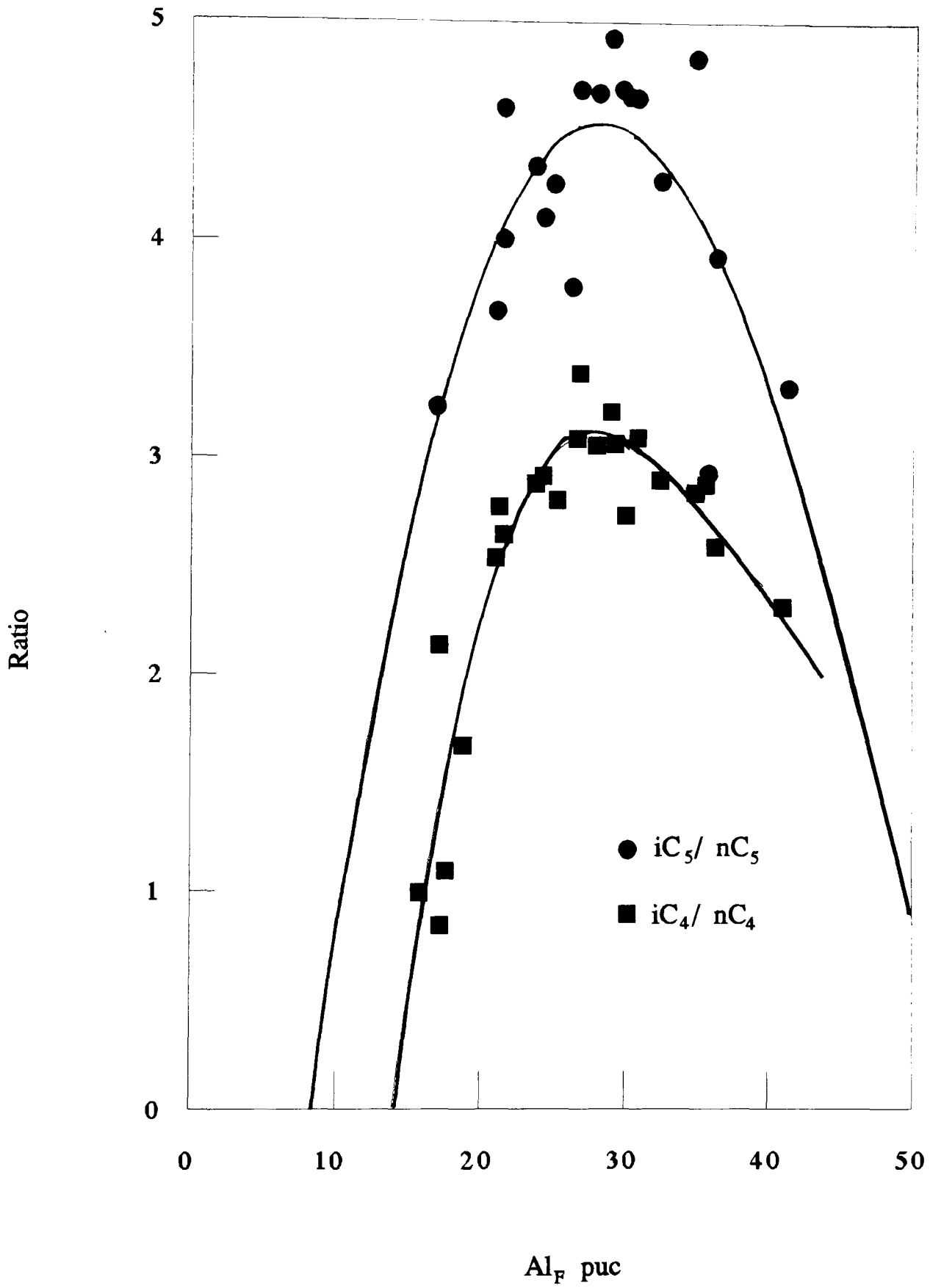

Figure 4.23: Isomerisation ratios.

There is a linear relationship between the amount of n-hexane cracked in the first pulse and the amount of isobutane therein, with the exception of those samples with an activity of less than $1.2x10^{19}$ molecules g^{-1} (figure 4.13). These samples have high values for the CMR and thus a greater contribution from protolytic cracking. To emphasis the data obtained from the less active catalysts, figure 4.13 has been replotted using the natural logarithm of the amount of n-hexane consumed in the first pulse (figure 4.24). The activity as measured by total n-hexane consumed initially increases at a faster rate than that as measured by iC_4. At higher conversions there is essentially no difference in the gradients. Furthermore, the stable t-butyl carbenium ion cannot crack by ß-scission, for it has no bond ß to the charge, and so can only be consumed in bimolecular reactions, or by isomerisation to the straight chain isomer.[283] Although studies have been conducted using isobutane as a feed stock [250,276,283,284,285,286] it would seem that monitoring isobutane would give a good indication of the initial hydride abstraction activity as it is the most stable of the products formed. Therefore, for catalysts which have similar CMR values, ie. when the reaction proceeds predominately by the same mechanism, comparing the production of single products is valid. Figure 4.25 shows the production of isobutane over all the catalysts.

Deactivation

The amount of retained coke on each catalyst, reported in table 3.41, cannot directly account for the drop in activity already noted. Most catalysts suffered a drop in activity to around two thirds of the initial activity after fifteen pulses. The exceptions are those with high CMR ratios and concurrent low activities which underwent less than ten percent deactivation over the same time period, and NH_4YAS which essentially did not deactivate. The extracted catalysts suffered similar extents of deactivation to the unextracted catalysts, with the exception of catalysts HYST 923Ex to HYST 1073Ex, which now suffered similar deactivation to the rest of the extracted catalysts.

The extent of deactivation can, therefore, in the first instance be related to the activity of the samples, in as far as there is a threshold activity below

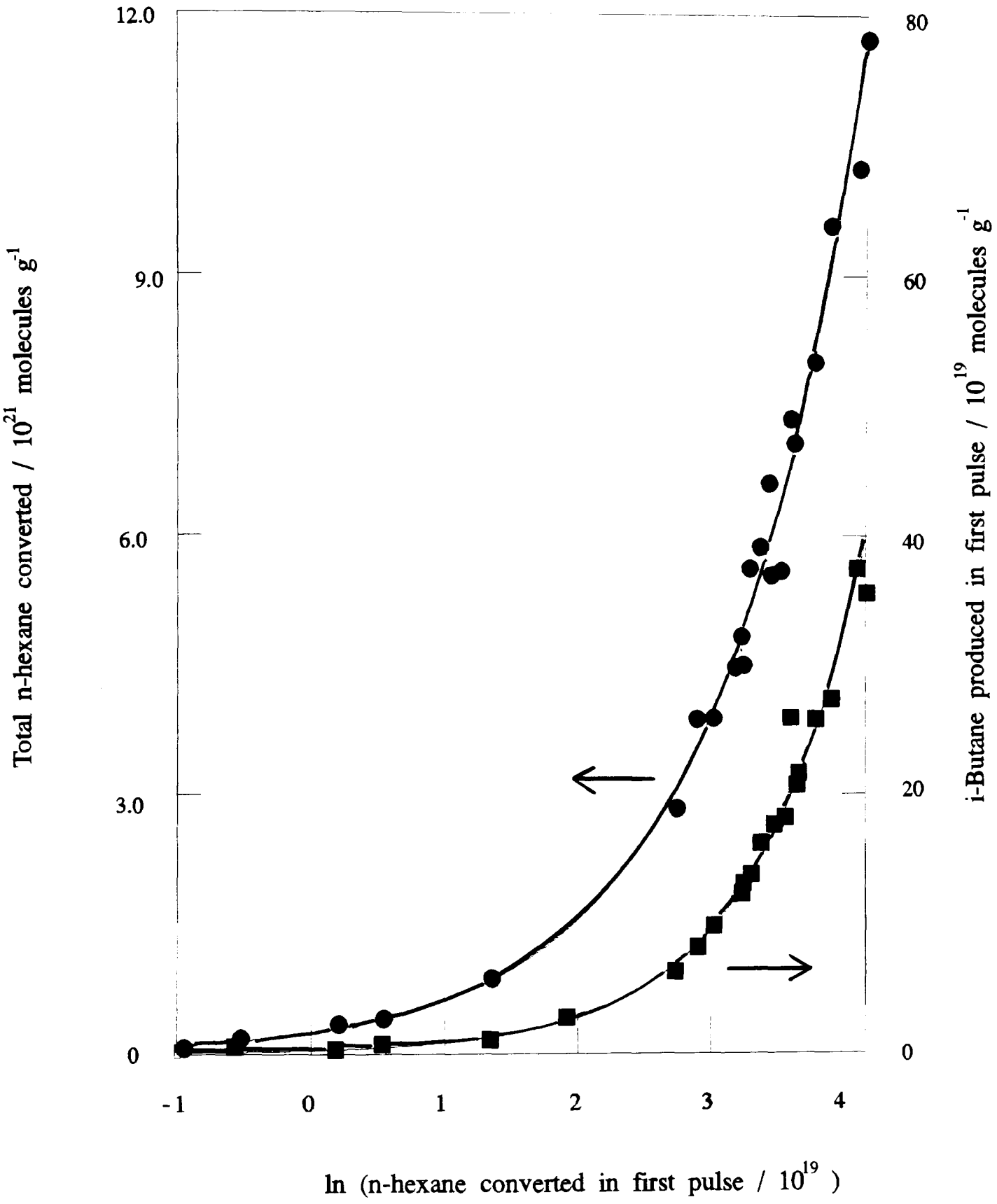

Figure 4.24: Comparison of different methods of denoting activity II.

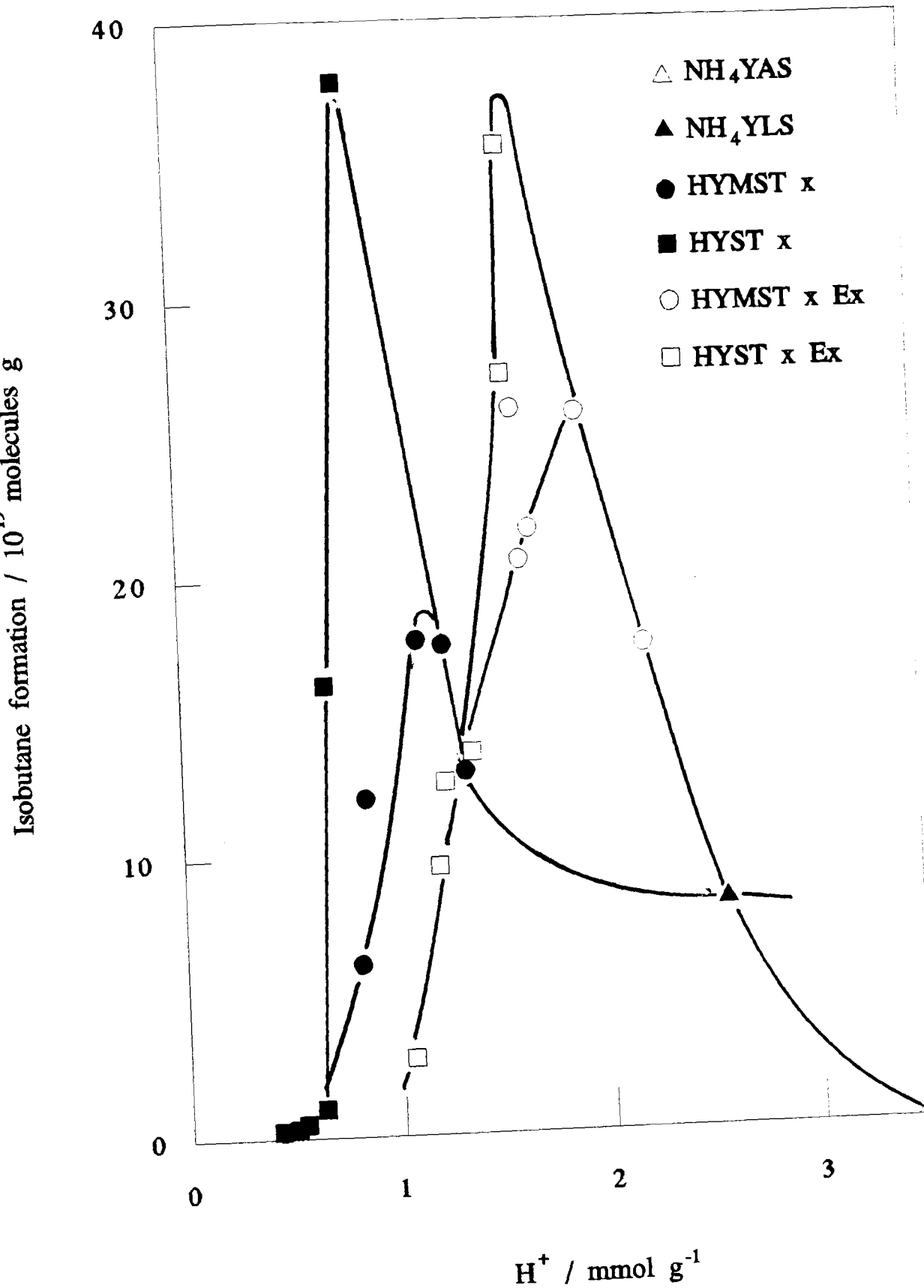

Figure 4.25: Isobutane produced in the first pulse.

which deactivation occurs to a much lesser extent. These more inactive catalysts are those which have a greater contribution from the protolytic pathway and are less able to support hydride chain transfer. Hammon *et al*[221] related extent of deactivation to the aluminium content of the framework, but incorrectly conjectured that crystals which had a framework aluminium content below a certain value were more resistant to coking. The results obtained here show that a subtle change in the balance of the reaction mechanisms is more likely to lead to the difference in deactivation. It is tempting to suggest that the chain transfer mechanism has a higher coking function than protolytic cracking. Hydride transfer to adsorbed species from a feedstock molecule, a process integral to the continuation of the chain mechanism, followed by desorption would, by definition, decrease the carbon content of the catalysts. However, it has to be recalled that these catalysts have a much higher activity and an increase in deactivation could be due to a increase in the rate of the coking reaction and that the amount of coke found does not differ from sample to sample in the unextracted series. Therefore a similar amount of coke can have a disproportionate effect on the activity in some catalysts.

There are two well documented causes of deactivation,[287] namely active site suppression and pore filling. The first eliminates the catalytic activity by interfering with the action of the active sites, and the second prevents diffusion of reactant to, and products away, from them. The very low coke content of the spent catalysts indicates that pore filling has a negligible contribution, being perhaps one tenth the level of coking found in these samples for other reactions.[201] Assuming that the coke has a hydrogen/carbon ratio of 1.9, as was found in a study of n-hexene cracking over ultrastable Y zeolite[188] and 2-methylpentane cracking over HY,[282] a one weight percent coke loading corresponds to approximately ten carbon atoms per unit cell. Given that the coke does not exist as entities with individual carbon atoms, the implications arise that active site suppression cannot account for the observed deactivation unless a small proportion of the structural sites are active, and that the sites must be deactivated within the first fifteen pulses. The influence of one coke molecule could extend beyond one framework Brønsted site, possibly through

electronic interactions with the framework, which have been shown to exist using ^{29}Si masnmr.[189] The amount of coke deposited after sixteen hours corresponds to that of the carbon contained in less than half of one pulse, and so it is not unreasonable to assume that the majority of the coke could be laid down in this initial period.

When HYST 823, which had previously been subjected to ten pulses of n-hexane at 673K, was heated to 703K for half an hour and then allowed to cool to 673K, a noticeable rise in activity was observed (figure 4.26). A similar rise in activity was noted when the sample was left for sixteen hours under flowing helium at 673K. In both cases it seems that a small amount of material has been desorbed from the surface, freeing some sites. However, this effect is soon cancelled out by further pulses. It is proposed that as the reaction proceeds, these strongly adsorbed species are progressively dehydrogenated, supplying hydrogen for use in producing saturated product molecules. The proportion of paraffinic molecules in the product stream in this instance cannot be as high as has been claimed elsewhere[247] as, unless the production of (unresolved) acetylinic compounds is invoked, the amount of coke produced is insufficient to have supplied enough hydrogen. The maximum possible paraffin/olefin ratio, if one assumes one cracking event per n-hexane molecule, is one; any greater ratio requires more hydrogen to be abstracted from the coke. As dehydrogenation of the surface bound molecules continues, desorption into the gas phase becomes less favourable, thus explaining why the increase in activity on heating, or evacuating for an extended period of time, does not return the activity to the initial level. The majority of the coke, or at least the majority of the coke which is effective in deactivating the catalysts, is therefore laid down within the first few pulses. This is in complete agreement with Groten *et al*[189] who concluded that HY has practically deactivated under the conditions employed in twenty seconds due to coke deposition. They found that the level of coke within the catalyst did not change thereafter and further rearrangements of the coke served only to minimise the energy of the surface layer.

There is a slight increase in the CMR after fifteen pulses which implies

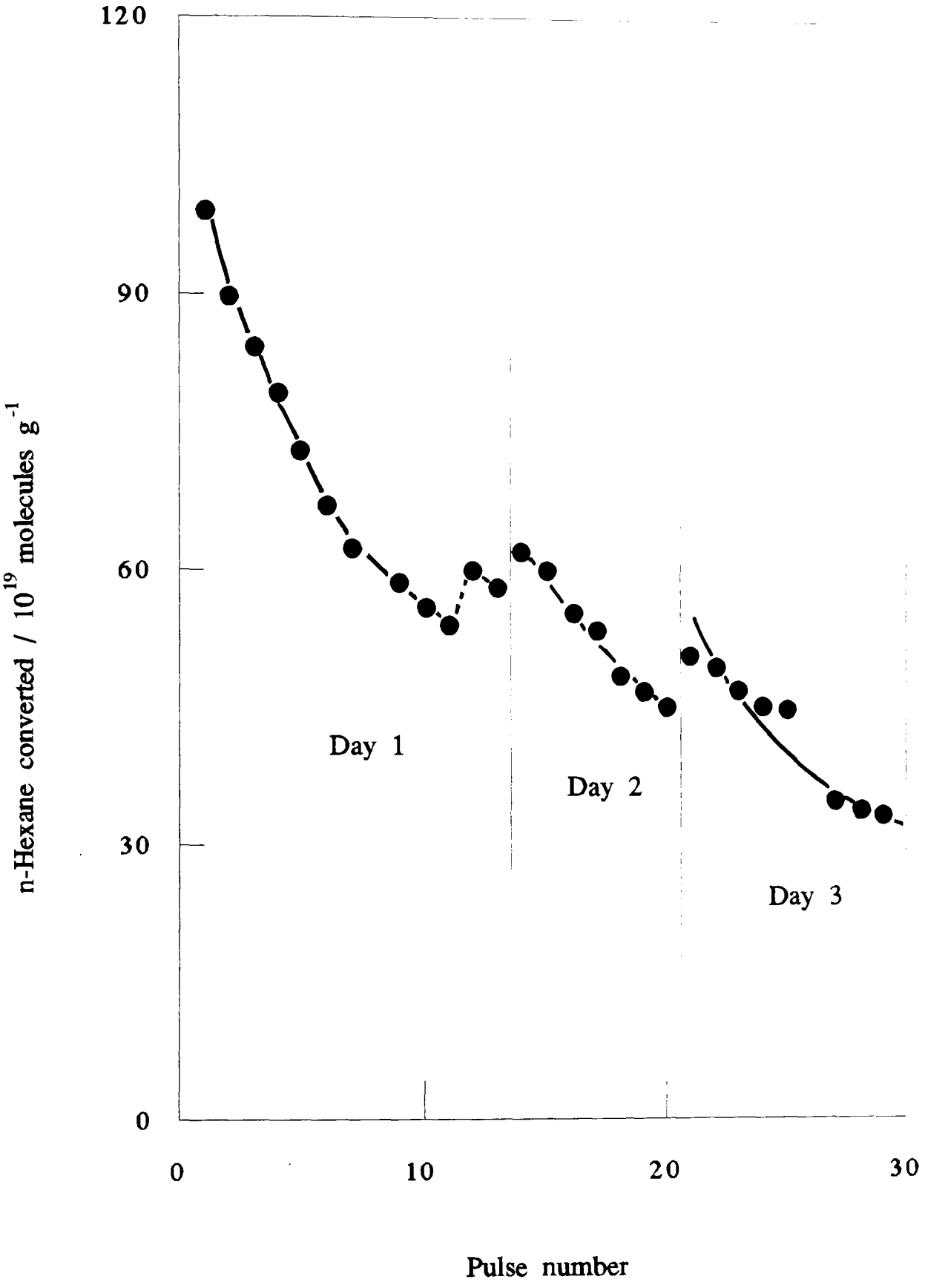

Figure 4.26: Effect of pulse interval and temperature rise on n-hexane cracking activity - HYST 823.

that the reaction mechanism profile has changed with slightly less emphasis on charge transfer/β-scission. This corroborates the idea that some sites have become blocked and the chain transfer process becoming less favourable is likely to be the greatest contributor of the drop in activity (cf the dramatic rise in activity when more sites are made available on extraction). In addition a small drop in activity might be expected due to the loss in number of sites available to initiate the reaction by protonation of the paraffin to form a pentacoordinated carbonium ion. Small amounts of coke blocking pore entrances would have a disproportionate effect on the activity. However, as this would in effect simply reduce the mass of the active catalyst, no change in the CMR would be expected. The discrete removal of sites by coke is therefore the favoured explanation of deactivation which may imply that a small proportion of the total framework aluminiums are active,[252] even only those on the crystallite surface.[189] Alternatively, the removal of acid sites by coking could hinder the hydride transfer step of the reaction, thus shortening the chain length. This would reduce the activity as less molecules of reactant are cracked for a similar number of initiation events.

Catalyst HYST 873 exhibits a threefold increase in the CMR between the initial pulse and sixteen hours. This is the most aluminous catalyst not to have a high (ie. >0.3) initial CMR and confirms other evidence which suggests that as the reaction proceeds sites are progressively removed, or rendered unable to participate in the reaction. HYST 873 has a critical number of sites such that during the initial stages of the reaction there are sufficient adjacent sites for the β-scission mechanism to predominate, but after adsorption/coking there is just few enough to effect the mechanism causing a shift towards protolytic cracking dominance. However, it must be remembered that the CMR by definition is a noncalibrated measure and so the absolute contributions from the two mechanisms cannot be assessed.

At this stage it is necessary to draw comparisons with previous work[201] which studied these catalysts under continuous flow conditions. In that work rapid deactivation was observed in the first hour, and then more gradual deactivation seen in the next three to four hours with a final steady activity

achieved after twenty four hours. It has to be remembered that, as well as the previous work being studied under continuous flow conditions, the catalyst bed geometry was slightly different. If, as postulated above, loss in activity is due to the adsorption of reactant/product molecules onto active sites, a continuous flow of n-hexane is going to exacerbate the situation. Pulses, which deliver the same amount of reactant as about six seconds of continuous flow, arrive at approximately thirty minute intervals. This gives any strongly adsorbed material longer to desorb than if the pulses had no interval, ie. the flow was continuous. This has two consequences; firstly, a higher activity would be observed as a desorption/adsorption equilibrium would not have been established, and secondly a cleaner surface is presented to the pulse than after a zero minute interval, yielding a higher conversion. Therefore, one would expect the rate of deactivation observed during pulse experiments to be less than for the equivalent time of a continuous flow experiment. Continued deactivation of the samples in the previous continuous flow experiments is thus proposed to be due to a build up of n-hexane on the surface of the zeolite. Excess n-hexane diminishes the pore volume of the catalyst, leading to a reduction in the diffusion pathlength. This deactivation is not seen in the present study when pulse measurements were made after sixteen hours on stream because the samples were flushed for two hours prior to the second pulse measurements being taken, to avoid confusion between retained products desorbing from the surface and products from the reactant pulse. The apparatus would have to be further modified before more detailed examination of this phenomen could be attempted. Different deactivation could also be witnessed due to more reaction taking place in the pulse experiments which could lead to different rates of the coking reaction. Unfortunately, due to the sampling procedure and other experimental differences, further comparisons cannot be drawn.

Extraction of nonframework aluminium

It has already been noted in the present study that extraction of non framework aluminium increases the activity of the catalysts. The effect of

extrastructural aluminium on the activity of HY zeolites has been studied elsewhere with various conclusions being drawn, depending in part on the reactant used in the study, and in part the amount of extrastructural material remaining in the extracted catalysts. Contrary results have been obtained by Wang *et al*[247] who reported no difference in activity between samples which had less than $20Al_F$ puc and more than $25Al_{NF}$ puc and those which had less than $10Al_{NF}$ puc. However, samples which had more than $20Al_F$ puc and $25Al_{NF}$ puc were found to be more active than the samples with an equivalent framework composition but which had less than $10Al_{NF}$ puc. Biaglow *et al*[251] found that steamed samples had a higher activity than chemically dealuminated samples, and that acid extraction reduced their activity to that of the appropriate chemically dealuminated sample, thus concluding that the enhanced cracking activities of the steamed samples are not due to an increase in the acidity of the hydroxyl groups. The presence of non framework aluminium has three discrete physical effects:

i) acting as charge balancing cations, thus lowering the proton content,[288,289]

ii) physically filling the pores, shielding the protonated sites,

iii) synergistic effects leading to the strengthening of the framework Brønsted sites,[151,247] or the polarising effects of the nonframework aluminium acting as Lewis sites on the reactant.[66]

In addition there is the possibility of the presence of acidic groups on the non framework alumina.[170,290,291]

For the highly dealuminated unextracted samples, by implication those with a large amount of non framework aluminium, the increase in activity seen on extraction is dramatic, figure 4.27, and associated with a concomitant decrease in the CMR, such that the values for the extracted samples are almost constant. The similarity between figures 4.21 and 4.27 is quite marked, showing that the change in relative contributions of the two mechanisms dramatically increases the extent of the reaction. Thus it can be concluded that the hydride abstraction/ß-scission pathway offers a much more efficient means

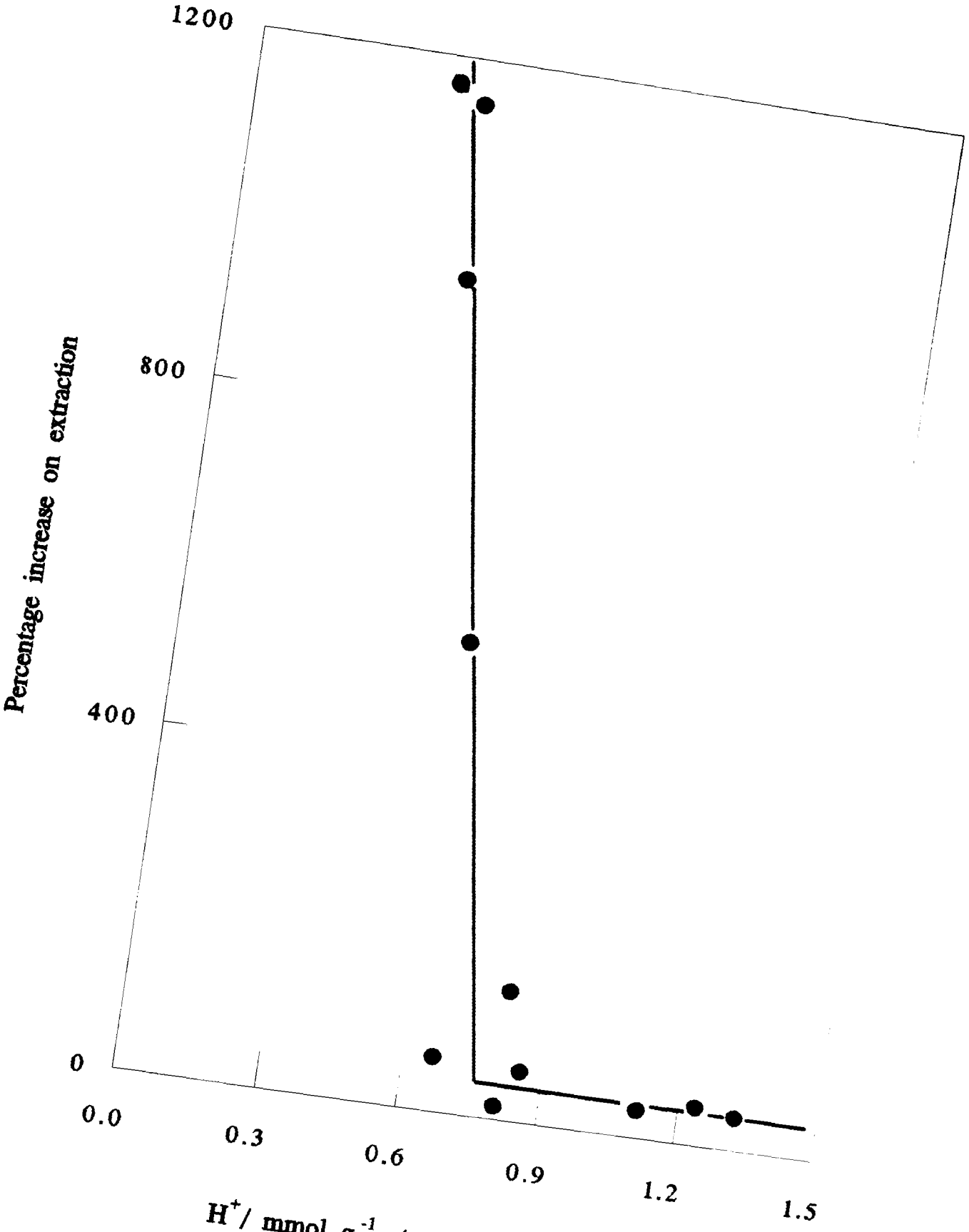

Figre 4.27: Increase in total activity on extraction.

of reaction, when conditions permit it. This is only reasonable as it permits far more molecules of reactant to be cracked per initiation event. A drop in the capacity of zeolites to adsorb olefins, and a decrease in the relative olefin/paraffin adsorption ratio has been advanced as an alternative explanation for the decrease in hydride transfer activity on dealumination.[248] This effect is only marked at framework aluminium concentrations of less than ten per unit cell and so can be discounted when considering the catalysts used in this study.

If, as proposed by Banwenda[290] in the case of the cracking of 2,3-dimethylbutane, extraframework aluminium extraction merely freed more sites to take part in the reaction, the change in activity would be directly related to the change in acidity as probed by ammonia temperature programmed desorption, but figures 4.21 and 4.27 have a clear discontinuity, corresponding to between 40 and 45 Al_{NF} puc. The physical effects of extrastructural aluminium are obviously proportional to the extent of the dealumination, and since this is clearly not the case, there is a physical or mechanistic reason for this change. It has been proposed that ß-scission requires two adjacent sites,[217] or close Brønsted sites or a Brønsted site close to another type of cation,[248] whereas protolytic cracking takes place on a single site.[217] Hydride transfer, which carries the chain reaction, requires the two participating molecules to come within close proximity. With the carbenium ion already anchored to one site, a n-hexane molecule can be induced towards a neighbouring site and if the second site is close enough hydride transfer occur. Thus it is not ß-scission itself which is disproportionately enhanced by the increased availability of sites on extraction, as there is no logical reason why protolytic cracking rates would not also be thus affected, but rather the continuation of the chain by hydride transfer, leading to a dramatically increased amount of reaction products from a similar number of initiation events. Therefore, β-scission does not require two sites, whereas chain transfer probably does. However, the dramatic rise in activity upon extraction of the highly dealuminated samples is not sufficient to give an activity similar to an unextracted sample of the same acidity, figure 4.15. This implies that acidity *alone* does not define the activity of the catalyst and that other factors have contributory roles. As outlined here, acidity

merely initiates the reaction and the other factors may have a controlling influence on the other parts, eg hydride transfer, of the reaction. This is also evident in the very steep rise in activity of the unextracted and extracted samples which have similar values of the CMR: their gradients far exceed one, which one would expect if an increase in initiation events, as caused by an increase in Brønsted sites was the sole contributory factor to the increase in activity. The shift of the peak maximum to higher acidity on extraction adds further credence to this idea. Rather, it seems that chain lengths are still increasing rapidly, under the influence of something other than acidity. It is worth noting that the value of the CMR which corresponds to equality between the two initiation reactions must be immense as the highly dealuminated unextracted samples show a doubling in activity for no more than a 30% increase in acidity, indicating that these 'other' effects are still quite strong. This also explains the non negligible amount of iC_4 formed by these catalysts. Although the amount of coke retained increases on extraction, which could reflect partly the increased strength of adsorption of product molecules[290] and partly the adsorption on sites which previously contained extraframework aluminium, no discernible increase in rate of deactivation was found.

To summarise, the direct protonation of an alkane molecule, followed by protolysis of a carbon-carbon bond to form a carbenium ion is the preferred method of initiation in all samples studied herein. However, in most samples, ie. those with very little extraframework aluminium, and the unextracted samples with less than $40Al_{NF}$ puc the reaction can proceed by bimolecular reactions involving hydrogen transfer and subsequent ß-scission. In a few samples, those unextracted with more than 40 Al_{NF} puc, bimolecular reactions are unfavourable and so chain lengths rapidly decrease and initiation products form a greater percentage of the total products. This would explain the high activation energy found for similar samples.[213] Extraction of nonframework aluminium from the highly dealuminated catalysts permits increased hydride transfer allowing the chain length to assume the levels found in the other extracted samples, which dramatically increases their activity over the highly dealuminated unextracted samples. In all cases some deactivation is noticed

after fifteen pulses, corresponding to ninety seconds on stream, but the amount of coke retained after sixteen hours on continuous stream suggests that pore filling cannot be responsible for the observed deactivation, and that one to one active site suppression can only account for the loss in activity if only a very few of the Brønsted sites are catalytically active, or electrons within the deposited coke perturb the electronic structure within the framework to render all sites less active. Deactivation is thought to be due to selective site removal resulting in a disturbance of the reaction mechanism, in particular, increasing the hindrance of the hydride transfer step. Differences between the pulse flow and continuous flow methods have been suggested.

4.3 Toluene Disproportionation

4.31 Pulse Flow

The activity of the catalysts was assessed using the disproportionation of toluene as a test reaction. The samples were activated for sixteen hours in flowing helium at the reaction temperature of 673K before pulses of toluene were passed over the sample at regular intervals. Five minutes were allowed for the reaction products and unreacted toluene to desorb from the sample and condense in the liquid nitrogen trap. Benzene, meta- and para-dimethylbenzene and ortho-dimethylbenzene were the major products, together with a very small amount aliphatic carbon; no trimethylbenzene was detected, whilst methane was not detected because it will not condense into the liquid nitrogen trap. A diagram of the major reaction pathways is shown in figure 4.28.

The initial activity, shown in figure 4.29 plotted against the Brønsted acid content of the catalysts as determined by the temperature programmed desorption of ammonia, exhibits three interesting features. There is an increase in activity with decreasing acid site concentration down to 0.9 mmol g^{-1} whereupon there is a more marked and linear decrease in activity. Closer examination reveals that the mildly steamed samples display slightly different behaviour, with a lower activity to site ratio than would be expected on the basis of the strongly steamed samples for those catalysts with a site concentration of less than 0.9 $mmolg^{-1}$. Catalyst HYST 873, which accentuates the difference between the two activity profiles, could be considered to have given erroneous results, but repetition of the experiment and data from other reactant systems suggest that the results are valid. Extraction of non framework material removes the distinction between the two methods of preparation, by decreasing the activity of the most active samples and increasing the activity of those samples with medium activity. Samples with a low initial activity will be treated separately. In all cases there is a benzene excess, as reported by a number of groups in the study of this reaction over ZSM-5.[292,293,294,295] However, there seems to be no consistent pattern to this excess.

There is clearly a relationship between strong acid sites and toluene disproportionation activity as the activity profile, figure 4.29, closely follows

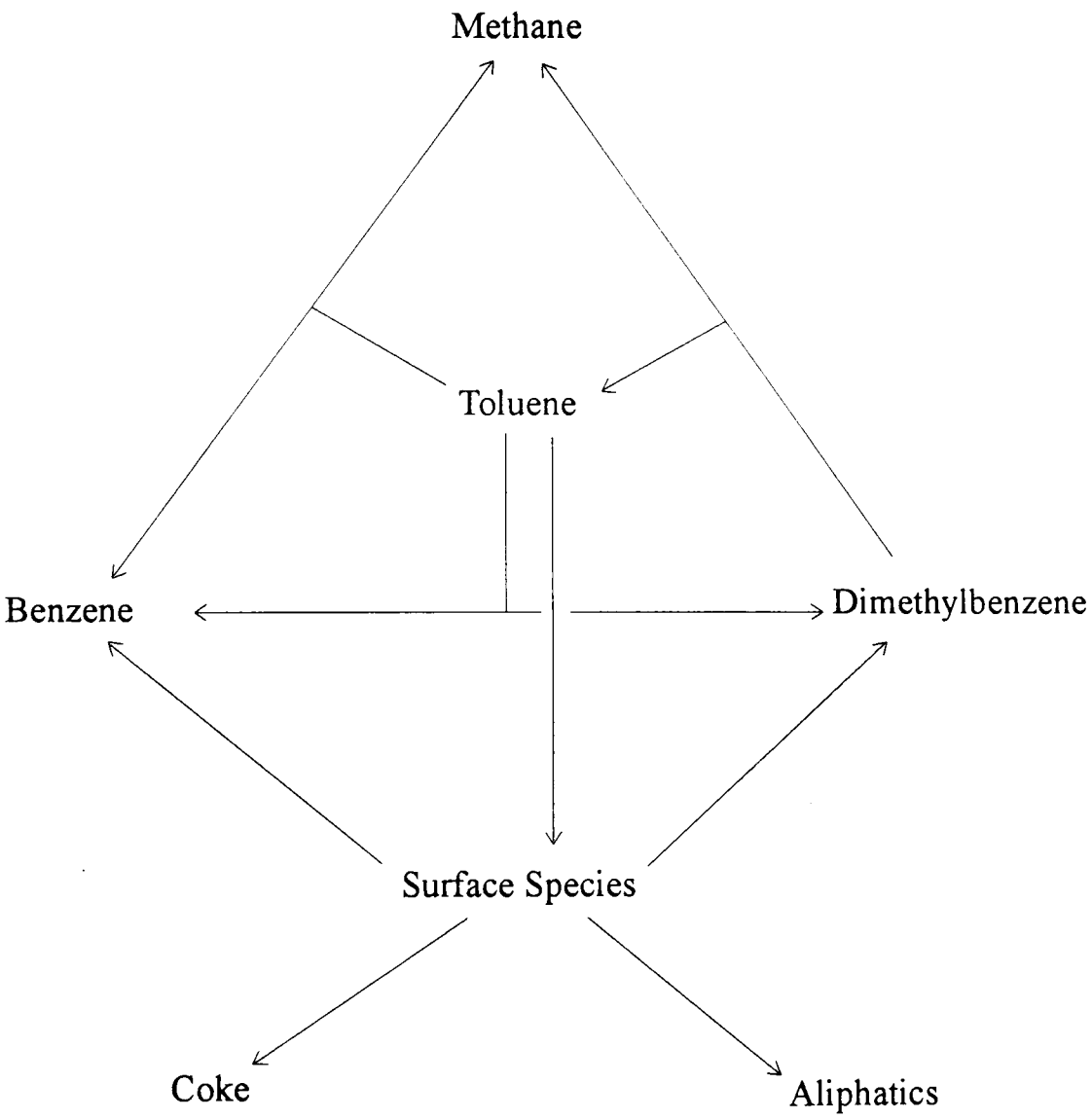

Figure 4.28: Toluene reaction scheme summary.

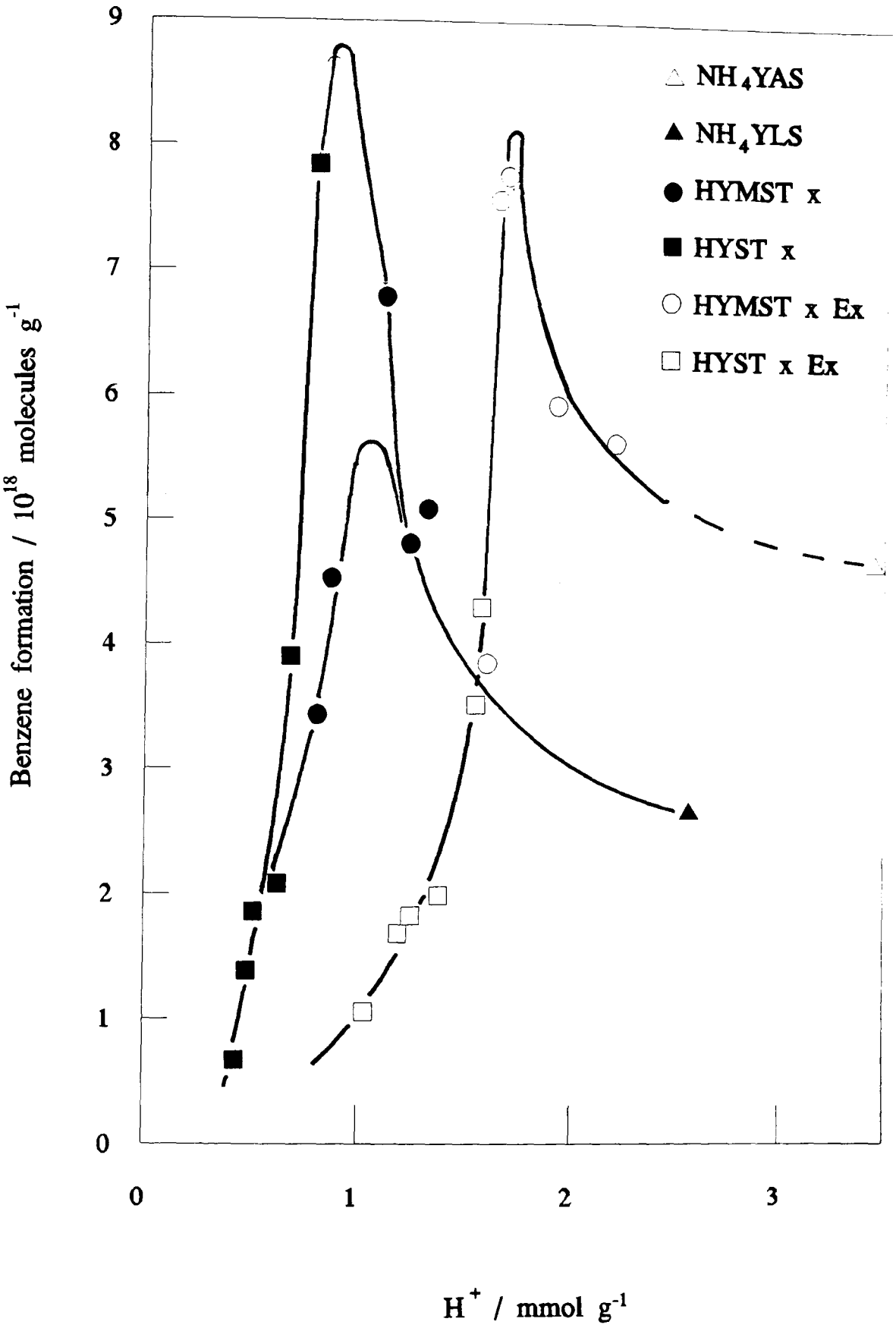

Figure 4.29: Toluene disproportionation.

the volcano curve shape of the theoretical predictions of strong site concentration;[77] this augments previous evidence[184,203,204,296] which, although implying the necessity of strong site acidity, stops some way short of definitive experimental proof.

The seat of the activity cannot be the Brønsted sites alone, as extraction has been show to have differing effects. Starting from HYST 1073, in which extraction almost doubles the activity, there is a progressive drop in activity enhancement on extraction, whereas catalysts HYST 973 to HYST 823 show a decrease in activity on extraction. The conflicting properties of nonframework aluminium can be shown to account for this contrasting behaviour. At high loadings the presence of non framework aluminium could be detrimental, as it might result in physical blocking of sites. Removal leads to an increase in activity roughly proportional to the increase in number of available sites. However, the decrease in activity on extraction of the most active unextracted catalysts could imply that the non framework aluminium might itself be catalytically active. Additional experiments by Rhodes,[201] in which he activated HYST 873Ex at 823K, resulted in an increase in activity which can be traced to the generation of more Lewis acid sites, and hence more Lewis/Brønsted site pairs.

Catalytically active non framework species were discounted by Rhodes,[201] who noted a decrease in activity on dehydroxylation of a sample, ie. on production of more Lewis sites at the expense of the pre-existing Brønsted sites. This decrease in activity was put down to a decrease in the number of Brønsted acid/Lewis acid pairs, which had previously been suggested[297] to be the site of maximum activity in the disproportionation of alkylaromatics. A similar decrease in Lewis site acidity can be affected by the extraction of extraframework material, as in the present work, and when the detrimental effect of this aspect of extraction outweighs the beneficial effect of 'unblocking' the catalyst, an overall decrease in activity can be expected. Furthermore, the overall effect should be proportional to the total amount of extrastructural aluminium present.

The mildly steamed samples exhibit different behaviour, with extraction

having less of a detrimental effect. Indeed, for catalysts HYMST 798Ex and HYMST 848Ex a dramatic enhancement of activity over the unextracted analogues is recorded. Although this may, in part, be linked to the drop in number of strong Brønsted sites which are capable of forming beneficial synergic interactions with the non framework aluminium in the first place, it is proposed that it is the removal of cationic extrastructural aluminium which accounts for these observations. During hydrothermal treatment the non framework species produced migrate to the external surfaces or mesopores[175] of the crystallites, this process is enhanced by the severity and duration of steaming.[174,298,299] It was concluded that high temperature steaming resulted in the production of only neutral species. Therefore, short duration, low intensity steaming seems more likely to produce highly dispersed[151] cationic extraframework species.[172] Numerous studies[236,249,250,251] have shown that strongly acidic sites are preferentially poisoned and therefore this cationic nonframework aluminium can be expected to carry out such a function.

Catalysts which maximise both the above criteria, ie. have strongly acidic sites and relatively large amounts of cationic extrastructural aluminium, namely HYMST 798 and HYMST 848, experience the largest positive change in activity. This implies that the liberation of the strong sites has a greater effect on the activity than the removal of some of the synergic effect, and thus the reaction proceeds to a greater extent via the strong sites.

As it has been established that the catalytic activity of the samples is due to their Brønsted acidity, albeit altered in nature by extraframework material, it is apposite to discuss mechanisms by which the reaction may proceed. Two mechanisms have been recently postulated[60] and they will be examined in turn.

The first mechanism[292] begins with protonation of the *ipso*-carbon on the toluene by a zeolitic proton, weakening the methyl bond, figure 4.30. Interaction between the protonated molecule and another molecule of toluene forms a charged transition state which releases a benzene molecule and a dimethylbenzene cation by cleavage of the original methyl bond; this can either return a proton to the zeolite surface, or protonate another toluene

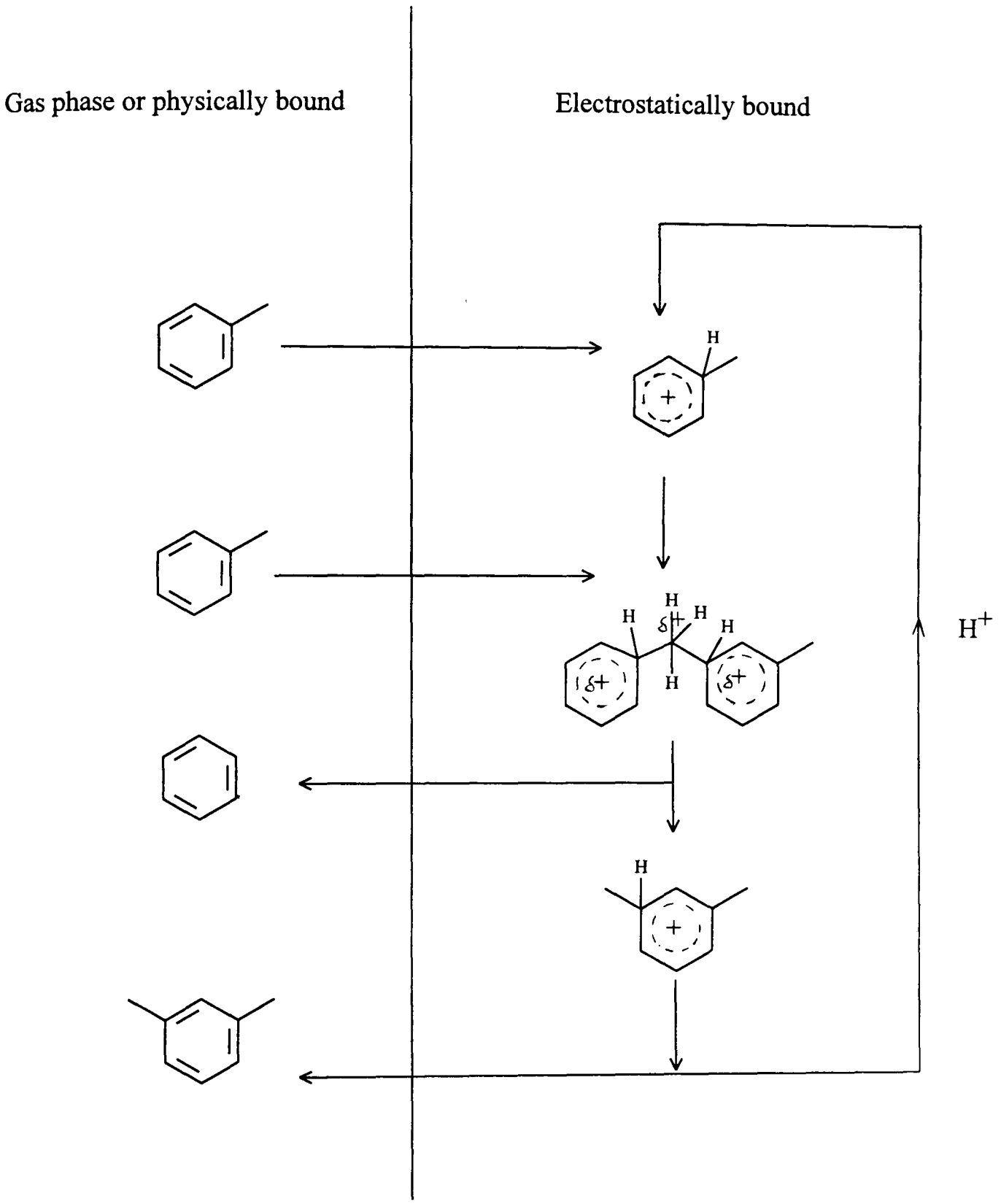

Figure 4.30: Toluene disproportionation - direct mechanism

molecule. Although this mechanism accounts for the major products observed, and the need for the strong Brønsted acidity in the protonation of the aromatic ring, it fails to account for the dimethylbenzene deficiency and the limited formation of carbonaceous residue on the catalyst surface, unless the assumption that both the products desorb off of the surface is questioned: it is a clean disproportionation mechanism.

The second mechanism, figure 4.31, is initiated by hydride abstraction from the methyl group, followed once again by the addition of another toluene molecule. The diphenylmethane cation thus produced, which has been observed using UV spectroscopy by Chen *et al*,[300] can either loose a proton to form a diphenylmethane molecule, or immediately dissociate into benzene and dimethylbenzene. The diphenylmethane can then be reprotonated and crack, or progress towards a polyaromatic compound. The isomers of dimethylbenzene can easily be produced by varying the position of addition of the second toluene molecule. The absence of any evidence of trimethylbenzene, which would be formed by the addition of a dimethylbenzene molecule in the second step of either reaction, can be explained by the relatively low concentration of the disubstituted aromatic in the product stream.

Although disproportionation is the main reaction, it is worth considering the implications of the dealkylation reaction. Dealkylation, producing benzene and methane from toluene and toluene and methane from dimethylbenzene, which has been claimed to occur on the strong sites of ZSM-5[294] could easily account for the excess of benzene in the product stream. However, these reactions are net consumers of hydrogen, and so if occurring must use the dehydrogenation of coke precursors as a source of hydrogen. Using HZSM-5, Bhaskar and Do[293] showed dealkylation to be inhibited by the use of nitrogen as a carrier gas with respect to hydrogen as expected, but also that large crystal size favours dealkylation, thought to be due to the longer diffusion path available promoting dealkylation of the dimethylbenzenes.

Conclusive proof of the existence or otherwise of the dealkylation reaction cannot be provided, as any methane produced would not condense into the cold trap and so cannot be detected. Although the coke loading of the spent

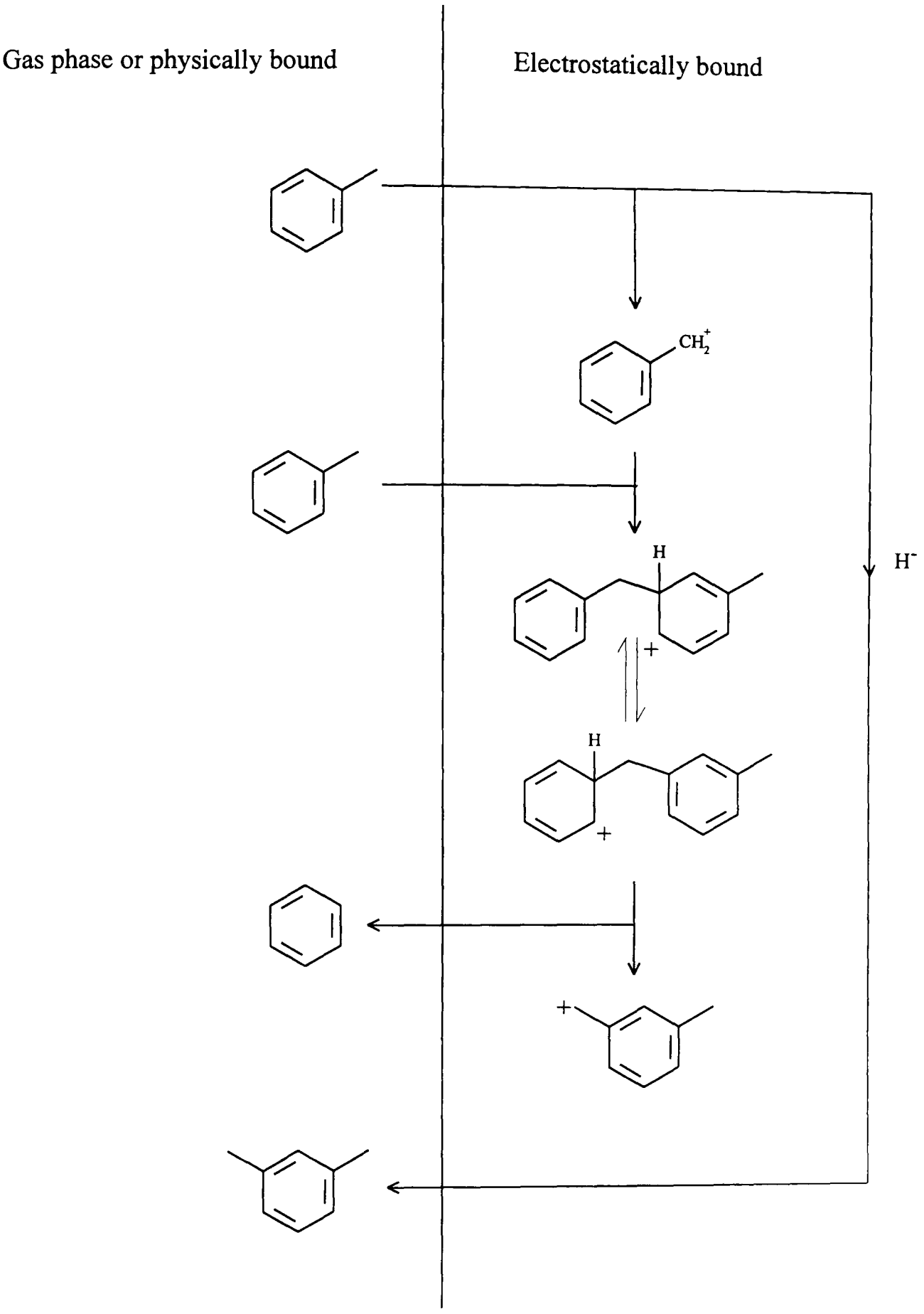

Figure 4.31: Toluene disproportionation - hydride abstraction mechanism

samples are low, typically corresponding to less than one percent of the toluene in each pulse, it is enough material to provide the necessary hydrogen to balance the requirement of the dealkylation reaction. Therefore, it is proposed that the dimethylbenzene deficiency is caused in part by the retention of the substituted aromatic product, and in part by dealkylation, although it is impossible to establish whether the toluene or the dimethyl benzene is undergoing dealkylation.

4.32 Continuous Flow

The inconsistent nature of the results from the continuous flow experiments, especially when compared with similar experiments conducted earlier,[201] prompted an investigation of possible catalyst or reactant contamination. These results, together with a brief description can be found in Section 3.23. Slowing the dehydrogenation of the coke by using hydrogen as the carrier gas was found to be effective in increasing the lifetime of the catalysts. This, when combined with the observation of a *rise* in activity on successive pulses of toluene over NH_4YAS, led to the realisation that the amount of coke present on the catalyst could have a crucial role in determining the disproportionation activity.

The results from the precoking set of experiments suggest that pre-treating the catalyst sample with toluene has an effect on the total reaction and activity profile of the sample. This is probably due to either the presence of adsorbed reactant and/or coke as the profile is critically dependant on the amount of coke which is allowed to form prior to the catalyst being exposed to a continuous flow of the helium stream saturated with toluene at 273K. The exact nature of this coke, and of its interaction with the reactant molecules is therefore of prime importance.

If the activity profile for a clean surface is taken as a reference point, then the effect of gradually precoking the surface can be seen in figure 4.32. As the Coke on Surface (*COS*) value increases the total reaction can be seen to increase at first before decreasing. It has to be emphasised that this is not a reaction or activity profile, merely a graphical representation that has no

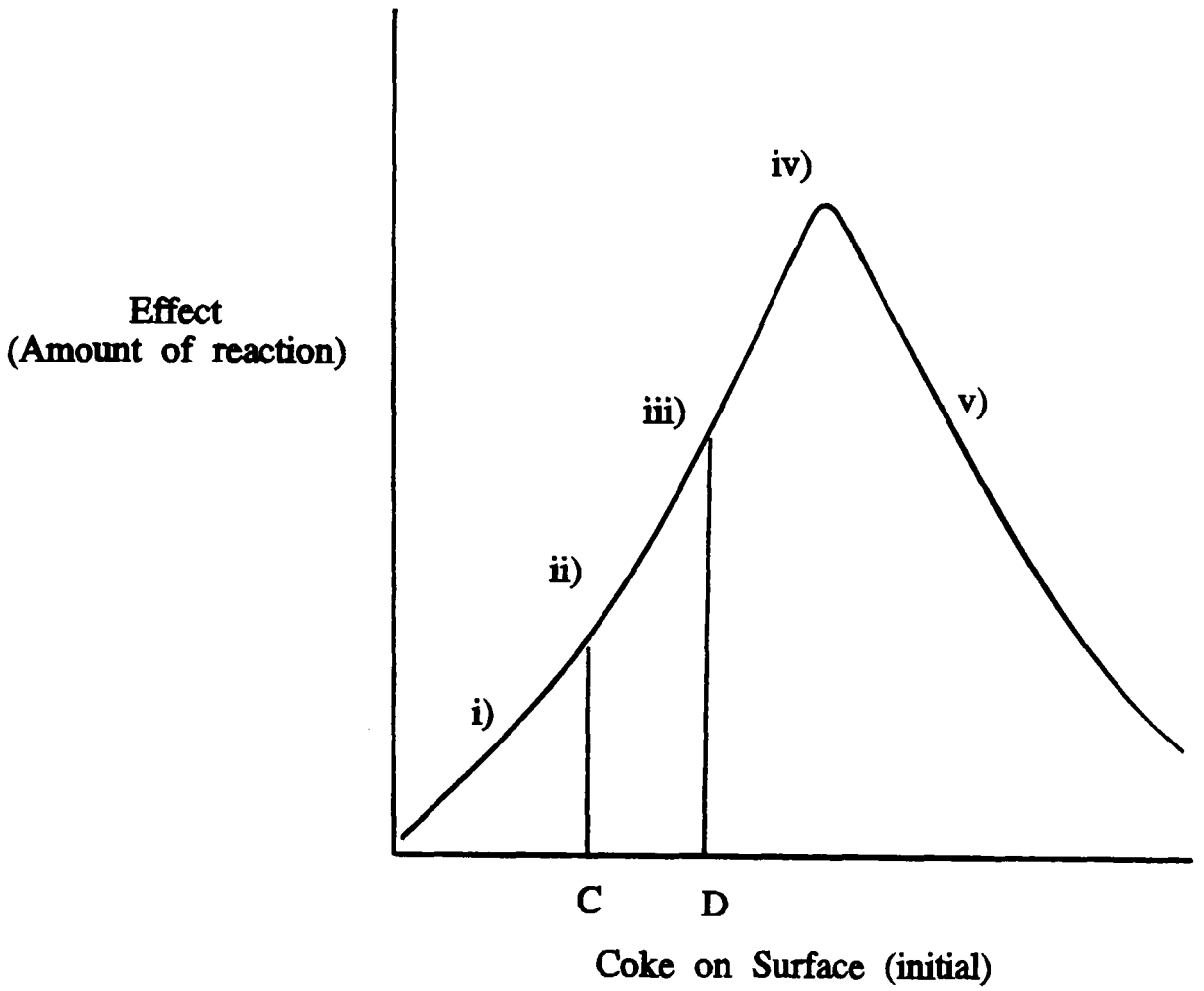

Figure 4.32: Effect of initial coke loading.

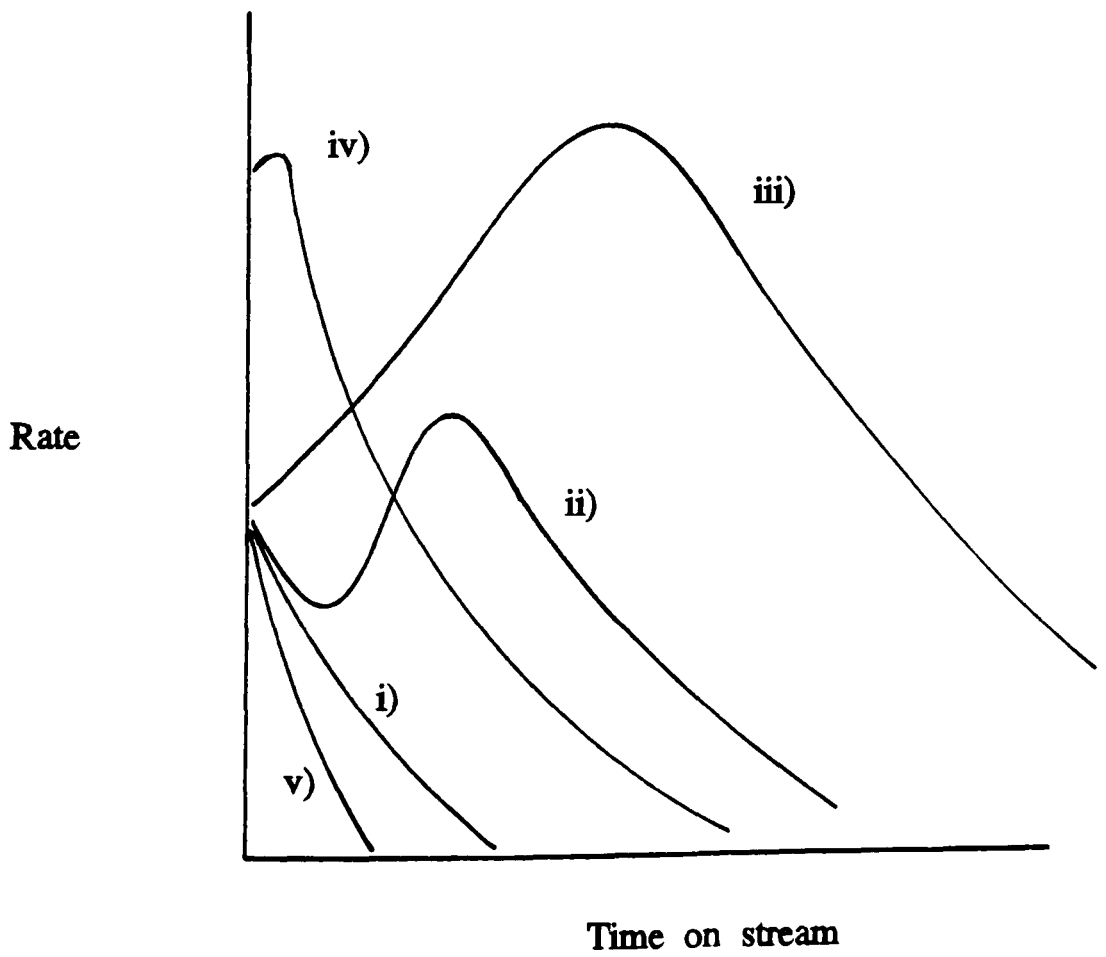

Figure 4.33: Effect of initial coke loading on reaction profile.

physical or experimental justification. For low *COS* values there is only a slight increase in the amount of reaction until point C is reached. At *COS* values C and greater a peak in activity occurs, but more coke may be required and so there is an induction period which may encompass a slight fall in activity. Point D can be termed the spontaneous point where immediate increased activity is observed. The peak of the diagram correlates with the conditions which are required to bring about very high activity and almost spontaneous deactivation, and any higher *COS* values result in a lower initial activity and immediate deactivation. These points are illustrated in figure 4.33.

Although the coke content of the totally deactivated catalyst is the same, ie *ca.* 15 wt%, the values for C and D need not necessarily be the same from catalyst to catalyst, as the former are under physical constraints whereas the latter are under chemical concentration constraints. If the initial acid sites are strong then more coke might be required to dissipate their strength than if they were weaker, prompting a change in the expected activity profiles with, at a constant initial coke loading, a progression from shape iv) to shape i) with increasing acidity.

Mechanisms relating to the formation of the products via disproportionation have already been discussed in the preceding section, but it is now necessary to account for the observed deficiency in benzene. For each catalyst sample the amount of benzene detected in the product stream was exceeded by that of the total of the dimethylbenzene isomers. This is in contradiction to the one to one ratio demanded by clean disproportionation, and the initial activity results obtained from the pulse flow method, presented earlier. Therefore either coke is being formed preferentially by the benzene over the substituted aromatics, which would seem contrary to logic as the molecules with side chains should have the greater steric hindrance, lower diffusivity and so be more susceptible to irreversible adsorption than the benzene, or that the benzene is being used up in a further reaction.

Closer examination of HYST 873Ex pellets/bulb experiment, figure 4.34, chosen because it has a well defined peak, shows that the benzene deficit increases until the peak in activity, in a similar manner to the increase

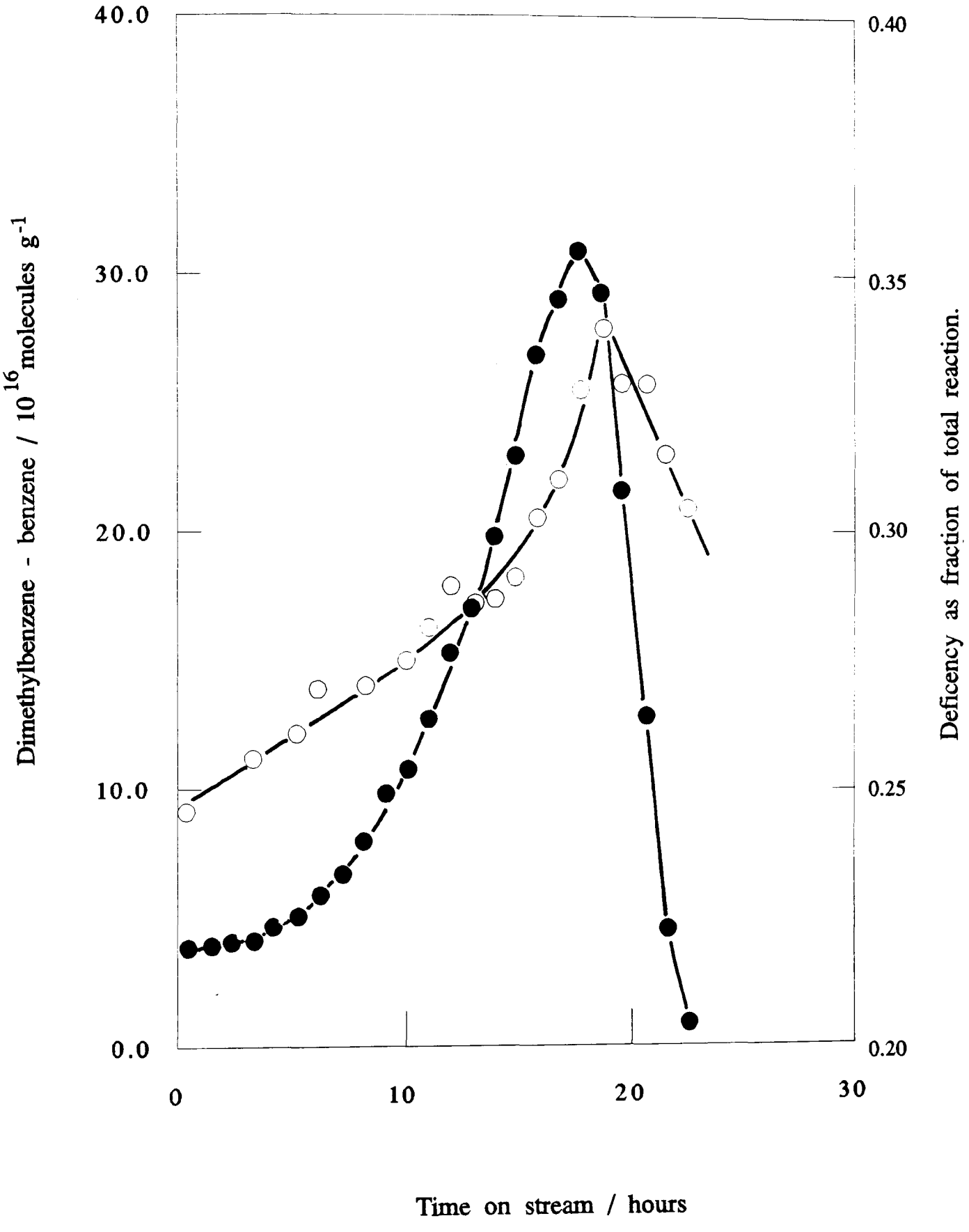

Figure 4.34: Benzene Deficency - catalyst HYST 1073Ex (pellets, tube format)

of the coke on the surface.[60] The benzene deficiency must therefore be caused by a reaction on the surface which is dependant on the amount of coke deposited. This clearly shows the interventionalist behaviour of the coke during the reaction, and that the perceived product imbalance is an experimental observation and not an artifact of the calibration.

The second mechanism (figure 4.31) does not allow the aromatic ring that will eventually form the free benzene to be protonated, and thus be directly attached to the zeolite framework, whilst the first mechanism (figure 4.30) requires the positive charge to be spread across the two phenyl rings via the methyl bridge. It is reasonable to suggest that these reaction mechanisms are operating in tandem and a balance is established between:

i) reaction on a clean surface,

ii) reactions of components on the surface,

iii) reactions between products of ii) and feedstock toluene.

Reaction i) has to proceed to allow a high enough surface concentration of adsorbed species to allow reaction ii) to be significant, as has been highlighted earlier. However, the vital factor is the rate of deposition of the carbonaceous material, because if the toluene is being supplied faster than the surface species can rearrange and desorb, one can conceive of a build up of excess carbonaceous material which will render the catalyst inactive. Aromatic surface species may ring-open and crack, as has been claimed by Chambellan *et al*[301] in a study of self alkylation of benzene over steamed HY zeolites, and by Anderson *et al*[302], who studied the residual coke after benzene had been passed over HZSM-5. If ring-opening occurs before the surface is inundated with more material, ie. reaction i), driven by the supply of toluene, is slower than or nearly equal to reaction ii) then the majority of the coke can be converted into desorbable products, thus prolonging the lifetime of the sample and resulting in an increasing deficit of benzene. Additionally, the cracked surface species may be able to alkylate the feedstock, causing an excess of disubstituted products. This would permit the presence of other substituted aromatic compounds in the product stream, for instance ethylbenzene, and although no traces of these compounds were found in the

present study, they might have been present but obscured by the major product peaks.

Finally, if this coke is catalytically active, that is it enhances the toluene disproportionation, then once formed a rise in the production of both major products would be expected. Hydride abstraction from a polyaromatic coke molecule by the dimethyl cation formed in the second mechanism, followed by abstraction from a toluene molecule, would produce a phenyl cation without recourse to the framework. In this way hydrogen is transferred from reactant to product without either coming into contact with the zeolite framework. This would avoid strong interactions which might lead to irreversible adsorption and deactivation.

Once formed, the coke may take part in a radical mechanism. Chen *et al*[300] have detected the presence of benzyl radicals on HY, although to a very low extent. Although the production of benzyl radicals would be linked to the amount of charge contained on the surface, the coke, with its high aromatic component, may be more amenable to hydrogen atom and electron transfer than the inorganic framework. This might lead to a more facile route to the production of the phenyl cation than that proposed in the second mechanism. If radical production occurs rapidly on sodium ions, an explanation of the totally anomalous behaviour of NH_4YAS can be found. It has a higher activity than would be expected on the basis of its acidity concentration, especially when it is remembered that any strong acid sites present will be poisoned by sodium. This was the only sample to show an undisputed rise in activity during the pulse experiments, a fact confirmed by the multiple pulse experiment. If radical production can commence straight away, without the necessity of deposition of carbonaceous material, the conditions for immediate enhancement exist.

The rate of accumulation of the coke can be influenced by lowering the vapour pressure of the toluene, or the coke can be given time to modify by cutting off the toluene supply altogether or by exposing the surface to small amounts of reactant at regular time intervals. When these experiments were performed deviations from the normal experimental results were seen.

However, it proved very difficult to quantify or to ensure the same amount of coke on the surface, and, as noted earlier, it was unknown what amount of coke was required to 'start' the reaction. It would appear that reaction i) is very much faster than reaction ii) as all attempts to slow it sufficiently, other than in the pulse flow system, have failed to produce dramatically enhanced activity.

The disproportionation of toluene has been shown to be a complex reaction, being dependent on the nature, as well as the number, of acid sites and extraframework aluminium species present. In the very initial stages of the reaction a simple disproportionation reaction is proposed, with the excess of benzene observed due to retention of dimethylbenzene and a small amount of dealkylation. The amount and nature of the extrastructural aluminium has been shown to have a profound effect on the activity of the catalyst. Continuing reaction results in a buildup of carbonaceous material, the role of which is vital as it had previously been linked to an increase in activity.[60] Conclusive proof has been presented that the amount of coke present on the surface influences the activity, and an explanation has been proposed. Upon enhancement of activity a change in the product profile was noted, with a dimethylbenzene excess becoming more predominant, which was linked to a surface reaction resulting in the consumption of benzene and/or the production of dimethylbenzene and increased activity of the catalyst.

4.5 Cumene Dealkylation

Cumene dealkylation has fallen out of favour as a model test reaction for cracking activity mainly because the 'superacids' available today catalyse a wider range of interesting reactions. Nevertheless, cumene remains a useful probe for the study of weaker acidity.

The complete range of zeolite samples was used in studies of cumene cracking using the pulse flow technique. The samples were activated at 673K for 16 hours in flowing helium, and then allowed to cool to the reaction temperature of 448K. Pulses of cumene were passed over the sample at ten minute intervals allowing five minutes for trapping of reaction products and unreacted cumene in the cold trap.

A general reaction scheme is shown in figure 4.35 where the products detected in this study are marked with an asterisk(*). The main reaction is assumed to be dealkylation of cumene to form benzene and propene with the other primary reactions, isomerisation to n-propylbenzene and disproportionation forming benzene and di-isopropylbenzene, and ethylbenzene and either isopropyltoluene or butene isomers, constituting the inner circle. Toluene, coke, and butanes arise from secondary reactions, together with those primary products which can also be formed via a secondary route, are found in the outer circle. Once formed, the other substituted aromatic compounds can in principle undergo further disproportionation and isomerisation reactions, to form numerous minor products. Since these were not detected the mechanism leading to their formation will not be discussed.

The major products detected were unresolved aliphatic compounds and benzene; the aliphatic compound peak was not resolved on the chromatographic column used, but detailed analysis of one sample showed it to consist of entirely C_3 hydrocarbons and C_4 hydrocarbons: there was no evidence for the formation of any other straight chain aliphatic compounds. Minor products formed, in order of decreasing amount, were ethylbenzene, toluene and a multi-branched alkane, probably dimethylbutane. Some evidence for limited reactant isomerisation to n-propylbenzene was found, but this was not treated as a product. Neither isopropyltoluene nor di-isopropylbenzene were

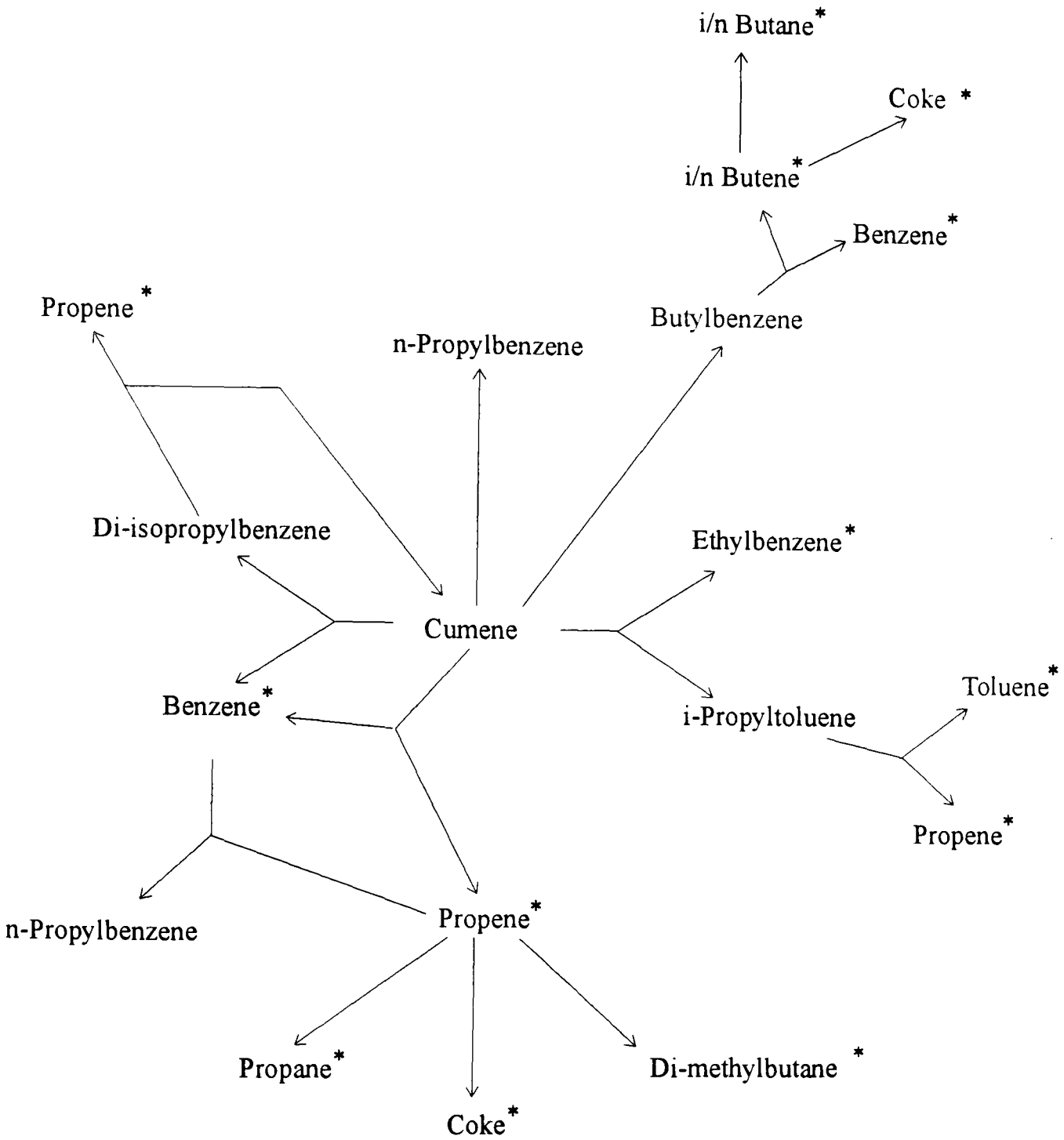

Figure 4.35: Cumene reaction scheme summary.

observed, probably due to the combined effect of very low concentrations and no resolution from the reactant peak, and coupled with the instability for the latter.[303]

The results of the catalyst tests are summarised in figures 4.36 and 4.37 with either aliphatic carbon or benzene production defining activity. Figure 4.38 shows that there is a linear relationship between the detected amounts of aliphatic and aromatic molecules, with possibly a slight bias towards aromatic at very high activities. However, although both representations are included here for the sake of completeness, that derived from benzene is preferred, as it follows a single product. Furthermore, this product is not thought to be involved in the coking process, and therefore it can be used with greater confidence as an indicator of activity.

The acidity contents of the catalysts used to produce figures 4.36 and 4.37 are those derived from the partially dehydrated temperature programmed desorption studies. It has been shown that extended evacuation of the catalyst in flowing helium at atmospheric pressure decreases the catalysts' capacity for ammonia as measured by temperature programmed desorption. The cumene experiments were run under conditions more similar to the partially dehydrated temperature programmed desorption experiments in that the samples were cooled from 673K to 448K in flowing helium. This has been shown to cause a change in the degree of hydration of the catalyst due to the extraction of water vapour from the helium. It is reasonable to suppose that as the hydrated surface can adsorb, and therefore protonate more ammonia, it can also protonate more cumene, and thus give a slightly higher activity for cumene cracking than if the helium had been vigorously dried.

It can be seen from figure 4.37 that NH_4YAS has very little activity, and that NH_4YLS has an activity an order of magnitude higher. There is a subsequent smaller rise of approximately 50% to the most active dealuminated samples and then a gradual decrease in activity on dealumination, which, on extrapolation, implies a direct acid site to activity correlation. This agrees favourably with the findings of DeCanio *et al.*[208]

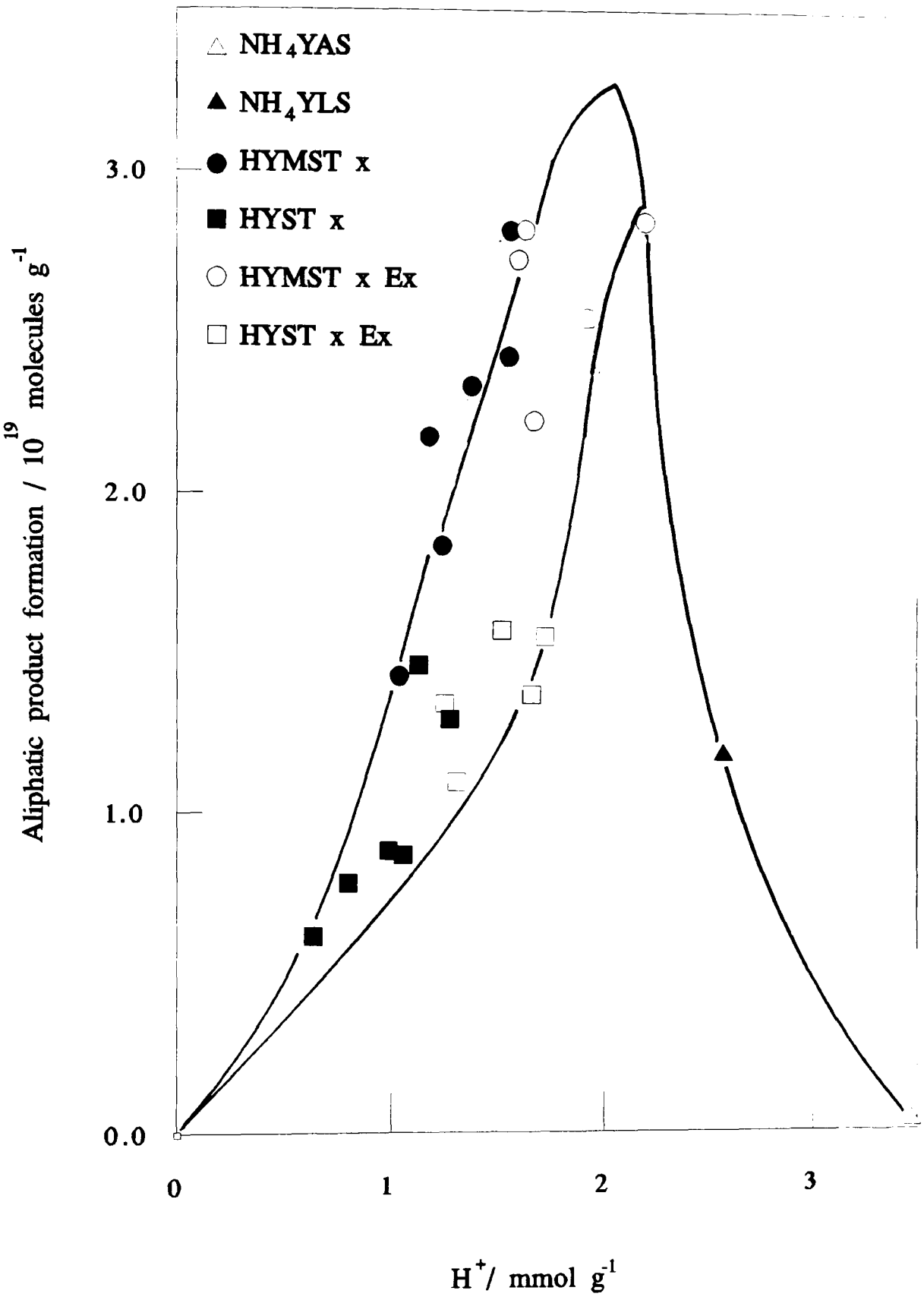

Figure 4.36: Cumene dealkylation - aliphatic products.

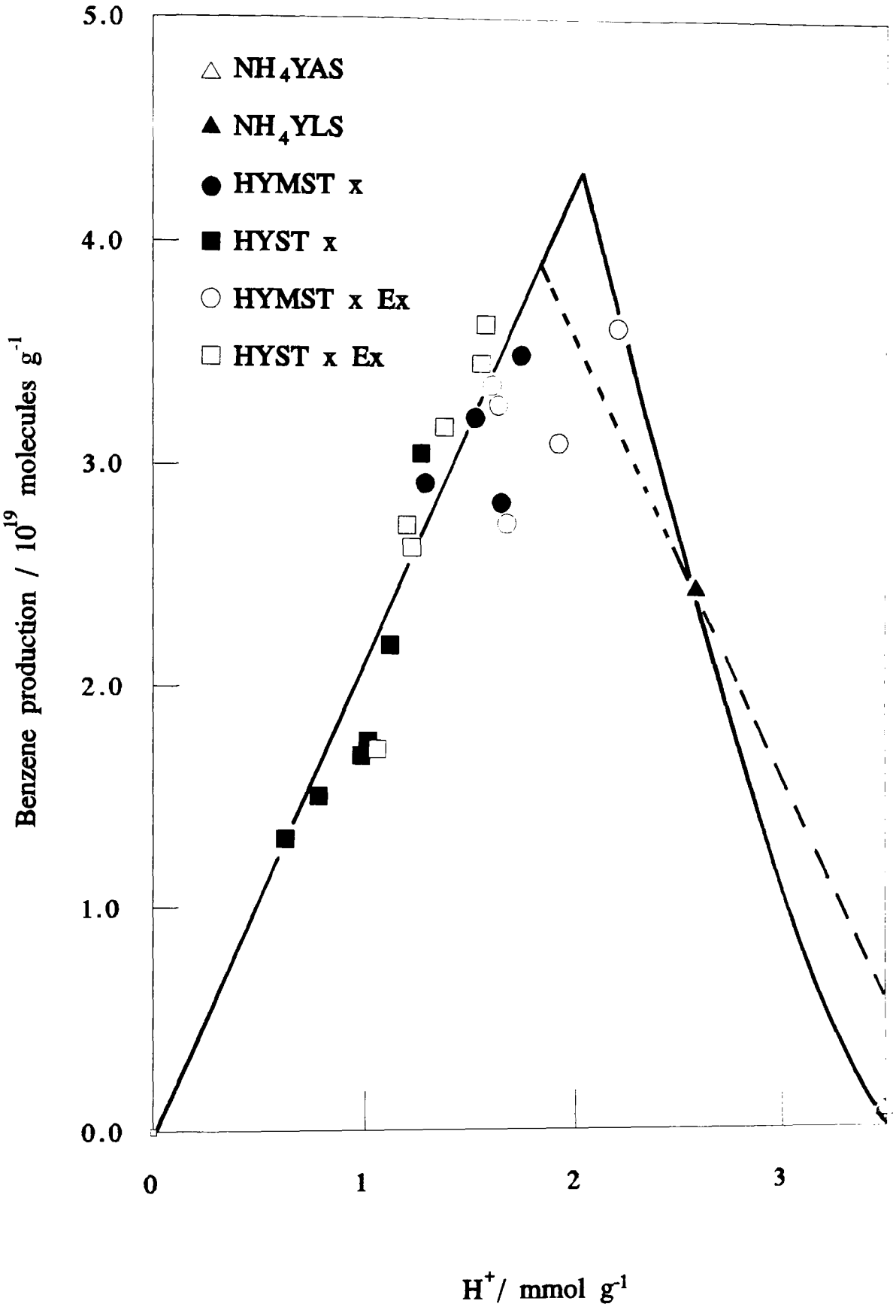

Figure 4.37: Cumene dealkylation - benzene production.

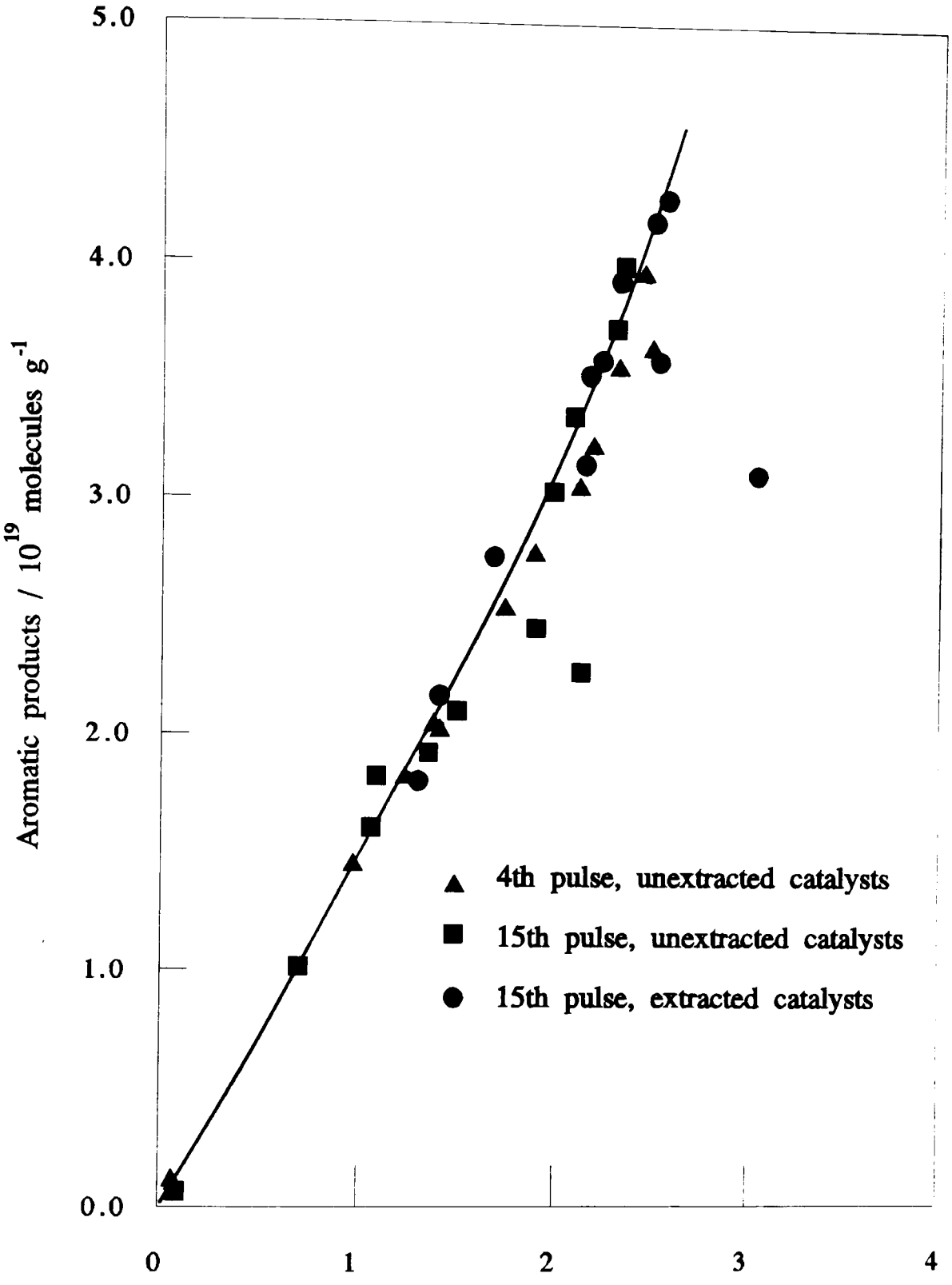

Figure 4.38: Aliphatic deficency in cumene dealklyation products.

NH_4YLS differs from NH_4YAS in three respects:

i) it has virtually no sodium ions present, ie. it is almost 100% exchanged,

ii) it has less structural aluminium as a consequence of the repeated thermal exchange procedure, and therefore,

iii) it also has extrastructural aluminium present.

Although each of these factors can enhance the activity of a selected catalyst the extent of their efficacy will vary. Of these factors, the removal of sodium ions, allowing access to the strongest sites, is probably the most important. Studies on the degree of cation exchange[202,304,305] have shown a disproportionate rise in activity for cumene cracking at high levels of exchange. Corma and Wojciechowski[202] observed a rapid increase in cumene dealkylation activity when the proton exchange level exceeded 85%. This they linked to admission of protons into the hexagonal prisms. Similarly, Nock and Rudham[306] found a non-linear increase in cumene cracking activity at high levels of exchange, and, noting a corresponding drop in activation energy, attributed this to an increase in acid strength of the zeolite. This appears to be in contradiction to Bielanski and Malecka[307] who reported a curved increase in activity with decreasing activation energy, and no sudden increase at exchange levels greater than 70%. However, the extent of reaction in the latter study was very high (ca.90%) and so meaningful conclusions cannot be drawn.

The maximum activity of NH_4YAS on removal of sodium, but without structural dealumination, can be estimated by the utilisation of the gradient from the origin to 2.0 mmol H^+/g in figure 4.37. This gives a value of approximately 0.7 $x10^{19}$ molecules g^{-1}; the difference between this and the experimentally obtained activity is therefore due to sodium poisoning. Reasonable agreement is thus obtained with studies where HY was poisoned with pyridine[308] to remove strong sites, which concluded that at 600K 23% of the reaction occurred on weak sites.

Removal of some of the framework aluminum produces more framework sites with no second neighbour aluminium, commonly regarded as strong sites. This will also enhance the activity, but the inclusion of

nonframework species, unless active in a promoting role on the framework Brønsted sites, should result in a retardation of activity. The combination of these effects therefore is responsible for the additional increased activity of NH_4YLS over NH_4YAS.

The unextracted samples, both mildly and strongly dealuminated, describe an almost linear decrease in activity, passing through the origin. This strongly implies that once a certain threshold strength of acidity has been achieved the activity of the sample is directly related to its structural aluminium content, a fact which is confirmed by poisoning studies.[309] On extraction the activity of every sample increases without exception. This is consistent with accepted ideas that extraction removes charged extrastructural framework aluminium which is poisoning the sites by location on cation positions, and neutral species which are sterically hindering the diffusion of reactant and product molecules through the crystallite or screening the sites. However, this is contrary to the findings of Jacobs *et al* [296] who stated that "the extrastructural aluminium has a favourable effect on the cracking activity".

Extraction of the non framework material, although increasing the activity of the catalysts, does not result in a disproportionate rise in activity, as was the case when n-hexane was the reactant; nor did it cause a drop in activity on the basis of the adsorbed ammonia measurements as was found for some catalysts in the study on toluene disproportionation. This implies that the reaction proceeds on a single site, ie. it is essentially unimolecular, there is no beneficial bimolecular path available, and that the removable extraframework aluminium has no beneficial effect on the reaction other than the numerical effect of freeing more sites. Furthermore, this suggests that dealkylation constitutes the majority of the reaction as disproportionation reactions would be favoured by the presence of more adjacent sites.

Neither the unextracted nor the extracted samples alone exhibited a maximum in activity; it is only when NH_4YLS and NH_4YAS are taken into consideration does a maximum appear at a value corresponding to 38-40Al_F puc. This is in good agreement with Shauki *et al*[310] who observed a maximum in activity with a sample of HY zeolite containing 42 Al_F puc. Other

workers have reported peaks at framework aluminium contents of 21.5 Al_F puc,[311] 23 Al_F puc[254] and the work of DeCanio *et al*[208] could be reinterpreted to include a peak at 40 Al_F puc but insufficient samples were provided in the 15-40 range. However, in the work of Shauki *et al*[310] the samples had a relatively low extent of exchange (71%), and the extent of ion exchange after EDTA treatment was not mentioned. It is possible that the slow increase in activity that they reported between 65 and 42 Al_F puc can be attributed to the gradual loss of sodium ions. The very sharp drop in activity in samples of aluminium content less than 42 per unit cell would seemingly be due to loss of crystallinity of the samples on acid treatment. X-ray crystallography has proved that the crystal integrity of the samples is retained across the range studied and has also noted the breakdown of crystal structure due to H_4EDTA treatment of the mildly steamed, ie. less acid stable samples.

An important conclusion can be drawn from the general trend in activities already outlined. As the peak in activity is at higher framework aluminium concentrations than the maximum number of strong sites (compare with Sections 4.2 n-Hexane Cracking and 4.3 Toluene Disproportionation) either the same strength of acidity is shared by all sites, the reaction requires so weak an acidity that all sites before dealumination are sufficiently strong, or there is a heterogeneity of sites, with a third intermediate strength between strong and weak acidity. If the reaction proceeds on all sites it is only poisoning of NH_4YAS (by sodium) and NH_4YLS, combined with the lack of synergic interaction with nonframework aluminium promoting the acidity of the framework Brønsted sites which causes their low activity.

There is enough nonframework aluminium in NH_4YLS to interact with forty percent of the framework aluminum on a one to one basis: if the activity is due to such pairs then a maximum activity of 250% of the observed value can be obtained for NH_4YLS under 'optimum' conditions. This promotes the favoured benzene activity into line with the activities of the other catalysts. The other samples which have more than half of the aluminium in framework positions would also require a similar, but less drastic correction.

Unfortunately there is an experimental contradiction to this simplistic

argument. Extraction of most of the non framework aluminium increases the activity, rather than suppresses it as it would if the above were true. There is enough nonframework material present in NH_4YLS to populate the sodalite units to the extent proposed by Lónyi and Lunsford,[85] so either it is in the wrong place and/or state in this catalyst, or the activity deficit is due to a different factor.

If dealumination increases the acid strength of the catalyst in a linear fashion, rather than producing individual, isolated strong sites at the expense of more cluttered weak sites, the results observed are fully explained. NH_4YLS, although possessing some sites of higher acid strength than NH_4YAS, does not have enough sufficiently strong sites to catalyse the reaction to the full extent. The number of acid sites with one or fewer aluminium near neighbours is between thirty five and forty per unit cell,[77] and, if it is accepted that heterogeneity exists in the strength of the hydroxyl groups,[80,312] an explanation of the activity profile has been achieved. X-ray data has shown the framework concentration of HYMST 748 to be $36Al_F$ puc, confirming this catalyst to have the maximum number of such sites, and therefore it is expected that this catalyst, in the extracted form, would exhibit the highest activity for this reaction.

The reaction of cumene is clearly very complicated and in elucidating mechanisms certain assumptions have to be made. In using the smallest viable amount of catalyst secondary reactions were kept to a minimum. However, it is recognised that the reactor certainly cannot be described as differential, and the possibility of some secondary reactions needs to be appreciated, leading to the absence of unstable minor products. This allows the complex range of possible reactions and products to be reduced to a simple 'delta' scheme shown in figure 4.39. This is similar to that proposed for high temperatures.[313] One mechanism, or more correctly group of mechanisms, can be considered to apply to all the catalysts in this study and furthermore, the selectivity of the mechanisms operating does not change markedly with dealumination, extraction, or deactivation as measured within these experiments, as can be drawn from figure 4.38.

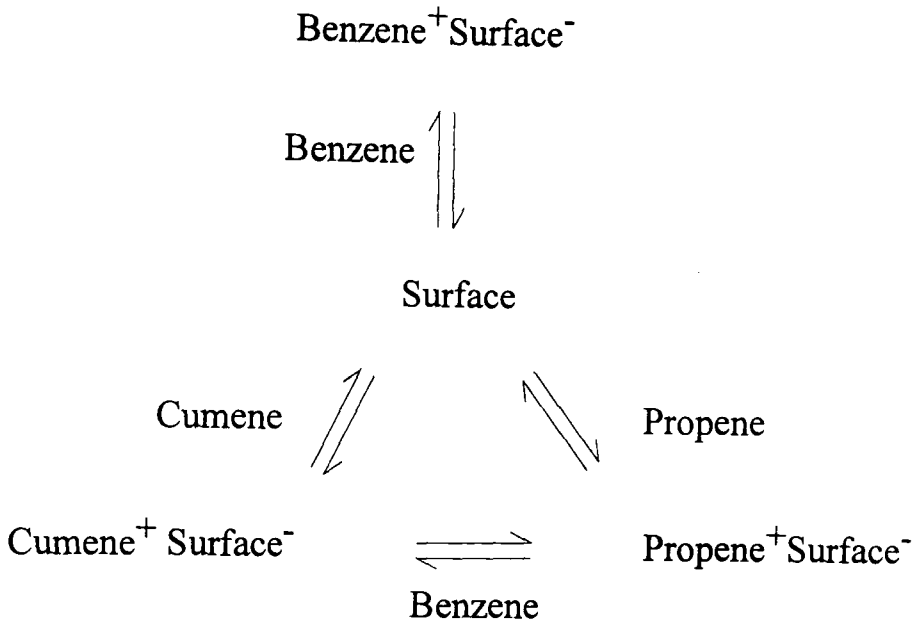

Figure 4.39: The delta mechanism.

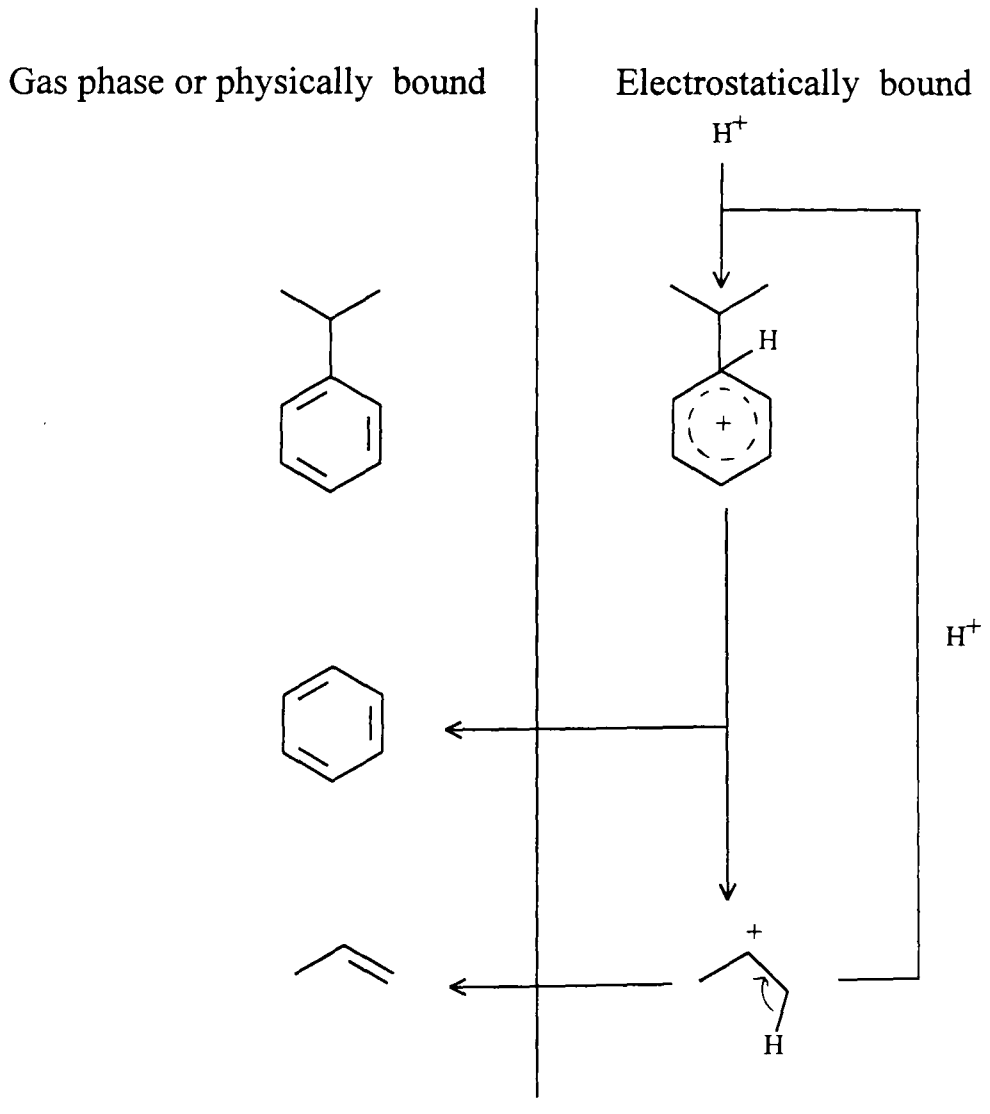

Figure 4.40: Simple dealkylation mechanism.

Mechanism one, shown in figure 4.40, deals with the simple cumene dealkylation process. The aromatic ring is protonated at the *ipso* position leading to an electrostatically bound carbenium ion. Cracking of the alkylaromatic bond then ensues, freeing a benzene molecule into the gas phase and leaving an adsorbed propenium ion. This can desorb from the surface of the catalyst as a propene molecule, freeing a proton which is available to continue the reaction, thus completing the simplest catalytic cycle. The decomposition of the carbenium ion is thought to be the rate determining step,[314] rather than the protonation of the aromatic ring. This explains the overall behaviour of the catalysts in the present study. Once the sites are sufficiently acidic they will protonate the cumene; increasing the strength of the acid sites still further has no additional effect as the rate of protonation is already at a maximum and the reaction is limited by the cracking of the alkylaromatic bond.

Instead of desorption, the propenium ion can abstract a hydride ion from another cumene molecule as in mechanism two, shown in figure 4.41, leaving a surface bound carbenium ion, and desorb as a propane molecule. ß-scission will release a propene molecule and a benzene cation which can abstract a hydride ion from another cumene molecule thus completing the second, more complicated catalytic cycle. This would probably have to be a concerted process as rapid equilibrium between the two types of possible cation will be established. Interaction between the alkylaromatic carbenium ions and another cumene molecule to form a charged intermediate is also feasible (figure 4.41). Methyl group transfer results in formation of an electrostatically bound ethylbenzene cation and an butylbenzene molecule, which is considered to be unstable.[313] Intramolecular hydrogen transfer yields a molecule of butene and of benzene. If the initial carbenium ion combines with benzene, toluene and ethylbenzene are produced.

The agent for hydride abstraction could in principle be either a Lewis acid site and/or a carbenium ion. However, the results obtained suggest that this role is not played by Lewis acid sites, associated with the nonframework aluminium, for three reasons. Extraction of the extrastructural aluminium, and

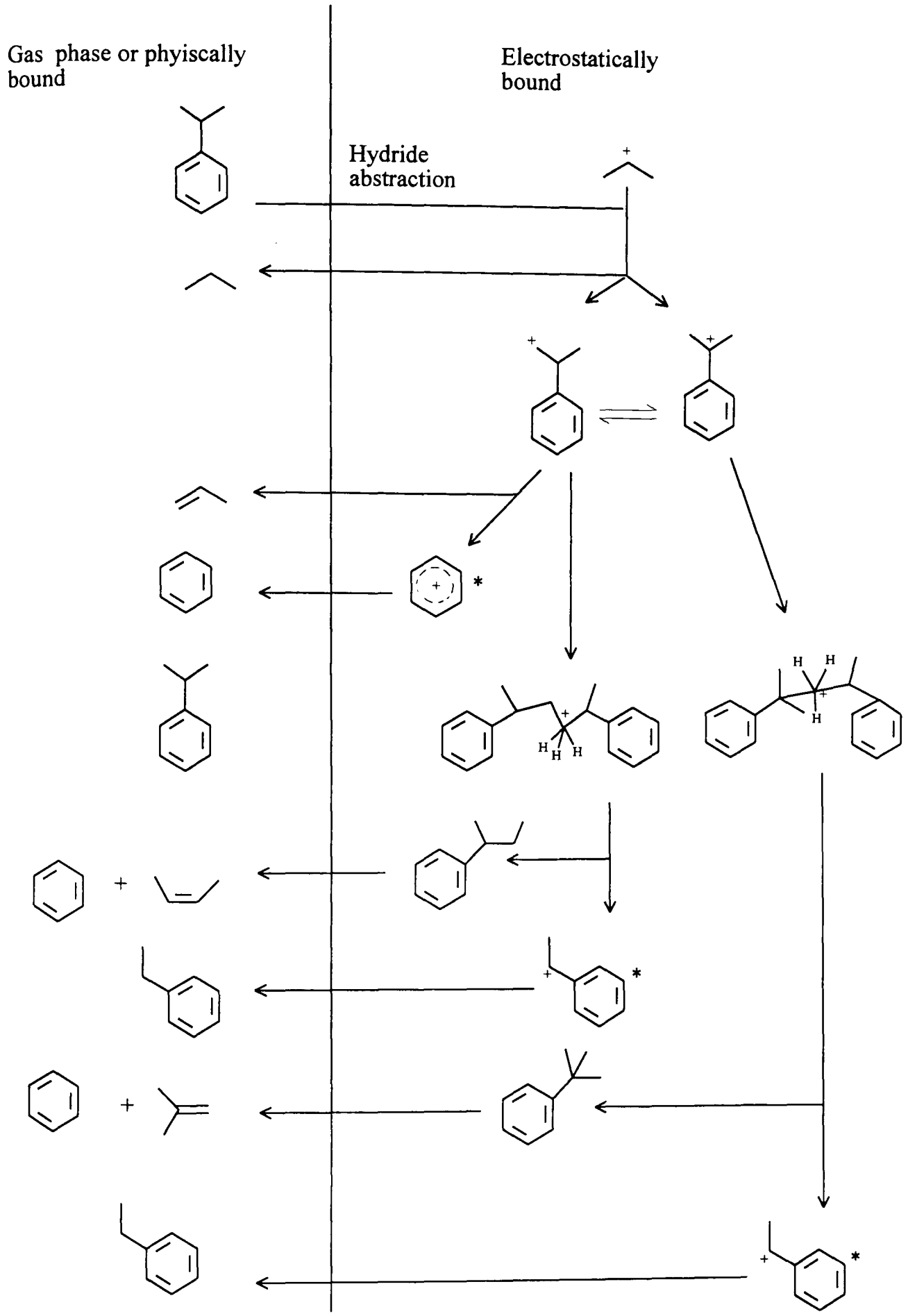

Species marked (*) can abstract a hydride ion from another molecule, usually cumene, to prorduce the appropriate gas phase molecule.

Figure 4.41: Hydride abstraction mechanism.

hence the Lewis acid sites, leads to an increase and not a decrease in the amount of ethylbenzene produced. Secondly, the amounts of ethylbenzene and toluene produced decreased with dealumination and coincident Lewis acid site generation, rather than increased as would be the case if the Lewis acid sites were the seat of the reaction. Finally, the production of ethylbenzene increases with pulse number, with the first pulse frequently producing very little or none of this product. Rather, the general pattern of ethylbenzene formation from catalyst to catalyst mimics that of benzene and so it would seem reasonable, as Bielanski and Malecka have also concluded,[307] that the hydride abstraction is performed by a carbenium ion alone, the concentration of which would be higher in the more active samples and after the first pulse.

When the total number of aliphatic molecules is compared to that of aromatic products a clear deficiency in aliphatic material is noted, as shown in figure 4.38. This is in agreement with other workers.[306,309,315,316,317] The total of aromatic products does not include n-propylbenzene as cumene isomerisation does not result in the production of a aliphatic molecule. However, this finding disagrees with those of Best and Wojciechowski,[318] who, although recognising more benzene than propene, put this down to an excess of benzene due to its formation from reactions other than straight dealkylation, namely the reactions resulting in butene/butane and ethylbenzene.

However, when the work of Best and Wojciechowski[318] is considered as a whole, there is still an 'aliphatic' deficiency. It therefore seems probable that at least some of the propene is consumed during coke formation, especially considering that the introduction of styrene as an aromatic coking agent did not cause a significant rise in the coking rate. In subsequent papers,[319,320] this group have admitted the coke is formed exclusively by propene polymerisation.

Polymerisation of propene is thought to be the initial step in the process culminating in the formation of coke,[319,320,321] generating studies of the reaction of propene over HY zeolites.[194,195,196] This fits in with the generic coking mechanism for all reactants proposed by Wolf[322] of initial dehydrogenation followed by addition polymerisation and cyclisation of hydrogen deficient

fragments. Using infrared spectroscopy, Jacobs *et al*[309] detected the presence of a νCH_2 band in the spectrum of adsorbed cumene and Ghosh and Kydd[196] have shown that the oligomer formed on HY at temperatures below 473K is highly branched and nonaromatic in nature. This evidence dismisses the possibility of propene dimerisation and subsequent dehydrogenation giving benzene, a route which could account for the benzene excess already noted.

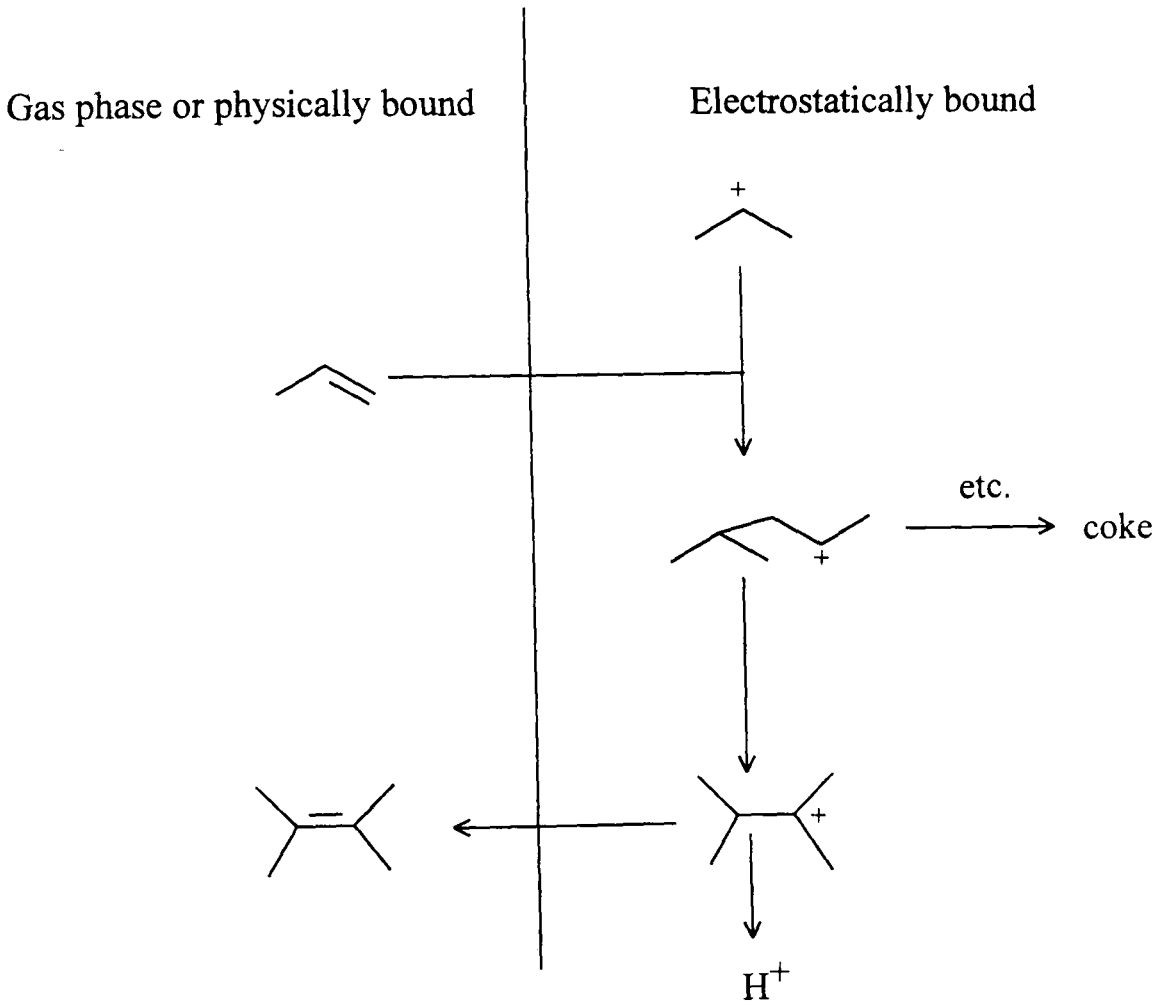

Figure 4.42: Dimethylbutene and coke formation.

Haw *et al*[194] have proposed a mechanism for the polymerisation of propene. At any stage in the process the oligomer can abstract a hydride ion from another molecule and desorb as a paraffin molecule, or desorb without further reaction as an olefin molecule. The likelihood of desorption or

movement through the crystallite drops rapidly with increasing chain length, and desorption of the dimer postulated in the mechanism of Haw would produce methylpentane, a molecule not detected in the present study. Therefore rearrangement of the dimer cation is proposed, forming the more stable dimethylbutene cation shown in figure 4.42.

In any discussion of deactivation it has to be remembered that any observations can be as much a reflection on the physical nature of the reactor as on the chemical nature of the reaction.[323] Any parallels drawn between different sets of experiments, especially those carried out by different workers, should be treated with the utmost caution. Nevertheless, meaningful correlations between the presently observed and other data are possible.

Three modes of deactivation have been outlined by Reyes and Scriven,[324] namely competitive adsorption, site coverage and pore blockage, being respectively dynamic, chemical and structural in nature. Langner[195] was of the opinion that deactivation below 573K is caused by strongly adsorbed coke precursors on active sites within the pores and at higher temperatures by exterior coke blocking the pore mouths. Bellare *et al*[325] concluded that at low temperatures the reaction is considered to take place primarily within the pores of the crystallites leading to deactivation by pore choking, followed by site suppression at higher coke levels. At higher temperatures the rate of reaction exceeds that of diffusion, and the reaction proceeds on the surface causing deactivation by pore blockage. This is partly corroborated by Choudhary and Akolekar[308] with the experimental observation that at 600K deactivation is due to deactivation of active sites by coke deposition, with a contribution from pore mouth blockage. The style of the deactivation observed in the present study can therefore be assumed to be taking place within the pores of the crystallites, although whether the coke remains on the sites or diffuses away slightly and causes pore blockage is open to conjecture.

The deactivation of each sample was defined as the percentage drop in benzene production between the third and fifteenth pulses, or pulses representative thereof. Benzene was used as the indicator of deactivation as it is thought not to be consumed in the primary coking reaction, although it

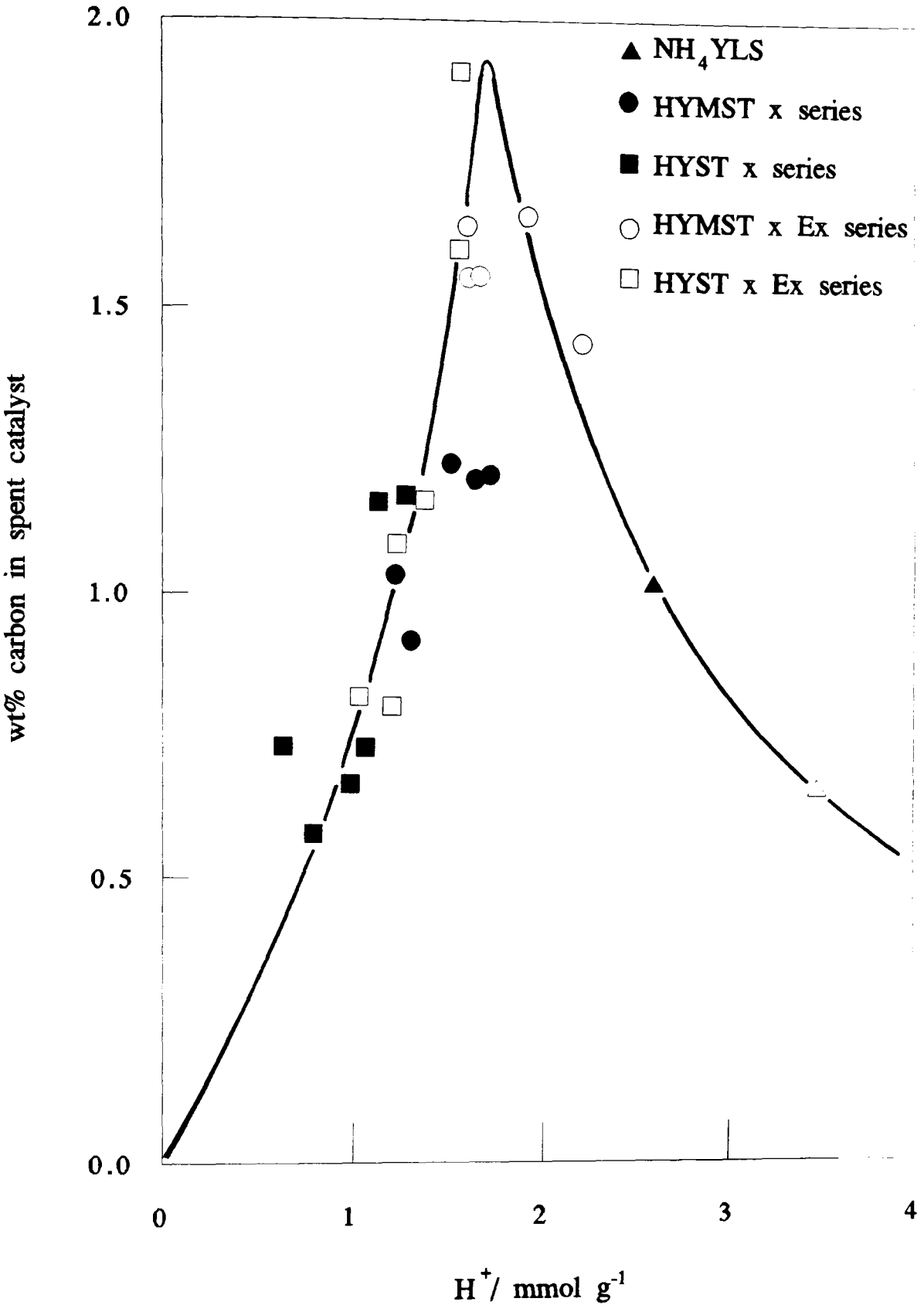

Figure 4.43: Carbon content of spent catalysts - cumene dealkylation.

might contribute in the later stages of deactivation as it becomes increasingly unable to diffuse from the crystallites.

Deactivation should be a function of the total amount of reaction, with the most active samples deactivating the quickest. Catalysts with a higher initial activity have been found to deactivate faster than those with a lower activity.[172] A five fold increase in coke was found for a 50% rise in the number of acid sites which lead to the authors[172] to conclude that the coking reaction becomes less favoured as the acid sites become more isolated.

In the broadest terms, the initial deactivation of the unextracted samples follows their activity, with the maximum value returned for HYST 823. NH_4YAS was found to have a low constant activity, and NH_4YLS deactivated by about 10%. It is known that the extrastructural aluminium occupies an appreciable amount of the available pore volume[176,201] and that under more severe hydrothermal treatment conditions the extraframework material agglomerates. These facts inescapably lead to the conclusion that, if the pore blockage theory is correct, deactivation will be both a function of the activity and of the extraframework material. NH_4YAS has no extrastructural aluminium and very little activity, and so suffers no deactivation, whereas NH_4YLS has aluminium in non framework positions and substantial activity, and so deactivation is observed. HYST 923, a sample of similar activity to NH_4YLS, suffers approximately twice the deactivation, possibly confirming the crucial role in deactivation played by extrastructural aluminium.

Carbon analysis of the spent samples reveals that the amount of coke retained by the samples has a strong dependency on the acid nature of the catalyst. There is enough difference between figure 4.43 and figures 4.36 and 4.37 to suggest that reaction leading to coke formation is favoured by stronger sites than that responsible for the dealkylation of cumene. This is not in agreement with the opinion of Fleisch *et al*[172] who claimed that the coking reaction is not favoured by isolated sites. If indeed the reaction was enhanced by adjacent sites a change in gradient along with higher coke contents for catalysts with proton contents in excess of 2.0 mmol/g would be expected. Deactivation is therefore not a function of coke content alone, but a

combination of coke content and extraframework aluminium. NH_4YLS has a greater number of active sites than HYST 923 and after fifteen pulses contains slightly more coke, but HYST 923 deactivates faster because as it contains more nonframework aluminium the combined effect of the two is greater.

Consideration of the deactivation of the extracted samples confirms this hypothesis. Those samples which previously contained large amounts of extrastructural aluminium now do not deactivate as fast even though they contain more coke. Additionally, the mildly dealuminated samples deactivate faster when the extrastructural aluminium has been removed. This could be due to a dehydrogenating function of the extraframework aluminium in the mildly dealuminated catalysts, which is more likely to be cationic. Alternatively, the enhancement in activity which produces coke could more than offset the effect of increasing the porosity of the catalysts which could be low due to the more highly dispersed nature of the extraframework species in these samples.

The rate of the coking reaction has been shown to be contributory to the rate of deactivation in the very initial stages of the reaction, but it is by no means the controlling factor. Further, it seems that in the dealkylation reaction the coke is associated with the extrastructural aluminium, although its production seems to be enhanced by slightly stronger sites than those required for the dealkylation reaction. These results support the pore mouth blockage theory.

Although there is an overall deactivation over fifteen pulses, there is an increase in the products detected over the first two or three peaks. If the length of the interval between the pulses was increased, a drop in activity was noted. Initially, the sample adsorbs a large proportion of the products; subsequently, these desorb slowly from the surface into the gas stream. The free capacity of the sample for adsorption is defined here as the 'apparent' adsorption capacity. This is dependent on the length of time since the previous pulse; the longer the time interval the more desorption from the surface that will have occurred and so the higher the 'apparent' adsorption capacity. The influence of temperature on this capacity cannot be neglected: a rise in temperature will increase the rate of desorption from the sample thus increasing the 'apparent' adsorption

capacity.

Alternatively, the initial increase in activity could be due to the adsorbed species enhancing the activity of the catalyst,[309] possibly through a hydride transfer function as has been postulated for toluene disproportionation, both here and elsewhere.[60] On a very clean surface, the population of adsorbed species is by definition very low and hence the low activity. As the reaction starts, hydride extracting species are deposited and the activity rises; increased desorption after extended intervals would also diminish the amount of this active coke. Unfortunately it is impossible to distinguish between product saturation of the sample and catalytic enhancement of the surface, although the former is certainly the more likely at the very early stages of the lifetime of the catalyst.

Additional information about the adsorbed species could have been obtained by desorption at a higher temperature, in effect flushing the surface. but the coke content under the operating conditions was required, and given the amount of substituted aromatics present, raising the temperature would also promote more cracking of the adsorbed surface species, thus altering the retained product distribution.

Analysis of the products desorbed up to an hour after, but not including, the last pulse, was undertaken. Whilst a totally quantitative appraisal of the results is unjustified, a qualitative examination produces some interesting results. The distribution of the products, as is shown in figure 4.44 for catalyst HYMST 768, differs markedly from that of the experimental run, and provides a valuable insight into the population of the surface as presented to each pulse of reactant.

The product distribution in the retained products is a function of the different adsorption qualities of the components of the product stream, and not of the catalytic nature of the catalyst. The proportion of benzene in the retained products is very low, but that of the substituted aromatic products is higher than that collected after each pulse. This can be rationalised by noting that the substituted molecules suffer hindered desorption from the catalyst. While almost all the benzene produced in a pulse diffuses from the catalyst in the

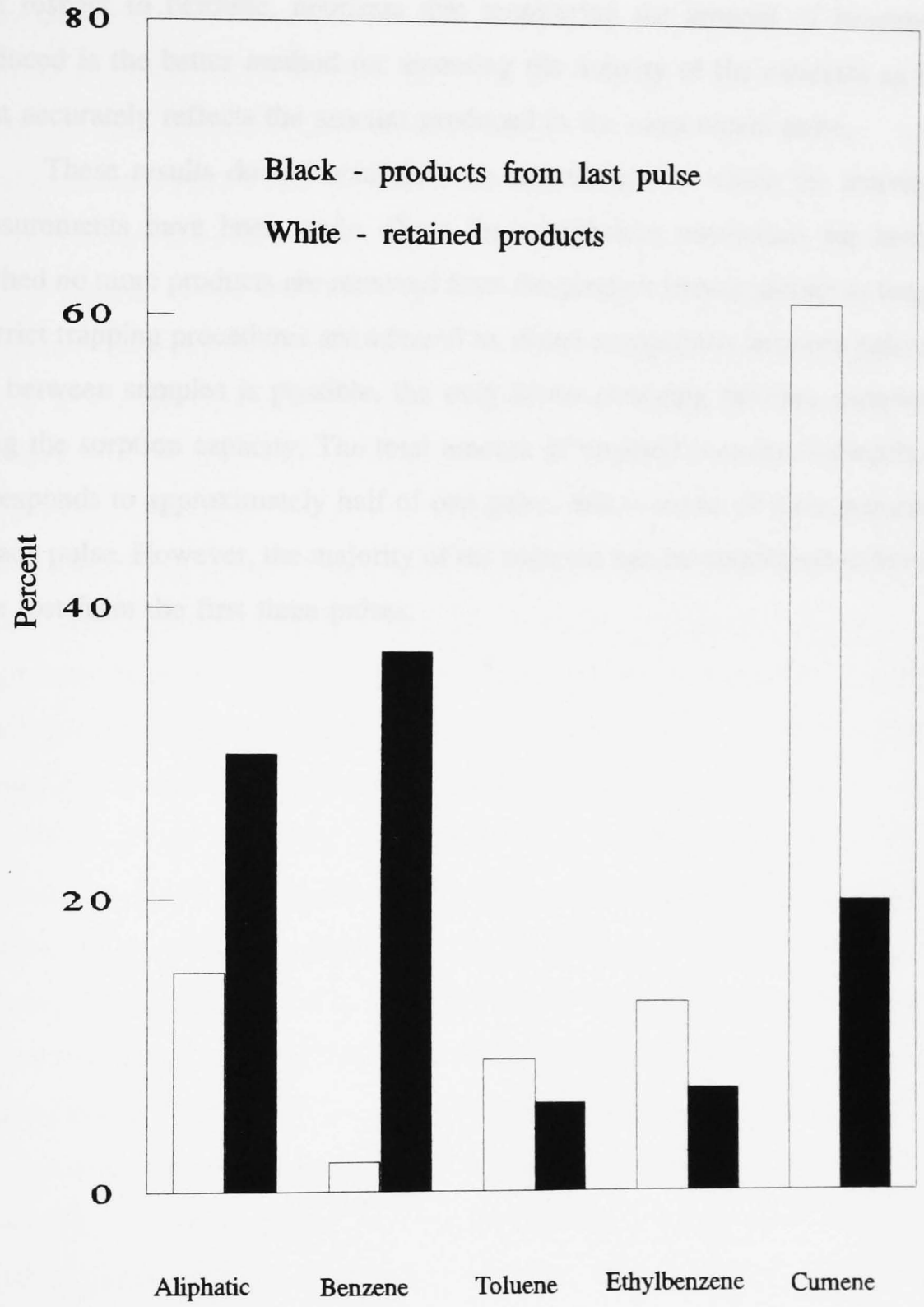

Figure 4.44: Comparison between the products of the fifteenth pulse and those desorbed from the surfacce up to one hour after the fifteenth pulse.

time allowed, the rates of diffusion of the toluene, ethylbenzene and cumene preclude total desorption. Thus, an accumulation of the substituted molecules can be envisaged. A similar explanation can account for the change in relative concentration of the aliphatic molecules. However, the less pronounced drop, with respect to benzene, confirms that monitoring the amount of benzene produced is the better method for assessing the activity of the catalysts as it most accurately reflects the amount produced in the most recent pulse.

These results do not invalidate the assumption on which the activity measurements have been made. Once the equilibrium adsorption has been reached no more products are removed from the product stream and so, as long as strict trapping procedures are adhered to, direct comparison between pulses and between samples is possible, the only factor changing between samples being the sorption capacity. The total amount of retained aromatic molecules corresponds to approximately half of one pulse, that is a loss of three percent of each pulse. However, the majority of the material can be considered to have been lost from the first three pulses.

4.6 Propan-2-ol Dehydration.

The dehydration of alcohols,[208,326] is a long established test reaction which is now widely seen as a reaction that is catalysed by even the weakest acid sites present in a catalyst.[187,208,327] Propan-2-ol is perhaps the most commonly studied alcohol,[187,327,328,329,330,331,332] and has been used in this study to assess the total acidity of the catalysts. Given that the reaction proceeds cleanly at low temperatures, yielding propene and di-isopropylether, the specific reaction rates obtained should bear close relation to the amount of available Brønsted acidity within the catalyst, irrespective of strength.

Previous work in this laboratory[187,333] has established a linear relationship between the amount of available Brønsted acidity and dehydration activity in a series of ion exchanged Y zeolites. Furthermore, the removal of acid sites by organic base poisoning was seen to decrease the activity in an almost linear manner. A logical extension of this work is to apply the same activity test to dealuminated samples, wherein the acid strength increases to a plateau while the number of sites decreases in a well established fashion. Any comparison between the present work and that which preceded it must therefore take into account the changing acidity spectrum of the catalysts, and important information regarding the reaction may become accessible.

The effects of both temperature and reactant pressure on the dehydration reaction were studied in a continuous flow system at atmospheric pressure. Experiments in which the partial pressure of propan-2-ol was gradually raised from 0.9kPa to 1.4kPA, resulted in a large drop in the rates of product formation. This departure from ideal zero order behaviour is probably due to the pores of the catalyst becoming blocked with reactant as the partial pressure rises. Diffusion of products and reactant through the crystallites is hindered, thus diminishing the activity of the catalyst. A very slow buildup of reactant partial pressure, or stepwise experimentation, might have alleviated this problem, but allowing the reaction to stabilise at a higher partial pressure before continuous reduction in the partial pressure was found to be the most reliable method of obtaining results.

The results from those experiments where the pressure of propan-2-ol

was allowed to fall from 1.40kPa to 1.00kPa, presented in Section 3.25, figures 3.38 and 3.39, confirm that in the range studied the reaction is almost independent of reactant pressure, with an increase in the rate of formation of propene of typically six percent and four percent for the ether. The dehydration of propan-2-ol, under the present conditions of temperature and pressure, has been shown to zero order with respect to reactant, in agreement with other workers.[227,228,334] The pressure dependant experiments have served the dual purpose of confirming that the reaction is independent of reactant pressure, therefore the measured reaction rates are maximum experimental values, and that the temperature dependant measurements were taken under valid conditions.

Intramolecular dehydration to propene was found to be the dominant reaction, with a contribution from intermolecular dehydration yielding di-isopropylether: there was no evidence of dehydrogenation leading to the formation of propanone. The presence of the water in the product stream could not be established due to the method of detection employed.

The activation energies measured across the range of samples and the zero order rate constants at 373K are presented in table 3.136. The two products show consistent activation energies, with the energy difference between the two being about 15 $kJmol^{-1}$ in three out of the four groups. The exception is the group of mildly steamed unextracted samples where, although the propene activation energy is commensurate with the other groups, at 137$kJmol^{-1}$, that for di-isopropylether is low, 93$kJmol^{-1}$. Similar activation energies obtained for both groups of extracted samples suggest that the reaction proceeds by a similar mechanism as the aluminium content of the framework decreases. However, the high activation energies for the formation of both propene and di-isopropylether over the severely steamed unextracted catalysts seem to imply the involvement of the extra structural aluminium. It has already been noted in preceding sections that the nature of this material is likely to change with the severity of hydrothermal treatment; the associated change in activation energies is possibly due to a slight change in the interaction between framework and nonframework species. The similarities in

activation energies between the catalysts are sufficient to treat the derived zero order rate constants with confidence as no change in mechanism is implied. The following general series of reaction pathways for alcohol dehydration is well established:

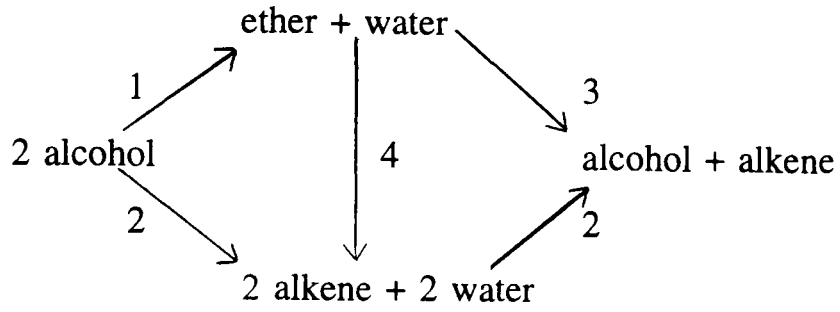

The simultaneous appearance of both products at the start of the reaction can be taken as evidence of the parallel pathway (1): the dehydration of ether only becomes apparent at higher temperatures. In this reaction, the total activity of the catalysts can be deduced from the detected products. Therefore the rate of conversion of propan-2-ol equates to the rate of production of propene plus twice that of the ether. It is inappropriate to use this approach for the other reactions, as they produce an unquantifiable amount of coke. In addition, there is less certainty in the quantitative detection of the disubstituted products in the disproportionation reactions. This method of analysis removes the effects of any changes in selectivity on dealumination or extraction.

The temperature at which the dehydration reaction was studied was the lowest of the test reactions employed in the present work, reflecting the facile nature of the reaction. Consequentially, the hydration level of the samples is relatively high, especially when the partial pressure of water in the gas diluent is considered. Therefore, as with cumene dealkylation, Section 4.4, the results obtained from the partially dehydrated temperature programmed desorption are used in the activity plots, figures 4.45 to 4.47. However, there is an unacceptable degree of scatter within the points as plotted. The quality of the data from the temperature dependence experiments is reasonably high, generating confidence in the derived activities used and furthermore, deactivation on the timescale of the experiments was absent, a fact confirmed

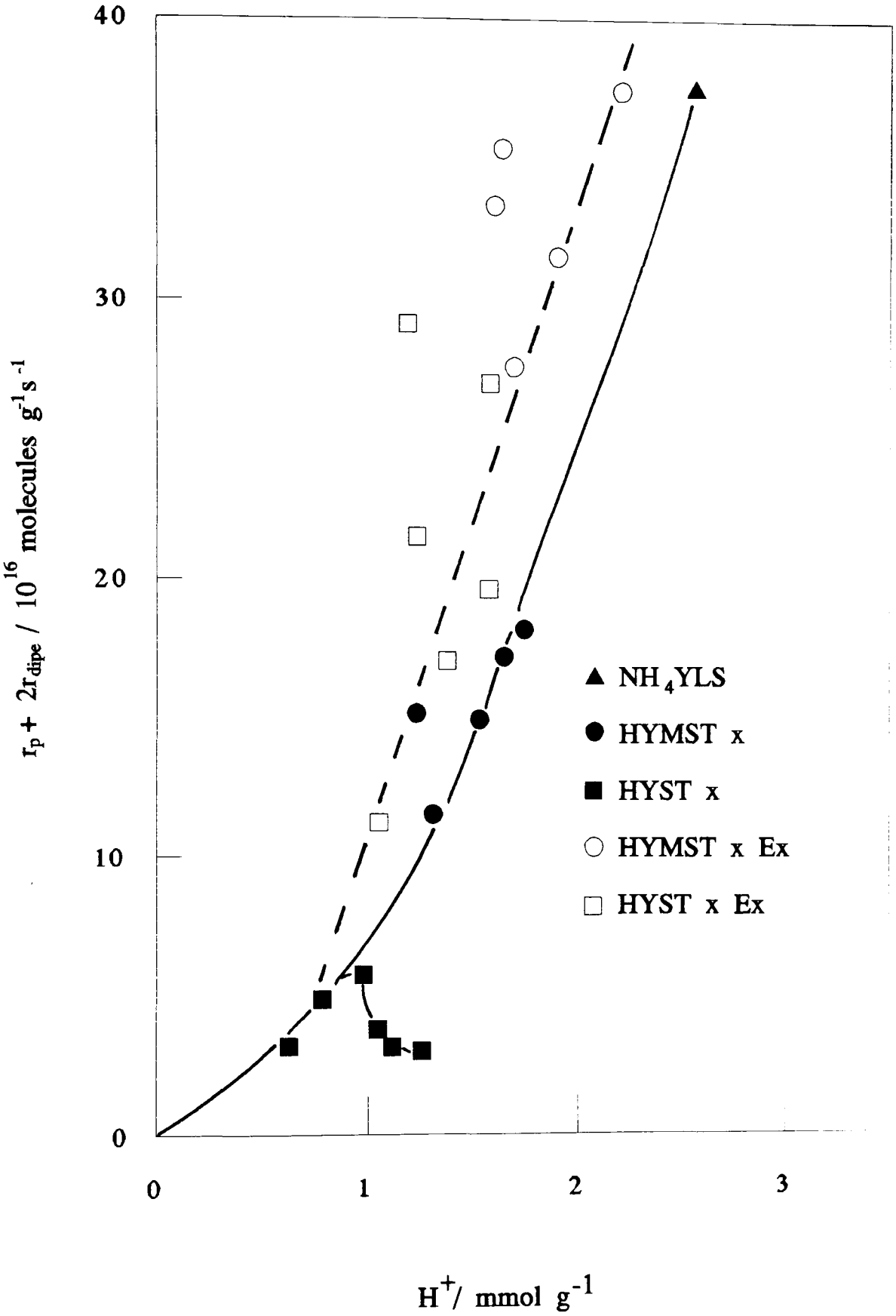

Figure 4.45: Propan-2-ol dehydration.

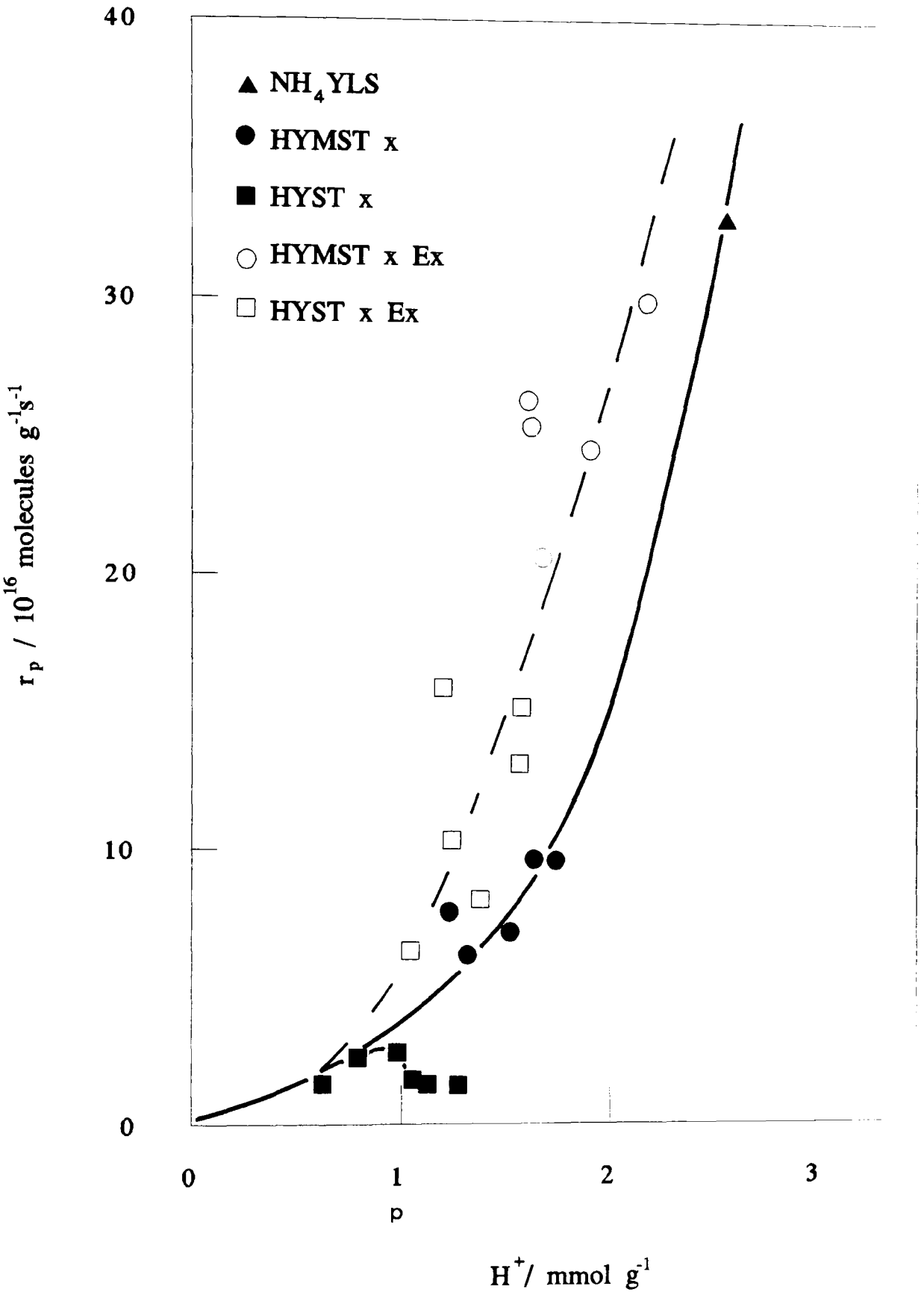

Figure 4.46: Propan-2-ol dehydration - propene formation.

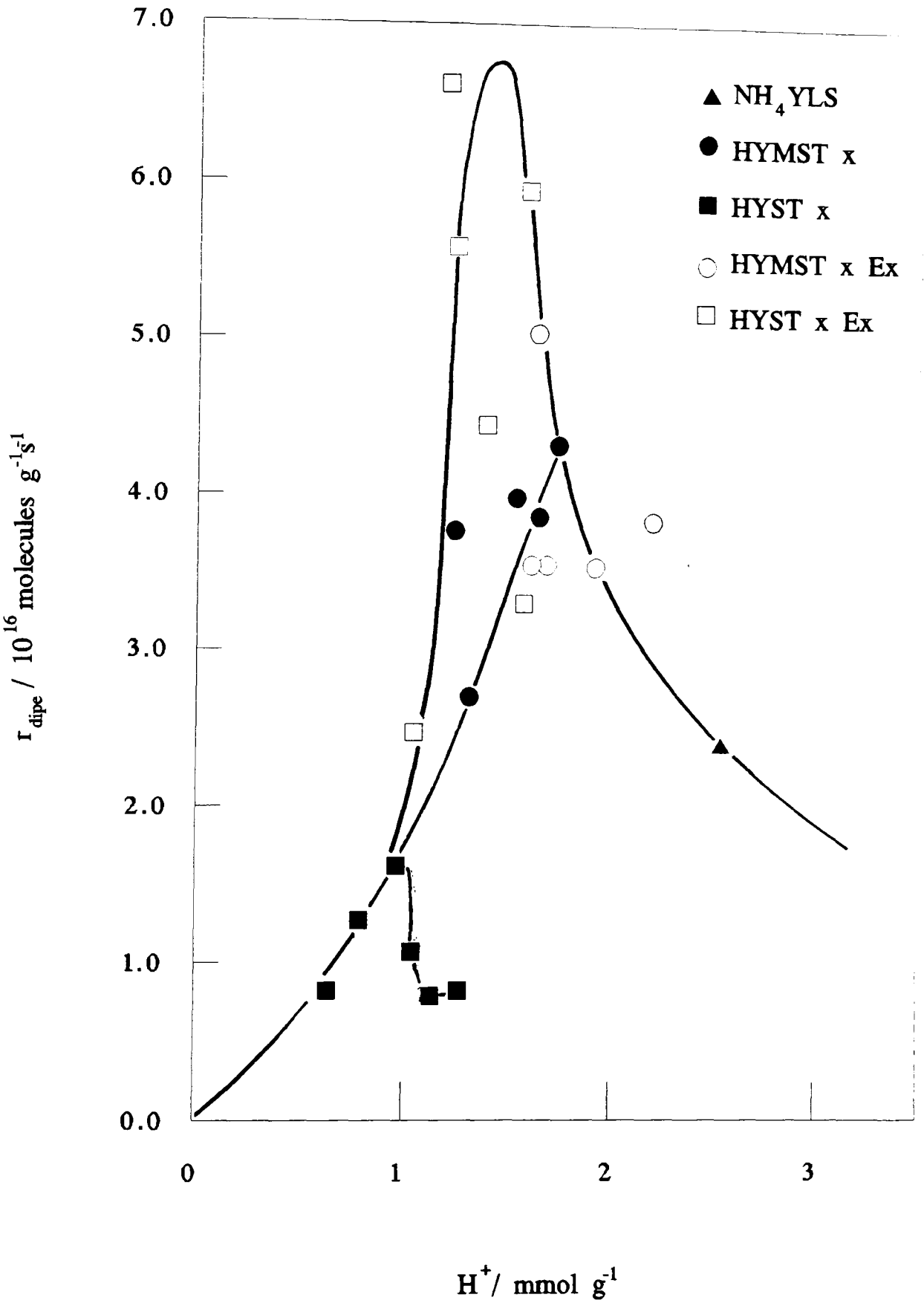

Figure 4.47: Propan-2-ol dehydration - di-isopropylether formation.

by the longer pressure dependant experiments. It is proposed that the hydration level of the catalysts is crucial to this reaction, in concordance with the conclusions of Nock.[227]

Nevertheless, there is a strong dependence between activity and proton content of the unextracted samples, as found with methanol dehydration,[208] with the exception of catalysts HYST 823 to HYST 923. Therefore this reaction is purely a measure of the number available sites with all sites, or a constant fraction of all sites, contributing in the same manner to the reaction. The turnover frequency (TOF) increases on extraction, implying that the extracted samples are more efficient in promoting the reaction. This can probably be related to changes in the transport capabilities of the catalysts on extraction of the extraframework material.

It is important to note that NH_4YLS is the most active of the unextracted samples: this was not the case for the other reactant requiring weaker acidity, cumene. The implication is that cumene dealkylation requires sites of a stronger nature than propan-2-ol dehydration. This adds further credence to the hypothesis postulated in the preceding section that there is a certain degree of heterogeneity in the strength of the acid sites. The pre-existing sites in the catalyst before high temperature hydrothermal dealumination are sufficiently acidic to promote propan-2-ol dehydration to the maximum extent and no benefit is to be gained from increasing the acidity of the individual sites.

The pressure dependence results confirm an interesting anomaly seen in the temperature dependence results. In both types of experiment, the least active catalyst was HYST 823, a catalyst which has twice the number of acid sites as HYST 1073. Furthermore, the trend is continued, showing a maximum at approximately 1.0 mmol H^+ g^{-1}, which is present in both products. The underlying reason for this behaviour is not immediately obvious, although the observations that it is removed on extraction, and not shared by the mildly steamed unextracted catalysts, indicate the involvement of the strongly steamed extraframework material. Synergic interaction with the framework can be disregarded, as the observed activities are less than would be expected on the

basis of the other catalysts, and not more, as would be the case if there was a beneficial interaction. A possible explanation is that the combined effect of the extrastructural aluminium and the partial pressure of the propan-2-ol result in the pores of the catalyst becoming blocked, in much the same way as described earlier in the initial pressure dependant experiments. The nature of the extraframework species, in particular the extent of agglomeration, is dependent on the manner of hydrothermal treatment. Although more extraframework material is present in catalysts HYST 973 to HYST 1073, it may be concentrated in different areas of the crystallites and so have less effect on the activity. Hydrogen bonding of propan-2-ol to these hydroxylated aluminohydroxy species would increase the effective size of the nonframework aluminium. In this way, the internal transport properties of the samples can be envisaged as being dependant on the nature, amount and position of the extraframework material.

Although the overall activity of each catalyst has been defined as a combination of the rate constants of both products it is worth considering the two products separately. Even after due account is taken of the scatter the activity profiles of the two products, figures 4.46 and 4.47, are markedly different. Whilst the propene profile follows that of the overall activity, figure 4.45, as expected for the dominant product, that for the ether has more in common with those seen for reactions which are known to require strong sites. The most salient point is that the rate of formation of di-isopropylether for NH_4YLS is only about one third that of the most active sample, whereas it is the most active in the production of propene. This is not a manifestation of the high conversion rate of this sample diminishing the amount of propan-2-ol in the reactant stream, favouring the unimolecular reaction, as conditions were employed to keep the level of conversion within accepted limits, and results from the pressure dependence experiments confirm zero order over the range of the reaction studied.

Extraction of nonframework aluminium was found to increase the activity of the catalysts to a greater extent than would be expected on the basis of the increase in available acid sites alone, as is reflected in the different

product turnover numbers of the extracted and unextracted catalysts. Removal of nonframework species will undoubtedly aid the diffusion of the reactant into and the products from the catalyst crystallites. This will be more apparent in the highly dealuminated samples, ie. those with more non framework aluminium. In addition figure 4.48 shows that there is a change in product selectivity with a dramatic drop in the di-isopropylether/propene ratio on extraction. This is entirely opposite to what would be expected on the grounds of transport properties alone. The unextracted catalysts, ie. those with more congested pores and channels, are much more efficient at producing the large di-isopropylether than the extracted catalysts. A drop in selectivity was also noted by Hey *et al*[335] in a study of a series of strongly dealuminated Y zeolites, which although having the same framework aluminium content, had progressively less extraframework aluminium. It was concluded that the ether formation involves both the Brønsted acidity of the hydroxyl groups and the Lewis acidity of the nonframework aluminium. Removal of the nonframework aluminium by acid treatment enhanced the propene production, presumably due to the freeing of more sites and the improvement of the transport properties, to a greater extent than the ether formation, which was claimed to be affected by the drop in the amount of nonframework aluminium. Unfortunately, no data was presented regarding the number of available sites before and after extraction, precluding a more exact analysis of these results. The change in selectivity in both this and the present study is likely to be due to the increased total acidity and change in acidity spectrum on extraction, and not extraction *per se*, as NH_4YLS, which has high acidity and extraframework aluminium has a selectivity ratio comparable to the mildly dealuminated extracted samples.

These facts, when combined with the information from the activity profiles of each product, lead to the unavoidable conclusion that the reaction culminating in the production of the ether is different in nature to that resulting in propene. Strong acid sites promote the reaction forming the ether; note that the rate of formation of the ether did not increase on extraction of the HYMST series, but only when the HYST series was extracted. When this is combined with the observation that NH_4YLS, which has more extraframework aluminium

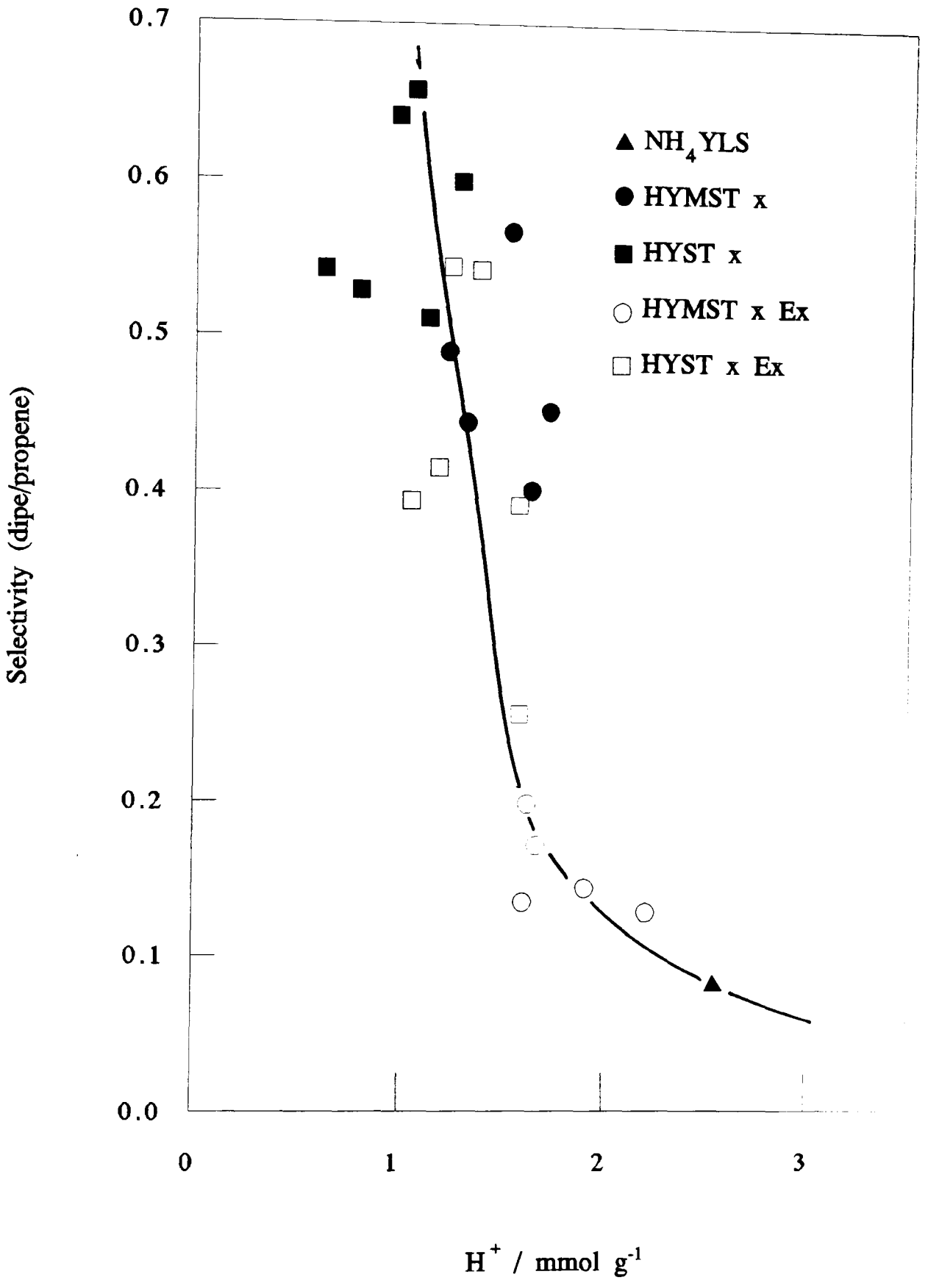

Figure 4.48: Selectivity of propan-2-ol dehydration.

than the HYMST x Ex samples, has a lower selectivity for the ether, the theory of ether production requiring both Brønsted and Lewis acidity can be dismissed. It is therefore not sufficient merely to state that di-isopropylether results from an interaction between a surface bound carbenium ion and a propan-2-ol molecule without reference to the acidity and distribution of the sites within the catalyst.

The change in selectivity, figure 4.48, can be traced to a relative change in the rate of production of each product. The percentage increase in propene is roughly dependant on the increased number of available acid sites, with the strongly steamed samples benefiting proportionally to a greater extent than those steamed under mild conditions. In contrast, the mildly dealuminated samples actually suffer a drop in ether production on extraction whilst the other samples exhibit a strong rise.

These results can be appreciated using the information that the product formation is favoured by acid sites of differing strength. Extraction of any material enhances the rate of production of propene, as it always results in more sites becoming accessible. For some samples, those with pores partially blocked with such material this enhancement is disproportionately large, large enough to bring the overall activity in line with the other extracted samples.

Ether production, it has already been established, is favoured by strong acid sites. Extraction of the mildly treated samples does not enhance ether production as no strong sites are freed because there are none present to be freed. However, weak sites are freed and so the rate of propene production increases. In contrast, extraction of the strongly dealuminated samples does provide additional strong sites, and so the rates of production of both ether and propene increase. When these activity changes are combined in the selectivity ratio, the selectivity to ether is seen to drop with decreasing site strength (and not due to the concurrent increasing total acidity).

Before detailed consideration of the interaction between catalyst and reactant can be attempted, a reaction mechanism has to be discussed. In the following, protons will be treated as existing as discrete entities, although it must be remembered that under the operating conditions, and with the

production of water during the reaction, some protons may exist as hydroxonium ions.

The simple intramolecular dehydrogenation reaction requires protonation of a propan-2-ol molecule, shown in figure 4.49, which can, by an E_1 elimination step result in the formation of a carbenium ion and a water molecule. The carbenium ion is free to desorb as a propene molecule transferring the proton back to the surface of the catalyst, or interact directly with a further propan-2-ol molecule; either process continues the catalytic cycle.

Intermolecular dehydration, also shown in figure 4.49, proceeds via addition of the carbenium ion to a second molecule of propan-2-ol. Subsequent desorption of the ether molecule allows the proton to be recycled in the same way as above. Recombination of ether and water to form propan-2-ol, propene and water, or direct dehydration of ether to two molecules each of propene and water, is thought not to occur in this instance due to the low operating temperature. The simultaneous appearance of ether and propene in the product stream is taken as evidence of the operation of the parallel, and not the consecutive reaction pathway.[334]

A theory of solvated protons (hydroxonium ions) contained in ceramic pots (zeolite framework) has been advanced to explain the activity of Y zeolite.[187] By necessity the protons are assumed to become divorced from the framework, loosing their original identity, with the framework having no influence over them. On the basis of the present work this theory can be dismissed as incorrect, as it accounts for neither the shape of the ether activity profile nor the increased activity on extraction, other than the availability of more protons in larger ceramic pots than in the first place.

A two site mechanism for the formation of ether has been postulated before[186] with this reaction over X zeolite. Similar results were obtained by Stockwell[334] working on Y zeolite, with the conclusion that the two site mechanism is less favourable, due to the relative scarcity of acid sites in Y zeolite and the improbability of reaction between to entities of the same charge. In this study, an increase in the site density has been shown to

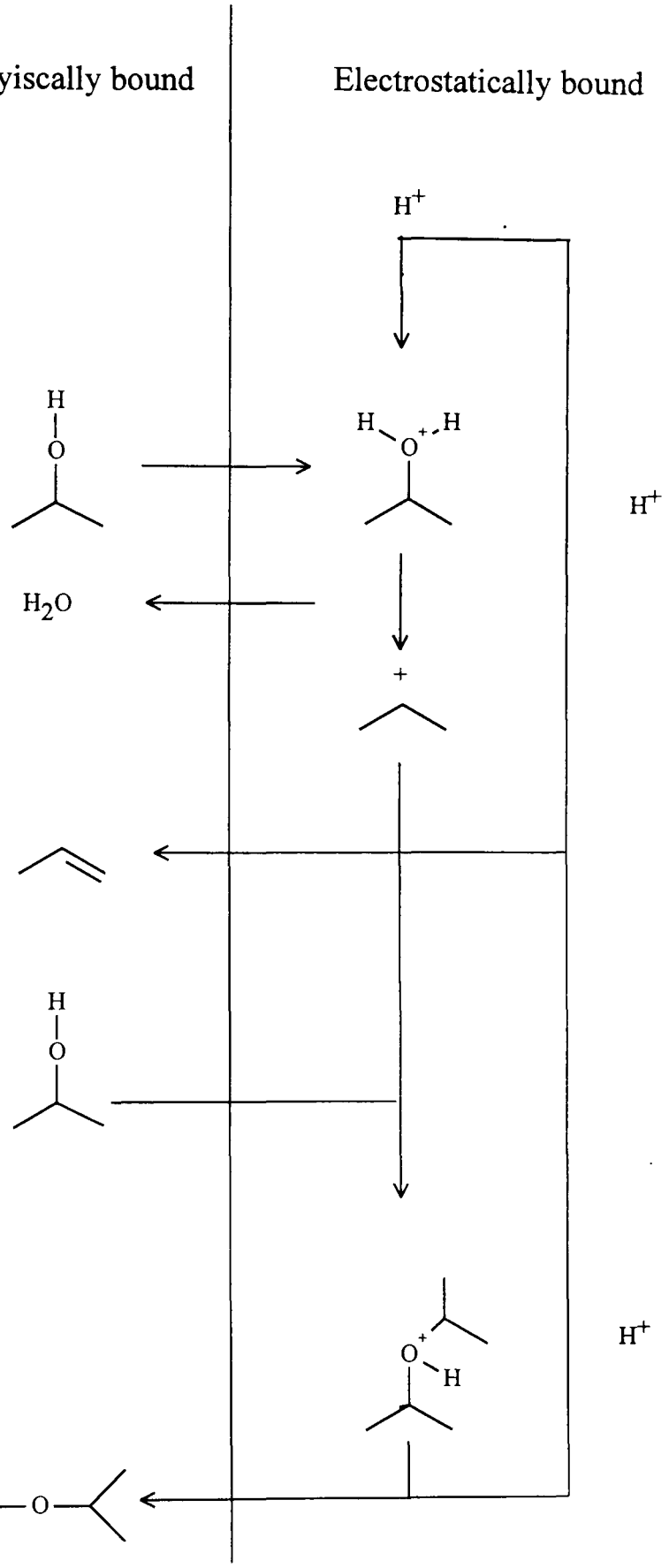

Figure 4.49: Propan-2-ol dehydration mechanism.

decrease the rate of formation of the ether, implying that the ether does not form via a two site mechanism. However, it must be remembered that in the present research the effects of an increase in site density are indistinguishable from those arising from simultaneous changes in the acidity spectrum. Extraction leads to an increase in the TOF, but as this is constant in all samples it is probably linked to changes in the transport capabilities of the samples, with extraction of non framework material leading to faster diffusion through the crystallites.

If, as claimed above, both products are formed from a common intermediate, then the action of a higher density of sites would be to bring the second molecule close and in a favourable orientation for the reaction to proceed. Protonation of the second molecule may not be necessary, and indeed could be disadvantageous if dehydration yielding a carbenium ion is almost instantaneous. Additionally, protonation would necessitate the close interaction of two similarly charged species, a clearly unfavourable situation. If density of sites was the controlling factor in the production of ether the most weakly dealuminated samples would have the highest activity: there would be very little difference in the activity profiles for the two products, possibly with the ether profile having a more rapidly increasing gradient.

Strong sites will hinder the desorption of the carbenium ion, giving it a longer lifetime on the surface. Thus, unless the turnover frequency is so high that it renders the surface continually populated by adsorbed carbenium ions, the chances of a favourable interaction between an adsorbed species and another propan-2-ol molecule are increased if the carbenium ion is adsorbed on a strong site. Therefore, the generation of a greater number of strong sites will be seen to increase the production of di-isopropylether. It is also predicted that the selectivity of the reaction towards ether will decrease with increasing temperature, as this will also shorten the lifetime of the adsorbed carbenium ion. This agrees with the activation energies, where a drop in ether selectivity with increasing temperature is duly noted.

Earlier in this discussion the hydration level of the sample was invoked to explain the scatter observed in the experiment results. Whilst the theory of

'acids in pots' has been dismissed, the presence of hydroxonium ions cannot be discounted, and in some respects is necessary at these temperatures. However, it is doubtful whether the hydroxonium ions produced ever totally dissociate themselves from the framework, as the evidence of the ether formation implies otherwise. In reality they may be better described as adsorbed water molecules, retaining some characteristics of the original protons.

Protons thus adsorbed will not protonate propan-2-ol to the same extent as 'free' protons, resulting in differences in the observed activity. The extent of hydration, although influenced by the changes in structure of the catalysts, is dominated by the water content of the helium diluent. Any changes in this will far outweigh the more subtle structural changes. Information regarding the effect of hydration on the activity could obtained from pulse flow experiments. Temperature control could be used to ensure that the surface of the catalyst was dehydrated before each pulse.

Coking Experiments

Activation of the extracted catalysts at 673K to remove the exchanged ammonia produced samples which underwent noticeable deactivation during the normal temperature dependence experiments, such that meaningful activation energies could not be obtained. This problem was entirely removed by rehydrating the sample at room temperature before proceeding with the same activation sequence as used for the unextracted samples. This suggests that the hydration level of the samples plays an important part in determining the overall activity and deactivation characteristics of the catalyst.

Deactivation of the sample is most likely to be caused by polymerisation of propene on the surface, resulting in the loss of activity by active site suppression or pore choking. The carbenium ion has an appreciable lifetime on the surface due to the low temperatures used in the dehydration reaction combined with the strong interaction between the adsorbed carbenium ion and the framework when the sample is in a highly dehydrated state. If this lifetime is long enough to allow addition polymerisation of a second propene

molecule a polymer will build up on the surface. With the addition of each successive propene molecule the polymer molecule is less likely to desorb or move away from the active site, culminating in deactivation.

This is, of course, a similar argument to that advanced earlier for the formation of the ether, as it relies on the lifetime of the adsorbed carbenium ion to be commensurate with the statistical probability of interaction with another molecule. Obviously in the reaction conditions employed in the present study the second molecule is far more likely to be propan-2-ol, resulting in di-isopropylether than propene resulting in polymerisation. Affecting the lifetime of the adsorbed carbenium ion will therefore change the nature of the experiment. Rehydrating the sample by exposure to nitrogen saturated with water vapour (pressure 2.3kPa) was found to prevent deactivation in all the extracted samples, allowing activation energies to be determined.

Differing activity profiles were obtained when the catalyst sample was treated with propan-2-ol at elevated temperatures prior to the start of the catalytic runs, figure 4.50. In every case an enhancement of activity was noted, although the extent was dependant on the temperature of the pretreatment. In addition, the shape of the profile changes from almost constant activity over nineteen hours, to having a distinct maximum, or continuous linear deactivation.

Considering the initial activity in greater detail, the enhancement is tenfold at pretreatment temperatures between 419K and 582K, falling off slightly to sevenfold at 673K. The reaction of propan-2-ol at these temperatures tends towards complete conversion to propene, which is subject to polymerisation. The larger molecules thus formed are less likely to desorb from the sample, and with increasing temperature are more likely to dehydrogenate to a highly carbonaceous material. It seems that this material plays a supporting, if not crucial role in the catalysis. High temperature pretreatment diminishes the effect of this coke, leading to the reasonable assumption that there is an optimum level of dehydrogenation of coke; the lowest temperature pretreatment, although having an activity higher than the unpretreated sample at all times, underwent the most dramatic deactivation.

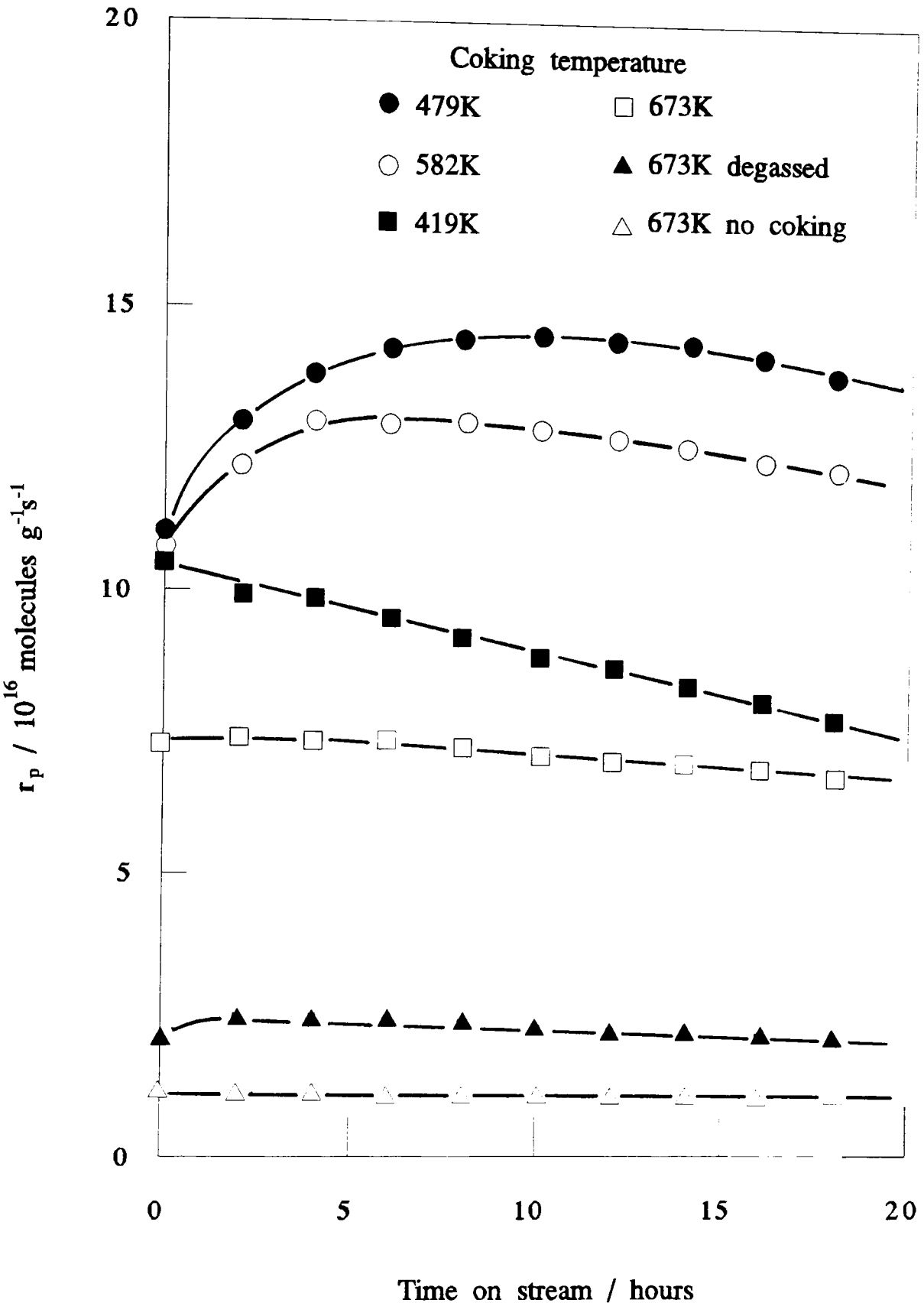

Figure 4.50: Effect of different pretreatments on propan-2-ol dehydra activity - HYST 1073.

Careful control of the sample conditions is required, as it has been shown that it is possible to reduce the efficacy of the coke formed. When the sample was degassed at 673K, removing all the desorbable material, before being cooled to the reaction temperature in flowing helium, only a small increase in the initial activity was observed. However, a distinct rise in activity, which was absent in the equivalent non degassed experiment was seen, resulting in a 18% increase over the initial activity after 2 hours.

There are two possible explanations for these observations, which are to some extent linked as the presence of coke is essential to both. Maximum initial activity requires that there be adsorbed propan-2-ol on the surface. This is lacking in the degassed experiment, but the small amount of coke present produces a modest rise in the initial activity. As the experiment progresses the surface becomes increasingly populated with propan-2-ol/coke species and so a maximum in activity ensues. The second theory is that the coke itself is always active, but its activity is dependant on the level of dehydrogenation. The consequence of too drastic a dehydrogenation can be seen in the reduced activity of the highest temperature pretreated sample. The continuing reaction, ie. no degassing, prevents the surface from becoming too carbonaceous, thus providing a more active surface at the start of the reaction at 376K.

An enhancement in activity due to the level of coke on the surface has already been claimed in the disproportionation of toluene over the same catalysts. It is necessary to consider the action of this coke in promoting the dehydration reaction. Promotion of the zeolitic protons, allowing easier protonation of the reactant molecule, is unlikely considering the ease of protonation of the alcohol in the first place. The generation of more protons from the reactant via the coke is equally unlikely, as this would necessitate the production of an equal amount of negative charge, presumably on the coke, to maintain electronic neutrality. Rather, it seems that the most reasonable explanation is that the coke increases the turnover frequency of the original protons, possibly by preventing the return of the protons to zeolitic framework. It may be helpful to consider the transfer of the proton to and from the coke as a propagation step, rather than a termination/initiation process.

The amount of coke detected on the spent catalysts is roughly in line with the total amount of reaction. This has the interesting result that the sample which suffered the greatest deactivation was not that with the greatest coke loading. Therefore, if the assumption that coke causes deactivation by pore chocking is valid, either the coke in this sample is different in nature, or the deactivation is really a progressive decrease in activation. Higher temperatures are known to effect the distribution of coke throughout the pore system of the catalyst, but, as the majority of all the reactions were conducted at 376K, it seems rational to suppose that the coke is of similar nature in all samples. Progressive loss of activity due to reorganisation of the coke layer is therefore favoured.

The selectivity of the reaction changes on pretreatment, with proportionately far more propene produced when the sample has been exposed to propan-2-ol at high temperatures. The selectivity to propene is slightly less for the degassed sample, confirming the differences noted earlier. It can thus be concluded that the presence of coke favours the unimolecular reaction, possibly by reducing the lifetime of the adsorbed carbenium ion. The chances of a favourable interaction with another propan-2-ol molecule are thereby reduced resulting in increase selectivity towards propene. Alternatively, the presence of the coke could reduce the strength of the acidity of the Brønsted sites, thus making the ether reaction less favourable.

5 Conclusions

The present research has shown that mild hydrothermal dealumination of Y zeolite using a partial pressure of water vapour produces catalysts with a framework aluminium content in the range 28-36 Al_F puc. These catalysts were compared with those produced by dealumination under a 100% steam atmosphere. A gradual progression in the acid content of the catalysts, as measured by the temperature programmed desorption of ammonia, was found to be dependant solely on the temperature of the dealumination process. Extraction of the nonframework material was achieved using an ammonium salt of EDTA. It was found possible to carry out this procedure at an intermediate acidity, high enough to remove the extraframework aluminium into solution, but low enough to prevent breakdown of the zeolite framework.

The catalysts were studied in a modified temperature programmed desorption system which permitted the simultaneous monitoring of the deammoniation, dehydration and dehydroxylation processes. Destruction of hydroxyl groups at elevated temperatures was shown to be directly linked to the reduction in the acidic content of the catalysts. Dealumination was shown to produce hydroxyl groups which dehydroxylate at higher temperatures, thus confirming a shift to higher acidity. In contrast, the presence of extraframework aluminium was seen to reduce the temperature of the maximum rate of dehydroxylation, suggesting that the nonframework material interferes with the acidity of the remaining structural hydroxyl groups. This effect was reduced on the extraction of the majority of the nonframework material. Dehydroxylation energies, which were substantially lower in the extracted catalysts, support the view that nonframework aluminium interacts with and affects the properties of the framework hydroxyl groups.

The catalytic properties of the modified zeolites were investigated by using a series of catalytic reactions which are known to have differing acid site strength requirements. The cracking of n-hexane was confirmed to require acid sites of the highest strength, with catalysts possessing a framework content of $\approx 25Al_F$ puc returning the highest activity. The acid site concentration in these catalysts is similar to that required for the maximum theoretical number of

strong sites, 30 Al_F puc.[77] However, a clear distinction between the mildly dealuminated and strongly dealuminated catalysts was found. Mildly steamed unextracted catalysts of a similar framework aluminium content to the highly active catalysts were found to have a much lower activity than was expected on the basis of their framework content alone. This anomaly lessened on extraction, prompting the suggestion that the nature of the extraframework material depends on the conditions of dealumination. A progression from individual charged species to neutral conglomerates with increasing hydrothermal treatment has been suggested.

More detailed study reveals a change in mechanism on dealumination, and on extraction. The cracking mechanism ratio, cmr, a measure of the relative contributions of the protolytic and hydride transfer reaction pathways, was found to suddenly increase rapidly for highly dealuminated unextracted samples. This increase, which implies progressive dominance of the protolytic pathway, is removed on the extraction of the nonframework material. It is suggested that this is indicative of the hydride transfer process being suppressed by increasingly isolated sites. The removal of extraframework material decreases the isolation of the sites, either by allowing greater access to existing sites, or by the release of sites poisoned by cationic debris. The decrease in the cmr is simultaneous with a dramatic increase in the activity of these catalysts. It is suggested that the low density of strong sites hinders the process of hydride transfer, and thus the chain reaction mechanism. After extraction, far more molecules can be cracked from a similar number of initiation events. This is best exemplified by the highly dealuminated extracted catalysts, where the unhindered progress of the hydride transfer mechanism results in a massive increase in activity over the equivalent unextracted catalysts. This increase is far greater than in the catalysts dealuminated to a lesser extent, as the smaller amount of nonframework aluminium does not isolate as many acid sites. Therefore, it seems probable that in all cases the reaction is initiated by protolytic cracking of the feedstock. Where conditions permit, the reaction continues by hydride transfer and ß-scission steps. In catalysts which cannot support these steps, far fewer feedstock molecules are

converted per initiation step, resulting in an increase in the preponderance of the products of protolytic cracking. This reasoning also accounts for the lack of a direct relationship between the activity and acid site concentration. As the acid sites become increasingly more isolated the chain reaction ceases; below a critical concentration all the products are formed by protolytic cracking, and the activity is so low as to be negligible.

A similar distribution of activity with acid site concentration was found in the study of the disproportionation of toluene, another reaction known to require sites of high acid strength. The distinction in activities between the mildly and strongly steamed samples was again apparent, and was removed on the extraction of the nonframework material. However, an important departure from the behaviour noted in the n-hexane cracking was observed; extraction *reduced* the activity of some of the most active strongly dealuminated catalysts, but increased the activity of the mildly dealuminated catalysts. This was taken as further evidence of the difference in nature of the extrastructural aluminium in the catalysts prepared using different conditions, and that this material plays an important part in the reaction. It is suggested that the presence of extrastructural aluminum has a number of effects:

i) blocking of sites (steric),

ii) interaction with framework acid sites (synergic),

iii) cationic poisoning of framework acid sites (electrostatic).

These effects are respectively detrimental, beneficial and detrimental to the overall activity of the catalysts. Therefore, extraction will have different effects on the activity depending on the amount and nature of the nonframework material present. Increasing the severity of dealumination, both conditions and temperature, causes the effect of the nonframework aluminium to change in nature from iii) to i) above as the degree of agglomeration increases; this change is reflected in the activity changes.

The nature of the toluene disproportionation reaction was found to change during the lifetime of the catalyst. In the very initial stages of the reaction an excess of benzene was noted in the product stream. This was linked to the greater steric hindrance of the dimethylbenzene isomers resulting

in their restricted diffusion from the catalysts, and possibly the existence of a small amount of dealkylation. However, in the continuous flow experiments, a deficiency in the rate of benzene production was noted, which increased as the reaction progressed. This was linked to reactions on the surface of the catalysts, possibly involving ring opening of benzene. When allied to the alkylation of toluene this could account for the observed results. Additional verification of the importance of the surface reactions was provided by the observation that pretreating the catalyst samples with toluene by various methods was found to increase the lifetime of the catalyst. Thus, confirmation was given concerning the important role of coke in this reaction.

The dealkylation of cumene is a less demanding reaction, and is catalysed by weaker sites. Indeed, the activity was found to be directly proportional to the number of acid sites in all catalysts with acid site concentrations below 2.0 mmol g^{-1}; only the very aluminous catalysts had lower activity than would be expected on their acid site concentration alone. The first of these facts suggests that the reaction proceeds on one site, and that there is no favourable effect of adjacent sites. This is in contrast to the results from the n-hexane cracking and toluene disproportionation studies. Extraction of the nonframework material has neither an overtly beneficial nor detrimental effect on the activity; it merely increases the activity to that which would be expected from the acid content alone. The lower than expected values for the two most aluminous catalysts suggest that the weakest sites are not capable of promoting this reaction. This in turn implies that dealumination does not convert weak sites to strong sites without passing through an intermediate strength of acid site. This heterogeneity in acid site strength results from a progressive change in the environment of a particular structural aluminium atom.

The final reaction studied, the dehydration of propan-2-ol, is catalysed by any structural acid site. There is slight evidence to suggest that isolated sites are not as efficient in catalysing this reaction. Study of the rates of formation of the individual products reveals that propene formation indeed proceeds on any site, regardless of strength, but that the formation of

di-isopropylether is favoured by strong sites. This is best exemplified in the change in selectivity with acidity. Increased strength of acidity was proposed to lengthen the lifetime of the carbenium ion on the catalyst surface, creating a greater statistical chance of interaction with another propan-2-ol molecule. This reasoning is the same as used for the coke production in the cumene dealkylation studies. In that instance, the same carbenium ion interacts with a propene molecule, leading to the formation of polymeric species. The dehydration of propan-2-ol was found to be influenced by pretreating the catalyst sample with reactant at various elevated temperatures. The formation of coke, possibly polymeric in nature, dramatically increased the activity of the catalysts, whilst at the same time shifting the selectivity of the reaction almost entirely towards propene.

The present research has shown the necessity of employing more than one catalytic reaction to fully characterise a range of acidic zeolites. The activity of a catalyst for any particular reaction was found to be dependant primarily on the number of acid sites present, and their acidity distribution. However, the importance of extrastructural aluminium, its electronic state, degree of agglomeration and distribution throughout the crystallites, has been emphasised. This material can modify the acidity site strength distribution and the acid site density. It can also effect the transport properties within the catalyst particles. Further structural studies of the preparative methods and their effect on the nature and location of the extraframework aluminium, when combined with catalytic measurements, will help in furthering the understanding of the chemistry involved in this area of heterogeneous catalysis.

References

1 Dyer,A., *An Introduction to Zeolite Molecular Sieves,* London, Wiley, 1988

2 Breck,D.W., *Adv.Chem.Ser.*, 1971, **101**, 1

3 Barrer,R.M., *J.Chem.Soc.*, 1948, 2158

4 Breck,D.W., Eversole,W.G., Milton,R.M., Reed,T.B. and Thomas,T.L., *J.Am.Chem.Soc.,* 1956, **78**, 5963

5 Barrer,R.M., *Zeolites*, 1981, **1**, 133

6 Barrer,R.M. and Denney,P.J., *J.Chem.Soc.*, 1961, 971

7 Whyte,T.E. and Dalla Betta,R.A., *Cat.Rev-Sci.Eng*, 1982, **24**, 567

8 Wilson,S.T., Lok,B.M., Messina,C.A., Cannan,T.R. and Flanigen,E.M., *J.Am.Chem.Soc.,* 1982, **104**, 1146

9 Lok,B.M., Messina,C.A., Patten,R.L., Garek,R.T., Cannan,T.R. and Flanigen E.M., *J.Am.Chem.Soc.*, 1984, **106**, 6092

10 Loewenstein,W., *Am.Mineral*, 1954, **39**, 92

11 Dempsey,E., Kühl,G.H. and Olson,D.H., *J.Phys.Chem.*, 1969, **73**, 387

12 Schroder,K-P. and Sauer,J., *J.Phys.Chem.*, 1993, **97**, 6579

13 Takaishi,T., Kato,M. and Itabashi,K., *J.Phys.Chem.*, 1994, **98**, 5742

14 Feher,F.J., Weller,K.J. and Ziller,J.W., *J.Am.Chem.Soc.*, 1992, **114**, 9686

15 Breck,D.W., *Zeolite Molecular Sieves*, Wiley, 1974

16 Breck,D.W., *J. Chem. Ed,* 1964, **48**, 678

17 Smith,J.V., *Adv.Chem.Ser.*, 1971, **101**, 171

18 Smith,J.V., In: *Zeolite Chemistry and Catalysis*, Rabo,J.A. (ed) *ACS Monongraph*, 1976, **171**, 1

19 Kramer,G.J., de Man, A.J.M. and van Santen, R.A., *J.Am.Chem.Soc.*, 1991, **113**, 6435

20 Kassab,E., Seiti,K. and Allavena,M., *J.Phys.Chem.*, 1988, **92**, 6705

21 Herrero,C.P., *J.Chem.Soc: Faraday Trans.*, 1991, **87**, 2837

22 Bolton,A.P., *Experimental Methods in Catalytic Research. Vol.2*, Anderson,R.P. and Dawson,P.T.,(eds) New York Academic, 1976,1

23 ASTM Handbook, Easton USA, American Society for the Testing of Materials 1989

24 Sohn,J.R., DeCanio,S.J., Lunsford,J.H. and O'Donnell,D.J., *Zeolites*, 1986, **6**, 225

25 Breck,D,W. and Flanigen,E.M., *In: Molecular Sieves*, Barrer,R.M.,(ed) London: Soc Chem.Ind., 1968, 47

26 Beyer,H.K., Belenykaja,I.M., Hange,F., Tielen,M., Grobet,P.J. and Jacobs, P.A., *J.Chem.Soc: Faraday Trans.*, 1985, **81**, 2889

27 Kerr,G.T., *Zeolites*, 1989, **9**, 350

28 Fritz,P.O., Lunsford,J.H. and Fu,C-M., *Zeolites*, 1988, **8**, 205

29 Rubio,J.A., Soria,J. and Cano,F.H., *J.Coll.Int.Sci.*, 1980, **73**, 313

30 Anderson.M.W. and Klinowski,J., *J.Chem.Soc: Faraday Trans I*, 1986, **82**, 1449

31 Kubelková,L., Seidl,V., Borbély,G. and Beyer, H.K., *J.Chem.Soc: Faraday Trans.*, 1988, **84**, 1447

32 Pichat,P., Beaumont, R. and Barthomeuf,D., *J.Chem.Soc: Faraday Trans.*, 1974, **70**, 1402

33 Dutta,P.K. and Twu,J., *J.Phys.Chem.*, 1991, **95**, 2498

34 Brémard,C. and Le Maire,M., *J.Phys.Chem.*, 1993, **97**, 9695

35 Flanigen,E.M., Khatami,H. and Szymanski,H.A., *Adv.Chem.Ser.*, 1971, **101**, 201

36 Flanigen,E., *Adv.Chem.Ser.*, 1976, **171**, 80

37 de Man,A.J.M. and van Santen,R.A., *Zeolites*, 1992, **12**, 269

38 Datka,J., Geerlings,P., Mortier,W. and Jacobs,P., *J.Phys.Chem.*, 1985, **89**, 3483

39 Smirnov,K.S. and Bougeard,D., *J.Phys.Chem.*, 1993, **97**, 9434,

40 Datka,J., Geerlings,P., Mortier,W. and Jacobs,P., *J.Phys.Chem.*, 1985, **89**, 3488

41 Dwyer,J., Fitch,F.R., Machado,F., Qin,Q., Smyth,S.M. and Vickerman,J.C., *J.Chem.Soc: Chem.Comm*, 1981, 422

42 Choi-Feng,C., Hall,J.B., Huggins,B.J. and Beyerlein,R.A., *J.Catal*, 1993, **140,** 395

43 Klinowski,J., Thomas,J.M., Audieer,M., Vasadevan,S., Fyfe,C. and Hartman,J., *J.Chem.Soc: Chem.Comm*, 1981, 570

44 Lippmaa,E., Mägi, M., Samoson,A., Engelhardt,G. and Grimmer,A.R., *J.Am.Chem.Soc.*, 1980, **102**, 4889

45 Kokotailo,G.T., Fyfe,C.A., Gobbi,G.C., Kennedy,G.J., Deschutter,C.T., Ozubko,R.S. and Murphy,W.J., In: *Zeolites*, Drzaj,B., Hocevar,S. and Pejovnik,S. (eds), *Stud.Surf.Sci.Catal.*, 1985, **24**, 219

46 Nagy,J.B. and Derouane,E.G., *Perspectives in Molecular Sieve Science*, *ACS Symposium Series*, 1988, **368**, Chp.1

47 Thomas,J.M., Klinowski,J., Ramdas,S., Anderson,M.W., Fyfe,C.A. and Gobbi,G.C., In: *Intrazeolite Chemistry*, Stucky,G.D., and Dwyer,F.G., eds, *ACS Symposium Series* 1983, **218**, 159

48 Lippmaa,E., Mägi,M., Samoson,A., Tamarak,M. and Engelhardt,G.,*J.Am.Chem.Soc.*, 1981, **103**, 4992

49 Thomas,J.M. and Klinowski,J., *Adv.Catal.*, 1985, **33**, 199

50 Ramdas,S., Thomas,J.M., Klinowski,J., Fyfe,C.A. and Hartman,J.S., *Nature*, 1981, **292**, 228

51 Klinowski,J., Ramdas,S., Thomas,J.M., Fyfe,C.A. and Hartman,J.S., *J.Chem.Soc: Faraday Trans II*, 1982, **7**,1025

52 Newsam,J.M., *J.Phys.Chem.*, 1985, **89**, 2002

53 Grobet,P.J., Geerts,H., Martens,J.A. and Jacobs,P.A., *J.Chem.Soc: Chem.Comm*, 1987, 1688

54 Kobe,J.M., Gluszak,T.J. Dumesic,J.A., and Root,T.W., *J.Phys.Chem.*, 1995, **99**, 5485

55 Ghosh,A. and Curthoys,G., *J.Chem.Soc: Faraday Trans I*, 1984, **80**, 99

56 Ward,J.W., In: *Zeolite Chemistry and Catalysis*, Rabo,J.A. (ed) *ACS Monongraph*, 1976, **171**, 118

57 Mirodatos,C., Pichat,P. and Barthomeuf,D., *J.Phys.Chem.*, 1976, **80**, 1335

58 Otsuka,K., Wada,Y., Tanaka,K. and Morkawa,A., *Bull.Chem.Soc.Jpn*, 1979, **52**, 3443

59 Angell,C.L. and Howell,M.V., *J.Phys.Chem.*, 1970, **74**, 2737

60 Rhodes,N.P. and Rudham,R., *J.Chem.Soc: Faraday Trans.* 1994, **90**, 809

61 Larsen,J.G. and Hall,W.K., *J.Am.Chem.Soc.,* 1968, **90**, 851

62 Angell,C.L. and Schaffer,P.C., *J.Phys.Chem.*, 1965, **69**, 3463

63 Eberly,P.E. *J.Phys.Chem.*, 1967, **71**, 1717

64 Ward,J.W., *J.Phys.Chem.*, 1968, **72**, 4211

65 Jacobs,P.A. and Uytterhoeven,J.B., *J.Chem.Soc: Faraday Trans.*, 1973, **69**, 359

66 Janin, A., Lavalley,J.C., Macedo,A., Raatz,F., In: *Perspectives in Molecular Sieve Science, ACS Symposium Series*, 1988, **368**, 117

67 Gil,B., Broclawik,E.,Datka,J. and Klinowski,J., *J.Phys.Chem.*, 1994, **98**, 930

68 Ward,J.W., *J.Catal*, 1968, **10**, 34

69 Hughes,T.R. and White,H.M., *J.Phys.Chem.*, 1967, **71**, 2192

70 Ward,J.W., *J.Catal*, 1967, **9**, 225

71 Eberly,P.E., *J.Phys.Chem.*, 1968, **72**, 1042

72 Parker,L.M., Bibby,D.M. and Burns,G.R., *J.Chem.Soc: Faraday Trans.*, 1991, **87**, 3319

73 Batamack,P., Doremieux-Morin,C., Vincent,R. and Fraissard,J. *J.Phys.Chem.*, 1993, **97**, 9779

74 Dempsey,E., *J.Catal.*, 1974, **33**, 497

75 Dempsey,E., *J.Catal.*, 1975, **39**, 155

76 Mikovsky,R.J. and Marshall,J.F., *J.Catal*, 1976, **44**, 170

77 Beagley,B., Dwyer,J., Fitch,F.R., Mann,R. and Walters,J., *J.Phys.Chem.*, 1984, **88**, 1744

78 Kramer,G.J. and van Santen,R.A., *J.Am.Chem.Soc.* 1993, **115**, 2887

79 Dombrowski,D., Hoffmann,J. and Fruwert,J., *J.Chem.Soc: Faraday Trans.I,* 1985, **81**, 2257

80 Datka,J. and Gil,B., *J.Catal*, 1994, **145**, 372

81 Makarova,M.A. and Dwyer, J., *J.Phys.Chem.*, 1993, **97**, 6337

82 Lunsford,J.H., *J.Phys.Chem.*, 1968, **72**, 4163

83 Mirodatos,C. and Barthomeuf,D., *J.Chem.Soc: Chem.Comm*, 1981, 39

84 Beyerlein,R.A., McVicker,G.B., Yacullo,L.N. and Ziemak,J.J., *J.Phys.Chem.*, 1988, **92**, 1967

85 Lónyi,F. and Lunsford,J.H., *J.Catal*, 1992, **136**, 566

86 Sherry,H.S., *Adv.Chem.Ser.*, 1971, **101**, 350

87 Cremers,A., In: *Molecular Sieves II,* Katzer,J.R., (ed) *ACS Symposium Series* 1977, **40**, 179

88 Townsend,R.P., *Chemistry and Industry,* 1984, 246

89 Gallezot,P. and Imelik,B., *Adv.Chem.Ser.,* 1973, **121**, 66

90 Lai,P.P. and Rees,L.V.C., *J.Chem.Soc: Faraday Trans.,* 1976, **72**, 1827

91 Ozin,G.A., Baker,M.D., Godber,J. and Gil,C.J., *J.Phys.Chem.*, 1989, **93**, 2899

92 Ozin,G.A., Baker,M.D., Helwig,K. and Godber,J., *J.Phys.Chem.*, 1985, **89**, 1846

93 Edgell,M.J., Paynter,R.W., Mugford,S.C. and Castle,J.E., *Zeolites*, 1990, **10**, 51

94 Jelinek,R., Özkar,S. and Ozin,G.A., *J.Am.Chem.Soc.,* 1992, **114**, 4907

95 Verhulst,H.A.M., Welters,W.W.J., Vorbeck,G., van de Ven,L.J.M., de Beer,V.H.J., van Santen,R.A. and de Haan,J.W., *J.Phys.Chem.*, 1994, **98**, 7056

96 Verhulst,H.A.M., Welters,W.W.J., Vorbeck,G., van de Ven,L.J.M., de Beer,V.H.J., van Santen,R.A. and de Haan,J.W., *J.Chem.Soc: Chem.Comm*, 1994, 639

97 Welsh,L.B. and Lambert,S.L. *Perspectives in Molecular Sieve Science, ACS Symposium Series*, 1988, **368**, 33

98 Harjula,R., Dyer,A., Pearson,S.D. and Townsend,R.P., *J.Chem.Soc: Faraday Trans.I*, 1992, **88**, 1591

99 Naccache,C. and Tarrit,Y.B., *ACS Symposium Series,* 1977, **40**, 156

100 Schmidt,F., Gurnsser,W. and Adolph,J., In: *Molecular Sieves II* Katzer,J.R., (ed) *ACS Symposium Series*, 1977, **40**, 291

101 Bremmer,H., Morke,W., Schodel,R. and Vogt,F., *Adv.Chem.Ser.,* 1973, **121**, 249

102 Augul,N.N., Bezus,A.G. and Dzhigit,D.M., *Adv.Chem.Ser.*, 1971, **102**, 184

103 Tsutumi,K., Fuji,S. and Takahasi,H., *J.Catal*, 1972, **24**, 8

104 Tsutumi,K., Fuji,S. and Takahasi,H., *J.Catal*,1972, **24**, 146

105 Hansford,R.C. and Ward,J.W., *Adv.Chem.Ser*, 1971, **102**, 354

106 Ward,J., *Adv.Chem.Ser.*, 1971, **101**, 380

107 Freude,D., Oehme,W., Schmiedel,H., Staudte,B., *J.Catal*, 1974, **32**, 137

108 Uytterhoeven,J.B., Christner,L.G. and Hall,W.K., *J.Phys.Chem.*,1965, **69**, 2117

109 Bosáček,V., Freude,D., Frohlich.T, Pfiefer,H. and Schiedel,H. *J.Coll.Int.Sci.*, 1982, **85**, 502

110 Kühl,G.H., In: *Molecular Sieves*, Uytterhoeven,J.B.,(ed), Leuven University Press, 1973, 277

111 Datka,J., *J.Chem.Soc: Faraday Trans.*, 1981, **77**, 2877

112 Ward,J., *J.Catal*, 1968, **11**, 251

113 Jacobs,P.A. and Beyer,H.K., *J.Phys.Chem.*,1979, **83**, 1174

114 Bosáček,V. and Freude,D., In: *Innovations in Zeolite Material Science*, Grobet,P.J., Mortier,W.J., Vansant,E.F. and Schulz-Ekloff,G., (eds), *Stud.Surf.Sci.Catal.*, 1988, **37**, 231

115 Freude,D., Froühlich,T., Hunger,M., Pfeifer,H. and Scheler,G., *Chem.Phys.Lett.* 1983, **98**, 263

116 Cattanach,J., Wu,E.L. and Venuto,P.B., *J.Catal*, 1968, **11**, 342

117 Wang,Q.L., Giannetto,G., Torrealba,M., Perot,G., Kappenstein,C. and Guisnet,M., *J.Catal*, 1991, **130**, 459

118 Jacobs,P. and Uytterhoeven,J., *J.Chem.Soc.Faraday Trans.I*, 1973, **69**, 373

119 Uytterhoeven,J.B., Jacobs,P.A., Makay,K. and Schoonheydt,R., *J.Phys.Chem.*, 1968, **72**, 1768

120 Maher,P.K., Hunter,F.D. and Scherzer,J., *Adv.Chem.Ser.*, 1971, **101**, 266

121 Lohse,U., Löffler,E., Hunger,M., Stöckner,J. and Patzelovà,V., *Zeolites*, 1987, **7**, 11

122 Ward,J., *J.Catal*, 1967, **9**, 326

123 Delprato,F., Guth,J., Huve,L. and Delmotte,L., *Zeolites*, 1990, **10**, 546

124 Newsam,J.M., Treacy,M.M., Vaughan,D.E.W., Strochemaier,K.J., and Mortier,J., *J.Chem.Soc: Chem.Comm*, 1989, 493

125 Barrer,R.M. and Coughlan,B., In: *Molecular Sieves*, Barrer,R.M., (ed) London: Soc Chem.Ind., 1968, p141

126 Barrer,R.M. and Makki,M.B., *Can.J.Chem.*, 1964, **42**, 1481

127 Kerr,G.T., *J.Phys.Chem.*, 1968, **72**, 2594

128 Kerr,G.T., *J.Phys.Chem.*, 1969, **73**, 2780

129 Beaumont,R. and Barthomeuf,D., *J.Catal*, 1972, **27**, 45

130 Corma,A., Fornés,V., Kolodziejski,W. and Martinéz-Triguero,L.J., *J.Catal*, 1994, **145**, 27

131 Kerr,G.T., *J.Catal*, 1969, **15**, 200

132 Kerr,G.T., *J.Phys.Chem.*, 1967, **71**, 4155

133 McDaniel,C.V. and Maher,M.K., In: *Molecular Sieves*, Barrer,R.M.,(ed) London: Soc Chem.Ind., 1968, 186

134 Ward,J.W., *J.Catal*, 1972, **27**, 157

135 Gallezot,P., Beaumont,R. and Barthomeuf,D. *J.Phys.Chem.*,1974, **78**, 1550

136 Vedrine,J.C., Abou-Kais,A., Massardier,J. and Dalmai-Imelik,G., *J.Catal*,1973, **29**, 120

137 Chen.N.Y., Mitchell,T.O., Olson,D.H. and Peirine,B.P., *Ind.Eng.Chem.Prod.Res.Dev.*, 1977, **16**, 247

138 Van Brockhoven,E.H., Daamen,S., Smeink,R.G., Wijngaards,H. and Nieman,J., In: *Zeolites: Facts, Figures, Future.*, Jacobs,P.A. and van Santen,R.A., (eds) *Stud.Surf.Sci.Catal.*, 1988, **49**, 1291

139 Bodart,P., Nagy,J.B., Debras, G. and Jacobs, P.A. and Gabelica,Z. *J.Phys.Chem.*, 1986, **90**, 5183

140 Pelemenschikov,A.G., Paukshtis,E.A., Edisherasvili,M.O. and Zhidomirov,G.M., *J.Phys.Chem.*,1992, **96**, 7051

141 Sulikowski,B. and Klinowski,J., *J.Chem.Soc: Faraday Trans.*, 1990, **86**, 199

142 Englehardt,G., Lohse,U., Patzelová,V., Mägi,M. and Lippmaa,E., *Zeolites*, 1983, **3**, 233

143 Gregg,S.J. and Sing, K.S.W., *Adsorption, Surface Area and Porosity*, Ac.Press London, 1982

144 Mange,F., Auroux,A., Couridle,J.C., Englehard,P., Gallezot,P. and Grossmangin,J., In: *Catalysis by Acids and Bases* ,Imelik,,B., Naccache,N., Coudurier,G., Ben Taarit,Y. and Vedrine,J.C.,(eds) *Stud.Surf.Sci.Catal.*, 1985, **20**, 91

145 Beyer,H.K. and Belenykaja,I., In: *Catalysis by Zeolites*, Imelik,,B., Naccache,N., Ben Taarit,Y., Vedrine,J.C., Coudurier,G. and Praliaud,H., (eds) *Stud.Surf.Sci.Catal.*, 1980, **5**, 203

146 Klinowski,J., Thomas, J.M., Fyfe,C.A. and Gobbi,G.C., *Nature*, 1982, **296**, 533

147 Klinowski,J., Thomas,J.M., Gobbi,G.C. and Hartman.J.S., *Inorg.Chem.*, 1983, **22**, 63

148 Grobet,P.J., Jacobs,P.A. and Beyer,H.K., *Zeolites*, 1986, **6**, 47

149 Anderson, M.W. and Klinowski,J., *Zeolites*, 1986, **6**, 455

150 Martens,J.A., Geerts,H., Grobet,P.J. and Jacobs,P.A., *J.Chem.Soc: Chem.Comm*, 1990, 1418

151 Shertukde,P.V., Hall,W.K., Dereppe,J-M. and Marcelin,G., *J.Catal*, 1993, **139**, 468

152 Skeels,G.W. and Breck,D.W., *Proc 6th Int. Zeolite Con.*, Olson,D.H. and Bisio,A, (eds), Butterworth, 1984, 87

153 Neuber,M., Dondur,V., Karge,H.G., Pacheo,L., Ernst,S. and Weitkamp,J. In: *Innovation in Zeolite Materials Science,* Grobet,P.J., Morteir,W.J., Vansant,E.F. and Schulz-Ekloff,G., (eds) *Stud.Surf.Sci.Catal.*, 1988, **37**, 461

154 Garralón,G., Fornés,V. and Corma,A., *Zeolites*, 1988, **8**, 268

155 Wang,Q.L., Giannetto,G. and Guisnet,M., *Zeolites*, 1990, **10**, 301

156 Chauvin,B., Boulet,M., Massiani,P., Fajula,F., Figueras,F., and Des Courières,T., *J.Catal.*, 1990, **126**, 532

157 He,Y., Li,C. and Min,E., In: *Zeolites: Facts, Figures, Future.*, Jacobs,P.A. and van Santen,R.A., (eds) *Stud.Surf.Sci.Catal.*, 1988, **49**, 189

158 Kerr,G.T., *Adv.Chem.Ser.*, 1973, **121**, 219

159 Scherzer,J., *ACS Symposium Series*, 1984, **248**, 157

160 Klinowski,J., *J.Chem.Soc: Faraday Trans I*, 1985, **81**, 3003

161 Bosáček,V. and Mastikhin,V.M., *J.Phys.Chem.*, 1987, **91**, 260

162 Gilson,J.P., Peters,A.W., Rajagopalan,K., Wormsbecher,R.F., Roberie,T.G. and Shatlock,M.P., *J.Chem.Soc: Chem.Comm*, 1987, 91

163 Samoson,A., Lippmaa,E., Englehardt,G., Lohse,U. and Jersachkewitz, H.G., *Chem.Phys.Lett.*, 1987, **134**, 589

164 Sanz,J., Fornes,V. and Corma,A., *J.Chem.Soc: Faraday Trans.I,* 1988, **84**, 3113

165 Peri,J.B., In: *Proc. 5th Int.Cong.Cat.*, Hightower,J.W.(ed), London, North Holland, 1973, 329

166 Haddix,G.W., Narayana,M., Gillespie,W., Georgellis,M. and Wu.Y., *J.Am.Chem.Soc.,* 1994, **116**, 672

167 Yang,X., *J.Phys.Chem.*, 1995, **99**, 1276

168 Patzelová,V., Drahorádová,E., Tvaruzková,Z. and Lohse,U., *Zeolites*, 1989, **9**, 74

169 Jacobs,P.A. and Uytterhoeven,J., *J.Catal*, 1971, **22**, 193

170 Garralón,G., Corma,A. and Fornés,V., *Zeolites*, 1989, **9**, 84

171 Fritz,P.O. and Lunsford,J.H., *J.Catal*, 1989, **118**, 85

172 Fleisch,T.H., Meyers,B.L., Ray,G.J., Hall,J.B. and Marshall,C.L., *J.Catal*, 1986, **99**, 117

173 Corma,A., Meto,F.V. and Rawlence,D., *Zeolites*, 1992, **12**, 264

174 Dwyer,J., Fitch,F.R., Qin,Q., Vickerman,J.C., *J.Phys.Chem.*, 1982, **86**, 4574

175 Addison,S.W., Cartlidge,S., Harding,D.A. and McElhiney,G., *Applied Catalysis*, 1988, **45**, 307

176 Rhodes,N.P. and Rudham,R., *J.Chem.Soc: Faraday Trans,* 1993, **89**, 2551

177 Shannon,R.D., Gardner,K.H., Staley,R.H., Bergeret,G., Gallezot,P. and Auroux,A., *J.Phys.Chem.*,1985, **89**, 4778

178 Chevreau,T., Chambellan, A., Lavalley,J.C., Catherine,E., Marzin,M., Janin,A., Hémidy,J.F. and Khabtou,S., *Zeolites*, 1990, **10**, 226

179 Dwyer,J., Karim,K., Smith,W.S., Thompson,N.E., Harris,R.K. and Apperley,D.C., *J.Phys.Chem.*, 1991, **95**, 8826

180 Wiesz,P.B., *Pure and Applied Chemistry*, 1980, **52**, 2091

181 Corma,A., Miguel,P.J., Orchillés,A.V. and Koermer,G., *J.Catal*, 1992, **135**, 45

182 Corma,A., Miguel,P.J., Orchillés,A.V. and Koermer,G., *J.Catal*, 1994, **145**, 181

183 Kaeding,W.W., *J.Catal*, 1989, **120**, 409

184 Jacobs,P.A., *Carboniogenic Activity of Zeolites*, Elsevier, Amsterdam, 1977

185 Venuto,P.B. and Landis,P.S., *Adv. Catal.*, 1968, **18**, 259

186 Gentry,S.J. and Rudham,R., *J.Chem.Soc. Faraday Trans.I,* 1974, **70**, 1685

187 Rudham,R., Spiers,A. and Winstanley,A., *Zeolites*, 1991, **11**, 850

188 Groten,W.A. and Wojciechowski,B.W., *J.Catal*,1990, **122**, 362

189 Groten,W.A., Wojciechowski,B.W. and Hunter B.K.,*J.Catal* 1990, **125**, 311

190 Chevalier,F., Guisnet,M. and Manrel,R., *Proc. 6th Int.Cong.Cat.*, Bond,G.C., Wells,P.B., Tomkins,F.C., (eds) Pub. C.S. London. 1977, 478

191 Jacobs,P.A., Declerck,L.J., Vandamme,L.J., and Uytterhoeven,J.B., *J.Chem.Soc.Farad.Trans.I*, 1975, **71**, 1545

192 Pines,H., *J.Catal*, 1986, **78**, 1

193 Weeks, T.J. and Bolton,A.P., *J.Chem.Soc.Farad.Trans.I*, 1974, **70**, 1676

194 Haw,J.F., Richardson,B., Oshiro,I., Lazo,N. and Speed,J., *J.Am.Chem.Soc.*, 1981, **111**, 2052

195 Langer,B.E., *Ind.Eng.Chem.Prod.Des,Rev.*, 1981, **20**, 326

196 Ghosh,A.K. and Kydd,R.A., *J.Catal*, 1985, **100**, 185

197 White,J.L., Lazo,N.D., Richardson,B.R. and Haw,J.F., *J.Catal*, 1990, **125**, 260

198 Kaeding,W.W. and Holland,R.E., *J.Catal*, 1988, **109**, 212

199 Weeks, T.J. Bolton,A.P., Angell,C.L. and Ladd,I.R., *J.Catal*, 1974, **33**, 256

200 Venuto,P.B., *Ad.Chem.Ser.*, 1971, **102**, 260

201 Rhodes,N.P., *Ph.D.Thesis*, Nottingham University. 1991

202 Corma,A. and Wojciechowski,B.W., *Catal. Rev.-Sci.Eng.*, 1982, **24**, 1

203 Wang,K.M. and Lunsford,J.H., *J.Catal*, 1972, **24**, 262

204 Benesi,H.A., *J.Catal*,1967, **8**, 368

205 Karge,H.G., Hatada,K., Zhang,Y. and Fedorow,R., *Zeolites*, 1983, **3**, 3

206 Karge,H., Ladebeck,J., Sarbak,Z. and Hatada,K., *Zeolites,* 1982, **2**, 94

207 Neuber,M., Dondur,V., Karge,H.G., Pacheo,L., Ernst,S. and Weitkamp,J., In: *Innovation in Zeolite Material Science*, Eds. Grobet,P.J., Mortier,W.J., Vansant,E.F. and Schulz-Ekloff,G., *Stud.Surf.Sci.Catal.* 1988, **37**, 461

208 DeCanio,S.J., Sohn,J.R., Fritz,P.O. and Lunsford,J.H., *J.Catal*, 1986, **101**, 132

209 Absil,R.P.L., Butt,J.B. and Dranoff,J.S. *J.Catal*, 1985, **95**, 220

210 Absil,R.P.L., Butt,J.B. and Dranoff,J.S. *J.Catal*, 1984, **85**, 415

211 Brown,H.C. and Smoot,C.R., *J.Am.Chem.Soc.,* 1956, **78**, 2176

212 Hopkins,P.D., *J.Catal*, 1968, **12**, 325

213 Anderson,M.W., Klinowski,J., Thomas,J.M. and Barlow,M.T. *J.Chem.Soc.Faraday.Trans.*, 1989, **85**, 1945

214 Sohn,J.R., DeCanio,S.J., Fritz,P.O. and Lunsford,J.H., *J.Phys.Chem.*, 1986, **90**, 4847

215 Kramer,G.M., McVicker,G.B. and Ziemiak,J.J., *J.Catal*, 1985, **92**, 355

216 Abbot,J. and Wojciechowski,B.W., *J.Catal*, 1989, **115**, 1

217 Wielers,A.F.H., Vaarkamp,M. and Post,M.F.M., *J.Catal*, 1991, **127,** 51

218 Riekert,L. and Zhou,J-Q., *J.Catal*, 1992, **137**, 437

219 Groten,W.A. and Wojciechowski,B.W., *J.Catal*, 1993, **140**, 262

220 Shendye,R.V. and Rajahyaksha,R.A., *Chem.Eng.Sci.*, 1992, **47**, 661

221 Hammon,U., Kokotailo,G.T., Riekert,L. and Zhou,J-Q., *Zeolites*, 1988, **8**, 338

222 Bassir,M. and Wojciechowski,B.W., *J.Catal*, 1994, **150**, 1

223 Abbot,J. and Wojciechowski,B.W. *Can.J.Chem.Eng.*, 1988, **66**, 825

224 Weisz,P.B. and Miale,J.N., *J.Catal*, 1965, **4**, 527

225 Miale,J.N., Chen,N.Y. and Weisz,P.B., *J.Catal*, 1966, **6**, 278

226 In: *Selected Mass Spectroscopy Data*, Thermodynamic Research Centre, Texas A and M University, 1974

227 Nock,A., *Ph.D.Thesis*, Nottingham University. 1985

228 Winstanley,A., *Ph.D.Thesis*, Nottingham University. 1992

229 Cvetanovic,R. and Amenomiya,Y., *Cat.Rev.*, 1972, **6**, 21

230 Hunger,M., Freude,D., Pfeifer,H., *J.Chem.Soc.Faraday Trans.*, 1991, **87**, 657

231 Kubelková,L., Dudihová,L., Bastl,Z., Borbély,G. and Beyer,H., *J.Chem.Soc.Faraday Trans,* 1987, 83, 511

232 Niwa,M., Iwanoto,M. and Segawa,K., *Bull.Chem.Soc.Jpn,* 1986, **59**, 3735

233 Lok,B.M., Markus,B.K. and Angell,C.L., *Zeolites,* 1986, **6,** 185

234 Dima,E. and Rees, L.V.C. *Zeolites*, 1990, **10**, 8

235 Chadanai,N. and Romanowskii,B., *Kin.Katal*, 1980 , **23**, 677

236 Hidalgo,V.C., Itoh,H., Hattori,T., Niwa,N. and Murakami,Y., *J.Catal*, 1983, **85**, 362

237 Chu,P., *J.Catal*, 1976, **43**, 346

238 Mavrodinova,V., Penchev,V., Lohse,U. and Gross,T., *Zeolites*, 1989, **9,** 203

239 Miessner,H., Kosslick,H., Lohse,U., Parlitz,B., and Tuan,V., *J.Phys.Chem.*, 1993, **97**, 9741

240 Karge,H., Dondur,V. and Weitkamp,J., *J.Phys.Chem.*, 1991, **95**, 283

241 Guimon,C., Zouiten,A., Boreave,A., and Pfister-Guillouzo,G., Schulz,P., Fitoussi,F. and Quet,C., *J.Chem.Soc.Faraday Trans.*, 1994, **90**, 3461

242 Malet,P., In: *Chemisorbtion of Probe Molecules*, *Stud.Surf.Sci.Catal.*, 1990, **57B,** 333

243 Auroux,A., Boris,V., Védrine,J., Gravelle,P., Wierzchowshi,P., Derouane,E, Nagy,N., Gilson,J., van Hooff,J., van den Berg,J. and Wolthuizen,J., *J.Chem.Soc.Faraday Trans.*, 1978, **75**, 2544

244 Védrine,J.C, Auroux,A., Bolis,V., Defaifve,P., Naccache,C., Wierzchowski,P., Derouane,E.G., Nagy,J.B., Gilson,J-P., van Hooff,J.H.C., van der Berg,J.P., and Wolthuizen,J., *J.Catal*,1979, **59**, 248

245 Hacul,D. and Brenner,A., *J.Catal*, 1979, **56,** 134

246 Dima,E., and Rees,L.V.C., *Zeolites*, 1987, **7**, 219

247 Wang,Q.L., Giannetto, G. and Guisnet,M., *J.Catal.,* 1991, **130**, 471

248 Corma,A., Faraldos,M., Martinez,A. and Mifsud,A., *J.Catal*, 1990, **122**, 230

249 Pine,L.A., Maher, P.J. and Wachter,W.A., *J.Catal*, 1984, **85**, 466

250 Englehardt,J. and Hall,W.K., *J.Catal,* 1990, **125**, 472

251 Biaglow,A.I., Parrillo,D.J., Kokotailo,G.T. and Gorte,R.J. *J.Catal*, 1994, **148**, 213

252 Lombardo,E.A., Sil,G.A. and Hall,W.K., *J.Catal,* 1989, **119**, 426

253 Haag,W.O., Lago,R.M. and Weisz,P.B. *Nature*, 1984, **309**, 589

254 Tsutsumi,K., Kajiwara,H. and Takahashi,H., *Bull.Chem.Soc.Jpn.*, 1974, **47**, 801

255 Mota,C.J.A., Nogeuria,L., Menezes,S.C., Alekstich,V., Pereira,R.C.L. and Kover,W.B., In: *New Frontiers in Catalysis*, Guczi,L., *et al* (eds), *Stud.Surf.Sci.Catal,* 1993, **75**, 463

256 Hattori,H., Takahashi,O., Takagi,M. and Tanabe,K., *J.Catal,* 1981, **68**, 132

257 Haag,W,O. and Dessau,R.M., In: *"Proc.8th Int.Cong.Catalysis"*, 1984, **2**, 309, Varlag Chemie Winheim

258 Corma,A., Planelles,J., Sanchez-Marin,J. and Tomas,F., *J.Catal*, 1985, **93**, 30

259 Marczewski,M., *J.Chem.Soc.Faraday Trans I*, 1986, **82**, 1687

260 Abbot,J. and Head,J.D., *J.Catal*, 1990, **125**, 187

261 Abbot,J., *App.Catal*, 1990, **57**, 105

262 Lombardo,E.A., Pierantozzi,R. and Hall,W.K. *J.Catal,* 1988, **110**, 171

263 Xu.T., Munson,E.J. and Haw,J.F., *J.Am.Chem.Soc.*, 1994, **116**, 1962

264 Xu,T. and Haw,J.F., *J.Am.Chem.Soc.*, 1994, **116**, 10188

265 Umansky,B., Englehardt,J. and Hall,W.K., *J.Catal*, 1991, **127**, 128

266 Sommer,J., Hachoumy,M., Garin,F. and Barthomeuf,D., *J.Am.Chem.Soc.*, 1994, **116**, 5491

267 Sommer,J., Hachoumy,M., Garin,F. and Barthomeuf,D., *J.Am.Chem.Soc.*, 1994, **117**, 1135

268 Mota C.J.A., Nogueira,L., Kover,B., *J.Am.Chem.Soc.,* 1992, **114**, 1121

269 Mota C.J.A. and R.L.Martins, *J.Chem.Soc.Chem.Comm.*, 1991, 171

270 Pansing,W.F., *J.Phys.Chem.*,1965, **69**, 392

271 Anufriev,D.M., Kuznetsov,P.N. and Ione,K.G., *J.Catal*, 1980, **65**, 221

272 Abbot,J. and Wojciechowski,B.W., *J.Catal*, 1987, **104**, 80

273 Magnotta,V.L. and Gates,B.C., *J.Catal*, 1977, **46**, 266

274 Shendye,R.V. and Rajadhyaksha,R.A., *Chem.Eng.Sci*, 1992, **47**, 661

275 Nace,D.M., *Ind.Eng.Chem.Prod.Res.Dev.*, 1969, **8**, 24

276 Shertukde,P.V., Marcelin,G., Sill,G.A. and Hall,W.K., *J.Catal.*, 1992, **136**, 446

277 Gerberich,H.R., Larson,J.G. and Hall,W.K., *J.Catal*, 1965, **4**, 523

278 Ozaki,A. and Kimura,K., *J.Catal*, 1964, **3**, 395

279 Haag,W.O., LagoR.M. and Wiesz,P.O., *Faraday Disc*, 1981, **72,** 317

280 Lukyanov,B.D., *J.Catal*,1994, **147**, 494

281 Lukyanov,D.B., *J.Catal*, 1994, **145**, 54

282 Zhao,Y., Bamwenda,G.R. and Wojciechowski,B.W., *J.Catal*, 1993, **142**, 465

283 McVicker,G., Kramer,G.M. and Ziemiak,J.J., *J.Catal*, 1983, **83**, 286

284 Wojceichowski,B.W. and Bassir,M.M., *J.Catal*, 1994, **147**, 352

285 Lombardo,E.A., Hall,W.K., *J.Catal*, 1988, **112**, 565

286 Corma,A., Martinez,A. and Martinez,C., *J.Catal*, 1994, **146**, 185

287 Derouane,E.G., In: *Catalysis by Acids and Bases.* Imelik,B., Naccache,C., Coudurier,G., Ben Taarit,Y. and Vedrine,J.C. (eds.) *Stud.Surf.Sci.Catal,* 1985, **20**, 221

288 Kubelková,L., Beran,S, Malecka,A., Mastikhin,V.M., *Zeolites*, 1989, **9,** 12

289 Macedo,A, Auroux,A. Raatx,F., Jacquinot,E. and Boulet,R. In: *Perspectives in molecular sieve science, ACS Symposium Series*, 1988, **368**,

290 Bamwenda,G.R., Zhao,Y.X. and Wojciechowski,B.W., *J.Catal*, 1994, **150,** 243

291 Lohse,U., Parlitz,B. and Patzelová,V. *J.Phys.Chem.*, 1989, **93**, 3677

292 Kaeding,W., Chu,C., Young,L.B. and Butter,S.A., *J.Catal*, 1981, **69**, 392

293 Bhasker,G.V. and Do,D.D., *Ind.Eng.Chem.Res.,* 1990, **29,** 355

294 Meshram,N.R., Hedge,S.G., Kulkarmi,S.B. and Ratnasamy P., *App.Catal.,* 1983, **8**, 359

295 Kulkarni,S.B., Kulkarni,S.J., Ratnasamy,P., Hattori,H. and Tanabe,K., *App.Catal.*, 1983, **8**, 43

296 Jacobs,P.A., Leeman,H.E., and Uytterhoeven,J.B., *J.Catal.*, 1974, **33**, 31

297 Csicsery,S. and Hickson,D., *J.Catal*, 1970, **19**, 386

298 Gross,T., Lohse,U., Englehardt,G., Richter,K. and Patzelová,V., *Zeolites*, 1984, **4,** 25

299 Lohse,U., Englehardt,G. and Patzelová,V., *Zeolites*, 1984, **4,** 163

300 Chen,F., Coudurier,G. and Naccache,C., In: *Zeolites: Facts, Figures, Future.,* Jacobs,P.A. and van Santen,R.A., (eds) *Stud.Surf.Sci.Catal.*, 1988, **49**, 1387

301 Chambellan,A., Cherveau,T., Khabtou,S., Marzin,M. and Lavalley,J., *Zeolites,* 1992**, 12**, 306

302 Anderson,J., Dong,Q., Chang,Y. and Western,R., *J.Catal*, 1991, **127**, 113

303 Corma,A. and Wojciechowski,B.W., *Can.J.Chem.Eng.*, 1980, **58**, 620

304 Tsutsumi,K. and Takahashi,H., *J.Catal*, 1972, **24**, 1

305 Zhavoronkov,M.N., Rosolovskaya,E.N. and Topchieva,K.V. *Kinet.Katal.*, 1971, **12**, 672

306 Nock,A. and Rudham.R., *Zeolites*, 1987, **7**, 481

307 Bielanski,A. and Malecka,A., *Zeolites*, 1986, **6**, 249

308 Choudhary,V.R. and Akolekar,D.B., *J.Catal*, 1990, **125**, 143

309 Jacobs,P.A., Leeman,H.E. and Uytterhoeven, J.B., *J.Catal*, 1974, **33**, 17

310 Shauki,M.K., Kuznetsov,O.I., Panchenkov,G.M. and Tolkacheva,E.I., *Kin.I.Kat.*, 1976, **18**, 1583

311 Topchieva,K.V. and T'huoang,H.S., *Kin.I.Kat.*, 1970, **11**, 490

312 Datka,J., Boczar,M. and Gil,B., *Langmuir*, 1993, **9**, 2496

313 Corma,A. and Wojciechowski,B.W., *Catal Rev. Sci Eng.*, 1985, **27**, 29

314 Campbell,D.R., and Wojciechowski,B.W., *J.Catal*, 1971, **20,** 217

315 Rabo,J.A., *Adv.Chem.Ser.*, 1971, **102**, 284

316 Plank,C.J. and Nace,D.M., *Ind.Eng.Chem.*, 1955, **47**, 2374

317 Pansing,W.F. and Malloy,J.B., *Ind.Eng.Chem.Proc.Des.Dev.*, 1965, **4**, 181

318 Best,D. and Wojciechowski,B.W., *J.Catal*,, 1977, **47**, 11

319 Marczewski,M. and Wojciechowski, B.W., *Can.J.Chem.Eng*, 1982, **60**, 617

320 Marczewski,M. and Wojciechowski, B.W., *Can.J.Chem.Eng*, 1982, **60**, 622

321 Pines,H., *The Chemistry of Catalytic Hydrocarbon Conversions*, Academic Press, 1981

322 Wolf,E. and Alfani,F., *Catal.Rev. Sci Eng.*, 1982, **24**, 329

323 Dadyburjor,D.B. and Liu,Z., *Chem.Eng.Sci.*, 1992, **47,** 645

324 Reyes,S.C. and Scriven,L.E., *Ind.Eng.Chem.Res.*, 1991, **30,** 71

325 Bellare,A. and Dadyburjor,D.B., *J.Catal*, 1993, **140**, 510

326 Gryazonova,Z.V., Ermilova,M.M, Tsitsishvili,G.V., Andronikashvili,T.G. and Krupennikova,A.Y., *Kin.Katal*, 1969, **10**, 1336

327 Jacobs,P.A., Tielen,M. and Uytterhoeven,J.B., *J.Catal*, 1977, **50**, 98

328 Levchuk,V.S. and Dzis'ko, V.A., *Kin.Katal.*, 1969, **10**, 124

329 Levchuk,V.S. and Dzis'ko, V.A., *Kin.Katal.*, 1969, **10**, 1289

330 Levchuk,V.S. and Ione,K.J., *Kin.Katal.*, 1971, **13**, 949

331 Topchieva,K.V. and T'huoang,H.S., *Kin.Katal.*, 1973, **14**, 398

332 Topchieva,K.V. and T'huoang,H.S., *Kin.Katal.*, 1973, **14**, 1491

333 Rudham,R. and Stockwell,A., In: *Catalysis by Zeolites*, Imelik,B., Naccache,C., Vedrine,J., Goudurier,G. and Praliaud,H., (eds) *Stud.Surf.Sci.Catal*, 1980, **5**, 113

334 Stockwell,A., *PhD Thesis*, Nottingham University, 1978

335 Hey,M.J., Nock,A., Rudham,R., Appleyard,I.P., Haines,G.A.J., and Harris,R.K., *J.Chem.Soc.Faraday Trans I*,1986, **82**, 2817

Appendix

The programs contained in this appendix are written in the GW-Basic language, and can be run separately or through the menu program.

1 MENU Program

```
10 REM ***** menu program *****
20 SCREEN 9
30 CLS
40 PRINT:PRINT:PRINT:PRINT
50 PRINT TAB(20)"Temperature Programmed Desorption Series"
60 PRINT:PRINT:PRINT:PRINT
70 PRINT TAB(26)"Nick Stanbridge, 1991-1995"
80 TIME$="00:00:00"
90 WHILE TIME$<"00:00:03"
100 WEND
110 CLS
120 PRINT TAB(15)"1  Run a TPD experiment"
130 PRINT:PRINT
140 PRINT TAB(15)"2  Check on the sample temperature"
150 PRINT:PRINT
160 PRINT TAB(15)"3  Integrate a trace"
170 PRINT:PRINT
180 PRINT TAB(15)"4  Differentiate a trace"
190 PRINT:PRINT
200 PRINT TAB(15)"5  Plot a trace"
210 PRINT:PRINT
220 PRINT TAB(15)"6  Subtract one trace from another"
230 PRINT:PRINT
240 PRINT TAB(15)"7  Exit program"
250 PRINT:PRINT
260 PRINT TAB(15)"Chose one number from the above list"
270 REM ***** waiting!!! ******
280 A$=INKEY$:IF LEN(A$)=0 THEN GOTO 270
290 IF ASC(A$)=49 THEN GOSUB 1000
300 IF ASC(A$)=50 THEN GOSUB 3000
310 IF ASC(A$)=51 THEN GOSUB 4500
320 IF ASC(A$)=52 THEN GOSUB 6000
330 IF ASC(A$)=53 THEN GOSUB 7500
340 IF ASC(A$)=54 THEN GOSUB 8500
350 IF ASC(A$)=55 THEN GOTO 500
370 GOTO 270
500 CLS
510 END
```

2 SCAN program

```
1000 '***** tpd scan program *****
1010 CLEAR,60000!
1020 TIME$="00:00:00"
1030 DIM B(501),MS(253)
1040 DIM TP(10),TC(250),FINALAREA(10)
1050 DIM MF(2),ML(2),P(2),K%(2),PF(2),PL(2),PP(2)
1060 DIM K(2),X(2,250),T(2,250),TEMP(300)
1070 GOTO 2220
1080 Q%=0
1090 Y=(FT-IT)/TR/BS/60                    'number of scans
1100 OPEN "o",#2,(B$)
1110 PRINT#2,E$;F$;G$;IT;FT;TR;C$;BS;WT
1120 '
1130 '              Set Up Program to Accept Commands
1140 Z=60000!:BLOAD"AS.BIN",Z              'Load Support Program
1150 DATAOUT=Z:DATAIN=Z+3:STATUS=Z+6   'Set offsets for Calls
1160 AD%=&H500                             'Card Base Address
1170 S=0
1180 TEMP=0
1190  CMD$="F20,PA10000,G0,I1,QS1,QD1,QE,T"'collects data from
      thermocouple
1200 CALL DATAOUT(AD%,CMD$,ST%)
1210 CALL STATUS(AD%,ST%)
1220 IF ST%<>0 THEN 1210
1230 CMD$="PA10000,QI"
1240 CALL DATAOUT(AD%,CMD$,ST%)
1250 CMD$="T"
1260 CALL DATAOUT(AD%,CMD$,ST%)
1270 CALL DATAIN(AD%,D%(0),D%(0),ST%)
1280 TEMP=D%(0)+TEMP
1290 IF S=1 THEN GOTO 1550
1300 CMD$="R00"            'initiates relay
1310 CALL DATAOUT(AD%,CMD$,ST%)
1320 SOUND 300,3
1330 TIME$="00:00:00"
1340 CMD$="R01"
1350 CALL DATAOUT(AD%,CMD$,ST%)
1360 WHILE TIME$<"00:00:00"
1370 WEND
1380 IF R=1 THEN CMD$="F0,PA10000,G0,I0,QS200,QD2,QE,T" ELSE
      CMD$="F0,PA10000,G1,I0,QS200,QD2,QE,T" 'collects data from mass
      spec
1390 '
1400 CALL DATAOUT(AD%,CMD$,ST%)            'Send Output
1410 '
1420 '                Wait for Process to Complete
```

```
1430 CALL STATUS(AD%,ST%)                    'Ask for Card Status
1440 IF ST%<>0 GOTO 1430
1450 CMD$="PA10000,QI"
1460 CALL DATAOUT(AD%,CMD$,ST%)
1470 FOR I=1 TO 200                          'read data from card
1480 CMD$="T"
1490 CALL DATAOUT(AD%,CMD$,ST%)
1500 CALL DATAIN(AD%,D%(0),D%(0),ST%)
1510 W=D%(0)
1520 MS(I)=D%(0)
1530 NEXT
1540 S=1:GOTO 1190
1550 '***** peak identification and integration program *****
1560 ' REM to identify start and end of peaks
1570 Y%=0
1580 FOR A = 1 TO 2
1590 Y%=Y%+1
1600 IF Y%>200 THEN GOTO 1800
1610 IF MS(Y%)>50 AND MS(Y%+1)>50 AND MS(Y%+2)>50 THEN
       MF(A)=MS(Y%) ELSE GOTO 1590
1620 PF(A)=Y%
1630 Y%=Y%+1
1640 MAX = MS(Y%)
1650 Y%=Y%+1
1660 IF Y%>200 GOTO 1710
1670 IF MS(Y%)<0 GOTO 1710
1680 IF MS(Y%)>MAX OR MS(Y%)=MAX THEN
       MAX=MS(Y%):PP(A)=Y%
1690 IF MS(Y%)>MAX OR MS(Y%)=MAX THEN PP(A)=Y%
1700 GOTO 1650
1710 IF A=1 AND MAX<.03*P(1) THEN  GOTO 1590
1720 IF A=2 AND MAX<.03*P(2) THEN GOTO 1590
1730 P(A)=MAX
1740 Y%=PP(A)
1750 Y%=Y%+1
1760 IF Y%>200 THEN GOTO 1790
1770 IF MS(Y%)<10  AND MS(Y%+1)<10  AND MS(Y%+2)<10 THEN
       ML(A)=MS(Y%) ELSE GOTO 1750
1780 PL(A)=Y%
1790 '
1800 NEXT A
1810 '***** T0 INTEGRATE COMPUTER RECOGNISED PEAKS *****
1820 A=1
1830 IF A>2 THEN GOTO 2020
1840 IF P(A)-MF(A)<5 THEN A=A+1: GOTO 1830
1850 K%(A) =(PL(A)-PF(A))          'REM NO. DATA POINTS
1860 IF K%(A)=0 THEN GOTO 2020
1870 FOR I=0 TO K%(A)
```

```
1880 X(A,I)=MS(PF(A)+I)
1890 NEXT I
1900 TOTALR=0:TOTALT=0
1910 FOR I = 1 TO K%(A)
1920 AREA =X(A,I)*TIM
1930 TOTALR=TOTALR +AREA
1940 T(A,I)=X(A,I)-X(A,I-1)
1950 TAREA=T(A,I)*TIM/2
1960 TOTALT =TOTALT+TAREA
1970 NEXT I
1980 BASE=(MS(PF(A))+(MS(PL(A))-MS(PF(A)))/2)*(PL(A)-PF(A))*TIM
1990 FINALAREA(A)=TOTALT+TOTALR-BASE
2000 IF A=2 THEN CLOSE#0:GOTO 2020
2010 A=A+1:GOTO 1830
2020 ' ***** to store the data on the hard disc and print to screen *****
2030 IF C$="l" OR C$="L" THEN X=.00247:Y=-.881
2040 IF C$="r" OR C$="R" THEN X=.002464:Y=-.756
2050 TEMP =(TEMP/2*X+Y)/.0412
2060 Q%=Q%+1
2070  IF R=0 THEN PRINT#2,P(1)/WT,P(2)/WT,TEMP,Q% ELSE
      PRINT#2,P(1)*10/WT,P(2)*10/WT,TEMP,Q%
2080 IF R=0 THEN U=150 ELSE U=15
2090 PSET((TEMP-IT)*480/(FT-IT)+25,255-P(2)/U),7
2100 PSET((TEMP-IT)*480/(FT-IT)+25,255-P(1)/U)
2110 PSET((TEMP-IT)*480/(FT-IT)+25,255-(P(1)-.23*P(2))/U),8
2120 TG=(FT-TEMP)/TR
2130 PRINT TEMP,INT(P(1)/WT-.23*P(2)/WT),P(2)/WT,TG
2140 WHILE TIME$<"00:00:13"
2150 WEND
2160 IF P(1)>27000 OR P(2)>27000 THEN R=1
2170 IF R=1 AND P(1)<2700 AND P(2)<2700 THEN R=0
2180 TIME$="00:00:00"
2190 WHILE TIME$ <"00:00:bs-4"
2200 WHEN
2210 IF TEMP>FT  THEN STOP ELSE GOTO 1170
2220 CLS
2230 '***** read in parameters *****
2240 PRINT:PRINT:PRINT:PRINT
2250 PRINT TAB(30)" Data Aquisition"
2260 PRINT:PRINT:PRINT:PRINT
2270 PRINT TAB(20)"Temperature Programmed Desorption Series"
2280 PRINT:PRINT:PRINT:PRINT:
2290 PRINT TAB(30)"by Nick Stanbridge"
2300 TIME$="00:00:00"
2310 WHILE TIME$<"00:00:01"
2320 WEND
2330 CLS
2340 SCREEN 9
```

```
2350 INPUT "date";E$
2360 INPUT "sample";F$
2370 INPUT "probe";G$
2380 INPUT "initial temp";IT
2390 INPUT "final temp";FT
2400 INPUT "ramp rate";TR
2410 TT=(FT-IT)/TR
2420 INPUT"interval between scans";BS
2430 INPUT "sample mass (g)";WT
2440 INPUT "name of file for data to be stored in";B$
2450 INPUT "thermocouple used (L/R)";C$
2460 CLS
2470 PRINT:PRINT
2480 PRINT TAB(69) "Date"
2490 PRINT TAB(70) E$
2500 PRINT TAB(69) "Sample"
2510 PRINT TAB(70) F$
2520 PRINT TAB(69) "Probe"
2530 PRINT TAB(70) G$
2540 PRINT TAB(69) "Temp range"
2550 PRINT TAB(69) IT;"-";FT
2560 PRINT TAB(69)"Ramp rate "
2570 PRINT TAB(70)TR
2580 PRINT TAB(69)"Data File"
2590 PRINT TAB(70) B$
2600 PRINT TAB(70) ""
2610 PRINT TAB(73)
2620 PRINT TAB(70) ""
2630 PRINT TAB(73)
2640 PSET(0,0)
2650 DRAW"bd255;br25;r480;bl480;u255;bd255"
2660 FOR I = 1 TO INT((FT-IT)/10)
2670 X=INT(480/(FT-IT)*10+.5)
2680 DRAW"br=x;u2;d2;"
2690 NEXT
2700 G=INT((FT-IT)/10)*INT(480/(FT-IT)*10+.5)
2710 DRAW"l=g;"
2720 X=X*10
2730 FOR I = 1 TO INT((FT-IT)/100)
2740 DRAW"br=x;u4;d4;"
2750 NEXT
2760 PRINT:PRINT
2770 FOR F=0 TO FT/100-1
2780 X=INT(480/(FT-IT)*100*F/8)+2
2790 PRINT TAB(X)IT+100*F;
2800 NEXT
2810   PRINT:PRINT:PRINT    "          Temp","Ammonia","Water","Time
      remaining"
```

```
2820 VIEW PRINT 23 TO 24
2830 GOTO 1080
2840 WEND
2850 RETURN
```

3 READOUT Program

```
3000 '***** Large scale readout of sample temperature *****
3010 CLEAR,60000!
3020 SCREEN 9
3030 CLS
3040 KEY OFF
3050 INPUT "Which thermocouple";Z$
3060 IF Z$="l" OR Z$="L" THEN V=.00247:W=-.881
3070 IF Z$="r" OR Z$="R" THEN V=.002464:W=-.756
3080 TIME$="00:00:00"
3090 Q%=0
3100 '
3110 '***** reads thermocouple *****
3120 '                    Set Up Program to Accept Commands
3130 Z=60000!:BLOAD"AS.BIN",Z              'Load Support Program
3140 DATAOUT=Z:DATAIN=Z+3:STATUS=Z+6 'Set offsets for Calls
3150 AD%=&H500                         'Card Base Address
3160 S=0
3170 TEMP=0
3180  CMD$="F20,PA10000,G0,I1,QS1,QD1,QE,T"      'collects data from
        thermocouple
3190 CALL DATAOUT(AD%,CMD$,ST%)
3200 CALL STATUS(AD%,ST%)
3210 IF ST%<>0 THEN 3200
3220 CMD$="PA10000,QI"
3230 CALL DATAOUT(AD%,CMD$,ST%)
3240 CMD$="T"
3250 CALL DATAOUT(AD%,CMD$,ST%)
3260 CALL DATAIN(AD%,D%(0),D%(0),ST%)
3270 TEMP=D%(0)+TEMP
3280 TEMP =(TEMP*V+W)/.0412
3290 '***** draws numbers *****
3300 A$(1)="    *        "
3310 A$(2)="*********    "
3320 A$(3)="        *    "
3330 A$(4)="*            "
3340 A$(5)="*       *    "
3350 A$(7)="     *       "
3360 Y=TEMP
3370 DIFF=TEMP-PRETEMP
3380 PRETEMP=TEMP
3390 IF Y<100 THEN P=1
3400 IF P=0 THEN K=100
3410 IF P=1 THEN K=10
```

```
3420 IF P=2 THEN K=1
3430 IF P=3 THEN K=.1
3440 X=INT(Y/K)
3450 IF X=2 OR X=0 OR X=3 OR X=5 OR X=7 OR X=8 OR X=9 THEN
B$(1)=B$(1)+A$(2)
3460 IF X=1 THEN B$(1)=B$(1)+A$(1)
3470 IF X=6 THEN B$(1)=B$(1)+A$(4)
3480 IF X=4 THEN B$(1)=B$(1)+A$(5)
3490 IF X=2 OR X=3 OR X=7 THEN B$(2)=B$(2)+A$(3)
3500 IF X=4 OR X=8 OR X=9 OR X=0 THEN B$(2)=B$(2)+A$(5)
3510 IF X=5 OR X=6 THEN B$(2)=B$(2)+A$(4)
3520 IF X=1 THEN B$(2)=B$(2)+A$(1)
3530 B$(3)=B$(2)
3540 B$(4)=B$(2)
3550 IF X=1 THEN B$(5)=B$(5)+A$(1)
3560 IF X=0 THEN B$(5)=B$(5)+A$(5)
3570 IF X=7 THEN B$(5)=B$(5)+A$(7)
3580 IF X=2 OR X=3 OR X=4 OR X=5 OR X=6 OR X=8 OR X=9 THEN
B$(5)=B$(5)+A$(2)
3590 IF X=1 OR X=7 THEN B$(6)=B$(6)+A$(1)
3600 IF X=2 THEN B$(6)=B$(6)+A$(4)
3610 IF X=0 OR X=8 OR X=6 THEN B$(6)=B$(6)+A$(5)
3620 IF X=3 OR X=4 OR X=5 OR X=9 THEN B$(6)=B$(6)+A$(3)
3630 B$(7)=B$(6)
3640 B$(8)=B$(6)
3650 IF X=1 OR X=7 THEN B$(9)=B$(9)+A$(1)
3660 IF X=4 OR X=9 THEN B$(9)=B$(9)+A$(3)
3670 IF X=2 OR X=5 OR X=3 OR X=6 OR X=8 OR X=0 OR X=5  THEN
B$(9)=B$(9)+A$(2)
3680 Y=Y-X*K
3690 P=P+1
3700 CLS
3710 IF P=3 THEN GOTO 3740
3720 IF P=4 GOTO 3840
3730 GOTO 3400
3740 B$(1)=B$(1)+"       "
3750 B$(2)=B$(2)+"       "
3760 B$(3)=B$(3)+"       "
3770 B$(4)=B$(4)+"**     "
3780 B$(5)=B$(5)+"**     "
3790 B$(6)=B$(6)+"       "
3800 B$(7)=B$(7)+"       "
3810 B$(8)=B$(8)+"       "
3820 B$(9)=B$(9)+"       "
3830 GOTO 3400
3840 FOR Z=1 TO 9
3850 PRINT "                "+B$(Z)
3860 B$(Z)=""
```

```
3870 NEXT
3880 '***** draws bar *****
3890 P=0
3900 X=DIFF*100
3910 IF X>0 GOTO 3950
3920 DRAW"r=x;"
3930 DRAW "l=x;d20;r=x;u20;"
3940 IF X<0 GOTO 3960
3950 DRAW "R=x;d20;l=x;u20;"
3960 DRAW"bl=x;bd40"
3970 DRAW"u10;d10;r200;l400;"
3980 FOR SC= 1 TO 9
3990 DRAW"u5;d5;br50;"
4000 NEXT
4010 '***** waits ten seconds *****
4020 TIME$="00:00:00"
4030 WHILE TIME$<"00:00:10"
4040 WEND
4050 GOTO 3130
4060 RETURN
```

4 INTEGRAT Program

```
4500 '***** Integration program *****
4510 CLS
4520 DIM A(4040),B(700),C(700),D(700),E(700),T(700),A$(20)
4530 DIM J(20),K(20)
4540 PRINT:PRINT:PRINT:PRINT
4550 PRINT TAB(30)"Peak integration"
4560 PRINT:PRINT:PRINT:PRINT:
4570 PRINT TAB(20)"Temperature Programmed Desorption Series"
4580 PRINT:PRINT:PRINT:PRINT:
4590 PRINT TAB(30)"by Nick Stanbridge"
4600 TIME$="00:00:00"
4610 WHILE TIME$<"00:00:01"
4620 WEND
4630 SCREEN 9
4640 '***** input parameters *****
4650 CLS
4660 INPUT "number of files",FILE
4670 FOR H= 1 TO FILE
4680 INPUT"filename";A$(H)
4690 NEXT
4700 INPUT"initial temperature";IT
4710 INPUT "final temperature";FT
4720 INPUT"peak to be integrated";C$
4730 INPUT"number of integrations";N
4740 FOR R = 1 TO N
```

```
4750 INPUT "start,end of integration";J(R),K(R)
4760 NEXT R
4770 CLS
4780 '***** draws trace *****
4790 PRINT:PRINT:PRINT:PRINT:PRINT:PRINT:PRINT:PRINT:PRINT
       :PRINT:PRINT:PRINT:PRINT:PRINT:PRINT:PRINT:PRINT
4800 DRAW"bl350;bu160;r525;d290;l525;u290;"
4810 DRAW"bd255;br25;r480;bl480;u255;bd255"
4820 FOR I = 1 TO INT((FT-IT)/10)
4830 X=INT(480/(FT-IT)*10+.5)
4840 DRAW"br=x;u2;d2;"
4850 NEXT
4860 G=INT((FT-IT)/10)*INT(480/(FT-IT)*10+.5)
4870 DRAW"l=g;"
4880 X=X*10
4890 FOR I = 1 TO INT((FT-IT)/100)
4900 DRAW"br=x;u4;d4;"
4910 NEXT
4920 PRINT:PRINT
4930 FOR F= 0 TO FT/100-1
4940 X=INT(480/(FT-IT)*100*F/8)+2
4950 PRINT TAB(X)IT+100*F;
4960 NEXT
4970 FOR H= 1 TO FILE
4980 OPEN "i",1,(A$(H))
4990 FOR X=1 TO 10
5000 INPUT#1,K(X)
5010 NEXT
5020 Z%=0
5030 IF EOF(1) THEN 5110
5040 INPUT #1,A(Z%),B(Z%),D(Z%),E(Z%)
5050 PSET((D(Z%)-IT)*480/(FT-IT)+34,268-A(Z%)/150)
5060 PSET((D(Z%)-IT)*480/(FT-IT)+34,268-(A(Z%)-.23*B(Z%))/150)
5070 PSET((D(Z%)-IT)*480/(FT-IT)+34,268-B(Z%)/150)
5080 Z%=Z%+1:GOTO 5030
5090 GOTO 5040
5100 IF C$="17" OR C$="18" GOTO 5160
5110 FOR A%=1 TO Z%
5120 A(A%)=A(A%)-.23*B(A%)
5130 NEXT
5140 ***** INTEGRATES PEAKS *****
5150 LPRINT "Initial T,  Final T,  Area,  Base,   Rectangle, Triangle"
5160 IF C$="17" OR C$="17c" GOTO 5200
5170 FOR Q%=1 TO Z%
5180 A(Q%)=B(Q%)
5190 NEXT
5200 LPRINT A$(H)
5210 X=0
```

```
5220 X=X+1
5230 IF D(X)<FT GOTO 5220
5240 Z%=X
5250 FOR R=1 TO N
5260 AB=0:AT=0:YZ=0:AL=0
5270 X=0
5280 X=X+1
5290 IF D(X)<J(R) GOTO 5280 ELSE 5300
5300 L=X
5310 X=X+1
5320 IF D(X)<K(R) GOTO 5310 ELSE 5330
5330 M=X
5340 TOTALR=0:TOTALT=0
5350 FOR I = L TO M-1
5360 AREA =A(I)*(D(I+1)-D(I))
5370 TOTALR=TOTALR +AREA
5380 NEXT
5390 FOR I = L+1 TO M
5400 T(I)=(A(I)-A(I-1))*(D(I+1)-D(I))/2
5410 TOTALT =TOTALT+T(I)
5420 NEXT I
5430 W%=0
5440 FOR I=1 TO 10
5450 IF A(I)<.1*A(I+1) OR A(I)<.1*A(I+2) THEN W%=W%+1:GOTO 5470
5460 AT=AT+A(I)
5470 NEXT
5480 AB=AT/(10-W%)
5490 W%=0
5500 FOR I=Z%-10 TO Z%
5510 IF A(I)<.1*A(I-1) OR A(I)<.1*A(I-2) THEN W%=W%+1:GOTO 5530
5520 AL=AL+A(I)
5530 NEXT
5540 YZ=AL/10
5550 GRAD=(YZ-AB)/(D(Z%-5)-D(5))
5560 CONSTANT=FIRST-GRAD*D(5)
5570 BASE=((D(M)+D(L))*GRAD+2*CONSTANT)*(D(M)-D(L))/2
5580 BASE=ABS(BASE)
5590 FINALAREA=TOTALT+TOTALR-BASE
5600 LPRINT J(R);K(R);FINALAREA;BASE;TOTALR;TOTALT
5610 NEXT R
5620 CLOSE#1
5630 NEXT H
5640 RETURN
5650 FOR Y%=1 TO Z%
5660 A(Y%)=B(Y%)
5670 NEXT
5680 GOTO 5140
```

5 DIFF Program

```
6000 '***** Differentiation program *****
6010 CLS
6020 SCREEN 9
6030 AB=1:CD=1
6040 DIM DIFF(2000)
6050 DIM TEDI(2000),G(200,2)
6060 DIM A(1620),B(1620),C(1620),D(1620),E(1620),T(1620)
6070 PRINT:PRINT:PRINT:PRINT
6080 PRINT TAB(28)"Differentiation Program"
6090 PRINT:PRINT:PRINT:PRINT:
6100 PRINT TAB(20)" Temperature Programmed Desorption Series"
6110 PRINT:PRINT:PRINT:PRINT
6120 PRINT TAB(30)"by Nick Stanbridge"
6130 Z%=Z%+1
6140 TIME$="00:00:00"
6150 WHILE TIME$<"00:00:03"
6160 WEND
6170 CLS
6180 SCREEN 9
6190 ' ***** enter parameters *****
6200 INPUT "filename";A$
6210 INPUT"Save to hard disc";Q$
6220 INPUT"initial temperature";IT
6230 INPUT "final temperature";FT
6240 CLS
6250 IF QWE=1 THEN GOTO 6290
6260 VIEW PRINT 21 TO 24
6270 INPUT"coarseness (1=raw)";SX
6280 INPUT "Point ratio (1 to x)";F
6290 '***** WORK OUT DIFFERENTIAL *****
6300 OPEN "i",1,(A$(1))
6310 Z%=0
6320 FOR X= 1 TO 10
6330 INPUT #R,Z$
6340 NEXT
6350 IF EOF (1) THEN GOTO 6380
6360 INPUT #R,A(Z%),B(Z%),D(Z%),E(Z%)
6370 Z%=Z%+1: GOTO 6350
6380 LAST=INT(Z%/F)
6390 OPEN "i",2,(A$(2))
6400 Z%=0
6410 FOR X= 1 TO 10
6420 INPUT #2,Z$
6430 IF EOF (2) THEN GOTO 6460
6440 INPUT #R,A(Z%),B(Z%),D(Z%),E(Z%)
6450 Z%=Z%+1: GOTO 6350
```

```
6460 LAST=INT(Z%/F)
6470 CO=0
6480 AX(CO)=0:AY(CO)=0
6490 FOR X =(1+CO*F+AB*F-SX/2)TO (CO*F+AB*F+SX/2)
6500 AY(CO)=AY(CO)+A(X)
6510 AX(CO)=AX(CO)+D(X)
6520 NEXT
6530 AY(CO)=AY(CO)/SX
6540 AX(CO)=AX(CO)/SX
6550 IF CO= 1 THEN GOTO 6580
6560 CO = 1
6570 GOTO 6480
6580 DIFF(CD)=(AY(1)-AY(0))/(AX(1)-AX(0))
6590 TEDI(CD)=(AX(1)+AX(0))/2
6600 CD=CD+1
6610 AB=AB+1
6620 IF AB=LAST THEN GOTO 6650
6630 GOTO 6470
6640 '***** plots points *****
6650 PSET (34,170)
6660 DRAW"r600"
6670 DRAW "BL600; r80;u100;d200;u100;r40;u100;d200;u100;r40;u100;d200
6680 IF Q$="n" GOTO 6760
6690 INPUT "New filename";R$
6700 OPEN "a",2,(R$)
6710 FOR BC = CD-AB TO CD
6720 PSET((TEDI(BC)-IT)*480/(FT-IT)+34,170-DIFF(BC))
6730 PRINT#2,DIFF(BC),TEDI(BC)
6740 NEXT
6750 CLOSE
6760 SX=SX-1:F=F-1:QWE=1:AB=1
6770 IF SX=5 THEN GOTO 6790
6780 GOTO 6250
6790 INPUT "range for fitting x,y";A,B
6800 FOR X= 1 TO 1000
6810 IF TEDI(X)<A GOTO 6860
6820 IF TEDI(X)>B GOTO 6860
6830 C=C+1
6840 G(C,1)=TEDI(X)
6850 G(C,2)=DIFF(X)
6860 NEXT
6870 X=0
6880 FOR A = 1 TO C
6890 X=X+G(A,1)
6900 Y=Y+G(A,2)
6910 XY=XY+G(A,1)*G(A,2)
6920 XX=XX+G(A,1)^2
```

```
6930 NEXT
6940 GRAD=(C*XY-X*Y)/(C*XX-X^2)
6950 CONS=(Y-GRAD*X)/C
6960 TMAX=-CONS/GRAD
6970 MEAX=X/C
6980 MEAY=Y/C
6990 FOR A = 1 TO C
7000 CYY=CYY+(G(A,2)-MEAY)^2
7010 CXX=CXX+(G(A,1)-MEAX)^2
7020 TOP=TOP+(G(A,1)-MEAX)*(G(A,2)-MEAY)
7030 NEXT
7040 BOT =(CXX*CYY)^.5
7050 CC=TOP/BOT
7060 PRINT"Points gradient constant Tmax r^2"
7070 LPRINT C,GRAD,CONS,TMAX,CC
7080 CLS
7090 RETURN
```

6 SUBTRACT Program

```
7500 '***** Subtraction Program *****
7510 CLS
7520 DIM A(900,2),B(900,2),D(900,2),E(900,2),NA(700,2)
7530 PRINT:PRINT:PRINT:PRINT
7540 PRINT TAB(25)"Subtraction Program"
7550 PRINT:PRINT:PRINT:PRINT:
7560 PRINT TAB(15)" Temperature Programmed Desorption Series"
7570 PRINT:PRINT:PRINT:PRINT
7580 PRINT TAB(25)"by Nick Stanbridge"
7590 TIME$="00:00:00"
7600 WHILE TIME$<"00:00:03"
7610 WEND
7620 SCREEN 9
7630 PRINT"first file will be subtracted from second file"
7640 INPUT"first filename";A$(1)
7650 INPUT"second filename";A$(2)
7660 INPUT" Save results to hard disc?",Q$
7670 CLS
7680 FOR R = 1 TO 2
7690 OPEN "i",R,(A$(R))
7700 SOUND 300,5
7710 Z%=0
7720 FOR X= 1 TO 10
7730 INPUT #R,Z$
7740 NEXT
7750 IF EOF (R) THEN GOTO 7810
7760 INPUT #R,A(Z%,R),B(Z%,R),D(Z%,R),E(Z%,R)
```

```
7770 GOTO 7790
7780 PSET((D(Z%,R))*480/700+34,268-A(Z%,R)/50)
7790 Z%=Z%+1:GOTO 7750
7800 GOTO 7760
7810 FOR V=100 TO 700 STEP 10
7820 X=X+1
7830 IF D(X,R)<V THEN GOTO 7820
7840 GRAD=(A(X+1,R)-A(X-1,R))/(D(X+1,R)-D(X-1,R))
7850 CONST=A(X+1,R)-GRAD*D(X+1,R)
7860 NA(V,R)=GRAD*V+CONST
7870 PSET((V)*480/700+34,268-NA(V,1)/50)
7880 NEXT V
7890 NEXT
7900 FOR V=100 TO 700
7910 SUB(V)=NA(V,2)-NA(V,1)
7920 PSET((V)*480/700+34,268-SUB(V)/50)
7930 NEXT
7940 IF Q$="y" OR Q$="Y" THEN GOTO 7950 ELSE STOP
7950 INPUT "filename";R$
7960 OPEN "O",2,R$
7970 FOR X=100 TO 700
7980 PRINT#2,V;SUB(V)
7990 NEXT
8000 RETURN
```

7 PLOT Program

```
8500 '***** Plot Program *****
8510 CLS
8520 DIM A(4040),B(900),C(900),D(900),E(900),T(900)
8530 PRINT:PRINT:PRINT:PRINT
8540 PRINT TAB(38)"Plot Program"
8550 PRINT:PRINT:PRINT:PRINT:
8560 PRINT TAB(25)" Temperature Programmed Desorption Series"
8570 PRINT:PRINT:PRINT:PRINT
8580 PRINT TAB(35)"by Nick Stanbridge"
8590 TIME$="00:00:00"
8600 WHILE TIME$<"00:00:03"
8610 WEND
8620 SCREEN 9
8630 '***** input parameters *****
8640 CLS
8650 INPUT "number of files";Q
8660 FOR R=1 TO Q
8670 INPUT"filename";A$(R)
8680 INPUT"Ammonia",Q$
8690 INPUT"Water";R$
8700 NEXT
```

```
8710 INPUT"initial temperature";IT
8720 INPUT "final temperature";FT
8730 CLS
8740 ' ***** Draws trace *****
8750 PRINT:PRINT:PRINT:PRINT:PRINT:PRINT:PRINT:PRINT:
       PRINT:PRINT:PRINT:PRINT:PRINT:PRINT:PRINT:PRINT:PRINT
8760 DRAW"bl350;bu160;r525;d290;l525;u290;"
8770 DRAW"bd255;br25;r480;bl480;u255;bd255"
8780 FOR I = 1 TO INT((FT-IT)/10)
8790 X=INT(480/(FT-IT)*10+.5)
8800 DRAW"br=x;u2;d2;"
8810 NEXT
8820 G=INT((FT-IT)/10)*INT(480/(FT-IT)*10+.5)
8830 DRAW"l=g;"
8840 X=X*10
8850 FOR I = 1 TO INT((FT-IT)/100)
8860 DRAW"br=x;u4;d4;"
8870 NEXT
8880 PRINT:PRINT
8890 FOR F= 0 TO FT/100-1
8900 X=INT(480/(FT-IT)*100*F/8)+2
8910 PRINT TAB(X)IT+100*F;
8920 NEXT
8930 FOR R = 1 TO Q
8940 OPEN "i",R,(A$(R))
8950 SOUND 300,5
8960 Z%=0
8970 FOR X= 1 TO 10
8980 INPUT #R,Z$
8990 NEXT
9000 IF EOF (R) THEN GOTO 9090
9010 INPUT #R,A(Z%),B(Z%),D(Z%),E(Z%)
9020 PSET((D(Z%)-IT)*480/(FT-IT)+34,268-E(Z%)/2)
9030 IF Q$="n" AND R$="y" GOTO 9060
9040 PSET((D(Z%)-IT)*480/(FT-IT)+34,268-(A(Z%)-.23*B(Z%))/50)
9050 IF Q$="y" AND R$="n" GOTO 9000
9060 PSET((D(Z%)-IT)*480/(FT-IT)+34,268-B(Z%)/50)
9070 Z%=Z%+1:GOTO 9000
9080 GOTO 9010
9090 NEXT
9100 STOP
9110 RETURN
```